



ABB Impell Corporation

**OYSTER CREEK NUCLEAR GENERATING STATION
STRUCTURAL EVALUATION OF THE
SPENT FUEL POOL**

Prepared for:

GPU Nuclear Corporation
One Upper Pond Road
Parsippany, NJ 07054

Prepared by:

ABB Impell Corporation
770 Cochituate Road
Framingham, MA 01701

Report No. 03-0370-1341

Revision 0

June 29, 1992

DOCUMENT APPROVAL COVER SHEET



DOCUMENT NUMBER: 03-0370-1341

TITLE: Oyster Creek Nuclear Generating Station
Structural Evaluation of the Spent Fuel Pool

DOCUMENT TYPE:
 CALCULATION
 SPECIFICATION
 REPORT
 DOCUMENT PER
 QP-3.11

CLIENT: GPU Nuclear Corporation

PROJECT: Evaluation of the Spent Fuel Pool

PROJECT NUMBER: 0370-187

SUMMARY DESCRIPTION:

This report documents the Structural Analysis of the Spent Fuel Pool (SFP), at Oyster Creek Nuclear Generating Station (OCNGS), for consolidated and high density fuel rack loads in addition to normal and abnormal plant operating loads. The structural analysis considered the change in stiffness due to concrete cracking and reductions in embedment length of reinforcing steel bars.

The evaluation concluded that the SFP walls (East, West, North and South), SFP slab, girders RD, RE and R6 and Column C6 were in compliance with the requirements of ACI 349-80 code for high density racks and consolidated fuel racks. These are the only components of the SFP structure that would be affected by the addition of Spent Fuel loads.

REV.	REVISION DESCRIPTION	NO. PAGES	ORIGINATOR/ DATE	VERIFIER/ DATE	APPROVER/ DATE
0	Original Issue		G. S. Bjorkman <i>[Signature]</i> 6/29/92	A. I. S. Sain <i>[Signature]</i> 6/29/92	J. F. Rich <i>[Signature]</i> 6/30/92

PAGE 1 CONT ON 1

	PAGE
3.2 Description of Analysis Cases	38
3.2.1 Analysis Case A	38
3.2.2 Analysis Case B	38
3.2.3 Analysis Case C (Licensed Condition)	38
3.2.4 Analysis Case D	38
3.3 Load Combinations	38
3.3.1 Analysis Cases A and B	39
3.3.2 Analysis Cases C and D	39
3.4 Material Properties and Section Capacity	40
4.0 SPENT FUEL POOL BEHAVIOR	
4.1 Basic Considerations	42
4.2 The Evaluation Process	42
4.2.1 Reactor Building Structural Response	42
4.2.1.1 Design Intent and the Primary Supporting Members	43
4.2.1.2 Effect of Thermal and Mechanical Loads on Floor Slabs	43
4.2.1.3 Influence of Floor Slabs on SFP Response	45
4.2.1.4 Conclusions Regarding Floor Slab Behavior	46
4.2.1.5 Effect of Temperature Conditions on Shield Wall and SFP Cracking	46
4.2.2 Analysis Strategy	47
4.2.3 Application of the Cracking Methodology Using the Branson Equation	49
4.2.4 Load Application and Stiffness	51
4.2.4.1 Incorporating Seismic Loads	52
4.2.4.2 Selection of Critical Seismic Load Directions	53
4.3 The Cracking Iteration Process	54
4.3.1 SFP Behavior and the Iteration Process	55
4.3.1.1 Analysis Case C - High Density Storage	55
4.3.1.2 Analysis Case D - Consolidated Fuel Storage	61
4.3.2 Description of Cracking Iterations for Analysis Case C	62
4.3.3 Description of Cracking Iterations for Analysis Case D	68
5.0 SUMMARY OF RESULTS	
5.1 The Evaluation Process	119
5.2 Evaluation of Critical Sections	120
5.2.1 Evaluation of Girders and Columns	122
5.2.1.1 High Density Fuel Storage - Analysis Case C	122
5.2.1.2 Consolidated Fuel Storage - Analysis Case D	124

	PAGE
5.2.2 Evaluation of the SFP Slab	125
5.2.2.1 High Density Fuel Storage - Analysis Case C	125
5.2.2.2 Consolidated Fuel Storage - Analysis Case D	129
5.2.3 Evaluation of the SFP Walls	130
5.2.3.1 High Density Fuel Storage - Analysis Case C	130
5.2.3.2 Consolidated Fuel Storage - Analysis Case D	130
5.2.4 Example Code Check Evaluations	131
5.2.4.1 Girder RE Evaluation Example	131
5.2.4.2 SFP Slab Evaluation Example	137
5.3 Correlation of Analysis Results with Observed Cracking	140
5.3.1 Crack Beneath the SFP North Wall in the Floor Slab at Elevation 75'	141
5.3.2 Cracks in the Shield Wall and Pool Walls	143
5.3.3 Cracking of Floor Slabs at Elevations 75', 95', and 119'	148
5.3.4 Cracks in Girder RE	150
5.4 Conclusions	155
6.0 REFERENCES	282

APPENDIX

- A. ANSYS Input File Listings
- B. Analysis Criteria Document, Revision 1

LIST OF FIGURES

- Figure 2.1 Plan View; North Half of Reactor Building
- Figure 2.2 Elevation View; North Half of Reactor Building
- Figure 2.3 SFP Finite Element Model Plot; Shield Wall
- Figure 2.4 SFP Finite Element Model Plot; Shield Wall and Girders
- Figure 2.5 SFP Finite Element Model Plot; Shield Wall, Girders and SFP Slab
- Figure 2.6 SFP Finite Element Model Plot; Shield Wall, Girder, SFP Corners and SFP Slab
- Figure 2.7 SFP Finite Element Model Plot; SFP Walls
- Figure 2.8 SFP Finite Element Model Plot; Walls and Solid Elements at Elevation 75'-3"
- Figure 2.9 Support Frame for Column C6 Plot
- Figure 2.10 SFP Finite Element Model Plot; SFP Walls and Floors
- Figure 2.11 SFP Finite Element Model Plot; SFP Walls, Floors and Columns

- Figure 2.12 SFP Finite Element Model Plot; SFP Walls, Floors and Columns Viewed from Northwest
- Figure 2.13 SFP Finite Element Model Plot; SFP Walls, Floors and Columns Viewed from Southeast
- Figure 2.14 SFP Finite Element Model Plot; Full Model
- Figure 2.15 Geometry Plot; Slice Through Girder RD; Viewed From East
- Figure 2.16 Geometry Same as Figure 2.15; Closer Look
- Figure 2.17 Geometry Plot; Slice Through Girder RE; Viewed From East
- Figure 2.18 Shield Wall Interface with the Girders and Column C5
- Figure 2.19 Shield Wall; Girders; SFP Slab at Elevation 75'-3" and Exterior Columns; Viewed from Northwest Below
- Figure 2.20 Geometry Plot; Shield Wall; SFP Walls and Slab; Girders and Walls Corners; Viewed from Northwest Below
-
- Figure 4.1 Floor at Elevation 119'-3"
- Figure 4.2 Principal Stresses (SIG1); Floor at Elevation 119'-3"; Case C Iteration 0; Winter Temperature
- Figure 4.3 Principal Stresses (SIG1); Floor at Elevation 119'-3"; Case A Iteration 2; Equation "a"
- Figure 4.4 Principal Stresses (SIG1) for Figure 4.1; Iteration 0
- Figure 4.5 Principal Stresses (SIG1); Floor at Elevation 119'; Case C Iteration 0; DL+LL+T_w
- Figure 4.6 Principal Stresses Vector Plot; Floor at Elevation 119'; Case C Iteration 0; DL+LL
- Figure 4.7 Principal Stresses Vector Plot; Floor at Elevation 119'; Case C Iteration 0; DL+LL+T_w
- Figure 4.8 Horizontal Displacement (UX); FE Model; Case C Iteration 2; Concrete Dead Load
- Figure 4.9 Vertical Displacement (UZ); FE Model; Case C Iteration 2; Concrete Dead Load
- Figure 4.10 Principal Stresses (SIG1); FE Model Viewed From East; Case C Iteration; Concrete Dead Load 0
- Figure 4.11 Principal Stresses (SIG1); FE Model Viewed from East; Case C Iteration 0; Hydrostatic + Rack High Density + Cask
- Figure 4.12 Principal Stresses (SIG1); FE Model Viewed from East; Case C Iteration 0; Winter Temperature (T_w)
- Figure 4.13 Principal Stresses (SIG1); FE Model Viewed from East; Case C Iteration 1; Concrete Dead Load
- Figure 4.14 Principal Stresses (SIG1); FE Model Viewed from East; Case C Iteration 1; Hydrostatic + High Density Rack + Cask
- Figure 4.15 Principal Stresses (SIG1); FE Model Viewed from East; Case C Iteration 1; Winter Temperature (T_w)
- Figure 4.16 Principal Stresses (SIG1); Girder RE Viewed from East; Case C Iteration 0; Winter Temperature (T_w)

ABB Impell Corporation

- Figure 4.17 Principal Stresses (SIG1); Girder RE Viewed from East; Case C Iteration 1; Winter Temperature (T_w)
- Figure 4.18 Temperature Distribution; FE Model Viewed from East; Winter Temperature (T_w)
- Figure 4.19 Temperature Distribution; FE Model Viewed from East; Summer Temperature (T_s)
- Figure 4.20 Principal Stresses (SIG1); FE Model Viewed from Southwest; Case C Iteration 0; Summer Temperature (T_s)
- Figure 4.21 Principal Stresses (SIG1); FE Model Viewed From Northeast; Case C Iteration 0; Summer Temperature (T_s)
- Figure 4.22 Principal Stresses (SIG1); FE Model Viewed from Southwest; Case C Iteration 0; Winter Temperature (T_w)
- Figure 4.23 Principal Stresses (SIG1); FE Model Viewed from Northeast; Case C Iteration 0; Winter Temperature (T_w)
- Figure 4.24 Principal Stresses (SIG1) Above 400 PSI; FE Model Viewed from Southeast; Case C Iteration 0; Summer Temperature (T_s)
- Figure 4.25 Principal Stresses (SIG1) Above 400 PSI; FE Model Viewed from Southeast; Case C Iteration 0; Winter Temperature (T_w)
- Figure 4.26 Principal Stresses (SIG1); FE Model Viewed from Southwest; Case C Iteration 1; Load Combination "b"
- Figure 4.27 Principal Stresses (SIG1); FE Model Viewed from Southeast; Case C Iteration 1; Load Combination "e"
- Figure 4.28 Geometry Plot of FE model; Viewed from Northwest Below
- Figure 4.29 Principal Stresses (SIG1); FE Model Viewed from Northwest Below; Case C Iteration 1; Load Combination "e" (Stresses 0-720)
- Figure 4.30 Principal Stresses (SIG1); FE Model Viewed from Northwest Below; Case C Iteration 2; Concrete Dead Load
- Figure 4.31 Principal Stresses (SIG1); FE Model Viewed from Northwest Below; Case C Iteration 2; Hydrostatic + High Density Rack + Cask
- Figure 4.32 Principal Stresses (SIG1); FE Model Viewed from Northwest Below; Case C Iteration 2; Design Live Load
- Figure 4.33 Principal Stresses (SIG1); FE Model Viewed from Northwest Below; Case C Iteration 2; Winter Temperature (T_w)
- Figure 4.34 Principal Stresses (SIG1); FE Model Viewed from Northwest Below; Case C Iteration 2; Cask Drop Accident
- Figure 4.35 Principal Stresses (SIG1); FE Model Viewed from Northwest Below; Case C Iteration 0; Concrete Dead Load
- Figure 4.36 Principal Stresses (SIG1: 0-1120); FE Model Viewed from Northeast Below; Case C Iteration 2; Load Combination "e"
- Figure 4.37 Stresses in X-direction (SX) for Figure 2.15; Case C Iteration 2; Load Combination "e"
- Figure 4.38 Shear Stresses (SXZ); Close View of Figure 4.37
- Figure 4.39 Stresses (SX); Slice Through Girder RE; Case C Iteration 2; Load Combination "e"

- Figure 4.40 Shear Stress (SX); Slice Through Girder RE; Case C Iteration 2; Load Combination "e"
- Figure 4.41 Stress (SX) at Both Faces of Girder RE; Case C Iteration 2; Load Combination "b"
- Figure 4.42 Shear Stresses (SXZ) at Both Faces of Girder RE; Case C Iteration 2; Load Combination "b"
- Figure 4.43 Principal Stresses (SIG1); FE Model Viewed from Northwest Below; Iteration 3RB; Load Combination "e"
- Figure 4.44 Same as Figure 4.49; Stresses Limited to 1040 psi
- Figure 4.45 Stresses (SX) Slice Through Girder RD; Case C Iteration 2; Concrete Dead Load
- Figure 4.46 Stresses (SX) Slice Through Girder RD; Case C Iteration 3RB; Concrete Dead Load
- Figure 4.47 Stresses (SX); SFP Slab and Girders RD, RE and R6
- Figure 4.48 Same as Figure 4.47, but Stress Limited to 124 psi
- Figure 4.49 Stresses in X-direction (SX); FE Model Viewed from Northeast; Case C Iteration 4; Load Combination "a"
- Figure 4.50 Same as Figure 4.41 but Stresses Range (0-400 psi)
- Figure 4.51 Vertical Displacement (UZ); Girders RD, RE and R6, and Columns C6, D7, E7 and F6
- Figure 4.52 Stresses (SZ); Girders RD, RE, and R6, and Columns C6, D7, E7 and F6
- Figure 4.53 Vertical Displacement (UZ); SFP Slab and Girders RD, RE and R6; Case C Iteration 2; Concrete Dead Load
- Figure 4.54 Stresses in Y-direction (SY); SFP Slab and Girders; Case C Iteration 2; Concrete Dead Load
- Figure 4.55 Same as Figure 4.47 Stresses Limited to 87 psi
- Figure 4.56 Shear Stresses (SYZ); FE Model; Case C Iteration 3US; Seismic In + Y + Hydrodynamic
- Figure 4.57 Shear Stresses (SXY); FE Model; Case C Iteration 3US; Seismic In + Y + Hydrodynamic
- Figure 4.58 Principal Stresses (SIG1); FE Model; Case C Iteration 3US; Seismic In + Y + Hydrodynamic
- Figure 4.59 Stresses (SX); SFP Slab and Girders Viewed from Below; Case C Iteration 3US; Seismic In - X + Hydrodynamic
- Figure 4.60 Stresses (SX); SFP Slab and Girders Viewed from Below; Case C Iteration 3US; Seismic In + Y + Hydrodynamic
- Figure 4.61 Stresses (SX); SFP Slab and Girders Viewed from Below; Case C Iteration 3US; Seismic In + Z + Hydrodynamic

- Figure 5.1 Critical Section Locations in the SFP Slab and Girders
- Figure 5.2 Location in the Slab Where Linearized Stresses Computed Through the Slab Thickness for Bending Evaluation
- Figure 5.3 Portions of Girders RD and RE between the SFP North Wall and Exterior Walls

- Figure 5.4 Node Numbers at the East Face of Girder RE
 Figure 5.5 Node Numbers at the West Face of Girder RE
 Figure 5.6 Girder RE "Linearized Stresses Plot at the East Face" at the Critical Section for Moment
 Figure 5.7 Girder RE "Linearized Stresses Plot at the West Face" at the Critical Section for Moment
 Figure 5.8 Load-Moment Interaction Diagram for Girder RE
 Figure 5.8A Girder RE Moment Capacity Plot vs. Factored Moment
 Figure 5.9 Geometry Plot Plan View for the Girders RD, RE and R6 and the Shield Wall
 Figure 5.10 Displacement Plot for Figure 5.9; Case C Iteration 3R; Loading = DL+LL+T_w
 Figure 5.11 Shear Stress Distribution (SXY); at Elevation 75'-3"; Case C Iteration 2; Loading = DL+LL+T_w
 Figure 5.12 Shear Stress Distribution (SXY); at Elevation 75'-3"; Case C Iteration 0; Loading = DL+LL+T_w
 Figure 5.13 Same as Figure 5.12 but Stress Limited to 150 psi
 Figure 5.14 Load-Moment Interaction Diagram for the SFP Slab; Case C Iteration 3R
 Figure 5.15 Half of the Reactor Building Plot; Showing Location of Cracks in Slab at Elevation 75'-3"
 Figure 5.16 Principal Stresses (SIG1); FE Model Viewed from Northwest Below; Case C Iteration 2; Load Combination "e"
 Figure 5.17 Principal Stresses (SIG1); FE Model Viewed from Northwest Below; Case C Iteration 2; Load Combination "b"
 Figure 5.18 Geometry Plot; Floor Slab at Elevation 75'-3"; Viewed from Southeast
 Figure 5.19 Stresses (SX); Floor Slab at Elevation 75'-3"; Case C Iteration 2; DL+LL+T_w
 Figure 5.20 Stresses (SX); Limited to 520 P.; Case C Iteration 2; DL+LL+T_w
 Figure 5.21 Geometry Plot; Slab at Elevation 75'-3" Interface with the SFP Wall
 Figure 5.22 Stresses (SX); Slab at Elevation 75'-3" and Corner of SFP Wall; Case C Iteration 2; DL+LL+T_w
 Figure 5.23 Stresses (SX); Slab at Elevation 75'-3"; Case C Iteration 2; DL+LL+T_w
 Figure 5.24 Reinforcement in Slab at Elevation 75'-3"
 Figure 5.25 Lack of Bars Embedment in Slab at Elevation 75'-3"
 Figure 5.26 Crack in Slab at Elevation 75'-3"
 Figure 5.27 Displacement (Hz); Slab at Elevation 75'-3"; Case C Iteration 2; Load Combination "b"
 Figure 5.28 Geometry Plot of Shield Wall and SFP Wall Viewed from West
 Figure 5.29 Geometry Plot of Shield Wall and SFP Wall Viewed from East
 Figure 5.30 Principal Stresses (SIG1); SFP Walls and Shield Wall Viewed from Southwest Above; Case C Iteration 0; DL+LL
 Figure 5.31 Principal Stresses Vector Plot; SFP Walls and Shield Wall Viewed from West; Case C Iteration 0; DL+LL

- Figure 5.32 Principal Stresses (SIG1); SFP Walls and Shield Wall Viewed from West; Case C Iteration 0; DL+LL+T_w
- Figure 5.33 Principal Stresses Vector Plot; SFP Walls and Shield Wall Viewed from West; Case C Iteration 0; DL+LL+T_w
- Figure 5.34 Principal Stresses (SIG1); SFP Walls and Shield Wall Viewed from West; Case C Iteration 0; DL+LL+T_s
- Figure 5.35 Principal Stresses Vector Plot; SFP Walls and Shield Wall Viewed from West; Case C Iteration 0; DL+LL+T_s
- Figure 5.36 Principal Stresses (SIG1); SFP Walls and Shield Wall Viewed from West; Case C Iteration 1; DL+LL
- Figure 5.37 Principal Stresses Vector Plot; SFP Walls and Shield Wall Viewed from West; Case C Iteration 1; DL+LL
- Figure 5.38 Principal Stresses (SIG1); SFP Walls and Shield Wall Viewed from West; Case C Iteration 1; DL+LL+T_w
- Figure 5.39 Principal Stresses Vector Plot; SFP Walls and Shield Wall Viewed from West; Case C Iteration 1; DL+LL+T_w
- Figure 5.40 Principal Stresses (SIG1); SFP West Wall and Shield Wall Viewed from West; Case C Iteration 1; DL+LL+T_s
- Figure 5.41 Principal Stresses Vector Plot; SFP West Wall and Shield Wall Viewed from West; Case C Iteration 1; DL+LL+T_s
- Figure 5.42 Principal Stresses (SIG1); SFP East Wall and Shield Wall Viewed for East; Case C Iteration 0; DL+LL
- Figure 5.43 Principal Stresses Vector Plot; SFP East Wall and Shield Wall Viewed from East; Case C Iteration 0; DL+LL
- Figure 5.44 Principal Stresses (SIG1); SFP East Wall and Shield Wall Viewed from East; Case C Iteration 0; DL+LL+T_w
- Figure 5.45 Principal Stresses Vector Plot; SFP East Wall and Shield Wall Viewed from East; Case C Iteration 0; DL+LL+T_w
- Figure 5.46 Principal Stresses (SIG1); SFP East Wall and Shield Wall Viewed from East; Case C Iteration; 0 DL+LL+T_s
- Figure 5.47 Principal Stresses Vector Plot; SFP East Wall and Shield Wall Viewed from East; Case C Iteration 0; DL+LL+T_w
- Figure 5.48 Principal Stresses (SIG1); SFP East Wall and Shield Wall Viewed from East; Case C Iteration; 1 DL+LL
- Figure 5.49 Principal Stresses Vector Plot; SFP East Wall and Shield Wall Viewed from East; Case C Iteration 1; DL+LL
- Figure 5.50 Principal Stresses (SIG1); SFP East Wall and Shield Wall Viewed from East; Case C Iteration 1; DL+LL+T_w
- Figure 5.51 Principal Stresses Vector Plot; SFP East Wall and Shield Wall Viewed from East; Case C Iteration 1; DL+LL+T_w
- Figure 5.52 Principal Stresses (SIG1); SFP East Wall and Shield Wall Viewed from East; Case C Iteration 1; DL+LL+T_s
- Figure 5.53 Principal Stresses Vector Plot; SFP East Wall and Shield Wall Viewed from East; Case C Iteration 1; DL+LL+T_s

- Figure 5.54 Geometry Plot; SFP East Wall and Shield Wall Viewed from East
- Figure 5.55 Geometry Plot; SFP Wall and Shield Wall Plan View; Case C Iteration 0; Winter Temperature (T_w)
- Figure 5.56 Principal Stresses (SIG1); SFP Wall and Shield Wall Plan View
- Figure 5.57 Principal Stresses (SIG1); SFP East Wall and Shield Wall Viewed from East; Case C Iteration 1; Winter Temperature (T_w)
- Figure 5.58 Stresses (SZ); SFP East Wall and Shield Wall Viewed from East; Case C Iteration 0; Winter Temperature (T_w)
- Figure 5.59 Stresses (SZ); SFP East Wall and Shield Wall Viewed from East; Case C Iteration 1; Winter Temperature (T_w)
- Figure 5.60 Stresses (SY); SFP East Wall and Shield Wall Viewed from East; Case C Iteration 0; Winter Temperature (T_w)
- Figure 5.61 Stresses (SY); SFP East Wall and Shield Wall Viewed from East; Case C Iteration 1; Winter Temperature (T_w)
- Figure 5.62 Principal Stresses (SIG1); SFP Walls and Shield Wall Plan View; Case C Iteration 0; Winter Temperature (T_w)
- Figure 5.63 Principal Stresses (SIG1); SFP Walls and Shield Wall Plan View; Case C Iteration 1; Winter Temperature (T_w)
- Figure 5.64 Stresses (SY); SFP Walls and Shield Wall Plan View; Case C Iteration 0; Winter Temperature (T_w)
- Figure 5.65 Stresses (SY); SFP Walls and Shield Wall Plan View; Case C Iteration 1; Winter Temperature (T_w)
- Figure 5.66 Displacement Plot; SFP Walls and Shield Wall Plan View; Case C Iteration 0; Winter Temperature (T_w)
- Figure 5.67 Displacement Plot; SFP Walls and Shield Wall Plan View; Case C Iteration 1; Winter Temperature (T_w)
- Figure 5.68 Linearized Stress Plot Through the Shield Wall Thickness; Case C Iteration 0; Winter Temperature (T_w)
- Figure 5.69 Linearized Stress Plot Through the Shield Wall Thickness; Case C Iteration 1; Winter Temperature (T_w)
- Figure 5.70 Principal Stresses (SIG1); SFP West Wall Viewed from West; Case C Iteration 0; DL+LL+ T_w
- Figure 5.71 Principal Stresses and Vector Plot; SFP West Wall Viewed from West; Case C Iteration 0; DL+LL+ T_w
- Figure 5.72 Principal Stresses (SIG1); SFP West Wall Viewed from West; Case C Iteration 1; DL+LL+ T_w
- Figure 5.73 Principal Stresses Vector Plot; SFP West Wall Viewed from West; Case C Iteration 1; DL+LL+ T_w
- Figure 5.74 Principal Stresses (SIG1); SFP East Wall Viewed from East; Case C Iteration 0; DL+LL+ T_w
- Figure 5.75 Principal Stresses Vector Plot; SFP East Wall Viewed from East; Case C Iteration 0; DL+LL+ T_w
- Figure 5.76 Principal Stresses (SIG1); SFP East Wall Viewed from East; Case C Iteration 1; DL+LL+ T_w

- Figure 5.77 Principal Stresses Vector Plot; SFP East Wall Viewed from East; Case C Iteration 1; DL+LL+T_w
- Figure 5.77A Stresses (SX); SFP Wall and Shield Wall Plan View; Case C Iteration 1; Winter Temperature (T_w)
- Figure 5.78 Geometry Plot; SFP North Wall Viewed from North
- Figure 5.79 Principal Stresses (SIG1); SFP North Wall Viewed from North; Case C Iteration 0; DL+LL+T_w
- Figure 5.80 Principal Stresses Vector Plot; SFP North Wall Viewed from North; Case C Iteration 0; DL+LL+T_w
- Figure 5.81 Principal Stresses (SIG1); SFP North Wall Viewed from North; Case C Iteration 1; DL+LL+T_w
- Figure 5.82 Principal Stresses Vector Plot; SFP North Wall View from North; Case C Iteration 0; DL+LL+T_w
- Figure 5.83 Predicted Crack Pattern on the West Face of the Spent Fuel Pool and Shield Wall
- Figure 5.84 Predicted Crack Pattern on the East Face of the Spent Fuel Pool and Shield Wall
- Figure 5.85 Predicted Crack Pattern for the North Face of the Spent Fuel Pool
- Figure 5.86 Observed Cracks on the West Face of the Spent Fuel Pool and Shield Wall
- Figure 5.87 Observed Cracks on the East Face of the Spent Fuel Pool and Shield Wall
- Figure 5.88 Observed Cracks on the North Wall of the Spent Fuel Pool
- Figure 5.89 Principal Stresses (SIG1); Floor at Elevation 119'; Case C Iteration 0; DL+LL+T_w
- Figure 5.90 Principal Stresses (SIG1); Range (400-1000) Floor at Elevation 119'; Case C iteration 0; DL+LL+T_w
- Figure 5.91 Principal Stresses Vector Plot; Floor at Elevation 119'; Case C Iteration 0; DL+LL+T_w
- Figure 5.92 Principal Stresses Vector Plot; Floor at Elevation 119' (Pool Walls and Shield Wall Excluded); Case C Iteration 0; DL+LL+T_w
- Figure 5.93 Geometry Plot Floor at Elevation 95'
- Figure 5.94 Principal Stresses (SIG1); Floor at Elevation 95'; Case C Iteration 0; DL+LL+T_w
- Figure 5.95 Principal Stresses Vector Plot; Floor at Elevation 95'; Case C Iteration 0; DL+LL+T_w
- Figure 5.96 Principal Stresses (SIG 1); Floor at Elevation 95'; Case C Iteration 0; DL+LL+T_w
- Figure 5.97 Geometry Plot; Floor at Elevation 75'
- Figure 5.98 Geometry Plot; Floor at Elevation 75'; Viewed from Northwest Above
- Figure 5.99 Principal Stresses (SIG1); Floor at Elevation 75'-3"; Case C Iteration 0; DL+LL+T_w
- Figure 5.100 Principal Stresses Vector Plot; Floor and Elevation 75'-3"; Case C Iteration 0; DL+LL+T_w

- Figure 5.101 Predicted Crack Pattern for Floor Slab at Elevation 119'
- Figure 5.102 Predicted Crack Pattern for Floor Slab at Elevation 95'
- Figure 5.103 Predicted Crack Pattern for Floor Slab at Elevation 75'
- Figure 5.104 Observed Cracks in Floor at Elevation 119'
- Figure 5.105 Observed Cracks in Floor at Elevation 95'
- Figure 5.106 Observed Cracks in Floor at Elevation 75'
- Figure 5.107 Geometry Plot; Girder RE East and West Faces
- Figure 5.108 Principal Stresses (SIG1); Girder RE East and West Faces; Case C Iteration 0; Winter Temperature (T_w)
- Figure 5.109 Principal Stresses Vector Plot; Girder RE East and West Faces; Case C Iteration 0; Winter Temperature (T_w)
- Figure 5.110 Principal Stresses (SIG1); Girder RE East and West Faces; Case C Iteration 0; Summer Temperature (T_s)
- Figure 5.111 Principal Stresses Vector Plot; Girder RE East and West Faces; Case C Iteration 0; Summer Temperature (T_s)
- Figure 5.112 Principal Stresses (SIG1); Girder RE East and West Faces; Case C Iteration 0; DL+LL
- Figure 5.113 Principal Stresses Vector Plot; Girder RE; Case C Iteration 0; DL+LL
- Figure 5.114 Principal Stresses (SIG1); Girder RE East and West Faces; Case C Iteration 0; DL+LL+ T_w
- Figure 5.115 Principal Stresses Vector Plot; Girder RE; Case C Iteration 0; DL+LL+ T_w
- Figure 5.116 Principal Stresses (SIG1); Girder RE East and West Faces; Case C Iteration 0; DL+LL+ T_s
- Figure 5.117 Principal Stresses Vector Plot; Girder RE; Case C Iteration; 0 DL+LL+ T_s
- Figure 5.118 Principal Stresses (SIG1); Girder RE East and West Faces; Case C Iteration 1; DL+LL
- Figure 5.119 Principal Stresses Vector Plot; Girder RE; Case C Iteration 1; DL+LL
- Figure 5.120 Principal Stresses (SIG1); Girder RE East and West Faces; Case C Iteration 1; DL+LL+ T_w
- Figure 5.121 Principal Stresses Vector Plot; Girder RE; Case C Iteration 1; DL+LL+ T_w
- Figure 5.122 Principal Stresses (SIG1); Girder RE East and West Faces; Case C Iteration 1; DL+LL+ T_s
- Figure 5.123 Principal Stresses Vector Plot; Girder RE; Case C Iteration 1; DL+LL+ T_s
- Figure 5.124 Principal Stresses (SIG1); Girder RE East and West Faces; Case C Iteration 2; DL+LL
- Figure 5.125 Principal Stresses Vector Plot; Girder RE; Case C Iteration 2; DL+LL
- Figure 5.126 Principal Stresses (SIG1); Girder RE East and West Faces; Case C Iteration 2; DL+LL
- Figure 5.127 Principal Stresses Vector Plot; Girder RE; Case C Iteration 2; DL+LL
- Figure 5.128 Principal Stresses Vector Plot; Girder RE Portion Between the SFF North Wall and Column E7; Case C Iteration 0; DL+LL+ T_w
- Figure 5.129 Principal Stresses Vector Plot; Girder RE Portion Between the SFF North Wall and Column E7; Case C Iteration 0; DL+LL+ T_s

- Figure 5.130 Predicted Crack Pattern on the West Face of Girder RE; Case C Iteration 2; DL+LL+T_w
- Figure 5.131 Predicted Crack Pattern on the West Face of Girder RE for Case C DL+LL+T_w Based on Average Crack Orientation Between Iteration 0 and 2
- Figure 5.132 Observed Crack Pattern on the West Face of Girder RE
- Figure 5.133 Observed Crack Pattern on the East Face of Girder RE
- Figure 5.134 Observed Crack Pattern on the East Face of Girder RE MIRROR IMAGE OF FIGURE 5.133
- Figure 5.135 Vertical Displacement (UZ); Floor at Elevation 95'; Case C Iteration 0; DL+LL+T_w
- Figure 5.136 Principal Stresses (SIG1); Floor at Elevation 95'; Case C Iteration 0; DL+LL+T_w
- Figure 5.137 Vertical Displacement (UZ); Floor at Elevation 119'; Case C Iteration 0; DL+LL+T_w
- Figure 5.138 Principal Stresses (SIG1); Floor at Elevation 119'; Case C Iteration 0; DL+LL+T_w

LIST OF TABLES

- 4.1 Steps in the Cracking Iteration Process for Case C
- 4.2 Steps in the Cracking Iteration Process for Case D
- 4.3 Brief Description for Cracking Iteration for Case C
- 4.4 Brief Description for Cracking Iteration for Case D
- 4.5 Vertical Shear Forces (Kips) in Girder RD at Face of Column D7
- 4.6 Vertical Shear Forces (Kips) in Girder RE at Face of Column E7
- 4.7 Vertical Shear Forces (Kips) in Girder R6 at Face of Column F6
- 4.8 Vertical Forces (Kips) in Column C-6 at Bottom of Girder R6
- 4.9 Vertical Shear Forces (Kips) in Girder RD at Face of Column D7
- 4.10 Vertical Shear Forces (Kips) in Girder RE at Face of Column E7
- 4.11 Vertical Shear Forces (Kips) in Girder R6 at Face of Column F6
- 4.12 Vertical Forces (Kips) in Column C6 at Bottom of Girder R6
- 4.13 Cracking Status Array for Analysis Iterations

- 5.1a Load Combination Equations
- 5.1b Load Combination Equations Specifically Developed to Show Compliance with ACI 349-80 Section 9.23.
- 5.2a Shear Capacity Margin In Girders RD, RE and R6 Analysis Case C
- 5.2b Shear Capacity Margin (%) in the Girders for Load Combinations in Table 5.1b Analysis Case C, Iteration 4S
- 5.3a Moment Capacity Margin In Girders RD, RE and R6 Analysis Case C
- 5.3b Moment Capacity Margin (%) in the Girders for Load Combinations in Table 5.1b Analysis Case C, Iteration 4S
- 5.4 Moment Capacity Margin In Column C6 Analysis Case C

ABB Impell Corporation

- 5.5 Moment Capacity Margin In Girders RD, RE and R6 Analysis Case D
- 5.6 Shear Capacity Margin In Girders RD, RE and R6 Analysis Case D
- 5.7a Shear Capacity Margin In The SFP Slab For Analysis Case C
- 5.7b Shear Capacity Margin (%) in the SFP Slab for Load Combinations in Table 5.1b Analysis Case C, Iteration 4S
- 5.8a Moment Capacity Margin In the SFP Slab For Analysis Case D
- 5.8b Moment Capacity Margin (%) in the SFP Slab for Load Combinations in Table 5.1b Analysis Case C, Iteration 4S
- 5.9 Shear In Southeast Slab (Kips) For Analysis Case C
- 5.10 Gaps At The Uncoupled Nodes In The SFP Slab
- 5.11 Shear Capacity Margin In The SFP Slab (Kips) For Analysis Case D
- 5.12 Moment Capacity Margin In The SFP Slab (Kips) For Analysis Case D
- 5.13 Shear Capacity Margin In The SFP Walls Analysis Case C
- 5.14 Moment Capacity Margin In The SFP Walls Analysis Case C
- 5.15 Linearized Stresses Girder RE Section (930, 210), Case C Iteration 3R Equation C
- 5.16 Linearized Stresses Girder RE Section (940, 310), Case C Iteration 3R Equation C
- 5.17 RCBEAM Evaluation For Girder RE Case C Iteration 3R
- 5.18 East and West Face Bending Stresses In Girder RE
- 5.19 Linearized Stresses Girder RE Mid-Span Sections, Case C Iteration 3R, Equation C
- 5.20 Linearized Stresses for Girder RE from Table 5.19
- 5.21 Summary of Linearized Stresses For SW Slab Iteration 3R, Case C
- 5.22 RCBEAM Evaluation For SW Slab Case C Iteration 3R
- 5.23 Summation of Forces SW Slab In SW Slab East Section Case C Iteration 3R Equation a
- 5.24 Tensile Stresses (PSI) at the Maximum Moment Section of Girder RE

1.0 INTRODUCTION

1.1 Objectives

A structural evaluation of the Spent Fuel Pool (SFP) at the Oyster Creek Nuclear Generating System (OCNGS) was initiated under GPUN Contract No. PC-082008 (Reference 1). The purpose of this effort was to evaluate the SFP concrete structure for consolidated and unconsolidated fuel loads with other design basis loads. The general technical requirements for this evaluation are defined in GPUN Specification SP-1302-53-047, Revision 1 (Reference 2). These requirements were followed to develop an Analysis Criteria Document (Reference 3) which provides the detailed direction for their implementation.

The analysis considers the effects of dead load, live load, thermal gradients, seismic load and cask drop accident using prescribed loads and load combinations. The specific evaluation of section capacities and stresses was performed in accordance with ACI-349 (Reference 4). A detailed finite element model of the SFP concrete structure with connecting and supporting members was generated in order to consider all required loads, load combinations, and specific features of the SFP which cannot be effectively analyzed by less rigorous methods. Specifically, these features are (1) the reduced embedment length of bottom reinforcing bars connecting the SFP slab to the supporting beams/walls, (2) the integral connection of the floor slabs and shield wall with the SFP structure, and (3) cracks on the concrete girder along Column Line FE, and the bottom of the floor slab beneath the SFP north wall (Reference 8) and cracks on areas of the shield wall connection to the SFP wall observed during field walkdowns. The model was developed to predict this cracking and consider the effects of internal force redistribution. This report describes the process followed by ABB Impell to meet these analytical requirements, resulting in an evaluation of the SFP for design basis and increased fuel loads, considering specific as-built and observed features of the structure.

This report focuses on the results of Analysis Cases C and D, described in Section 3.2. Analysis Cases C and D results envelop those of Case A and B, as described in Section 3 of this report.

1.2 Scope

The scope of work for the SFP evaluation, defined in the GPUN Specification, required the development of an Analysis Criteria Document prior to the initiation of any activities. This document (Reference 3) includes the definition of loads, load combinations, material properties, and evaluation criteria. It also establishes the methods to be used to consider concrete cracking, load redistribution, and details of the finite element model, including boundary conditions, model limits, and types

ABB Impell Corporation

of elements to be used. This document was approved by GPUN and is included as an attachment to this report (Reference 23).

Using these requirements, ABB Impell generated a detailed finite element model of the OCNGS SFP using the ANSYS computer program (Reference 5). This model was developed to meet the stated requirements of the SFP concrete structure evaluation for design basis and increased fuel loads, while considering specific observed and as-built features of the structure. The evaluation considered four analysis cases, as defined in Section 4.0 of Reference 2. This report provides a description of the SFP finite element model, the analytical work performed, the behavior of the SFP and a summary of results.

1.3 Brief Summary of Results

The results of the analyses described herein demonstrate that the OCNGS SFP meets the requirements of ACI 349-80 (Reference 4) for Load Combinations of the Analysis Cases prescribed in the GPUN Specification (Reference 2). A detailed discussion of the Code evaluation results and margins is contained in Section 5.2. The general pattern of cracks observed in the SFP and connected structures, as well as specific individual cracks, are predicted by this analysis. A detailed discussion of the correlation of analysis results with observed cracks can be found in Section 5.3. Conclusions are presented in Section 5.4.



ABB Impell Corporation

INTENTIONALLY LEFT BLANK

2.0 METHODS OF ANALYSIS

2.1 Description of the Reactor Building and SFP

The Reactor Building at OCNCS is a box-shaped concrete structure with plan dimensions 140'-0" by 109'-0" and height 95'-9" above the top of a concrete chamber which surrounds the reactor. The longer direction of the building is divided into six approximately equal spacings by seven column lines from R1 to R7. Similarly, the shorter side is divided into five spacings by six column lines from RA through RF. The northern half of the reactor building is shown in the plan view of Figure 2.1.

Figures 2.1 and 2.2 show that the reactor vessel centerline coincides with Column Line R4 and is 4'-9" to the west of Column RD. The vessel is enclosed by an axisymmetric reinforced concrete shield wall of varying thickness ranging from 5' to 10', shaped like an inverted light bulb and supported by a substantial concrete structure. The shield wall is connected to the exterior walls by slab and beam systems located at elevations 51'-3", 75'-3", 95'-3" and 119'-3" which will be referred to throughout this report as elevations 51', 75', 95' and 119'. Reinforced concrete columns are located between elevations to support these slabs.

The SFP is an elevated reinforced concrete tank cantilevered from the north side of the upper half of the shield wall between elevations 75' and 119' and supported from below by girders and columns. The exterior dimensions of the SFP measure 51'-3" in the east-west direction, 39' in the north-south direction, and 43'-11" vertically from the bottom of the pool slab to the top of the walls. The top of the SFP is open to the air. With 6' walls around the four sides, except for the 4'-6" upper portion of the west wall, the pool interior occupies a volume of 39'x27'x39'-5". The south wall of the pool is monolithically cast with the shield wall and contains the thickest concrete regions of the SFP. The bottom of the SFP is a 4'-6" thick slab supported by Girders RD and RE, and Girder R6. Girder R6, which carries a portion of the load from the SFP slabs, is supported by Girders RD and RE, and Columns CD and F6. Girders RD and RE are supported by the shield wall at their south ends and Columns D7 and E7, respectively, at their north ends.

2.2 The Finite Element Model

The established requirements for the structural evaluation of the OCNCS SFP necessitated the development of a detailed finite element model having the capability of predicting the cracking of the concrete and the resulting redistribution of internal forces and stresses. To accomplish this, it was necessary that the finite element model be of sufficient size and detail to allow for the internal redistribution of forces

over a relatively large region which included all potential load carrying mechanisms within the Reactor Building. A detailed description of the SFP model geometry is provided in Reference 25.

A review of the Reactor Building drawings shows that the entire structure is approximately symmetric with respect to Column Line R4. Using this symmetry, the finite element model consists of the northern half of the Reactor Building, which includes the region bounded by columns lines R4 to R7 and RA to RF, and vertically from elevation 23' to 119' (See Figures 2.1 and 2.2).

2.2.1 Global Coordinate Systems

Two global coordinate systems are used to define the ANSYS SFP model: a Cartesian system and cylindrical system. In the Cartesian coordinate system, the positive X-axis points to the north and the positive Y-axis to the west. Both X and Y coordinates are measured from the centerline of the reactor and the Z coordinate is chosen to be the same as the actual elevation, with positive Z pointing upward as shown in Figures 2.1 and 2.2.

The origin for the cylindrical coordinate system is the same as that of the rectangular cartesian coordinate system. The radial direction is measured from the center of the reactor, the Z coordinate is the same as the actual elevation, and the angular direction is positive when measured counterclockwise from a radial line pointing north.

2.2.2 Finite Elements Used

2.2.2.1 Finite Elements for Stress and Thermal Analysis

The ANSYS model of the SFP is composed of 5,071 nodes and 3,583 elements. Three different structural finite elements are employed:

1. 3-D solid element (STIF 45)
2. 3-D quadrilateral shell (STIF 63)
3. 3-D spar (truss) (STIF 8)

The 3-D solid elements (STIF 45) are used to model the SFP walls, the SFP slab, the supporting beams, girders and columns and the shield wall. Floor slabs at elevation 75', outside the SFP, from Column Lines R5 to R7 and RC to RF, are also modeled with 3-D solid elements.

Slabs and walls at other areas are modeled by using 3-D shell elements (STIF 63). These include the slabs at elevations 51', 75', 95' and 119', and

ABB Impell Corporation

exterior walls at Column Lines RA, RF and R7. By changing the thicknesses of these shell elements, various beams and columns which are monolithically cast with the slabs or walls are also modeled.

The third finite element used in the SFP is a 3-D spar (STIF 8). Column C6, which carries load from the SFP, is supported at its bottom end (elevation 23') by a concrete frame spanning over the torus. To incorporate the stiffness properties of the concrete frame, a separate model of the frame was constructed, (as described in Section 2.2.3) and its stiffness at the location of Column C6 was determined. This stiffness was converted to equivalent properties for spar elements that support the nodes at the bottom of Column C6.

The ANSYS structural finite element model described above was also used for thermal analysis by changing the ANSYS structural elements from STIF 45, 63 and 8 to ANSYS thermal elements STIF 70, 57 and 33. The thermal finite elements corresponding to the structural elements listed above are:

1. 3-D thermal solid (STIF 70)
2. 3-D thermal shell (STIF 57)
3. 3-D thermal bar (STIF 33)

2.2.2.2 ANSYS Element Types

In the ANSYS model, 20 ANSYS element types are used to identify groups of similar type elements within various regions. The ANSYS element types and the specific structural components they represent are listed below.

1. Types 1, 2 and 3 - Girders RD and RE
2. Type 4 - Shield Wall
3. Type 5 - South wall of the SFP, not included in Type 4
4. Type 6 - Shelves supporting the south wall of the SFP
5. Type 7 - SFP Floor Slab
6. Type 8 - SFP Walls (North, East and West)
7. Type 9 - Regions intersected by two SFP walls, or wall and slab, and Columns C6 and C5
8. Type 10 - Girder R6
9. Type 11 - Slabs outside the SFP, at Elevation 75', from Column Lines R5 to R7 and Column Lines RC to RF
10. Type 12 - Spar elements at bottom end of Column C6
11. Type 13 - Exterior walls at Column Lines RA, RF and R7, and slab at Elevation 51'. Some columns and beams embedded in these walls and slabs are also identified as Type 13.

ABB Impell Corporation

12. Type 14 - Columns B4, B5, B6, D7, E7, F5 and F6
13. Type 15 and 16 - Slabs at Elevation 75'
14. Type 17 and 18 - Slabs at Elevation 95'
15. Type 19 and 20 - Slabs at Elevation 119'

2.2.3 Modeling of Specific Regions

2.2.3.1 Drywell Shield Wall

The drywell shield wall is modeled using 3-D solid elements, with 2 elements across the thickness, 20 elements along the circumferential direction and 19 elements in the vertical direction. The mesh is finer in the upper cylinder to match the finer mesh of the SFP walls and coarser in the lower portion of the wall to reduce the total number of elements in an area where a finer mesh will not noticeably improve the accuracy of the results for the SFP.

Figure 2.3 shows the drywell shield wall model. As seen from the outside surface, the wall is composed of a smaller cylinder at the top, a larger cylinder at the bottom, and a conical portion in the middle connecting the two cylinders. From the inside surface, Figure 2.13 shows that the wall is formed by tapered cylinders at the top and a spherical bulb at the bottom. The narrow opening in the upper cylindrical portion of the model is the location of the removable concrete blocks.

Global cylindrical coordinates are used when generating these elements and nodes, and when specifying the boundary conditions at the bottom of the shield wall.

2.2.3.2 South Wall of the Pool

The south wall of the SFP is shown in Figure 2.3 and extends from elevation 75' to 119'. The south wall is monolithically cast with the drywell shield wall and contains the thickest concrete regions of the SFP.

Extending from the bottom of the south wall to the outer surface of the conical portion of the shield wall are the shelves supporting the wall. Due to the geometric complexity, this is the most difficult region of the SFP to model with solid elements. To ensure that warping of element faces was avoided, this region was modeled with a combination of eight noded solids and tetrahedrons, which are a degenerate form of the eight noded solid. In addition, a feature of the ANSYS program which allows mismatched nodes at adjacent element faces to be joined together by internally

generated constraint equations among the nodal degrees of freedom was used in the development of this portion of the model. The mismatched elements of the shelves and shield wall are shown in Figure 2.4. (This feature was also used to attach column C5 and the southern end of Girders RD and RE to the conical portion of the shield wall as shown in Figure 2.18.)

2.2.3.3 Girders RD, RE, R6 and Adjacent Floor Slab

Figure 2.4 shows the SFP, with Girders RD, RE and R6, the shield wall, and the SFP south wall. Due to the presence of flexure and flexure-shear cracks in the web and bottom face of Girder RE near Column Line R7 (Reference 8), the webs of Girders RD and RE are modeled with a relatively fine mesh of solid elements. Since no bending is expected about their vertical axis, only one element was used across the width. For Girders RD and RE, six elements were used through the depth of the 9 foot region, and eight elements in the 13'-6" deep region (see Figures 2.15, 2.16 and 2.17 and Section 2.2.3.7). One end of these girders is built into the shield wall, and the other end is supported by a column at Column Line R7.

Similar to RD and RE, Girder R6 is modeled with one element across the width. In the vertical direction six elements are used to model the 10'-7" deep region with four of these elements through the 6' deep web portion of the girder.

The floor slab at elevation 75' between Column Lines RE and RD contains a through thickness crack at the intersection with the SFP north wall and slab (Reference 8). This slab also forms the top flange of girders RE, RD and R6. Therefore the portions of the slab at elevation 75' which attach to girders RE, RD and R6 are modeled using solid elements to ensure that potentially complex behavior and load redistribution can occur. This slab is shown in Figure 2.8.

2.2.3.4 SFP Slab

The upper portion of Girders RD, RE and R6 are embedded in the SFP floor slab which has a depth of 4'-6". Figure 2.5 shows the location of the SFP slab and its connection with Girders RD, RE and R6. The slab is modeled using 3-D solid elements with 2 elements through the slab thickness. In those portions of the slab not embedded with girders, finer meshes are used to capture the more localized stresses in the slab.

One of the objectives in developing the finite element model was to be able to address the reduced embedment length of the bottom reinforcing bars connecting the SFP slab to the supporting beams and walls (see Section 1.1). To be able to simulate the effect of rebar pullout along the bottom edge of the slab an additional set of coincident nodes was defined at these locations (i.e., along the east, west and south edges of the southeast and southwest slabs and the north edge of the northeast and northwest slabs, see Figure 2.1). Rather than connecting the adjacent solid elements to the same node at these locations, each adjacent solid element (one in the slab and one on the supporting wall or girder) was connected to a different coincident node. In all analyses these coincident nodes were constrained to deform together, except for the analysis where rebar pullout was simulated (i.e., iteration 3U). In that case the degree of freedom in the direction of the rebar (perpendicular to the potential crack) was released to simulate the effect of rebar pullout.

2.2.3.5 Spent Fuel Pool Walls and Integral Columns

The solid elements forming the corners of the SFP walls and the intersection of the walls with the SFP slab are shown in Figure 2.6. With the east, west and north walls included in the model, the entire SFP becomes a rectangular tank, open to the air at the operating floor, as shown in Figure 2.7. Each wall is modeled with two solid elements through the wall thickness. Figure 2.7 shows that columns C5 and C6 are integrally connected to the east wall of the pool.

Column C5 is located at the intersection of the east and south walls. Figures 2.7 and 2.8 show that the nodes at the bottom of Column C5 do not coincide with the nodes on the outer surface of the shield wall (see also Figure 2.18). Using a special feature of the ANSYS program, the base of the column is attached to the conical portion of the shield wall by a set of internally generated constraint equations which couple the nodal degrees of freedom of the column and the nodal degrees of freedom of the shield wall. This effectively "glues" the column to the shield wall.

Column C6, which is monolithically cast with the SFP east wall and Girder R6, carries load directly from the wall and girder, as well as loads from various floors (see Figures 2.7 and 2.20). This column is modeled to elevation 23', where it is supported by a large concrete frame spanning over the tanks. The concrete structure below elevation 23' is not included in the overall SFP model, although the stiffness of the concrete frame has been incorporated at the base of the column using truss elements (acting as springs) of equivalent stiffness. The stiffness at the location of column

C6 was determined from the 3-D solid element model of the concrete frame shown in Figure 2.9.

2.2.3.6 Floor Slabs at Various Elevations

The floor slabs at elevations 119' and 95', and elevation 75', where 3-D solid elements are not used, are all modeled using 3-D shell elements as shown in Figures 2.10, 2.11, 2.12 and 2.13. Floor beams in these regions are also modeled using shell elements by increasing the shell thickness.

These floor slabs are included in the model because (1) they accurately distribute the vertical floor dead and live loads to the SFP structure, (2) they allow a determination of the extent to which the floors support the SFP, and (3) they provide lateral continuity between the shield wall and SFP, and the exterior walls.

The floor slab at elevation 51', consisting of a very coarse mesh of 3-D shell elements, is included in the model to provide a realistic boundary condition for the shield wall at elevation 51'. The plane of Elevation 51' is considered the effective boundary of the finite element model. In order to achieve as accurate a boundary condition as possible at this elevation, the shield wall, exterior wall and interior columns were extended to elevation 23'. The slab at Elevation 51' provides the lateral connection among these various structures and ensures that lateral loads are realistically distributed. This slab is shown in Figures 2.12 and 2.13.

Each node of a floor slab 3-D shell element contains three translation degrees of freedom and two rotational degrees of freedom about orthogonal axes which lie in the plane of the element. Unlike the 3-D shell elements, the 3-D solid elements, which comprise the shield wall and SFP walls, do not possess rotational degrees of freedom at their nodes. Therefore, at locations where the floor slab is connected to the SFP walls and shield wall, a hinge connection exists which can resist three components of force but no bending. This lack of bending restraint between the SFP walls and the floor slabs is not significant to the overall response of the SFP and only results in larger forces being transmitted to the primary members supporting the SFP. (Effectively this condition only exists in iteration 0, since in all other iterations the floor slab stiffness is reduced by a factor of 1000. See Sections 4.2.1.3 and 4.2.1.4.)

2.2.3.7 Exterior Walls and Columns

To provide the most accurate boundary conditions for girders RD and RE, the columns supporting the ends of these girders are modeled with two layers of solid elements through the thickness from elevation 23' to elevation 95'. Details of the model in this region can be seen in Figure 2.15, which shows a vertical slice taken through the entire model at the east face of Girder RD. Figure 2.16 is a closer view of the same slice, and Figure 2.17 shows a similar vertical slice taken along the east face of Girder RE. The ends of Girders R5 and R6 are supported by similar columns from elevation 23' to elevation 75'. All of these columns can be seen in Figures 2.12 (see also Figure 2.19). The exterior walls and remaining exterior columns, shown in Figure 2.14, are modeled with 3-D shell elements, with the columns having the same thickness as the exterior walls.

2.2.4 Boundary Conditions

Since the SFP model includes a large portion of the Reactor Building, boundary conditions are only required within the plane of Column Line R4 and the plane of elevation 23'. Within these planes the following boundary conditions were applied:

Column Line R4

Symmetric boundary conditions were applied to all nodes along Column Line R4 from Column Line RA to Column Line RF and between elevation 23' and elevation 119' (i.e., translation in X and rotation about Y and Z equal zero with all other degrees of freedom unrestrained). Antisymmetric boundary conditions were applied for the north-south (X) direction seismic analysis.

Elevation 23'

At elevation 23' the interior and exterior nodes of the drywell shield wall were restrained circumferentially but unrestrained radially to allow the shield wall to grow thermally through the thickness. At the shield wall middle surface, nodes were restrained radially and circumferentially. All other walls and columns were restrained in both horizontal translational degrees of freedom and all rotational degrees of freedom. All vertical (Z) degrees of freedom at elevation 23' were either fully restrained, or in the case of column C6, elastically restrained as discussed previously in this section.

ABB Impell Corporation

As explained in Section 2.2.3.6, the extension of the SFP model from elevation 51' to elevation 23' was done to ensure that accurate boundary conditions were applied to the model at elevation 51'. While other combinations of boundary conditions at elevation 23' may be plausible, their influence above elevation 51' will not be significant.

Except as specifically noted above, all other degrees of freedom are unrestrained.

2.3 Criteria for Cracked Stiffness Properties

2.3.1 Branson Equation Methodology

Bending moments which occur in a transversely loaded beam produce a relative rotation of adjacent cross sections. The amount of relative rotation per unit length of two adjacent cross sections is the curvature. Once the distribution of curvature along a beam is known, deflections can easily be calculated. For an elastic beam, the curvature is given by the expression M/EI where M is the applied moment and EI is the flexural stiffness of the cross section. In a reinforced concrete beam a wide disparity in flexural stiffness can exist from one cross section to another, due not only to whether cracking has or has not occurred, but also due to the severity of cracking once it has occurred.

In a reinforced concrete beam EI_u denotes the flexural stiffness of an uncracked cross section and EI_{cr} denotes the flexural stiffness of a fully cracked cross section. Between these two extremes intermediate values of EI exist which are dependent on the load level, i.e., the actual moment acting on the cross section. To express the transition from I_u to I_{cr} as a function of the load level, Branson (Reference 6) developed an empirical expression for an effective flexural stiffness, EI_E , based on a number of controlled experiments. The Branson Equation for the effective moment of inertia is:

$$I_E = \left(\frac{M_{cr}}{M_a} \right)^4 I_u + \left[1 - \left(\frac{M_{cr}}{M_a} \right)^4 \right] I_{cr}$$

Where:

M_{cr} = The cracking moment, $f_t I_g / Y_1$ (for pure bending).

M_a = Actual moment in the member at the load level for which the effective moment of inertia is being calculated.

ABB Impell Corporation

- f_r = Modulus of rupture = $7.5 \sqrt{f'_c}$
- f'_c = Ultimate compressive strength of concrete in psi.
- Y_t = Distance from centroid to extreme tension fiber.
- I_g = Gross (uncracked) moment of inertia.
- I_{cr} = Cracked transformed moment of inertia.
- I_E = Effective moment of inertia from Branson Equation.

In determining the flexural rigidity of partially cracked concrete sections the Branson Method provides a transition value between well defined limits in the uncracked and fully cracked states. The Branson Method is based on proportioning between these limits where the proportioning factor is a function of the ratio of cracking moment to actual moment.

The Branson Equation is the only expression explicitly recognized by ACI 349-80 (Reference 4) for the computation of the flexural rigidity of reinforced concrete members to account for the effects of cracking. The ACI Code recognizes the use of the Branson Equation to predict member stiffness changes due to cracking for both one-way construction (beams) and two-way construction (slabs and walls).

In the ACI Code, the Branson Equation uses the third power instead of the fourth power used here. The third power Branson Equation is intended to calculate an effective moment of inertia at the location of maximum moment as a single value for the entire span in the case of simply supported beams, or as a single value between points of inflection in continuous beams. However, to recognize the continuous variation of the moment of inertia along the span, which is the case when the moment of inertia is calculated at discrete locations along the span, Branson found that a fourth order equation gave best results (Reference 6). In this analysis, the Branson Equation is applied at all cracking locations. Hence, the Branson Equation may be applied at many locations in the same member. Therefore, use of the fourth order form is appropriate.

Since thermal and mechanical loads may introduce significant axial forces in the walls and slab of the SFP, the Branson Equation must be adapted to account for the influence of axial load on the flexural rigidity. This was done by defining the cracking moment to be the actual moment on the cross section which in combination with axial load produces an extreme

ABB Impell Corporation

fiber tensile stress equal to the modulus of rupture (Reference 7). Specifically, the cracking moment was modified as follows:

$$M_{cr} = (f_r - \sigma_m) I_g / Y_t$$

where:

σ_m = The membrane stress acting on the section.

In the SFP model, the thickness of the solid elements could not be changed to account for the changes in the effective moment of inertia due to cracking. Instead, the modulus of elasticity of each affected element was changed in proportion to the ratio of I_E to I_g to reflect the change in flexural stiffness, EI .

Since the SFP model is composed of solid elements, moments and axial forces, which act on the cross section of slab or beam members, cannot be output directly. Therefore, the moments and axial forces acting on any cross section were obtained by integrating the nodal stresses through the depth of the section. The resulting moments and axial forces were used in the Branson Equation to determine the section's effective flexural stiffness.

All solid elements in the SFP model incorporate cracking effects using changes to the directional elastic moduli perpendicular to the crack plane. Following the initial cracking of a slab or wall element, an effective element stiffness (elastic modulus) was calculated from the fourth order Branson Equation. The new value of elastic modulus perpendicular to the cracked plane was proportioned to reflect the relative stiffness changes predicted by the Branson Equation. The influence of tension stiffening due to the uncracked concrete still bonded to the steel adjacent to the crack is implicitly incorporated in the empirical formulation of the Branson Equation.

Reduced Rebar Embedment

Insufficient or reduced rebar embedment has the effect of lowering the moment capacity of a section by not allowing the yield stress of the reinforcement to be reached prior to bar pullout. At sections of the SFP slab where moment capacity could be affected by reduced embedment, separate element nodes were generated on either side of an element interface so that they could be uncoupled in the direction of the reinforcement at the location of the reinforcement (see Section 2.2.3.4).

The result of this uncoupling was to reduce the section's ability to resist moment so that a redistribution of forces could occur within the slab.

2.3.2 Fully Transformed Cracking Criteria

As moment is applied to the cross section of a reinforced concrete beam, the concrete tensile stresses increase until they reach the cracking stress (modulus of rupture), at which time the concrete cracks and tensile load previously resisted by the concrete is transferred to the tension reinforcement. As additional moment is applied, other sections crack and the steel and concrete stresses at all cracked sections increase in close proportion to the moment. At some level of moment, the steel yields and the concrete compressive stresses become nonlinear at the cracked section. This level of moment is usually close to the ultimate moment. It is between the stage when the concrete first cracks and when the proportionality between the applied moment and the steel and concrete stresses is no longer valid that the Branson Equation is intended to be used to compute an effective flexural stiffness.

As explained in Section 2.3.1, the Branson Method provides a transition value between the limits of an uncracked section and a fully cracked transformed section for determining the flexural rigidity of partially cracked concrete sections. The limits of uncracked and fully cracked transformed sections correspond to the limits of applied moment which vary between the cracking moment and a moment, less than ultimate, at which the tensile reinforcement yields.

As discussed further in Sections 2.3.2.1 and 2.3.2.2, there are two situations for which the Branson Equation does not perform adequately, i.e., provide a complete transition in stiffness from the uncracked moment of inertia (I_u) to the fully cracked transformed moment of inertia (I_{cr}). These situations occur in areas with low reinforcement ratios. One is in the SFP walls where the cracking moment exceeds the ultimate moment, and the other is in the SFP slab where the Branson Equation provides an incomplete transition in stiffness. In both the walls and the slab, the fully cracked transformed state is not achieved when the ultimate moment is reached. In the walls and slab, therefore, the Branson Method always over predicts stiffness (i.e., under predicts the level of cracking) which leads to very conservatively calculated moments. To resolve this problem for the walls and slab, fully transformed cracking criteria was developed. In these criteria when a section exceeds the cracking moment, rather than using the Branson Equation to compute stiffness, the cracked transformed properties are used.

2.3.2.1 Application to the SFP Walls

With respect to the discussion in Section 2.3.2, the use of the Branson Equation to compute cracked cross-section stiffness properties implies that the section under consideration has additional moment capacity beyond the moment which causes cracking. During the preliminary evaluation of the SFP it became apparent that this was not the situation for the SFP walls.

Specific provisions of the ACI Code (Reference 4, Section 10.5.1) recognize the desirability for the moment capacity to be greater than the cracking moment. However, the minimum reinforcement requirements for walls specified by the Code may provide less reinforcement than necessary to ensure a moment capacity greater than the cracking moment. Consequently, for walls so constructed, the Branson Equation will severely over predict member stiffness. This is particularly significant where thermal gradients are concerned, since the over prediction of stiffness results in higher thermal moments.

Therefore, for the SFP walls, where the cracking moment exceeds the moment capacity, alternate stiffness and cracking criteria were used. In these criteria, the stress at which cracking occurs was set equal to the value obtained by applying the ultimate moment to the uncracked section rather than the modulus of rupture, f_r . Thus, the moment which produces cracking can never be greater than the ultimate moment. Use of these criteria avoids the situation where the factored moment from a thermal load combination exceeds the moment capacity at a section which may not have cracked, or at a section for which the level of cracking had been underestimated. Where cracking did occur based on this criteria, fully cracked transformed properties were used for those sections, since no transition region exists between the cracking moment and the ultimate moment.

2.3.2.2 Application to the SFP Slabs

Referring to the discussion in Section 2.3.2, the use of the Branson Equation to compute cracked stiffness properties assumes that at or slightly below the ultimate moment, the stiffness properties of a section will have transitioned to the cracked transformed value. In the SFP slab this transition to the cracked transformed value at the ultimate moment does not occur. When the moment in the slab reaches the design capacity, the effective stiffness computed from the Branson Equation is more than 60% greater than the cracked transformed value. In regions of the slab where mechanical and thermal moments combine, a bending stiffness 60% greater than the cracked transformed value can produce an unrealistically

high combined moment because of the higher stiffness computed from the Branson Equation. To resolve this problem for the slab, the fully cracked transformed criteria was used.

2.3.2.3 Consistency in the Application of Cracking Criteria

Section 8.6.1 of ACI-349 requires that reasonable and consistent assumptions be adopted throughout the analysis for computing the relative stiffness of structural components. The use of the Branson Method throughout the analysis to compute member stiffness constitutes a consistent basis for determining relative stiffness. However, as explained in Sections 2.3.2.1 and 2.3.2.2, when the cracking moment exceeds the ultimate moment or when the proper transition in stiffness is not provided, the Branson Method is not applicable. To address the inability of the Branson Method to provide reasonable stiffness values in these situations, criteria were developed (see Section 2.3.2) to ensure that appropriate stiffness, consistent with the intent of the Branson Method, was applied.

2.4 Load Application

In accordance with Reference 3, the SFP analysis considered concrete dead load, hydrostatic and hydrodynamic pool loads, fuel rack loads, thermal gradients and seismic loads. A detailed description of the SFP loads and of how the loads were applied to the SFP model is provided in Reference 26. A summary description of the SFP model loads is provided below.

Concrete dead load was applied as a 1g vertical load on all structural elements. Hydrostatic and hydrodynamic pool loads were applied statically as element pressures to the slab and walls of the SFP. Hydrodynamic pool loads were calculated using the methodology given in Reference 11 and were based on the determination that the SFP walls and slab are essentially rigid, as demonstrated by calculations performed by GPUN (Reference 12). Static and dynamic fuel rack loads corresponding to the three conditions described in Section 3.1.1 and the cask drop load were applied statically to the pool slab as element pressures. Seismic inertia loads were applied statically to all structural elements of the SFP as a percent of gravity based on floor response spectra ZPA values.

The temperatures on the wet surface of the SFP and the inner and outer surfaces of the shield wall were explicitly applied at each node as specified in Table 3.2. Uniform ambient air temperature was applied at all the remaining surface nodes in the reactor building. Using the SFP thermal model (see Section 2.2.2.1) a steady state heat transfer analysis was performed to determine the temperatures at the intermediate

ABB Impell Corporation

nodes in the shield wall and the SFP walls and slab. The temperature at each node was stored on File 04 of the ANSYS heat transfer analysis and then retrieved in the thermal Load Step solution for the structural model.

The first step in performing a distinct analysis (i.e., iteration), was to apply each load separately to the entire model, assuming linear elastic behavior, to determine the general effect of each load, its relative severity with respect to other loads, and its participation in the load combination for the various structural components. These separate load cases (load steps) were then scaled and combined to produce results for each load combination.

Within this report, the following nomenclature is used to describe SFP model loads and load combinations:

(1) Loads and Load Steps

These are the individual loads applied to the SFP model, namely:

- Load Step 1 - Concrete Dead Load
- Load Step 2 - Hydrostatic, Fuel Rack, and Stored Cask Loads
- Load Step 3 - Design Live Load
- Load Step 4 - Winter Temperature Condition
- Load Step 5 - Summer Temperature Condition
- Load Step 6 - Cask Drop Load

(2) Analysis Case

These represent the four conditions prescribed by GPUN (Reference 2) referred to as Analysis Cases A, B, C, and D. Each Analysis Case is described in Section 3.2.

(3) Load Combination

This represents the combination of results from individual load steps with the appropriate load factors applied to each load step. Load Combinations (a, b, c, d, and e) are described for each Analysis Case in Section 3.3.

(4) Iteration or Cracking Iteration

This represents a distinct computer run where the SFP model is executed with material properties revised to reflect a stiffness change. In structural analysis, the word iteration normally refers to a change in load during the analysis process. However, in the SFP analysis, the word iteration refers to a change in stiffness with all loads held constant during the analysis process. Therefore,



ABB Impell Corporation

each cracking iteration (or iteration) represents a distinct stiffness configuration of the SFP to which loads are applied and results obtained based on a linear elastic analysis. The iteration process is described in detail in Section 4.3



ABB Impell Corporation

INTENTIONALLY LEFT BLANK

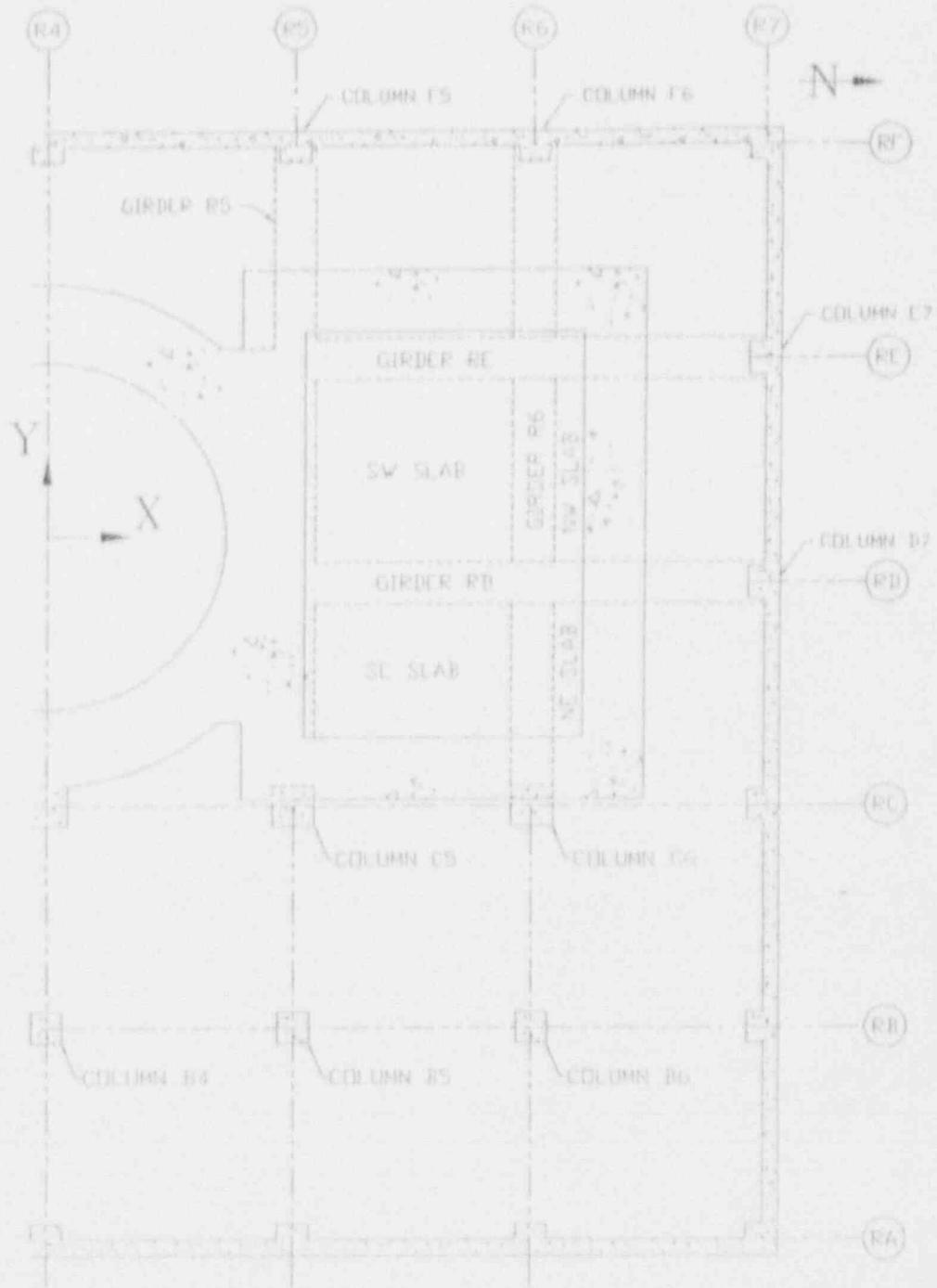


Figure 2.1

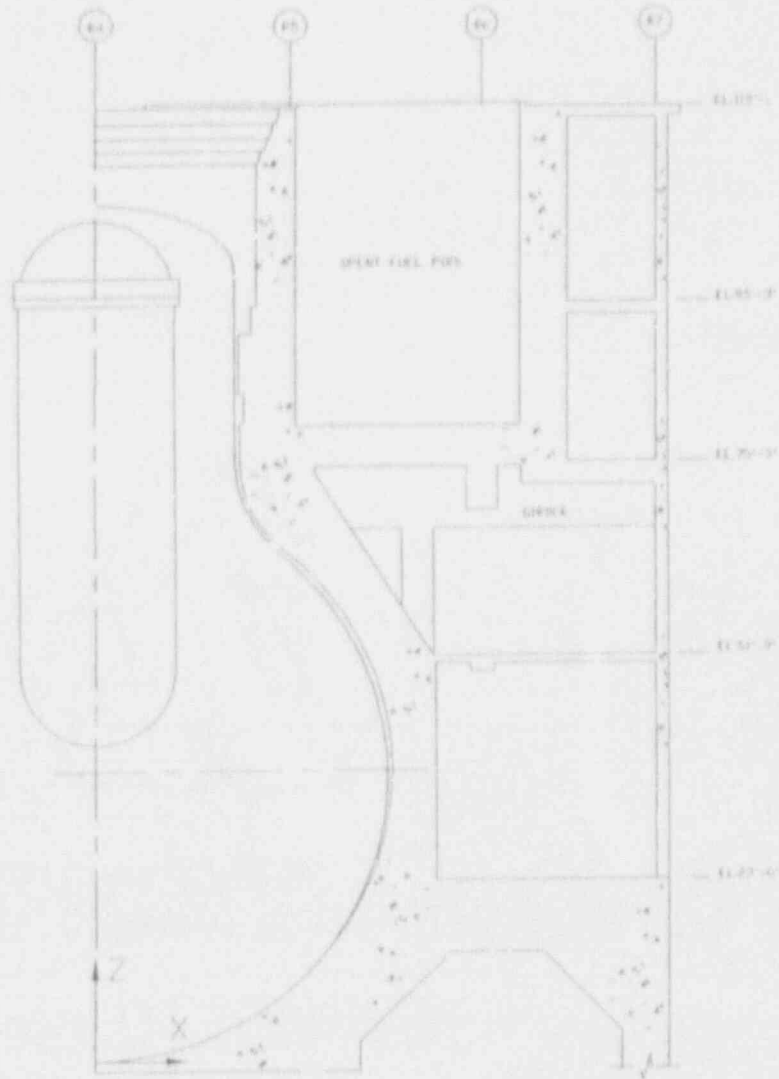


Figure 2.2

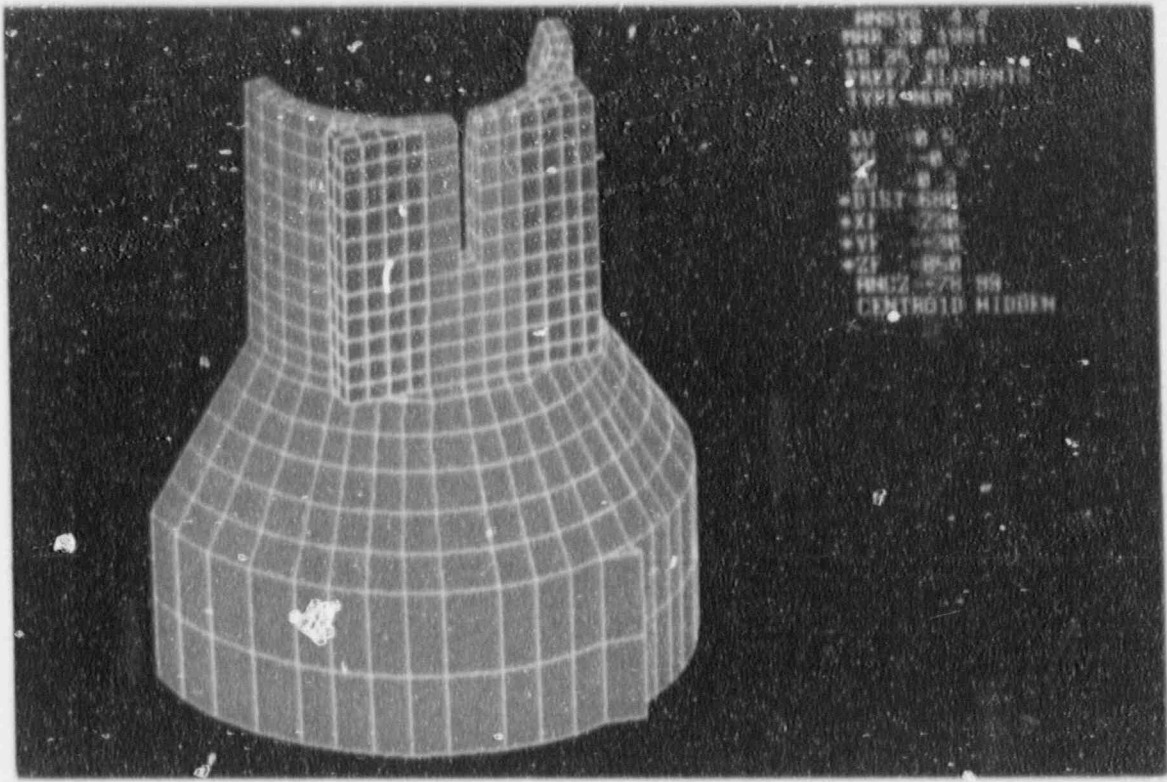


Figure 2.3

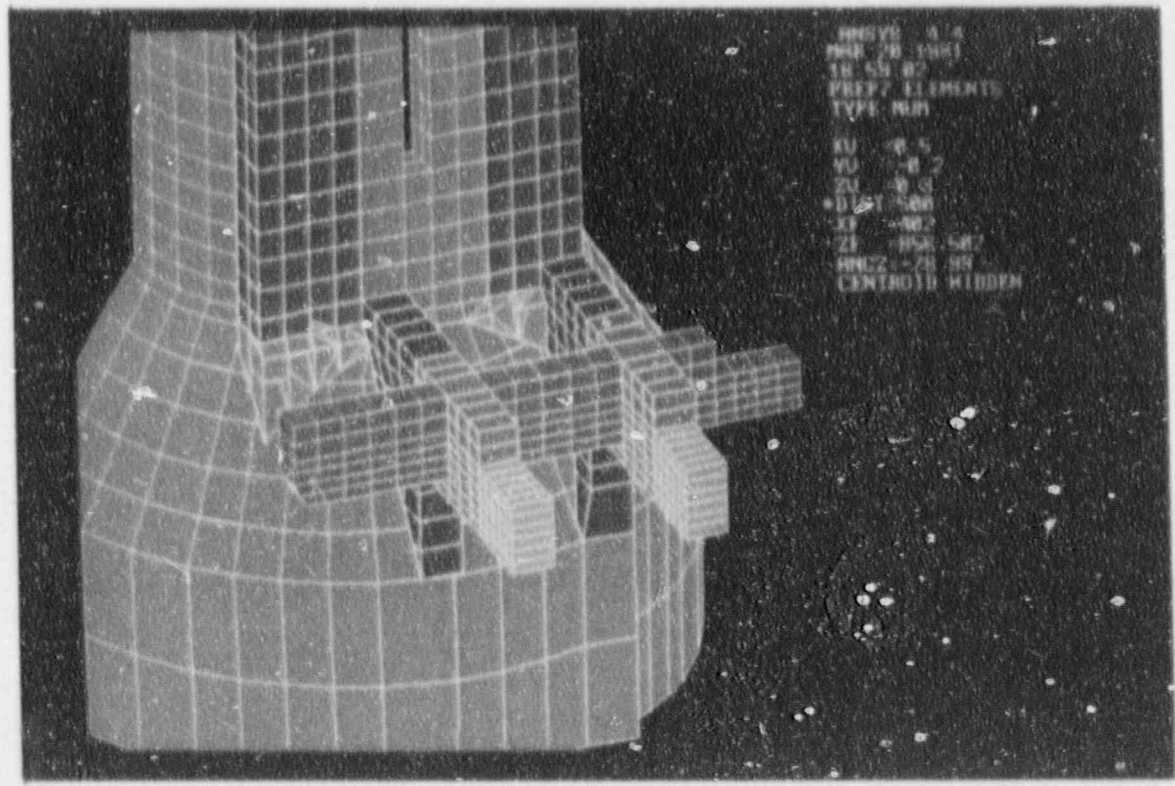


Figure 2.4

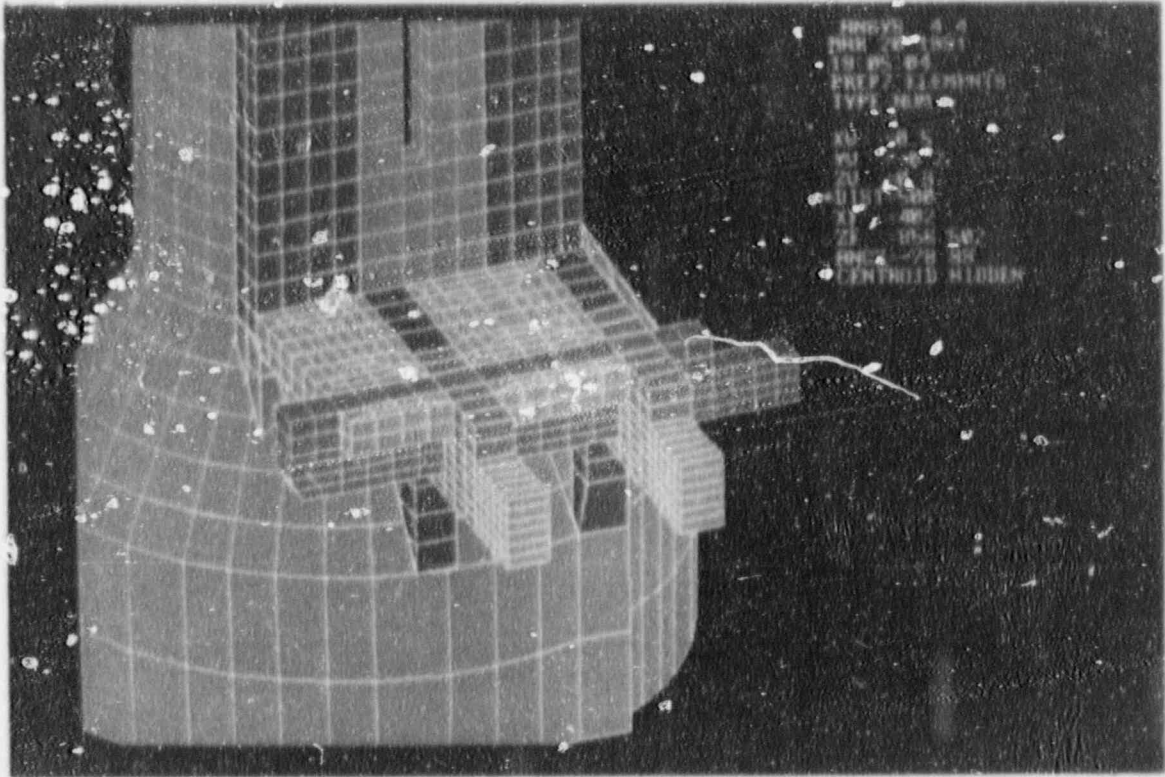


Figure 2.5

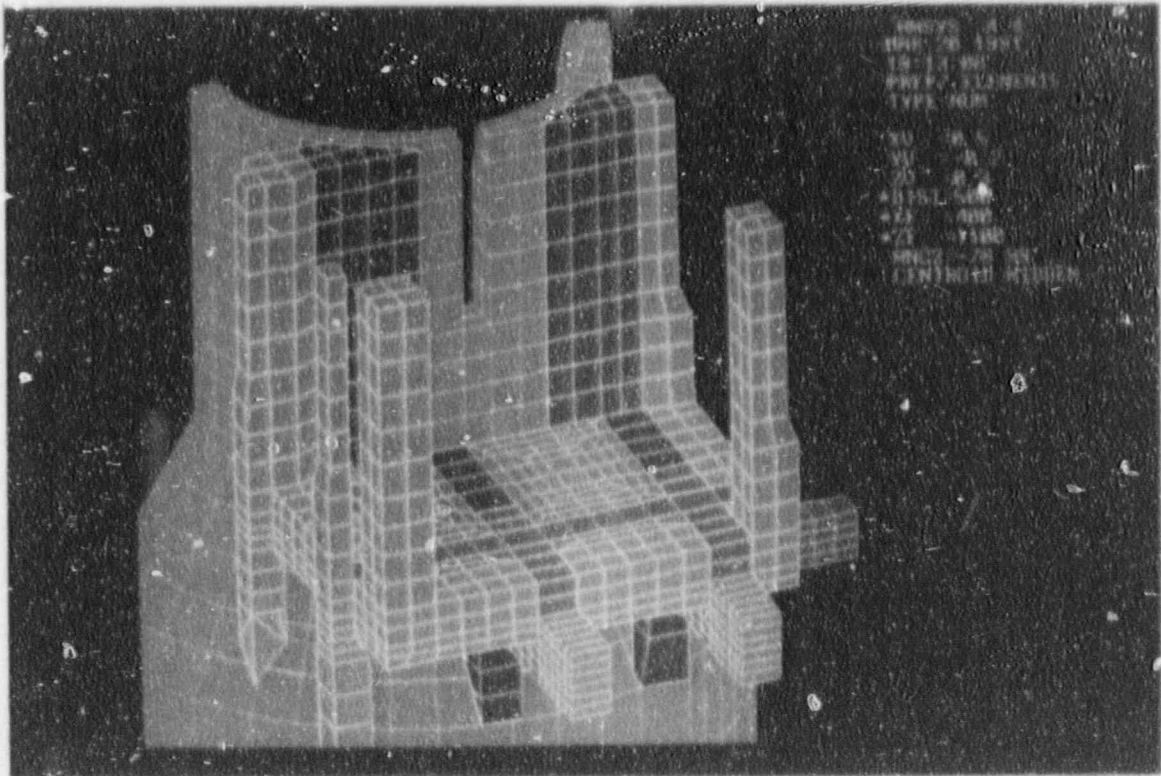


Figure 2.6

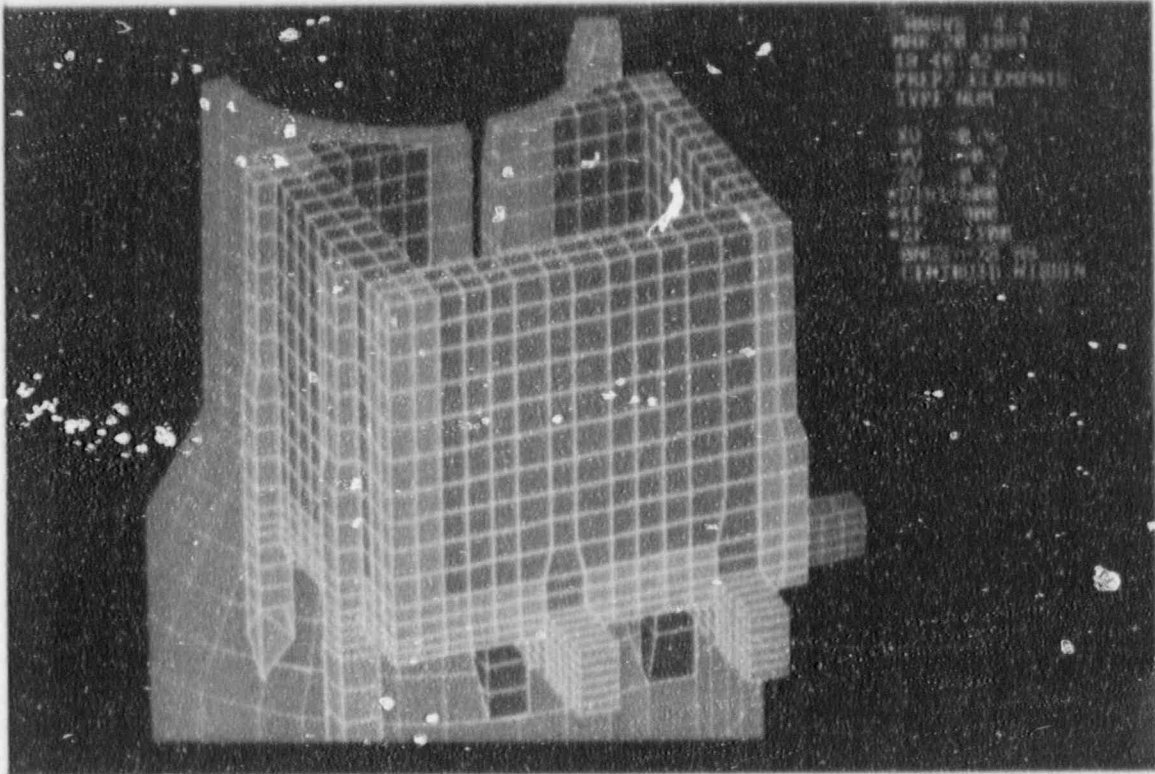


Figure 2.7

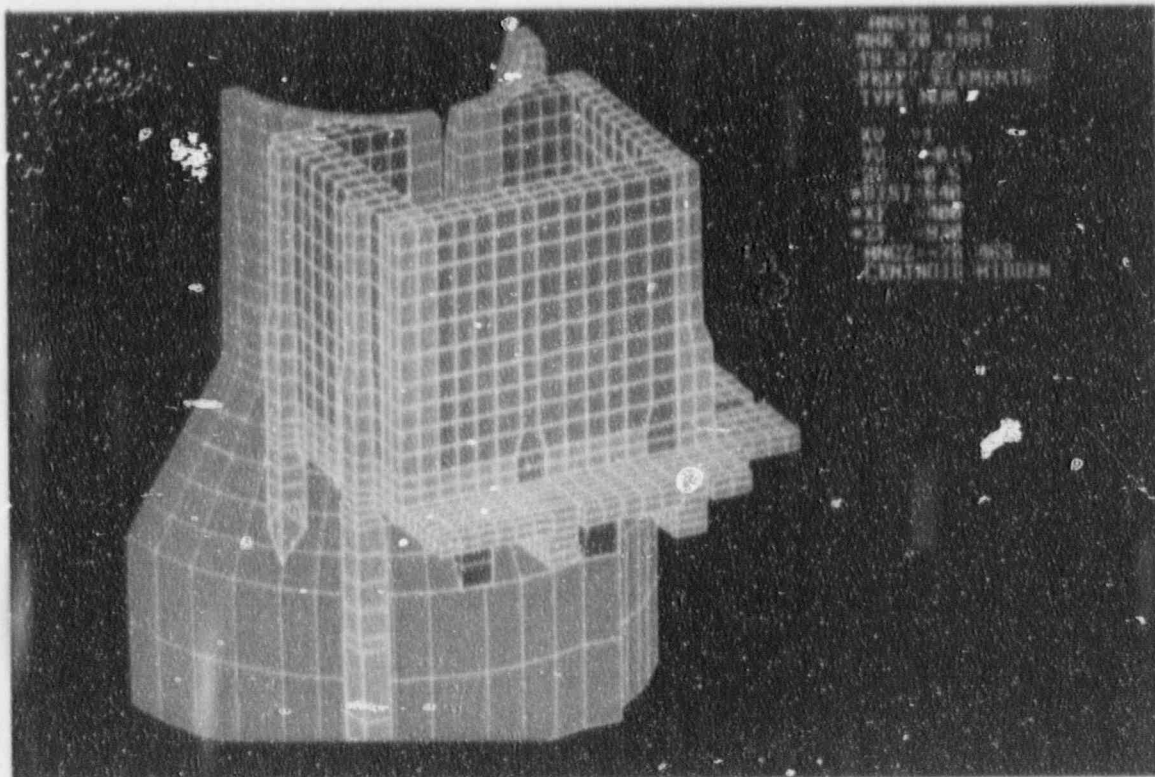
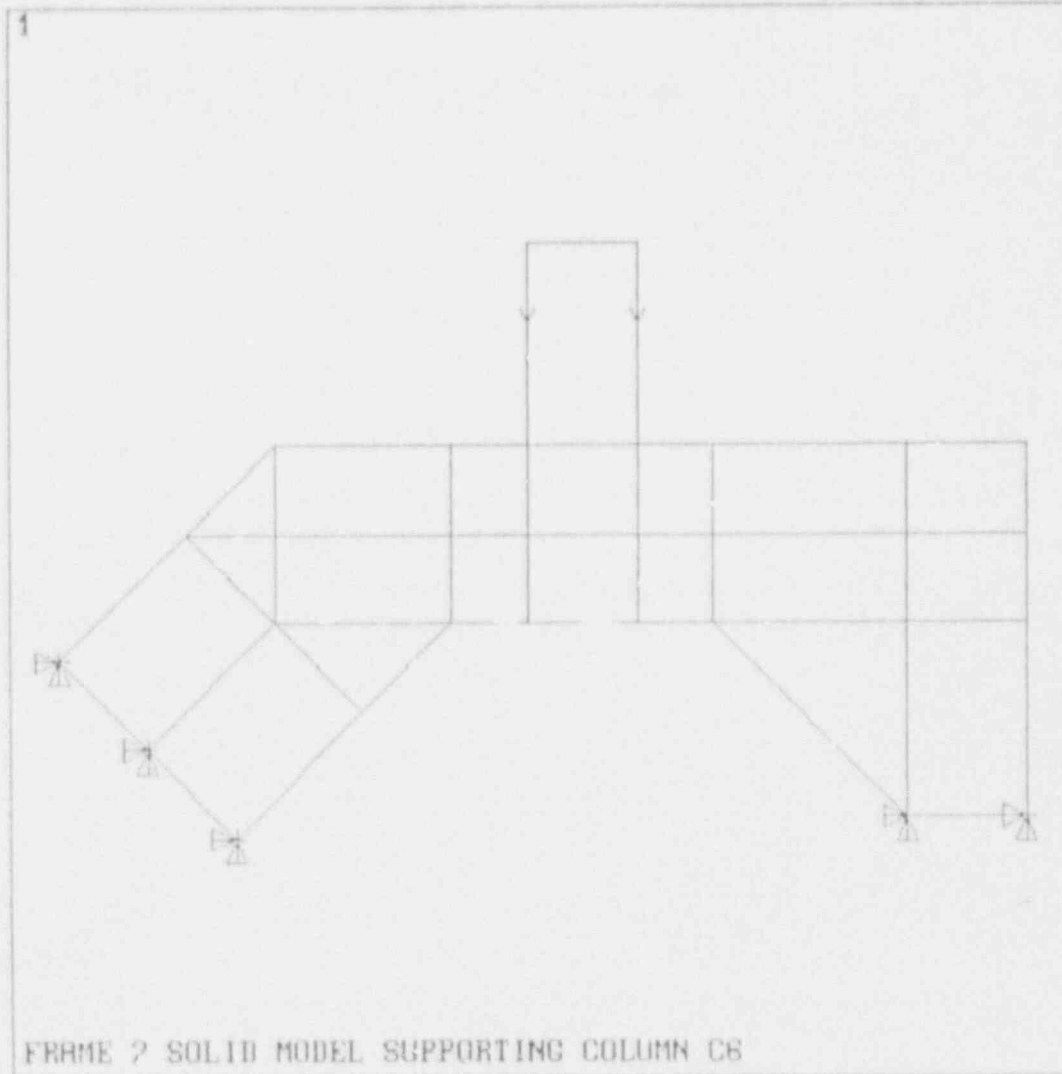


Figure 2.8



ANSYS 4.4
MAR 20 1991
16:30:54
PREP7 ELEMENTS
TYPE NUM
BC SYMBOLS

YU =-1
DIST=319
XF =583
YF =27
ZF =223.5
PRECISE HIDDEN

Figure 2.9

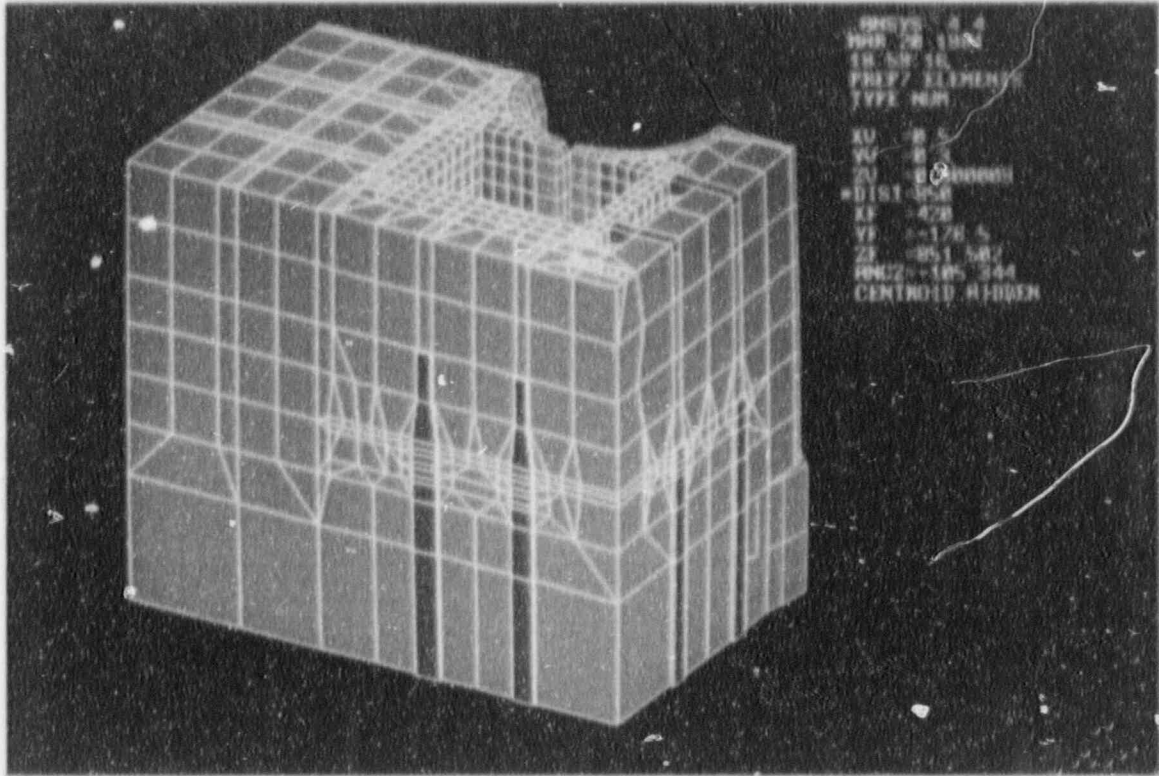


Figure 2.14

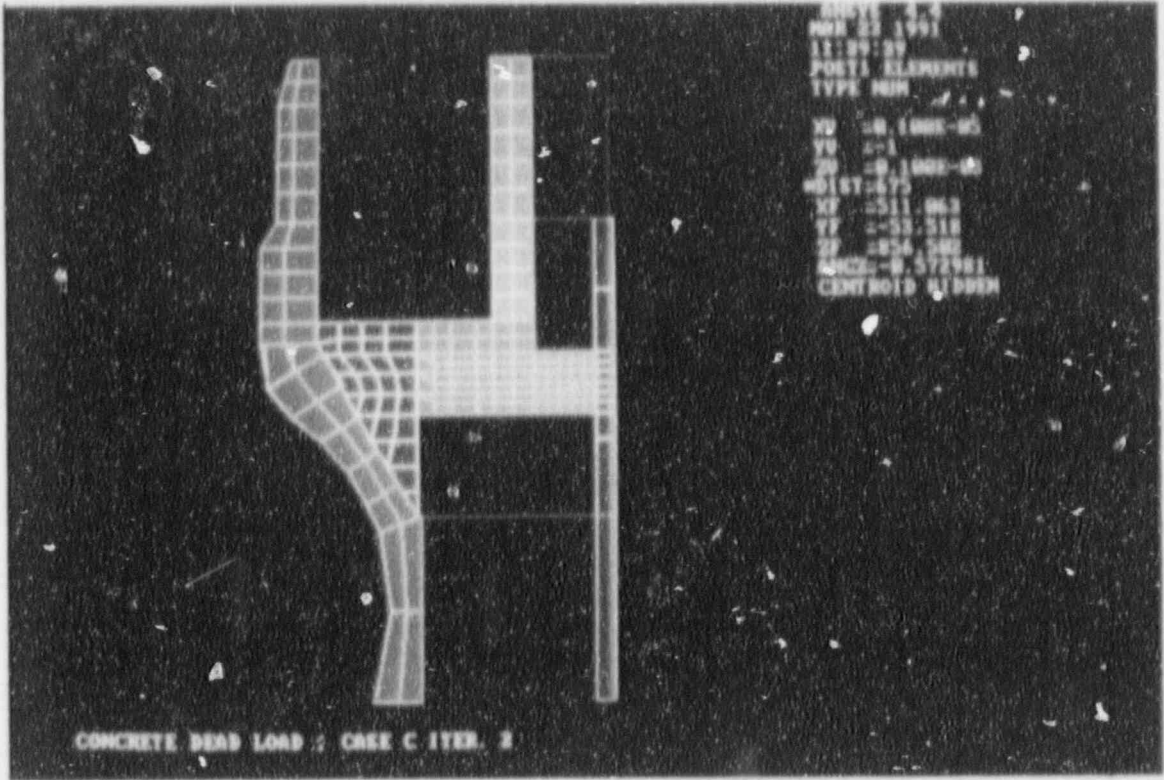


Figure 2.15

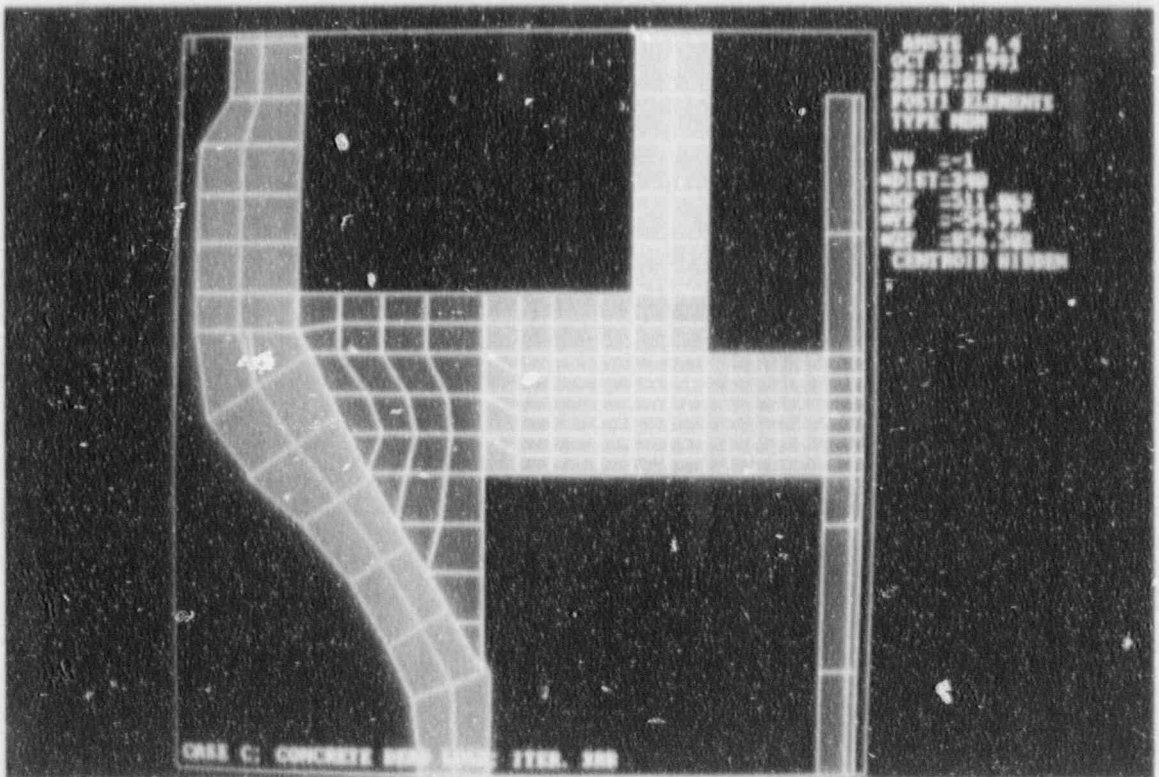


Figure 2.16

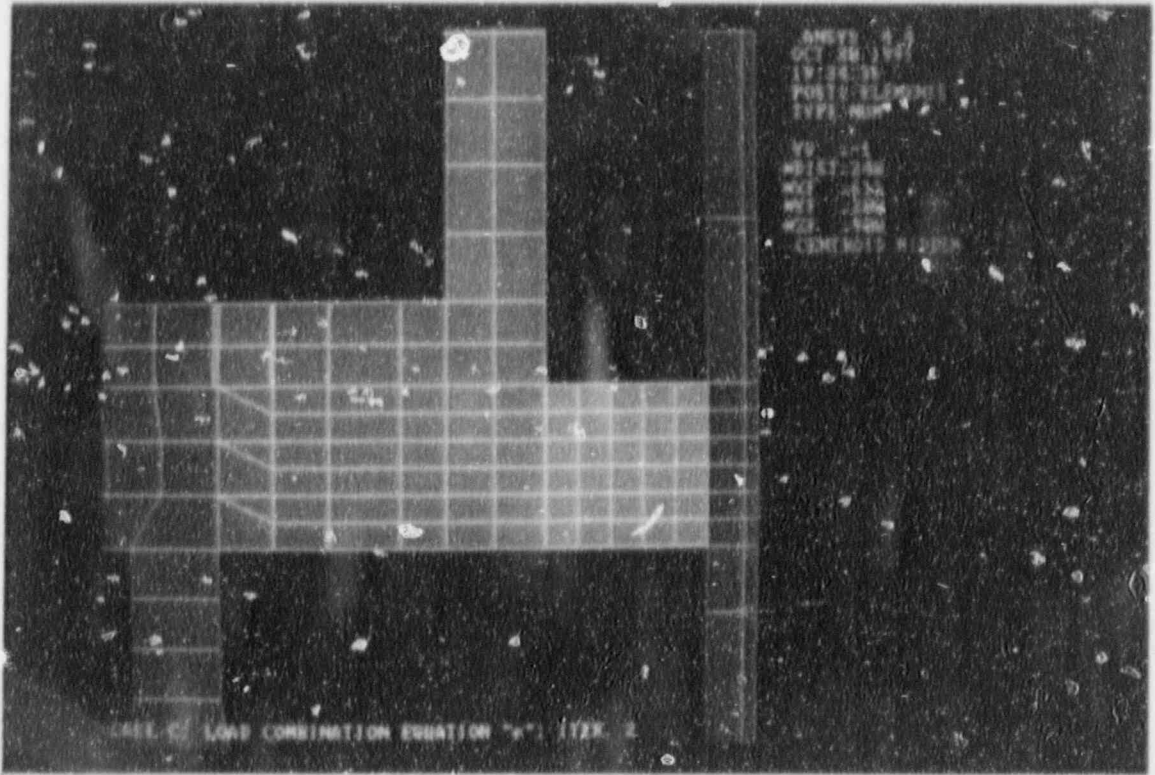


Figure 2.17

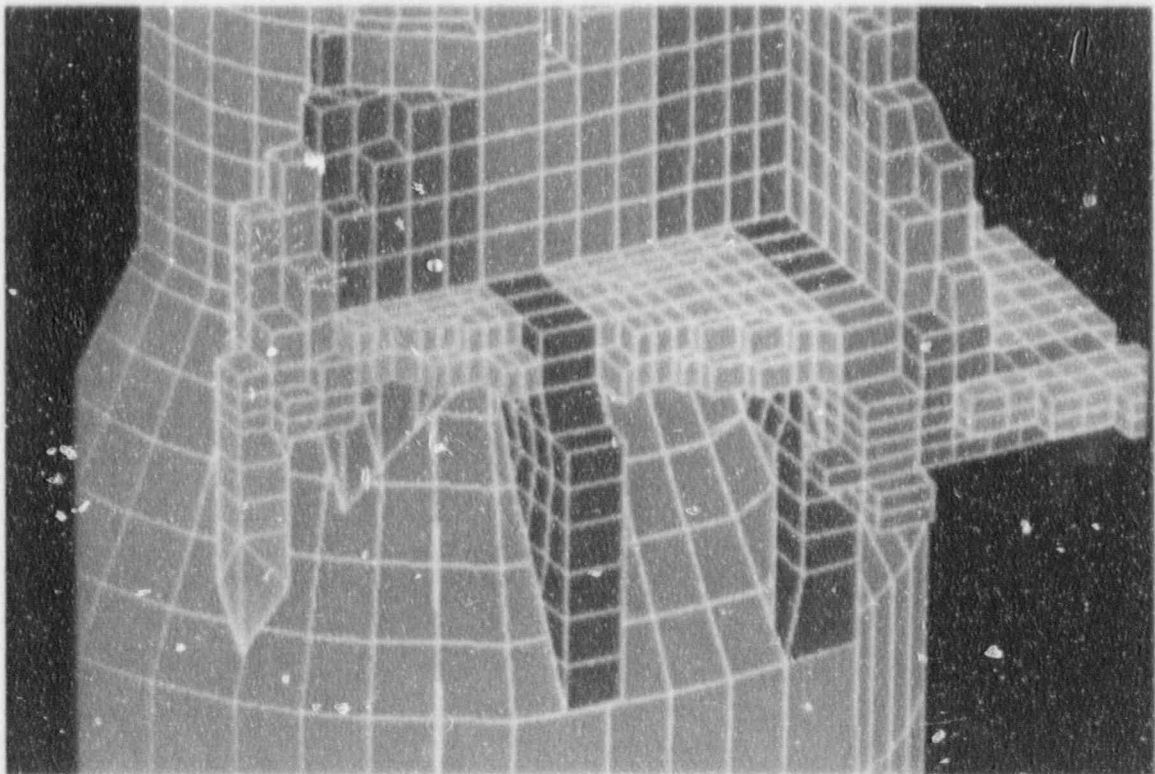


Figure 2.18

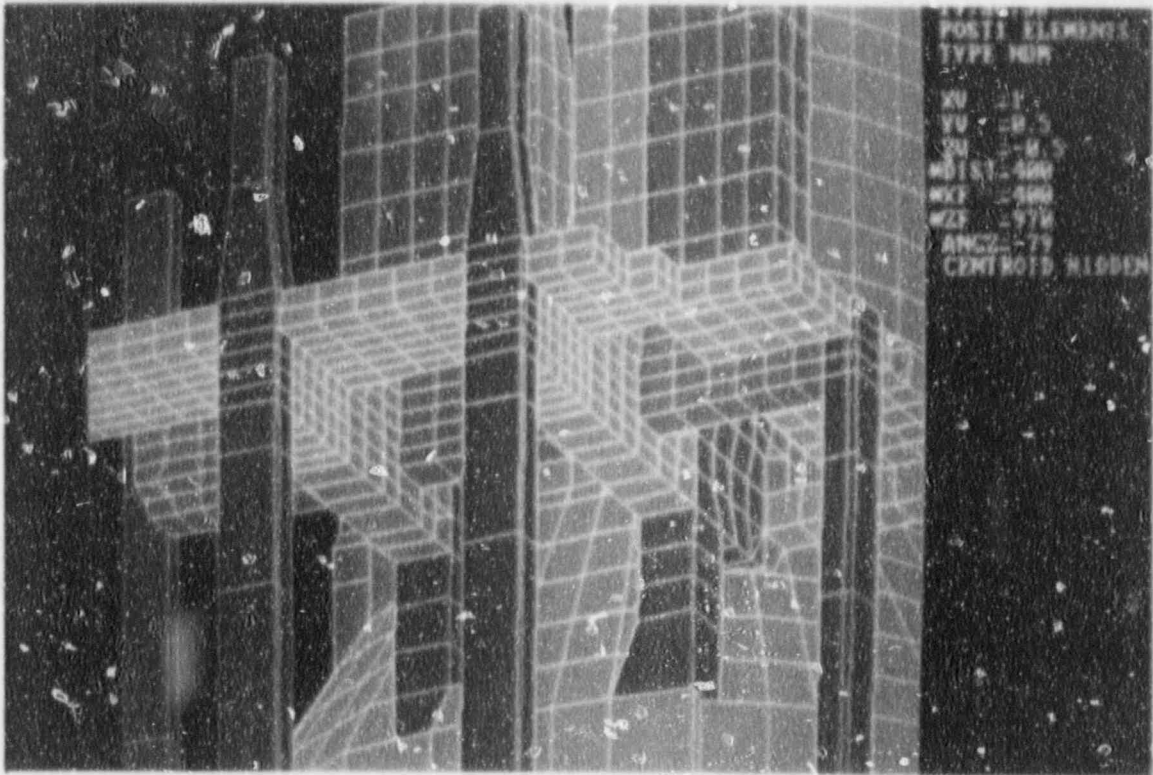


Figure 2.19

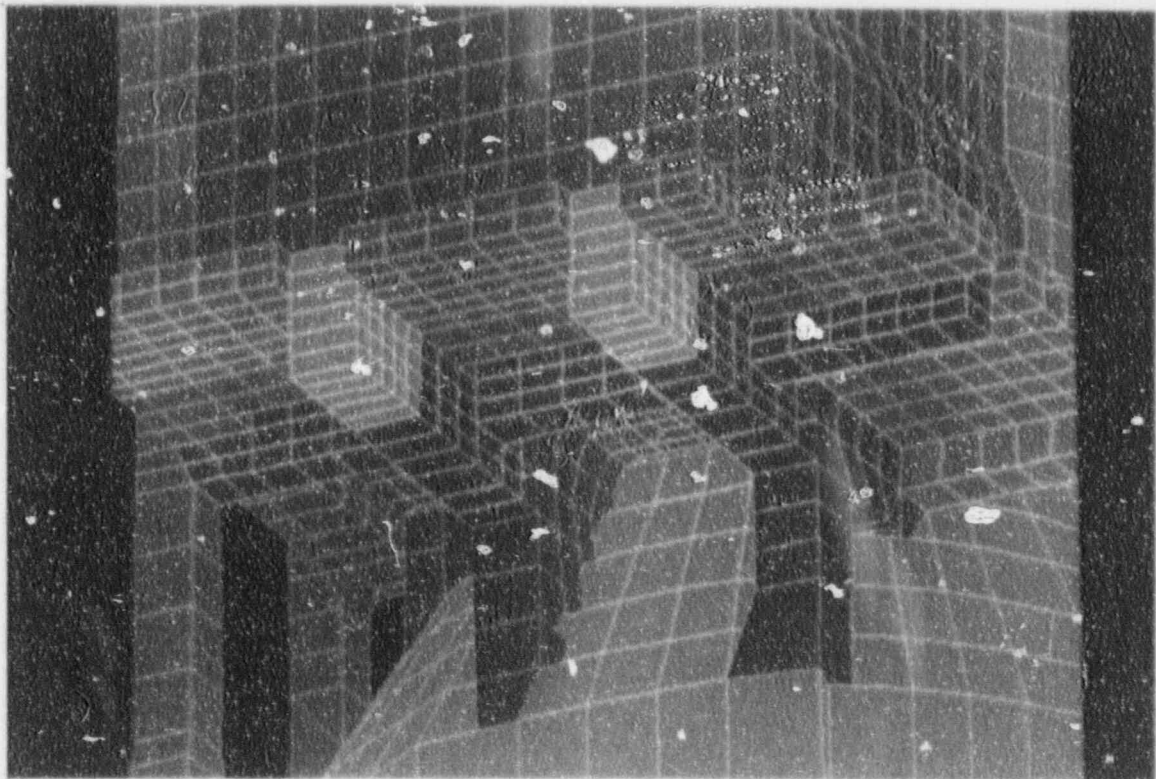


Figure 2.20

3.0 DESIGN CRITERIA

The loads and load combinations used in the evaluation of the SFP were developed and applied in accordance with Reference 3. Results were evaluated in accordance with ACI-349 (Reference 4). Per GPUN direction only results for Analysis Cases C and D were carried to completion (Reference 30). Results for Analysis Cases A and B are considered preliminary and are not reported. However, Analysis Cases A and B are bounded by the results of Analysis Cases C and D.

Dead load, live load, seismic load, thermal gradients, and cask drop load each constitute a separate load definition as described below.

3.1 Definition of Loads

The individual loads defined in this section were used in conjunction with the Analysis Cases described in Section 3.2 and combined in accordance with the load combinations given in Section 3.3. The details on how these loads were applied to the SFP model can be found in Reference 26.

3.1.1 Dead Load

The dead load applied to the SFP model consisted of the weight of reinforced concrete at a density of 150 lb/ft³, a 38'-9" column of water at a density of 62.4 pounds per cubic foot within the SFP, the submerged weight of fully loaded racks, and a local load in the northeast corner of the pool to simulate a 100 ton cask temporarily stored within the Cask Drop Protection System.

The 100 ton cask dead load was applied as a uniform pressure to the elements within the ten (10) foot diameter circle centered as shown in Figure IV-8 of Reference 13.

Three fuel rack conditions were considered:

1. Rack and fuel loads in place in 1983 were used. The rack loads were determined from the Wachter rack drawings listed in Reference 14. The Wachter racks are as located on Sketch No. 1 except that row 6 was never installed (Reference 15). Approximately 980 fuel assemblies were in the pool in 1983 located in rows 1, 2 and 3. The weight of one fuel assembly was 680 pounds and its net volume was 2326 cubic inches including the channel.

ABB Impell Corporation

2. The weights of the fully loaded high density racks presently in the pool are provided on Joseph Oat Drawing D-7475, Revision 4 (Reference 14) and their location within the pool is shown on Joseph Oat Drawing D-7472, Revision 2 (Reference 14). The volume of the racks was calculated from the Joseph Oat Drawings. The weight and volume of one fuel assembly were as specified for Condition 1 above.
3. The weight, volume, and out of the racks were the same as in Condition 2 above. The volume of a consolidated fuel assembly (128 fuel rods), including the canister, is 4158 cubic inches. The weight of one fuel assembly fully loaded was 1350 lbs. (Reference 16).

Fuel and rack loads were applied as equivalent uniform pressures to the pool slab elements located directly beneath the racks.

3.1.2 Live Loads

Design Live Loads

Design Live Load is summarized in Table 3.1 below:
(See Table 3.8.6 of Reference 17)

TABLE 3.1 - DESIGN LIVE LOAD

<u>Elevation</u>		<u>Load (psf)</u>
119'-3"	Columns A-C, 4-7	1000
119'-3"	Remainder	800
95'-3"	New Fuel Storage	800
95'-3"	Remainder	400+20 kips
(The 20 kip load was applied as a concentrated load between column line RD and RE).		
75'-3"	All Areas	400

Equipment Live Loads

Equipment Live Loads are as specified below (Reference 16 and 18):

Elevation 75'-3":

1. Two (2) Fuel Pool Heat Exchangers weighing 3200 lbs. each located near the junction of Column Lines R5 and RE-RF.

ABB Impell Corporation

2. Two (2) Spent Fuel Pool Pumps weighing 5000 lbs. each located near the junction of Column Lines R5-R6 and RE-RF.
3. One (1) Augmented Spent Fuel Pool Heat Exchanger weighing 31,700 lbs. located near the junction of Column Lines R7 and RD.
4. Two (2) Augmented Spent Fuel Pool Pumps weighing 5000 lbs. each located near the junction of Column Lines R7 and RE.

Elevation 95'-3":

1. Two (2) Emergency Condensers weighing 380,000 each located in the region of Column Lines R3-R5 and RA-RC.

3.1.3 Seismic Load

The Operating Basis Earthquake (OBE) horizontal acceleration used in both the north-south and east-west directions was 0.24g. The OBE vertical acceleration used was 0.10g (Reference 3).

The Safe Shutdown Earthquake (SSE) horizontal acceleration in both the north-south and east-west directions was 0.48g. The SSE vertical acceleration was 0.20g, per Reference 3.

The equivalent static seismic load of the reinforced concrete was equal to the weight of the concrete multiplied by the appropriate vertical and horizontal accelerations.

The vertical inertial load on the SFP slab was equal to the weight of the 38'-9" column of water multiplied by the SSE vertical acceleration. The hydrostatic pressure on the SFP walls was also increased by the vertical seismic acceleration. Statically equivalent hydrodynamic loads were applied to the SFP walls using the methodology of Reference 11 (References 22 and 26).

To account for fuel rack loads during a seismic event with the pool full of racks, the buoyant weight of fully loaded racks was multiplied by the vertical acceleration. No horizontal inertia load was applied (Reference 15).

The seismic loads were applied independently in each direction and the results were combined algebraically. Several different algebraic combinations were used in the load combination equations to produce the most conservative results (see Section 4.2.4.2).

3.1.4 Thermal Gradients

The thermal gradients for Analysis Cases C and D were assembled considering the Reactor Building air temperature varying from 40°F to 110°F, the pool water temperature from 85°F to 100°F, and the interior surface of the drywell concrete temperature varying with elevation as shown in Table 3.2 (References 3 and 21).

The above variations result in two critical thermal conditions which generate maximum thermal demand on the structure (Reference 21).

1. The winter condition with the Reactor Building air at 40°F and pool water at 100°F resulting in a thermal gradient of 60°F through the pool slab and the north, east and west pool walls. The interior drywell concrete shield wall temperatures were the lower bound operating temperatures given in Table 3.2 with surface temperatures interpolated linearly between elevations.
2. The summer condition with the Reactor Building air at 110°F and pool water at 85°F resulting in a thermal gradient of 25°F through the pool slab and the north, east and west pool walls. The interior drywell concrete shield wall temperatures were the upper bound operating temperatures given in Table 3.2 with surface temperatures interpolated linearly between elevations.

The temperatures on the wet surface of the SFP and the inner and outer surfaces of the shield wall for the two conditions described above were explicitly applied at each node of the SFP thermal model. Uniform ambient temperature was applied at all the remaining surface nodes in the reactor building. Using the SFP thermal model (see Section 2.2.2.1) a steady state heat transfer analysis was performed to determine the temperatures at the intermediate nodes in the shield wall and the SFP walls and slab. The temperature at each node was stored on File 04 of the ANSYS heat transfer analysis and then retrieved in the thermal Load Step solution for the structural model.

ABB Impell Corporation

All thermal gradients were considered to be steady state conditions.

TABLE 3.2 (Reference 21)
SPENT FUEL POOL ANALYSIS TEMPERATURES (°F)

<u>EL. (ft.)</u>	<u>INTERIOR SURFACE CONCRETE SHIELD WALL</u>	<u>FUEL POOL WATER</u>	<u>REACTOR BLDG. AMBIENT AIR</u>
<u>Winter Condition</u>			
50	105*	N/A	40
80	176*	100	40
92	200*	100	40
95	200**	100	40
110	200**	100	40
<u>Summer Condition</u>			
50	126*	N/A	110
80	176*	85	110
92	200*	85	110
95	200**	85	110
110	200**	85	110

* Calculated
 ** Measured

3.1.5 Cask Drop Accident

The effect of a cask drop accident was considered in the analysis using an equivalent static load of 1560 kips applied to the SFP slab (Reference 16). This load was uniformly distributed over the slab elements within a 10' diameter circle centered as shown in Figure IV-8 of Reference 13.

3.2 Description of Analysis Cases

3.2.1 Analysis Case A

The baseline analysis assumes normal plant operation loads, the rack and fuel loads in place in 1983, (Section 3.1.1, Rack Condition 1) and a thermal gradient as delineated in Section 3.1.4, Winter Condition. No seismic or cask drop loads were considered and only equipment live load (Section 3.1.2) was included for this case. Adequate embedment length of the rebar was assumed and pre-existing cracks were not included.

3.2.2 Analysis Case B

This analysis used the same loads as in Case A, except that a reduced embedment of the bottom slab rebar into the supporting beams and walls was included.

3.2.3 Analysis Case C (Licensed Condition)

This analysis assumed normal plant operating loads and the high density rack and fuel loads as given in Section 3.1.1, Rack Condition 2. Reduced rebar embedment and the existing crack as described in Reference 2 were included. The thermal gradients were as delineated in Section 3.1.4. Also included in this case were design live load, seismic load and cask drop load as described in Sections 3.1.2, 3.1.3 and 3.1.5. Analysis Case C is the licensed condition for the plant.

3.2.4 Analysis Case D

This analysis assumed normal plant operating loads and the maximum rack and consolidated fuel loads as given in Section 3.1.1, Rack Condition 3. Reduced rebar embedment and the existing crack as described in Reference 2 were included. The thermal gradients were as delineated in Section 3.1.4. Seismic, cask drop, and design live load were considered.

3.3 Load Combinations

In Sections 3.3.1 and 3.3.2 below, the load combinations for which the SFP is licensed and which were used in the analysis are presented. However, they do not constitute all of the load combinations for which the SFP must be evaluated in order to comply with an ACI 349-80 Code evaluation. Section 9.2.3 of the Code requires that where any load reduces the effects of other loads, the corresponding coefficient (load factor) for that load shall be taken as 0.9 if the load is always present or occurs

simultaneously with other loads. As discussed in Section 5.2, the primary concern is for the SFP slab where a reduction in dead load on the pool slab surface could reduce margins in load combinations which include thermal gradients. Thus, the load combinations below are not the complete set of all load combinations used in the analysis. The complete set of load combinations used to evaluate the SFP and to demonstrate compliance with Section 9.2.3 of the Code are presented in Section 5.2.

3.3.1 Analysis Cases A and B

The following load combinations were considered for Analysis Cases A and B (References 2 and 16).

- a. $1.4D + 1.7L$
- b. $0.75 (1.4D + 1.7L + 1.4T_o)$

Where: D = dead load as specified in Section 3.1.1, Rack Condition 1
 L = design live load as specified in Section 3.1.2
 T_o = thermal load due to temperature differential across the slab or wall as specified in Table 3.2

3.3.2 Analysis Cases C and D

The following load combinations were considered for Analysis Cases C and D (References 2 and 16).

- a. $1.4D + 1.7L \pm 1.9E$
- b. $0.75 (1.4D + 1.7L + 1.4T_o)$
- c. $0.75 (1.4D + 1.7L + 1.4T_o \pm 1.9E)$
- d. $D + L + T_o \pm E'$
- e. $D + L + T_o + C$

Where: D = dead load as specified in Section 3.1.1, Rack Conditions 2 and 3

L = design live load as specified in Section 3.1.2

T_o = thermal load due to temperature differential across the slab or wall. Two critical cases were considered as specified in Table 3.2

E = OBE seismic load as specified in Section 3.1.3

E' = SSE seismic load as specified in Section 3.1.3

C = Cask drop load as specified in Section 3.1.5

Due to the introduction of live load in each of these equations, the load combinations could not be conservatively simplified to take advantage of the fact that $E' = 2E$.

3.4 Material Properties and Section Capacity

Section capacities, stresses and properties were determined in accordance with ACI-349 (Reference 4) and standard engineering texts on reinforced concrete analysis and design (References 9, 10 and 20). Ultimate moment capacity was based on the fundamental assumptions of ACI-349 Section 10.2 and used the Whitney Stress Block for concrete as described in ACI-349 Section 10.2.7.

A yield strength of 40,000 psi was used for the reinforcing steel.

A compressive strength of 3000 psi was used for concrete.

The surrounding structural floor slabs at elevations 75', 95', and 119' in the SFP finite element model generated axial loads in the SFP walls and slab due to the restraint of axial thermal growth. Since compressive axial force has a significant effect on increasing moment capacity and tensile axial force has a significant effect on decreasing moment capacity, the calculation of the moment capacity of a member at critical sections must account for the effects of axial load. The calculation of moment capacity accounting for axial loads complied with ACI-349 Section 10.3.1. The influence of axial forces on shear capacity complied with ACI-349 Section 11.3.1.2 and 11.3.2.3.

The calculation of concrete and steel stresses at moments which are less than ultimate was based on the application of first principals (i.e., cross section equilibrium, linear strain distribution, strain compatibility, and the stress-strain curve for concrete and steel).



ABB Impell Corporation

INTENTIONALLY LEFT BLANK

4.0 SPENT FUEL POOL BEHAVIOR

4.1 Basic Considerations

The Spent Fuel Pool (SFP) occupies a prominent position in the Reactor Building because of its relatively large mass and its location high up in the structure. As shown in Figures 2.1 and 2.2, the SFP is integrally connected to the shield wall and the floor slabs at Elevations 119', 95' and 75', and supported from below by integrally cast concrete girders which are, in turn, supported by interior columns and exterior columns and walls. Because of this connectivity, the SFP's behavior is dependent on the relative supporting stiffness provided by all of these members. As the relative stiffness of these members change, due to the normal cracking of the reinforced concrete from mechanical loads and thermal gradients, so too does the amount of load that each of these members carries. It is this redistribution of the internal forces within the Reactor Building which leads to the intricate and complex behavior of the SFP. Section 4 is concerned with the behavior of the SFP structure and the evaluation process. The actual evaluation to demonstrate Code compliance and the determination of the significance of cracks in the SFP structure is provided in Section 5.

4.2 The Evaluation Process

The evaluation of the SFP structure integrates various analysis methods, criteria and strategies with structural behavior to form an overall evaluation process. The distinct components of this process include: (1) an understanding of the Reactor Building structural response to individual loads and the role of the major structural components in supporting the SFP, (2) an analysis strategy which addresses observed response and considers original design intent, (3) the application of a cracking methodology, and (4) load application and stiffness. The following sections discuss these interrelated components which together make up the evaluation process.

4.2.1 Reactor Building Structural Response

This section discusses what was learned from the results of iteration 0 (see Section 4.3.2) regarding the response of the SFP model to each load step defined in Section 2.4. The manner in which the SFP model responded to these loads formed the basis for the development of the analysis strategy in Section 4.2.2.

4.2.1.1 Design Intent and the Primary Supporting Members

As discussed in Section 2.1, the SFP is integrally connected to the reactor building shield wall and to three floor slabs at the top, mid-height and bottom of the pool walls. From below, the SFP is supported by integrally cast concrete girders and columns. This high degree of connectivity between the SFP structure and the Reactor Building makes the overall structure highly indeterminate and, as a consequence, many parts of the Reactor Building will resist loads from the SFP. However, in the original design this high degree of indeterminacy was not considered in the selection, sizing and reinforcing of structural members to resist loads from the SFP. Rather, the original designers selected (or designed) a specific set of major structural members to resist all of the vertical loads developed by the SFP and its contents. This specific set of major structural members includes Girders RD, RE and R6 and Column C6, as shown in Figure 2.1. These four members are referred to throughout this report as the "Primary Supporting Members." Insights into the behavior of the SFP can be revealed by examining the loads in each of these members at various phases in the analysis process.

It is the primary supporting members which were designed to carry the vertical loads from the SFP. That is, the primary supporting members were evaluated for load from the SFP and reinforced to resist those loads. However, due to the high degree of connectivity between the SFP and Reactor Building, it can be expected that other structural members, which were not designed to resist SFP load, will also carry significant load. Therefore, it is important to distinguish between those structural components which were designed to resist SFP load and are "qualified" load paths, and those structural components which were not specifically designed to resist SFP loads and are considered "unqualified" load paths. The concept of qualified load paths is an important part of the analysis strategy discussed in Section 4.2.2.

4.2.1.2 Effect of Thermal and Mechanical Loads on Floor Slabs

In the discussions that follow in this and other sections, photographs of stress contour plots will be used to illustrate various aspects of SFP response. For reference, each photograph contains a caption describing the analysis case, iteration number and load combination. In addition to the factored load combinations described by various letters (e.g., see section 3.3.2 and Table 5.1a), unfactored load combination results are also used in order to clearly distinguish response in terms of only sustained mechanical and thermal loads. When an unfactored load combination is used it is incorporated directly into the caption. "DL" represents dead load

ABB Impell Corporation

and includes concrete dead load, hydrostatic pool load and high density fuel racks as described in Section 3.1.1, "LL" represents floor design live load as described in Section 3.1.2, and " T_w " and " T_s " represent the winter and summer temperature conditions as described in Table 3.2.

The results for Analysis Case A indicated that the floor slabs at elevation 119', 95' and 75' have an important influence on the response of the SFP and, in particular, on the response of the primary supporting members. However, before discussing this influence specifically, it is important to understand why they have an influence and the factors that effect the degree to which they can influence the response of the primary supporting members.

The responses of the floor slabs to mechanical and thermal loads are quite different. To illustrate this difference for the floor slab at Elevation 119', which is shown in Figure 4.1, the principal tensile membrane stresses within the floor slab are plotted in Figure 4.2 for the unfactored load combination of dead load plus live load (DL+LL). Figure 4.3 is the same plot with the shield wall and SFP wall removed. For this combination of mechanical loads, the stress levels everywhere in the slab are well below the concrete cracking stress of 410 psi (410 psi is the modulus of rupture for concrete with a compressive strength of 3000 psi.). In Figure 4.4 the principal tensile membrane stresses in this same slab are plotted for the unfactored load combination of dead load, live load and winter temperature condition (DL+LL+ T_w). To better illustrate the tensile stresses in the floor slab for this load combination, Figure 4.5 shows only the stresses in the floor slab elements. In contrast to Figures 4.2 and 4.3, Figures 4.4 and 4.5 show much higher levels of membrane tensile stress. Thus, the winter temperature condition alone subjects the floor slab to significantly higher membrane stresses than all the mechanical loads combined. Also, as can be seen in the stress trajectory plots in Figures 4.6 and 4.7, the general direction of the tensile stresses in Figures 4.3 and 4.5 is the same.

Figures 4.3 and 4.5 show that when thermal loads are combined with mechanical loads, the resulting stresses are sufficiently in excess of 410 psi over wide regions of the floor slab at Elevation 119' to cause extensive concrete cracking. However, because of the self-limiting nature of thermal strain, the thermal stresses and the associated internal forces are substantially relieved after the slab's membrane stiffness has been reduced by the concrete cracking. This is not the situation for the stresses resulting from the mechanical loads which produce the stresses shown in Figure 4.3. The internal forces which cause the mechanical load stresses remain in the structure since they are not self-limiting or self-relieving. Thus these mechanical forces will redistribute after cracking has occurred due to the

thermal stresses. It is also apparent from Figure 4.6, which shows the direction of the principal tensile stresses given in Figure 4.3, that these stresses (forces) restrain the SFP, preventing the upper portion of the pool from moving in the northerly direction. This tendency of the upper portions of the pool to move in the northerly direction, and also rotate downward, under the action of mechanical load (e.g., concrete dead load) can be seen from the horizontal (x) and vertical (z) displacement contours plotted in Figures 4.8 and 4.9 respectively.

4.2.1.3 Influence of Floor Slabs on SFP Response

In Analysis Case C, iteration 0, the floor slabs were assumed to be fully effective (uncracked), but in iteration 1 the floor stiffness was reduced by several orders of magnitude to make the floor slabs ineffective as restraining membranes. The influence of reducing the floor slab stiffness from iteration 0 to iteration 1 on the redistribution of forces onto the primary supporting members is illustrated in Tables 4.5, 4.6, 4.7 and 4.8 for each load case. The vertical shear forces in the girders shown in these tables are unfactored values and are taken at the face of the embedded wall column. As these tables show, the result of reducing the floor slab stiffness was an increase in load in all primary supporting members. This load transfer is further illustrated by comparing the stress increase in Girder RE, as observed in Figures 4.10, 4.11 and 4.12 for iteration 0 and Figures 4.13, 4.14, and 4.15 for iteration 1 (see also Figures 5.112 and 5.118).

The actual significance of the floor slabs as restraining membranes which reduce the loads in the primary supporting members is probably underestimated by the results shown in Tables 4.5 to 4.8. In proceeding from iteration 0 to iteration 1, these tables reflect only the release of the floor slabs while the remainder of the Reactor Building and SFP structure are left completely uncracked. Had the floor slabs been released after the shield wall and SFP walls cracked, the resulting load in the primary supporting members would have been the same since the overall level of cracking would have been the same, however, a greater contribution of the total load due to the release of the floor slabs and the cracking of the shield wall and SFP walls would have been attributed to the release of the floor slabs.

Another observation to be made from Tables 4.5 to 4.8 is the significant effect that the floor slabs have on the response of the structure due to temperature conditions. For example, Tables 4.5 and 4.6 show that reducing the stiffness of floor slabs to simulate tensile cracking causes a significant load change in Girders RD and RE, so much so in fact, that load reversal occurs between iterations 0 and 1. This load change can also be

ABB Impell Corporation

observed in the stress change which takes place at the bottom of Girder RE between Figures 4.16 and 4.17.

4.2.1.4 Conclusions Regarding Floor Slab Behavior

Based on the discussion above, it is concluded that (1) the temperature condition will cause extensive cracking of the floor slabs, (2) the mechanical loads cause tensile membrane forces in the slabs which redistribute to other regions of the structure after the slabs crack, (3) the original design intent for the floor slabs would not have been designed to act as restraining membranes to support the mechanical loads of the SFP, and (4) as a consequence of (3) the continuity and development of the reinforcing steel may not be adequate to ensure that the slabs can function as restraining membranes. Therefore, it is important to reduce the membrane stiffness of the slabs so that they do not act as restraining membranes for the SFP.

A comparison of the influence of the winter versus summer temperature conditions on the cracking of the floor slab at elevation 119' showed that the winter condition dominates floor slab cracking. For the shield wall, SFP (see Section 4.2.1.5) and floor slabs, the winter temperature condition produces much higher tensile stresses over larger regions of the SFP model. As a result, load combinations with the winter temperature condition will produce far greater relative stiffness changes within the structure and more redistribution of internal forces onto the primary supporting members than will the summer temperature condition. Therefore, load combinations with the winter temperature condition were used in the cracking process for the entire model.

4.2.1.5 Effect of Temperature Conditions on Shield Wall and SFP Cracking

As discussed in Section 2.4 the temperature distribution throughout the SFP and Reactor Building structure for the winter and summer conditions was determined from a heat transfer analysis of the entire SFP finite element model. Figures 4.18 and 4.19 show the resulting winter and summer temperature distributions used in all analysis cases. The thermal stresses in the shield wall and SFP structure resulting from these temperature distributions in iteration 0 are shown in Figures 4.20 and 4.21 for the summer condition, and in Figures 4.22 and 4.23 for the winter condition. The plots in Figure 4.24 for the summer condition and in Figure 4.25 for the winter condition have the same stress contour range, and show that concrete cracking is far more extensive for the winter condition than the summer condition and, therefore, the winter temperature condition was used in the cracking process for the entire model.

4.2.2 Analysis Strategy

The objectives of the SFP analysis were to qualify the SFP for increased loads in accordance with the Code requirements of ACI-349 and to explain why cracks exist in the SFP structures. It is the analysis strategy which provides the means to achieve these objectives.

To confirm the licensed condition for High Density Fuel Storage (Analysis Case C), an analysis strategy was developed which provides high confidence in the safety of the SFP design. The implementation of the analysis strategy is the cracking process. The objective of the cracking process used for Analysis Case C was to ensure that the sequence of cracking and the resulting redistribution of internal forces maximized the forces in the primary supporting members of the SFP and the SFP slab. While the cracking sequence used in the evaluation could deviate from the actual, but unknown, cracking sequence, there is high confidence that the cracking process together with the evaluation process provide conservative results which can account for any variation in the cracking sequence that might be postulated.

However, an analysis strategy which only focuses on maximizing the forces in the primary supporting members and SFP slab may not achieve the objective of explaining why the cracks in specific members exist and what these cracks mean in terms of the magnitude of the loads that the primary supporting members may actually resist. Recognizing that unqualified load paths do participate in resisting SFP loads, the analysis strategy also quantified that portion of the response which was caused by unqualified load paths. It is here that the analysis strategy and the development of the finite element model cannot be separated, because in order to achieve this level of understanding of actual behavior, all significant load paths, including unqualified load paths, must be represented in the model. This was an objective in developing the model (see Section 2.2).

In consideration of these broad objectives, the analysis strategy employed a cracking sequence which deliberately allowed load to accumulate within the primary supporting members due to the cracking of other regions of the reactor building and SFP. In addition to accounting for the normal cracking of concrete under mechanical and thermal load, this cracking sequence also addressed the problem of SFP loads carried by unqualified load paths and the concerns for observed cracking. As implemented, therefore, the cracking sequence allowed the uncracked primary supporting members to accumulate all of the load relieved through the normal cracking of the shield wall and SFP and the release of unqualified load paths before the primary supporting members were cracked and allowed to redistribute load. With

ABB Impell Corporation

loads conservatively accumulated in the primary supporting members (see Section 4.3.1.1, iteration 3R), these members would then be cracked in accordance with the criteria of Section 2.3.1 and their load redistributed back (see Section 4.3.1.1, iteration 4) to structures which had cracked in previous iterations. These structures would then be checked for higher levels of cracking and if required cracked further and their internal forces redistributed in a subsequent iteration. The strategy of incorporating normal cracking with the sequential elimination of unqualified load paths and intentionally accumulating load in the primary supporting members resulted in a conservative assessment of the loads carried by the primary supporting members. This, in turn, led to a high confidence that the calculated loads (unfactored) are greater than the actual load to which the primary supporting members may be subjected. An additional benefit to this approach is that it also quantified the extent to which unqualified load paths participated in supporting the SFP.

The concepts of design intent and qualified load paths were introduced in Section 4.2.1. As already noted, these ideas formed an important part of the analysis strategy, and were used to ensure that load paths which support the SFP were designed and qualified for that purpose. Consequently, unqualified load paths identified during the analysis process were made inoperative. In subsequent iterations the load within these load paths was redistributed to qualified support components. Three unqualified load paths were identified during the analysis process: (1) the restraining membrane mechanism provided by the floor slabs at elevations 119', 95' and 75', (2) the bending resistance and flange action of the floor slab at elevation 75 near girders RD, RE and R6, and (3) the cantilevered support provided to the SFP by the upper elevations of the shield wall. Each of these mechanisms was separately released to understand its significance and to redistribute its load to the qualified structural components of the SFP. The first mechanism was released in iteration 1, the second in iteration 4 and the third in iteration 5. This is further explained below and also in Sections 4.3.1 and 4.3.2.

The influence of the floor slabs on the structural response of the SFP was discussed in Section 4.2.1. The support that these floors provide to the SFP was shown to be significant. Since the original design of these slabs did not envision that they would restrain the SFP by membrane action, the detailing and continuity of the reinforcing steel may not be adequate to provide this type of structural support. Therefore, as part of the analysis strategy this unqualified load path was released (i.e., membrane and bending stiffness reduced by a factor of 1,000) in iteration 1 and all subsequent iterations to ensure that it was not relied upon for SFP support.

The Muenow Report (Reference 8) quantified the cracks that had been observed in Girder RE and the floor slab between Girders RE and RD. The report concludes that the cracks in Girder RE do not penetrate the width of the girder and are confined to the first few inches of its surface. However, the floor slab at elevation 75', which is adjacent to girder RD and RE and forms their compression flange, contains a crack through its entire 3 foot thickness. The presence of this crack and its potential significance were included in the analysis process by the complete release of this slab (i.e., stiffness reduced by a factor of 1,000 in iteration 4 and all subsequent iterations).

A walkdown of the SFP conducted by the analysis team, prior to implementation of the analysis, identified the presence of cracks in the upper elevations of the shield wall which suggested that some structural support for the SFP may be coming from the shield wall. It was recognized that the integral and indeterminate nature of the SFP and shield wall would allow the shield wall to partially support the SFP through cantilever action. However, this load path was not a qualified support mechanism since the reinforcement between the shield wall and SFP south wall was never detailed to perform this function. Therefore, as part of the analysis process, the shield wall cantilever support mechanism was entirely removed and forces were allowed to redistribute to other load paths within the structure in iteration 5. (It should be pointed out that the shield wall was already cracked in iteration 2 and all subsequent iterations based on the application of the Branson Equation, as will be discussed in Section 4.2.3. Iteration 5 took a step beyond this to ensure that no support for the SFP would come from the shield wall.)

To achieve high confidence in the safety of the SFP design, the cracking process was interrupted for the purpose of examination to study structural behavior at critical iterations (see Sections 2.4 and 4.3). In this manner evaluations could be performed at each critical iteration to ensure that the most severe cases had been evaluated for each structural component of the SFP.

4.2.3 Application of the Cracking Methodology Using the Branson Equation

The cracking methodology which was used consistently throughout the cracking iteration process was based on the use of the Branson Equation as discussed in Section 2.3.1. The intent in using the Branson Equation was to have a reasonable and consistent basis to account for the changes in stiffness which occur due to concrete cracking. As originally derived, the Branson Equation is not intended to be applied in an incremental loading manner, as would be done in a tangent stiffness approach where stiffness

is updated at each successive load iteration. Rather, the Branson Equation is intended to predict deflection (flexural stiffness) at or near service load levels with the total service load applied in a single load iteration (Reference 6), as would be done in a secant stiffness approach.

To illustrate the method, the total service load would be applied to the uncracked structure and the internal forces computed from a linear elastic analysis. Based on these internal forces, a linear distribution of stress (the linearized stress) would be computed through the thickness of all SFP structural components (i.e., shield wall, SFP walls, SFP slab and girders). The entire model would be scanned and at locations where the linear stress levels exceeded the cracking stress, the associated forces (moments) would then be input to the computer program Branson (Reference 19) to determine new stiffness properties at these locations. The revised stiffnesses would then be used in a subsequent analysis (iteration) with the same total service load to determine the redistribution of internal forces due to the cracking which had occurred in the previous analysis (iteration). In the next iteration stresses would again be reviewed to determine if higher levels of cracking were appropriate at sections which had previously cracked. In all cases it was found that the moment causing first cracking was higher than the moment after cracking. This process would be repeated in successive iterations until no new cracking occurred.

In this process all concrete cracking (and the release of unqualified load paths) takes place at a constant load level. The process itself is divided into distinct linear elastic analyses which are called "iterations." Each of these iterations takes place at the same constant value of load. Stiffness is the only thing that changes from one iteration to the next. Therefore, iterations do not refer to changes in load, they refer to distinct changes in stiffness with load held constant. The stiffness changes which occurred with each iteration are described further in Section 4.3.

Since both load combinations "b" and "e", (Section 3.3.2) are close to service load levels it was decided that one of these load combinations would be used as the service load for the cracking process. Surface stress contours for each of these load combinations are shown in Figures 4.26 and 4.27 for different sides of the SFP. Both load combinations "b" and "e" produce very similar results even though they have somewhat different load factors. The real difference between these two load combinations is that "e" includes the cask drop load while "b" does not. The cask drop load has its major influence on the girders beneath the SFP, and its presence would transfer more load to other parts of the structure when the girders were cracked, since the level of cracking would be greater than if the cask drop load were not present. Since this was consistent with the analysis strategy

and since all of the load factors in load combination "e" were 1.0, load combination "e" was selected as the service load to be used in the cracking iteration process. However, as part of the evaluation process all load combinations were checked at critical iterations (see Section 5).

To implement the cracking process utilizing the Branson Equation, the total load for load combination "e" was applied to the SFP. Beginning with iteration 1, stresses in the entire SFP model were scanned, and in those regions where the concrete tensile stress exceeded 410 psi (the modulus of rupture for 3000 psi concrete) the stresses were integrated through the thickness of the shield wall, pool walls and pool slab to determine the moment and axial force acting on each cross section and the equivalent linear stress distribution. The resulting applied moment together with the section cracking moment were input to the Branson Equation to determine an effective directional concrete modulus to simulate the reduction in stiffness due to concrete cracking. As described in Reference 24, the two in-plane directional moduli calculated from the Branson Equation were compared to a predeveloped 3 x 10 x 10 material property matrix (array) to select the three digit ANSYS material number representing the rows and column of the matrix location which most closely approximated the actual set of directional moduli calculated from the Branson Equation. These sets of directional moduli were used in subsequent analyses (iterations) to reflect the cracking which took place. By the conclusion of the cracking iteration process, individual ANSYS material numbers had been applied to over 2300 of the 2889 solid elements to simulate the effect of stiffness reduction due to concrete cracking.

4.2.4 Load Application and Stiffness

The loads applied to the SFP structure during the cracking process include concrete dead load, hydrostatic pressure, fuel rack load, design live load and winter temperature condition. In addition, as explained in Section 4.2.3, the cask drop load was also included since it complemented the analysis strategy. The unfactored combination of all of these loads is load combination "e". This load combination was applied statically to the structure and tracked throughout the cracking process. As explained below, seismic inertia and hydrodynamic loads were not included in the cracking process. (They were included in the evaluation process.)

4.2.4.1 Incorporating Seismic Loads

Although seismic inertia and hydrodynamic loads were applied statically, they are still dynamic loads which produce oscillations about a static equilibrium position. As the structure moves in one direction, its stiffness changes as crack opening and closing occurs. When the structure moves in the opposite direction, cracks which opened on the previous half cycle now close and vice versa. In the absence of large moment reversals, the average structural stiffness accompanying this process can be assumed to be that which exists at the static equilibrium position. Therefore, the converged structural stiffness which exists at the end of the application of all actual sustained loads, including thermal gradient, was the stiffness used for the statically applied seismic loads.

It should be emphasized that analyses for seismic loads are not cracking iterations. Concrete cracking in this analysis only takes place under the application of sustained mechanical loads and thermal gradient. The cracked state (iteration) which results, is the cracked state to which the seismic inertia loads are applied. The only exception to this involves the floor slabs at elevations 75', 95' and 119' which were "cracked" (i.e., released) in iteration 1 because they were unqualified load paths for the membrane restraint of the SFP. These floor slabs were "put back" (uncracked) in the SFP model for all seismic analyses because they are qualified load paths for resisting and distributing seismic inertia loads. The lateral motion of the SFP due to seismic loads is intended to be resisted by the floor slabs at elevations 119', 95' and 75', and therefore their stiffness and mass were included in the seismic analysis of that cracked state (iteration). A rule which was applied consistently for all seismic analyses is that if the stiffness of a component is included in a seismic analysis, its inertial mass is also included, and if the stiffness of a component is not included (i.e., released as in the case of the floor slab at elevation 75' in iteration 3R and the shield wall in iteration 5) then its inertial mass is also not included in the associated seismic analysis for that iteration.

Very late in the analysis an error in the boundary conditions used for the seismic analyses was discovered. Specifically, the error was that symmetric boundary conditions at column line R4 were used for the north-south (X) seismic analyses rather than antisymmetric boundary conditions. All of the load combinations and evaluations in the Reference Calculations 24, 27 and 28 contain the error. This situation was investigated (Reference 34) by running the north-south seismic for the configuration of iteration 3F. This is conservative since it maximizes the loads to the primary support members. The following conclusions were drawn:

1. This error substantively affects only the loads and moments in girders RD and RE.
2. Seismic stresses in the structure are small and the conclusions above regarding stiffness and application of seismic inertia to the cracked state are still valid.
3. All of the descriptive material involving load combinations which include seismic came from References 24, 27, and 28, and therefore, contain the error.
4. The evaluation of girders RD and RE presented in Tables 5.2 through 5.6 contain the corrected values.

4.2.4.2 Selection of Critical Seismic Load Directions

Although seismic loads are not part of the cracking iteration process because they oscillate about an equilibrium configuration (see Section 4.2.4.1), they are an important load for the evaluation of the SFP. Therefore, it is appropriate to briefly discuss the general behavior of the SFP to seismic load and the selection of critical seismic load directions.

OBE level equivalent static seismic loads were applied to the entire Reactor Building finite element model in the two horizontal and one vertical direction. The stress results for seismic loads applied in the east-west direction (+Y acceleration direction) are shown in Figures 4.56 to 4.58. Of particular interest in these figures is the shear transfer which takes place between the exterior wall at R7 and the north wall of the SFP at elevations 75', 95' and 119'. The influence of each seismic load direction on the response of the girders is shown in Figures 4.59 to 4.61. The magnitude of the response to OBE seismic load relative to the response of other mechanical loads can be seen by comparing these figures to Figures 4.30, 4.31 and 4.32.

In the load combinations shown in Section 3.3.2, downward seismic acceleration (-Z) has the effect of reducing the 1.4 factor in front of the dead load term. For most of the SFP structure, this reduces the member loads and increases margins and thus was not considered for the bulk of the structure. However, since downward seismic acceleration has the same effect as reducing dead load, it could add to the response of the SFP slab from the winter and summer thermal gradients (see Sections 3.3 and 5.2), and therefore it must be included in the evaluation of the SFP slab. This evaluation was conducted for iteration 4S and the results are

ABB Impell Corporation

presented in Section 5.2.2. The results show that downward seismic acceleration in combination with winter and summer thermal gradients does not result in the minimum capacity margins in the SFP slabs. Minimum capacity margins are always produced by load combinations which include upward seismic acceleration.

From the three seismic directional cases, seismic load combinations were made to determine the most severe directional combinations for the primary supporting members, the SFP slab and SFP walls. The various seismic acceleration directions were summed algebraically, however, because downward seismic acceleration (-Z) opposes the sustained loads, and was considered in a separate evaluation for the SFP slab, it was not the focus in this evaluation. For the bulk of the SFP structure, the following seismic acceleration combinations were considered: (1) +X+Y+Z, (2) -X+Y+Z, (3) +X-Y+Z and (4) -X-Y+Z. Based on a review of results for the four combinations, combinations (2) and (4) contributed most to the response of the primary supporting members, SFP slab and SFP walls. Therefore only seismic combinations (2) and (4) were incorporated in the load combination equations for evaluation, except for analysis iteration 4S which also included combinations -X+Y-Z and -X-Y-Z.

4.3 The Cracking Iteration Process

As discussed in Section 4.2.2, the cracking iteration process is the implementation of the analysis strategy. The objective of the cracking iteration process was to ensure that the sequence of cracking and the resulting redistribution of internal forces maximized the forces in the primary supporting members of the SFP and the SFP slab. As the analysis proceeded the cracking process was interrupted to study structural behavior and to perform evaluations at critical iterations to ensure that the most severe cases had been evaluated.

A summary of the behavior of the SFP as described by the iterative process is given in Section 4.3.1. The distinct iterations in the cracking process are shown in Tables 4.1 and 4.2. A description of each iteration is given in Section 4.3.2 and summarized in Tables 4.3 and 4.4. Table 4.13 arranges the information in Table 4.3 into an array format for easy reference. Figures showing stresses for various load combinations are sometimes referred to in the discussion which follows. For easy reference, Table 5.1a summarizes all of the load combinations referred to in the figures.

4.3.1 Spent Fuel Pool Behavior and the Iteration Process

In discussing SFP behavior in general, and in particular as it relates to the cracking iteration process, constant reference will be made to Tables 4.5 through 4.8. These tables provide the descriptive information necessary to develop an understanding of SFP behavior. Tables 4.5 to 4.7 show the vertical shear force at the end of each girder where it intersects the face of the exterior wall columns, and Table 4.8 shows the axial force in Column C6 where it intersects the bottom of Girder R6. The forces in all of the tables are unfactored so that quantitative response comparisons can easily be made for the various types of load and for different iterations. For the purpose of discussing behavior, it is not necessary to tabulate moments or stresses since these are a direct consequence of (and proportional to) the forces shown in these Tables. (Tables 4.5 to 4.8 apply to Analysis Case C. Tables 4.9 to 4.12 display the same force information but apply to Analysis Case D.)

4.3.1.1 Analysis Case C - High Density Storage

Iteration 0

In iteration 0 the entire SFP model was uncracked. The results from this iteration, which were discussed in Section 4.2.1, showed that the temperature conditions had a significant impact on the cracking of the shield wall, the SFP walls and the floor slabs. As a result of the extensive cracking of the floor slabs caused by the temperature condition and the fact that the floor slabs were not a qualified load path (see Section 4.2.2) for providing support to the SFP, the floor slabs at elevations 119', 95' and 75' were cracked (i.e., released) except for the portion of the floor slab at elevation 75' from column lines R5 to R7 and RC to RF (see Section 2.2.3). iteration 1 contains the analysis results with these floor slabs cracked.

Iteration 1

As again discussed in Section 4.2.1, the cracking of the floor slabs in iteration 1 caused an increase in load carried by each of the primary supporting members. This load increase is shown in Tables 4.5 to 4.8. Based on the stress distribution for load combination "e" with the winter temperature condition, the shield wall, SFP walls and SFP slab were cracked (see Sections 4.2.1 and 4.2.3). However, consistent with the analysis strategy (see Section 4.2.2), Girders RD and RE were not cracked based on iteration 1 results even though stresses were above 410 psi (see Figures 4.28 and 4.29). The stresses which resulted from the redistribution

of internal forces due to shield wall, SFP walls and slab cracking in iteration 1 are given in iteration 2.

Iteration 2

The increase in load carried by each of the primary supporting members due to the concrete cracking which took place between iteration 1 and iteration 2 is again shown in Tables 4.5 to 4.8. From these tables it can be determined that in the cracking which took place between iteration 0 and iteration 2 the total sustained load redistributed to Girders RD and RE increased from 1268 kips (671 + 597) to 1793 kips (988 + 805). Of this 41% increase in load, 18% occurred between iterations 0 and 1, and 23% occurred between iterations 1 and 2. Principal tensile stresses in the girders and the floor slab at elevation 75' are shown in Figures 4.30 to 4.34 for each load step in iteration 2. For comparison to Figure 4.30, Figure 4.35 shows these same stresses for concrete dead load in iteration 0.

Figure 4.36 shows the principal tensile stresses for load combination "e" in iteration 2. Also, for load combination "e" of iteration 2, Figure 4.37 shows the normal stresses in the X direction (North-South) in Girder RD and Figure 4.38 shows the distribution of shear stresses. Figures 4.39 and 4.40 show the same stresses in Girder RE. For comparison to load combination "e", Figures 4.41 and 4.42 show the normal and shear stresses on the east and west faces of Girder RE for load combination "b" of iteration 2. Based on the results of iteration 2, the floor slab at elevation 75' adjacent to the SFP north and west walls was released. The resulting redistribution of internal forces and final stresses are given in iteration 3R.

Iteration 3R

Based on the Muenow Report (Reference 8), the floor slab at elevation 75' contains a crack along the outside edge of the SFP north wall between girders RD and RE through its entire three foot thickness (see Figure 5.15). As a consequence, the ability of this slab to resist significant load and, also, to act as a compression flange to produce Tee beam behavior in Girders RD and RE is questionable. Therefore, consistent with the objectives of the analysis strategy, the solid elements of this slab were cracked (i.e., reduced in stiffness by a factor of 1,000) along the entire north and west faces of the SFP extending from column lines RC to RF and R5 to R7. This cracked portion of the floor slab was intentionally made larger than the actual region containing the crack because of the uncertainty that the proper reinforcing details exist which would allow the floor slab to provide positive moment restraint at its connection to the SFP wall (see Section

5.3.1). As discussed in Section 4.2.2, this floor slab was never designed to resist SFP loads and therefore is considered an unqualified load path.

The cracking of the portion of the slab adjacent to the SFP at elevation 75' was the only change made in iteration 3R and, as such, it showed not only what portion of the applied loads were resisted by this slab, but also an upper bound on the loads that the primary supporting members would have to carry due to the functional limitations of this slab. From Tables 4.5 to 4.7 it can be seen that the sustained load in Girders RD, RE and R6 increased by 11%, 14% and 22% respectively when the floor slab at elevation 75' was released. These results show that the floor slab at elevation 75' along the north and west walls of the SFP can reduce a significant portion of load to the SFP primary supporting members. The principal tensile stresses in the girders for load combination "e" of iteration 3R are shown in Figure 4.43. Due to the magnitude of the loads accumulated in the girders, iteration 3R is a critical iteration for the evaluation of Girders RD and RE. (It is important to recognize that the loads accumulated in Girder RD and RE in iteration 3R are conservative, since the girders have not been cracked and therefore have not redistributed any portion of their load.) Based on the results of iteration 3R, Girders RD and RE were cracked. The resulting redistribution of internal forces and final stresses are given in iteration 4.

Iteration 4

Using the stress results of iteration 3R, Girders RD and RE were cracked. This cracking resulted in the state of stress given in iteration 4, which is shown in Figure 4.44 for load combination "e". The redistribution of forces to the primary supporting members which occurred when these girders cracked is again shown in Tables 4.5 and 4.6. The results show that due to the redistribution of internal forces, the combined sustained load in Girders RD and RE was reduced by 208 kips (1096+920-969-839), which constitutes a 10% reduction in load. As expected the reduction in load in Girder RD and RE resulted in an increase in load in Girder R6 and Column C6 (see Table 4.7 and 4.8). However, the 208 kip reduction is greater than the 75 kip (299+1444-276-1392) increase in load experienced by Girder R6 and Column C6. As discussed in the section below titled "Membrane Behavior of the SFP Slab," part of the load not distributed to Girder R6 and Column C6 was redistributed to the negative moment regions of Girders RD and RE which lie within the slab of the SFP (see Figures 2.15 and 2.16). Using the results from iteration 4 the shield wall was released. The resulting redistribution of internal forces and final stresses are given in iteration 5.

Iteration 5

As part of the normal cracking process, the shield wall was cracked in iteration 2 in accordance with the cracking criteria of Section 2.3.1 and the stress results from iteration 1. The shield wall between elevations 80' and 119' was never designed or intended to support the SFP, although, as explained in Section 4.2.1, the highly indeterminant nature of the SFP and Reactor Building structure makes it inevitable that some support for the SFP will be derived from the shield wall. Since this was never the design intent, the reinforcing details necessary to provide this support were not incorporated into the original design.

To address this issue, and to ensure that the objectives of the cracking process for Analysis Case C were met, the reactor shield wall was removed (i.e., stiffness reduced by 1000) between elevations 80' and 119' and from column line R4 to where the shield wall intersects the south wall of the SFP. This analysis was performed in iteration 5. As can be observed from Tables 4.5 to 4.8, additional load was redistributed to the primary supporting members. The amount of load increase between iterations 4 and 5 in Girders RD and RE was approximately 10%.

Iteration 5 concluded the cracking iteration process using the Branson Methodology to redistribute internal forces within the Reactor Building/SFP structure due to the normal cracking of concrete and the release of unqualified load paths. With the completion of iteration 5 the SFP became structurally isolated from all the load paths which had never been designed or intended to resist SFP loads. What the iteration process showed is the high degree of redundancy which exists in the Reactor Building/SFP structure and the unquantified margins which exist due to this redundancy.

Other iterations, such as iteration 3SU, addressed rebar embedment in the SFP slab by decoupling adjacent solid elements to assess the effect of rebar pull-out on the redistribution of internal forces in the SFP slab. Additional iterations using the fully transformed cracking criteria were conducted to address specific regions of the structure, such as the SFP walls and SFP slab (e.g., iteration 4S), where the Branson Methodology under-estimated the level of cracking associated with moments which approached the ultimate capacity of the structural component. Each of these secondary iterations, which focused on a more localized area, were based on one of the primary iterations (i.e., iteration 4) discussed earlier. What is important to emphasize, is that each of these iterations with its different variation in the stiffness of the Reactor Building/SFP structure were evaluated for their severity and impact on the structural components of the SFP.

Membrane Behavior of the SFP Slab

The negative moment resistance provided by Girder RD can be seen in Figure 4.45. This figure shows the positive and negative moment stresses in the X (North-South) direction in Girder RD and the deflection of the girder/pool system under concrete dead load for iteration 2. Figure 4.46 shows the same result as Figure 4.45 but for iteration 3R. Figure 4.47 shows the tensile stresses in the X direction on the surface of the pool slab due to concrete dead load and Figure 4.48 shows the same information with the stress range of interest better defined. The concrete dead weight load step is used to illustrate this behavior because no loads are applied directly to the pool surface. When loads are applied directly to the pool surface the same negative moment bending behavior in the girder occurs, but it is masked by the bending stresses on the slab surface and cannot be seen as easily. Thus, as these figures illustrate, the SFP slab acts as a tension flange within the negative moment region of Girder RD. This flange behavior induces membrane tension in the slab through shear transfer from the girder. With the fuel pool slab acting as a tension flange for the girder, the local negative moment bending in the pool slab due to hydrostatic pressure and rack load causes the south edge of the slab adjacent to the shield wall to be a critical location for the evaluation of negative moment bending and shear because the membrane tension in the slab significantly reduces the bending and shear capacity. This is illustrated in Figure 4.49 which shows the normal stresses in the X direction acting on the SFP slab surface for load combination "a" of iteration 4 and Figure 4.50 which shows the same information with the stress range of interest better defined.

The tension flange behavior of the SFP slab discussed above is the primary mechanism for the introduction of membrane tensile stresses into the slab in the X direction. Membrane tensile stresses also occur in the Y (East-West) direction as well. The Y direction membrane tension is caused by the greater circumferential thermal expansion of the reactor building shield wall relative to the thermal expansion of the SFP slab. Figure 5.97 is a plan view of elevation 75' where the section plane is taken at the mid-depth of the SFP slab. The composition of this plan view can be better seen in Figure 5.98 which is a 3-D view taken from the northeast just above elevation 75'. For the unfactored load combination of dead load (DL), design live load (LL) and winter temperature (T_w) in iteration 0, the principal stress contours in Figure 5.99 show that the stresses at the mid-depth of the slab (the membrane stresses) are on the order of 100 to 300 psi tension. Figure 5.100 shows that the principal stress trajectories are in the Y direction within the slab. While these stresses are significantly reduced due to the concrete cracking which takes place in subsequent cracking

iterations, they are, nonetheless, still present and have the effect of reducing the moment and shear capacity of the SFP slab.

Tipping Behavior of the SFP

As can be seen from Figure 4.9, the northeast corner of the SFP has a larger downward displacement than any other region of the pool. This tipping of the SFP toward the east end of Girder R6 is caused by the greater downward displacement of column C6 relative to the other supporting Columns D7, E7 and F6 (see Figure 2.1). The vertical displacement of these four columns is shown in the contour plot of Figure 4.51 for the sustained loads of load combination "a" in iteration 4. Column C6 has larger displacements than the other three columns for two reasons: (1) it is supported by a relatively flexible concrete frame spanning over the torus and (2) it has higher axial compressive stresses along its entire length, as shown in Figure 4.52, which causes a greater shortening of the column. The axial stresses in Columns D7, E7 and F6 are significantly lower than those of Column C6 because they are embedded in the Reactor Building exterior wall, to which they transfer significant load.

This tipping has two effects on the response of the SFP structure. The first, and most pronounced effect, is the increase in load in Girder RD. This contributes to Girder RD consistently being more heavily loaded than Girder RE for all sustained load cases (see Figures 4.30 to 4.32) and all iterations (see Figures 4.29, 4.36, 4.43 and 4.44 and Tables 4.5 and 4.6). The second, but more subtle effect, is the increase in bending stress in the Y direction of the southeast section of the SFP slab (see Figure 2.1). The vertical displacement of the primary supporting members and the SFP slab caused by concrete dead load in iteration 2 is shown in Figure 4.53. The relative downward displacement of the east side of the southeast slab relative to the west side causes tensile stress in the Y direction on the top of the west side of the slab and compression on the top of the east side of the slab. This can be observed in Figure 4.54 and in Figure 4.55 where the stress range of interest is better defined. The negative moment on the west side due to loads not directly applied to the slab (e.g., concrete dead load) adds directly to the negative moment caused by loads applied directly to the pool surface, to make this region an important location for evaluation.

[An inconsistency exists between Tables 4.5 to 4.8 and Tables 4.9 to 4.12 caused by an analysis error in Analysis Case C. The only difference between Analysis Case C and D is the increase in pool slab load. As such, only the load step for pool slab loads (i.e., hydrostatic + fuel racks + stored cask) should be different, since the same cracked states were used in both cases. Therefore, the results for concrete dead load, live load, temperature

conditions and cask drop should be the same for a specific iteration and structural component. As can be observed in these tables, this is not true. The difference in results arises because of an error in Case C for iterations 0, 1, 2, 3R, 4 and 5. The error was in the stiffness value used at the base of column C6 (elevation 23') to represent the stiffness of the deep girder which spans over the torus and upon which Column C6 rests. The incorrect value was 75% of the actual stiffness of the torus girder. However, due to the relatively high axial flexibility of Column C6 between elevations 23' and 70', the effect on pool response was very small. Using iteration 4 and concrete dead weight loading as a basis for comparison, the errors in response in Girder RD, RE and R6 and Column C6 are -0.5%, -0.8%, -2.2% and +4.5% respectively. Given the specific members that those errors effect, as well as the magnitude and direction of the error, it was not necessary to perform a reanalysis. The error was corrected in iteration 4S of Analysis Case C and all iterations of Analysis Case D.]

4.3.1.2 Analysis Case D - Consolidated Fuel Storage

The preceding discussion focused on the structural behavior and cracking iteration process for Analysis Case C. The general behavior of all SFP structural components in Analysis Case D was the same as their behavior in Analysis Case C. The only difference in response was caused by the loads applied directly to the pool slab which were higher in Analysis Case D.

Consolidated fuel storage in Analysis Case D increased the total sustained load on the SFP slab by 32% from the Analysis Case C loading for high density storage (Reference 26). For other portions of the SFP structure the increase in total sustained load was much less. For example, from Tables 4.5 and 4.9 the response of Girder RD to total pool slab loads for iteration 3R increased by 18% $[(373-315)/315 = 1.18]$, while the total sustained load in Girder RD only increased by 5% $[1146-1096]/1096 = 1.05]$. While the increase in sustained load carried by different structural components varies considerably, the actual significance of these increases must be judged in terms of the actual margins in the SFP slab and primary supporting members. From the standpoint of cracking, however, this overall load increase is relatively small, when considered in combination with other sustained loads and temperature. When viewed from the standpoint of the changes in stress which occurred in load combination "e" for Analysis Case D, the increase in SFP loads had a negligible influence on the cracking which had occurred in the iterations for Analysis Case C. Therefore, the same cracked states (iterations) were used for Analysis Case D as were used for Case C. The only change made in Case D was an increase in

pool surface load to reflect the weight increase for consolidated racks and fuel. The stiffness properties of all Case D iterations were unchanged from those of Case C.

4.3.2 Description of Cracking Iterations for Analysis Case C

A brief description of the stiffness characteristics of each iteration is given in Table 4.3. Table 4.13 displays this same information in an array format for easy reference. For a description of the cracking iteration process, the reason for performing each iteration, and SFP behavior, see Section 4.3.1.

Iteration 0 - Uncracked model.

The first analysis was performed with the entire structure uncracked. This iteration showed the relative importance of each individual load type and the distribution of stresses throughout the entire structure caused by each load. The load steps in this iteration were:

- L.S. 1 - Concrete Dead Load
- 2 - Hydrostatic + High Density Fuel Racks + Stored Cask
- 3 - Design Live Load
- 4 - Winter Temperature Condition
- 5 - Summer Temperature Condition
- 6 - Cask Drop

Since the winter temperature load step has a higher thermal gradient and produced higher thermal stresses with more extensive cracking than the summer temperature load step, the summer temperature load step was only included in this iteration and iterations 4W and 4S. (See discussion in Section 4.2.1.)

Iteration 1 - Floor Slabs cracked.

Based on the stress results from iteration 0, the stiffness of the floor slabs at elevations 75', 95' and 119' were reduced by a factor of one thousand (1000). The stiffness of the solid element portion of the floor slab at elevation 75' (see Section 2.2.3.3) was left unchanged to allow tee beam behavior in girders RD, RE and R6 and to determine the extent to which the slab carried load. The SFP load steps included were:

- L.S. 1 - Concrete Dead Load
- 2 - Hydrostatic + High Density Fuel Racks + Stored Cask

ABB Impell Corporation

- 3 - Design Live Load
- 4 - Winter Temperature Condition
- 5 - Cask Drop

The regions specifically cracked on the basis of this iteration include the shield wall, the SFP slab and the SFP walls.

Iteration 2 - Shield wall, SFP walls and SFP slab cracked, plus the cracked properties from Iteration 1.

Based on the stress results from iteration 1, the shield wall, SFP walls and SFP slab were cracked in accordance with the methodology described in Section 2.3.1. The analysis of the SFP structure was performed for the same load steps as in iteration 1:

- L.S. 1 - Concrete Dead Load
- 2 - Hydrostatic + High Density Fuel Racks + Stored Cask
- 3 - Design Live Load
- 4 - Winter Temperature Condition
- 5 - Cask Drop

In this iteration the portion of the slab at elevation 75' consisting of solid elements remained uncracked and was the only portion of the floor systems at elevation 75', 95' and 119' to carry load from the SFP structure.

Iteration 3SU - SFP Slab Uncoupled, plus the cracked properties from Iteration 2.

Under the action of mechanical load the SFP slab develops positive moment in the middle region and negative moment along the supporting edges. The SFP Slab is designed for such behavior. Under the winter thermal gradient, however, the bottom of the SFP Slab develops a constant positive moment which could overcome the negative moment along the supporting edges. Since the SFP Slab has a lack of positive moment rebar embedment along these supporting edges, which may not be able to resist a significant positive moment, the degrees of freedom in the direction of the rebar (perpendicular to the potential crack) were uncoupled along the bottom surface of the pool slab at the supporting edges to simulate rebar pullout, see Section 2.2.3.4. This iteration used the same element stiffness properties for the SFP model and the same load steps as iteration 2.

Iteration 3US - SFP Uncoupled for Seismic, plus the cracked properties from Iteration 2.

This iteration was the equivalent static seismic run used in combination with iteration 3SU. However the stiffness deviates slightly from iteration 3SU since, in a seismic event, the floor slabs are designed to transfer the horizontal inertia loads to the exterior walls and couple the response of the shield wall and SFP with the exterior walls. Hence, the stiffness of all the floor slabs, including the solid elements at elevation 75' were intact (uncracked). The following directions of seismic acceleration were applied to the model:

- L.S. 1 - Seismic -X and Hydrodynamic
- 2 - Seismic +Y and Hydrodynamic
- 3 - Seismic +Z and Hydrodynamic

The following combinations were considered and the various seismic directions were summed algebraically.

- L.S. 1 : + X + Y + Z
- 2 : - X + Y + Z
- 3 : + X - Y + Z
- 4 : - X - Y + Z

Based on a review of the four seismic acceleration load steps, load steps 2 and 4 were shown to contribute most to the forces in the primary supporting members. Hence, only load steps 2 and 4 were used for load combinations and evaluation (see discussion in Section 4.3.1).

Iteration 3R - Solid elements in the floor slab at Elevation 75' were cracked to allow for Rectangular beam behavior in the girders, plus the cracked properties from Iteration 2.

The floor slab at elevation 75' contains a crack along the edge of the pool wall between girders RD and RE through the entire three foot thickness (Reference 8). As a consequence, the ability of this slab to resist significant load and, also, to act as a compression flange to produce tee beam behavior in Girders RD and RE, is questionable. Based on this, and consistent with the objectives of the cracking process, the slab at elevation 75', extending from RC to RF and R5 to R7, was cracked (i.e., reduced in stiffness by a factor of 1,000). By so doing, this also determined the

portion of the applied loads which were resisted by these slabs. This was the only change made between iteration 2 and iteration 3R.

The stiffness of the slab solid elements at elevation 75' was reduced to maximize the loads in the supporting girders and determine the extent to which this floor slab was resisting mechanical load. The presence of the thru-thickness crack at the bottom surface of the slab made it essential to perform this iteration. Therefore, in iteration 3R the girders are resisting load as rectangular sections not as tee beams. The following load steps were included:

- I.S. 1 - Concrete Dead Load
- 2 - Hydrostatic + High Density Fuel Racks + Stored Cask
- 3 - Design Live Load
- 4 - Winter Temperature Condition
- 5 - Cask Drop

This iteration is referred to throughout this report as iteration 3R. The designations 3R and 3RB, which are used in the calculations (Reference 24), refer to the same iteration. This iteration formed the basis for cracking the girders in iteration 4.

Iteration 3SS - Stiffness and mass of Solid elements in the floor slab at Elevation 75' were neglected, plus the cracked properties from Iteration 2 for Seismic.

This iteration is the equivalent static seismic run used in combination with iteration 3R. Similar to iteration 3US, the stiffness of all the floor slabs is intact (uncracked) except for the solid elements at elevation 75' where the stiffness and mass were neglected to ensure rectangular beam behavior in the girders. The same seismic acceleration directions and load steps were used, as in iteration 3US.

Iteration 4 - Girders RE, RD and R6 cracked, plus the cracked properties from iteration 3R.

Based on the results of iteration 3R girders RD, RE and R6 were cracked and load was redistributed to other parts of the structure. Iteration 4 is identical to iteration 3R except for the revised (cracked) elastic moduli for girders RD, RE and R6. This iteration included the load steps shown below:

ABB Impell Corporation

- L.S. 1 - Concrete Dead Load
- 2 - Hydrostatic + High Density Fuel Racks + Stored Cask
- 3 - Design Live Load
- 4 - Winter Temperature Condition
- 5 - Cask Drop

Iteration 4SS - Same as iteration 3SS with girders RE, RD and R6 cracked as in iteration 4.

This iteration is the equivalent static seismic run to be used in combination with iteration 4. Similar to iteration 3SS, the stiffness of all the floors is intact except the solid elements at elevation 75' for which the stiffness and mass were neglected to ensure rectangular beam behavior of the girders. The same seismic acceleration directions and load steps were used as in iteration 3SS.

Iteration 5 - Shield wall stiffness above Elevation 80' neglected plus the cracked properties in iteration 4.

This iteration was done to assess the reliance of the SFP structure on the shield wall for support. The stiffness of the shield-wall from elevation 79'-10" to elevation 119'-3" and from column line R4 to where the shield wall intersects the south wall of the pool was reduced by a factor of one thousand. The stiffness of all other member is the same as iteration 4. The load steps included were:

- L.S. 1 - Concrete Dead Load
- 2 - Hydrostatic + High Density Fuel Racks + Stored Cask
- 3 - Design Live Load
- 4 - Winter Temperature Condition
- 5 - Cask Drop

Iteration 5S - Same as Seismic Iteration 4SS plus the crack properties from iteration 5.

This iteration is the equivalent static seismic run to be used in combination with iteration 5. Similar to iteration 4SS, the stiffness of all the floors is intact except the solid elements at elevation 75' where the stiffness and mass were neglected to ensure rectangular beam behavior in the girders. In addition, the shield wall was "disconnected" to be consistent with iteration

5. The same seismic acceleration directions and load steps were used as in iteration 4SS.

Iterations Using the Fully Transformed Cracking Criteria for Case C

The following iterations were performed using the fully transformed cracking criteria. This criteria is described in Section 2.3.2 and the methodology in Section 4.2.3.2. The summer temperature condition was included in the analysis because it effects the negative moment regions in the SFP east, west, and north walls and pool slab. The cracked properties of the walls and pool slab based on the fully transformed cracking criteria were added to iteration 4 to form iterations 4S and 4W.

Iteration 4W - SFP Walls have cracked properties based on the fully transformed cracking criteria plus the cracked properties from iteration 4.

Cracked properties for the SFP walls based on the fully transformed cracking criteria were used together with the cracked properties from iteration 4.

The load steps included in the analysis were:

- L.S. 1 - Concrete Dead Load
- 2 - Hydrostatic + High Density Fuel Racks + Stored Cask
- 3 - Design Live Load
- 4 - Winter Temperature Condition
- 5 - Cask Drop
- 6 - Summer Temperature Condition

Iteration 4WSS - Cracked properties for SFP Walls based on the fully transformed cracking criteria plus the cracked properties from iteration 4SS

This iteration is the seismic run used in combination with iteration 4W. The stiffness of all the floors is intact except the solid elements at elevation 75' for which the stiffness and mass were neglected to ensure rectangular beam behavior in the girders. The following seismic acceleration directions and load steps were used:

ABB Impell Corporation

- L.S. 1: Seismic -X and Hydrodynamic
- 2: Seismic +Y and Hydrodynamic
- 3: Seismic +Z and Hydrodynamic

Iteration 4S - Cracked transformed properties for the SFP Slab based on the fully transformed cracking criteria plus the cracked properties from iteration 4W.

In addition to the changes incorporated in iteration 4W, the cracked properties of the SFP slab based on the fully transformed cracking criteria were added. The same load steps of iteration 4W were used in this iteration.

Iteration 4SSS - Cracked transformed properties for the SFP Slab based on the fully transformed cracking criteria plus the cracked properties from iteration 4WSS.

This iteration is the seismic run to be used in combination with iteration 4S. The stiffness of all the floors is intact except the solid elements at elevation 75' for which the stiffness and mass were neglected to ensure rectangular beam behavior in the girders. The same load steps of iteration 4WSS were used in this iteration.

4.3.3 Description of Cracking Iterations for Analysis Case D

The cracking of the shield wall and SFP walls and slab, which resulted in the cracked properties for iteration 2 of Analysis Case C, was dominated by the winter temperature condition. It was therefore concluded that for Analysis Case D the addition of consolidated racks and fuel to the SFP slab would not appreciably change the cracking patterns or the level of cracking, as measured by the effective concrete moduli, used in iteration 2 (see Section 4.3.1). Hence, iterations 0 and 1 were not performed for Case D and the cracked properties from iteration 2 of Analysis Case C were used for iteration 2 of Analysis Case D.

Iteration 2 - Shield wall, SFP walls and SFP slab cracked, plus the cracked properties from iteration 1.

Element stiffnesses are based on cracked concrete properties developed from the iteration 1 results of Case C. The analysis of the SFP structure was performed for the same load steps as iteration 1:

- L.S. 1 - Concrete Dead Load
- 2 - Hydrostatic + Consolidated Fuel Racks + Stored Cask
- 3 - Design Live Load
- 4 - Winter Temperature Condition
- 5 - Cask Drop

In this iteration, the portion of the slab at elevation 75' consisting of solid elements is uncracked and is the only portion of the floor systems at elevations 75', 95' and 119' to carry load from the SFP structure.

Iteration 3SU - SFP Slab Uncoupled plus the cracked properties from iteration 2.

Under the action of mechanical load the SFP slab develops positive moment in the middle region and negative moment along the supporting edges. The SFP slab is designed for such behavior. Under the winter thermal gradient, however, the bottom of the SFP slab develops a constant positive moment which could overcome the negative moment along the supporting edges. Since the SFP slab has a lack of positive moment rebar embedment along these supporting edges which may not be able to resist a significant positive moment, the degrees of freedom in the direction of the rebar (perpendicular to the potential crack) were uncoupled along the bottom surface of the pool slab at the supporting edges (see Section 2.2.3.4). This iteration has the same element stiffness properties for the SFP model and the same load steps as iteration 2.

Iteration 3US - SFP Uncoupled for Seismic in addition to cracked properties from iteration 2.

This iteration was the equivalent static seismic run used in combination with iteration 3SU. However the stiffness deviates slightly from iteration 3US since, in a seismic event, the floor slabs are designed to transfer the horizontal inertia loads to the exterior walls and couple the response of the shield wall and SFP with the exterior walls. Hence, the stiffness of all the floor slabs, including the solid elements at elevation 75', were intact

ABB Impell Corporation

(uncracked). The following directions of seismic acceleration were applied to the model:

- L.S. 1 - Seismic -X and Hydrodynamic
- 2 - Seismic +Y and Hydrodynamic
- 3 - Seismic +Z and Hydrodynamic

The various seismic directions were summed algebraically. Based on a review of Case C the following combinations were considered (see Case C iteration 3US and Section 4.3.1):

- L.S. 1 - X + Y + Z
- 2 - X - Y + Z

Iteration 3U designates the combination of iterations 3SU and 3US to form load combinations for evaluation.

Iteration 3R - Solid elements in the floor slab at Elevation 75' were cracked to allow for Rectangular beam behavior in the girders, plus the cracked properties from Iteration 2.

The floor slab at elevation 75' contains a crack along the edge of the pool wall between girders RD and RE through the entire three foot thickness (Reference 8). As a consequence, the ability of this slab to resist significant load and, also, to act as a compression flange to produce tee beam behavior in Girders RD and RE, is questionable. Based on this, and consistent with the objectives of the cracking process, the slab at elevation 75', extending from RC to RF and R5 to R7, was cracked (i.e., reduced in stiffness by a factor of 1,000). By so doing, this also determined what portion of the applied loads were resisted by these slabs. This was the only change made between iteration 2 and iteration 3R.

The stiffness of the slab solid elements at elevation 75' was reduced to maximize the loads in the supporting girders and determine the extent to which this floor slab was resisting mechanical load. The presence of the thru-thickness crack at the bottom surface of the slab made it essential to perform this iteration. Therefore in iteration 3R the girders are resisting load as rectangular sections not as tee beams. The following load steps were included:

- L.S. 1 - Concrete Dead Load
- 2 - Hydrostatic + Consolidated Fuel Racks + Stored Cask

ABB Impell Corporation

- 3 - Design Live Load
- 4 - Winter Temperature Condition
- 5 - Cask Drop

This iteration formed the basis for cracking the girders in iteration 4.

Iteration 3SS - Stiffness and mass of Solid elements in the floor slab at Elevation 75' were neglected, plus the cracked properties from iteration 2 for Seismic.

This iteration is the equivalent static seismic run used in combination with iteration 3R. Similar to iteration 3US, the stiffness of all the floor slabs is intact (uncracked) except for the solid elements at elevation 75' where the stiffness and mass were neglected to ensure rectangular beam behavior in the girders. The same seismic acceleration directions and load steps were used as in iteration 3US.

Iteration 4 - Girders RE, RD and R6 cracked, plus the cracked properties from iteration 3RB.

Based on the results of iteration 3R girders RD, RE and R6 were cracked and load was redistributed to other parts of the structure. Iteration 4 is identical to iteration 3R except for the revised (cracked) elastic moduli for girders RD, RE and R6. This iteration included the load steps shown below:

- L.S. 1 - Concrete Dead Load
- 2 - Hydrostatic + Consolidated Fuel Racks + Stored Cask
- 3 - Design Live Load
- 4 - Winter Temperature Condition
- 5 - Cask Drop

Iteration 4SS - Same as iteration 3SS with girders RE, RD and R6 cracked as in iteration 4.

This iteration is the equivalent static seismic run to be used in combination with iteration 4. Similar to iteration 3SS, the stiffness of all the floors is intact except the solid elements at elevation 75' for which the stiffness and mass were neglected to ensure rectangular beam behavior of the girders. The same seismic acceleration directions and load steps were used as in iteration 3SS.

Iterations Using the Fully Transformed Cracking Criteria for Case D

The following iterations were performed using the fully transformed cracking criteria. This criteria is described in Section 2.3.2 and the methodology in Section 4.2.3.2. The summer temperature condition was included in the analysis because it effects the negative moment regions in the SFP east, west, and north walls and pool slab. The cracked properties of the walls and slab based on the fully transformed cracking criteria were added to iteration 4 to form iteration 4S.

Iteration 4S - SFP Walls and Slab have cracked properties based on the fully transformed cracking criteria, plus the cracked properties from iteration 4.

Cracked properties for the SFP walls based on the fully transformed cracking criteria were used together with the cracked properties from iteration 4.

The load steps included in the analysis are:

- L.S. 1 - Concrete Dead Load
- 2 - Hydrostatic + Consolidated Fuel Racks + Stored Cask
- 3 - Live Design Load
- 4 - Winter Temperature Gradient
- 5 - Cask Drop
- 6 - Summer Temperature Gradient

Iteration 4SSS - Cracked properties for the SFP walls and Slab based on the fully transformed cracking criteria, plus the cracked properties from iteration 4SS.

This iteration is the seismic run used in combination with iteration 4S. The stiffness of all the floors is intact except the solid elements at elevation 75' for which the stiffness and mass were neglected to ensure rectangular beam behavior in the girders. The following seismic acceleration directions and load steps were used:

- L.S. 1 - Seismic -X and Hydrodynamic
- 2 - Seismic +Y and Hydrodynamic
- 3 - Seismic +Z and Hydrodynamic



ABB Impell Corporation

INTENTIONALLY LEFT BLANK

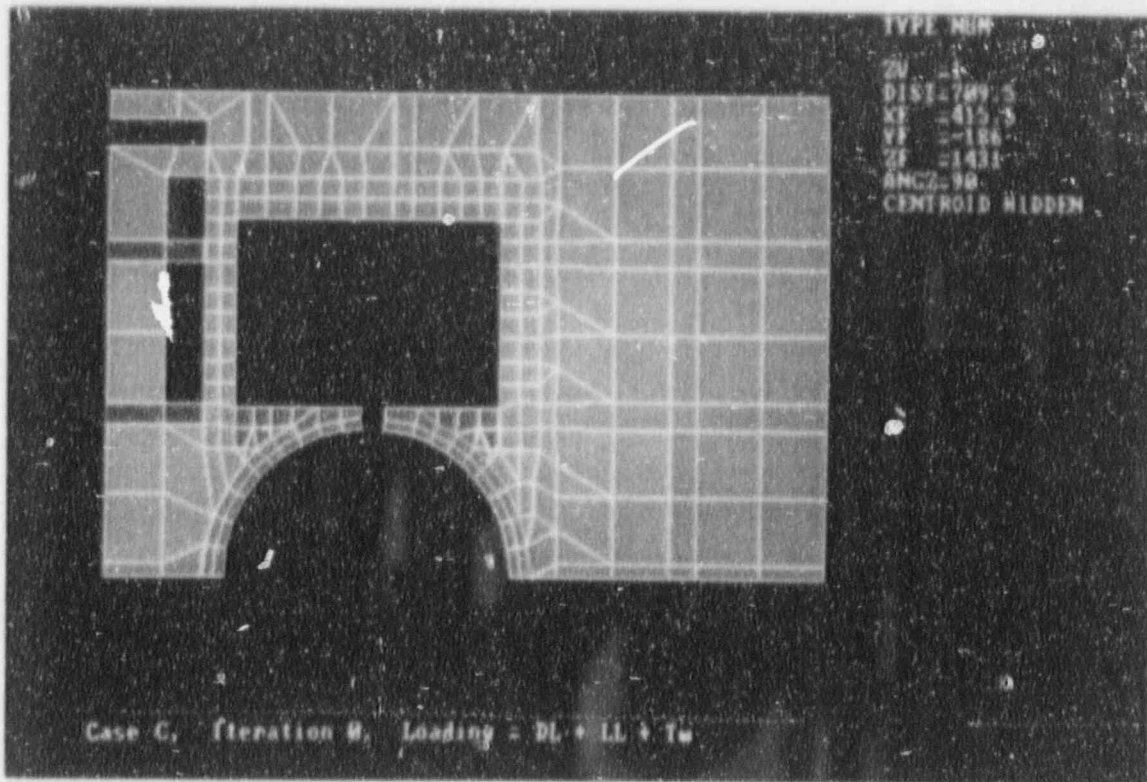


Figure 4.1

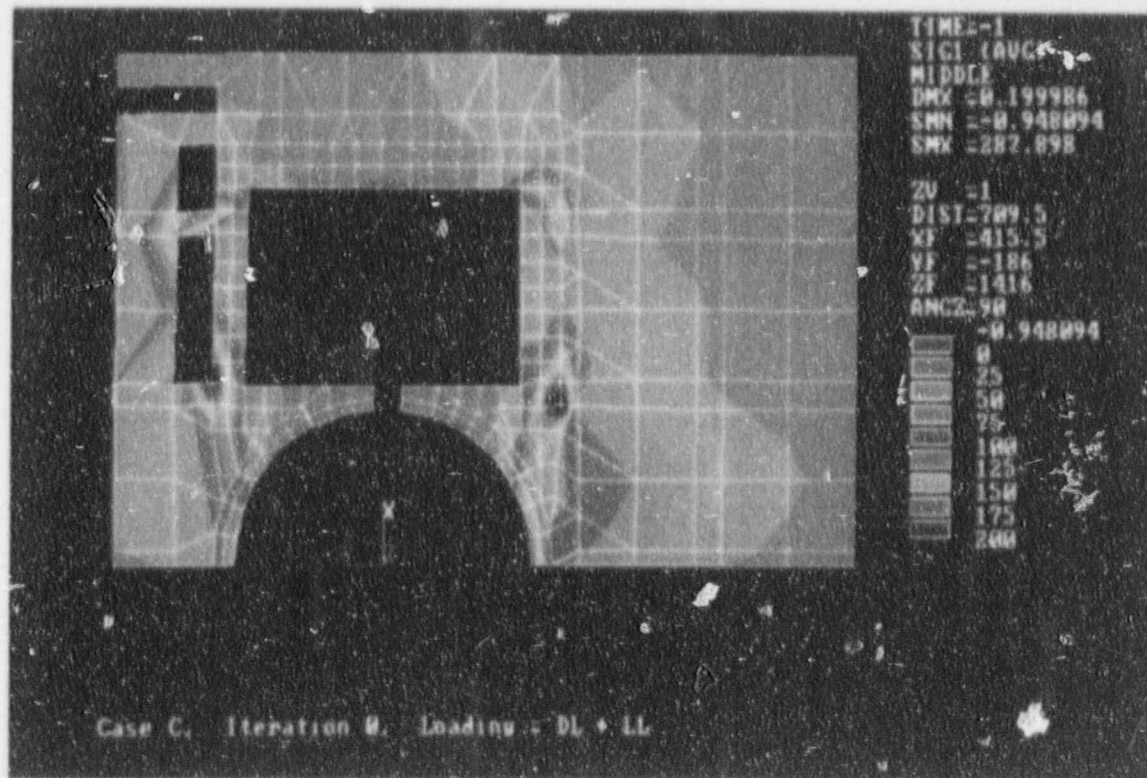


Figure 4.2

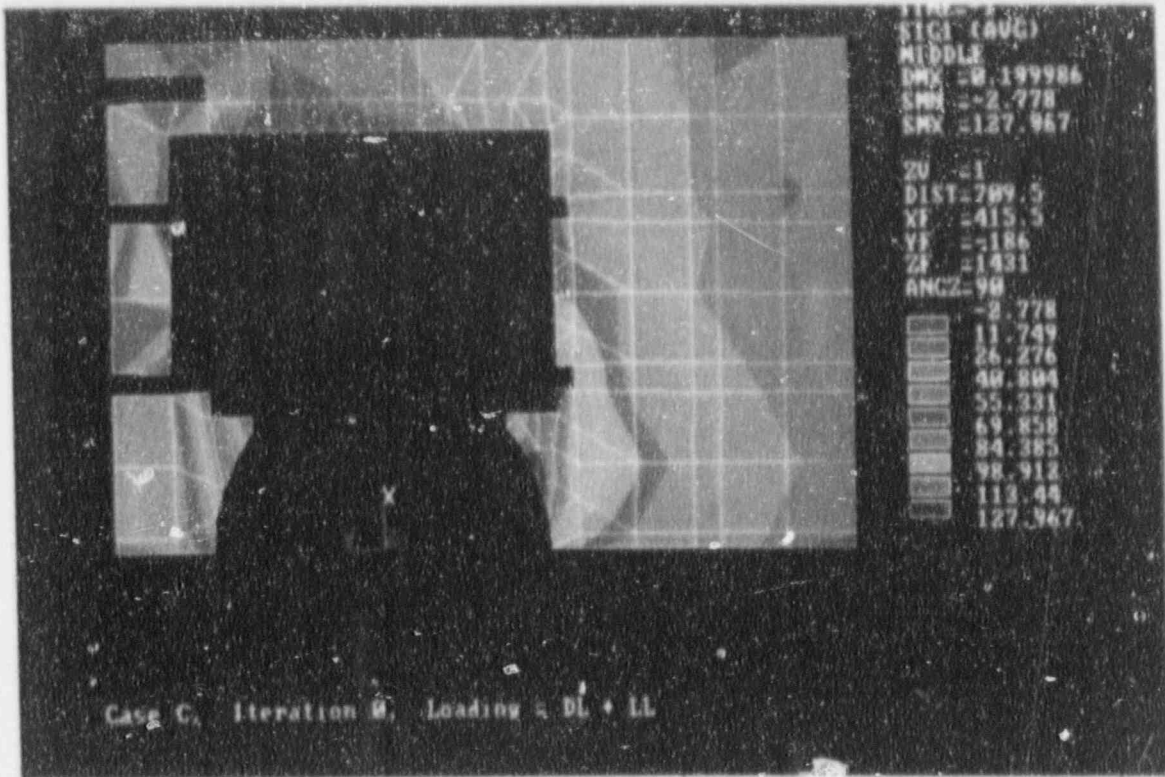


Figure 4.3

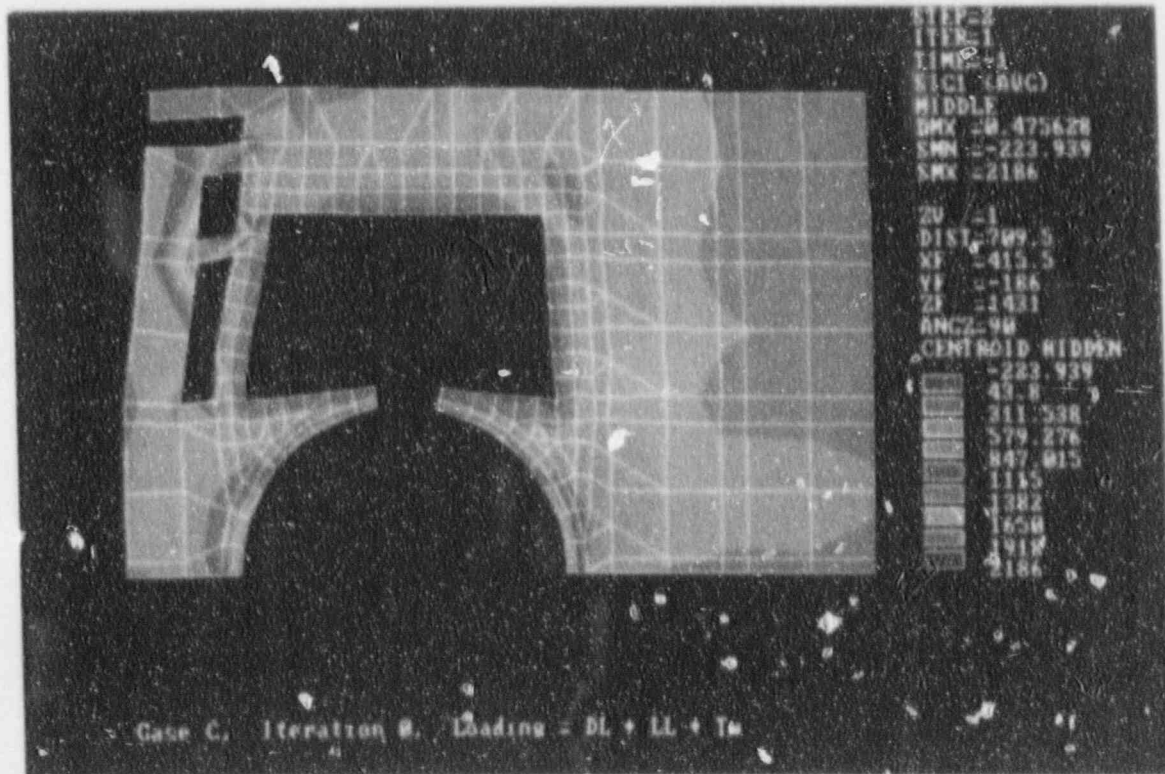


Figure 4.4

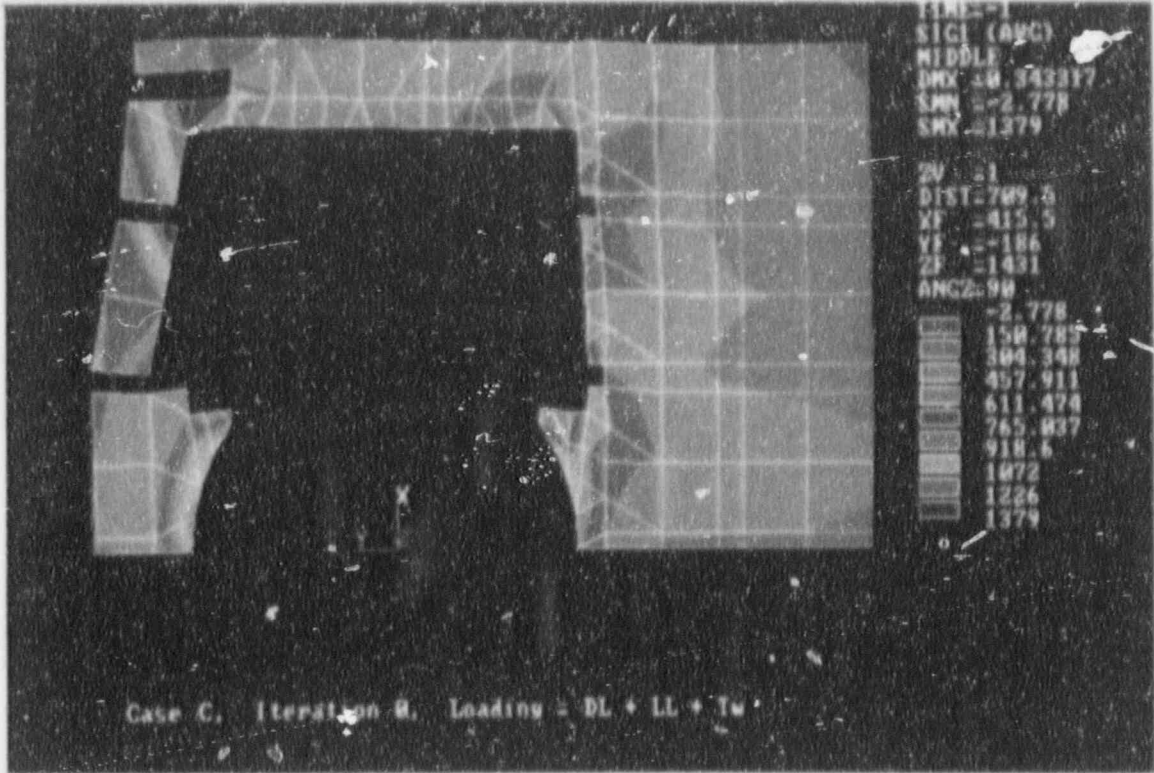


Figure 4.5

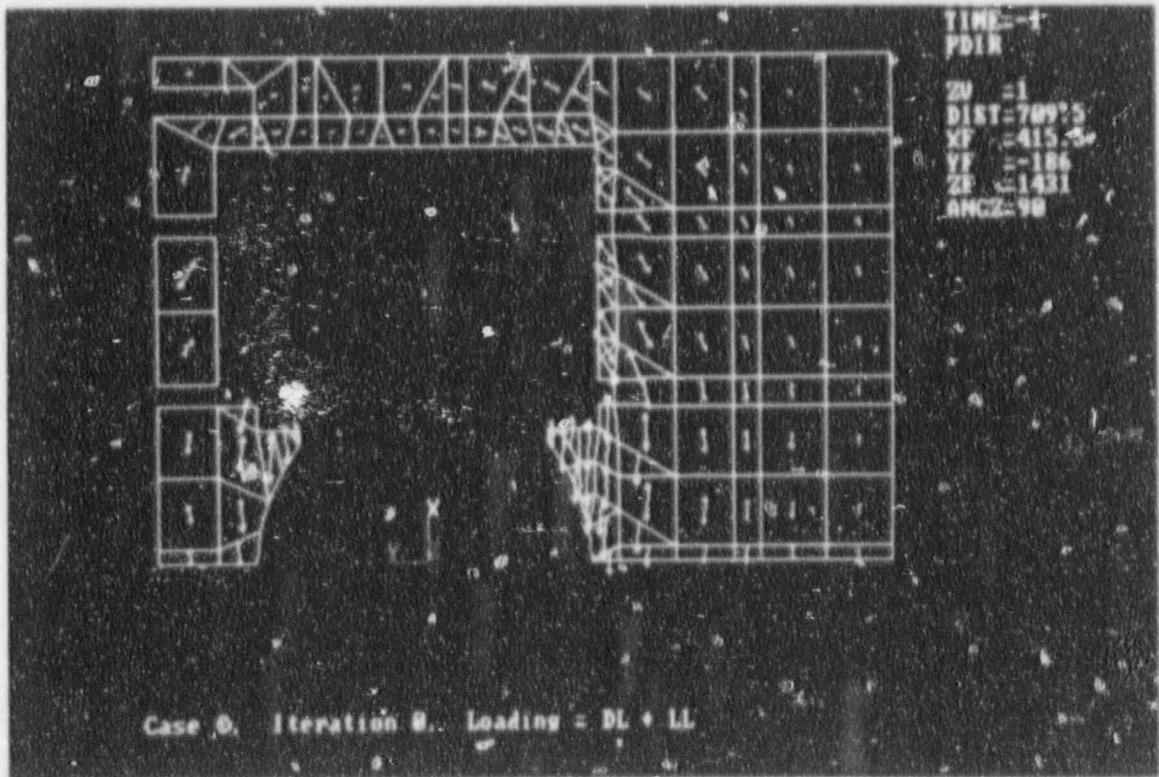


Figure 4.6

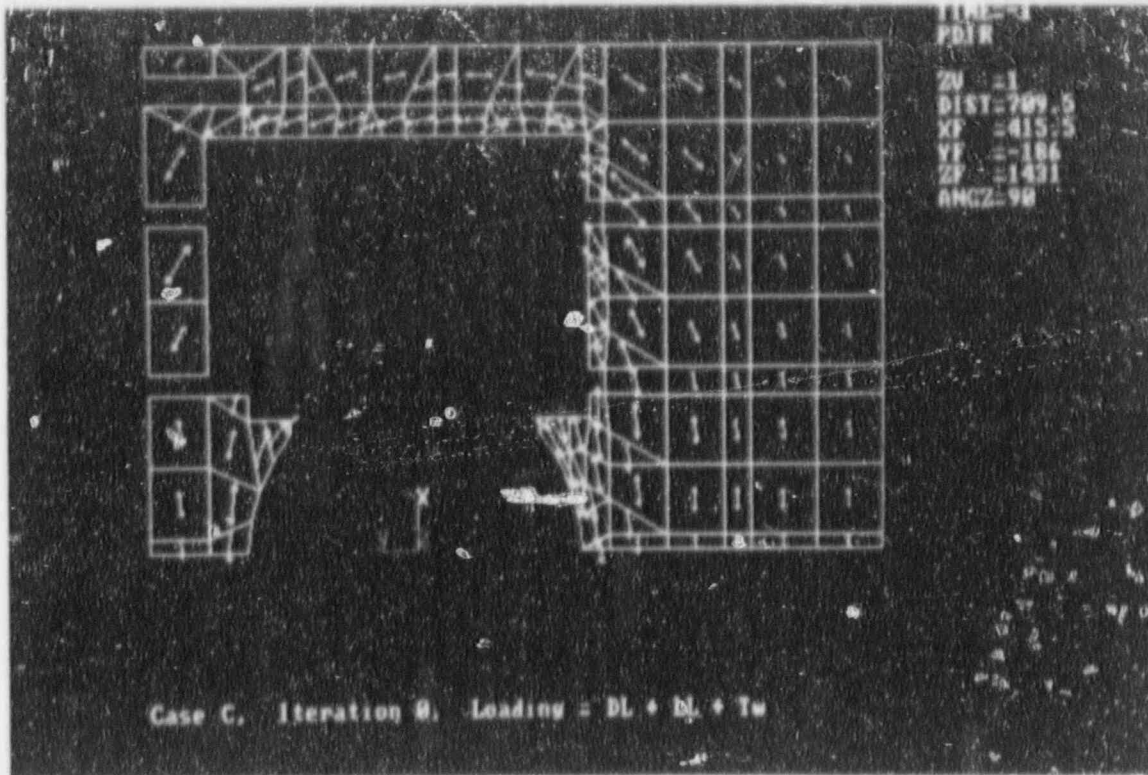


Figure 4.7

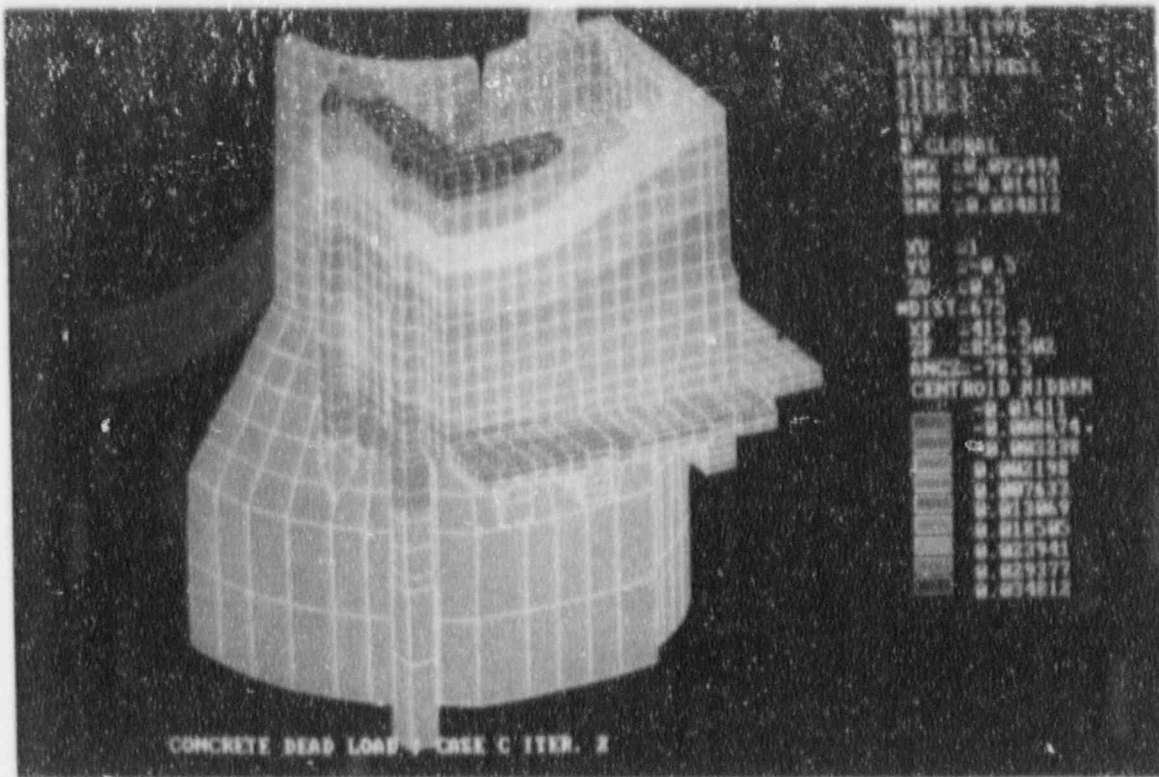


Figure 4.8

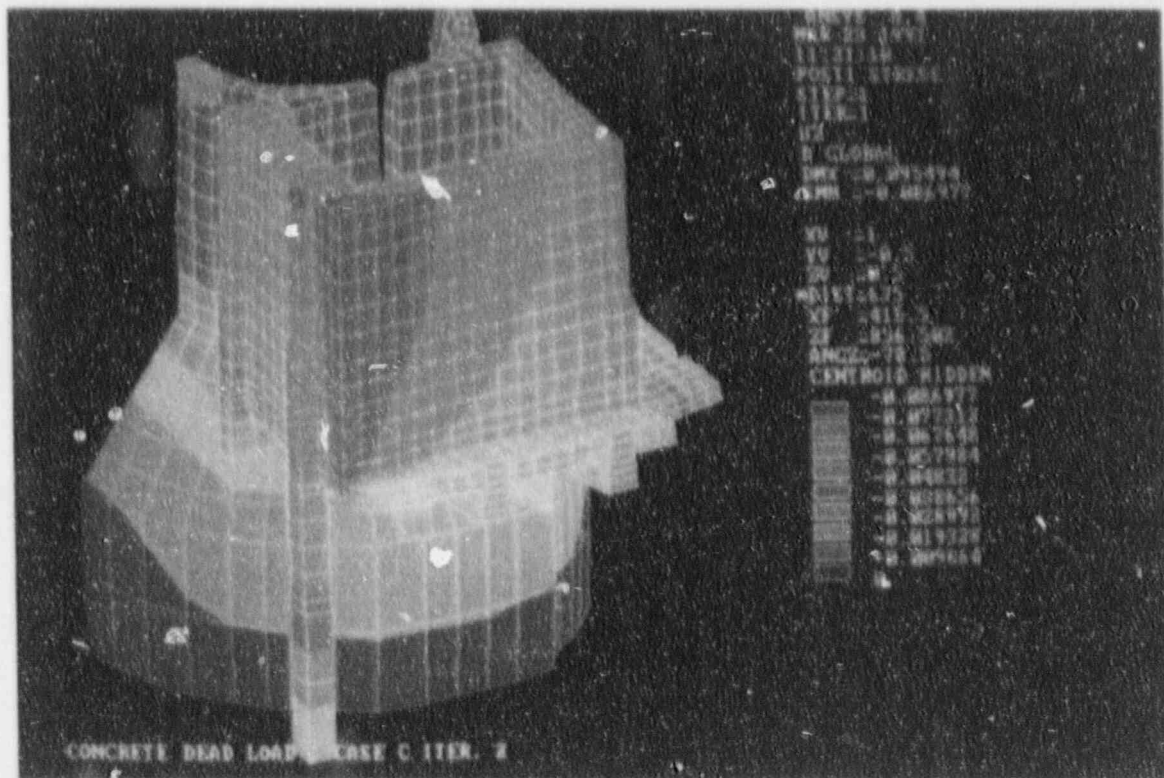


Figure 4.9

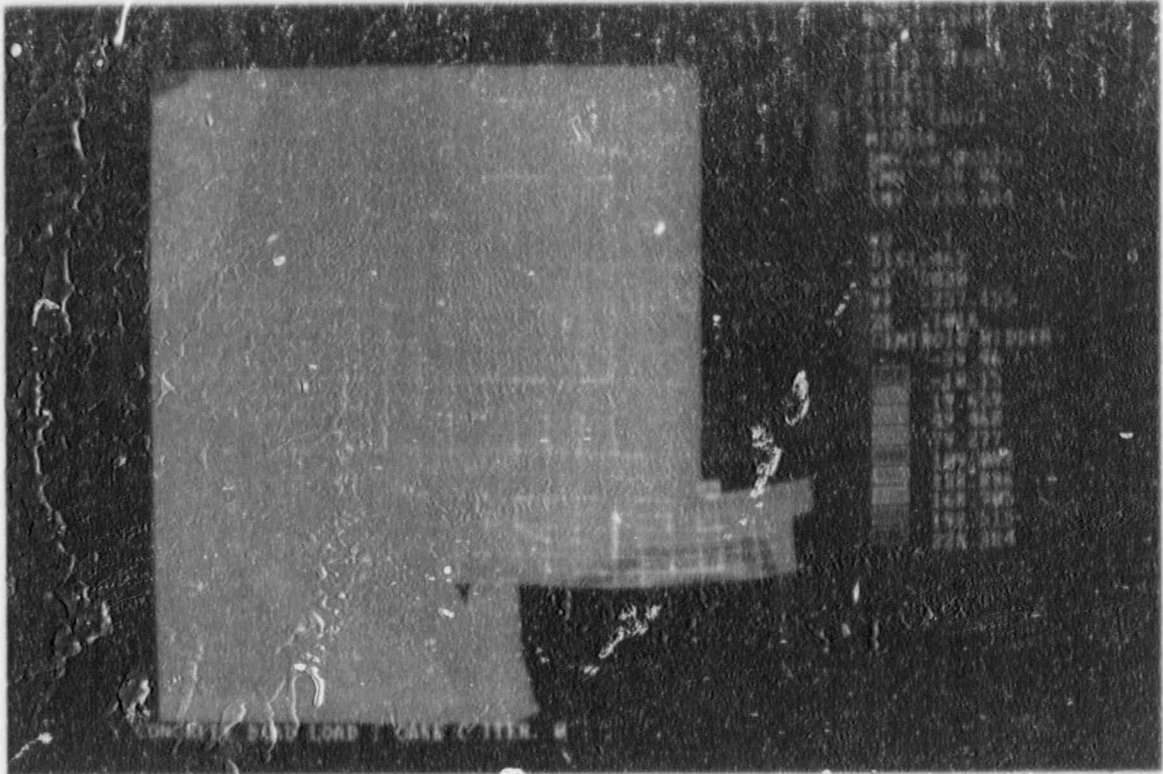


Figure 4.10

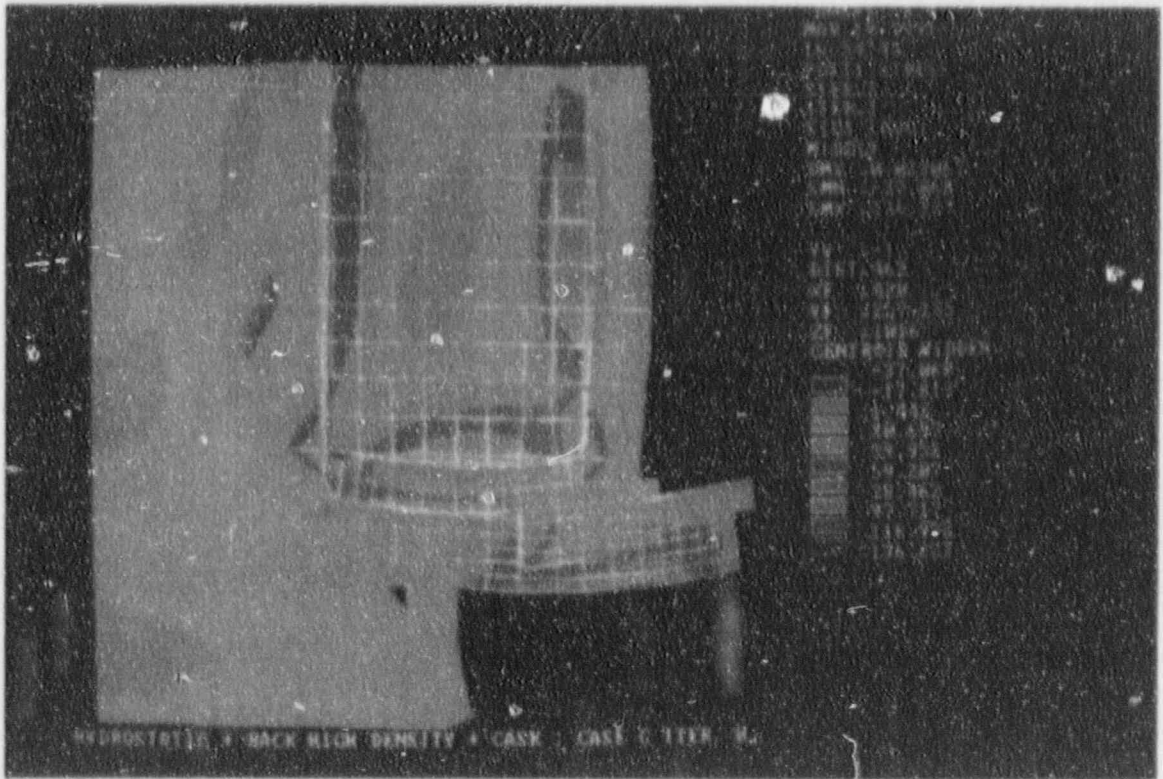


Figure 4.11

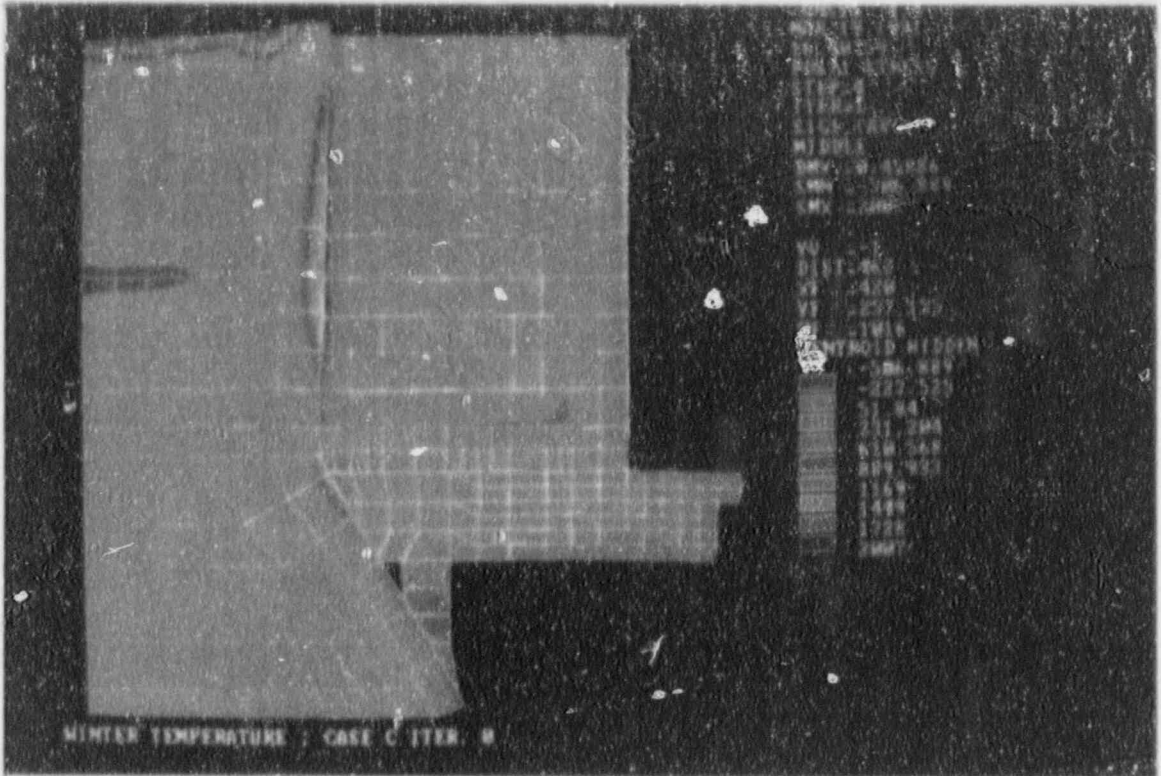


Figure 4.12

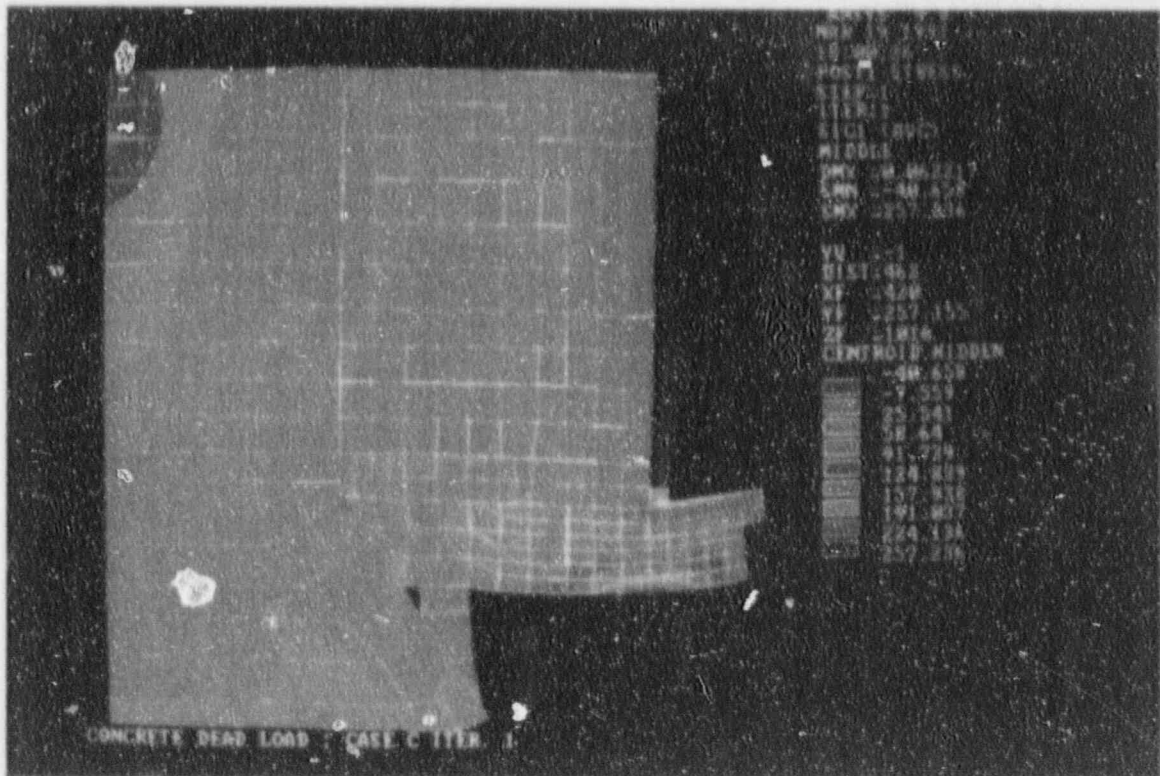


Figure 4.13

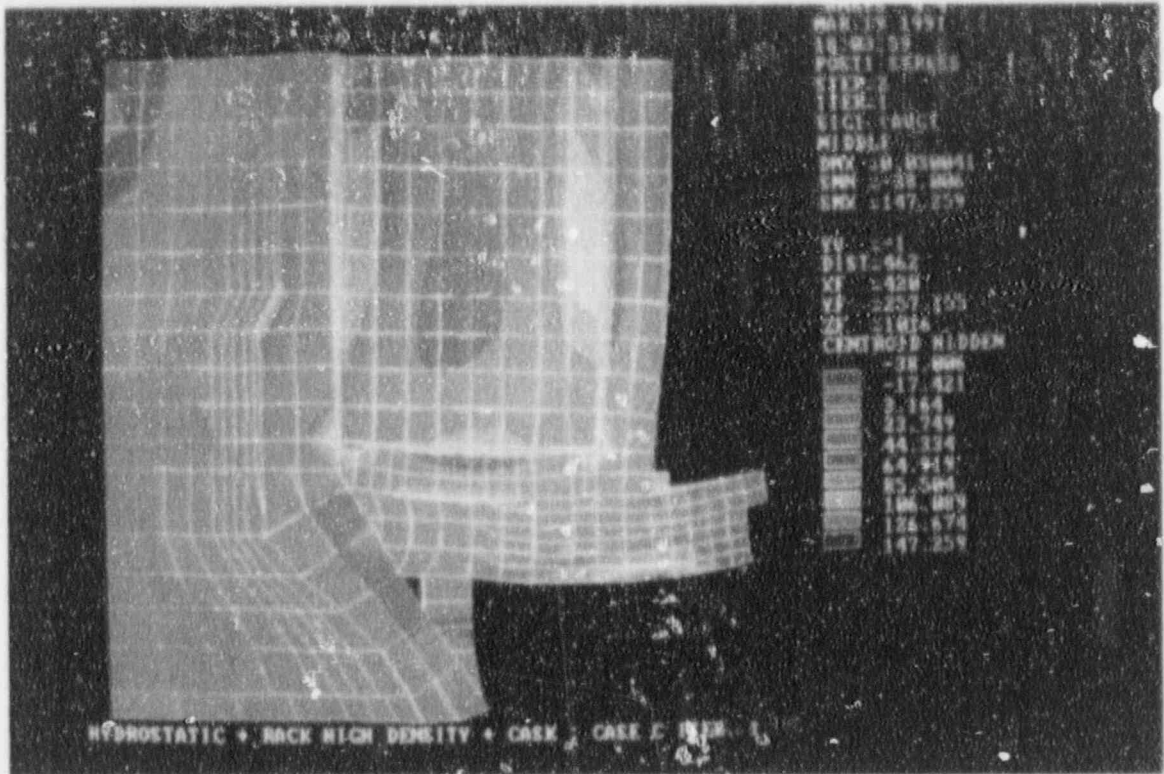


Figure 4.14

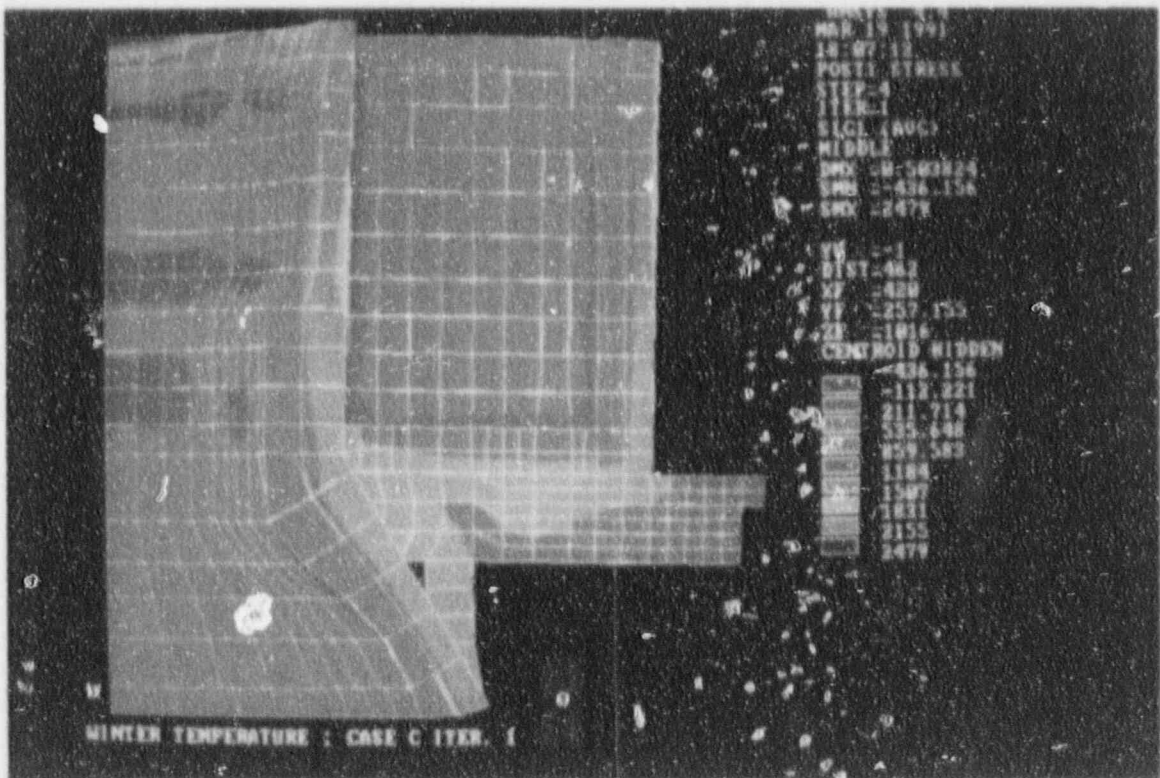


Figure 4.15

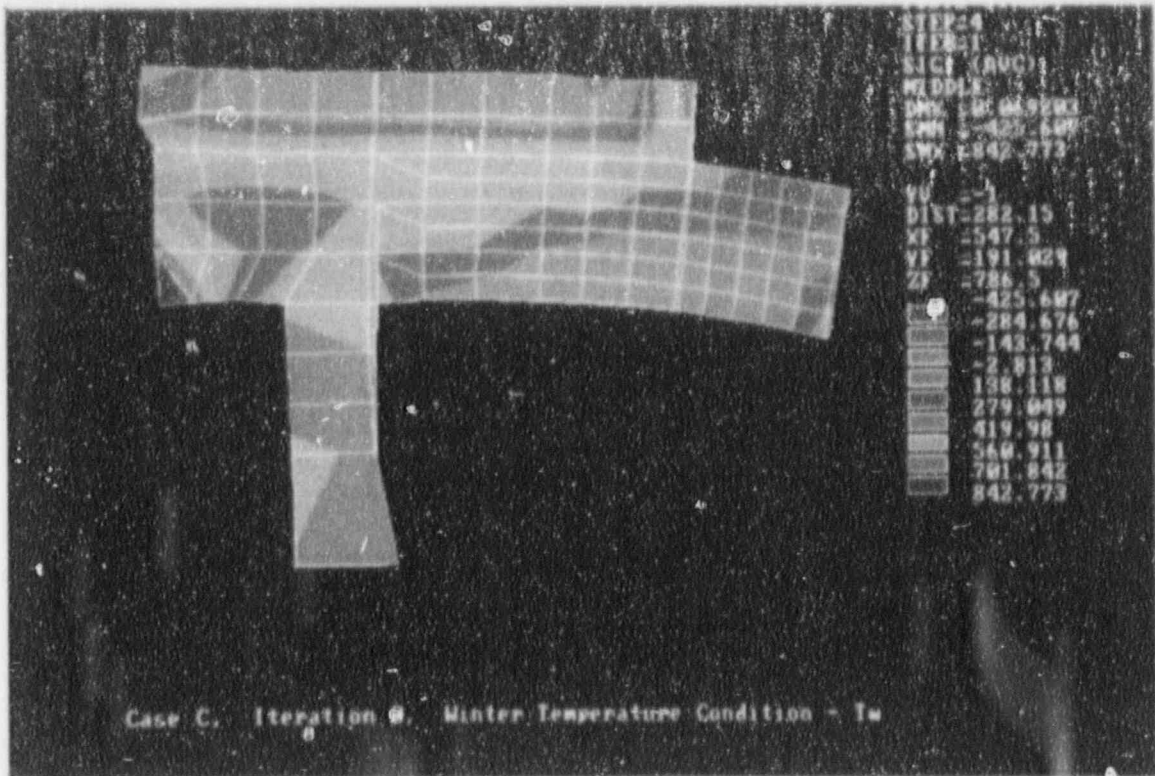


Figure 4.16

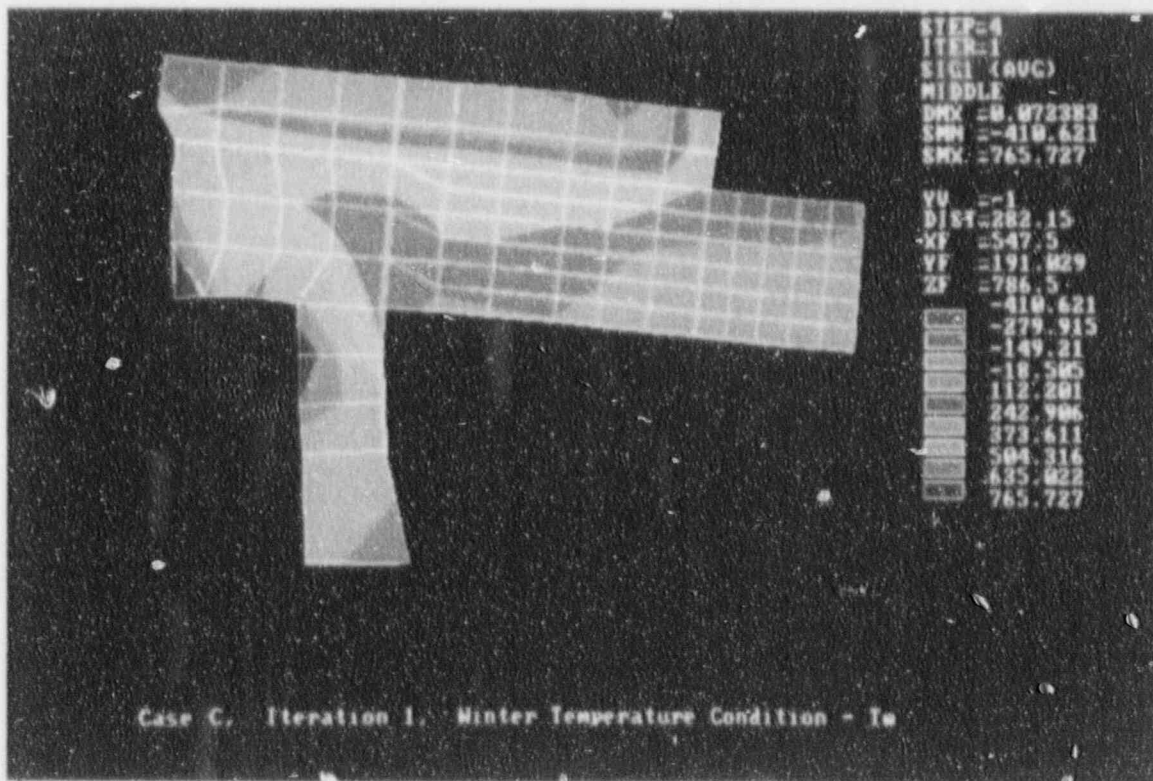


Figure 4.17

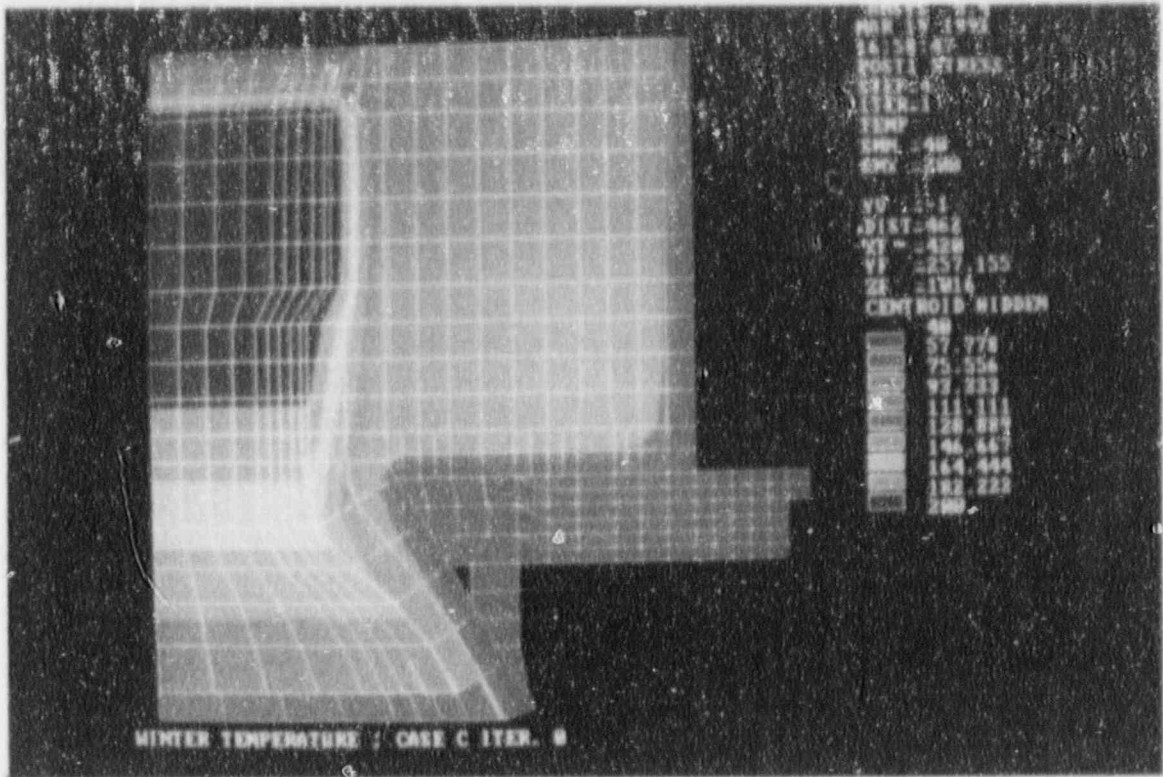


Figure 4.18

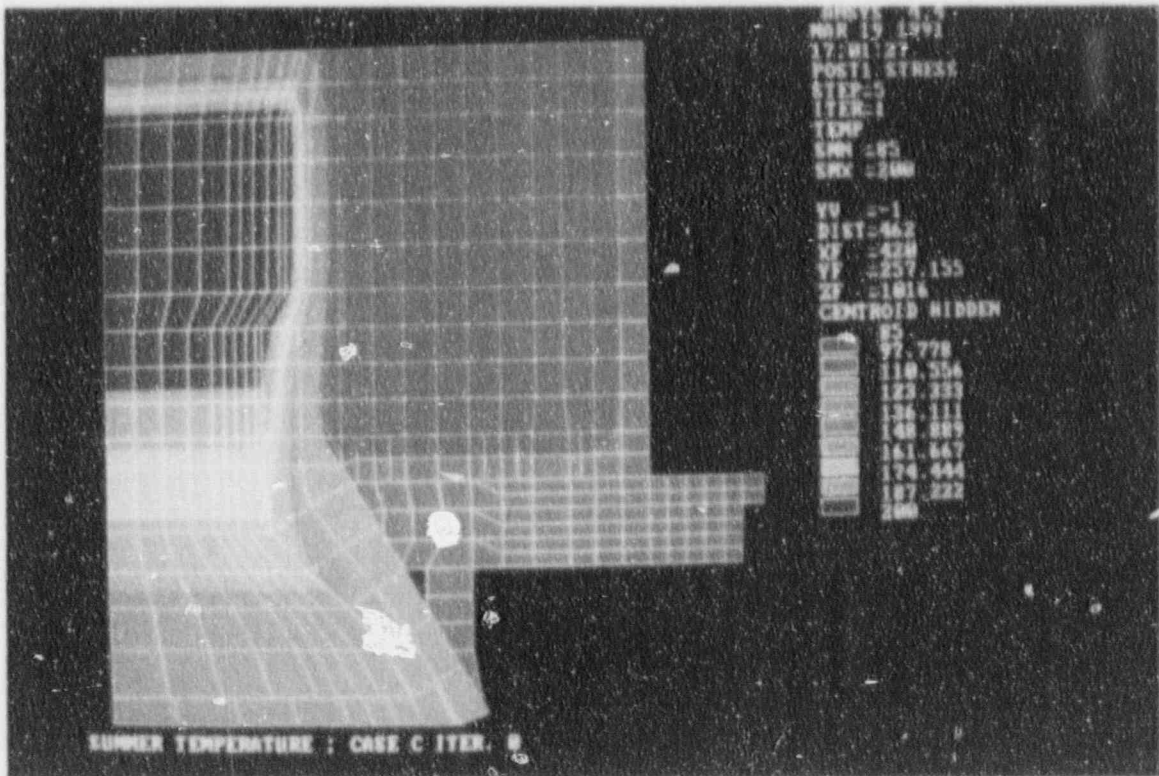


Figure 4.19

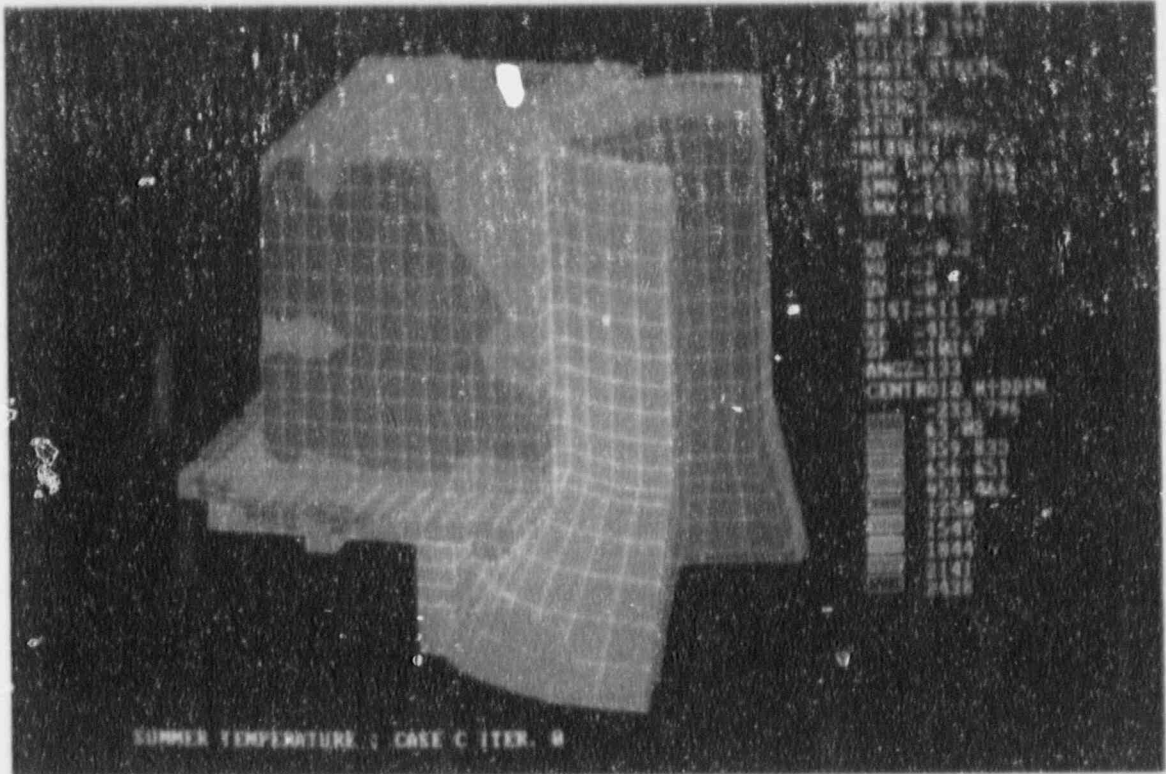


Figure 4.20

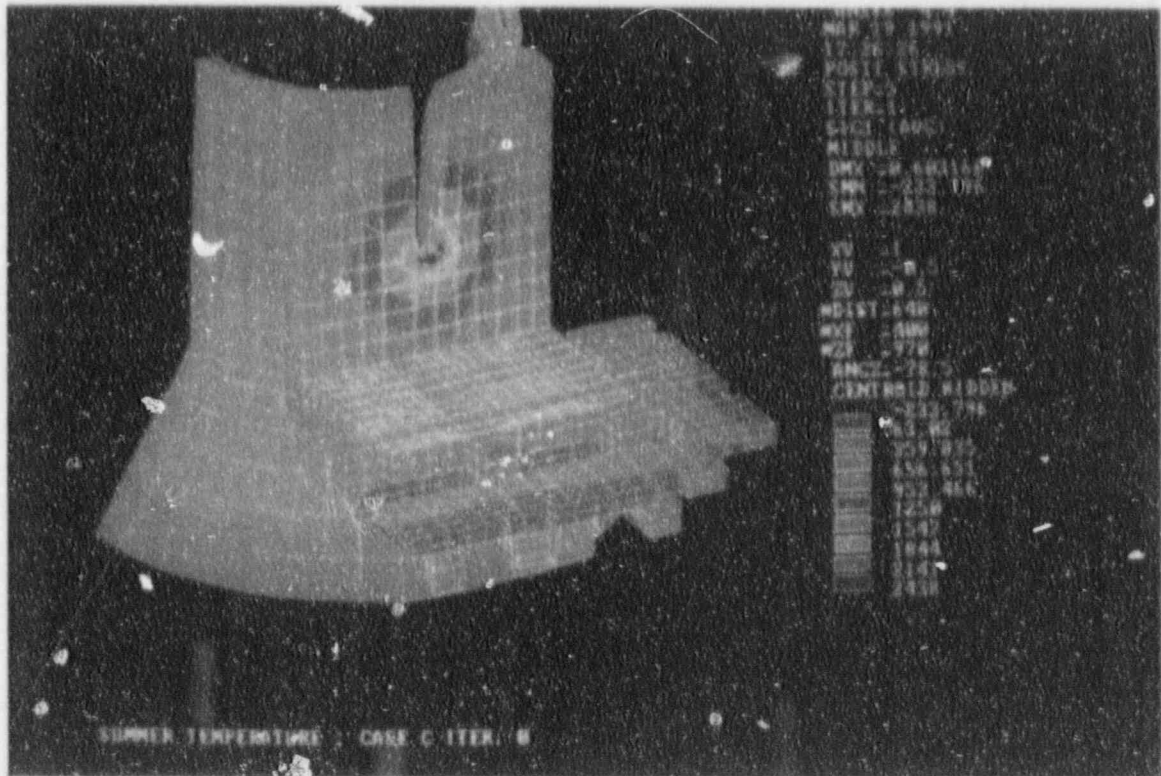


Figure 4.21

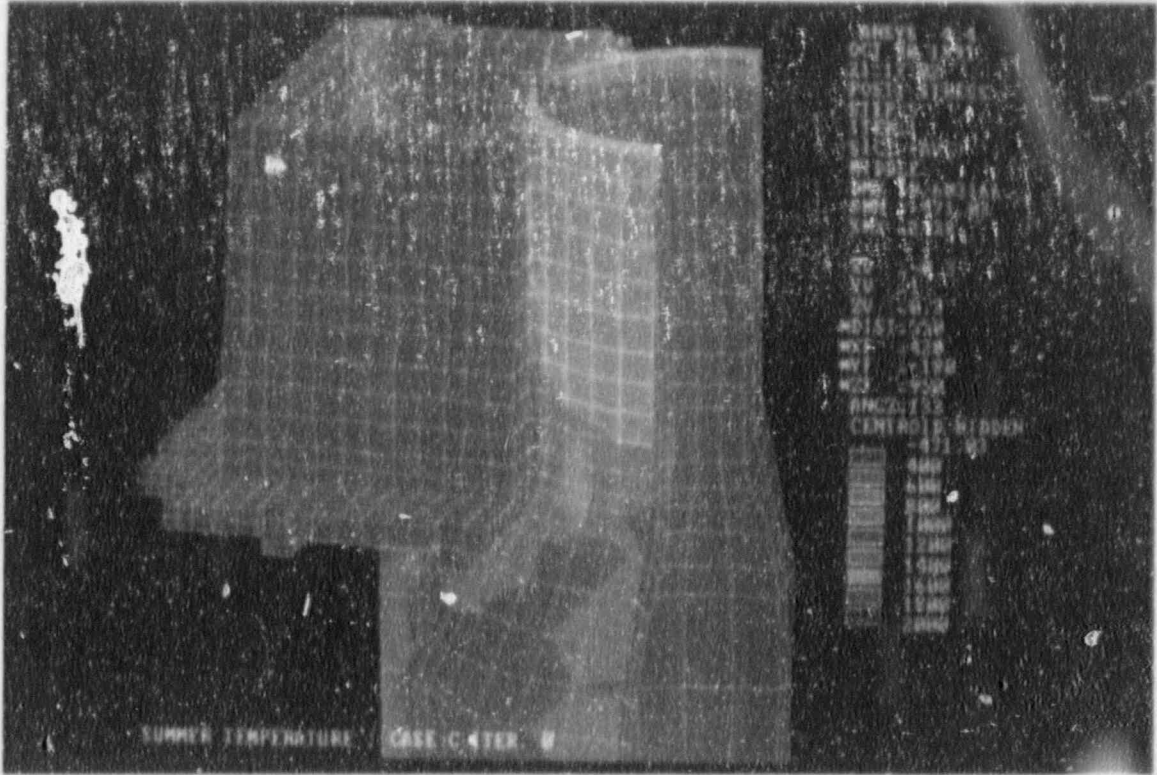


Figure 4.24

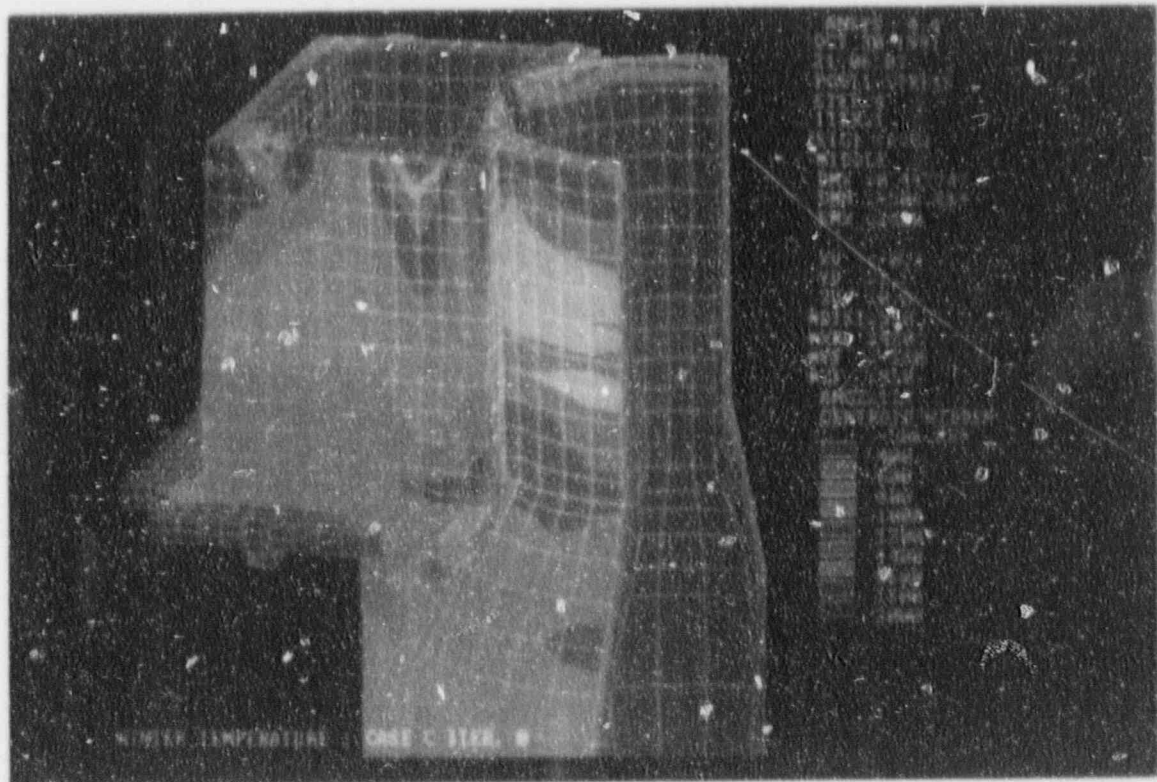


Figure 4.25

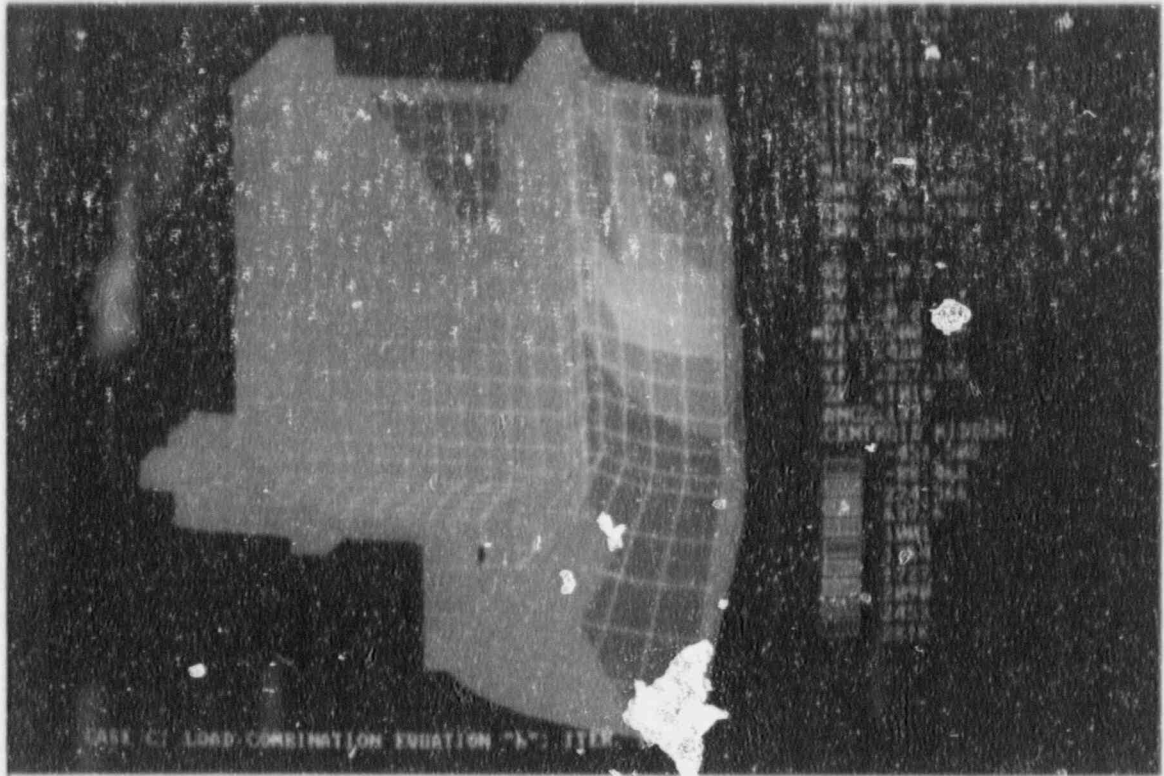


Figure 4.26

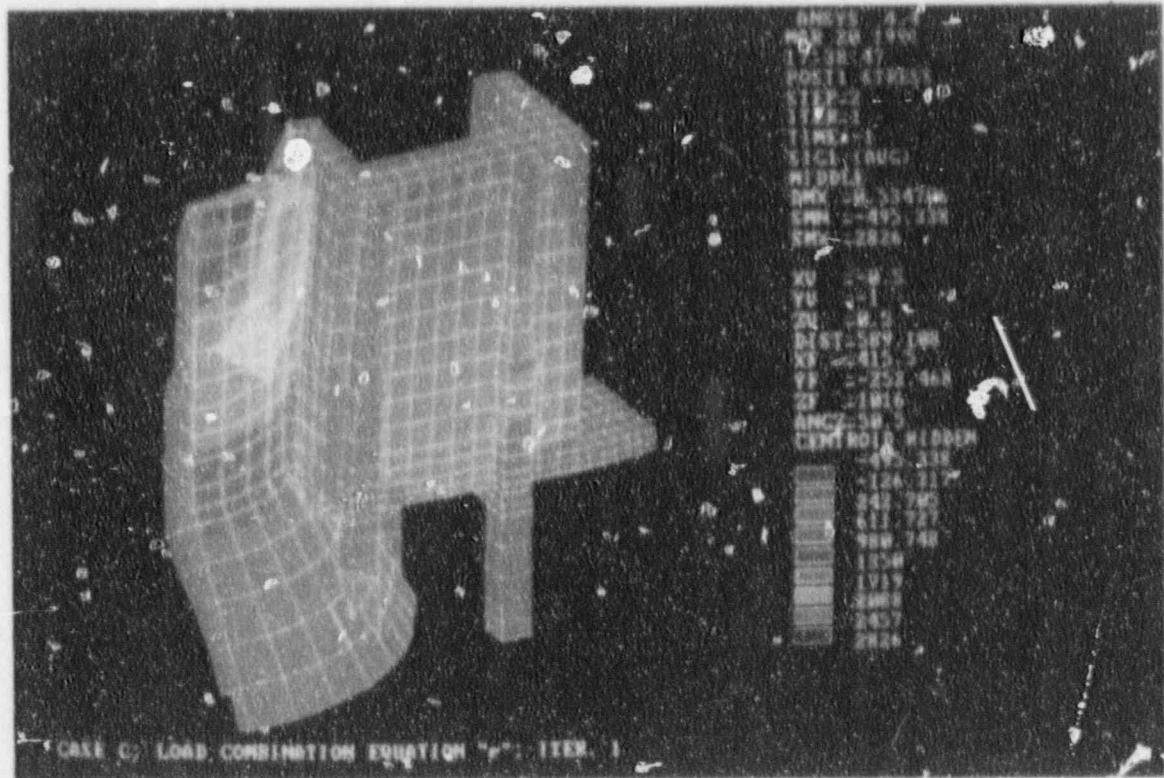


Figure 4.27

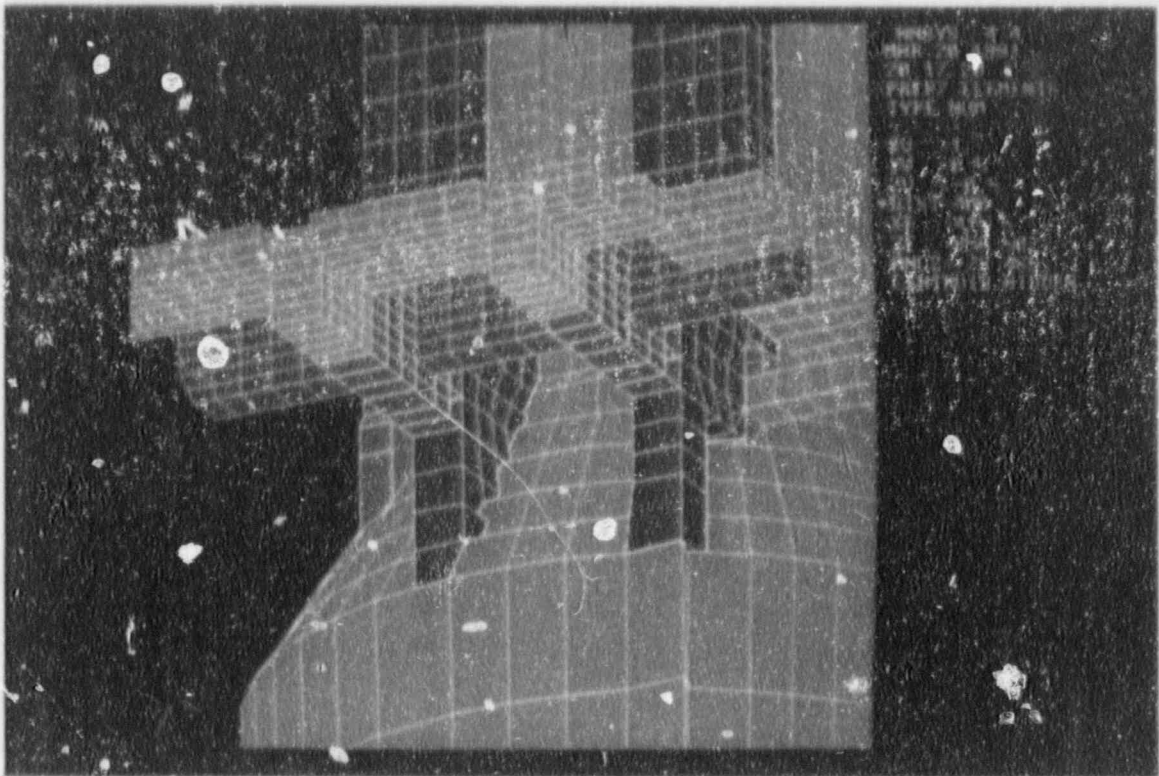


Figure 4.28

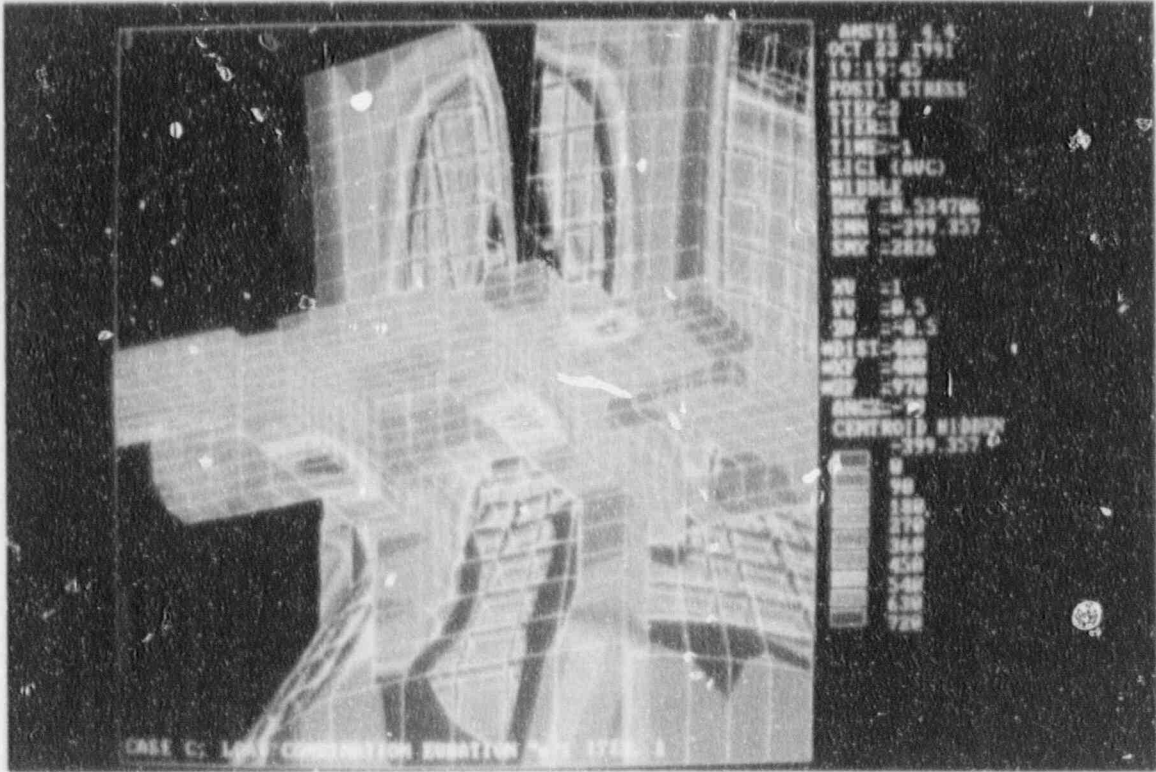


Figure 4.29

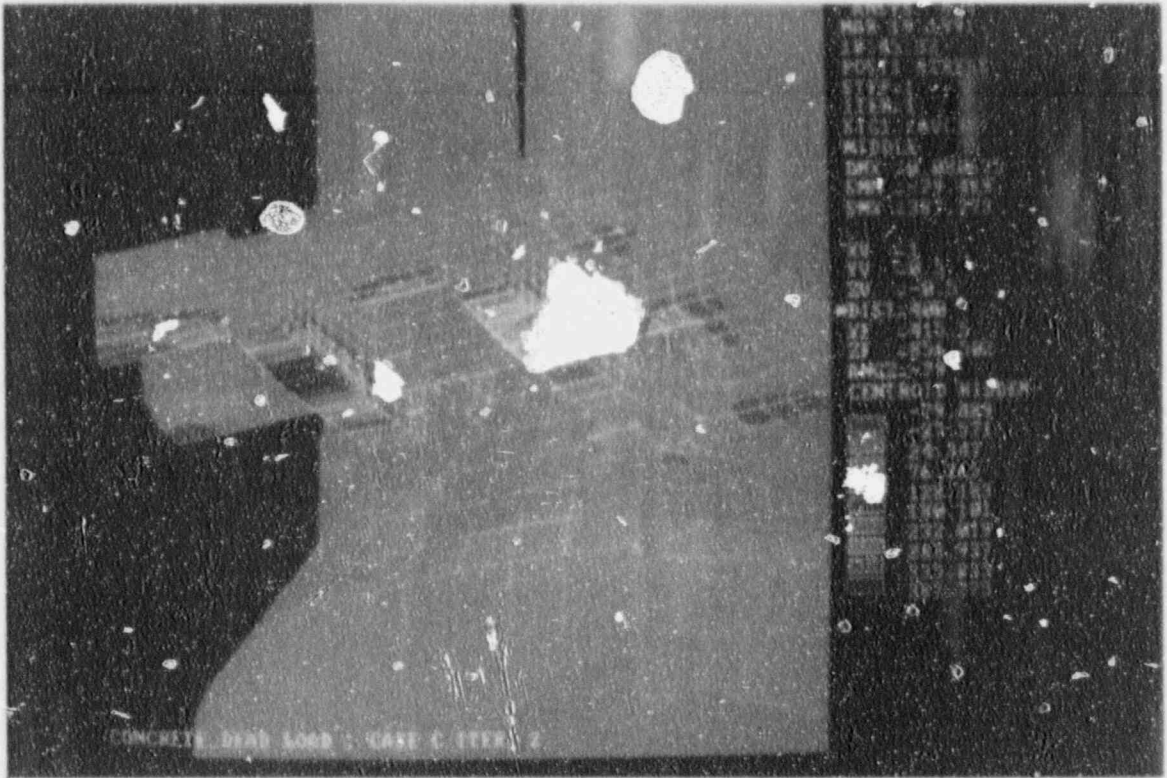


Figure 4.30

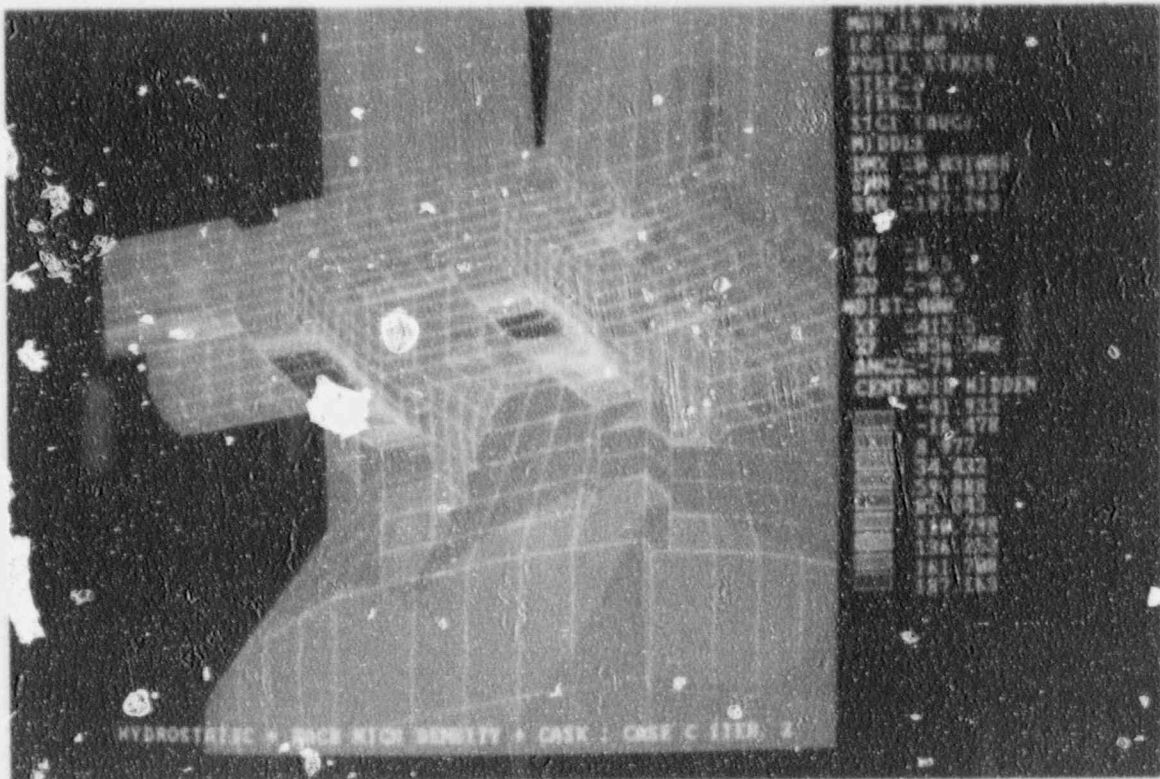


Figure 4.31

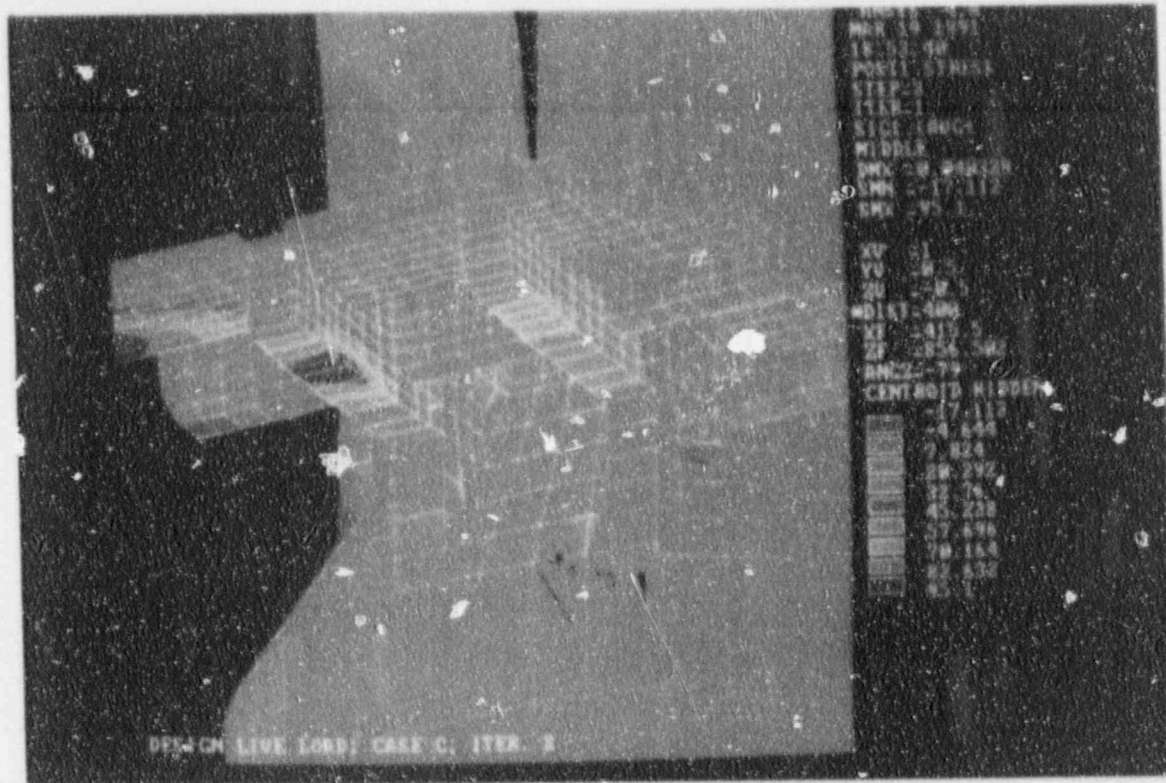


Figure 4.32

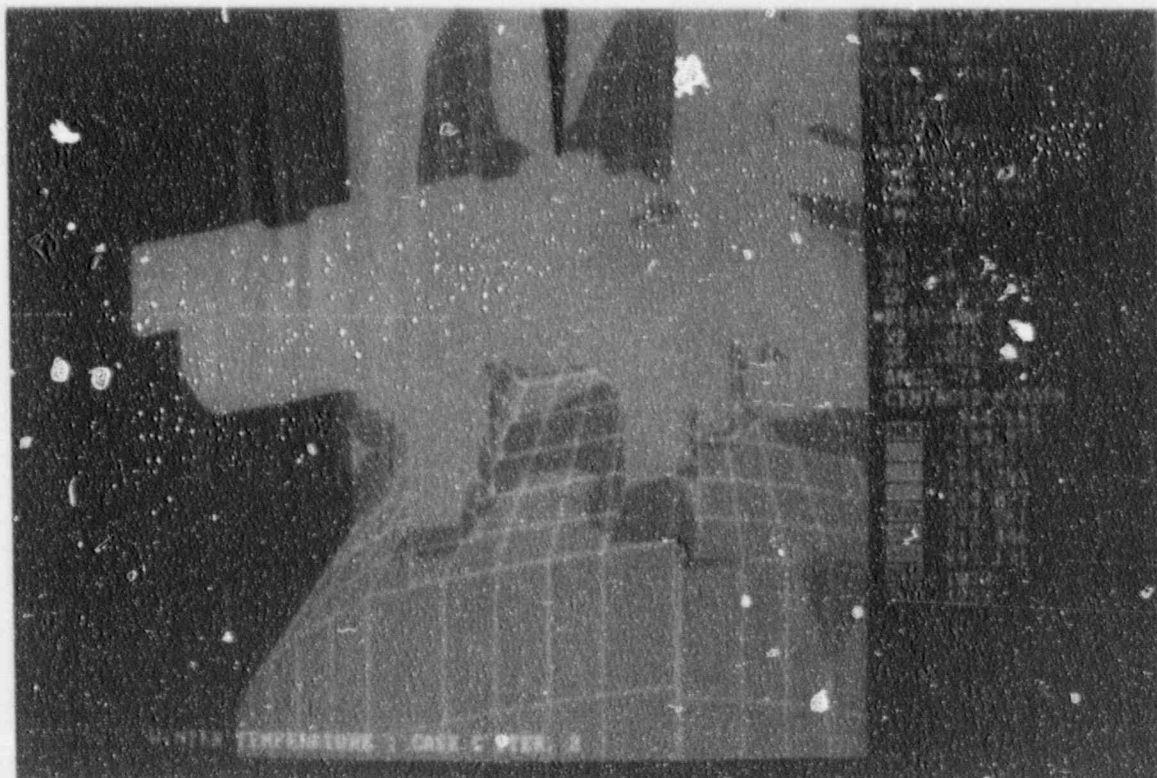


Figure 4.33

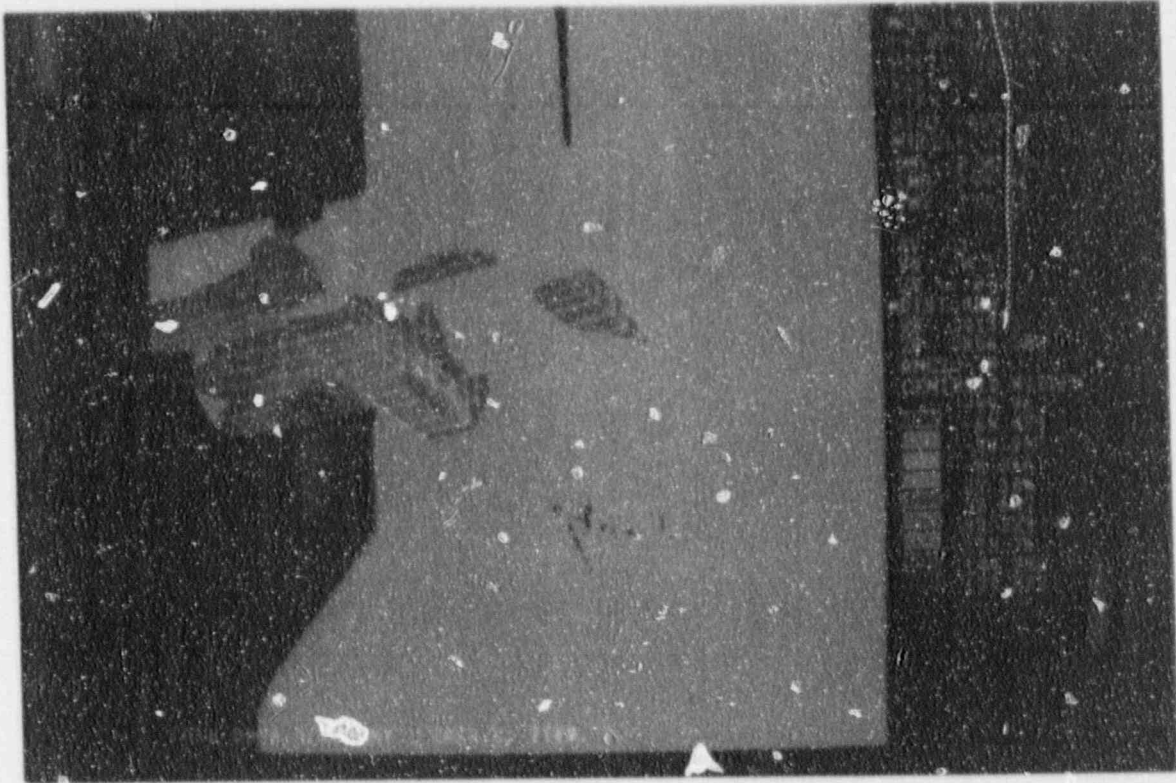


Figure 4.34

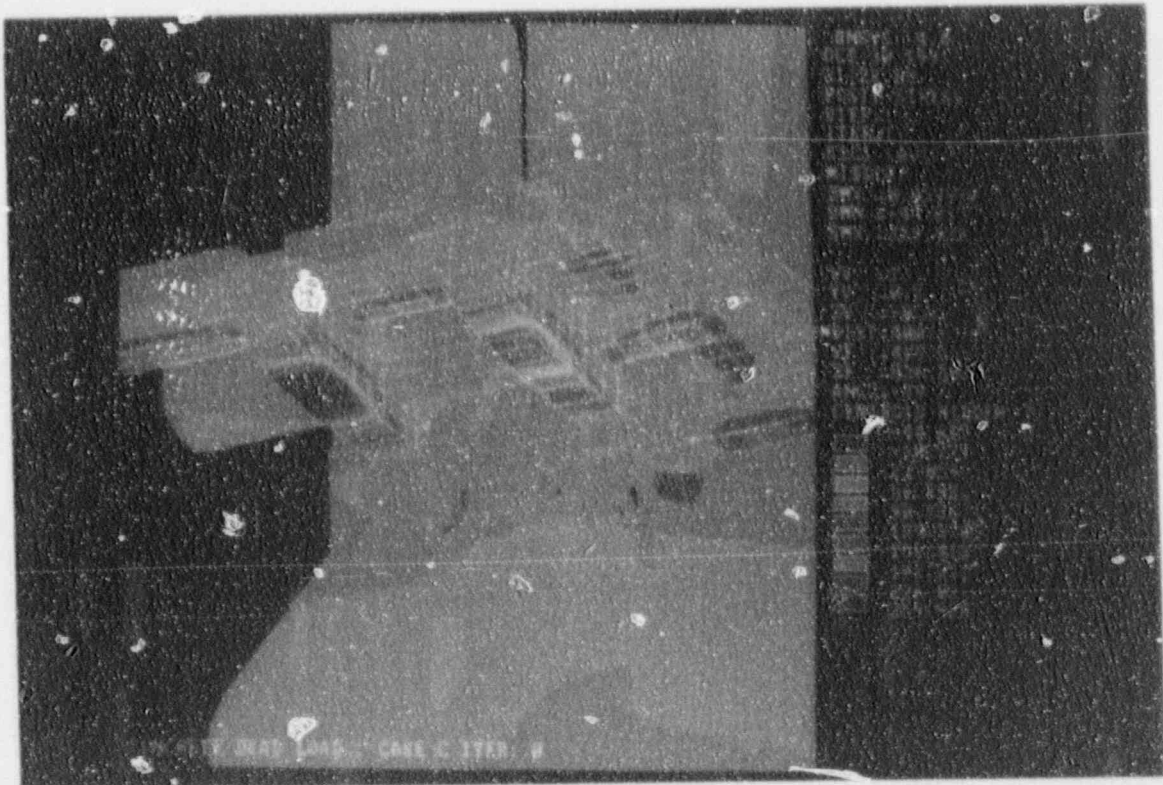


Figure 4.35

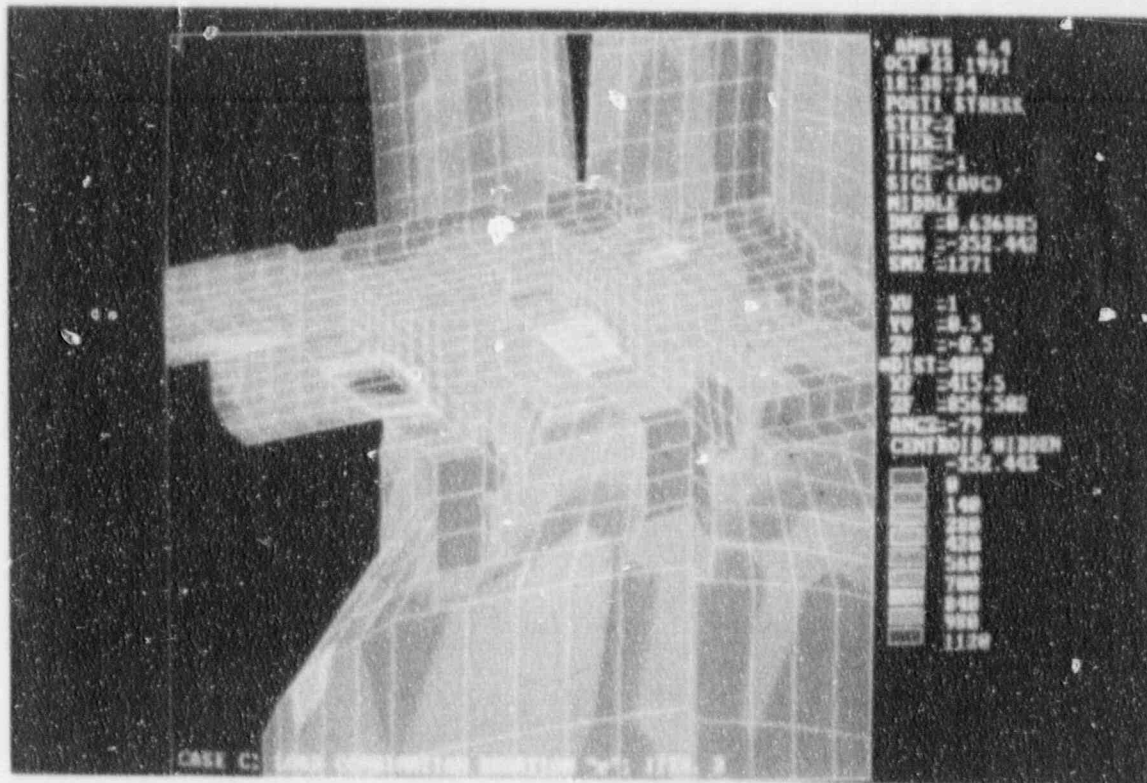


Figure 4.36

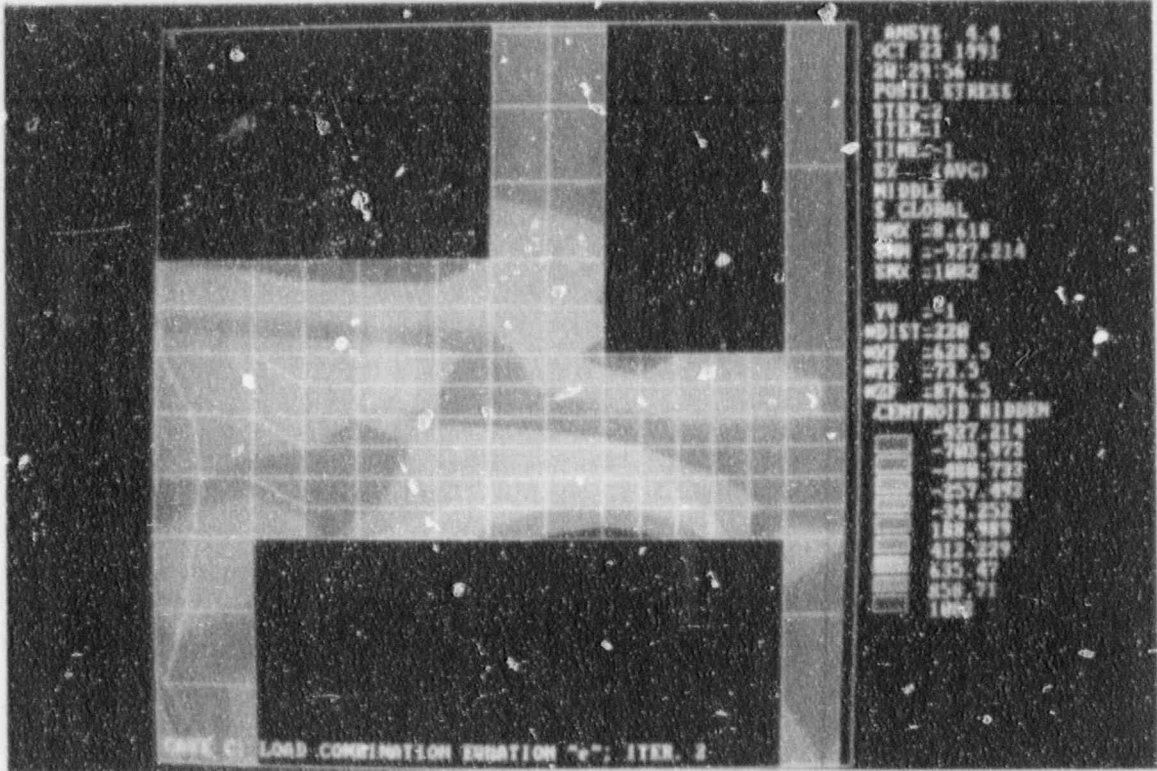


Figure 4.37

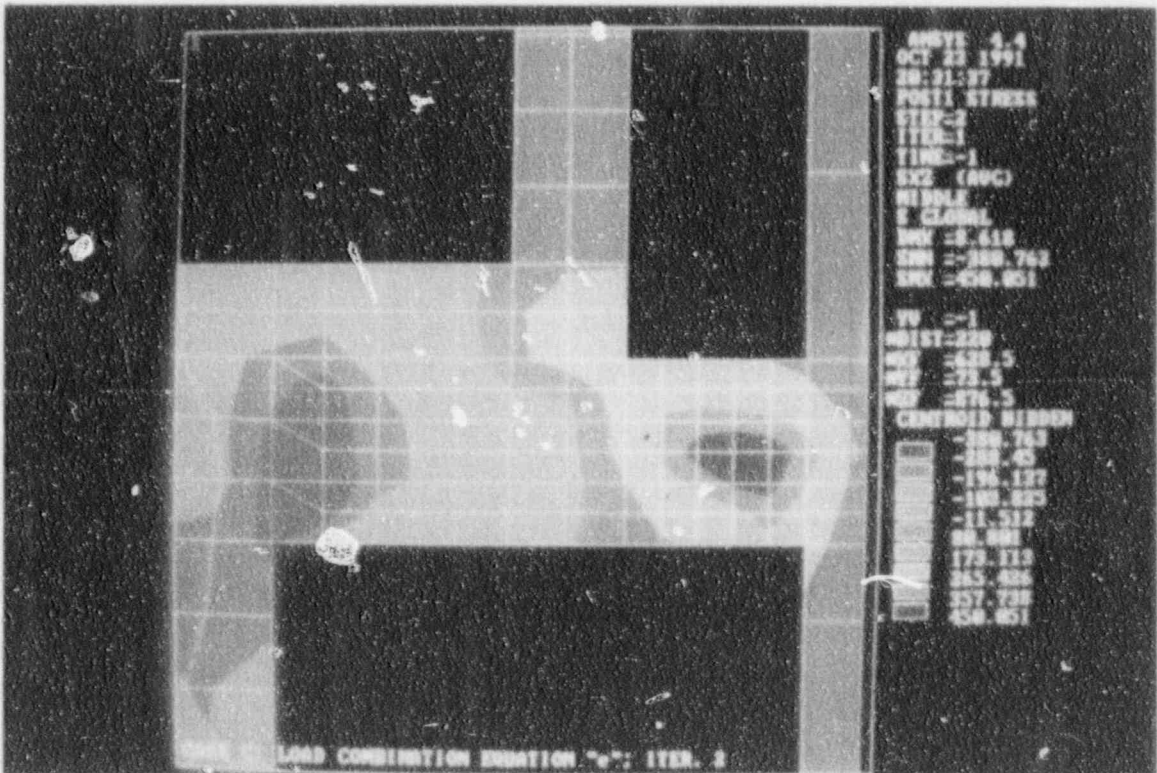


Figure 4.38

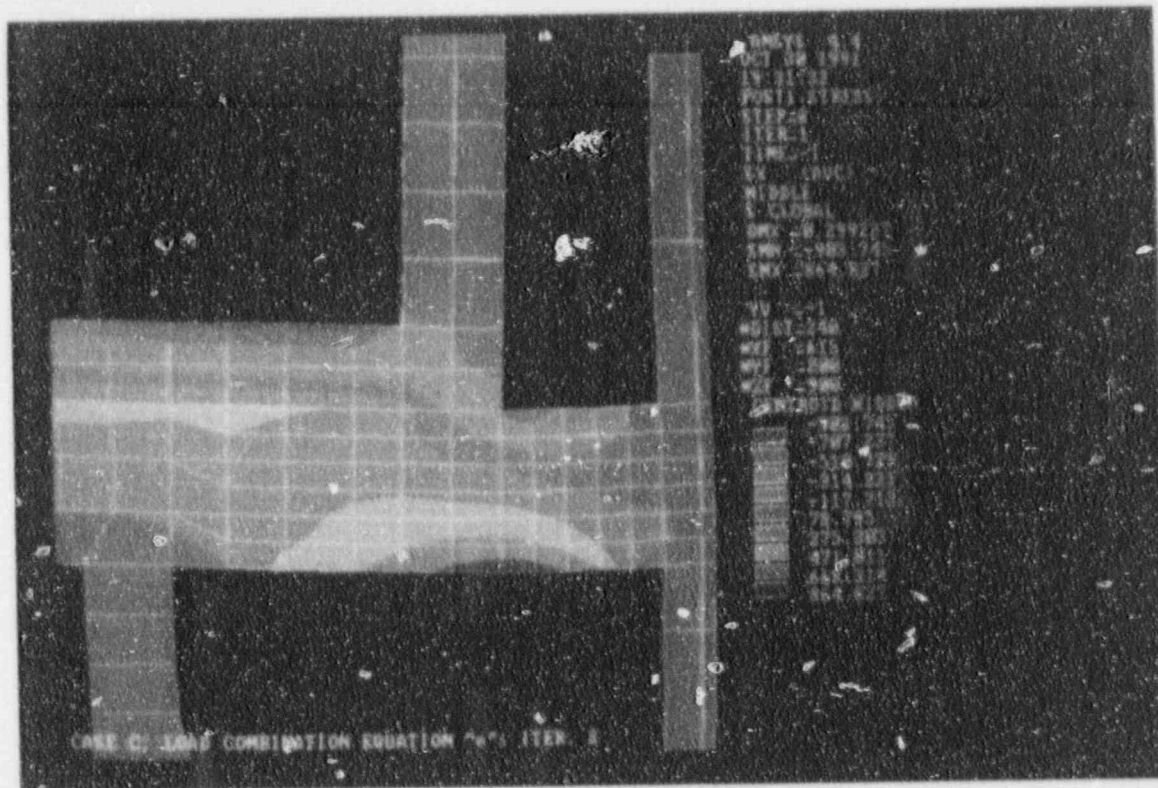


Figure 4.39

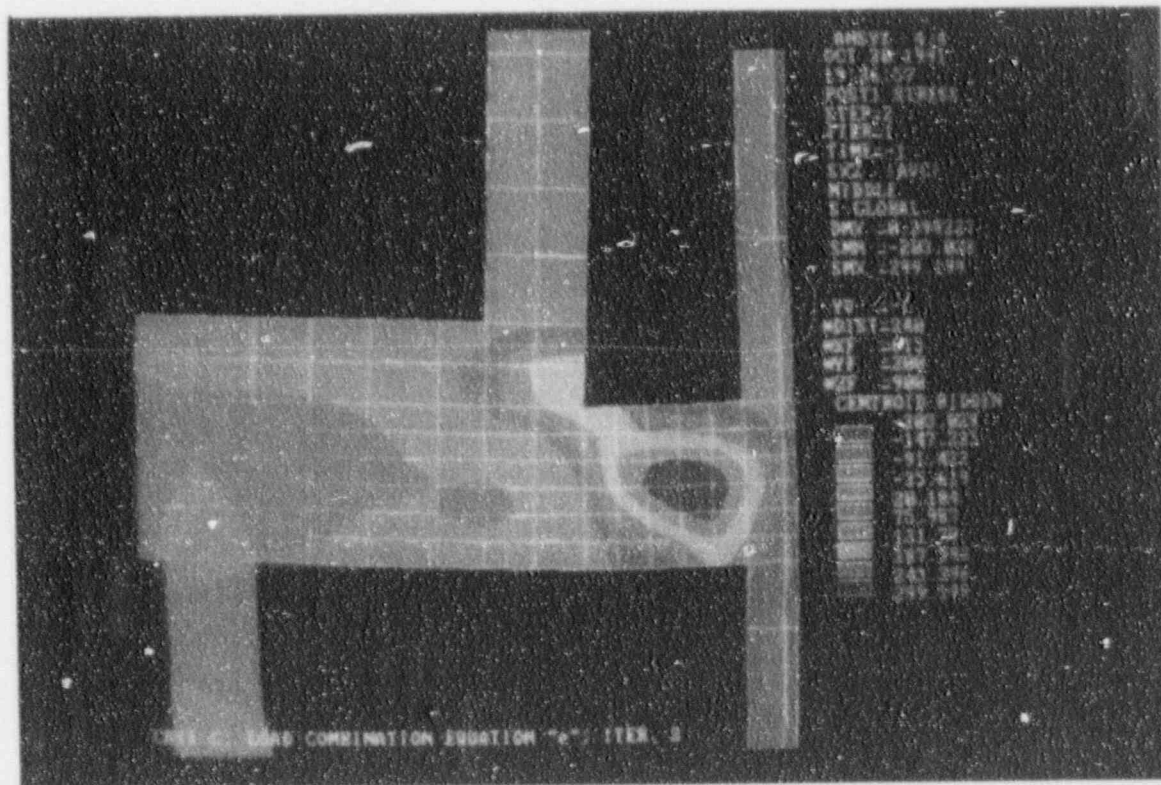


Figure 4.40

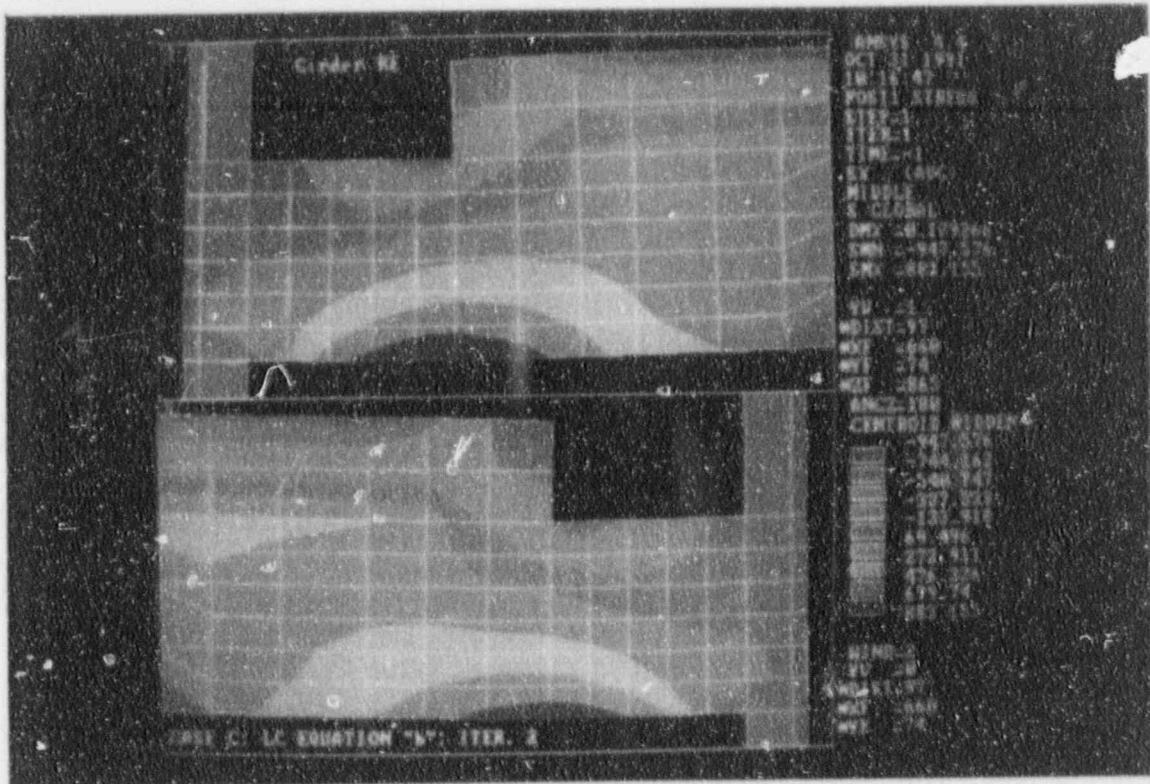


Figure 4.41

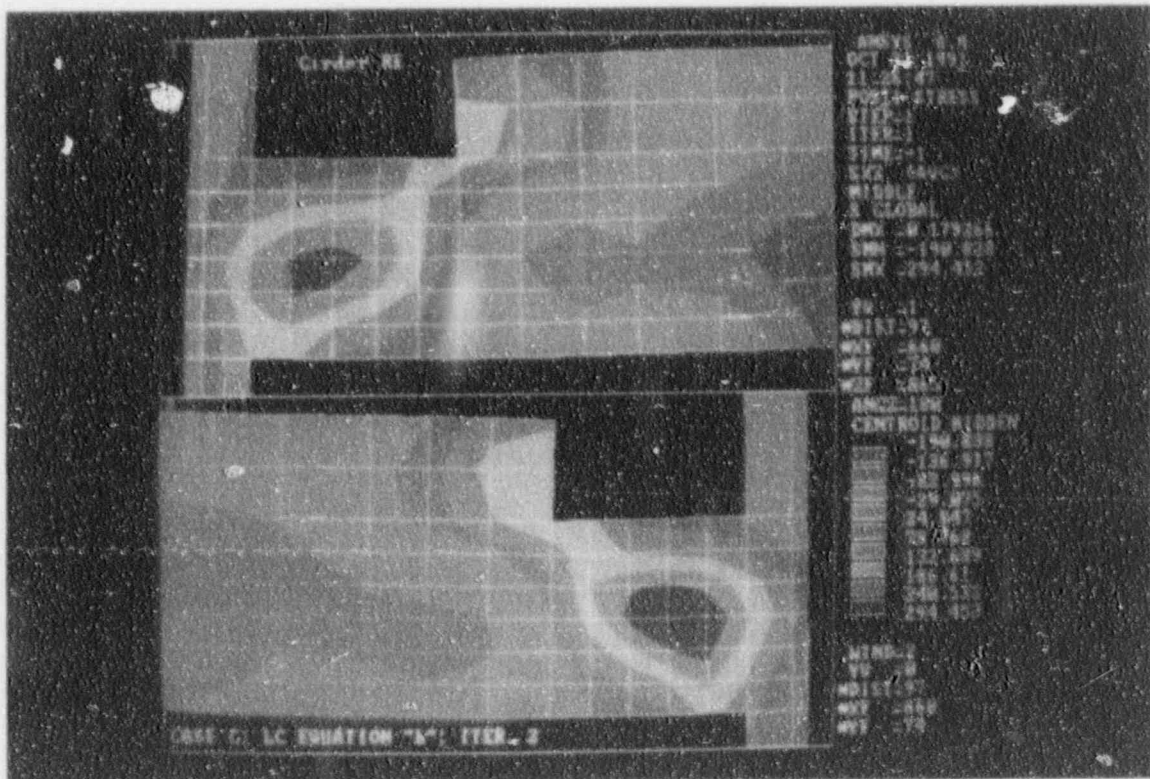


Figure 4.42

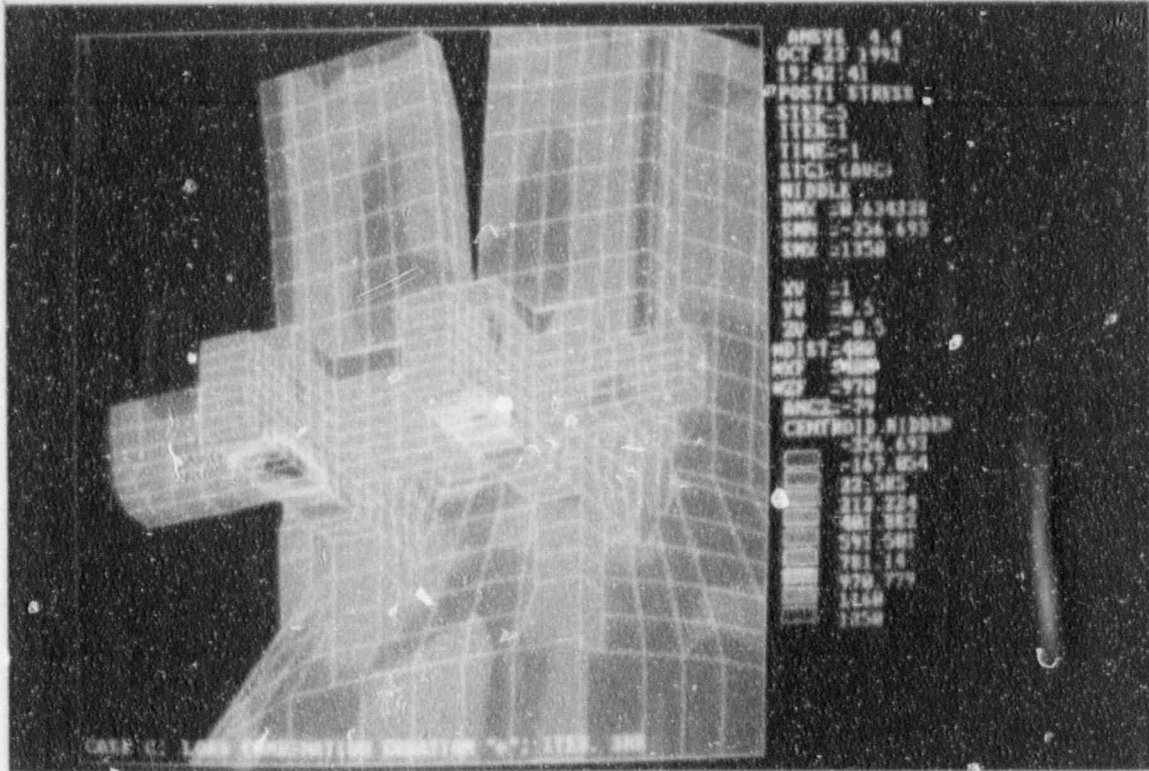


Figure 4.43

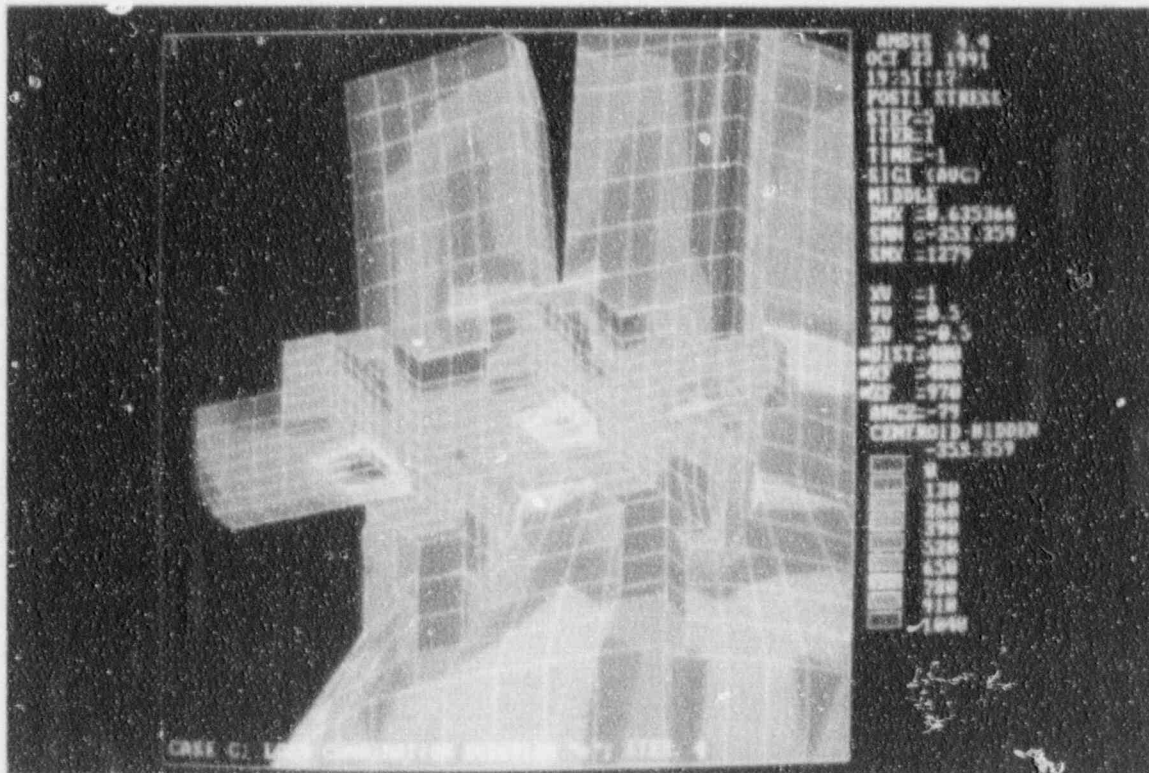


Figure 4.44

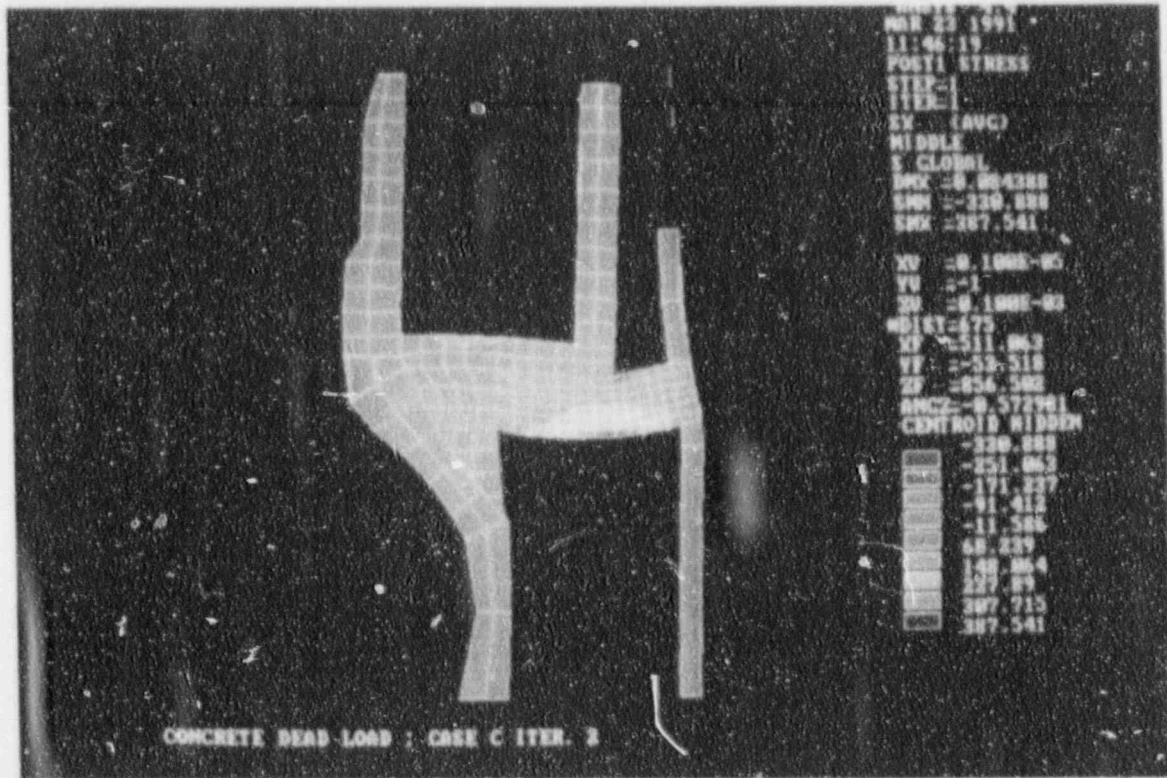


Figure 4.45

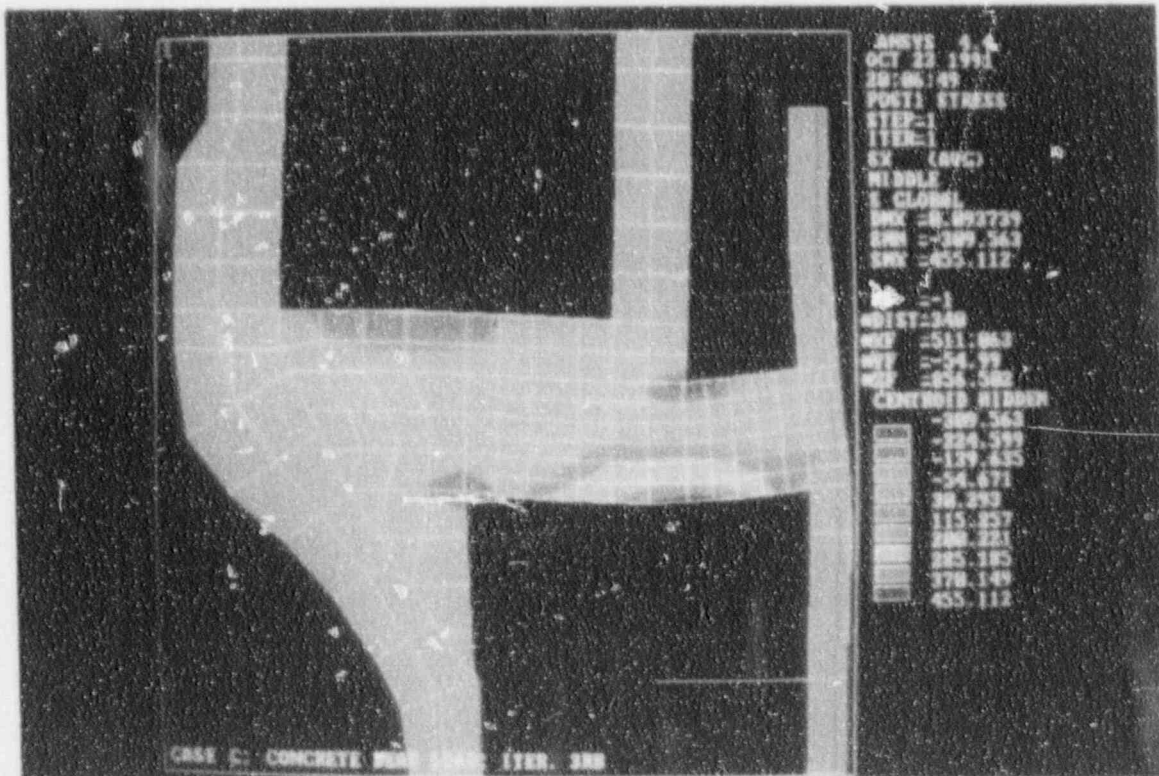


Figure 4.46

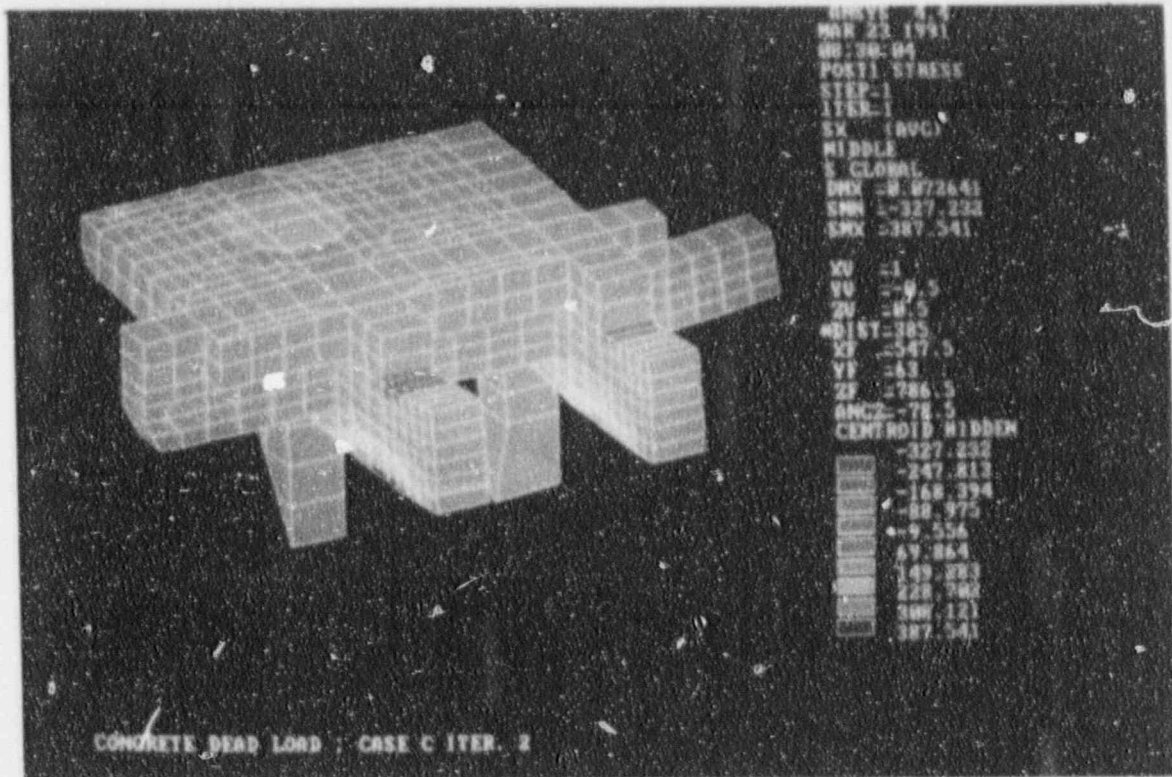


Figure 4.47

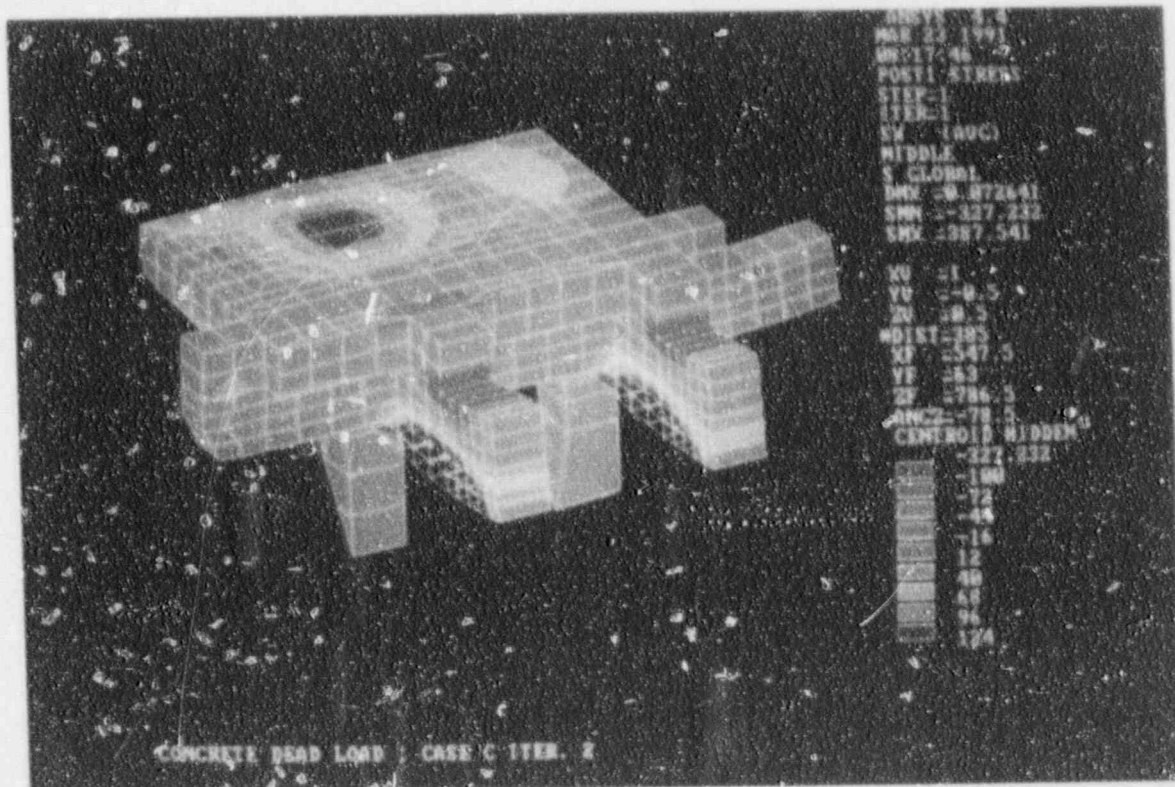


Figure 4.48

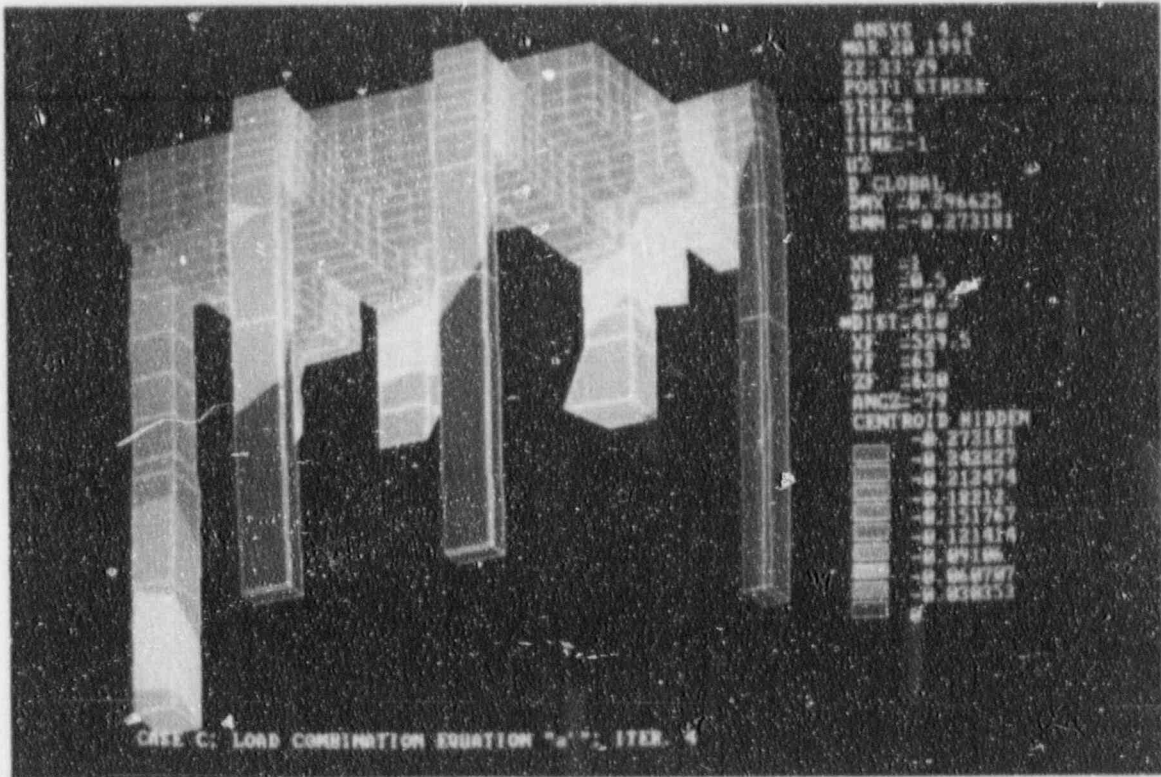


Figure 4.51

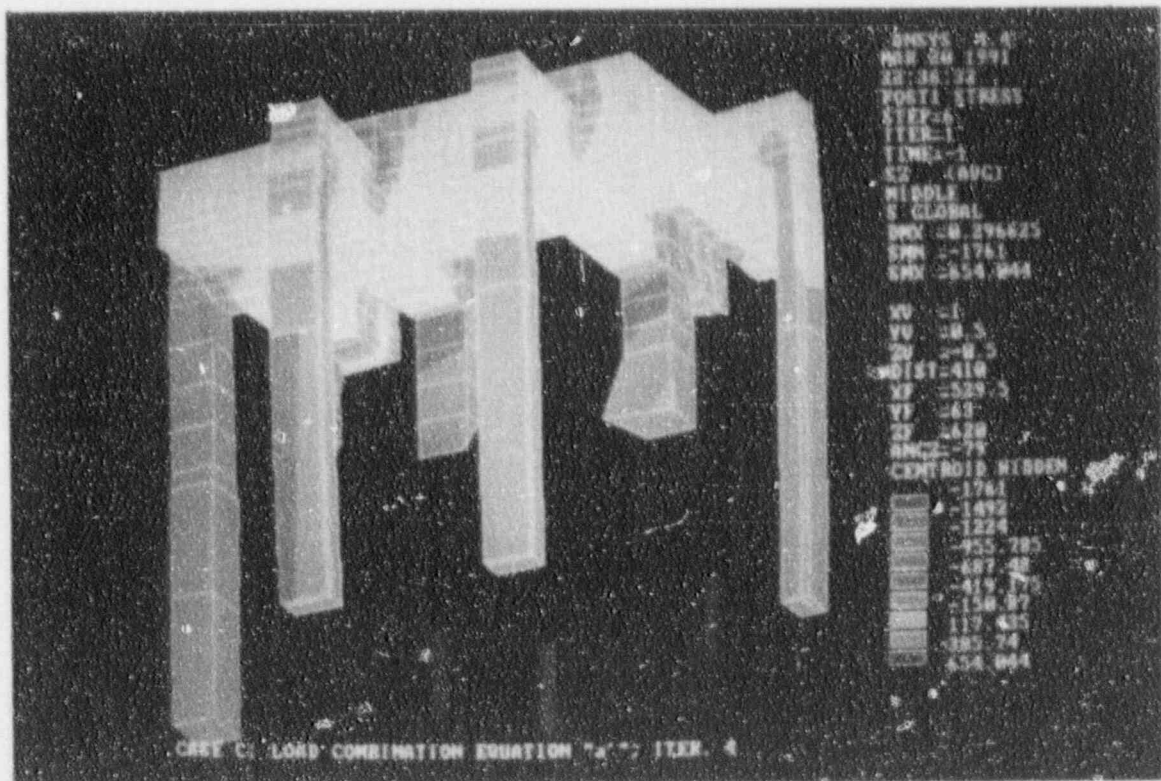


Figure 4.52

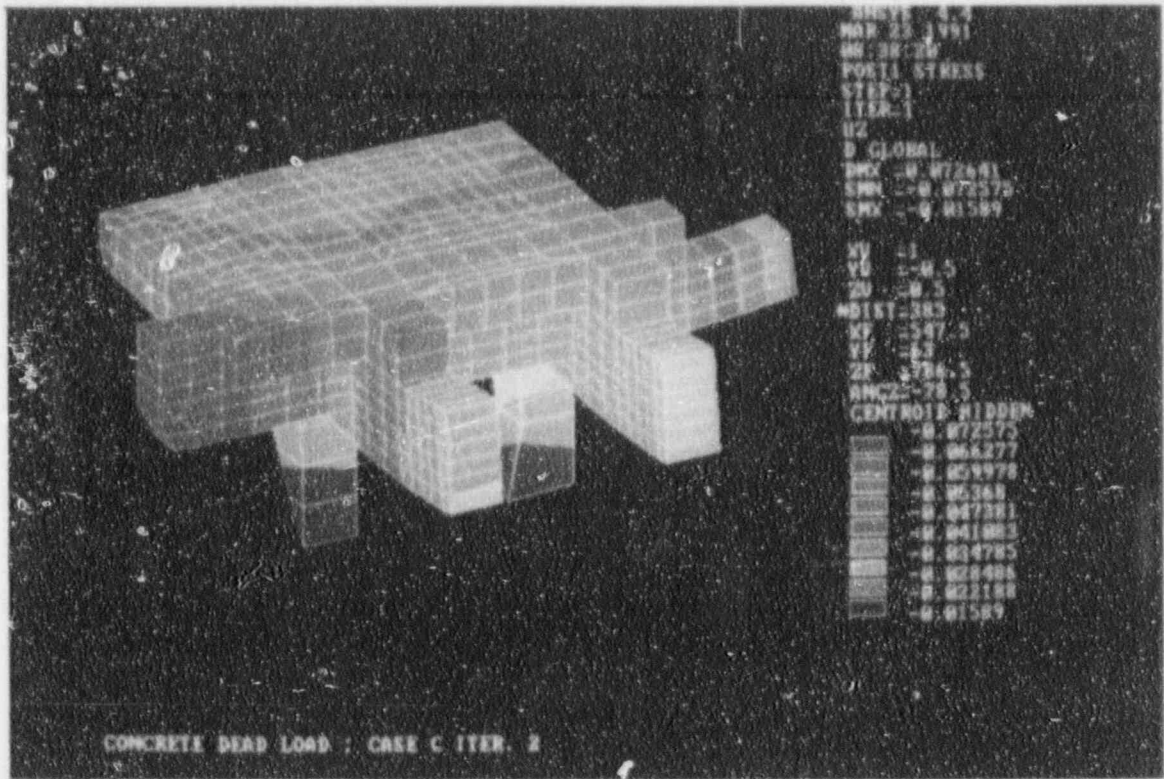


Figure 4.53

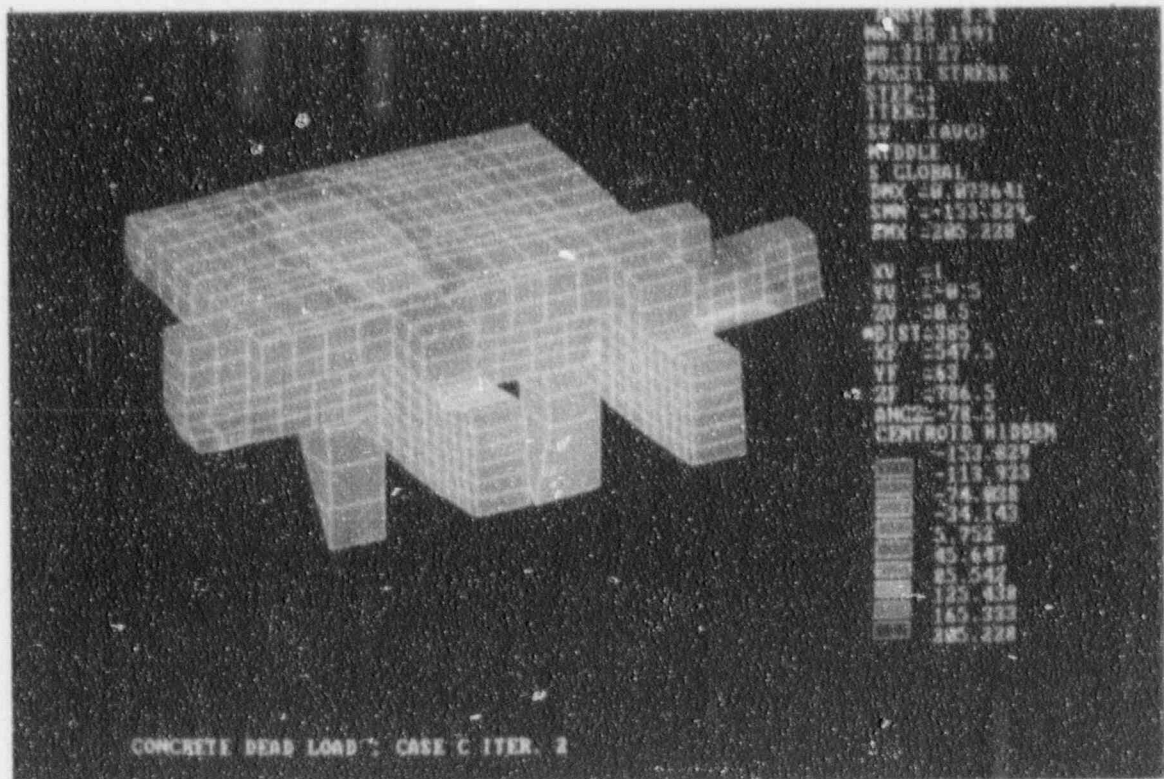


Figure 4.54

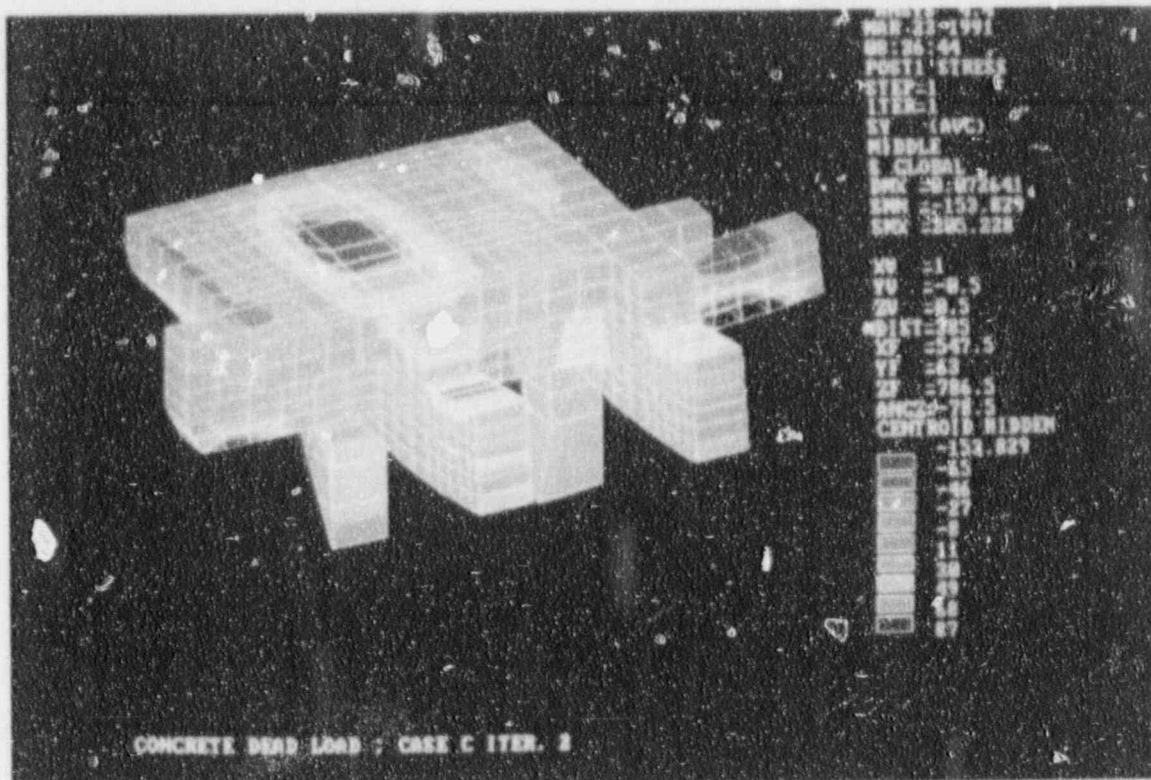


Figure 4.55

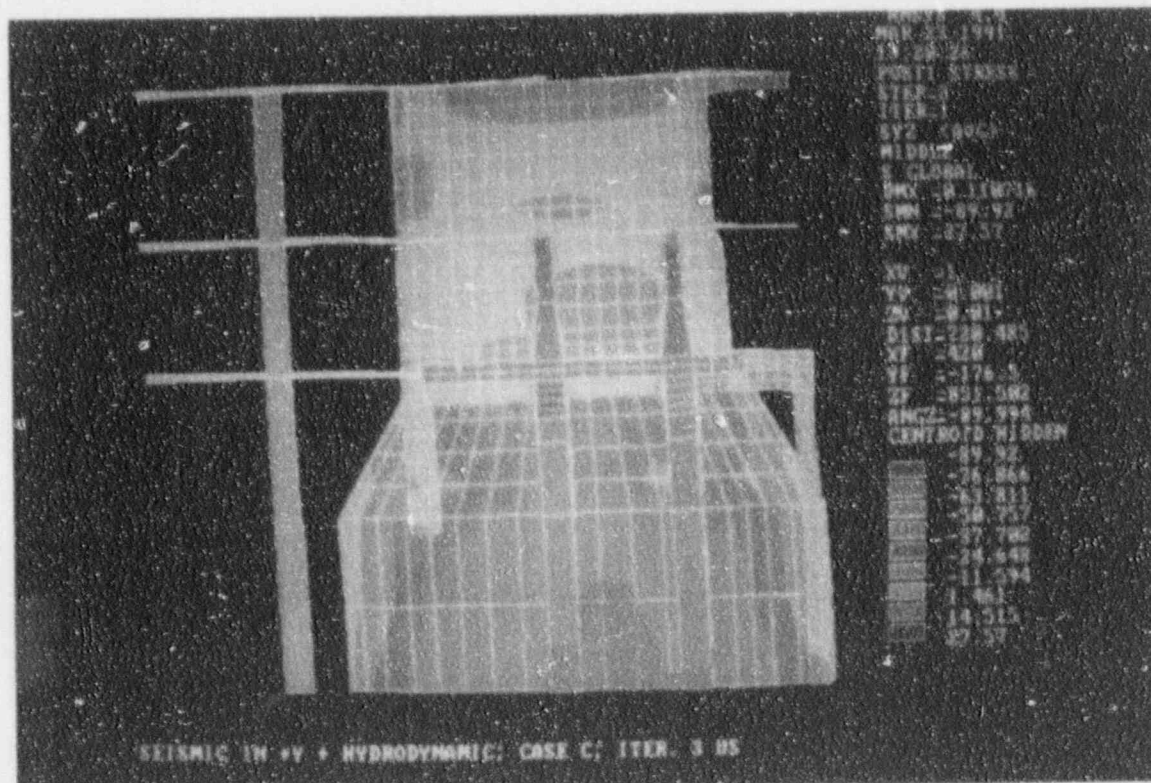


Figure 4.56

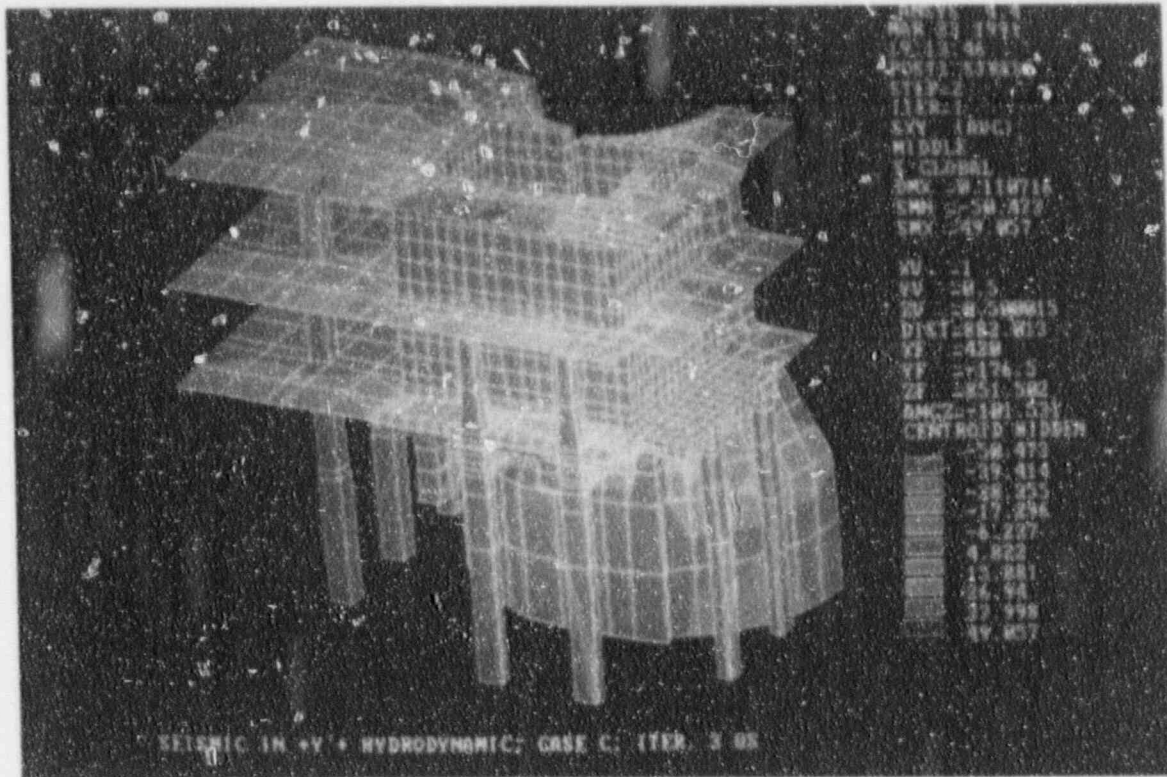


Figure 4.57

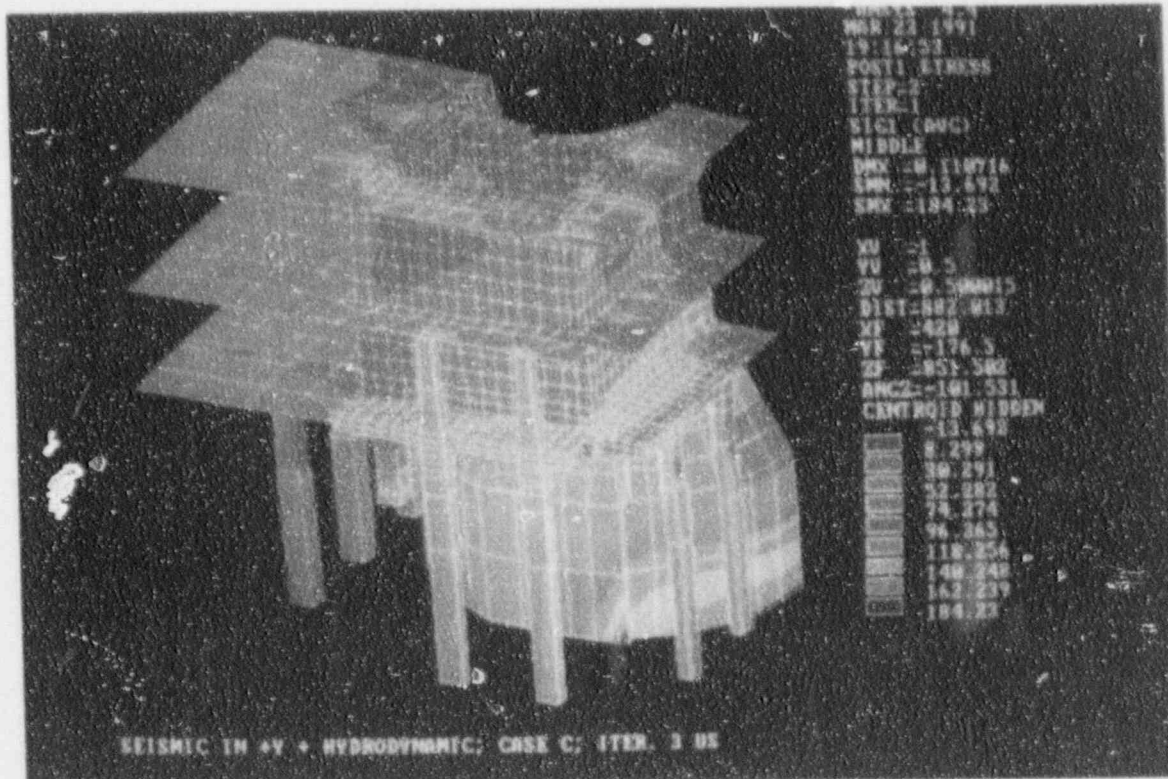


Figure 4.58

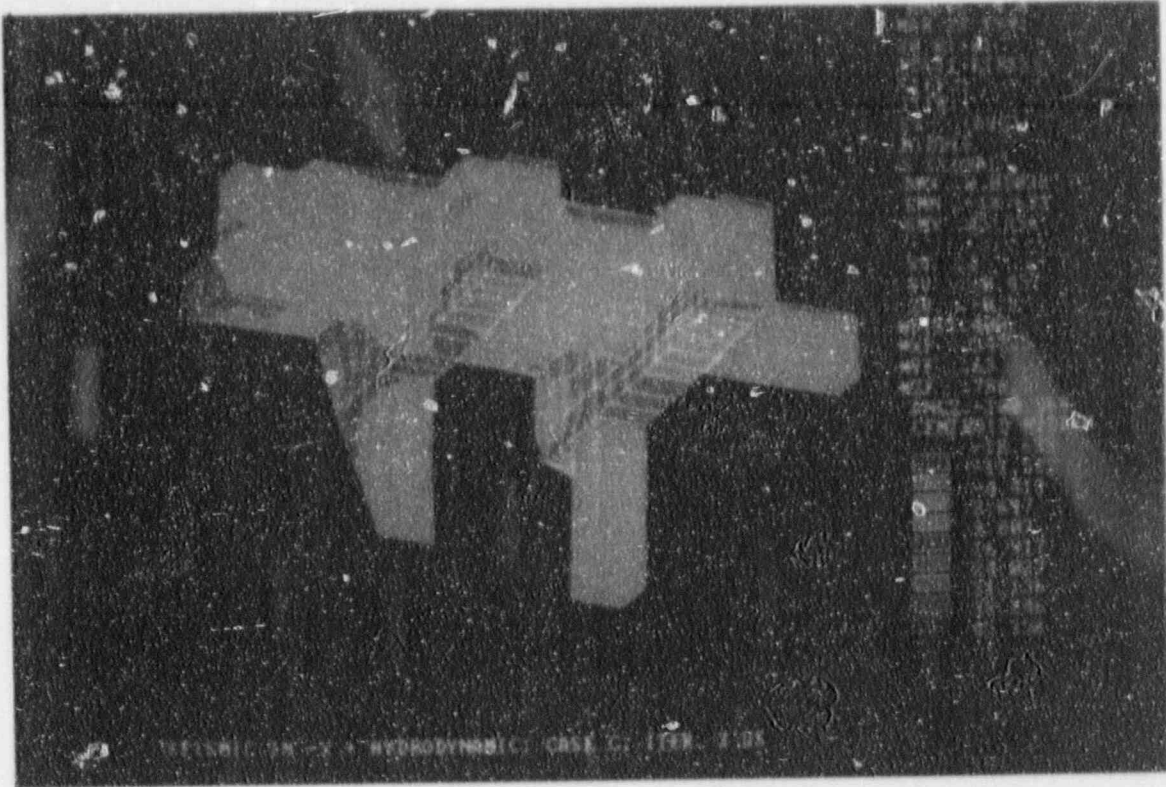


Figure 4.59

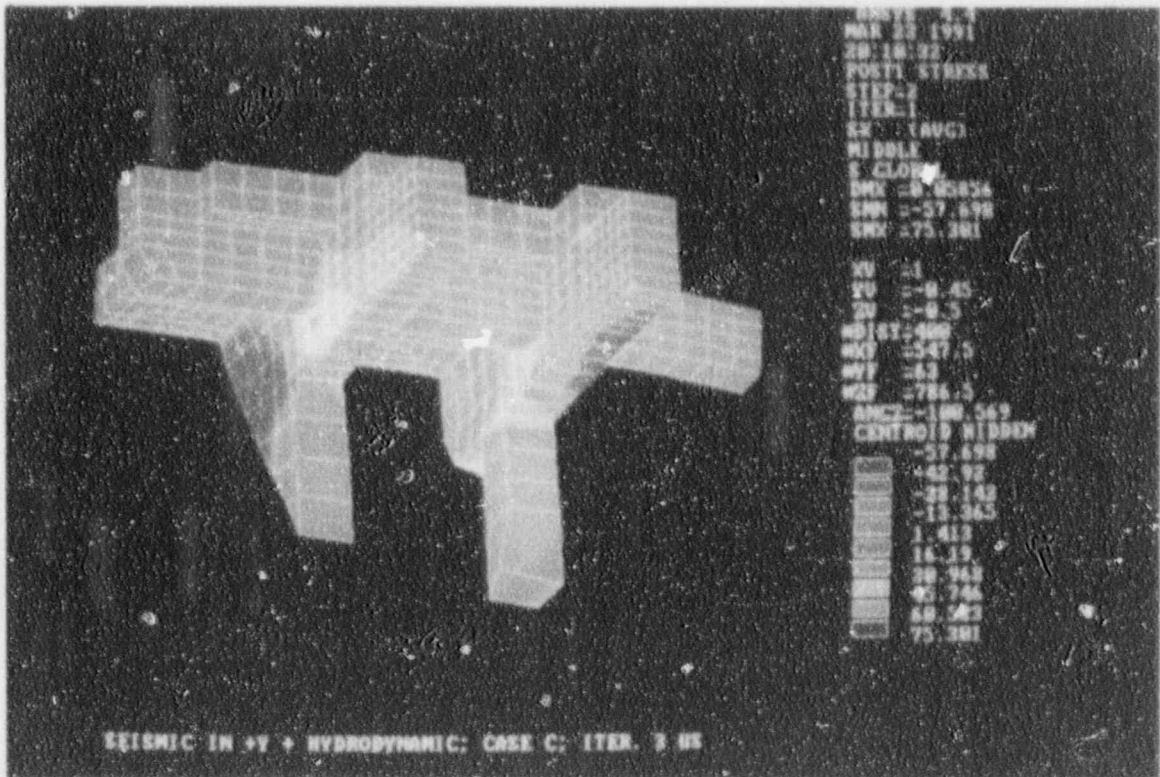


Figure 4.60

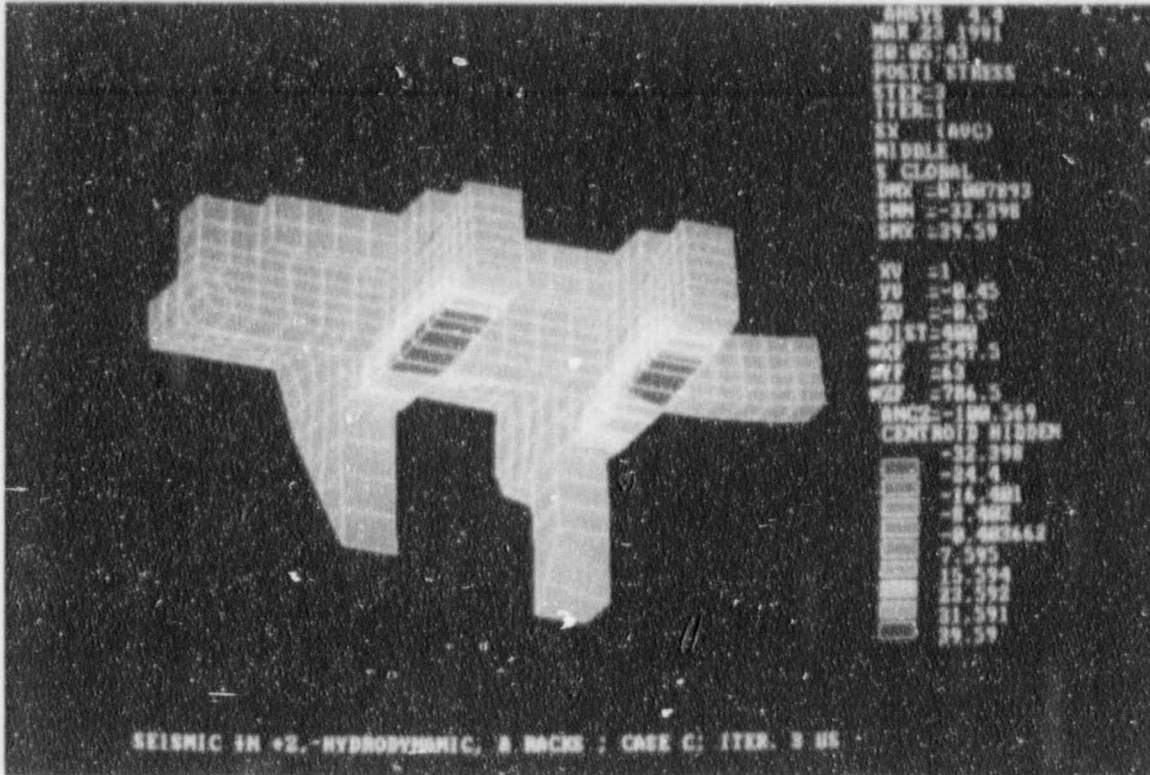


Figure 4.61

STEPS IN THE CRACKING ITERATION PROCESS FOR CASE C

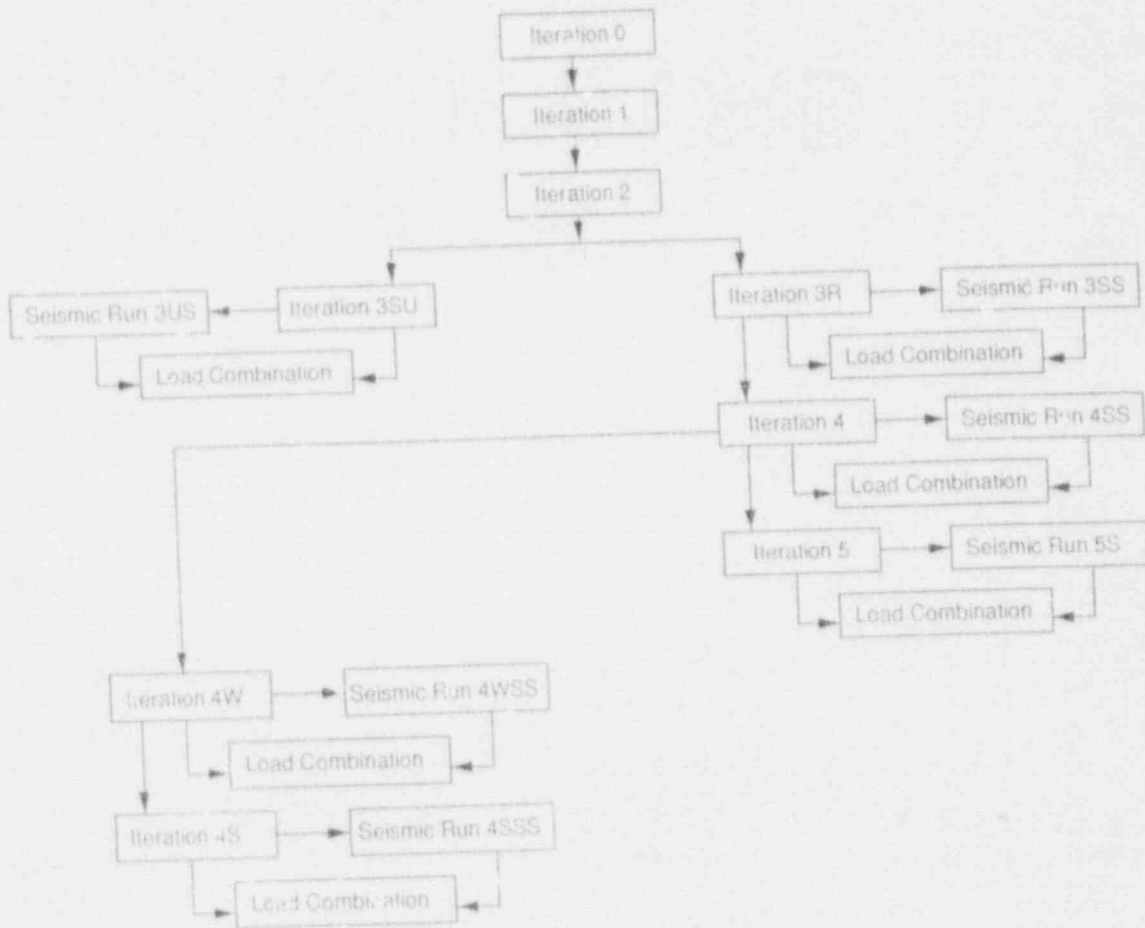


Table 4.1

STEPS IN THE CRACKING ITERATION PROCESS FOR CASE D

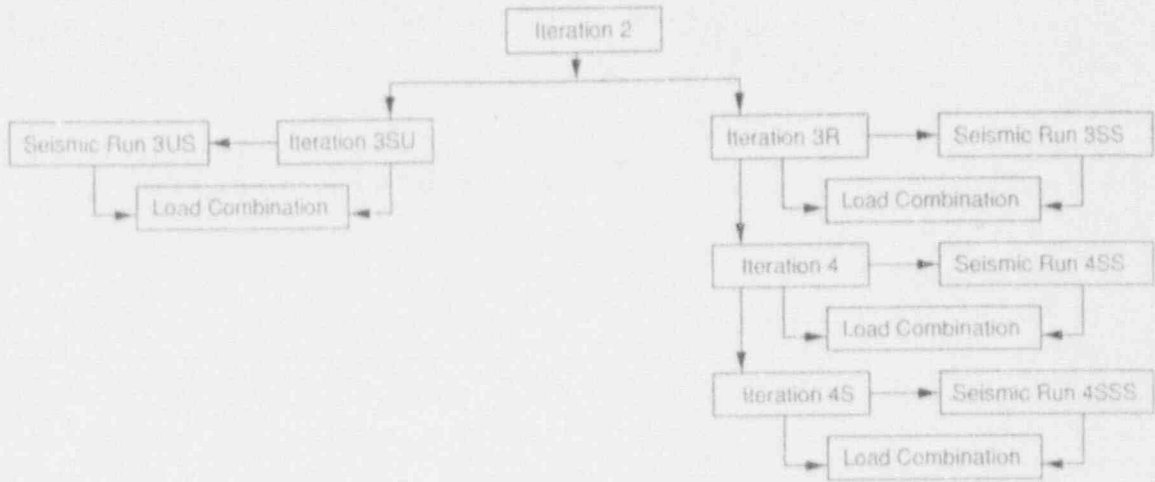


Table 4.2

ABB Impell Corporation

<u>ITERATION</u>	<u>BRIEF DESCRIPTION FOR CASE C</u>
0	Structural Analysis - Cracking Iteration 0 Entire model uncracked.
1	Structural Analysis - Cracking Iteration 1 Floors at Elevation 75', 95' and 119', except the solid elements at Elevation 75', had their stiffness reduced by a factor of one thousand.
2	Structural Analysis - Cracking Iteration 2 Shield Wall, SFP Slab and SFP Walls cracked.
3SU	Structural Analysis - Cracking Iteration 3SU The bottom edge of the SFP Slab is uncoupled, in addition to Iteration 2 stiffness properties. Floor Slab at 75' is active. "SU" denotes the SFP Slab in Uncoupled.
	Structural Analysis - Seismic Run 3US SFP Slab is uncoupled for seismic, in addition to Iteration 2 stiffness properties. All floor slabs including the solid elements at 75' were active. "US" denotes SFP Slab Uncoupled for Seismic.
3R	Structural Analysis - Cracking Iteration 3R Solid element of floor Slab at 75' are fully cracked, in addition to Iteration 2 stiffness properties. "R" denotes Rectangular beam behavior.
	Structural Analysis - Seismic Run 3SS All floors are active except the solid elements at Elevation 75' which had a reduced stiffness and mass by a factor of one thousand (1000) in addition to Iteration 2. "SS" denotes seismic with floors stiffness included.
4	Structural Analysis - Cracking Iteration 4 Girder RD, RE and R6 cracked in addition to Iteration 3R stiffness properties.
	Structural Analysis - Seismic Run 4SS Girders RD, RE and R6 cracked in addition to Seismic Run 3SS stiffness properties.
5	Structural Analysis - Cracking Iteration 5 Shield wall stiffness and mass were reduced by a factor of 1000, in addition to Iteration 4 stiffness properties.
	Structural Analysis - Seismic Run 5S Shield wall stiffness and mass above Elevation 79'-0" were reduced by a factor of 1000, in addition to Seismic Run 4SS.
4W	Structural Analysis - Cracking Iteration 4W Cracked transformed properties for SFP Walls, in addition to Iteration 4 properties.
	Structural Analysis - Seismic Run 4WSS Cracked transformed properties for SFP Walls, in addition to Seismic Run 4SS properties.
4S	Structural Analysis - Cracking Iteration 4S Cracked transformed properties for SFP Slab in addition to Iteration 4W properties.
	Structural Analysis - Seismic Run 4SSS Cracked transformed properties for SFP Slab in addition to Seismic Run 4WSS properties.

Table 4.3

ITERATION

BRIEF DESCRIPTION FOR CASE D

2	<p>Structural Analysis - Cracking Iteration 2 Shield Wall, SFP Slab and SFP Walls cracked.</p>
3SU	<p>Structural Analysis - Cracking Iteration 3SU The bottom edge of the SFP Slab is uncoupled, in addition to Iteration 2 stiffness properties. Floor Slab at 75' is active. "SU" denotes the SFP Slab in Uncoupled.</p> <p>Structural Analysis - Seismic Run 3US SFP Slab is uncoupled for seismic, in addition to Iteration 2 stiffness properties. All floor slabs including the solid elements at 75' were active. "US" denotes SFP Slab Uncoupled for Seismic.</p>
3R	<p>Structural Analysis - Cracking Iteration 3R Solid element of floor Slab at 75' are fully cracked, in addition to Iteration 2 stiffness properties. "R" denotes Rectangular beam behavior.</p> <p>Structural Analysis - Seismic Run 3SS All floors are active except the solid elements at Elevation 75' which had a reduced stiffness and mass by a factor of one thousand (1000) in addition to Iteration 2. "SS" denotes seismic with floors stiffness included.</p>
4	<p>Structural Analysis - Cracking Iteration 4 Girder RD, RE and R6 cracked in addition to Iteration 3R stiffness properties.</p> <p>Structural Analysis - Seismic Run 4SS Girders RD, RE and R6 cracked in addition to Seismic Run 3SS stiffness properties.</p>
4S	<p>Structural Analysis - Cracking Iteration 4S Cracked transformed properties for SFP Slab in addition to Iteration 4W properties.</p> <p>Structural Analysis - Seismic Run 4SSS Cracked transformed properties for SFP Slab in addition to Seismic Run 4WSS properties.</p>

VERTICAL SHEAR FORCES (kips) IN GIRDER RD AT FACE OF COLUMN D-7

LOAD STEP	ANALYSIS CASE C CRACKING ITERATIONS 0 THROUGH 5						
	0	1	2	3R	4	4S	5
Concrete Dead Load	403	485	565	623	551	600	607
Hydrostatic Pressure + High Density Racks + Stored Cask	171	221	281	315	277	320	304
Design Live Load	97	112	142	158	141	153	168
Sum of Sustained Loads	671	818	988	1096	969	1073	1079
Winter Temperature	-639	25	369	417	355	293	615
Summer Temperature	-523	*	*	*	*	-59	*
Cask Drop Accident	77	110	147	164	138	157	173

Notes:

1. The shear forces in the girder are unfactored values and are taken at the face of the embedded wall column.
2. The results reported in this table are in error by approximately -0.5% for all iterations except 4S (See Section 4.3.1 for discussion).

Table 4.5

VERTICAL SHEAR FORCES (kips) IN GIRDER RE AT FACE OF COLUMN E-7

LOAD STEP	ANALYSIS CASE C CRACKING ITERATIONS 0 THROUGH 5						
	0	1	2	3R	4	4S	5
Concrete Dead Load	363	396	455	520	475	530	515
Hydrostatic Pressure + High Density Racks + Stored Cask	168	204	257	294	264	285	285
Design Live Load	66	73	93	106	100	117	120
Sum of Sustained Loads	597	673	805	920	839	932	920
Winter Temperature	-534	97	366	395	344	304	585
Summer Temperature	-514	*		*	*	-85	*
Cask L p Accident	44	39	43	47	46	32	66

Notes:

1. The shear forces in the girder are unfactored values and are taken at the face of the embeded wall column.
2. The results reported in this table are in error by approximately -0.8% for all iterations except 4S (See Section 4.3.1 for discussion).

VERTICAL SHEAR FORCES (kips) IN GIRDER R6 AT FACE OF COLUMN F-6

LOAD STEP	ANALYSIS CASE C CRACKING ITERATIONS 0 THROUGH 5						
	0	1	2	3R	4	4S	5
Concrete Dead Load	118	115	140	169	182	195	192
Hydrostatic Pressure + High Density Racks + Stored Cask	48	53	64	77	84	85	90
Design Live Load	19	17	23	30	33	41	37
Sum of Sustained Loads	185	185	227	276	299	321	319
Winter Temperature	-253	-132	-51	-50	-37	-5	17
Summer Temperature	-206	*	*	*	*	-109	*
Cask Drop Accident	5	-5	-7	-9	-7	-12	-5

Notes:

1. The shear forces in the girder are unfactored values and are taken at the face of the embedded wall column.
2. The results reported in this table are in error by approximately -2.2% for all iterations except 4S (See Section 4.3.1 for discussion).

Table 4.7



ABB Impell Corporation

VERTICAL FORCES (kips) IN COLUMN C-6 AT BOTTOM OF GIRDER R6

LOAD STEP	ANALYSIS CASE C CRACKING ITERATIONS 0 THROUGH 5						
	0	1	2	3R	4	4S	5
Concrete Dead Load	484	591	737	792	822	974	893
Hydrostatic Pressure + High Density Racks + Stored Cask	179	231	289	316	330	360	360
Design Live Load	211	211	268	284	292	351	326
Sum of Sustained Loads	874	1033	1294	1392	1444	1685	1579
Winter Temperature	-1104	-657	-320	-260	-238	-230	16
Summer Temperature	-525	*	*	*	*	-159	*
Cask Drop Accident	125	184	238	260	269	325	313

Notes:

1. The axial forces in the column are unfactored values and are taken at the bottom of Girder R6.
2. The results reported in this table are in error by approximately +4.5% for all iterations except 4S (See Section 4.3.1 for discussion).

VERTICAL SHEAR FORCES (kips) IN GIRDER RD AT FACE OF COLUMN D-7

LOAD STEP	ANALYSIS CASE D CRACKING ITERATIONS 0 THROUGH 4S			
	2	3R	4	4S
Concrete Dead Load	560	617	548	600
Hydrostatic Pressure + Consolidated Racks + Stored Cask	335	373	329	372
Design Live Load	140	156	140	153
Sum of Sustained Loads	1035	1146	1017	1125
Winter Temperature	379	428	371	293
Summer Temperature	*	*	*	-59
Cask Drop Accident	146	162	138	157

Notes:

1. The shear forces in the girder are unfactored values and are taken at the face of the embeded wall column.
2. The results reported in this table are in error by approximately -0.5% for all iterations except 4S (See Section 4.3.1 for discussion).

VERTICAL SHEAR FORCES (kips) IN GIRDER R2 AT FACE OF COLUMN E-7

LOAD STEP	ANALYSIS CASE D CRACKING ITERATIONS 0 THROUGH 4S			
	2	3R	4	4S
Concrete Dead Load	458	524	479	530
Hydrostatic Pressure + Consolidated Racks + Stored Cask	329	375	336	354
Design Live Load	94	107	100	117
Sum of Sustained Loads	881	1006	915	1001
Winter Temperature	368	397	345	304
Summer Temperature	*	*	*	-85
Cask Drop Accident	43	47	46	32

Notes:

1. The shear forces in the girder are unfactored values and are taken at the face of the embedded wall column.
2. The results reported in this table are in error by approximately -0.5% for all iterations except 4S (See Section 4.3.1 for discussion).

VERTICAL SHEAR FORCES (kips) IN GIRDER R6 AT FACE OF COLUMN F-6

LOAD STEP	ANALYSIS CASE D CRACKING ITERATIONS 0 THROUGH 4S			
	2	3R	4	4S
Concrete Dead Load	143	173	186	195
Hydrostatic Pressure + Consolidated Racks + Stored Cask	87	104	112	108
Design Live Load	24	31	34	41
Sum of Sustained Loads	254	308	332	344
Winter Temperature	-54	-53	-48	-5
Summer Temperature	*	*	*	-109
Cask Drop Accident	-7	-8	-6	-12

Notes:

1. The shear forces in the girder are unfactored values and are taken at the face of the embeded wall column.
2. The results reported in this table are in error by approximately -0.5% for all iterations except 4S (See Section 4.3.1 for discussion).

Table 4.11

VERTICAL FORCES (kips) IN COLUMN C-6 AT BOTTOM OF GIRDER R6

LOAD STEP	ANALYSIS CASE D CRACKING ITERATIONS 0 THROUGH 45			
	2	3R	4	4S
Concrete Dead Load	775	831	861	974
Hydrostatic Pressure + Consolidated Racks + Stored Cask	357	386	401	409
Design Live Load	278	296	304	351
Sum of Sustained Loads	1410	1513	1566	1734
Winter Temperature	-351	-286	-282	-230
Summer Temperature	*	*	*	-159
Cask Drop Accident	247	270	275	325

Notes:

1. The axial forces in the column are unfactored values and are taken at the bottom of Girder R6.
2. The results reported in this table are in error by approximately +4.5% for all iterations except 4S (See Section 4.3.1 for discussion).

Table 4.12

CRACKING STATUS ARRAY FOR ANALYSIS ITERATIONS

REGIONS CRACKED	ITERATION**								
	0	1	2	3US	3R	4	4W	4S	5
Floor Slabs at el. 75', 95', 119'	no	yes ⁽¹⁾							
Floor slab at elev. 75' consisting of solid elements	no	no	no	no	yes*	yes*	yes*	yes*	yes*
Shield Wall	no	no	yes	yes	yes	yes	yes	yes	yes ⁽²⁾
SFP Slab	no	no	yes	yes	yes	yes	yes	yes**	yes
SFP Walls	no	no	yes	yes	yes	yes	yes**	yes**	yes
Girder R0	no	no	no	no	no	yes	yes	yes	yes
Girder 7	no	no	no	no	no	yes	yes	yes	yes
Girder R6	no	no	no	no	no	yes	yes	yes	yes
Lack of Rebar Embedment in the SFP Slab Considered	no	no	no	yes	no	no	no	no	no

* The modulus of elasticity was reduced by a factor of one thousand.
 ** The fully transformed cracking criteria was used (See Section 2.3.2).
 *** Yes = cracked, no = uncracked
 (1) Not cracked for seismic runs.
 (2) The modulus of elasticity was reduced by a factor of one thousand above elevation 80'.

Table 4.13



5.0 SUMMARY OF RESULTS

5.1 The Evaluation Process

The evaluation of the SFP structure, as discussed in Section 4.2, integrates various analysis methods, criteria and strategies with structural behavior to form an overall evaluation process. The objectives of that process were to requalify the SFP for existing high density rack loads considering existing cracks, to evaluate the SFP for consolidated fuel rack loads, and to explain why cracks exist in the SFP structures. As explained in Section 4.3, the cracking iteration process ensured that the sequence of cracking and the resulting redistribution of internal forces maximized the forces in the primary supporting members of the SFP and the SFP slab. As the analysis proceeded, the cracking process was interrupted to study structural behavior and to perform evaluations. Section 5.0 summarizes the results of those evaluations.

In the evaluation of a linear elastic structure for static load, the magnitude of the internal forces at a particular location can be determined for a variety of load combinations at the end of the analysis and then checked against code allowable values. However, this approach cannot be used for the evaluation of a structure which exhibits nonlinear behavior, such as the SFP. Due to the complex behavior of the SFP structure and due to the redistribution of internal forces which takes place as concrete cracking occurs, the most severe load condition for a structural component may not occur at the end of the cracking process. Therefore, to achieve high confidence in the analysis results, the cracking process was interrupted for the purpose of evaluating structural components at various stages within the process (see Section 4.3). In addition, iterations were added to the cracking process which were not directly related to actual levels of cracking. These added iterations allowed unintended support mechanisms, such as the floor slabs and shield wall, to be released during the iteration process to determine their influence on SFP response (see Section 4.2). Evaluations were performed for normal concrete cracking iterations and for those iterations which were added to account for the release of unintended support mechanisms (See Section 4.2.2). Whenever load combinations were formed for a particular iteration, as shown in Tables 4.1 and 4.2, evaluations were performed.

The iterations selected for evaluation of the primary supporting members, the SFP slab and SFP walls were based on a review of Tables 4.5 to 4.8, a comparison of stress contour plots for all iterations and specific load combinations and individual load cases, and an understanding of SFP structural behavior developed through the cracking iteration process, as discussed in Sections 4.2 and 4.3 and later in Section 5. The specific iterations selected for evaluation and the reasons for selecting them are discussed in Section 5.2. In addition, based on the examination of stress contour plots for each structural component for different iterations and load combinations, locations were selected within the component for processing and

tabulating internal forces and stresses (i.e. linearized stresses, see Section 5.2.4.1). Not only were specific locations of maximum stress selected, but also entire regions containing many individual locations where relatively high stresses were observed. For example, Figure 5.2 shows all of the locations within the SFP slab where extreme fiber surface stresses were processed for each load combination and then tabulated. As explained further in Section 5.2.4.2, stress criteria were developed to choose the most severe combinations of surface stresses from the tabulated data for code evaluation.

It is the combination of selecting internal forces and stresses at many locations for several cracking iterations and the processing of stress data for many load combinations which, together with stress screening criteria, constitutes the evaluation process. This process was used in the evaluation of the SFP slab, the SFP walls and the primary supporting members of the SFP.

5.2 Evaluation of Critical Sections

Table 5.1a shows all of the load combinations which were used to process stress data throughout the cracking iteration process. Combinations a, b, c, d and e (See Section 3.3.2) include the winter temperature condition and one of the critical directions of seismic load (see Section 4.2.4). Combinations a' and c' are the same as a and c except that they contain the second critical direction of seismic load. Combinations c_s, d_s, c'_s and d'_s correspond directly to combinations c, d, c' and d' except that they contain the summer temperature condition. Load combinations b and e were not evaluated for the summer temperature condition because their results were bounded by load combinations c_s and d_s.

Table 5.1b shows all of the load combinations which were specifically developed to demonstrate compliance with ACI 349-80, Section 9.2.3 (see Section 3.3). This code provision is directly applicable to the effects that combined dead load and thermal gradients have on the SFP slab. The winter and summer temperature conditions produce reversals in curvature in the SFP slab and dead load produces effects which both add to and subtract from the thermal response. In addition, both dead load and temperature produce axial tensile forces which reduce the moment and shear capacity. The concern is that, since the dead load and thermal conditions are always taken in the same proportion in the load combinations given in Table 5.1a, a slight change in that proportion could trigger a large response, because the response may be the result of a small difference between large numbers. Therefore, the Code requires that where any load (i.e., dead load) reduces the effects of other loads (i.e., thermal) the corresponding load factor for that load shall be taken as 0.9 if the load is always present. Since load combination c is a dominant contributor to the lowest margins in the SFP slab and girders, it was selected to monitor compliance with Section 9.2.3 of the Code (Reference 33). Downward seismic acceleration was also included in the load combinations of Table 5.1b, since this has the same effect as

reducing dead load and could result in even larger thermal responses in the SFP slab. The results of Code evaluations using the load combinations in Table 5.1b are discussed in Sections 5.2.1 and 5.2.2.

Evaluations of the SFP slab and girders were performed for cracking iterations 3U, 3R, 4, 4S and 5. The iterations for which load combinations were formed and processed are shown in Tables 4.1 and 4.2. Tables 4.5 to 4.8 show that iteration 3R, 4, 4S and 5 dominate the response of the girders. Based on this and a review of stress contour plots for all iterations, these iterations were selected for girder evaluation. A review of stress contour plots for the SFP slab for all iterations and specific load combinations showed that iterations 3R and 4 produced more severe results for thermal load combinations, due to increased axial forces, than iteration 2; and more severe results for mechanical load combinations than iterations 0 and 1. Therefore iterations 3R, 4, 4S and 5 were selected for SFP slab evaluation. In addition, iteration 3U was also evaluated for the SFP slab since this iteration simulated the effects of rebar pullout at locations along the edge of the slab where the bottom reinforcement could not be developed to full capacity.

The sections and locations of the girders and SFP slab where internal forces and stresses were processed for each load combination are shown in Figures 5.1 and 5.2. Not all twelve load combinations were tabulated from the processed data for each iteration and each component. A preliminary screen of the processed data usually eliminated several load combinations from consideration, although the specific load combinations not tabulated varied with structural component. In general, eight load combinations were tabulated for each component for the five iterations above. Based on a review of the tabulated data, together with stress screening criteria, the most severe combinations from each iteration were selected for code evaluation.

The additional loads applied to the SFP by high density and consolidated fuel racks do not increase the loads applied to the SFP walls. Therefore, the loads applied to the walls are the same as those for which the walls were originally designed. However, based on the results of the cracking iteration process (see Section 4.3), the shield wall provides some support to the SFP and relieves load in the primary supporting members. The mechanism, or load path, for this support is provided by the membrane forces in the SFP east and west walls. To ensure that the shield wall and SFP walls were not primary mechanisms for the support of vertical SFP loads, the shield wall stiffness was removed in iteration 5. As a consequence the horizontal membrane stresses in the SFP east and west walls decreased significantly. For example, at the south end of the SFP west wall the horizontal membrane forces acting on a vertical section through the height of the wall showed a 10% increase between iterations 3R and 4, and a 22% decrease between iterations 4 and 5 to the level required to restrain the hydrostatic pressure. These results show that in iteration 5 the walls were not restraining load intended for the primary supporting members. They also show that the stiffness configuration of the SFP structure in

iteration 4 produces the most severe results for the SFP walls as load is redistributed from the positive moment region of the girders in iteration 3R to the negative moment region of the girders and SFP slab, and into the shield wall through the SFP walls. Therefore the SFP walls were evaluated in iteration 4S. The ten most critical load combinations from Table 5.1a were tabulated at 85 locations in the walls. Based on a review of the tabulated data, together with stress screening criteria, the most severe locations were selected for code evaluation.

Both high density fuel storage (Analysis Case C) and consolidated fuel storage (Analysis Case D) are evaluated in this section. Since the only difference between the two cases is the higher rack loads in Case D, it is convenient to discuss the behavior and code evaluation of specific structural components for Analysis Cases C and D together.

5.2.1 Evaluation of Girders and Columns

5.2.1.1 High Density Fuel Storage - Analysis Case C

Tables 4.5 and 4.6 show that the maximum shear force carried by Girder RE is bounded by the results for Girder RD for all iterations, therefore, capacity margin results will only be discussed for Girder RD since both girders have the same cross-section dimensions, rebar size and reinforcing details. Table 4.5 shows that for unfactored loads, iteration 3R produces the highest sustained load shear forces in Girder RD, while for the combination of sustained load and temperature condition iteration 5 controls. Table 5.2a shows that the minimum shear capacity margin for Girder RD is 3% which occurred in iteration 3R. Table 5.3a shows that Girder RD has a moment capacity margin of 16% and is controlled by iteration 3R. Details of the methods used to obtain moments, shears and axial forces from the stress results in the finite element model, and details of the ACI Code evaluation performed on the girders are found in Section 5.2.4.

The results of nondestructive tests (Reference 8) conducted on Girder RE show the presence of 9 very large (i.e., greater than 2") diameter steel bars distributed across the width of the bottom surface of the girder. However, the structural drawings show 18 number 11 bars in each of the two layers distributed across the bottom surface. These results strongly indicate that the main tensile reinforcement at the bottom of the girder is bundled. If the 36 number 11 bars were grouped in 4 bar bundles, 9 very large diameter bars would be detected by a nondestructive examination. This is consistent with the test results and with the way the girder could have been constructed.

Bundled bars require additional embedment length to develop the yield strength of the bar. Thus, the presence of bundled bars could effect the moment capacity at specific sections along the girder. Therefore, in the evaluation of the girders, it was conservatively assumed that the reinforcement was grouped in 4-bar bundles, and evaluations were conducted at critical sections along the span of the girders based on development length requirements for 4 bar bundles. (No splices were assumed since the drawings do not show any.) The evaluation of embedment length effects along the girder span was conducted for load combination "c" of iteration 3R using the results from the more highly stressed Girder RD. Load combination c' of iteration 3R was used because it produced the lowest margin in the girders. The moment capacity diagram for the girder was constructed based on the embedment requirements for 4-bar bundles. This capacity diagram was compared to the moment diagram along the girder span in Figure 5.8A. This figure shows that the minimum capacity occurs at the maximum moment section. Therefore, embedment effects due to bar bundling do not effect girder capacity.

Other results from the nondestructive examination of Girder RE show the presence of low density material in a small pocket located in the bottom few inches of the girder at three to four feet from the face of column E7 (Reference 8). The location of the small pocket within the tension reinforcement region will not effect the shear capacity of Girder RE, however, it can have an effect on the moment capacity at various sections along the girder, because the rebar cannot develop additional forces along the length of the pocket. The location of the pocket is such that it does not effect the development of the bottom layer of reinforcement (18 bars), because this layer is embedded into the column and has already achieved its full development length before the pocket is encountered. However, the pocket could effect the development length required for the second (18 bars) and third (5 bars) layers of reinforcement. To evaluate the potential effect of this low density material on girder capacity, the required development length of the second and third layers of reinforcement was conservatively increased by 16", which is the maximum extent of the low density material along the length of the girder. (The 16" development length extension was in addition to the extension already included in the 4-bar bundle assumption.) This additional 16" development length requirement was included in the evaluation of Girder RE discussed in the previous paragraph. The results in Figure 5.8A and Table 5.3a show that the effect of the small pocket of low density material does not impact the minimum moment capacity margin.

Table 4.7 shows iteration 5 is critical for Girder R6 as load carried by Girders RD and RE in iteration 3R redistributes after they crack in

iteration 4, and as load is shed from the upper elevations of the shield wall due to its elimination as a supporting structure for the SFP in iteration 5. Table 5.3a shows that Girder R6 has a minimum moment capacity margin of 32% and Table 5.2a shows that it has a shear capacity margin of 46%. Table 5.4 shows that iteration 4S produced the lowest moment capacity margin in Column C6 of 77% (Column C6 was also checked for biaxial bending).

Influence of Reduced Dead Load and Downward Seismic Acceleration

As discussed in Section 5.2, evaluations were conducted to determine the influence of reduced dead load and downward seismic acceleration on the capacity margin of the girders. Specifically, the evaluations focused on the effect of (1) reducing dead load to 90% of its value in load combinations which include winter or summer temperature conditions and (2) reducing dead load to 90% of its value together with downward seismic acceleration in load combinations which include winter or summer temperature conditions. The results of these evaluations are summarized in Tables 5.2b and 5.3b for the load combinations shown in Table 5.1a and 5.1b.

These results show that reduced dead load and downward seismic acceleration from load combinations in Table 5.1b increase the capacity margins for shear and moment in the girders. Therefore, load combinations in Table 5.1a, which do not reduce dead load and do not include downward seismic acceleration, produce lower margins in the girders than the load combinations in Table 5.1b. Therefore, only the load combinations in Table 5.1a were used throughout the iteration process to evaluate the girders.

5.2.1.2 Consolidated Fuel Storage - Analysis Case D

The behavior of all SFP structural components in Analysis Case D was similar to their behavior in Analysis Case C. The only difference in response was caused by the pool slab load, which was higher in Analysis Case D. Since Cases C and D are so similar, the lessons learned in the screening and evaluation processes from Analysis Case C were used to more efficiently perform evaluations for Analysis Case D. Knowing the critical load combinations from Analysis Case C and knowing locations of highest responses within the structure, allowed for less information to be tabulated during the screening process. The fact that the only difference between the two analysis cases was the pool load enhanced the checking process by requiring that the observed differences in response be consistent with the difference in load.

The increase in rack loads from consolidated fuel seems high when compared directly to the rack loads from high density fuel, however, the overall response in the primary supporting members due to this increase is relatively small when considered in combination with all other loads. For example, while the total response in Girder RD to all pool slab loads increased by 18% (see iteration 3R in Tables 4.5 and 4.9, i.e., 373-315/315) the total sustained load in Girder RD only increased by 5%. However, as explained in Section 4, this increase must be viewed in the context of the actual margin involved. As Tables 5.5 and 5.6 show, the lowest moment capacity margin was 13% for Girder RD and the lowest shear capacity margin was 0%, also for Girder RD. It should be noted that the code evaluation for shear in deep girders (see Section 5.2.4.1) does not allow an increase in shear capacity due to the presence of an axial compressive force. Therefore, no credit was taken for any increase in shear capacity due to the presence of axial compression. Due to its high margin in Case C, Column C6 was not evaluated for Case D.

5.2.2 Evaluation of the Spent Fuel Pool Slab

5.2.2.1 High Density Fuel Storage - Analysis Case C

The SFP slab was evaluated for shear at all section locations shown in Figure 5.1 and for moment at all locations shown in Figure 5.2. The results of the evaluation are shown at the most severe locations in Tables 5.7a for shear and Table 5.8a for moment. As Table 5.8a shows, the lowest moment capacity margins range between 8 and 13% and result from load combinations which include the winter temperature condition. Load combinations which do not include temperature have margins of 18% or more.

Preliminary evaluations of iteration 4 for load combinations with summer temperature conditions resulted in negative margins. The negative margins were caused by the fact that the cracked properties of the slab were based on the Branson Equation using stress results from a load combination which included the winter temperature condition. This produced relatively low levels of cracking in the negative moment regions of the slab. (In fact, the south section of both the southeast and southwest SFP slabs did not crack.) Unlike the winter temperature gradient, the summer temperature gradient produces thermal moments which add to the negative moments from hydrostatic pressure and rack loads, thus producing considerably more cracking in these regions. To revise the cracked stiffness properties of the slab to reflect the higher levels of cracking which occur, the fully

transformed cracking criteria, discussed in Section 2.3.2, was used for the SFP slab in iteration 4S.

The results from iteration 4S (Reference 27) show substantial margins for moment of 32% or more in all areas of the SFP slab. The lowest margins at all sections result from the load combinations which include the summer temperature condition, even though the winter temperature condition has a higher gradient. This was expected since the summer temperature gradient produces negative moment in the slab which adds to the negative moment produced by the mechanical loads acting on the pool surface.

As Table 5.7a shows, significant margins exist for shear in the SFP slab for all iterations regardless of the cracking criteria used. In all cases the lowest margins occur for load combinations "a" and "a'", which do not contain temperature conditions. The lowest shear capacity margin anywhere in the slab is 30%.

A number of observations can be made from the results shown in Tables 5.7a and 5.8a:

- (1) For the south section of the southeast (SE) slab, load combination "a" in Table 5.8a shows a 50% decrease in moment between iteration 4 (Branson Equation based cracked properties) and iteration 4S (cracked transformed properties). Table 5.8a also shows a significant moment decrease between iterations 3U, 3R and 4, and iteration 4S for load combinations containing temperature. This is expected because of the increased flexibility of the slab in iteration 4S. However, the 50% moment decrease observed for mechanical loads was not expected and requires explanation. The decrease in mechanical load moment in the south section of the SE slab occurred, not because of the overall change in general stiffness properties, but, because of the relative change in directional stiffness properties between iterations 4 and 4S. In iteration 4 the SE slab's flexural stiffness properties were higher in the north-south (i.e., about the Y axis) direction than in the east-west (i.e., about the X axis) direction because the SE slab acts like a one-way slab in the east-west direction. Thus the moments in the east-west direction are higher, and as a consequence, the Branson Equation produces more cracking in the east-west direction. With the north-south direction stiffer than the east-west direction, the north-south direction attracts more moment in iteration 4 than it does in iteration 4S, where the flexural stiffness is the same in both directions.

- (2) The decreased stiffness of the slab in the north-south direction in iteration 4S decreases the net tension along the south section of the southwest (SW) slab. This is shown in Table 5.7a (South of SW) for load combination "a". Progressing from iteration 3R to 4, the tension forces in the north-south direction of the slab increase due to horizontal shear transfer between the negative moment region of Girder RE and RD and the slab. When the slab stiffness is reduced in iteration 4S, the pool slab, acting as the tension flange of the girders, is relieved and sheds load to the positive moment region of Girders RD, RE and R6, and to Column C6. The amount of tensile load relief can be seen by comparing equations "a" in iteration 4 and 4S. Although not shown in Table 5.7a, the same load reduction occurs for the south section of the SE slab. To demonstrate this, Table 5.9 shows that in the South section of the SE slab tensile loads are reduced from 840 kips to 575 kips for equation "a" and from 470 kips to 338 kips for equation "a" between iteration 4 and 4S.
- (3) Tensile membrane stress within the slab contributes to reducing the moment and shear capacities at many locations in the slab. The tensile stresses originate from the thermal expansion of the shield wall and the negative moment bending of Girders RD and RE within the pool region. This behavior was discussed in Section 4.3.1.1.

Evaluation of Slab Reinforcement Development Length

In several of the negative moment regions of the SFP slab the bottom reinforcement is not sufficiently embedded to be considered fully developed to resist positive moment (tension on the bottom of the slab). Since the winter temperature gradient produces positive moment in these regions, an analysis was performed which assumed that the bottom reinforcement was not effective. To implement this effect in the finite element model, adjacent nodes at specific slab boundaries were uncoupled (disconnected) in the displacement direction aligned with the reinforcement (see Section 2.2.3.4). The purpose of the analysis was to determine if the reduction in positive moment capacity in these regions could cause increased moments elsewhere in the slab, and also, to determine the maximum size of the crack which could form in these regions assuming the reinforcement was not effective. As shown in Tables 5.7a and 5.8a, this cracking iteration, 3U, was included in the evaluations of the SFP slab for moment and shear. Table 5.10 shows the size of the approximate gap between the adjacent nodes which were uncoupled. These numbers represent the maximum size



ABB Impell Corporation

of a crack which could exist in these regions assuming that all of the tensile strain accumulates in a single crack. (It should be noted that the gap size is dependent on slab stiffness and would be considerably less if the same analysis were performed for iteration 4S.) Most of the gap sizes are on the order of what could be expected for crack sizes in normal working concrete (i.e., 0.010" or less).

In the regions of the SFP slab where the reinforcement may not develop fully, iteration 3U estimated the upper bound on the size of the crack that might be expected if all of the tensile strain accumulated in a single crack. The size of many of these upper bound cracks is such that they would appear to be hairline cracks and, as such, the structure would show no visible signs of distress. However, considering that the rebar does have some embedment, all of the cracking may not accumulate in a single crack which would make the cracks very difficult to see.

Regardless of the extent to which this rebar can be developed, an evaluation was performed (iteration 3U) assuming no rebar development and it was shown in Tables 5.7a and 5.8a that the SFP slab can adequately sustain its licensed loads.

Influence of Reduced Dead Load and Downward Seismic Accelerations

As discussed in Section 5.2, evaluations were conducted to determine the influence of reduced dead load and downward seismic acceleration on the capacity margin of the SFP slabs. Specifically, evaluations focused on the effect of (1) reducing the dead load to 90% of its value in load combinations which include winter or summer temperature conditions and (2) reducing dead load to 90% of its value together with downward seismic acceleration in load combinations which include winter or summer temperature conditions. The results of these evaluations are summarized in Tables 5.7b and 5.8b for the load combinations shown in Tables 5.1a and 5.1b. Based on the results the following conclusions can be made:

1. Table 5.7b shows that reduced dead load and downward seismic acceleration increases or leaves unchanged the capacity margins for shear in the SFP slab.
2. Table 5.8b shows that reduced dead load and downward seismic acceleration decreases the moment capacity margin in the middle of the southeast and southwest SFP slabs only for load combinations with summer temperature condition. However, the minimum moment capacity margins in the middle of the SFP slabs are produced by load combinations with the winter temperature condition for which the

moment capacity margin increases when dead load is reduced and seismic acceleration is downward. Thus the minimum moment capacity margins produced by the winter temperature condition load combinations are lower than the reduced moment capacity margins produced by the summer temperature condition load combinations.

3. Table 5.8b shows that reduced dead load and downward seismic acceleration decreased the moment capacity margin on the north, south, east and west edges of the southeast and southwest SFP slabs only for load combinations with the winter temperature condition. However, the minimum moment capacity margin on the edges of the SFP slabs are produced by load combinations with the summer temperature condition for which the moment capacity margin increases when dead load is reduced and seismic acceleration is downward. Thus the minimum moment capacity margins produced by the summer temperature condition load combinations are lower than the reduced moment capacity margins produced by the winter temperature condition load combinations.
4. The results presented in 1, 2 and 3 above demonstrate that the load combinations in Table 5.1a, which do not consider reduced dead load or downward seismic acceleration, produce lower minimum capacity margins for the SFP slab than load combinations in Table 5.1b which reduce dead load and/or apply downward seismic acceleration. Therefore, the use of load combinations in Table 5.1a are sufficient for the evaluation of the SFP slab since they produce minimum margins.

5.2.2.2 Consolidated Fuel Storage - Analysis Case D

The same behavior already discussed for Analysis Case C can also be observed in Tables 5.11 and 5.12 for Analysis Case D. As in Case C, the moment capacity margins for the slab for Case D iteration 4S are high for all load combinations (Reference 32). The lowest moment capacity margin for iteration 4S is 36% which occurs in the west section of the SE slab and is again, like Case C, controlled by the summer temperature condition.

The shear capacity margin is controlled by mechanical loads. The lowest margin for iteration 4S is 14% and occurs at the east section of the SW slab for load combination "a".

moment capacity margin increases when dead load is reduced and seismic acceleration is downward. Thus the minimum moment capacity margins produced by the winter temperature condition load combinations are lower than the reduced moment capacity margins produced by the summer temperature condition load combinations.

3. Table 5.8b shows that reduced dead load and downward seismic acceleration decreased the moment capacity margin on the north, south, east and west edges of the southeast and southwest SFP slabs only for load combinations with the winter temperature condition. However, the minimum moment capacity margin on the edges of the SFP slabs are produced by load combinations with the summer temperature condition for which the moment capacity margin increases when dead load is reduced and seismic acceleration is downward. Thus the minimum moment capacity margins produced by the summer temperature condition load combinations are lower than the reduced moment capacity margins produced by the winter temperature condition load combinations.
4. The results presented in 1, 2 and 3 above demonstrate that the load combinations in Table 5.1a, which do not consider reduced dead load or downward seismic acceleration, produce lower minimum capacity margins for the SFP slab than load combinations in Table 5.1b which reduce dead load and/or apply downward seismic acceleration. Therefore, the use of load combinations in Table 5.1a are sufficient for the evaluation of the SFP slab since they produce minimum margins.

5.2.2.2 Consolidated Fuel Storage - Analysis Case D

The same behavior already discussed for Analysis Case C can also be observed in Tables 5.11 and 5.12 for Analysis Case D. As in Case C, the moment capacity margins for the slab for Case D iteration 4S are high for all load combinations (Reference 32). The lowest moment capacity margin for iteration 4S is 36% which occurs in the west section of the SE slab and is again, like Case C, controlled by the summer temperature condition.

The shear capacity margin is controlled by mechanical loads. The lowest margin for iteration 4S is 14% and occurs at the east section of the SW slab for load combination "a".

5.2.3 Evaluation of the SFP Walls

5.2.3.1 High Density Fuel Storage - Analysis Case C

A preliminary evaluation of the walls of the SFP was performed for iteration 4. The results showed that the moments from load combinations containing temperature conditions exceeded the moment capacity at several sections. Further investigation revealed that the moment capacity of the wall sections was actually less than the cracking moment. This meant that a cracked concrete model based on the Branson Equation, which uses the cracking moment as the starting point to initiate stiffness reductions, would result in a significant overestimate of cracked member stiffness. This led to thermal moments which were higher than the section could physically develop. Therefore, to achieve a cracked state more consistent with the actual situation which exists after cracking occurs, the cracked properties of the walls were set to the cracked transformed values in accordance with the criteria of Section 2.3.2. The resulting cracked stiffness properties for the walls were used in iteration 4S.

Tables 5.13 and 5.14 show the results of the SFP wall evaluations. The minimum moment capacity margin is 7% and occurs in the vertical section (i.e., moment about the Z axis) at the north end of the west wall. The 7% margin is controlled by sustained loads in load combination "a". In all cases axial tension plays a significant role in reducing moment capacity. In contrast to the moment results, the shear capacity margin everywhere is quite high with the lowest margin of 37% also occurring in the north section of the west wall. The upper portion of the west wall between elevations 95' and 119' tapers to a thickness of 4'-6". This is the thinnest region of any of the SFP walls and is where the lowest margins occur.

5.2.3.2 Consolidated Fuel Storage - Analysis Case D

No evaluations of the SFP walls were performed for Analysis Case D because (1) the hydrostatic and hydrodynamic loads on the walls from the pool did not change from Case C to Case D and (2) the lowest margins occurred in the upper regions of the walls where loads from the slab have little influence.

5.2.4 Example Code Check Evaluations

The output of the finite element analysis of the SFP model consists of nodal stresses and forces. Typically two or more solid elements are used through the thickness or depth of a member in the model. Nodal stress or force data by itself cannot be used to evaluate a structural component for compliance with the ACI Code (Reference 4). These stresses must first be translated into moments, shears and axial forces acting on a particular cross section in order to be used in a code evaluation. The intent of this section is to show step-by-step how raw data from the finite element model was translated into the information necessary to perform a code evaluation and how the code evaluation was performed.

In the sections which follow, typical moment and shear evaluations are performed for Girder RE and the SFP slab. For completeness ANSYS routine and filename terminology and actual filenames are used. For load cases (load steps) in a particular iteration analysis output (ANSYS File 12) refer to Section 4.3.2. For a listing of all analysis input files refer to Appendix A.

Since the code evaluation of the SFP walls is similar to the code evaluation for the SFP slab, it is not included as a specific example.

5.2.4.1 Girder RE Evaluation Example

Girder RE is evaluated for Analysis Case C, iteration 3R, load combination "c" (see Reference 24).

The results of ANSYS iteration 3R contained in output File 12 (CCI3RB.F12) and the File 12 (CCI3SS.F12) for the seismic run 3SS were placed in the same directory. File CCI3RB.F12 was renamed to FILE12.DAT and File CCI3SS.F12 to FILE40.DAT. Using ANSYS Post 27 and input file ECI3RLC.2F5, the unfactored load steps of iteration 3R and seismic run 3SS were added with the appropriate load factors applied to form all of the necessary load combinations. The load combinations were stored in file ECI3RLC.F10 in which load step 3 is load combination "c"

Using input file ECI3RLC.1F5, which read file ECI3RLC.F10, the elements pertaining to Girder RE between the north face of the SFP wall and column E7 were selected (see Figure 5.3). Figures 5.4 and 5.5 show the node numbers on the east and west faces of the selected portion of Girder RE. To this point the evaluation processes for both the moment and shear are the same. Beyond this point the evaluation processes are distinctly

ABB Impell Corporation

different for each and in the paragraphs below each is discussed separately.

Moment Evaluation

The bending stresses (SX) taken through a vertical section of each face at the location of maximum moment (see Section ME in Figure 5.1) are plotted in Figures 5.6 and 5.7. In Figure 5.6 the stresses are plotted from node 930 to node 210 and in Figure 5.7 from node 940 to node 310. These figures show that the actual bending stress distribution is nonlinear through the depth, particularly in the compression zone. This nonlinear bending stress distribution is integrated through the depth using the ANSYS Program (PLSECT Command) to obtain an equivalent linear stress distribution on the section. (The linear and nonlinear stress distributions are equivalent in the sense that they both produce the same resulting axial force and bending moment when integrated through the section.) These stresses are referred to as the "linearized stresses," and both the linear and constant (membrane) parts are given. The linearized stresses at the extreme fibers (i.e., the end point nodes) for all stress components are printed in Table 5.15 and 5.16 taken from output file ECI3RLCS.1F6.

Shown below are the top and bottom linearized bending stresses (SX) on the east and west faces (with the associated node in parentheses) as well as the average values at the top and bottom.

	East Face	West Face	Average
top	-1774(930)	-864(940)	-1319
bottom	1158(210)	1430(310)	1294

(Note: The difference between the stresses on the east and west faces shows that weak axis bending is occurring. This is discussed at the end of the Section.)

Using the computer program RCBEAM (Reference 31), the average linearized stresses, reinforcing details, and girder section properties are entered. From the linearized stresses and cross section geometry the program computes the moment and axial force acting on the cross section. The girder properties and reinforcing details entered are given below:

$$\begin{aligned}
 h &= 108" \\
 b &= 60" \\
 f_c &= 3,000 \text{ psi} \\
 f_y &= 40,000 \text{ psi}
 \end{aligned}$$

ABB Impell Corporation

<u>Rebar</u>	<u>Area</u>	<u>Distance from Comp. Face</u>
18#11 (1st layer)	$A_{s1} = 28.08 \text{ in}^2$	$d_1 = 104.5 \text{ in}$
18#11 (2nd layer)	$A_{s2} = 28.08 \text{ in}^2$	$d_2 = 101.7 \text{ in}$
5#11 (3rd layer)	$A_{s3} = 7.08 \text{ in}^2$	$d_3 = 98.9 \text{ in}$
18#11 (4th layer)	$A_{s4} = 28.08 \text{ in}^2$	$d_4 = 3.5 \text{ in}$

The output from the P.CBEAM program is given in Table 5.17 and summarized below.

Factored Moment = 12699. ft-kips
 Factored Axial Load = 81 kips (compression)

These values are plotted on the interaction diagram given in Figure 5.8.

From the interaction curve of Table 5.17, the Design Moment Capacity at 81 kips compressions is, $M = 18935 \text{ ft-kips}$. Therefore, the moment capacity margin of Girder RE is $100(18935-12699)/18935 = 33\%$. The results given above are those shown in Reference 24.

As mentioned earlier, the stress results for each face of Girder RE show the presence of weak axis bending. This bending can be easily seen from the displacement plot viewed from above the girders and shield wall shown in Figure 5.10 (See Figure 5.9 for reference). This weak axis bending is caused by the winter temperature condition and the unrestrained east-west thermal movement which occurs between the SFP north wall and the Reactor Building exterior wall due to the absence (reduced stiffness) of the slab at elevation 75'. The effect of reducing the stiffness of the floor slab at elevation 75' is clearly seen in Table 5.18. In iteration 3R the top and bottom stress on the east and west faces for the concrete dead load case are comparable in magnitude, where as for the winter temperature condition they are quite different and show the presence of significant weak axis bending.

With the slab at full stiffness this relative thermal growth is restrained by the shear stiffness of the slab. This can also be seen in Table 5.18 for iteration 2. For this iteration the concrete dead load stresses at the top and bottom of each face are almost the same, and the difference between the east and west face thermal stresses has been greatly reduced from what they were in iteration 3R. The restraint provided by the floor slab at elevation 75' can be seen from the inplane shear stresses (SXY) in Figure

5.11 for this same load combination in iteration 2 (see Figures 5.97 and 5.98 for reference). This figure also shows the high shear stress in the slab between the west SFP wall and the Reactor Building exterior wall due to the restraint of relative thermal growth in the north-south direction. The same inplane shear stresses are also shown in Figures 5.12 and 5.13 for iteration 0. The principal tensile stresses and predicted cracking of the floor slab at elevation 75' are discussed further in Section 5.3.3. For completeness the weak axis bending occurring in iteration 3R, although fictitious, was nonetheless evaluated and shown to be well within code limits.

Shear Evaluation

Girder RE was evaluated for shear in accordance with the Code provisions for deep flexural members found in Section 11.8 of ACI 349-80. The critical section for shear evaluation is located mid-way between the face of the supporting column and the north face of the SFP wall (see Section SE in Figure 5.1). Since the critical section location occurs half-way between nodal planes, the stress results from the adjacent nodal planes were averaged at the critical section. On the east face linearized stresses were determined at sections through nodes 282 and 212, and nodes 283 and 213 (see Figure 5.4), and on the west face through nodes 382 and 312, and nodes 383 and 313 (see Figure 5.5). The results are shown in Tables 5.19 from output file ECI3RLCS.1F6. The specific stress results needed from Table 5.19, as well as the final average values used, are shown in Table 5.20.

The section properties of the girder and the values of the ACI Code defined variables are given below:

$$h = 108", b_w = 60", d = 102.5",$$

$$\text{Section Modulus, } S = 116,620 \text{ in}^3,$$

$$A_g = b_w h = 6480 \text{ in}^2,$$

$$\rho_w = A_s / b_w h = 92.04 / 60 \times 102.5 = 0.0104,$$

$$\text{and } l_n = 117".$$

The span-to-depth ratio

$$l_n / d = 1.14 < 2.0,$$

ABB Impell Corporation

therefore the maximum nominal shear strength shall not be greater than

$$V_n(\max) = 8\sqrt{f'_c} b_w d = 2695 \text{ kips.}$$

From Table 5.20 the average bending stress at the top and bottom of the critical section are -744 psi and 696 psi, respectively. The average shear stress is 238 psi. The factored moment, M_u , axial load, P_u , and Shear, V_u , are converted from stresses as follows:

$$\begin{aligned} M_u &= (\text{Half the absolute sum of the top and bottom stresses})(\text{Section Modulus}), \\ P_u &= (\text{Half the algebraic sum of the top and bottom stresses})(\text{Gross Area}), \\ V_u &= (\text{Average shear stress})(\text{Gross Area}). \end{aligned}$$

Substituting into the above expressions gives,

$$M_u = (0.744 + 0.696)(116640)/2 = 83,980 \text{ in-kips,}$$

$$P_u = (-0.744 + 0.696)(6480)/2 = 156 \text{ kips (compression).}$$

$$V_u = (0.238)(6480) = 1,542 \text{ kips.}$$

The axial compressive force is taken as positive to comply with ACI Code convention.

The concrete contribution to shear capacity, V_c , is calculated from Code Equation 11-29

$$V_c = (3.5 - 2.5M_u/V_u d)(1.9\sqrt{f'_c} + 2500 \rho_w V_u d/M_u) b_w d$$

and results in

$$V_c = 2,041 \text{ kips.}$$

The expression

$$(3.5 - 2.5 M_u/V_u d) = 2.17$$

is less than the Code allowable maximum value of 2.5. In addition the Code requires that:

$$V_c \leq 6\sqrt{f'_c} b_w d = 2,021 \text{ kips.}$$

ABB Impell Corporation

Therefore, the concrete contribution to shear capacity at the critical section is $V_c = 2,021$ kips.

The shear reinforcement contribution to shear capacity, V_s , is calculated from Code Equation 11-30:

$$V_s = \left\{ \left(\frac{A_v}{S} \right) \left(\frac{1 + l_w/d}{12} \right) + \left(\frac{A_{vt}}{S_2} \right) \left(\frac{11 - l_w/d}{12} \right) \right\} f_y d,$$

where:

$$A_v = 2.2 \text{ in}^2 \text{ (5-#6 stirrups at 10")}$$

$$S = 10 \text{ in}$$

$$A_{vt} = 1.58 \text{ in}^2 \text{ (2-#8 bars, slab reinforcement neglected)}$$

$$S_2 = 25.7 \text{ in (5-#8 bars in each face conservatively spread over the total depth; bars are actually spaced at 10" in the girder web.)}$$

$$f_y = 40 \text{ ksi}$$

Substituting the above values in ACI Code Equation 11-30 gives:

$$V_s = 368 \text{ kips.}$$

The total shear capacity is the sum of the concrete and reinforcing steel contribution which is:

$$V_n = V_c + V_s = 2021 + 368 = 2,389 \text{ kip.}$$

This is less than the Code allowable maximum value of

$$V_n(\text{max}) = 2695 \text{ kips.}$$

Therefore the design shear capacity from ACI Code Equation 11-1 is $\phi V_n = (0.85)(2389) = 2,031$ kips, which exceeds the factored shear applied at the critical section of 1542 kips. The shear capacity margin of Girder RE is:

$$100(2031 - 1542) / 2031 = 24\%.$$

This is the value shown in Reference 24.

5.2.4.2 Spent Fuel Pool Slab Evaluation Example

In this section, the SFP slab is evaluated for Analysis Case C, iteration 3R. Moment is evaluated for load combination "c" and shear for load combination "a" (see Tables 5.7a and 5.8a). Following the same procedure described in Section 5.2.4.1, the factored load combinations for iteration 3R were formed. Load combinations "a" and "c" are load steps 6 and 7 respectively on ANSYS file ECI3RLC.F10.

Moment Evaluation

The solid elements representing the SFP slab (Type 7, Section 2.2.2.2) were selected by the ANSYS Post 1 input file ECI3RLCS.1F5, which computed linearized stresses in the X and Y directions (SX and SY) at the top (wet surface) and bottom (dry surface) of the SFP slab at all locations shown in Figure 5.2. The results, taken from output file ECI3RLC.1F6, are tabulated in Reference 24. Table 5.21 is an example of this tabulation at four of the node locations shown in Figure 5.2.

The SFP slab has #11's at 9" in both the east-west and north-south directions. For a 9" wide section of slab the program RCBEAM was used to create the design capacity moment/axial load interaction diagram shown in Figure 5.14 (see Table 5.22 for the specific numerical values). Based on the interaction diagram for this section a stress screening criteria was developed to scan the tabulated data to determine the most severe cases. From the interaction diagram (see also Table 5.22) it can be seen that for no axial load the section has a design strength in pure bending of 227 ft-kips, which is equivalent to a linear bending stress distribution of 622 psi acting on a 9"x54" section of slab. At a moment of 227 ft-kips, the compressive load capacity is 830 kips which is equivalent to a uniform compressive stress of 1708 psi. For no moment, the section has a capacity of 112 kips in tension and 949 kips in compression. These are equivalent to 231 psi in tension and 1953 psi in compression.

Based on the above results, slab sections which are in compression are satisfactory if the following two conditions are satisfied: (1) half of the algebraic sum (membrane stress) is less than 1708 psi, and (2) half of the absolute sum (bending stress) is less than 622 psi. For sections that were in net tension, three evenly spaced points on the tension portion of the interaction diagram (e.g., Figure 5.14) were chosen and the resulting moment and axial tension converted to three sets of equivalent membrane and bending stress pairs. Any tabulated stress data having membrane and bending stress values less than any one of the three screening criteria

stress pairs was satisfactory, since this meant that the stress state in the slab was within the design strength interaction diagram.

Stress data that came close to the screening values were flagged and checked using the RCBEAM program to determine actual margins. One such location which was flagged occurred at surface nodes 6398 and 6098 for stresses in the X-direction (see Table 5.21). The actual evaluation for this location, performed on the RCBEAM Program, is shown in Table 5.22. The results show that

the factored moment, $M_u = 229$ ft-kips,

the factored load, $N_u = 17$ kips (compression),

and that the design moment capacity is 250 ft-kips at this level of axial compression. At this location the moment capacity margin is:

$$100(250-229)/250 = 8\%.$$

These results are shown in Table 5.8a.

Shear Evaluation

In this section the southwest slab of the SFP (See Figure 2.1) is evaluated for the factored shear forces of load combination "a" at section E-E, also referred to as the "East Section of the SW Slab." (See Figure 5.1 and see Reference 4, Section 11.11.1.1 or Reference 9, Fourth Edition, pages 662 to 665 for an interpretation of section width for shear evaluation of slabs).

To determine the forces acting on the cross section, the southwest slab, cut at Section E-E, was selected using the ANSYS Post 1 input file, and the nodes along the section were isolated. The nodal forces were then summed in the vertical and axial directions to determine the resultant shear and axial force acting on the section. (The nodal line through which section E-E is taken is slightly less than a distance "d" from the west face of Girder RD, which results in slightly higher shear forces.) The factored shear and axial load are 771 kips and 80 kips (compression) respectively. These results can be seen in Table 5.23 from the ANSYS Post 1 output file ECI3RLCS.1F6.

ABB Impell Corporation

The geometric properties of section E-E are:

$$\begin{aligned} h &= 54", \\ b_w &= 243", \\ d &= 50.8", \end{aligned}$$

also,

$$A_g = b_w h = 13,122 \text{ in}^2, \text{ and } \sqrt{f'_c} = 54.77 \text{ psi.}$$

Shear is evaluated in accordance with the ACI Code Equation 11-4 of Section 11.3. The design shear strength of the section with axial compression acting is:

$$\phi V_c = \phi \{ 2(1 + N_u / 2000 A_g) \sqrt{f'_c} b_w d \}$$

where N_u is the axial compressive load. Substituting into the above equation gives:

$$\phi V_c = 1,153 \text{ kips}$$

which is also the design shear capacity of the section since shear reinforcement is not present. Thus, the shear capacity margin for the east section of the SW slab for load combination a of iteration 3R is

$$100(1153 - 771) / 1153 = 33\%.$$

This is the same result shown in Table 5.7a.

The SFP slab was also evaluated for shear in accordance with the provisions of ACI 349 Section 11.11.1.2 for two-way action. The shear evaluation in accordance with Section 11.11.1.2 of the Code produced significantly higher margins than the shear evaluation of Section 11.11.1.1. In addition, as part of the screening evaluation for shear in the SFP slab, the minimum shear capacity, corresponding to the maximum tensile stress on any of the critical sections, was found to exceed the applied shear on any section in all cases.

5.3 Correlation of Analysis Results with Observed Cracking

Prior to developing the SFP finite element model, GPUN personnel took the project team on an inspection tour of the Reactor Building and Spent Fuel Pool. The primary purpose of the inspection was to provide a clear understanding of the geometry of the SFP and Reactor Building as represented on the structural drawings from which the finite element model would be constructed. Another purpose of the inspection tour was to observe any significant visible cracks which had occurred in the SFP and primary supporting members. The project team's inspection included all accessible areas on elevations 51', 75', 95' and 119' in the vicinity of the SFP. The team observed cracks in the shield wall above elevation 95' and the SFP east and west walls. Vertical cracks were noticed at the intersection of the south SFP wall and the shield wall on both the east and west sides above elevation 95'. Cracks were also noticed in the floor slabs on elevations 75' and 95' on the north side of the SFP and on elevation 119' near the southeast and southwest corners of the SFP cavity. (Cracks were not observed at the northeast and northwest corners of the SFP at Elevation 119 because the floor in those areas was hidden from view by a paper covering.) The crack beneath the floor slab at elevation 75' and the cracks in Girder RE were closely inspected from scaffolding which had been erected to perform a nondestructive examination of the cracks (Reference 8).

All of the concrete surfaces inspected appeared to be heavily painted. As a result it is safe to say that minor hairline cracks which would be visible on unpainted concrete were probably not observed. In addition those cracks which were observed through the paint probably cycle in size with significant changes in the relative temperature distributions of the shield wall, SFP, and exterior Reactor Building walls. This will become clearer in the following sections.

Before beginning the discussions of crack prediction there are two topics which generally effect all of the discussions. The first is the surface stress level at which cracking should occur. This is generally considered to be equal to the modulus of rupture which is equal to 7.5 times the square root of the concrete compressive strength (See Section 2.3.1). While the design compressive strength is 3000 psi the insitu strength based on limited tests of Girder RE (Reference 8) is approximately 5000 psi. However, these higher insitu strengths may not consistently apply to all of the concrete in the Reactor Building. Therefore, for the purpose of crack prediction, cracking is expected to occur when surface stress levels are above 410 psi, which corresponds to a concrete strength of about 3000 psi.

Second, since cracks occur perpendicular to the direction of the maximum tensile stresses on the surface of the concrete, figures showing maximum tensile stress trajectories are used to predict crack direction. It is important to keep in mind that the trajectories in the figures are not shown at the element surface, but at the centroid of the element nearest the surface. Therefore, the number of elements

which occur through the width or thickness of a structural member will determine the depth from the observed surface at which the trajectory arrow is showing the direction of the maximum tensile stress. For example, this means that in most of the SFP walls the stress trajectory is showing the direction of the maximum tensile stress 18" below the surface, since the six foot wall has two elements through its thickness. Whenever either membrane or bending stresses dominate the response of a component the stress trajectories give a very accurate representation of maximum tensile stress direction. However, when bending stresses through the thickness of a structural component are comparable to the membrane stresses, the trajectories observed give a less accurate representation of maximum tensile stress directions on the surface. In general it is believed that most of the tensile stress trajectories shown in the figures approximate the actual surface trajectories.

5.3.1 Crack Beneath the SFP North Wall in the Floor Slab at Elevation 75'

At elevation 75', a three-foot thick floor slab spans between Girders RD and RE in the east-west direction and between the SFP north wall and the Reactor Building exterior wall, R7, in the north-south direction. At the bottom of this slab, just beneath the north wall of the SFP, there is a crack running in the east-west direction at approximately the location shown in Figure 5.15 (see Section 4.2.2). Physical examination of the crack (Reference 8) showed that the depth varied from 2.4' to 3.0' and that the crack width at the bottom of the slab varied from 0.040" midway between Girders RD and RE to about 0.003" near each of the girders (See Drawing No. 7 of Reference 8).

The tensile stress distribution at the bottom of the slab is shown in Figure 5.16 for load combination "a" of iteration 2 and in Figure 5.17 for load combination "b" of iteration 2. Both of these combinations represent service load conditions and give approximately the same stress results for the slab. Section A-A in Figure 5.15 passes through the crack plane. Taking this same section through the slab and girders of the finite element model and viewing it from the southeast results in the plot shown in Figure 5.18. The stress distribution along the entire face of the crack for the unfactored combination of dead load, live load, and winter temperature is shown in Figure 5.19. By better defining the stress range of interest, the contour plot of Figure 5.20 shows that the tensile stress level in the slab at the crack is about 500 psi under service load conditions. A better view of the stress distribution through the depth of the slab can be seen in Figure 5.22 which corresponds to Section B-B in Figure 5.15 (see also the geometry plot in Figure 5.21). Because of nodal stress averaging, the maximum stress in the slab shown in Figure 5.22 does not appear to occur under the north face of the north wall; however, by viewing only the slab

portion of the section, the nodal stress averaging with the wall elements is eliminated and a maximum stress of 482 psi is observed to occur below the face of the north wall in Figure 5.23. Figures 5.20 and 5.23 show that significant positive moment (i.e., tension at the bottom of the slab) exists at the section where the crack occurred, and that the stresses are sufficiently high (above 410 psi) to have produced cracking.

There are three cross-section details which show the reinforcement at the location where the slab at elevation 75' connects to the base of the SFP walls. They are Section P-P along the east wall, Section S-S along the west wall, and Section T-T along the north wall (Reference 29). The essential features of Section P-P are shown in Figure 5.24. In this section view, the top and bottom reinforcement have sufficient embedment where the slab joins the north wall to resist both positive and negative moment. The essential features of Section S-S and T-T are represented in Figure 5.25 which shows that sufficient embedment has been provided for the negative (top) reinforcement, but not for the positive (bottom) reinforcement.

Based on the above discussion, there are two reasons why a single, larger crack exists beneath the slab at elevation 75': (1) there is sufficient positive moment on the cross-section to cause cracking, and (2) all the positive moment reinforcement at the section is terminated just beyond the south face of the slab. Figure 5.25 (Section T-T) is the reinforcing detail that was used to join the slab to the north wall of the SFP. Since all of the positive reinforcement terminates in the maximum positive moment region, a stress concentration is created at the material discontinuity where the reinforcement ends. This can cause premature concrete cracking at stress levels well below the nominal cracking stress (although, as already discussed, analysis results show that the nominal stress is sufficiently high to cause cracking). Once the concrete cracks, the lack of continuous reinforcement through the positive moment region allows the concrete tensile strains to accumulate in a single, large crack rather than be distributed among several smaller cracks. Thus, it is expected that a single, large crack would occur near the termination of the bottom reinforcement as shown in Figure 5.26.

It is important to mention that this crack does not jeopardize the integrity of the SFP. In fact, cracking iteration 3R was developed specifically to address this issue, to ensure that no reliance would be placed on the floor slab at elevation 75' to carry any SFP load and to ensure that all loads which could be carried by the slab would be carried by the primary load carrying members of the SFP.

Figures 5.16, 5.17, 5.19 and 5.20 show that the slab between Girders RD and Column Line RC is more highly stressed than the slab between Girder RD and RE. This is consistent with the vertical displacement contours shown in Figure 5.27. Based on this, and knowing that all portions of the slab along the north wall were constructed in the same way, it must be concluded that a similar crack exists beneath the slab between Girder RD and Column Line RC. Since this area is not accessible, the existence of a crack has not been confirmed.

Figures 5.19 and 5.20 also show that the portion of the slab west of Girder RE is stressed to the same level as the slab between Girders RD and RE. However, large cracks in this region have not been observed. This may be due to the fact that the slab reinforcement was detailed in accordance with Section P-P due to the presence of local beam 3B33 (Reference 2).

5.3.2 Cracks in the Shield Wall and Pool Walls

The cracking of the shield wall and the east and west walls of the SFP is described using plots of maximum principal stress contours and plots of principal stress trajectories (directions) which are presented in pairs. The direction of a crack at a specific location is perpendicular to the direction of the arrows on the plots showing principal stress trajectories. In some cases these figures are augmented by figures showing the expected crack patterns for a particular iteration and load combination.

Two views of the SFP are provided: (1) the west view in Figure 5.28 shows the shield wall above elevation 53', Girder RE, and the west wall of the SFP, and (2) the east view in Figure 5.29 shows the shield wall above elevation 53', Girder RD, and the east wall of the SFP. The relevant cracking iterations are iteration 0 (no cracking anywhere) and iteration 1 (floor slabs at elevations 119', 95', and 75' completely cracked except for the floor slab at elevation 75' adjacent to the north and west walls of the SFP) since the shield wall and SFP walls are not cracked in these iterations and therefore the stresses that are calculated in these iterations are expected to cause cracking. The caption on each photograph in Figures 5.30 through 5.53 describes the Case C unfactored load combinations for which the stress results apply. "DL" represents dead load and includes concrete dead load, hydrostatic pool load and high density fuel racks, "LL" represents floor live load, "T_w" represents the winter temperature condition, and "T_s" represents the summer temperature condition.

Before discussing the shield wall and SFP walls separately, it should be mentioned that, except for a few very localized areas, Figures 5.30, 5.36, 5.42 and 5.48 show that there is no cracking in the shield wall or the east and west SFP walls due to dead load plus live load in either iteration 0 or 1. As discussed earlier in Section 4.2.1 and as will be observed in the following discussions, cracking is always dominated by load combinations containing a temperature condition.

Shield Wall

In iteration 0 for service load with winter temperature condition, Figure 5.32 and 5.33 show that the conical region of the shield wall between elevations 53' and 75' should contain vertical cracks. In fact, all figures from 5.32 to 5.53, which include a temperature condition, show that vertical cracking should occur on the east, west and north faces of the conical region of the shield wall. This vertical cracking pattern is presented in Figures 5.83 and 5.84 which show the predicted cracking patterns on the west and east faces of the shield wall for stress contours and trajectories corresponding to Figures 5.38 and 5.39 and Figures 5.50 and 5.51 respectively.

At the west portion of the shield wall between elevations 75' and 119', a comparison of Figures 5.32, 5.34, 5.36 and 5.38 show that, although cracking is predicted for the summer temperature condition, the winter temperature condition dominates. Between these elevations, Figures 5.33 and 5.39 show very similar cracking patterns for iterations 0 and 1 except that for iteration 1 cracks are more vertical at the junction of the south SFP wall with the west shield wall. Cracks near elevation 119' are very nearly vertical but begin to turn diagonally as they proceed down the wall to elevation 95'. Between elevations 95' and 75' the cracks farthest from the SFP have a nearly vertical orientation while cracks closest to the SFP, near the shield wall and pool wall intersection, are vertical at 119', turn diagonal at 95', and become nearly horizontal toward elevation 75'. The basic similarity in stress trajectories for iterations 0 and 1 means that it is expected that the same cracking patterns will exist regardless of the extent to which the floor slabs restrain the shield wall and SFP. As further discussions will show, the floor slabs on the west side of the shield wall and SFP provide relatively little restraint compared to the floor slabs on the east side. This can be seen in the deformed shape and stress contour plot of the floor slab at elevation 119' shown in Figure 4.5.

On the east portion of the shield wall, cracking is again dominated by the winter temperature condition. Unlike the west shield wall, however, crack orientation changes considerably between iterations 0 and 1, as shown in Figures 5.45 and 5.51. After the floors crack in iteration 1, the diagonal

cracks turn sharply toward the vertical from elevations 119' to 95' and then from nearly horizontal to almost vertical between elevations 95' and 75'. The great difference in stress trajectories between iterations 0 and 1 means that the orientation of cracks in the east shield wall will be dependent on the extent to which the floor slabs restrain the shield wall and SFP.

To clearly explain this difference in response between iterations 0 and 1, and to aid in the discussions which follow, a number of figures are required. Rather than breaking-up the discussion of the phenomenon with a concurrent explanation of the figures, most of the figures cited in the discussion are introduced here, accompanied by a brief explanation. Almost all of the descriptive information can be found in the figure itself, either in the title below it or in the ANSYS documentation block to the right. Figure 5.54 is a geometry plot of the shield wall and SFP viewed from the east, and Figure 5.55 is a cross-section of the shield wall and SFP taken at elevation 108'. All of the figures discussed below are derived from one of these two geometry plots. In addition, all figures pertain to the winter temperature condition only. Figures 5.56 and 5.57 show the principal tensile stress contours (SIG1) for iterations 0 and 1. Figures 5.58 and 5.59 show stresses in the vertical (SZ) direction for iterations 0 and 1, and Figures 5.60 and 5.61 show the circumferential stresses (SY in cylindrical coordinates) in the shield wall. Figures 5.62 and 5.63 show the principal tensile stresses (SIG1), Figures 5.64 and 5.65 show the circumferential stresses in the shield wall, and Figures 5.66 and 5.67 show deformed and undeformed displacement plots all for iterations 0 and 1, respectively.

Two important points need to be made concerning these results. First, the cracks become more vertical between iteration 0 and 1 in both the east and west shield walls as the floor slab stiffness is reduced with a much greater change occurring in the east shield wall. Second, in both the east and west shield walls, the thermal stresses increase on the surface of the shield wall from iteration 0 to iteration 1 which can be seen in the increase in principal stresses from Figures 5.56 to 5.57. Figures 5.58 and 5.59 show that the surface stress increase is not due to vertical stresses, but rather, is due to an increase in circumferential stresses, as observed in Figures 5.60 and 5.61. This is normally not expected, because as restraint of thermal deformation is released by the cracking of the floor slabs, thermal stresses would be expected to decrease. Instead, the shield wall surface stresses increase significantly.

This response is entirely related to the temperature condition. As the membrane stiffness of the floors is reduced in iteration 1, the shield wall expands, relieving most of the membrane thermal stress in the shield wall. This can best be seen in the linearized circumferential stress plots shown in Figures 5.68 and 5.69 for a nodal line in the east shield wall at elevation 108'. These plots show that the membrane compressive stress was reduced from approximately 350 psi through the shield wall to about 50 psi, while exterior surface bending stresses increased from 1000 psi to 1700 psi.

The greatest expansion in the shield wall and SFP occurs in the SFP south wall at the fuel transfer opening since this region provides the least restraint to thermal expansion. The east-west expansion of the SFP south wall rotates the southeast and southwest corners of the SFP because of the restraint provided by the SFP east and west walls. Figures 5.62 and 5.63 show the change in principal stresses and Figures 5.64 and 5.65 show the change in both the magnitude and the distribution of circumferential stresses in the shield wall as thermal expansion occurs and larger bending stresses are introduced into the shield wall near the intersection with the SFP south wall. Because the east wall is thicker than the west SFP wall, it provides more rotational restraint. In addition, because there is significantly less floor on the west side (and therefore less stiffness) less change occurs on the west side between iteration 0 and 1. This can be observed in the deformation plots of Figures 5.66 and 5.67. The restraint provided by the east SFP wall, rotates the southeast corner counterclockwise, thus increasing the circumferential bending stress in the east shield wall which results in an increase in the circumferential tensile stress on the shield wall exterior surface. Again, this is clearly seen in Figures 5.64 and 5.65. Since the circumferential tensile stresses now dominate, the tensile stress trajectories turn to the horizontal producing nearly vertical cracks in the shield wall.

Spent Fuel Pool Walls

Load combinations which include the summer temperature condition do not produce cracks on the exterior surface of the SFP east, west or north walls in either iteration 0 or iteration 1. This can be seen from Figures 5.34, 5.40, 5.46 and 5.52 for the east and west walls of the SFP.

Figures 5.70, 5.71, 5.72 and 5.73, which isolate the west wall in Figures 5.32, 5.33, 5.38 and 5.39, show that the most extensive cracking occurs between elevations 95' and 119' near the south end of the wall. In both iterations 0 and 1, Figures 5.71 and 5.73 predict the presence of vertical cracks between these elevations, however, because this portion of the wall

is behind the new fuel storage vault, many of these cracks were not observed. In the central region of the west wall, above and below elevation 95', these same figures show that large fluctuations in crack orientation occur between iteration 0 and iteration 1. Iteration 0 predicts nearly horizontal cracks in this region, while iteration 1 shows a distinct shift in orientation to vertical cracks. Since the mechanical loads have horizontal stress trajectories within this central region for both iterations, it is likely that vertical cracks will occur. These vertical cracks should be visible between elevation 85' and 95'. The predicted crack pattern for the west SFP wall is shown in Figure 5.83.

In the east wall of the SFP between Columns C5 and C6, Figures 5.74, 5.75, 5.76 and 5.77, which isolate the SFP wall in Figures 5.44, 5.45, 5.50 and 5.51, show many diagonal stress trajectories in iteration 0 but predominantly horizontal trajectories in iteration 1. This change in crack orientation between the two iterations can be attributed to the increase in horizontal bending stress which occurs in iteration 1. This is consistent with the bending restraint that the SFP east wall provides in resisting the thermal growth of the shield wall, as discussed in the previous section. These horizontal bending stresses (SX) in the east SFP wall at elevation 108' can be seen in Figure 5.77A for the winter temperature condition. Thus, in the region between columns it is expected that vertical cracks will begin at about elevation 80' and continue to elevation 119'. In the region of the east wall north of column C6 between elevation 80' and 105', both iterations 0 and 1 predict the presence of horizontal cracks. In addition, the stress trajectories and stress magnitudes in columns C5 and C6 for iteration 0, and to some extent iteration 1, strongly indicate that these columns should have horizontal cracks at possibly several elevations, with the most likely location being in Column C6 at about elevation 100'. The predicted crack pattern for the east wall of the SFP is shown in Figure 5.84.

A geometry plot of the north wall of the SFP is shown in Figure 5.78. The tensile stress magnitude on the surface of the north wall for iterations 0 and 1 are shown in Figures 5.79 and 5.81, and their associated stress trajectories are shown in Figures 5.80 and 5.82. These figures show that both iterations 0 and 1 predict very similar stress trajectory patterns over most of the wall. Based on these trajectories and the surface stress magnitudes, vertical cracks should occur between elevations 100' and 119', and horizontal cracks should occur between elevations 80' and 90'. The predicted crack pattern for the north wall is shown in Figure 5.85.

Correlation With Observed Cracks

The cracks observed in the shield wall and SFP walls have been sketched in Figures 5.86, 5.87 and 5.88. A comparison of these observed crack patterns with the predicted crack patterns shown in Figures 5.83, 5.84 and 5.85 shows good agreement. At all locations where cracks were observed, the analysis predicted the occurrence of cracks. Also, at almost all locations where cracks were observed the analysis predicted the same orientation of the cracks.

The only region where the observed crack orientation differed from predictions was in the lower region of SFP west wall just above elevation 75' where more diagonally oriented cracks were predicted. As explained in Section 5.3, the prediction of crack orientation is based on stress trajectories at the element centroid, which in this case is 18" below the surface. A review of the vertical and horizontal stress components on the surface of the west wall showed that the horizontal tensile stresses dominate the vertical stresses in this region. While the principal tensile stresses in this lower region are oriented diagonally, other influences, such as the extension of propagating vertical cracks from above (i.e., from elevation 95' down), could trigger vertical cracks in the biaxial tension field. Therefore, the presence of vertical surface cracks in this biaxial tension region is possible, based on the analysis results.

The only crack not predicted was the horizontal crack between Columns C5 and C6 in the east wall of the SFP; however, the vertical cracks in this region and the extension of the horizontal crack into the columns and the adjacent region of the east wall were predicted.

5.3.3 Cracking of Floor Slabs at Elevations 75', 95', and 119'

In Section 4.2.1 it was shown that mechanical loads (e.g., DL; LL) do not produce membrane stresses that are high enough to cause cracking of the floor slab at Elevation 119', but that thermal loads do produce membrane tensile stresses of sufficient magnitude to cause cracking over significant regions of the floor slab adjacent to the shield wall and SFP. In addition, it was demonstrated that the floor slabs provide a mechanism through membrane action to partially restrain the SFP and thereby reduce the loads in the supporting girders. It was the recognition of this behavior that led to the relaxation of the floor slabs at Elevation 75', 95', and 119' in iteration 1, and all successive iterations, to ensure that the floor slabs were not relied upon to resist SFP loads.

The maximum tensile stresses in the floor slab at Elevation 119' for an unfactored combination of dead load (DL), live load (LL) and winter temperature (T_w) are shown in the stress contour plot of Figure 5.89 and the refined contour plot of Figure 5.90, which highlights the tensile stresses between 400 and 1,000 psi. Figure 5.90 shows the large areas of the operating floor which are expected to crack due to the presence of membrane tensile stresses in excess of 400 psi. The direction of the tensile stress trajectories, shown with and without the SFP walls and shield wall, are shown in Figures 5.91 and 5.92. Based on the stress magnitudes in Figure 5.90 and the stress trajectory directions shown in Figure 5.91, the expected cracking pattern for the operating floor is shown in Figure 5.101. While the figure shows a great many cracks, it is anticipated that a much smaller number of the cracks will actually occur due to the relief of thermal stress as cracks initiate. The figure shows the regions where cracks can be expected to occur and their probable direction if they occur.

The elements comprising the floor slab at elevation 95' are shown in the geometry plot of Figure 5.93. The maximum membrane tensile stresses in the floor slab at Elevation 95' and their associated orientation are shown in Figures 5.94 and 5.95. Figure 5.96 is a refined contour plot showing the tensile stresses between 400 and 1,000 psi. Based on the stress magnitudes and the stress trajectory directions, the expected crack pattern for Elevation 95' is shown in Figure 5.102.

At Elevation 75', Figure 5.97 shows a plan view of the floor slab which includes the SFP wall and SFP slab taken at its mid-depth. The composition of this plan view can be better seen in Figure 5.98 which is a 3-D view taken from the northwest just above elevation 75'. The principal tensile stress contours in Figure 5.99 show the regions of the floor where the most cracking can be expected to occur. The trajectories for these tensile stresses are shown in Figure 5.100. Regions where cracks are expected and their anticipated directions are sketched in Figure 5.103.

The observed crack patterns in the floor slabs at Elevations 119', 95' and 75' are shown in Figures 5.104, 5.105, and 5.106, and were based on information supplied by GPUN. By comparing the existing cracks with the predicted crack patterns it can be seen that most of the observed cracks occur in regions where cracks are expected, and all of the cracks have orientations consistent with predicted results. The only exception is at the northeast corner of the SFP where cracks were observed in the floor slab at Elevations 75' and 95'. (Similar cracks were not observed at Elevation 119' because the floor in that area was hidden from view by a

paper covering.) As shown in Figures 5.96 and 5.99 these cracks occur in regions where membrane tensile stresses exist, but are below 400 psi. While membrane cracks are not predicted in this region, the observed cracks could be caused by tensile bending stresses on the top surface of the floor slab. Since the winter temperature condition causes the warmer shield wall and SFP to be displaced vertically to a much greater degree than the cooler exterior wall, the top surface of the slab between the SFP north wall and the exterior wall could be subjected to significant bending due to the differential vertical displacement. This displacement behavior is illustrated in Figures 5.135 and 5.137, which show the vertical displacement contours of the floor slabs at Elevations 95' and 119' for an unfactored load combination of $DL+LL+T_w$ in iteration 0. Figures 5.136 and 5.138 show the maximum tensile stress contours on the top surface of the floor slab at elevations 95' and 119' for the same load combination and iteration. These figures clearly show that the fan type cracking of the floor in the vicinity of both the northeast and northwest corners of the SFP should occur. Therefore these cracks should be observed on elevation 119' after the paper floor covering is removed. Figures 5.136 and 5.138 also show that surface cracks due to slab bending may be observed in other regions of the floors as well.

Figures 5.90, 5.96, and 5.99 show that the floor slabs at Elevations 119', 95' and 75' on the west side of the SFP and shield wall are more highly stressed than on the east side. This means that more relaxation of membrane restraint should occur on the west side than on the east side. This unequal relaxation of the membrane restraint provided by the floor slabs was not investigated in the analysis. However, the only effect that this could have on the analysis results would be a reduction in the load transferred to Girder RD and Column C6. Since the analysis assumes the complete release of the floor slabs as restraining membranes supporting the SFP, the resulting loads in Girder RD and the other primary supporting members have been conservatively estimated based on the expected behavior of the floor slab system.

5.3.4 Cracks in Girder RE

An elevation view of Girder RE as it exists in the finite element model is shown in Figure 2.17. This view, looking west, shows a portion of the north wall of the SFP and Column E7 which supports the north end of the girder. Figure 5.107 isolates just the girder elements and shows the west face in the top window and the east face below. Figures 5.108 through 5.127, which occur in pairs, show the maximum tensile stresses on each face and the associated tensile stress trajectories between faces (i.e., at

the element centroid) for iterations 0, 1 and 2 and different load combinations. For reference purposes, the specific iteration and load combination associated with each figure are shown at the bottom of the photograph. DL is dead load which includes concrete dead load, hydrostatic pressure and high density racks and fuel, LL is the floor live load, T_w is the winter temperature condition and T_s is the summer temperature condition. In the discussions which follow, attention is concentrated on the region of the girder between the north face at column E7 and the maximum moment section (i.e., section ME in Figure 5.1). This region coincides with the square area five elements long and six elements deep in Figure 5.107, where only the bottom four layers of elements are physically visible in the actual girder; the top two layers are embedded in the floor slab at elevation 75'.

Crack Orientation

In iteration 0 Figures 5.109 and 5.111 show that the winter and summer temperature conditions produce stress trajectory directions which are distinctly different from the load combination of dead plus live load (DL+LL) shown in Figure 5.113. The resulting combination of dead and live load plus either the winter or summer temperature condition produces very low stress levels between the north face of the girder and the maximum moment section, as shown in Figures 5.114 and 5.116. More importantly, when compared to the stress trajectories for DL+LL (Figure 5.113), the stress trajectories for load combinations which include temperature are very flat, as shown in Figures 5.115 and 5.117, and Figures 5.128 and 5.129 where the scale of the trajectory vector has been increased to clearly show the directions. From the discussion below, it will become apparent that the orientation of the stress trajectories in Figures 5.128 and 5.129, and Figure 5.113 bound the orientation of predicted and observed cracks in Girder RE.

In iteration 1 the stresses in the girder increase when the floor slabs at Elevation 75', 95' and 119' are reduced in stiffness to simulate complete release of their membrane load carrying capability (see discussion in Sections 4.2.1 and 4.2.2). This iteration produces the single most significant load change in the girder as the shear force from the winter temperature condition reverses direction. This shear force reversal between iterations 0 and 1 can be seen in Table 4.6 for the winter temperature condition. In contrast to iteration 0, the stress trajectories for DL+LL (Figure 5.119) and DL+LL+ T_w (Figure 5.121) now have the same orientation in iteration 1. However, for the load combination of DL+LL+ T_s (Figure 5.123) the stress trajectories are not as diagonally oriented at the north end of the girder as the trajectories for DL+LL or DL+LL+ T_w .

In iteration 2 the shield wall, SFP walls and SFP slab crack and additional load is redistributed to Girder RE. The stress trajectory orientations for DL+LL (Figure 5.125) and DL+LL+T_w (Figure 5.127) exactly coincide to those of iteration 1. It should be pointed out that the stress trajectories for DL+LL are always the same, in iterations 0, 1 and 2 and that only when temperature conditions are introduced do the stress trajectories change.

A review of Figures 5.113, 5.115, 5.117, 5.119, 5.121, 5.123, 5.125, 5.127, 5.128 and 5.129 for iterations 0, 1 and 2, show that the stress trajectory orientations in Figures 5.128 and 5.129 for DL+LL+T_w and DL+LL+T_s in iteration 0, and in Figure 5.125 for DL+LL in iteration 2 (as well as iterations 0 and 1) bound all of the stress trajectory orientations in the other figures. Thus, in the uncracked structure, before any significant thermal gradients occur, stress trajectories are oriented as shown in Figure 5.113. As the plant begins operation and thermal gradients increase, the trajectories become more horizontal as shown in Figures 5.128 and 5.129. As the floor slabs, shield wall, SFP wall and SFP slab crack, the orientation of the stress trajectories become less horizontal and more closely resemble those shown in Figures 5.125 or 5.127. Regardless of the extent or degree of cracking or the type and severity of the thermal gradients, the trajectory orientations predicted by the analysis fall between specific limits. The actual crack pattern which emerges in the girder will depend on what stage in the cracking process the surface stresses in the girder reach the tensile strength of the concrete. The crack pattern predicted from the stress trajectories in Figure 5.127 is sketched in Figure 5.130 for the west face of the girder. Similarly the crack pattern predicted from the average orientation of trajectories in Figures 5.127 and 5.128 is sketched in Figure 5.131.

The observed crack pattern on the east and west faces of the girder are shown in Figures 5.132 and 5.133. The pattern on the west face (Figure 5.132) compares well to the diagonally oriented crack pattern in Figure 5.130 which is the same for DL+LL in iterations 0, 1 and 2 or DL+LL+T_w in iterations 1 and 2. The pattern on the east face, shown in Figure 5.133 (and its mirror image in Figure 5.134) compares well to the more vertical crack pattern in Figure 5.131. What these comparisons show is that the observed crack patterns in Girder RE are within the predicted analysis bounds set by the successive cracking iterations and by the extreme limits of the thermal gradients. Therefore there is nothing unusual about either the orientation or pattern of cracks.

Interpretation of Analysis and Nondestructive Evaluation Results

The SFP analysis results show that for all load combinations and all iterations Girder RD is more highly stressed than Girder RE by about 10 to 20%, but since Girder RD is not visible no relative conclusions can be drawn between the observed cracks in Girder RE and the absence or presence of cracks in Girder RD. However, the physical examination and evaluation of the cracks in Girder RE, documented in Reference 8, revealed that all of the cracks penetrate only the first few inches of the girder's surface and that cracks on the east, west and bottom surfaces of the girder are probably related. Based on the analysis results and the results of the physical examination of the cracks two conclusions can be drawn.

First, in order to cause only surface cracking in a pattern which is consistent with the analysis results for mechanical and thermal loads, a relatively homogeneous isotropic tensile stress field must have existed within the first few inches of the surface of the girder at the time that significant mechanical and thermal loads were applied. (An isotropic stress field is a special case of a biaxial stress field where the stresses are the same in both directions, i.e., Mohr's Circle is a point.) The most reasonable way that such a surface stress field could have occurred is during the curing of the girder concrete at the time of construction. If the surface cured too rapidly relative to the interior of the girder, shrinkage would not occur uniformly through the width of the girder. This would result in a nonlinear residual stress distribution within the girder web. Tensile stresses would be highest on the east, west and bottom surfaces and would decrease rapidly within the first few inches to a much lower level of compression within the interior of the girder. Later, as mechanical and thermal loads were applied, the tensile stresses due to bending and shear would add to the isotropic tensile stresses on the surface until the tensile strength of the surface concrete was reached. A surface crack would initiate but only propagate a few inches below the surface as the tensile stresses decrease rapidly with distance from the surface. With an isotropic surface stress field, the resulting cracks would be oriented in exactly the same direction as the mechanical and thermal load stress trajectories. This is because the direction of these stress trajectories would not be altered by the presence of an isotropic stress field no matter what the magnitude of the isotropic field.

Second, the loads resisted by Girder RE do not produce sufficiently high shear or bending stresses to cause cracking through the entire width of the girder. Therefore, the combined effects of the magnitude of the load to which the SFP structure has been subjected and the degree to which

cracking has taken place in the SFP structure, must be consistent with this fact. It is reasonable to initially assume that the load levels that the SFP structure has actually been subjected to over its life time are close to the Case C dead load plus winter temperature condition. The maximum bending stresses in the girder for the load combinations of DL and DL+T_w are shown in Table 5.24 for iterations 0, 1 and 2. To determine when cracking might occur, these stresses must be related to the actual tensile stress at which the girder would be expected to crack. Nondestructive examination of the girder concrete showed that it had an average compressive strength of 4980 psi (Reference 8). This gives a modulus of rupture equal to 530 psi. Assuming that the isotropic tensile field on the surface of the girder was approximately 200 psi, the maximum bending stress in the girder must have exceeded 330 psi to cause surface cracks. Comparing this stress to the stresses in Table 5.21, it is concluded that the level of cracking and/or the extent of cracking was conservatively estimated in the analysis in iterations 1 and 2. This is quite possible, particularly for iteration 1. With the dramatic change in stress magnitude that occurs for the case of DL+T_w between iterations 0 and 1 (see Table 5.24), it is very probable that most of the conservatism lies in the complete release of the membrane restraint of the floors at Elevations 119', 95' and 75'. (See discussion in Sections 4.2.1 and 4.2.2 regarding the release of unqualified load paths.) Realistically these floors do participate in restraining the SFP and reducing the loads in Girders RE and RD. The effect of this participation by the floor slabs is one of the reasons why Girder RE does not have cracks through the web. Also, the fact that the two long vertical cracks nearest the maximum moment section in Figure 5.134 have an inclination similar to that predicted by the stress trajectories in Figures 5.128 and 5.129 further reinforces a conclusion that the actual level or extent of cracking is not too far from iteration 0. In addition, it is likely that the 40°F interior reactor building temperature used throughout the entire interior of the structure in the analysis may not have occurred at all elevations or for a sufficient duration to have caused as high a thermal gradient as used in the analysis. A lower thermal gradient would have resulted in less cracking and less load being redistributed to the girders.

Based on the results of the SFP analysis and the results of the nondestructive evaluation of Girder RE, it is concluded that the cracks in Girder RE are not a result of girder overload or other forms of distress. These cracks probably occurred as a result of tensile surface stresses in the girder produced during curing. These surface stresses added to the normal shear and bending stresses caused by mechanical and thermal loads which, in turn, caused premature cracking of the girder surface. The fact that these cracks are confined to the girder surface and are in a

normal crack pattern consistent with the analysis results, further supports this conclusion. In addition, this is consistent with the low number of observed cracks in the floor slabs at elevations 75', 95' and 119' discussed in Section 5.3.3, and it reinforces the conclusion that a significant portion of the SFP load is carried by structural systems not specifically designed to resist these loads, but due to the integral attachment to and connectivity with the SFP they provide redundant paths to divert load from the primary supporting members.

5.4 Conclusions

- (1) The finite element analysis of the Oyster Creek Spent Fuel Pool is valid, particularly as evidenced by the ability to match and explain the observed cracks in the SFP structure. The close correlation of analysis predictions with observed cracks indicates that even though the loading sequence in the analysis is not exact, the structure is not particularly sensitive to the loading sequence. This is due to the fact that little if any cracking takes place under the sustained mechanical loads and that it is the temperature conditions, applied after the sustained loads, which drive the cracking of the structure.
- (2) All observed cracks were shown not to be detrimental to the successful performance of the structure. The analysis showed that the prominent cracks are related to the high degree of connectivity within the structure and are a direct result of its kinematic behavior. As such, the cracks are not related to structural distress or other equilibrium issues. In correlating analysis results with observed cracks, it was shown that the existing cracks are predicted by the analysis and should be expected to occur as a result of normal operations within the envelope of licensed loads.
- (3) As a consequence of the high degree of redundancy and connectivity exhibited by the SFP structure, the analysis paid particularly close attention to the presence of unqualified load paths. As part of the analysis strategy these load paths were systematically released to ensure that the maximum loads were applied to the primary supporting members of the SFP. In addition, the analysis showed that the integral connectivity of the SFP slab with the shield wall and girders imposed significant biaxial membrane tension loads on the SFP slab which were accounted for in its evaluation. The evaluation showed that the SFP structure is in full compliance with ACI 349-80 for all loads for which the plant was licensed. Furthermore, the results of the Code evaluation and the excellent correlation of analysis results with observed cracks gives confidence that the SFP structure has not lost any structural capacity.



ABB Impell Corporation

- (4) The analytical results and Code evaluation show that the SFP structure can support consolidated fuel loads. However, the analysis also shows that Girder RD has only 0% margin when the pool is loaded with consolidated fuel. GPUN must be aware that (1) if consolidated fuel is added to the pool, Girder RE could crack further, which is undesirable, (2) Girder RD would have to be inspected and evaluated in detail prior to any decision, and (3) the bottom of the SFP slab would also have to be inspected. These points must all be considered and evaluated before a decision is made to increase SFP loads to consolidated levels.



ABB Impell Corporation

INTENTIONALLY LEFT BLANK

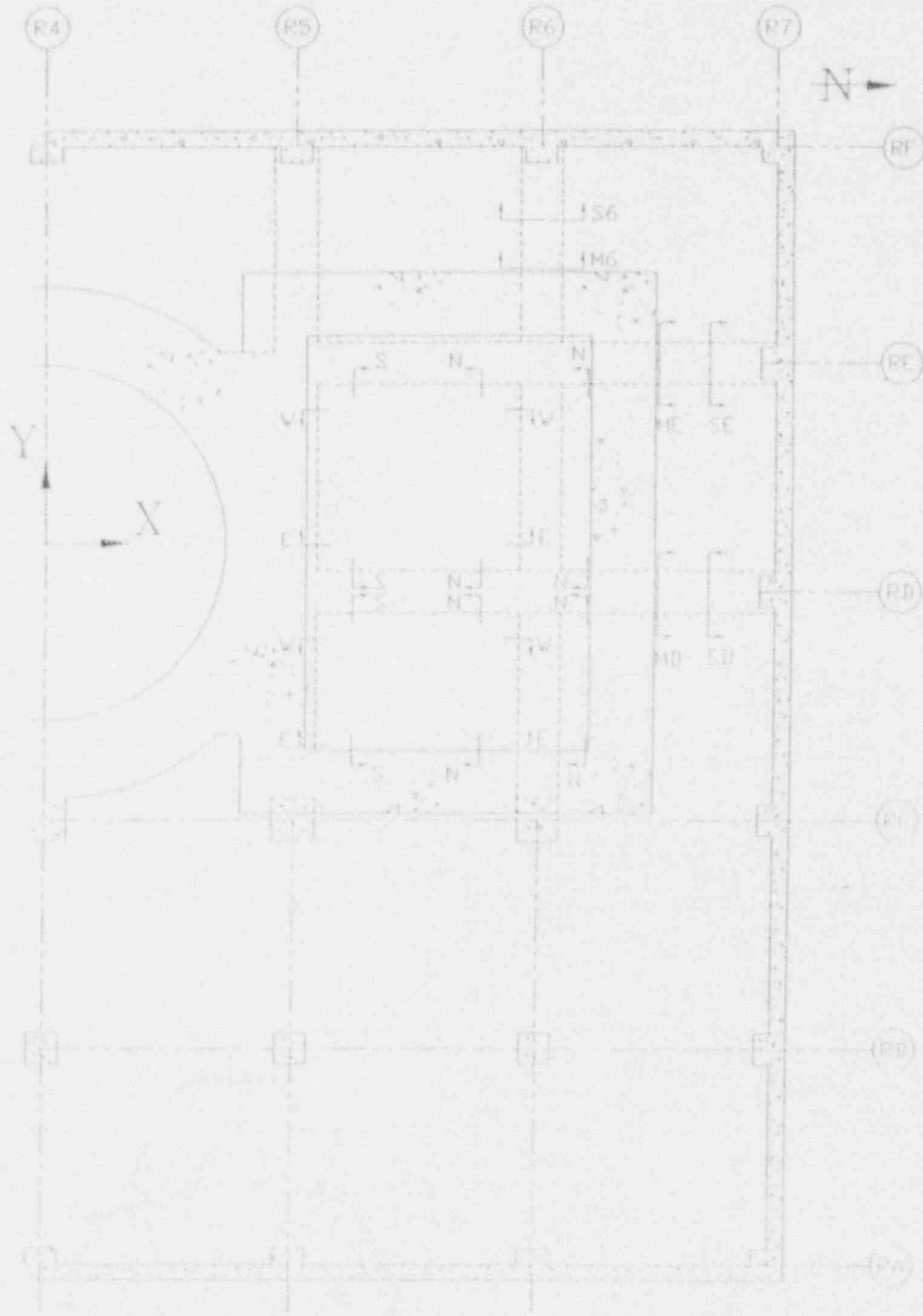


Figure 5.1

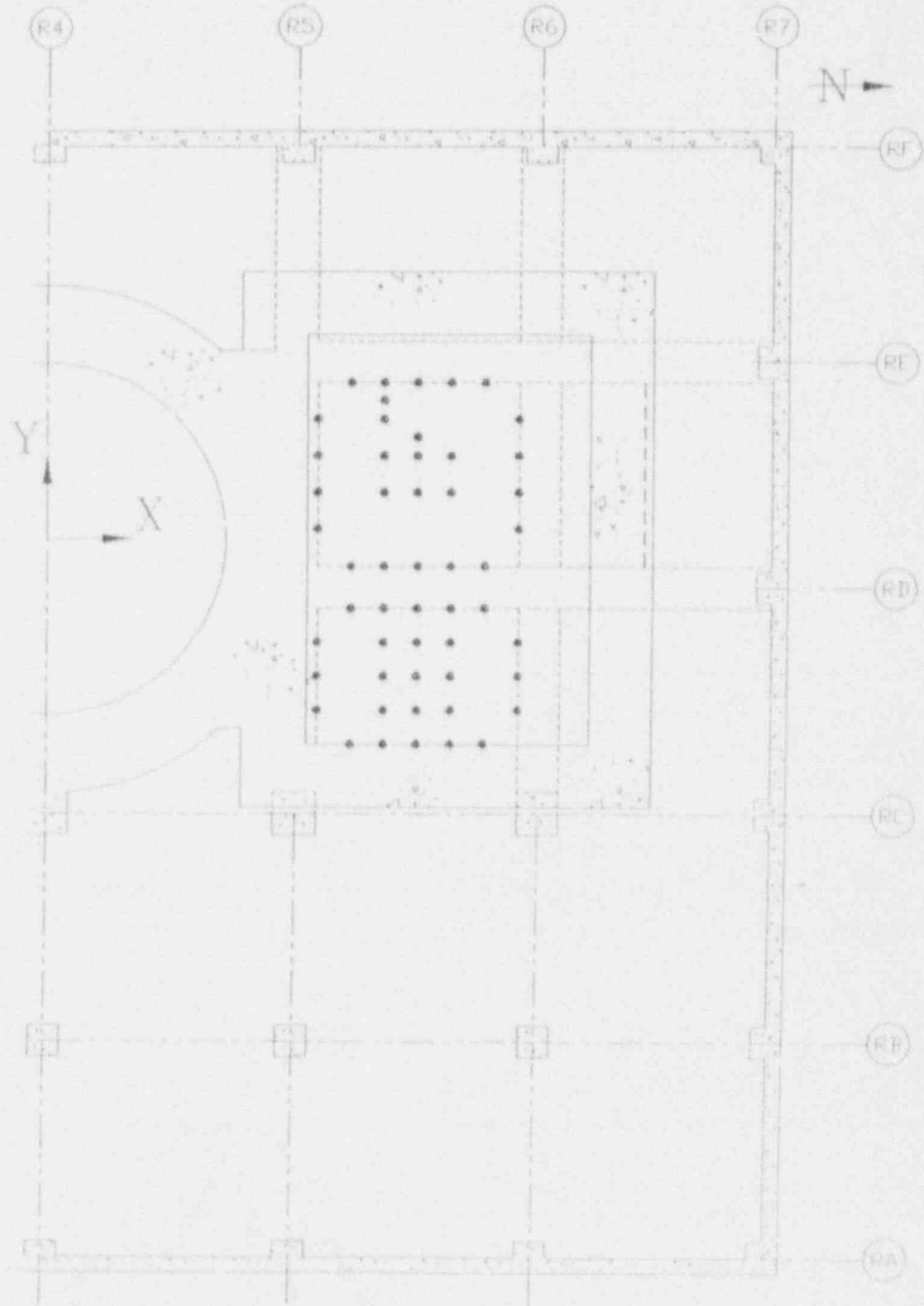
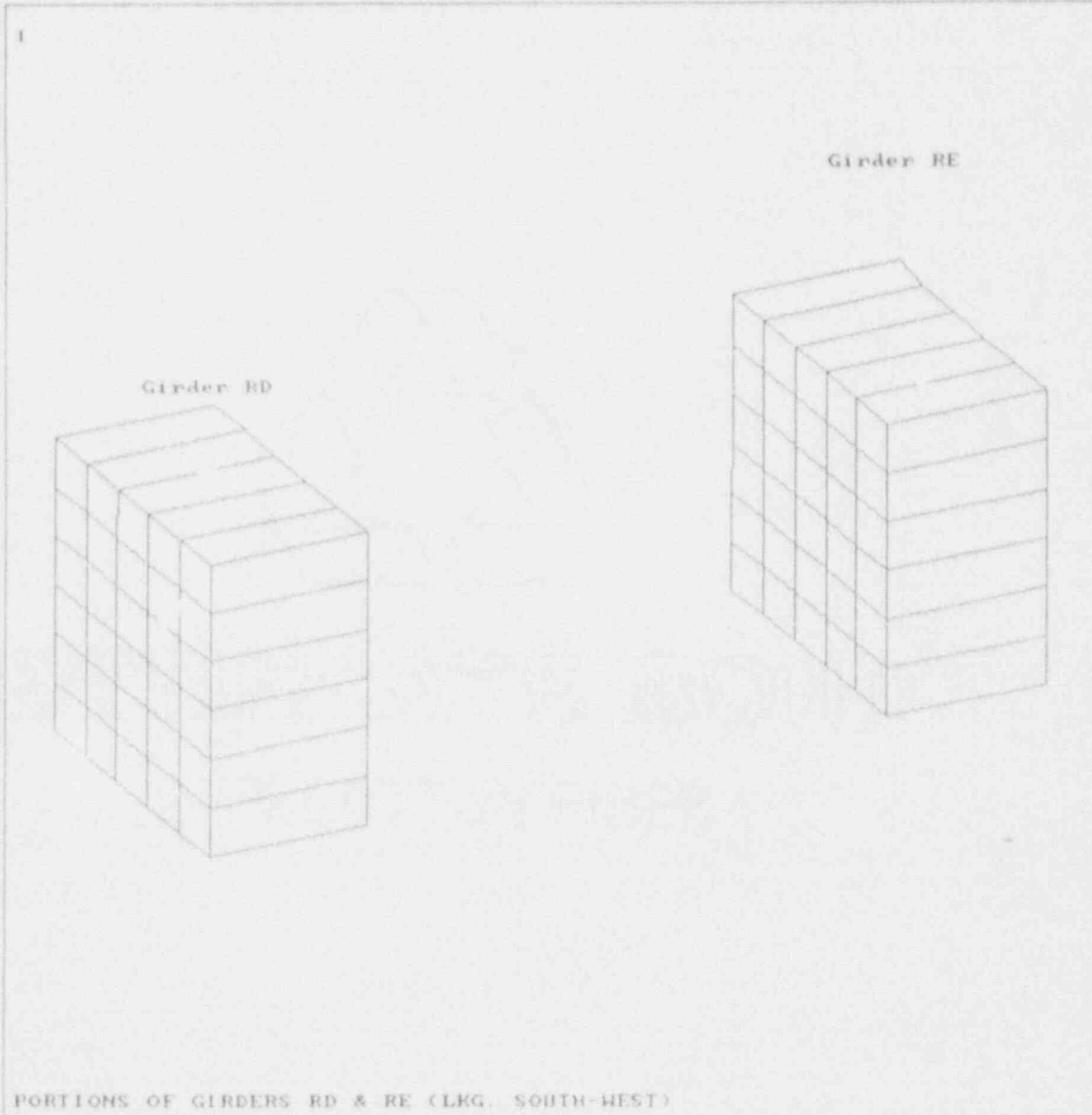


Figure 5.2



```
ANSYS 4.4  
NOV 20 1991  
15:15:31  
PLOT NO. 3  
POST1 ELEMENTS  
TYPE NUM  
  
XU =1  
YU =-0.5  
ZU =0.5  
DIST=186.73  
XF =745.5  
YF =73.5  
ZF =849  
ANGZ=-70.5  
PRECISE HIDDEN
```

Figure 5.3



ABB Impell Corporation

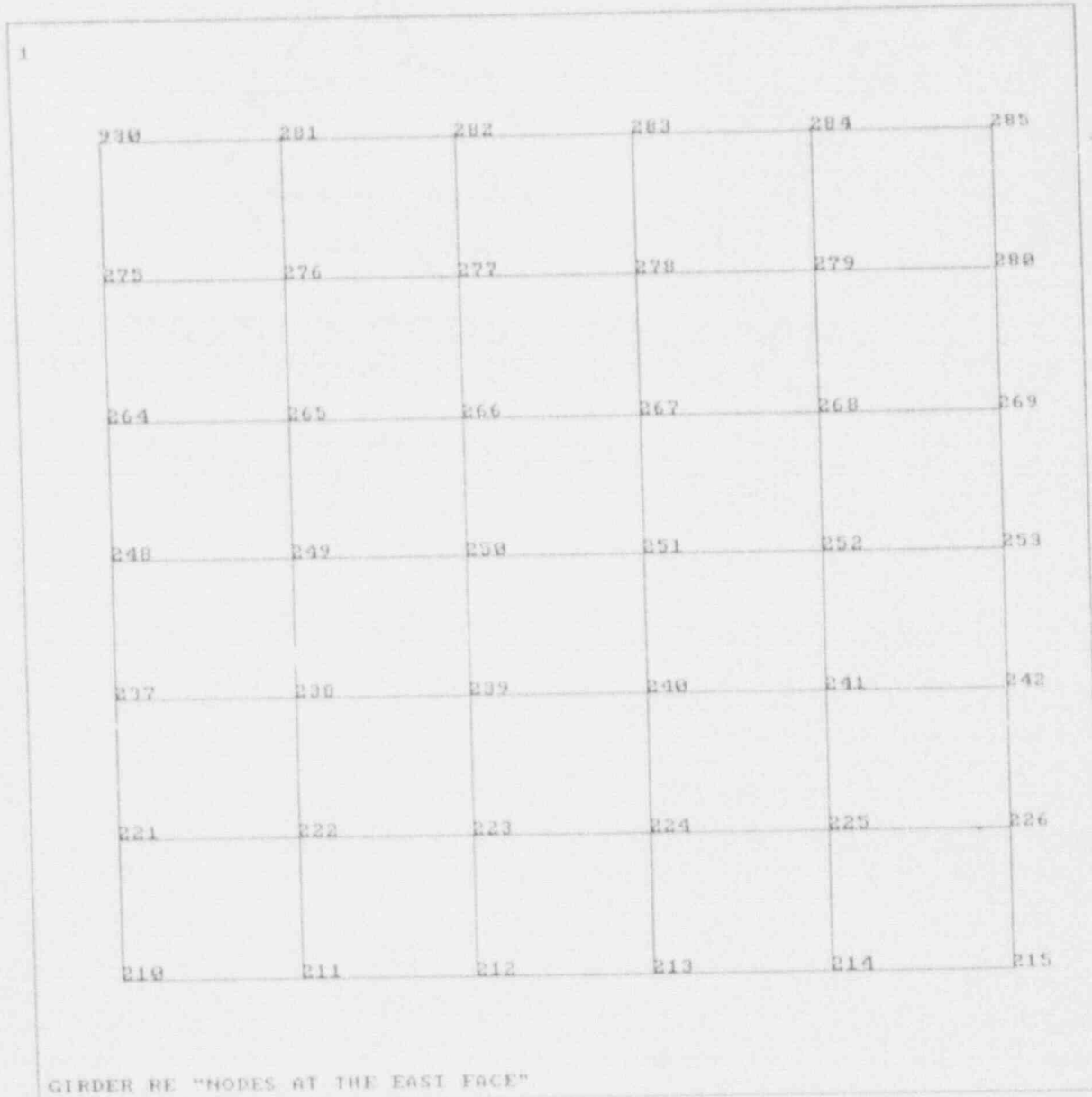
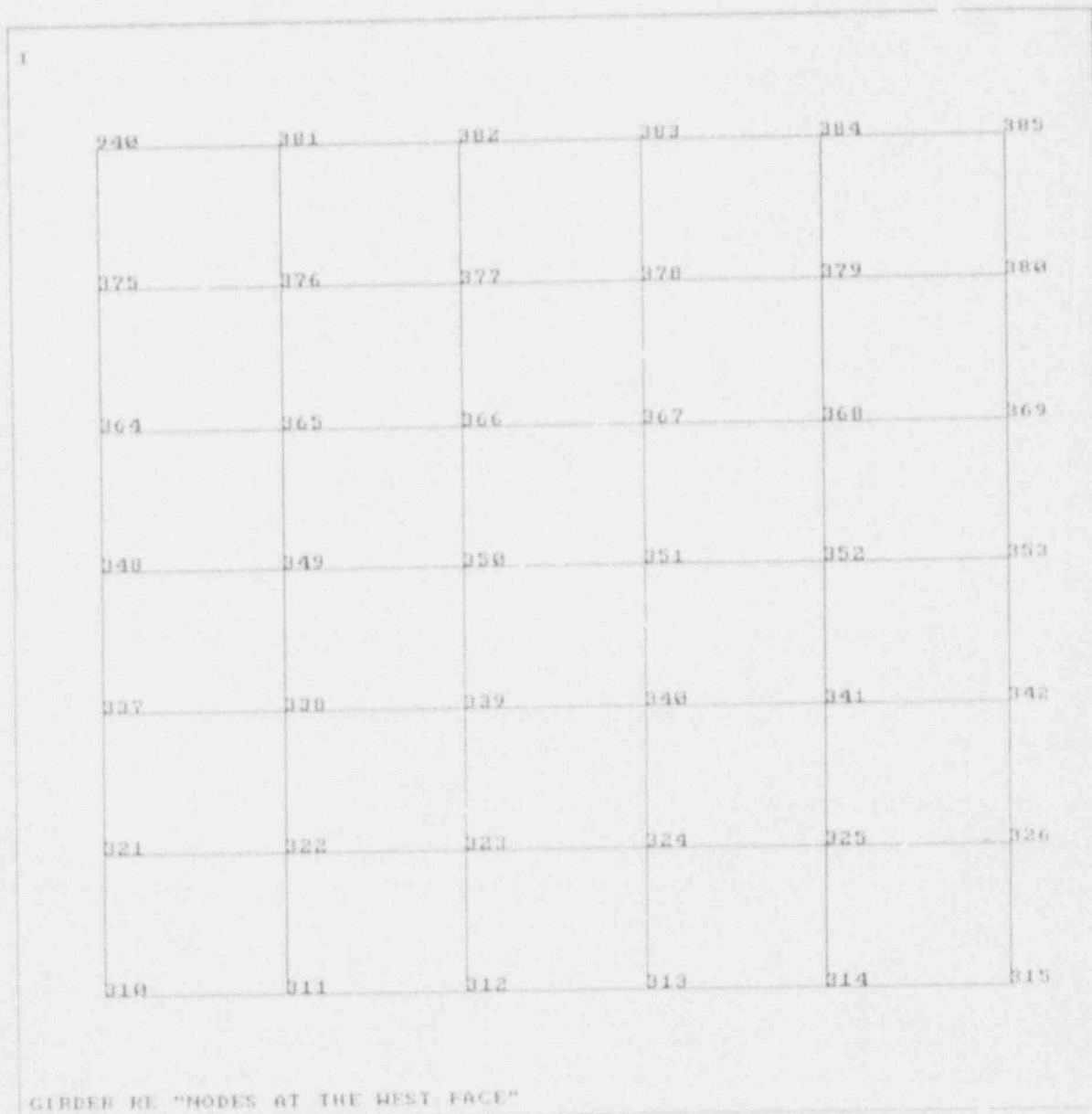


Figure 5.4



Appl Corporation



```

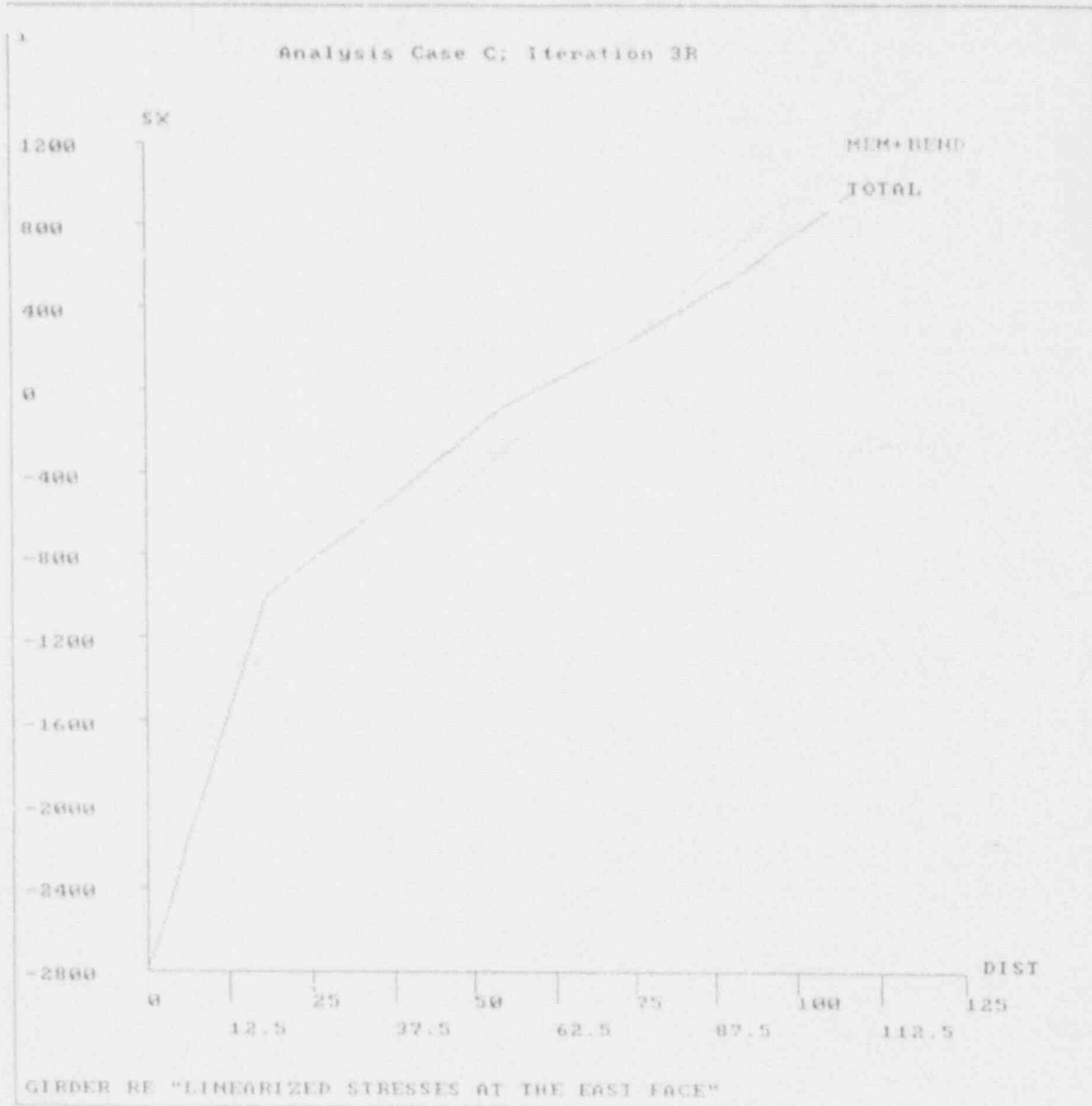
ANSYS 4.4
NOV 20 1991
11:53:55
PLOT NO. 2
POST1 ELEMEN
TYPE NUM
YU =-1
*DIST=74
XF =745.5
YF =232.5
ZF =049

```

Figure 5.5



ABB Impell Corporation



ANSYS 4.4
NOV 20 1991
14:57:31
PLOT NO. 1
POST1
STEP=3
ITER=1
TIME=-1
SECTION PLOT
MOD1=930
MOD2=210
SX
MIDDLE
STRESS GLOBA
ZU = 1
DIST=0.6666
XF = 0.5
YF = 0.5
ZF = 0.5

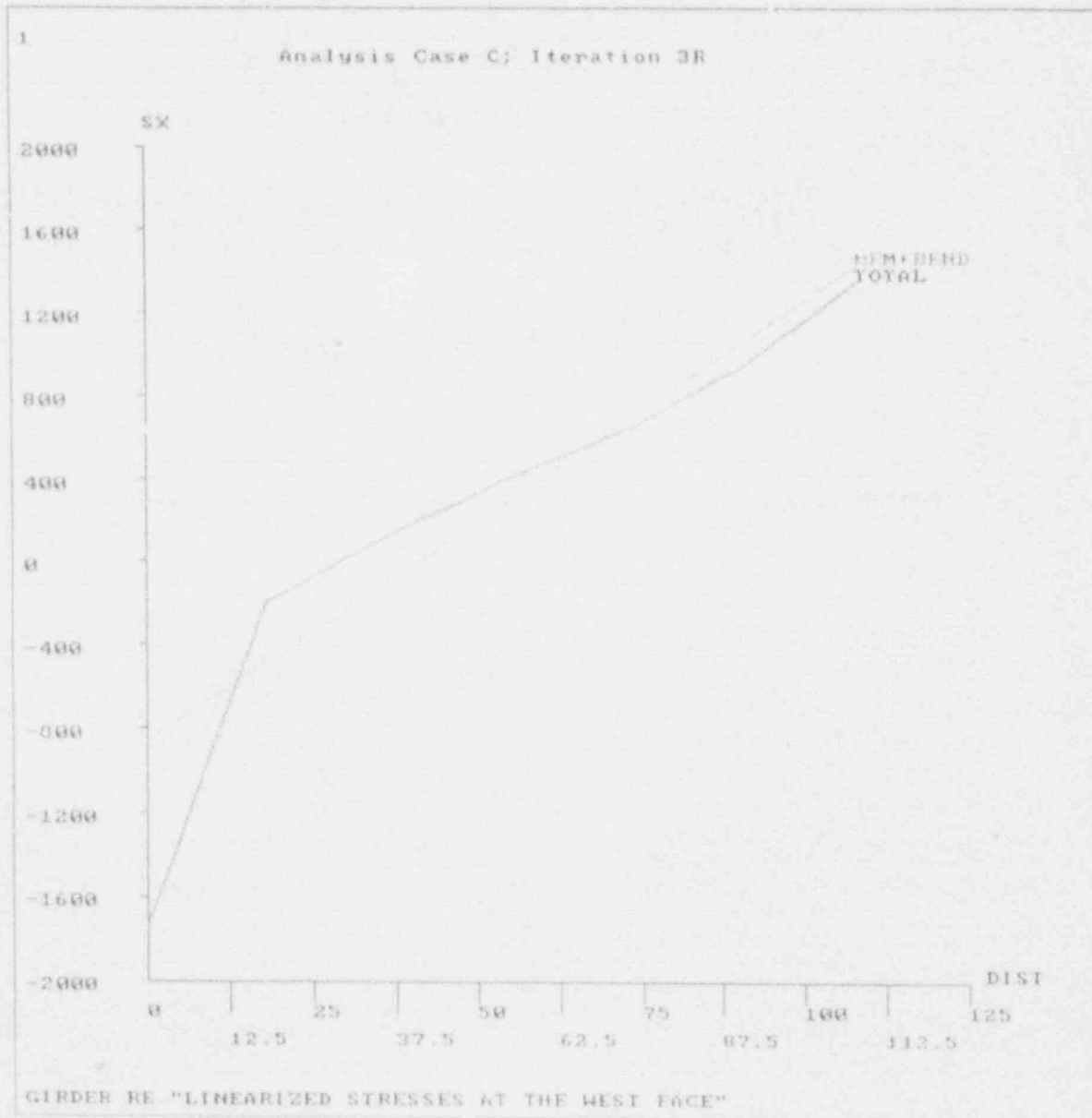
Figure 5.6



ABB Impell Corporation

Report No. 03-0370-1341

Revision 0



```
ANSYS 4.4
NOU 20 1991
14:58:56
PLOT NO. 2
POST1
STEP=3
ITER=1
TIME=-1
SECTION PLOT
MOD1=940
MOD2=310
SX
MIDDLE
STRESS GLOBR
ZU =1
DIST=0.6666
XF =0.5
YF =0.5
ZF =0.7
```

Figure .



ABB Impell Corporation

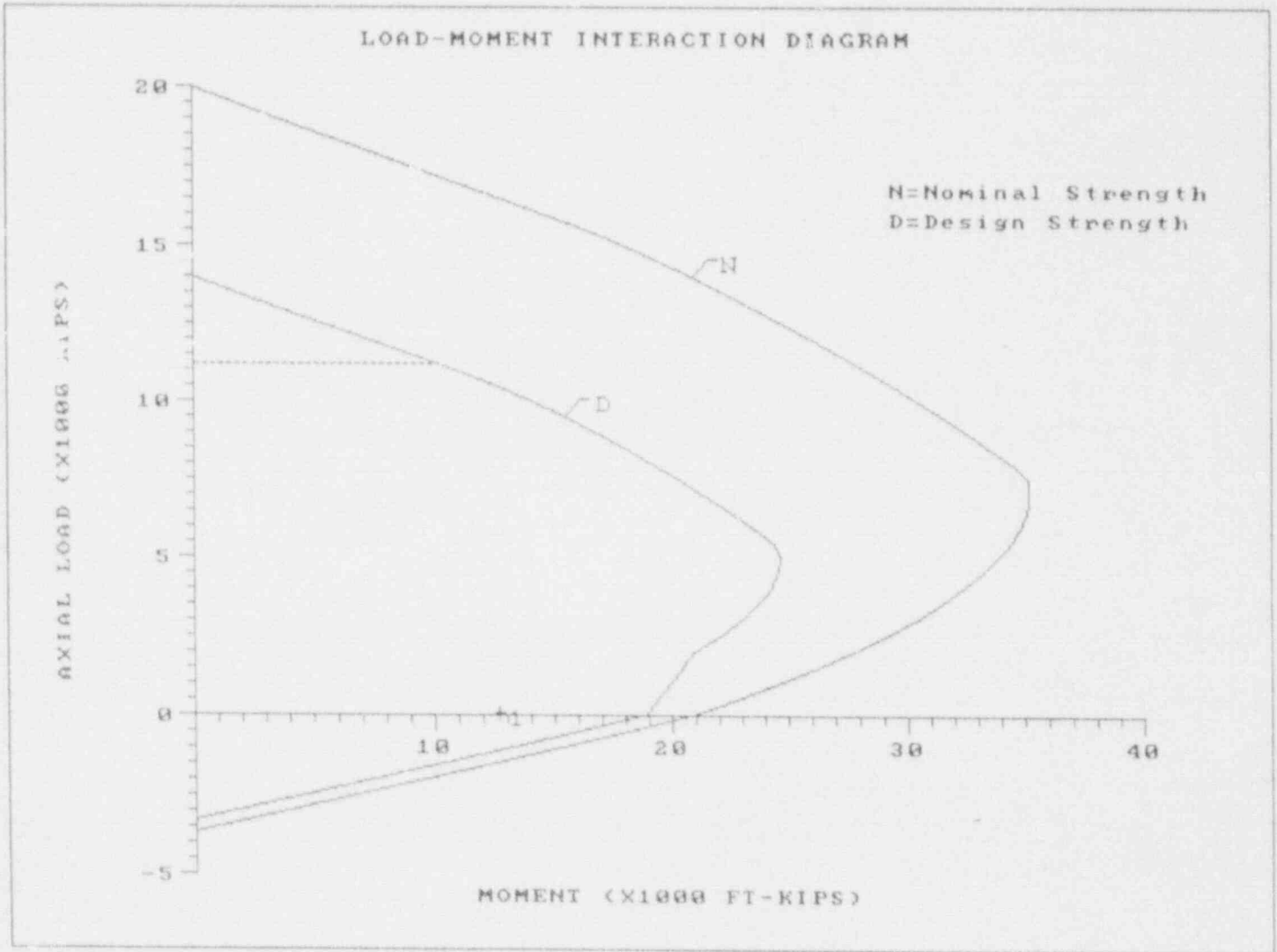


Figure 5.8

GIRDER RE MOMENT CAPACITY
 BASED ON REBAR DEVELOPMENT LENGTH
 (Factored Moment is Based on Girder RD)

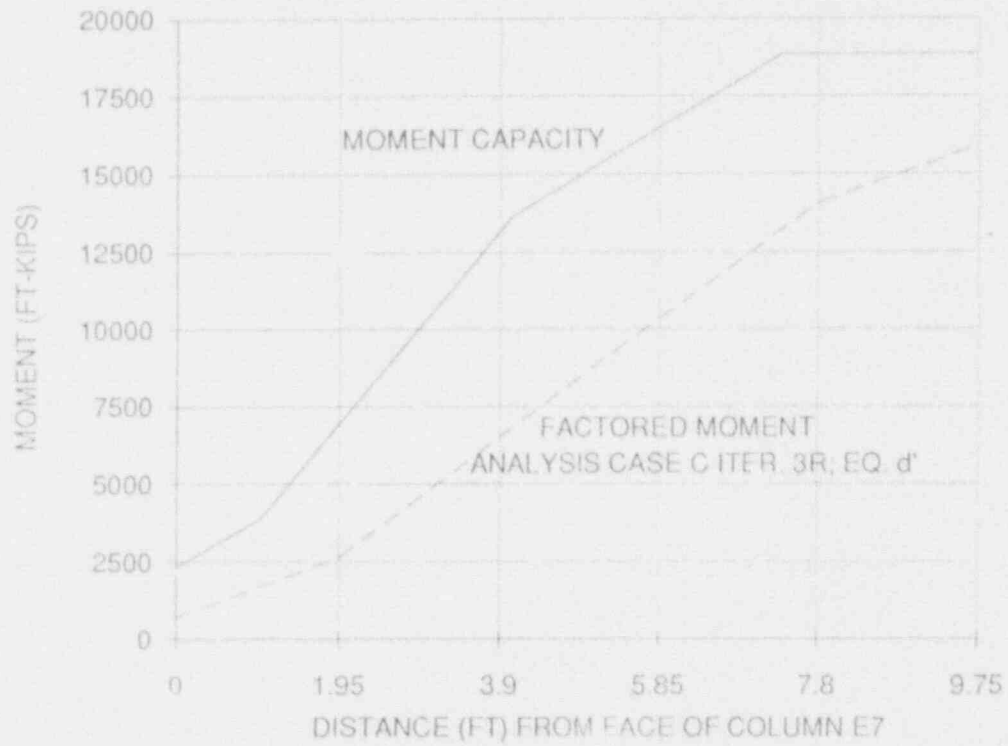


Figure 5.8A

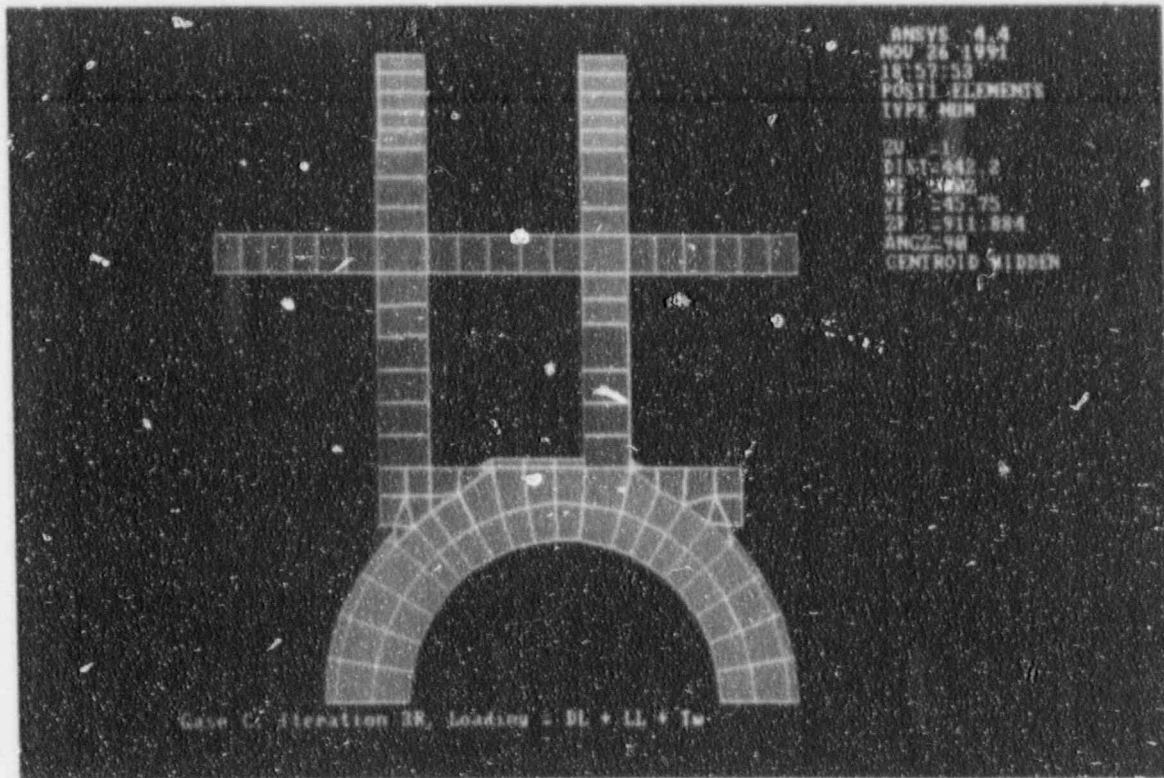


Figure 5.9

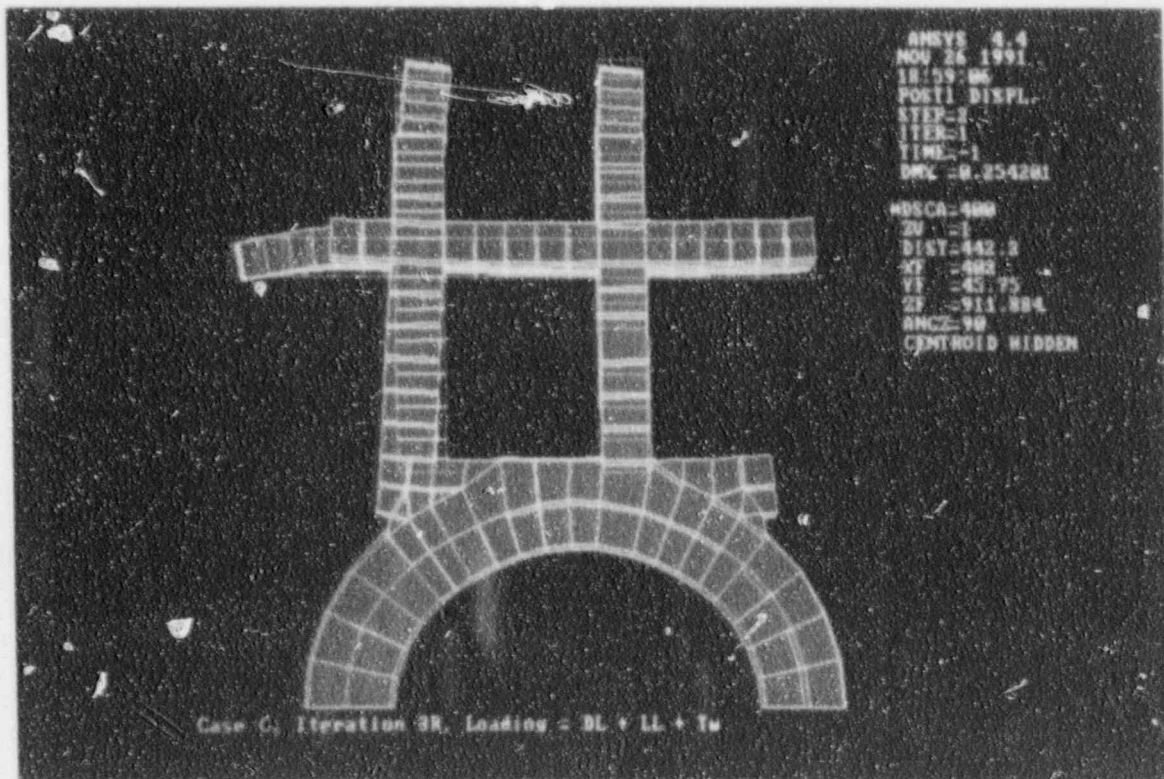


Figure 5.10

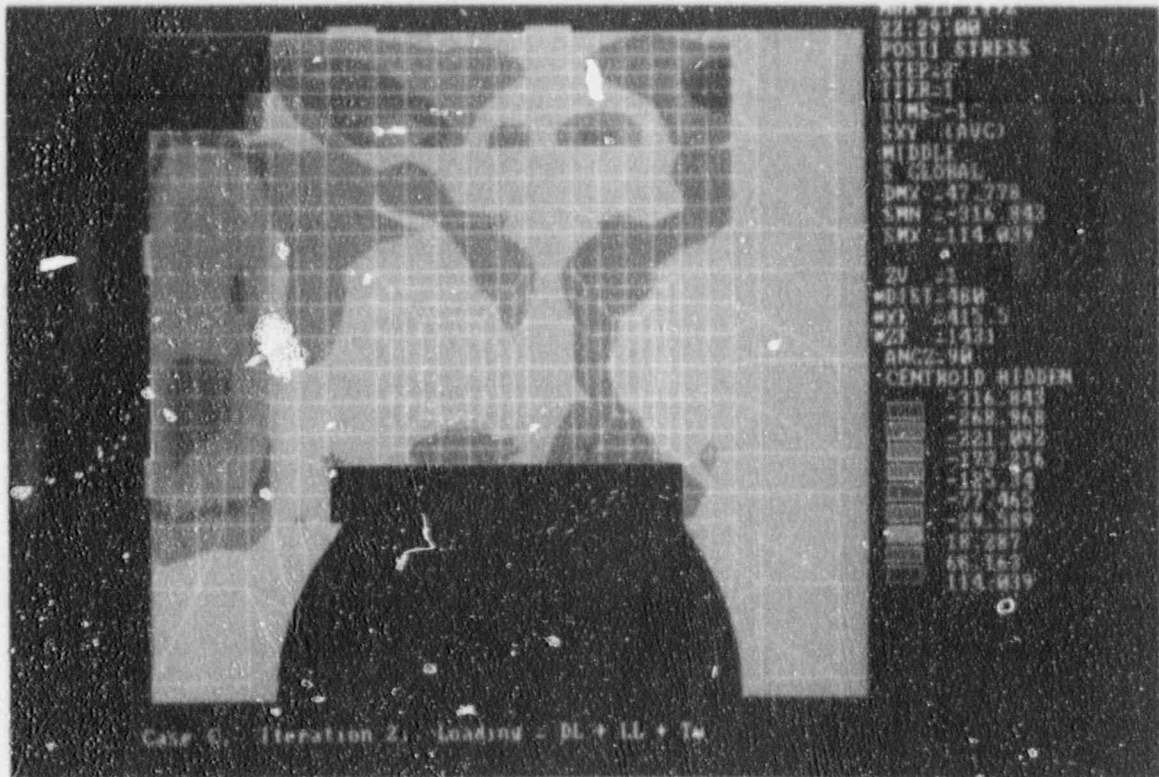


Figure 5.11

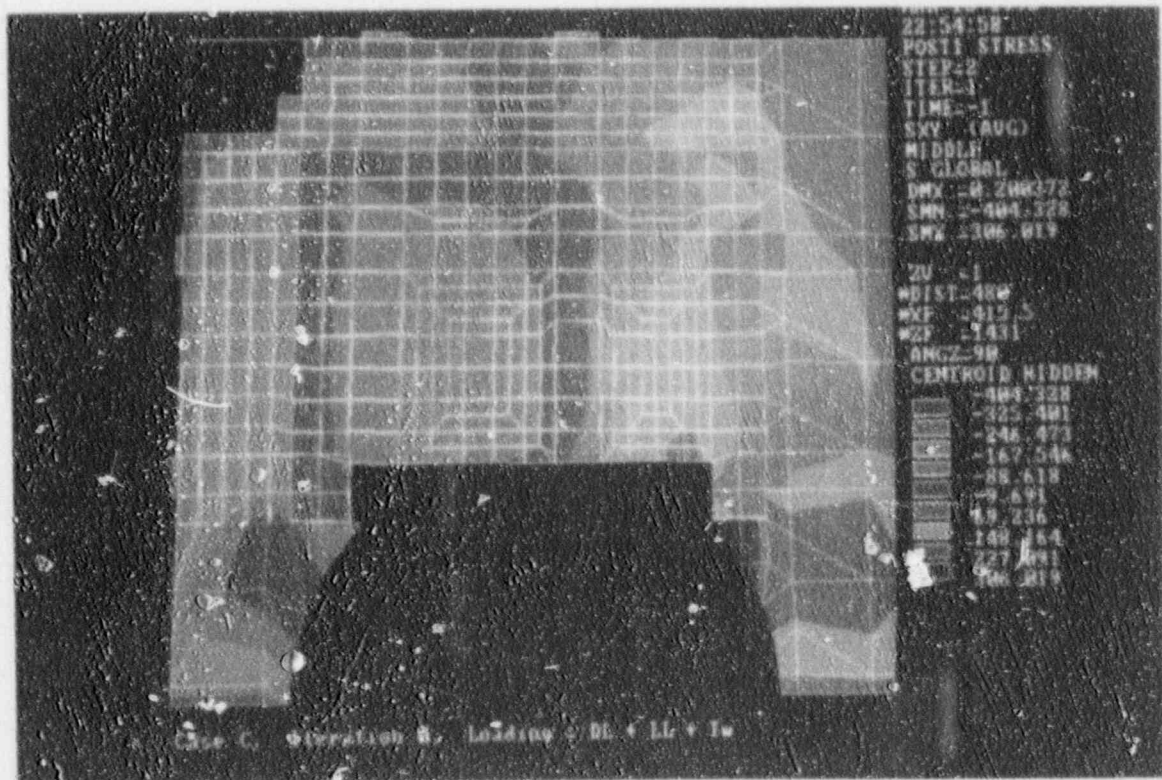


Figure 5.12

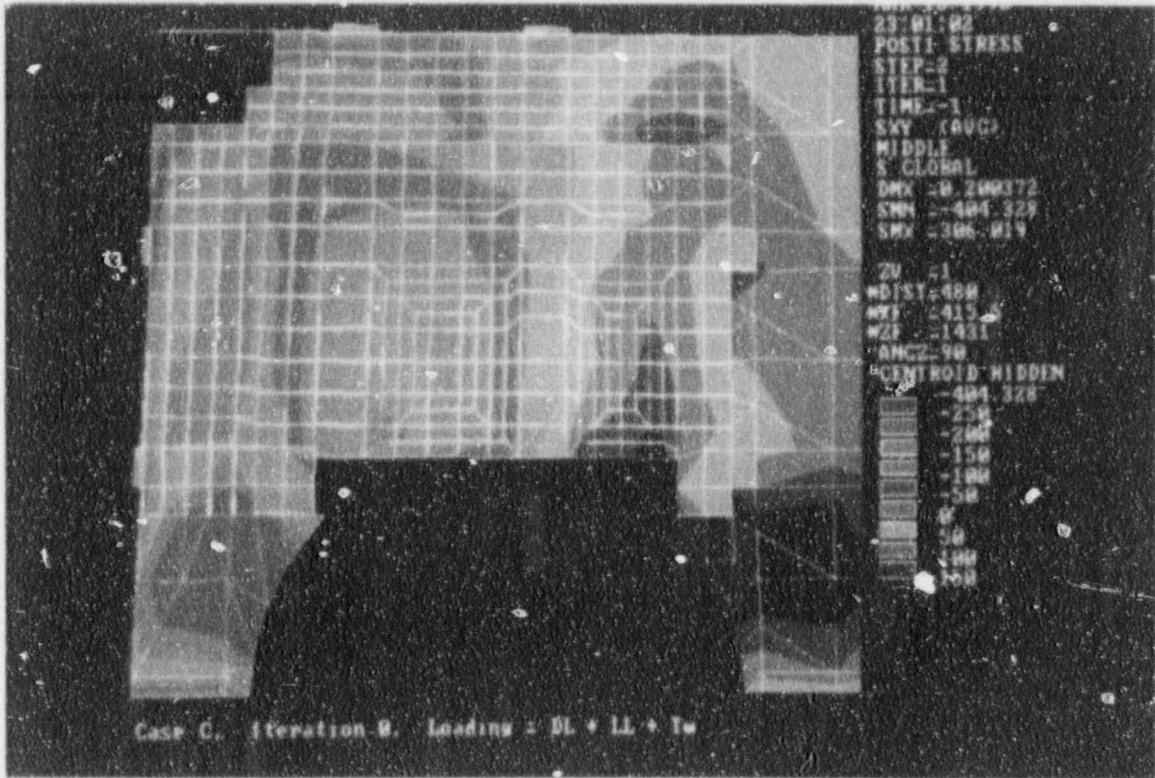


Figure 5.13



ABB Impell Corporation

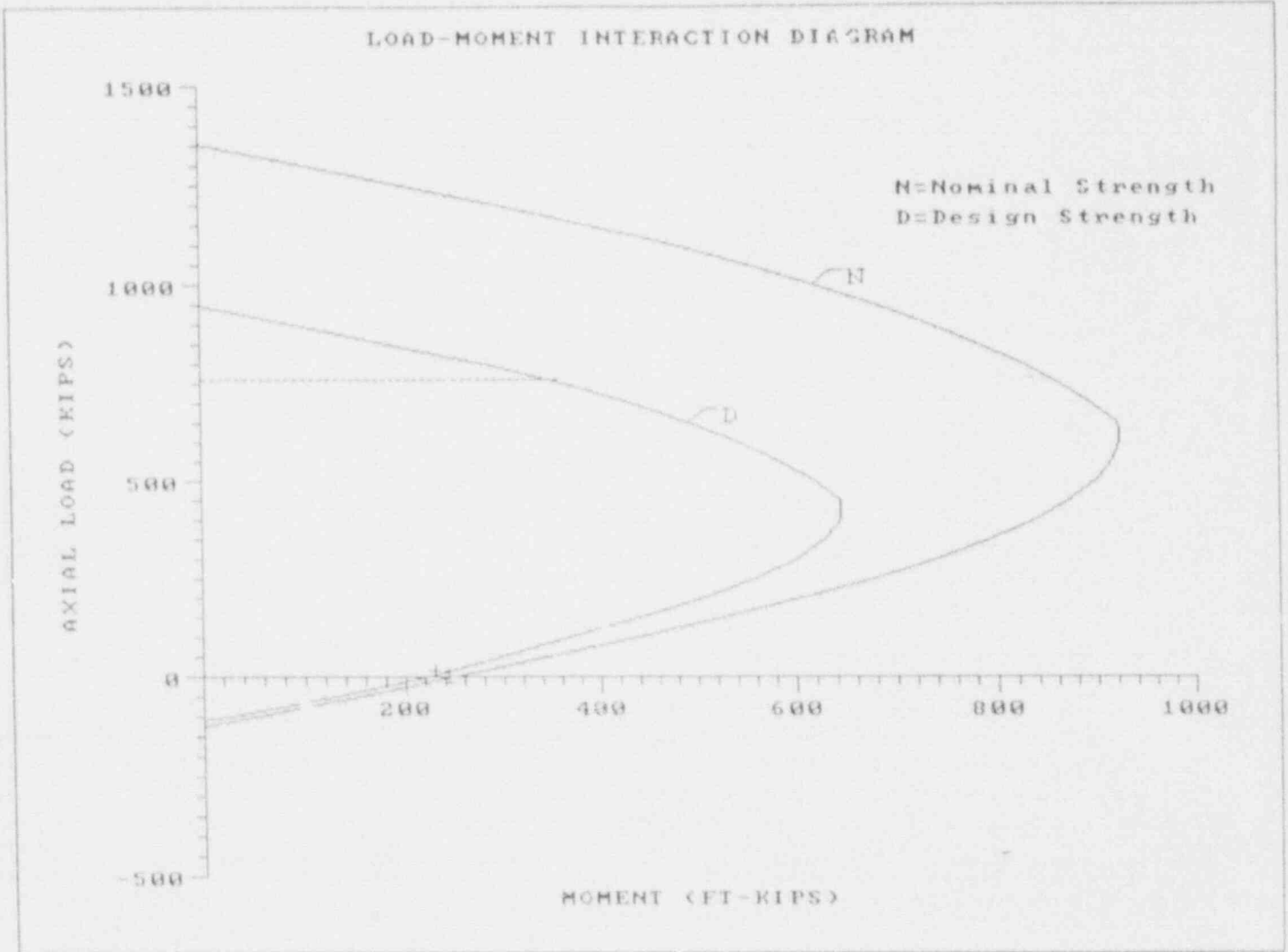


Figure 5.14

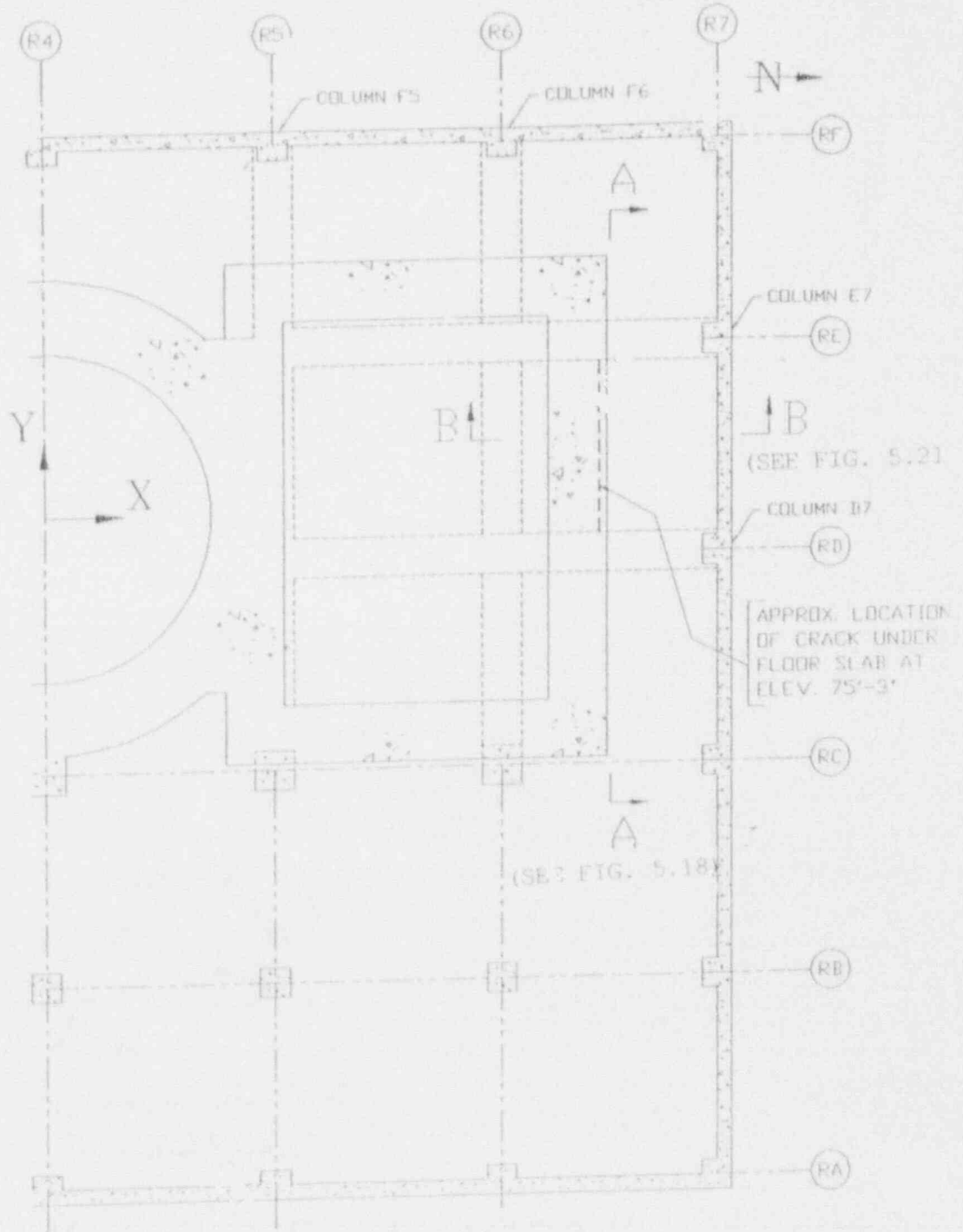


Figure 5.15

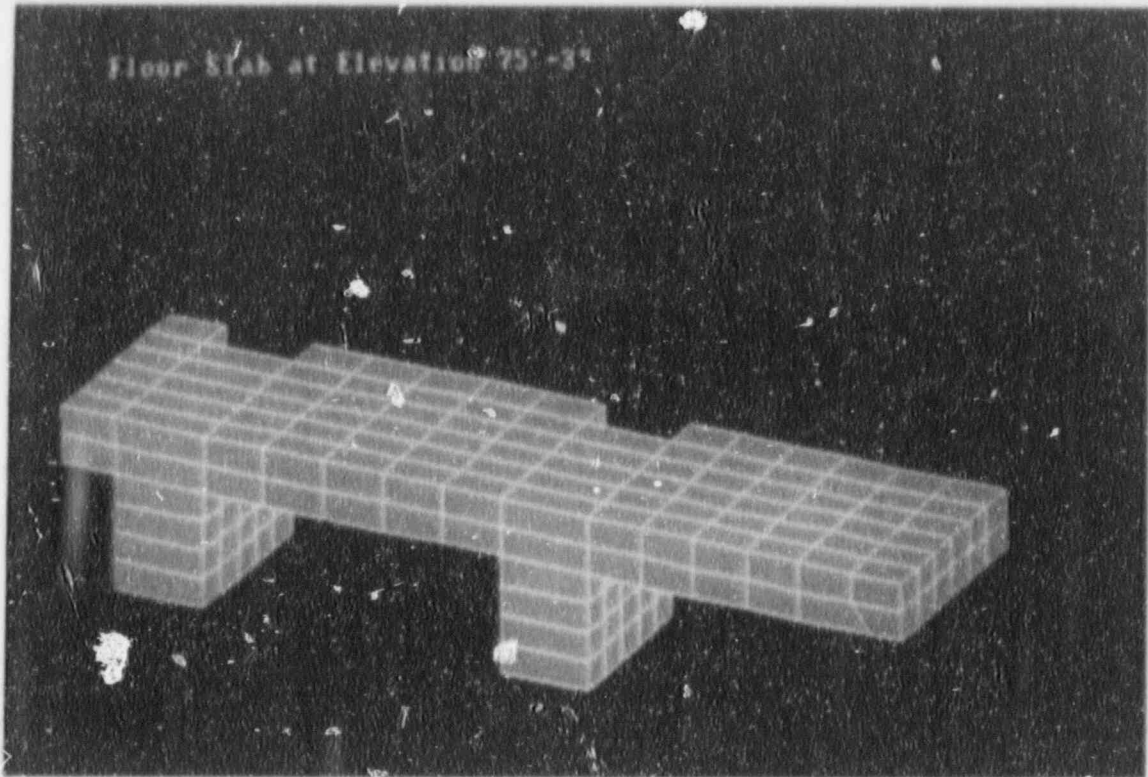


Figure 5.18

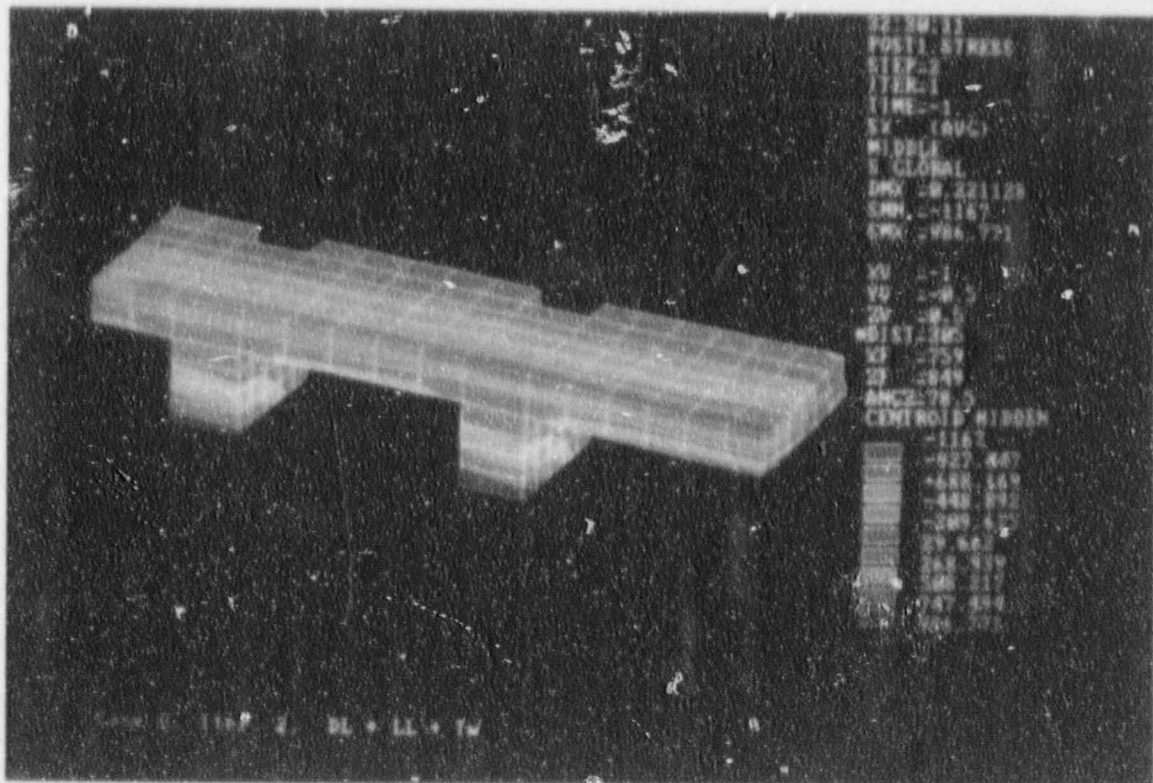


Figure 5.19

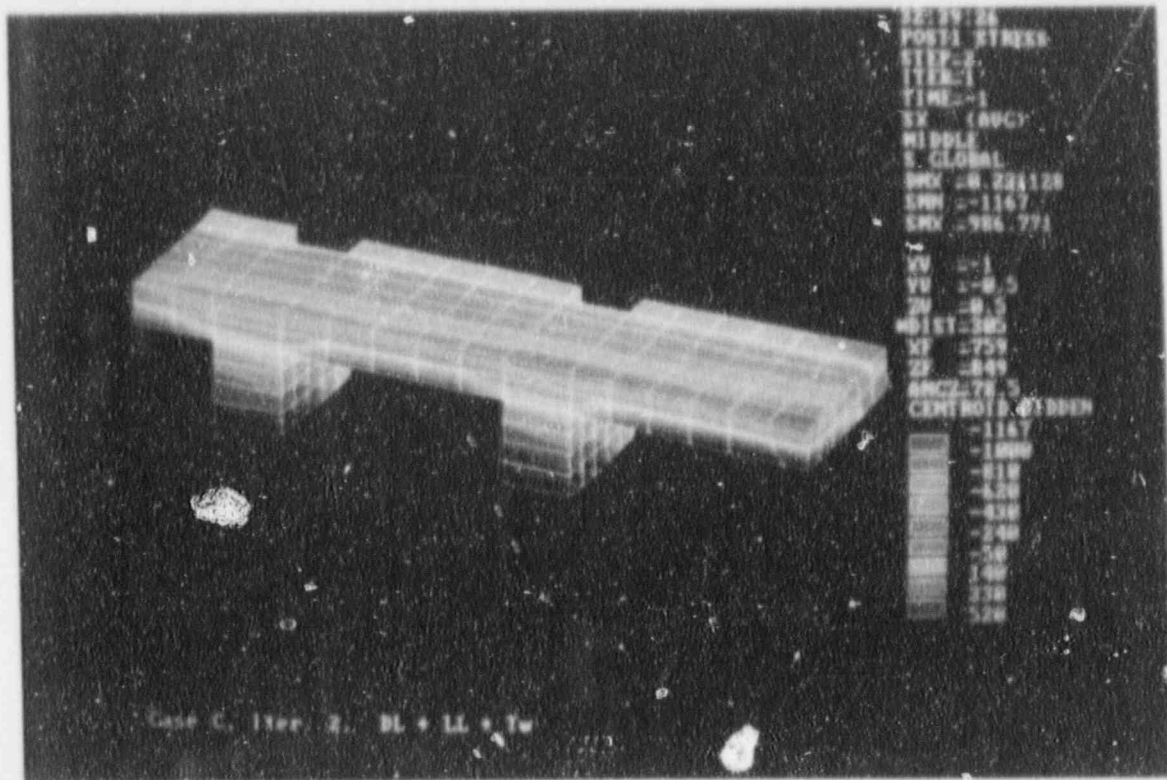


Figure 5.20

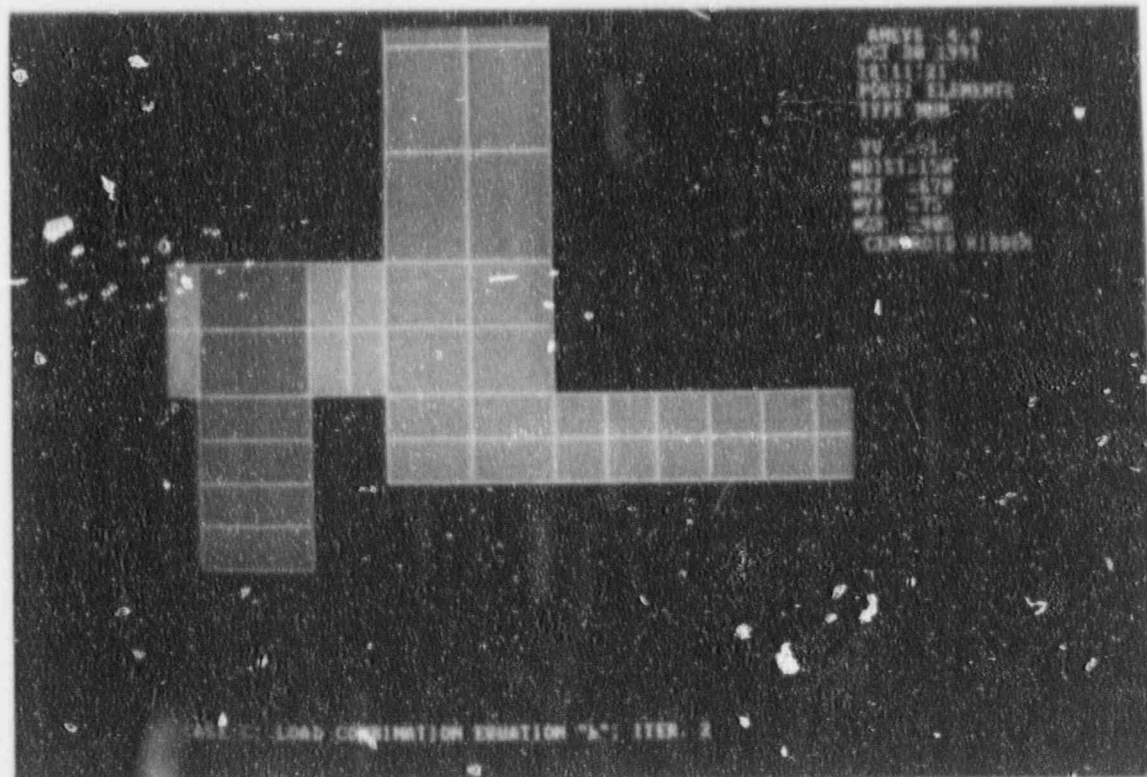


Figure 5.21

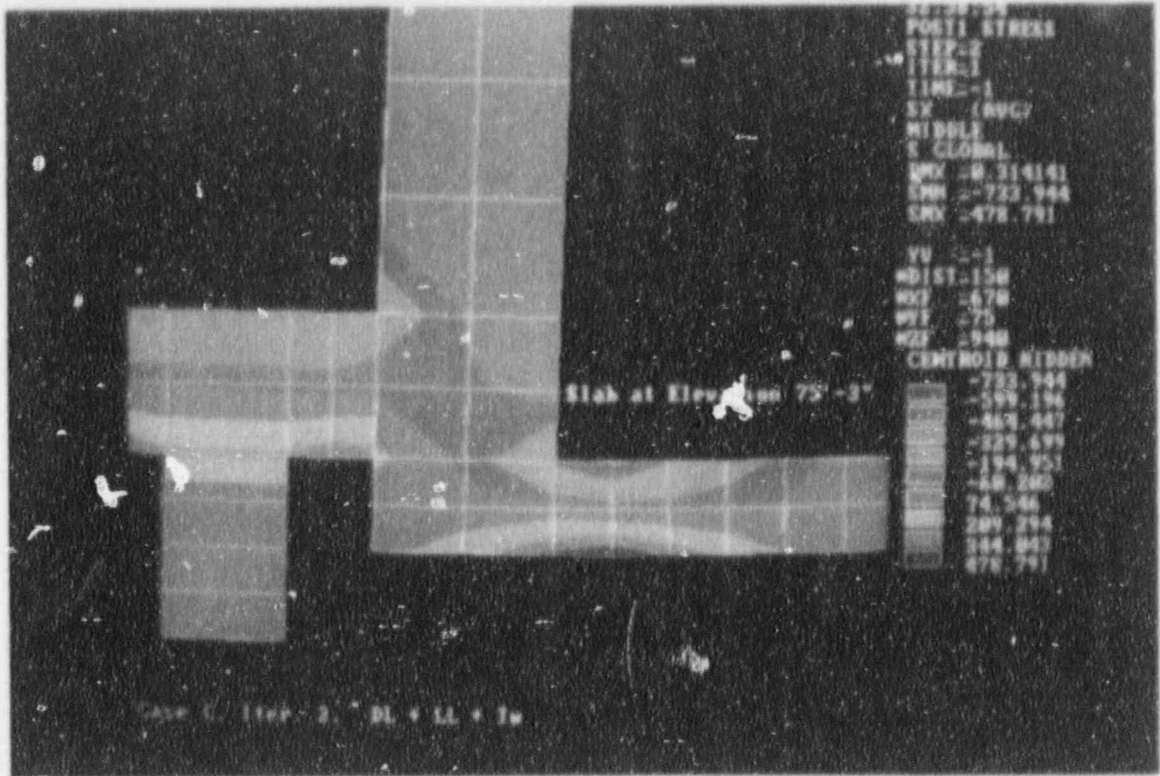


Figure 5.22

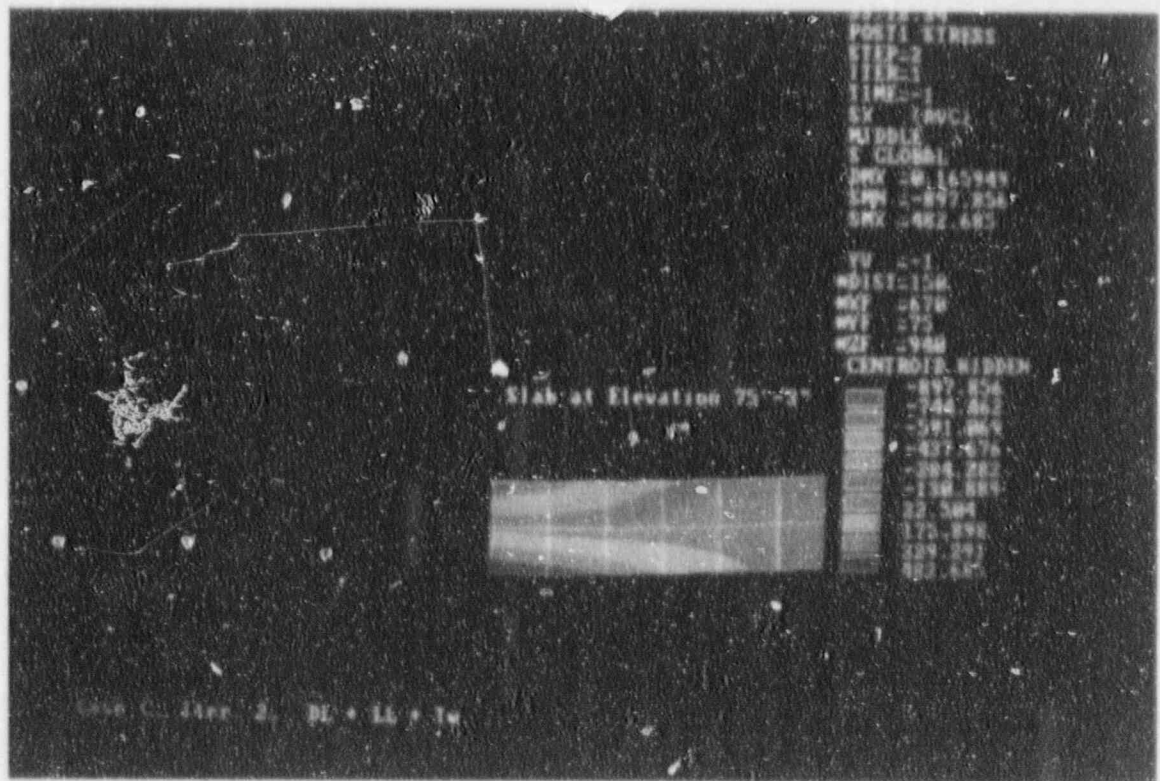


Figure 5.23

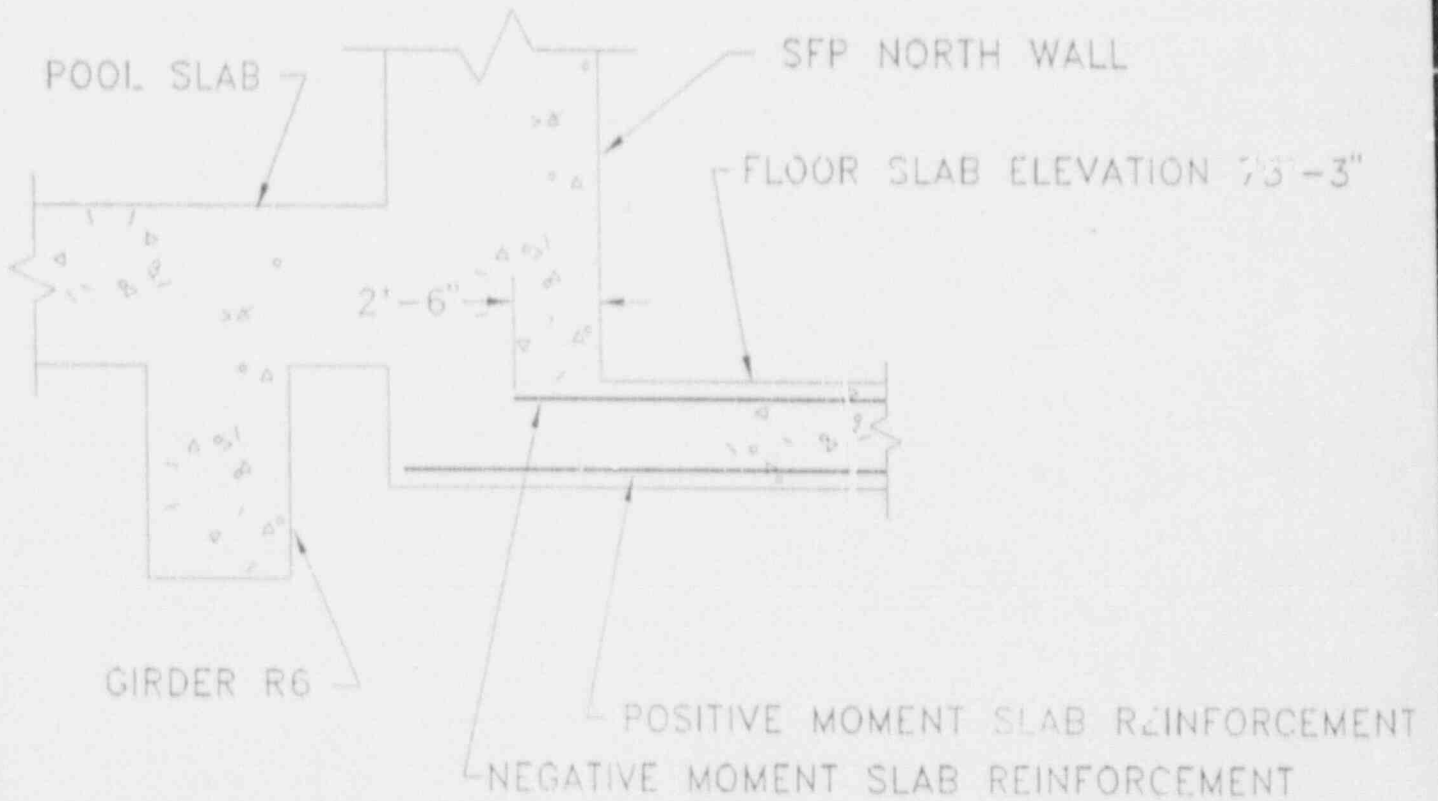


Figure 5.24

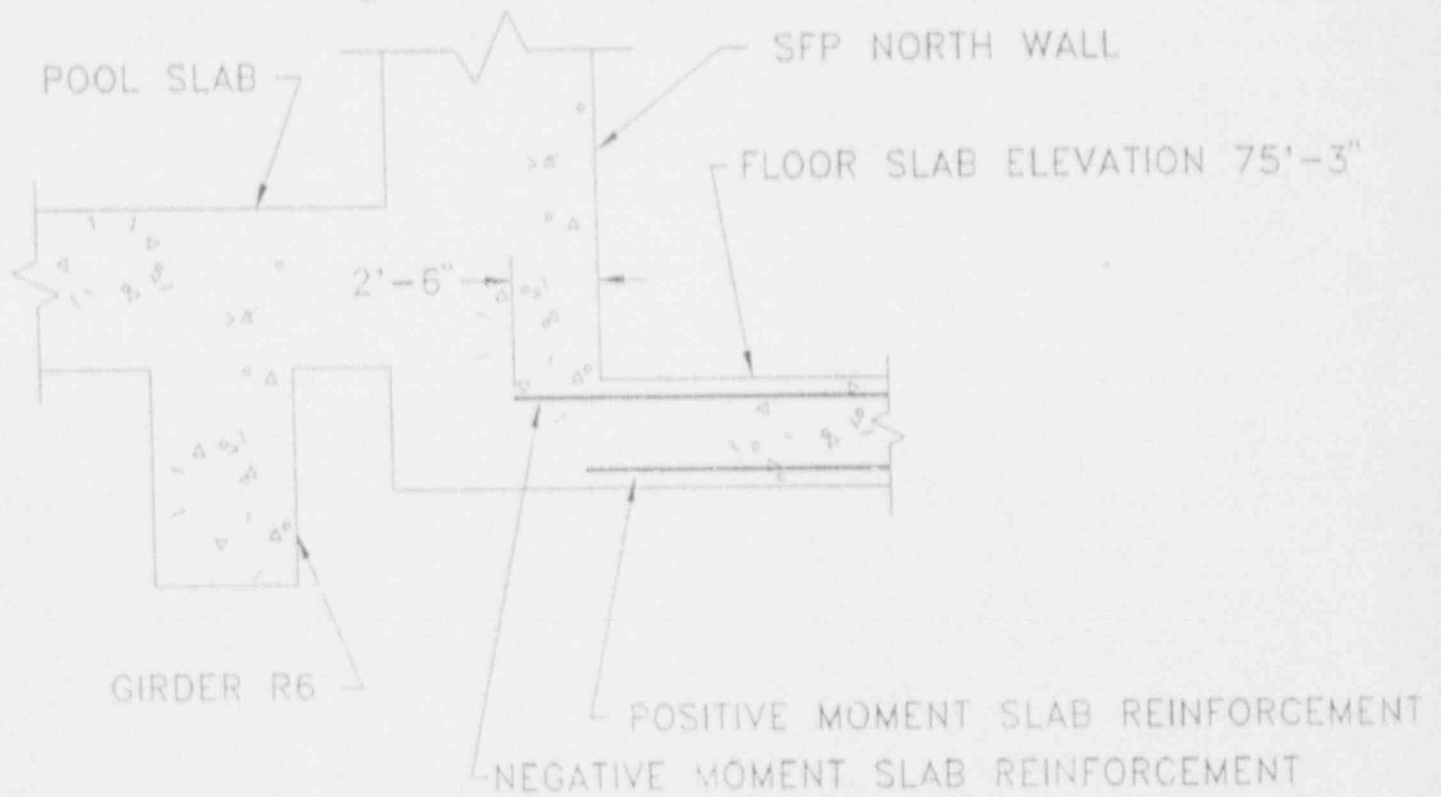


Figure 5.25

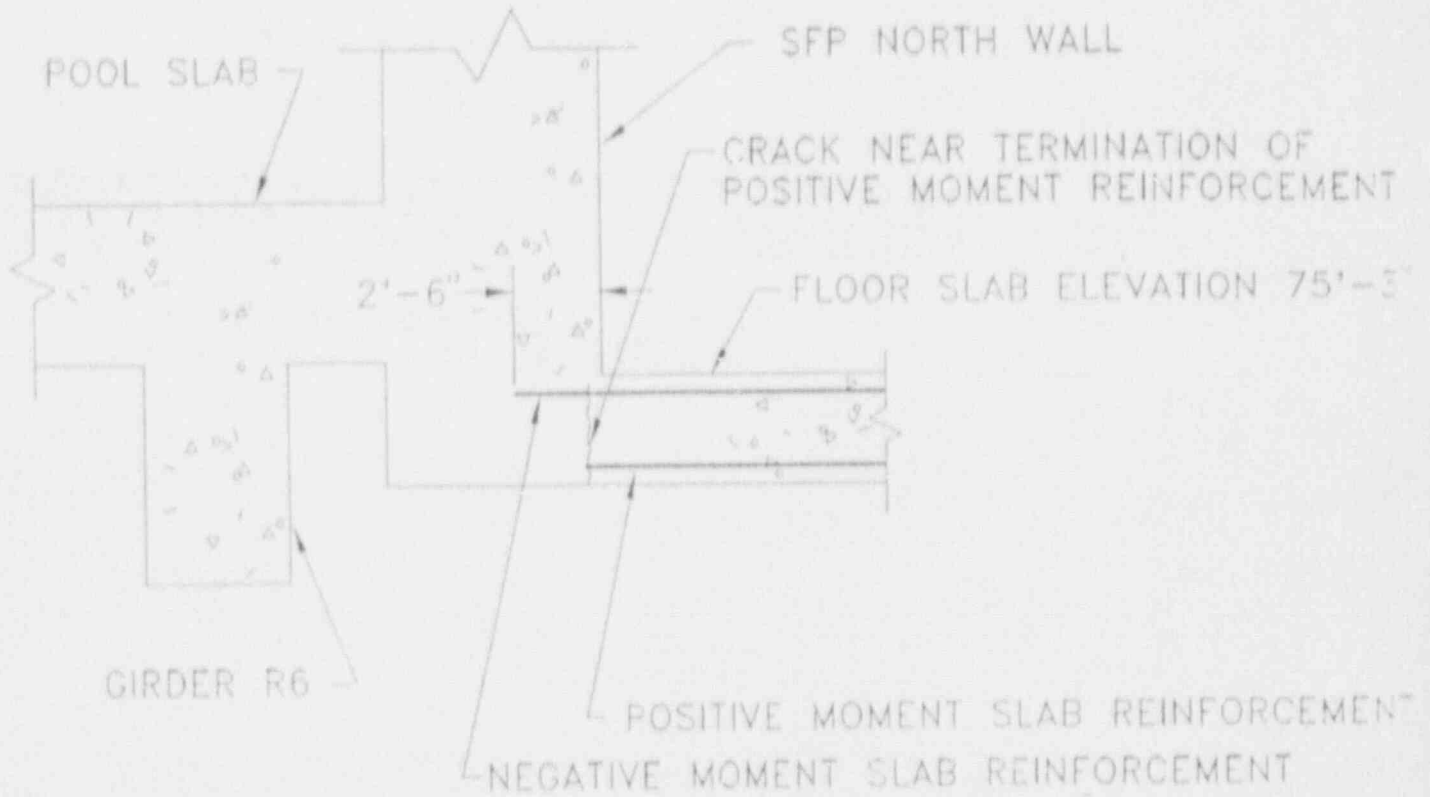


Figure 5 2C

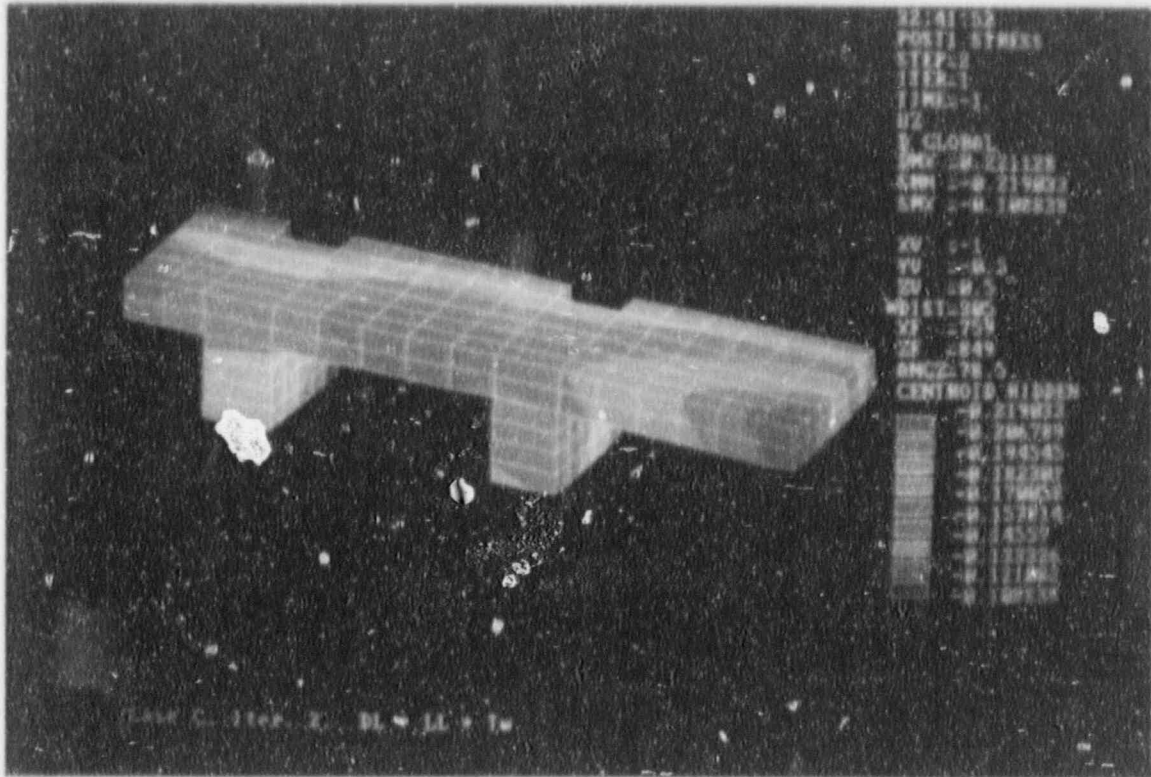


Figure 5.27

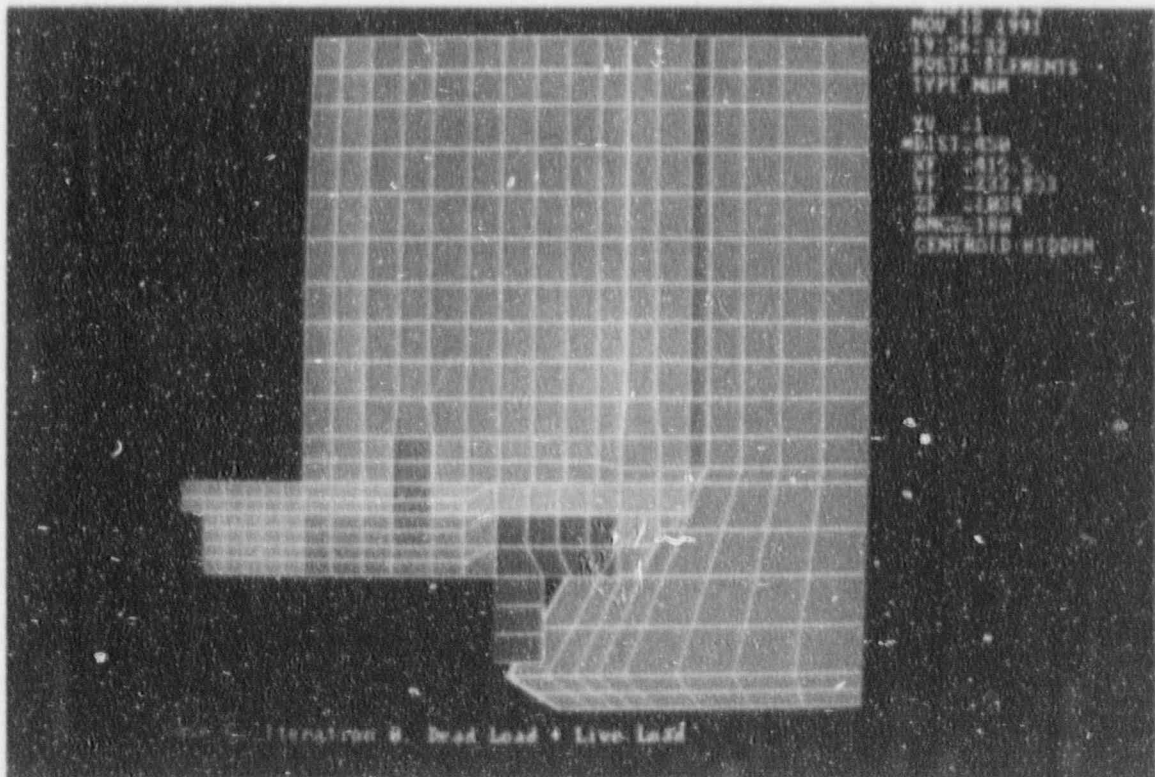


Figure 5.28

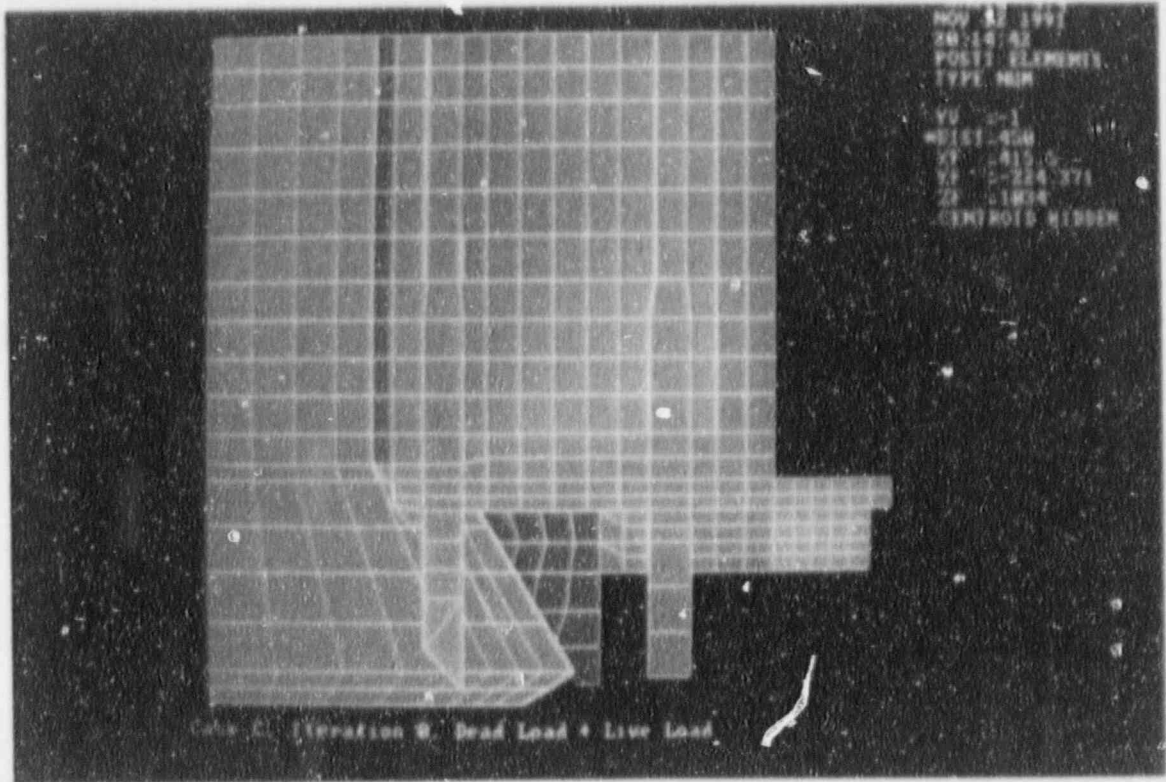


Figure 5.29

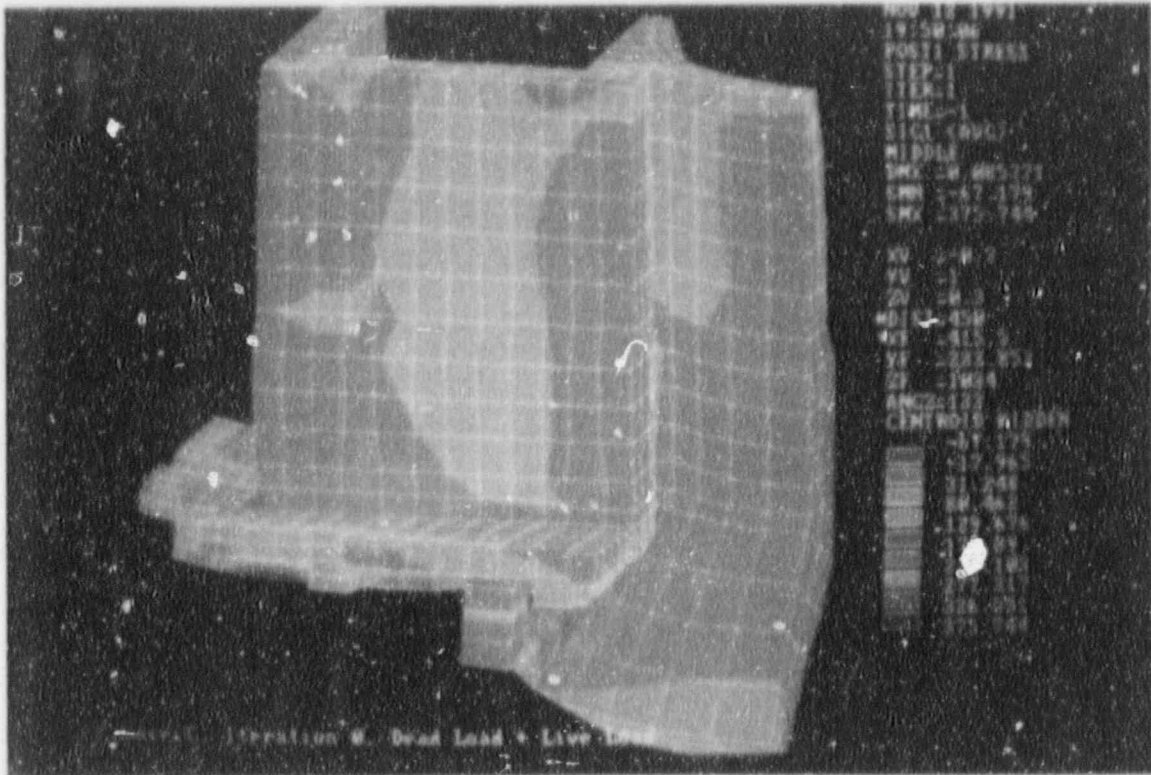


Figure 5.30

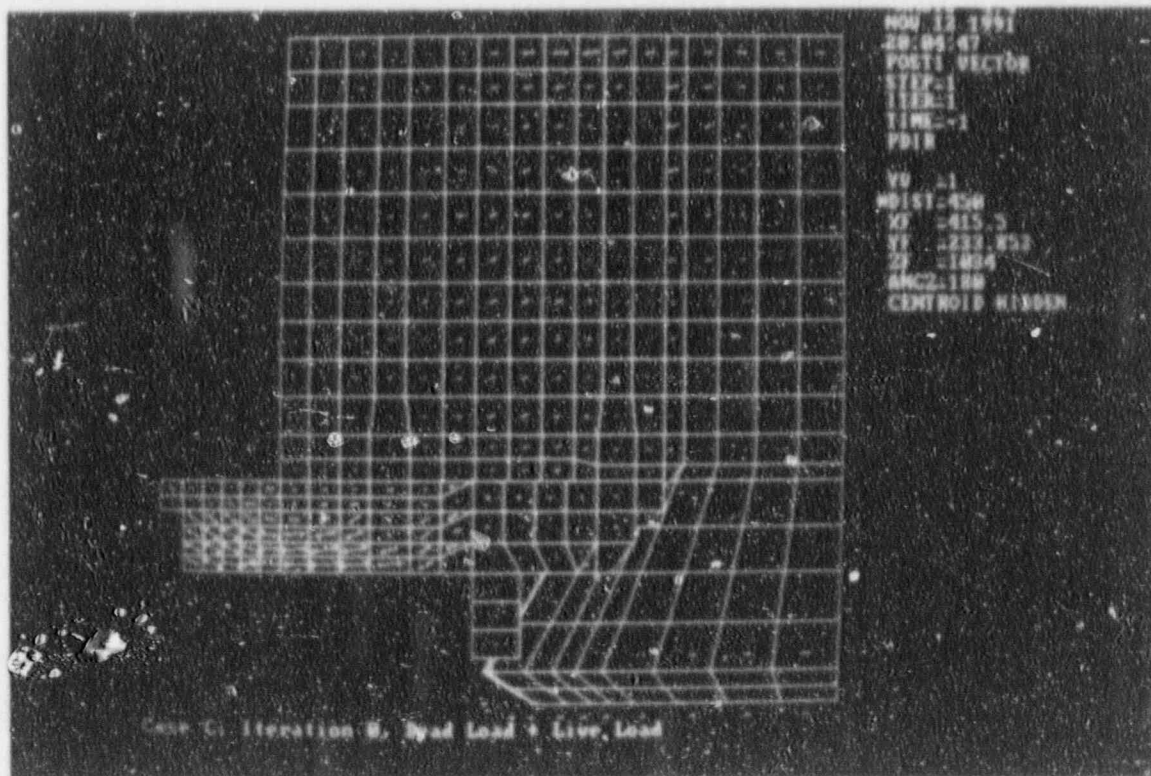


Figure 5.31

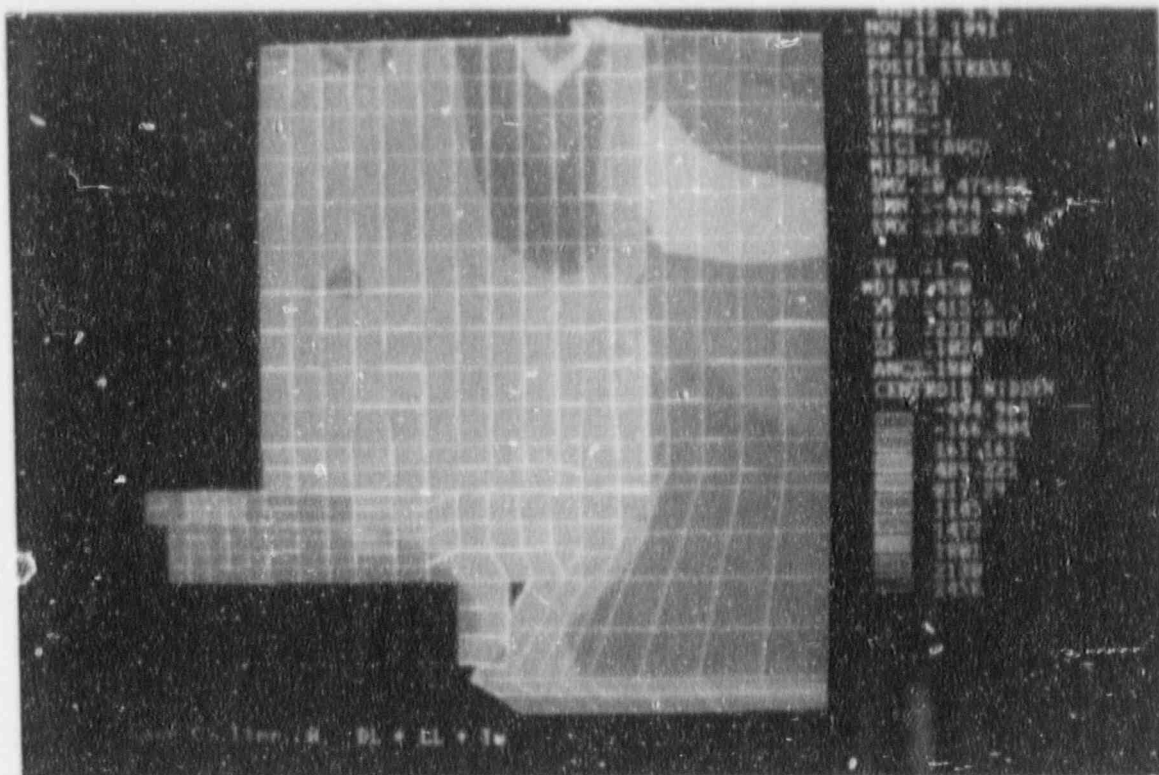


Figure 5.32

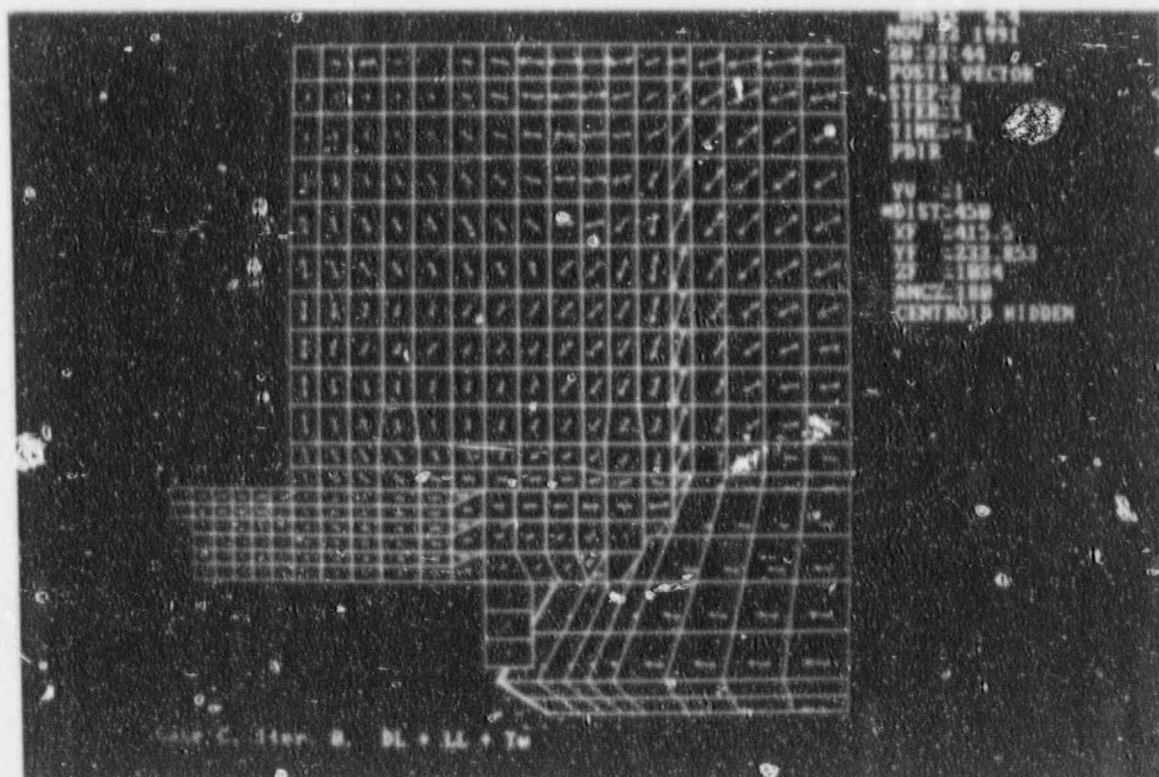


Figure 5.33

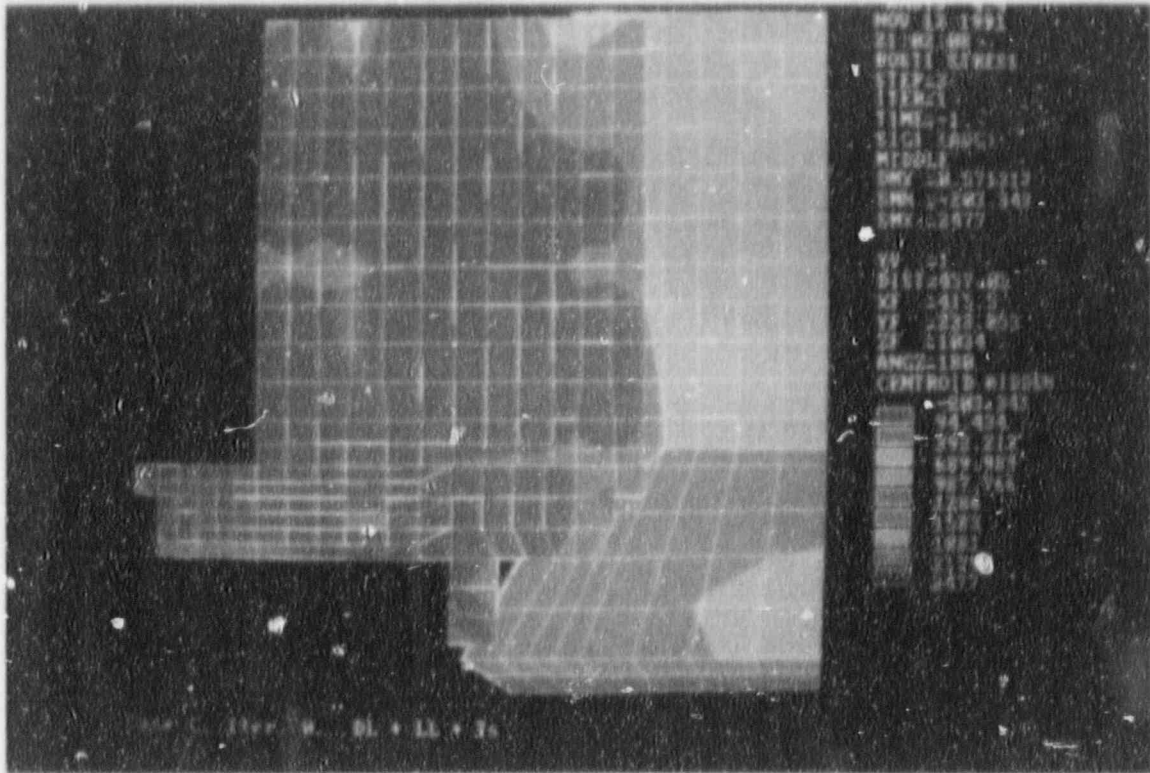


Figure 5.34

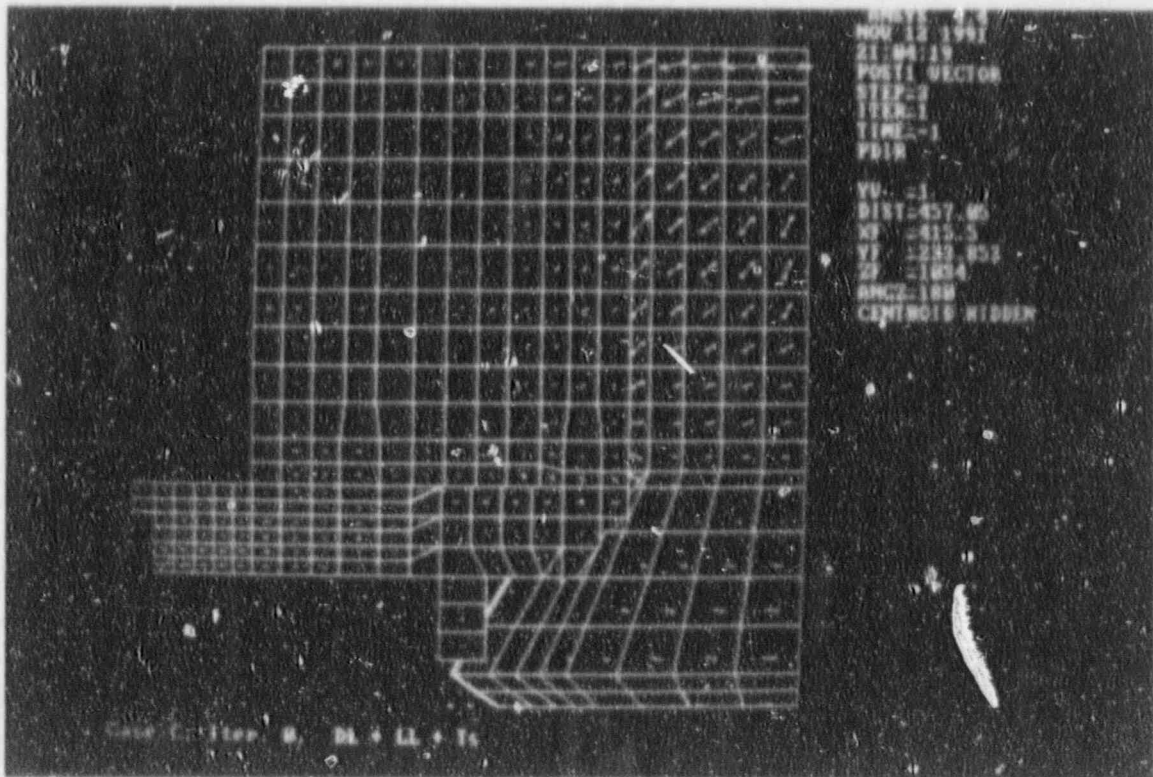
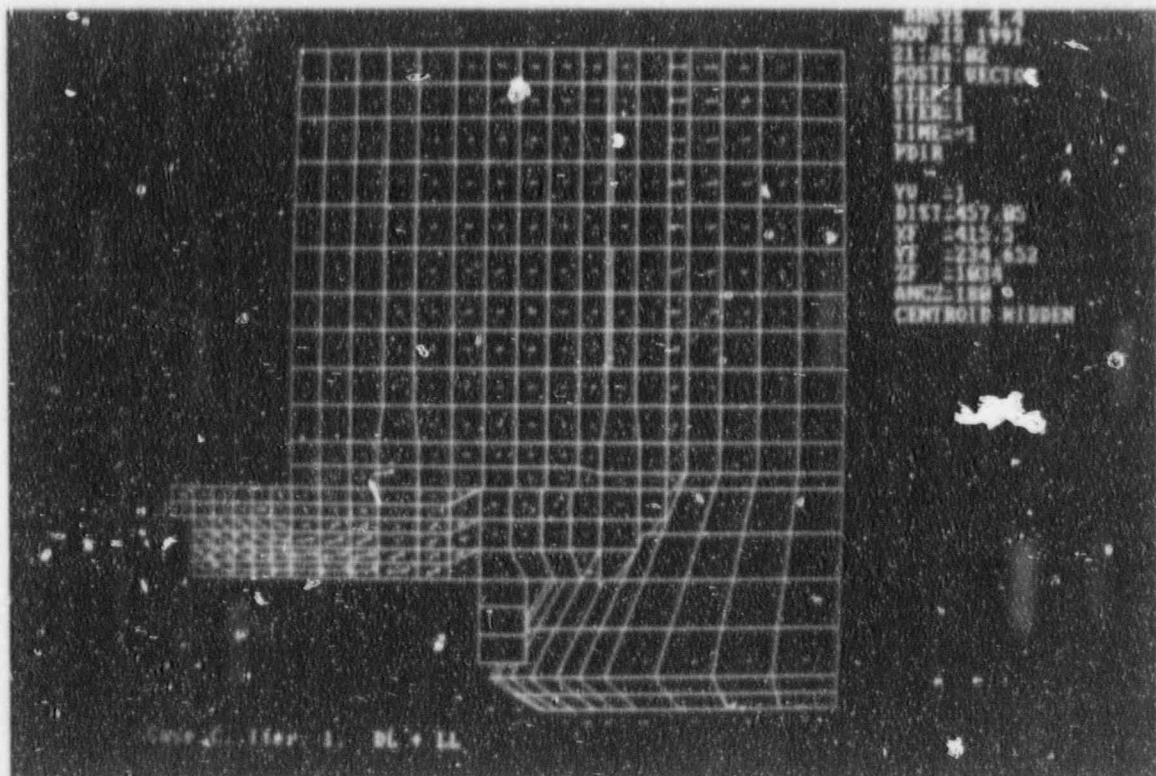
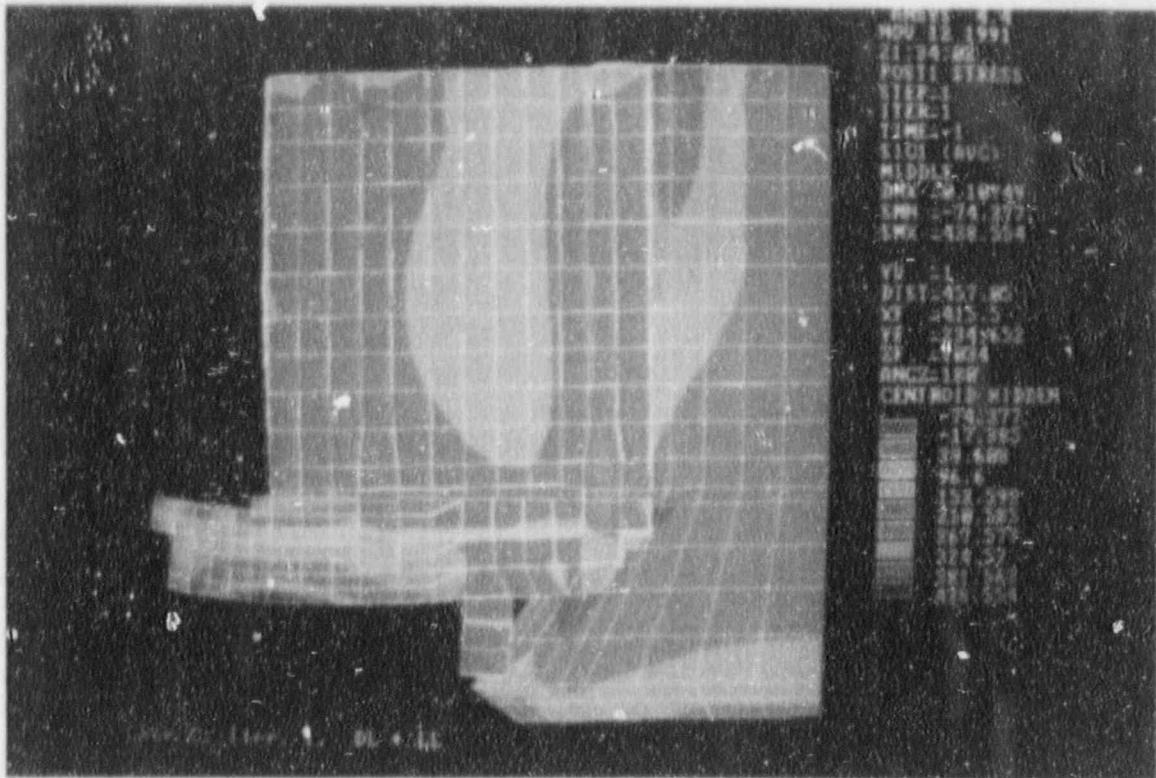


Figure 5.35



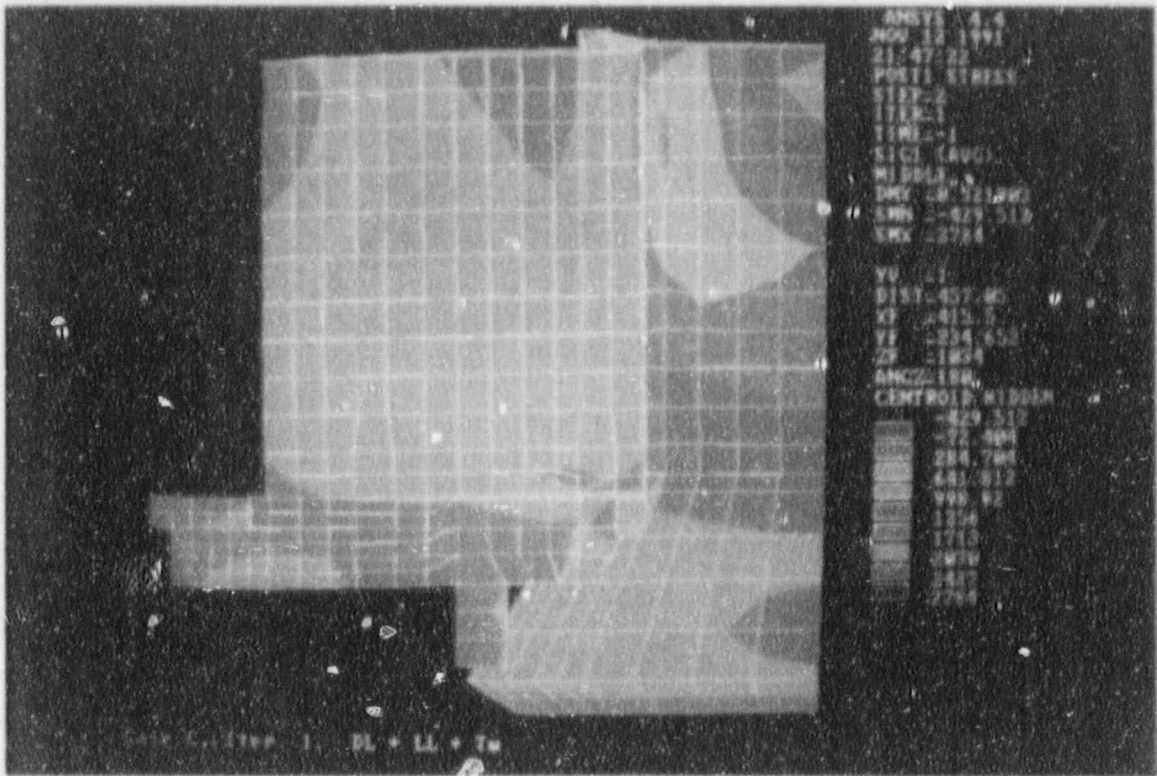


Figure 5.38

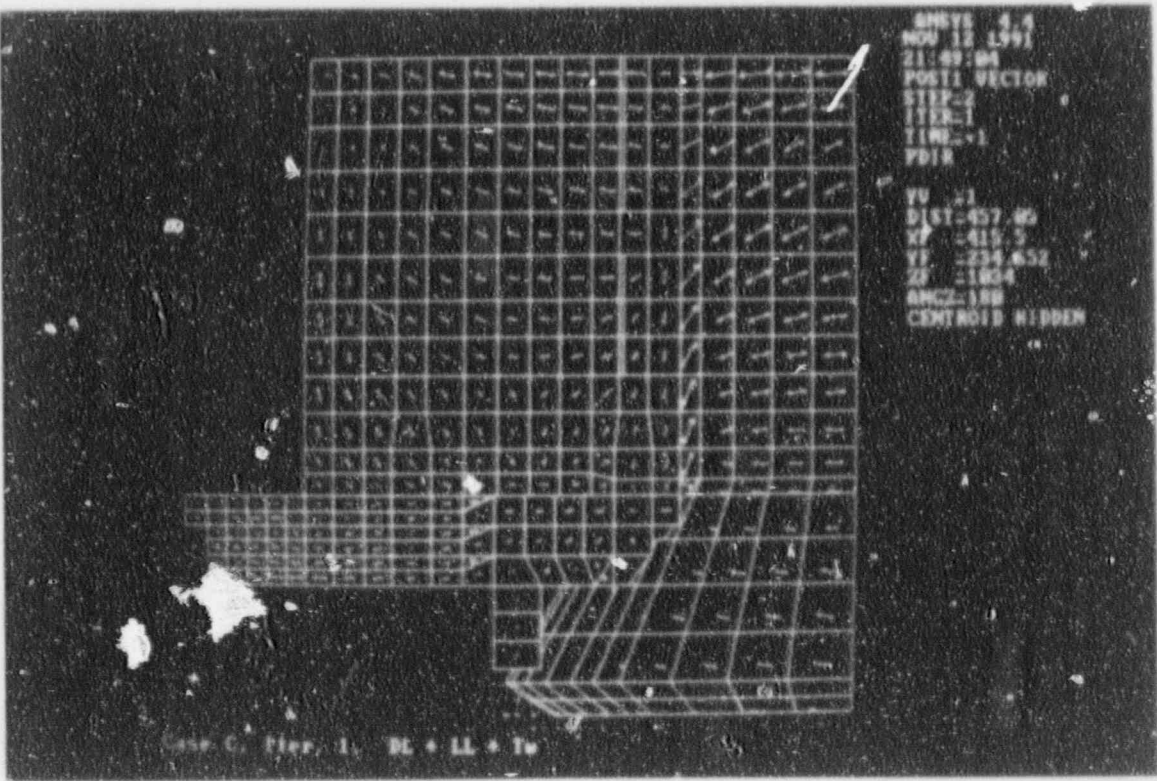


Figure 5.39

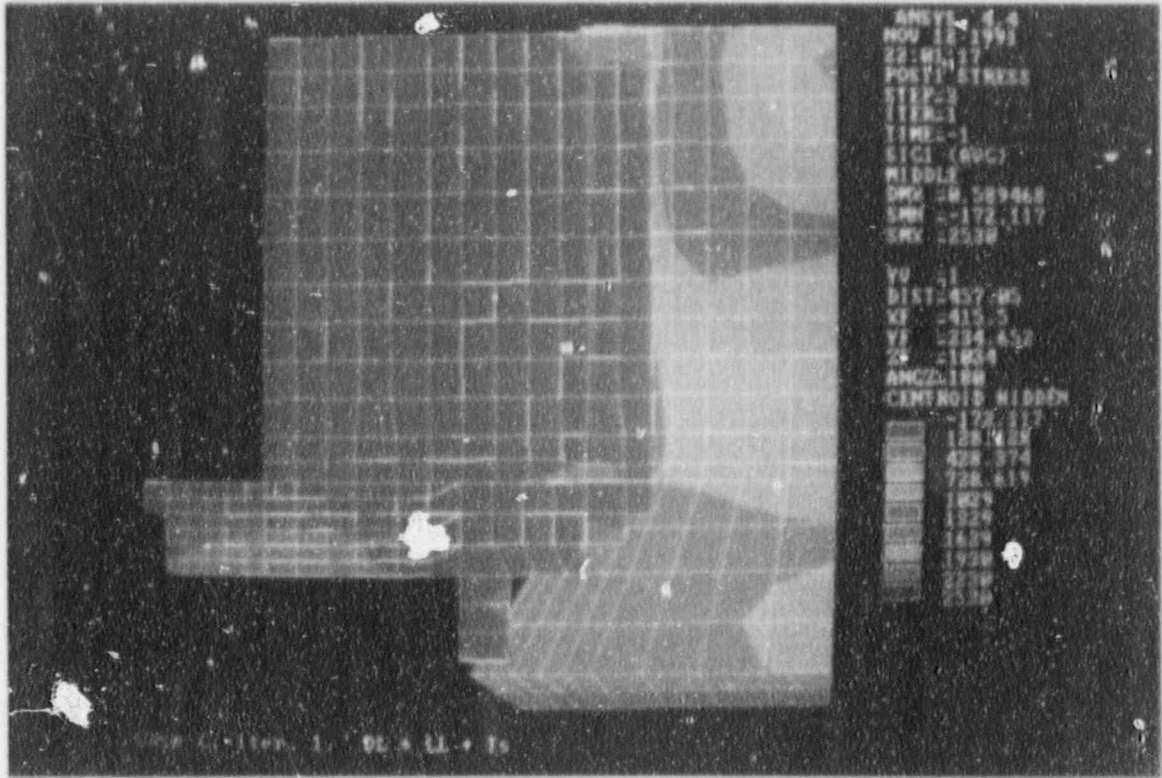


Figure 5.40

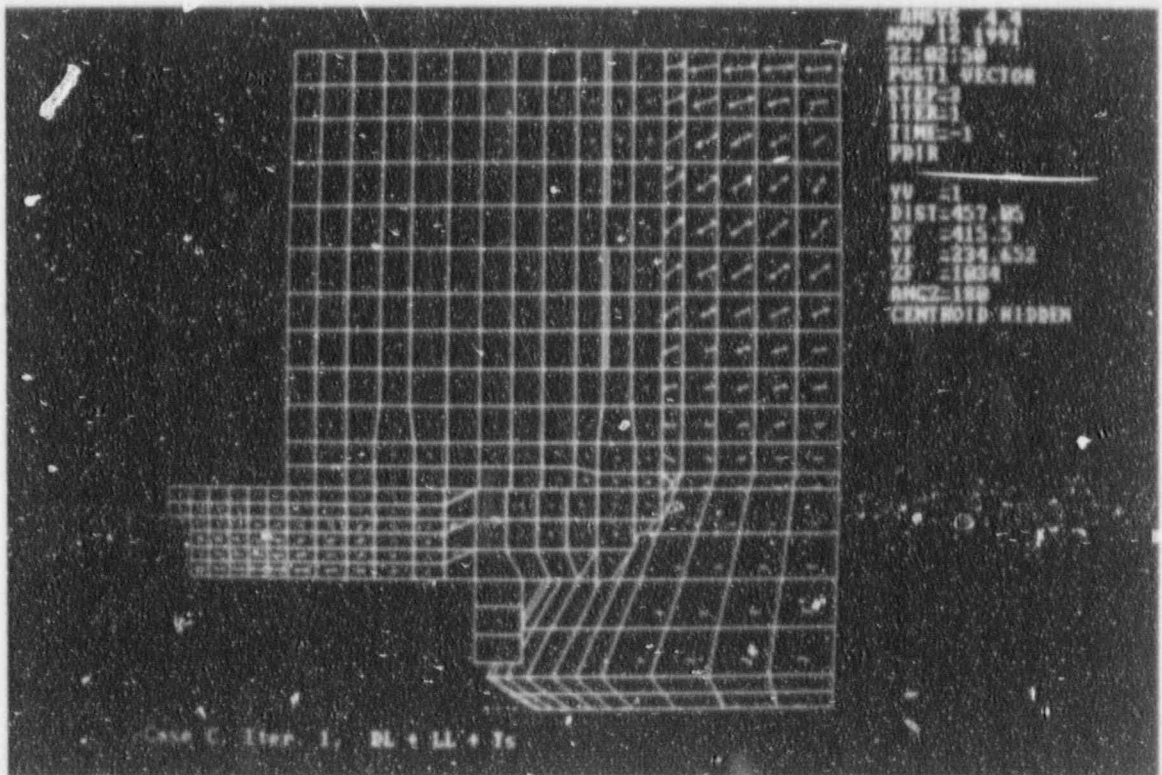


Figure 5.41

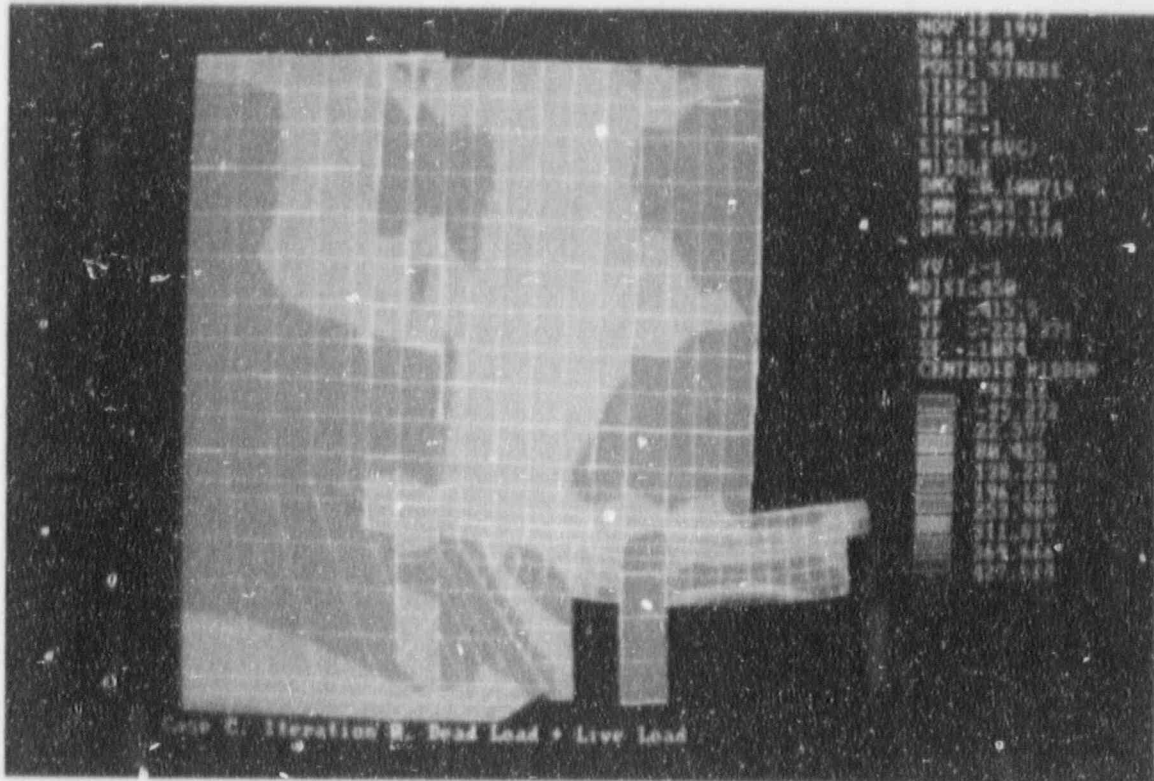


Figure 5.42

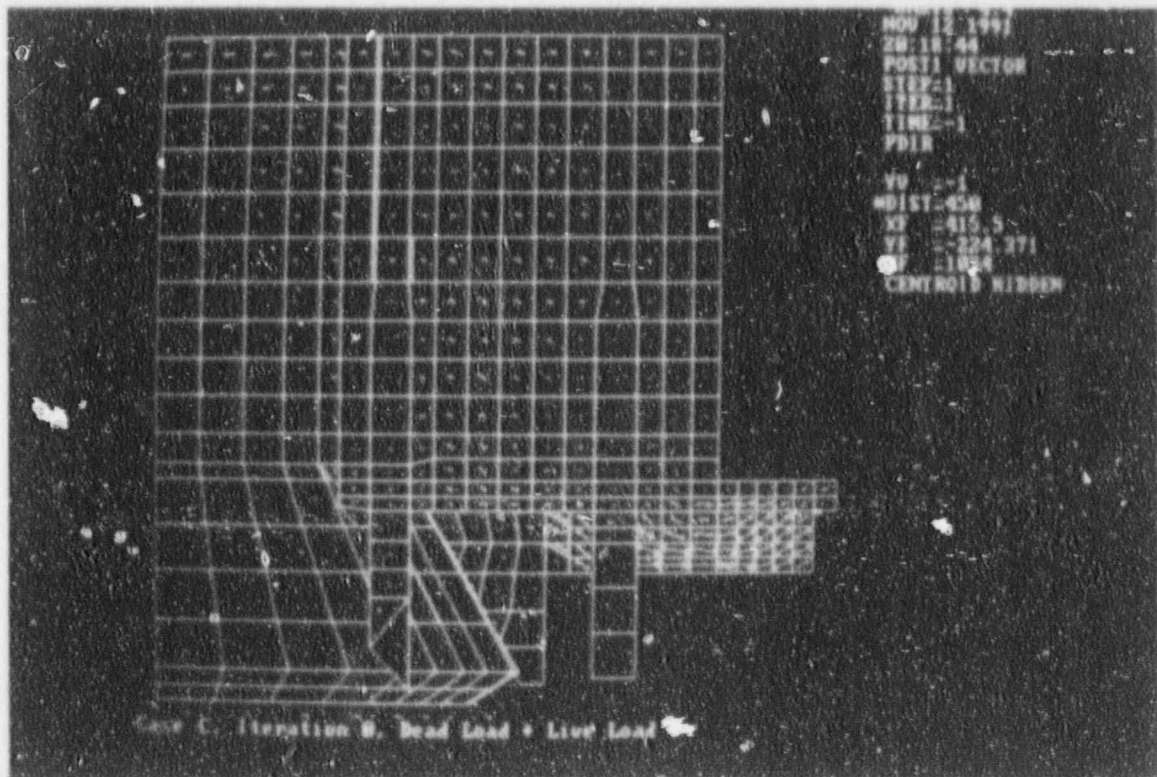


Figure 5.43

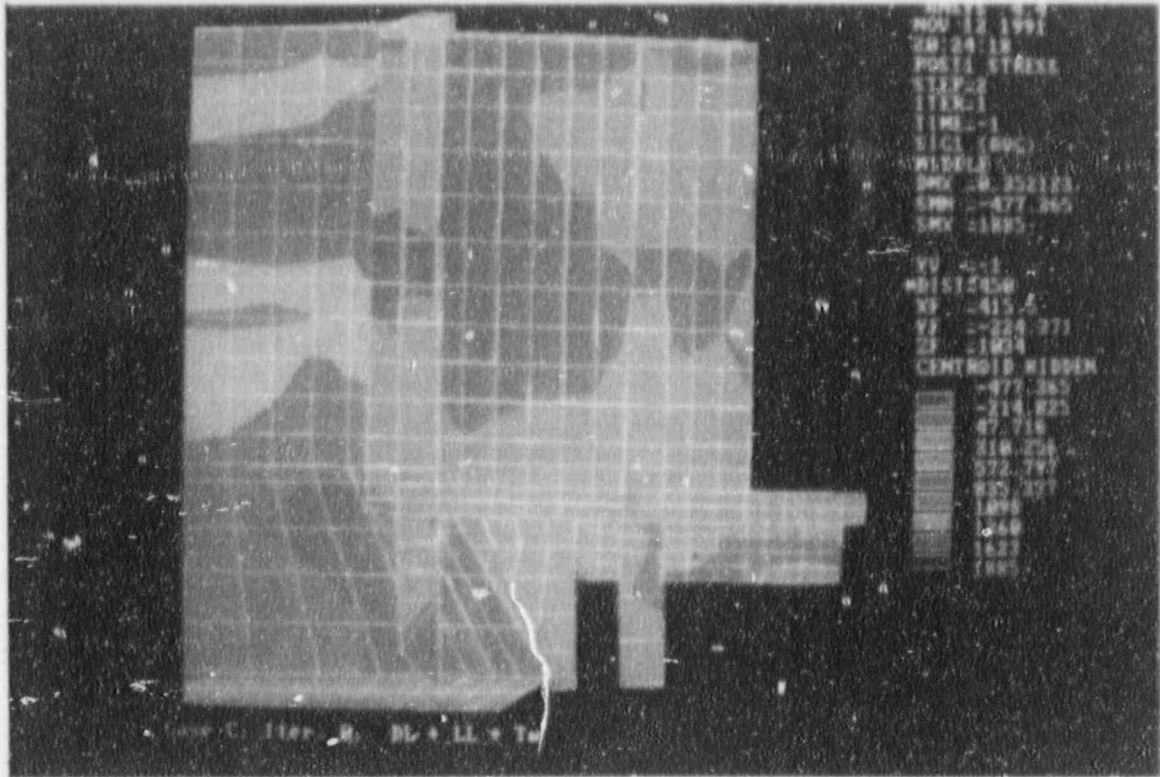


Figure 5.44

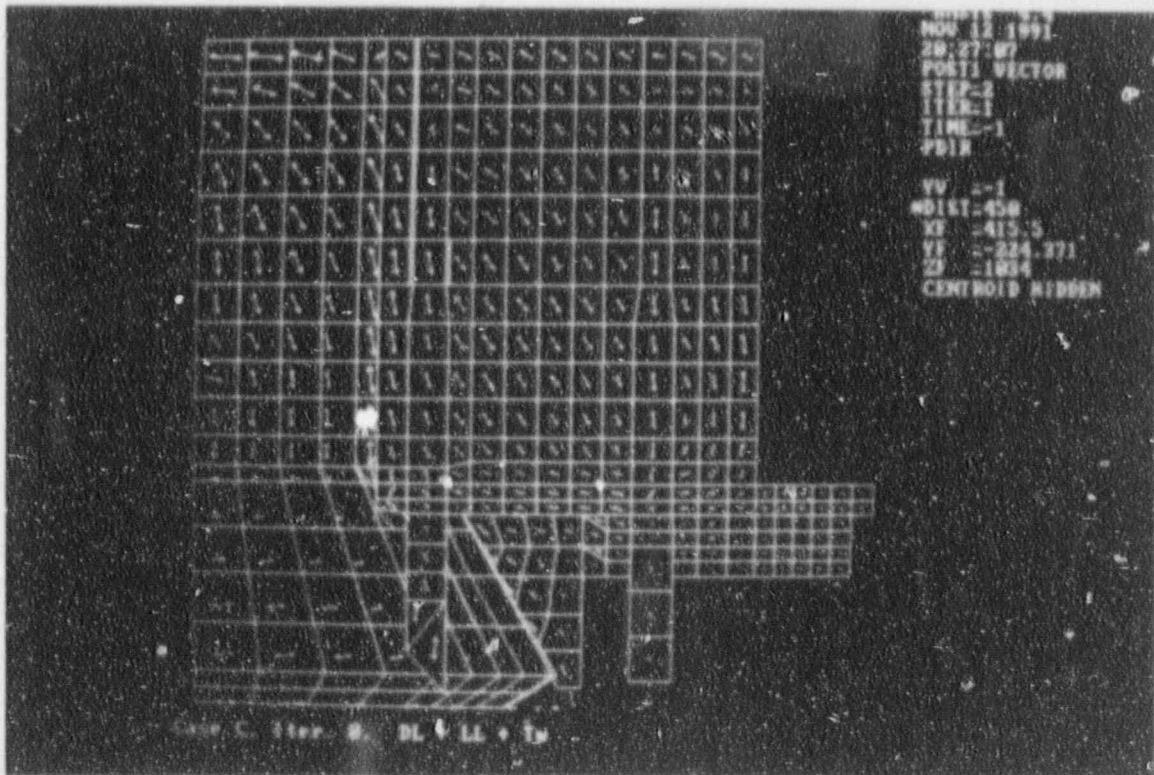


Figure 5.45

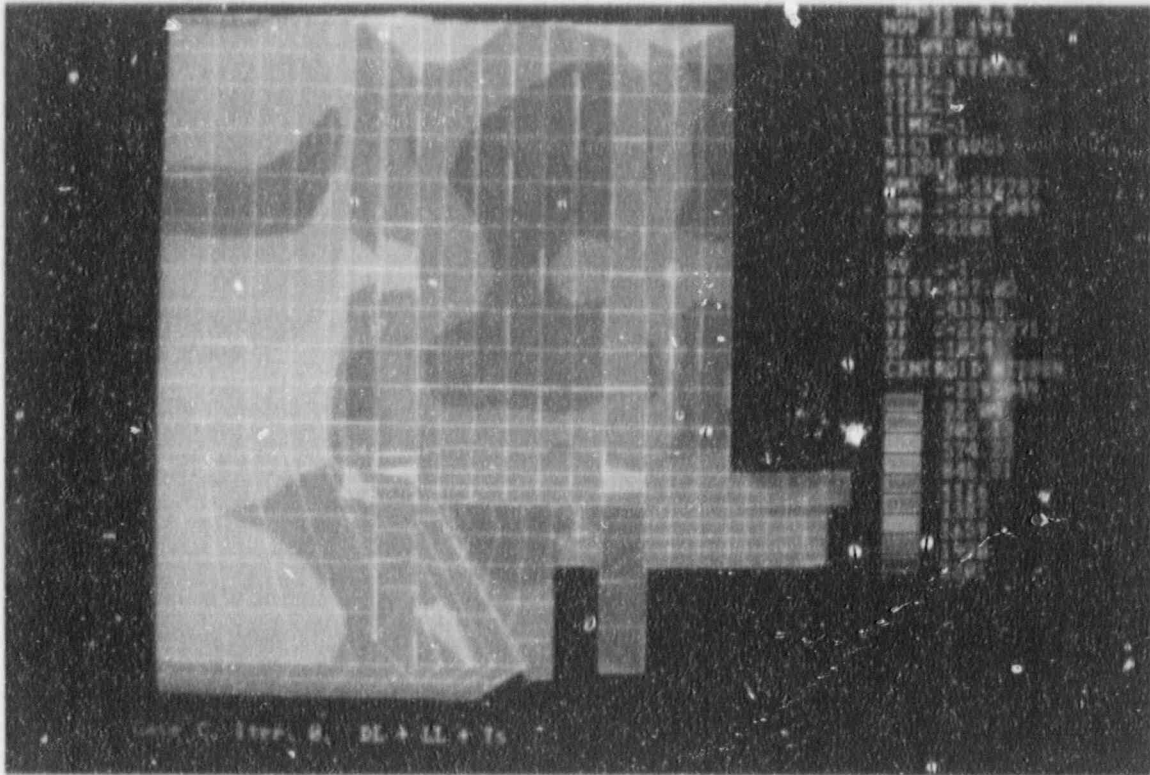


Figure 5.46

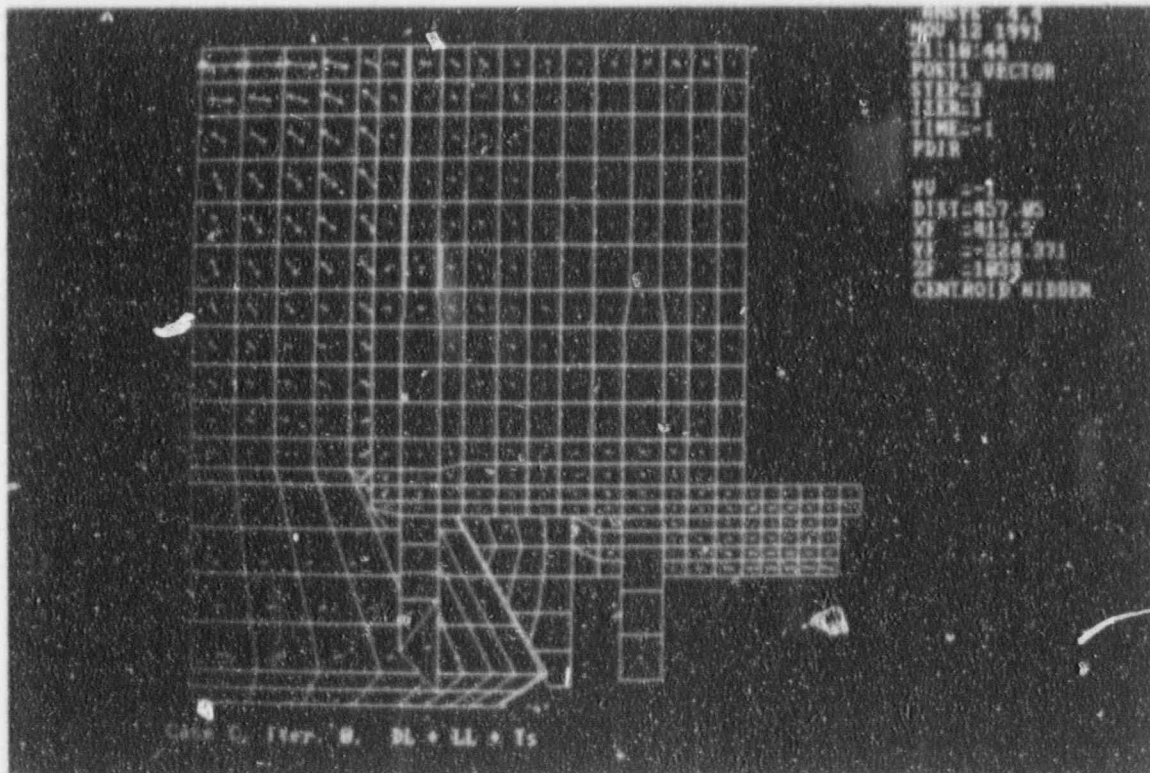


Figure 5.47

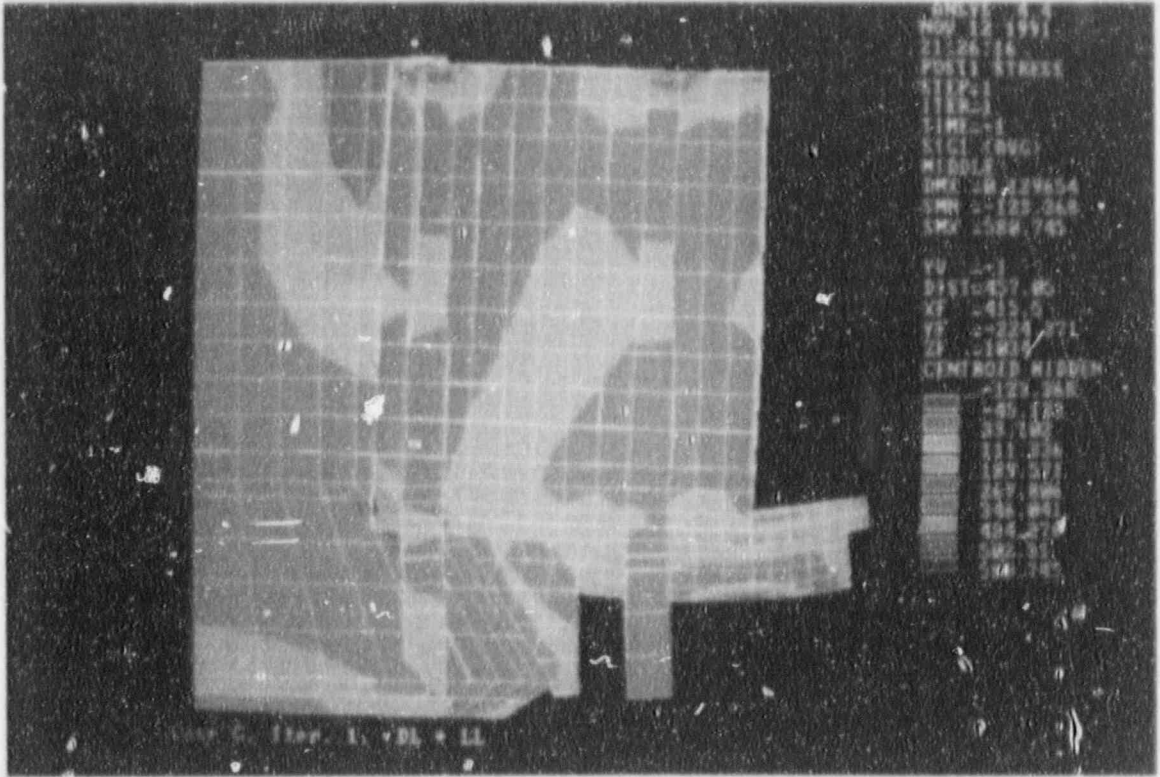


Figure 5.48

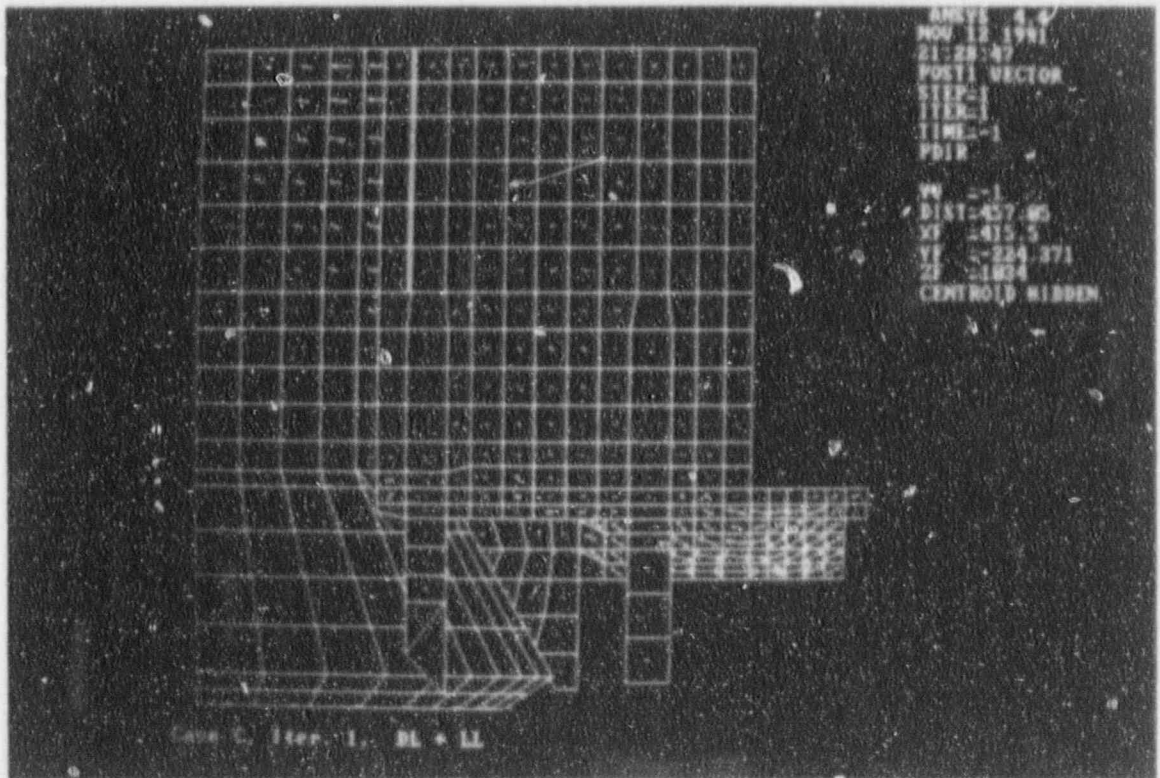


Figure 5.49

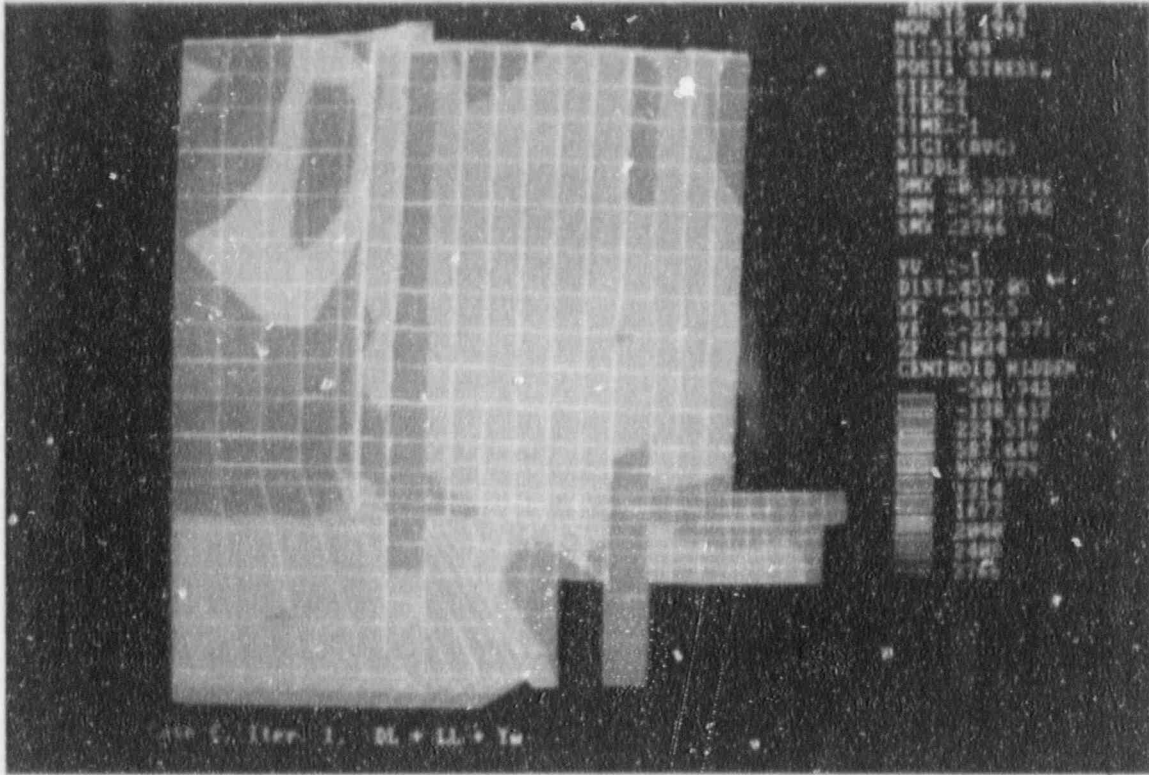


Figure 5.50

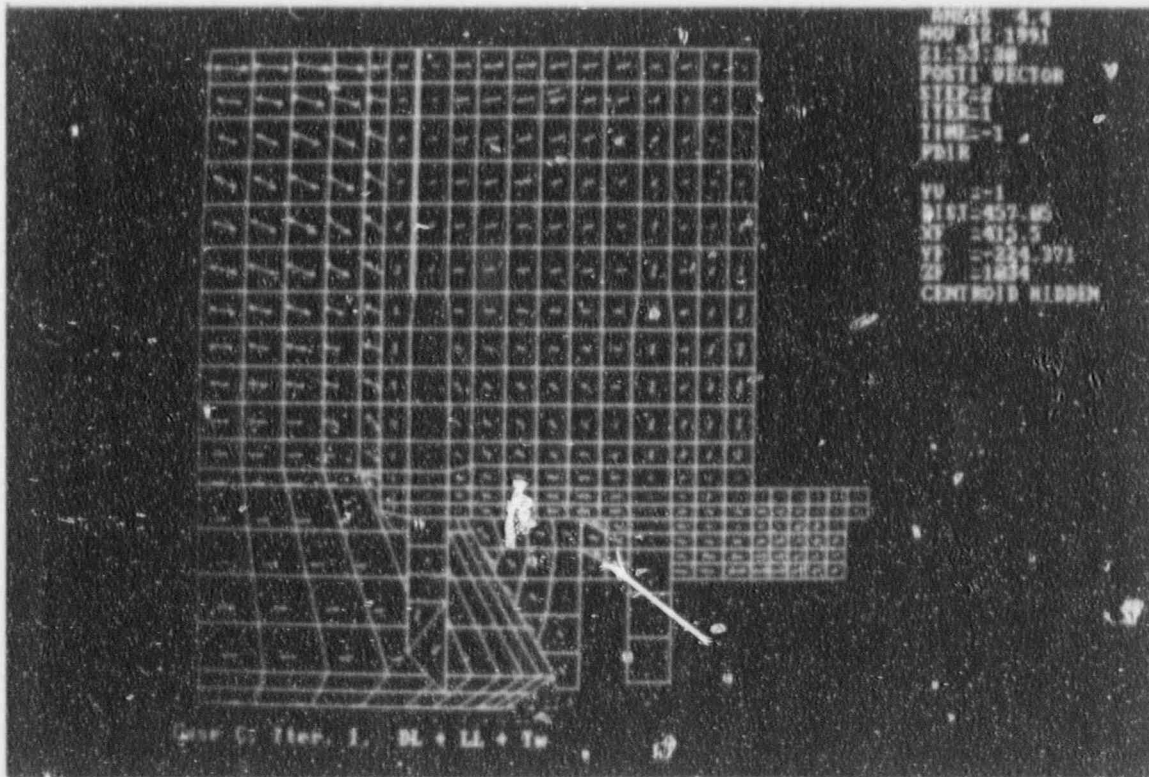


Figure 5.51

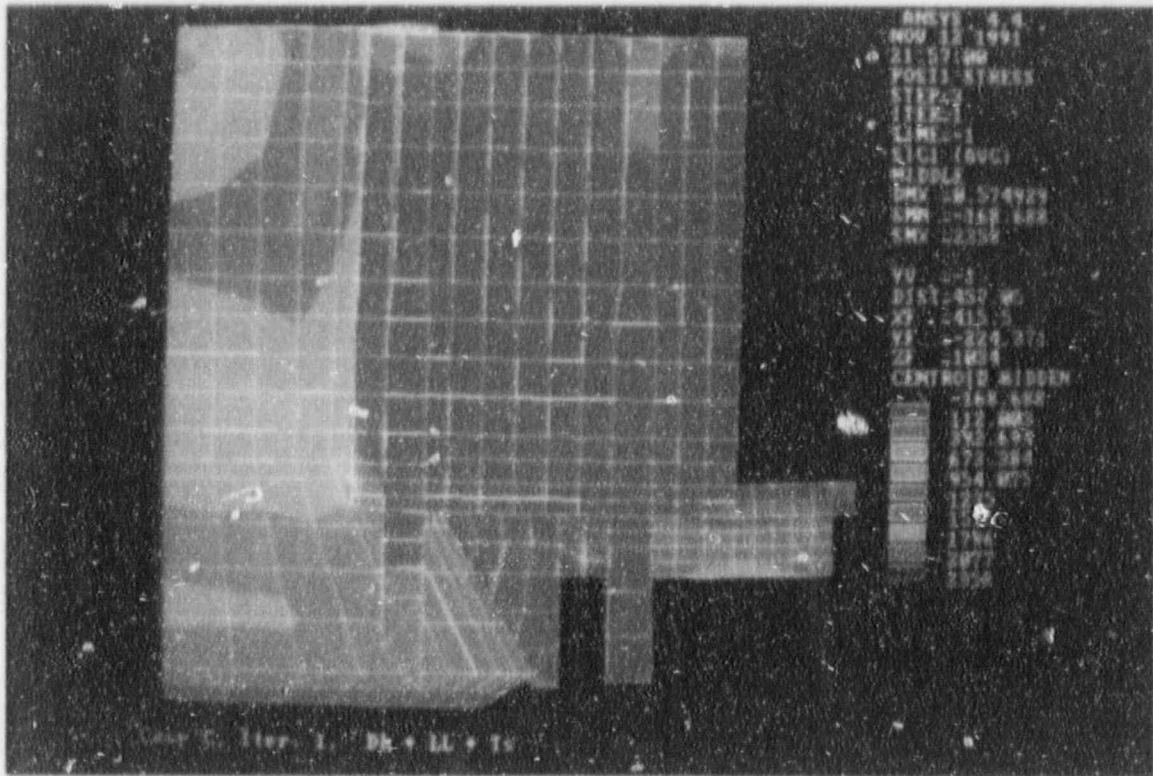


Figure 5.52

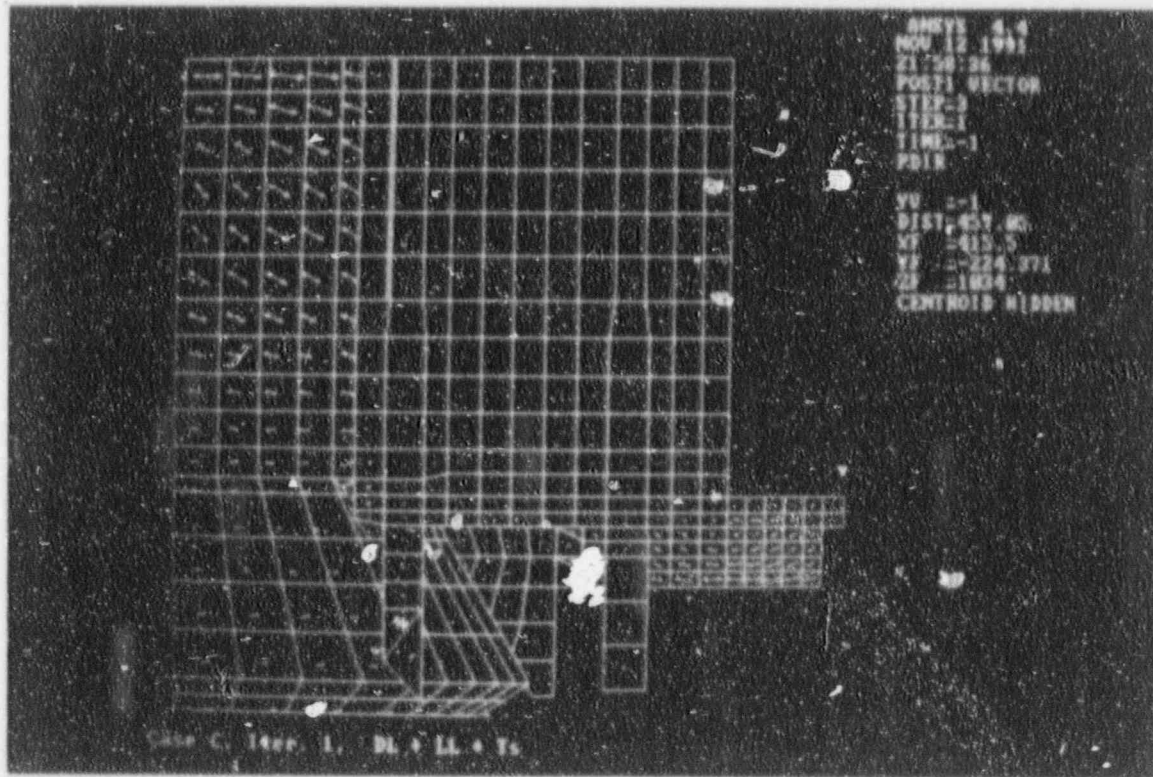


Figure 5.53

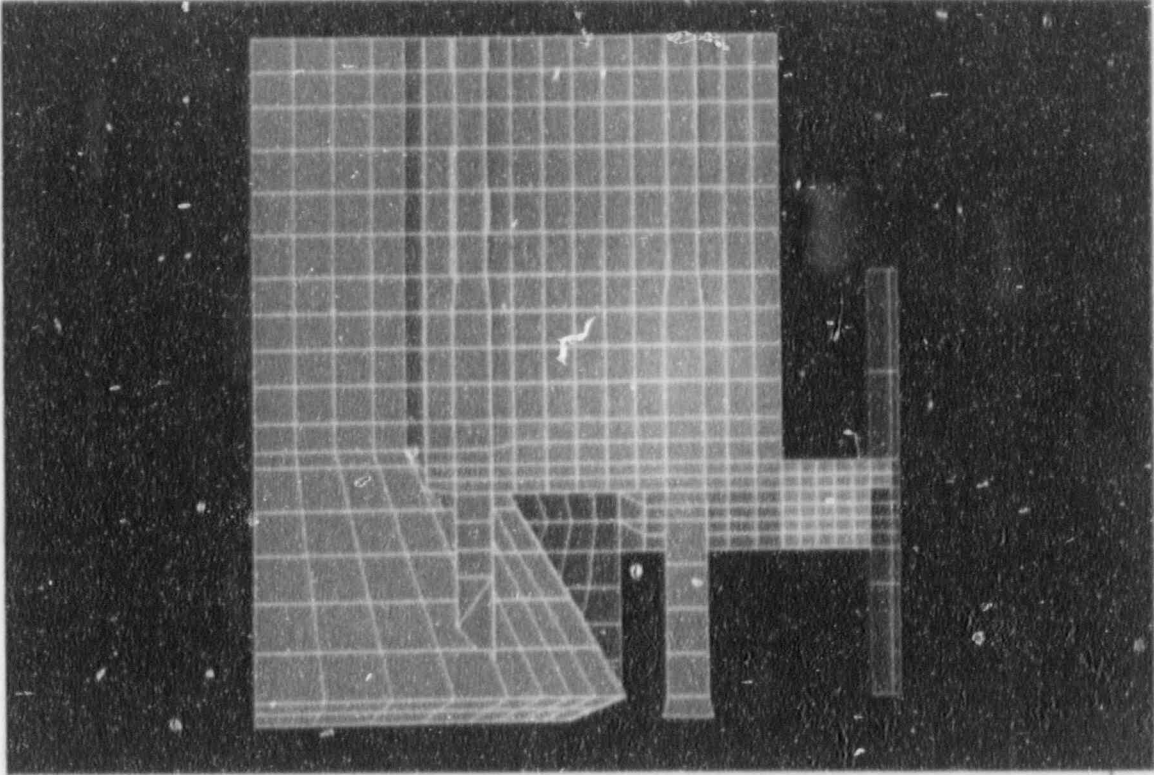


Figure 5.54

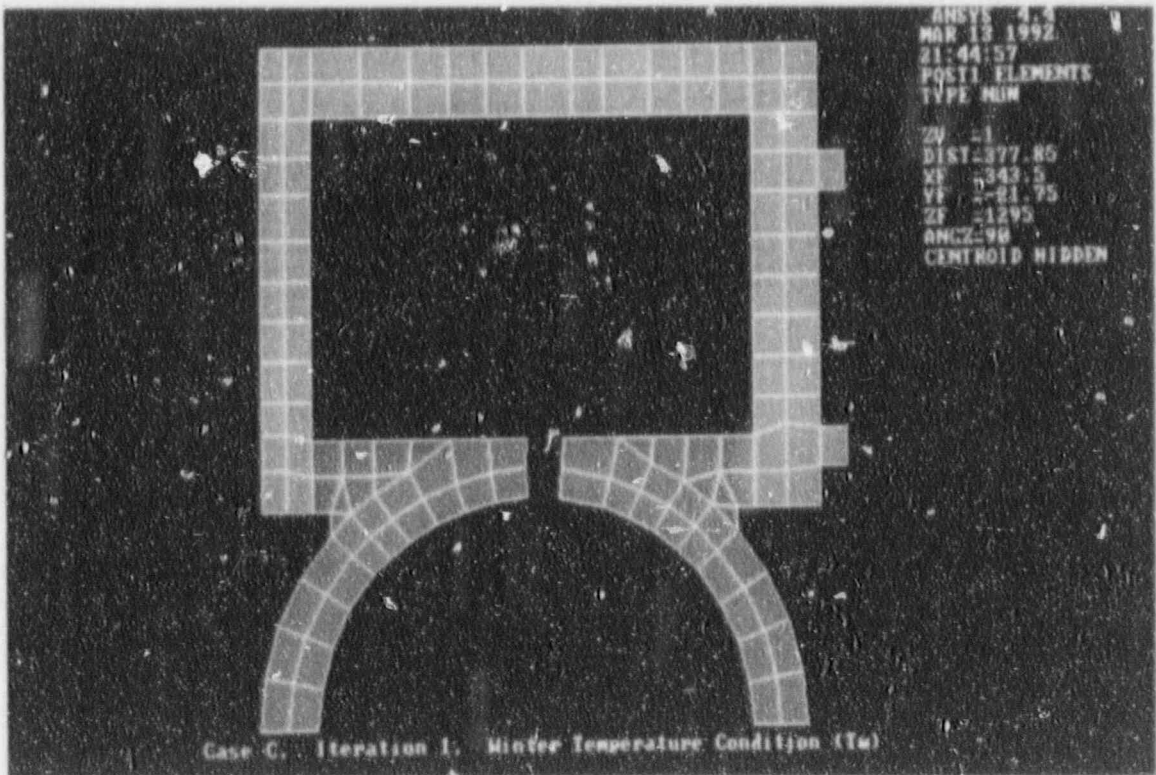


Figure 5.55

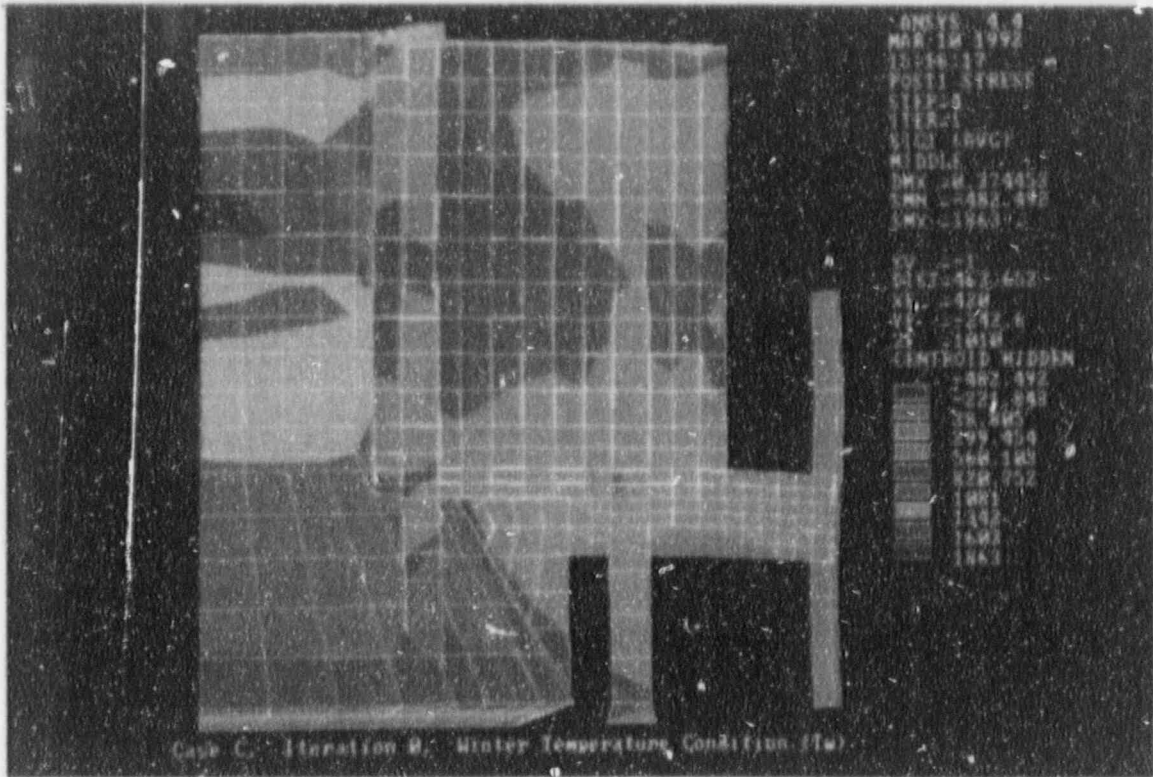


Figure 5.56

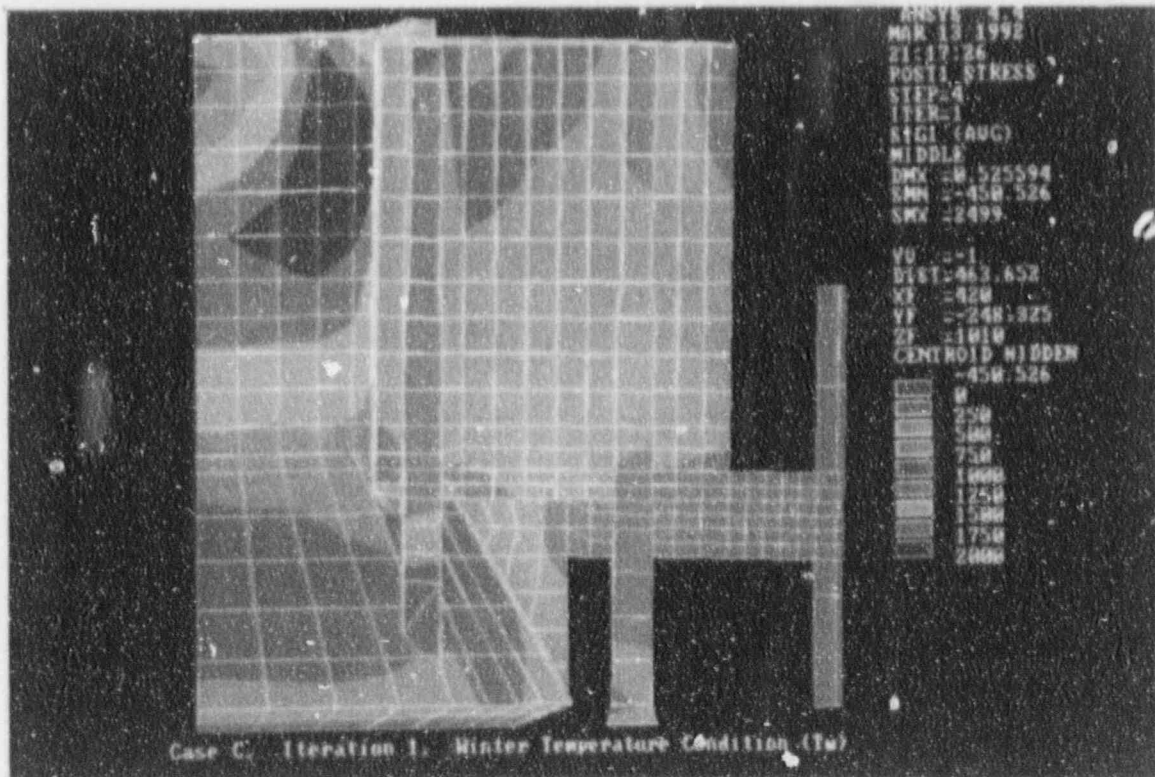


Figure 5.57

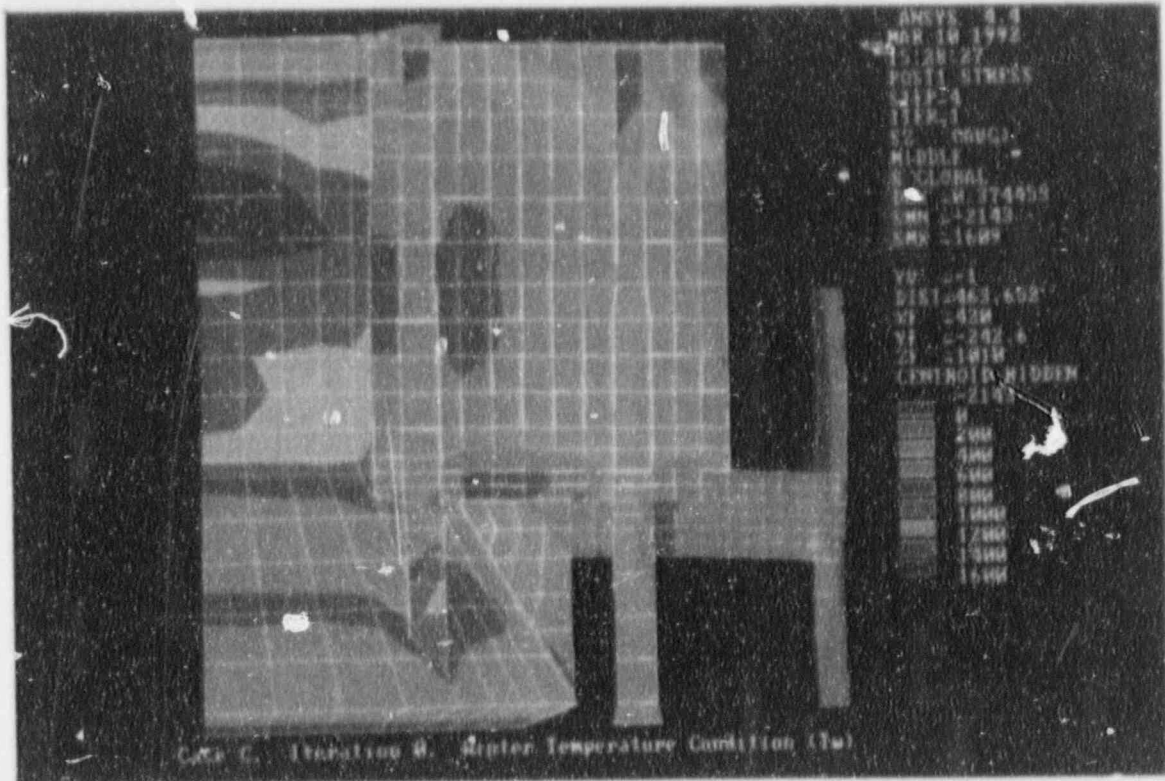


Figure 5.58

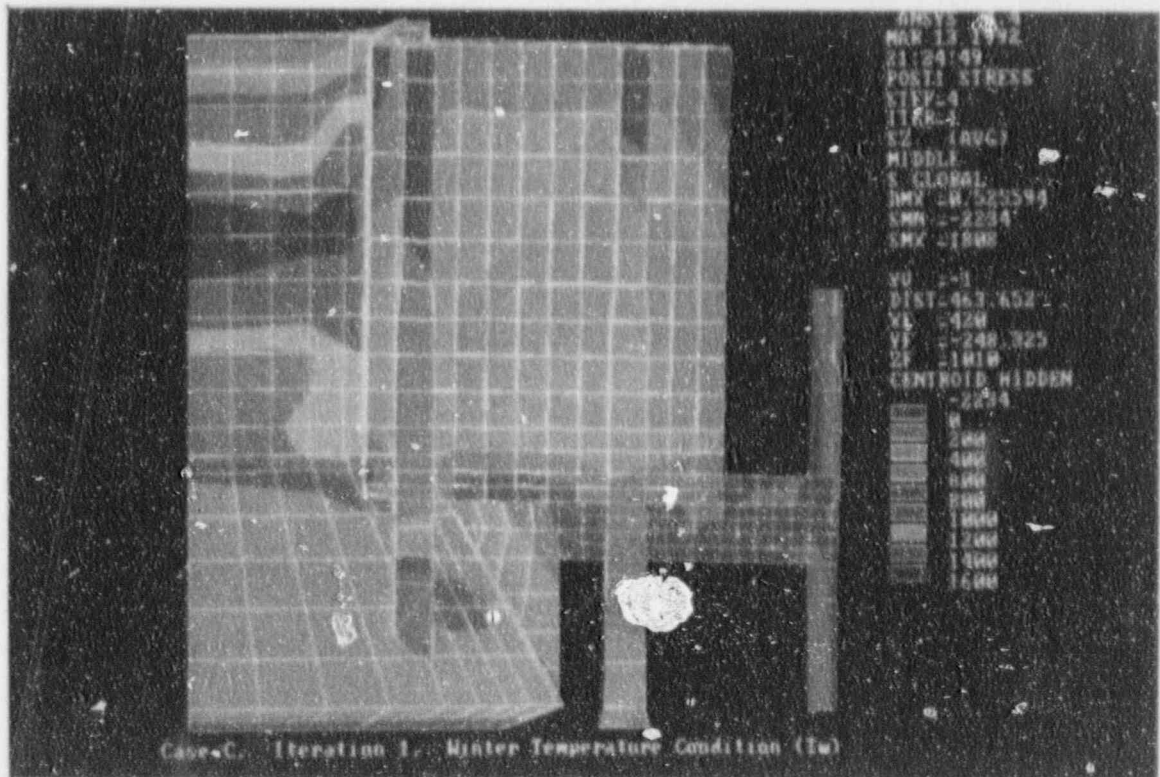


Figure 5.59

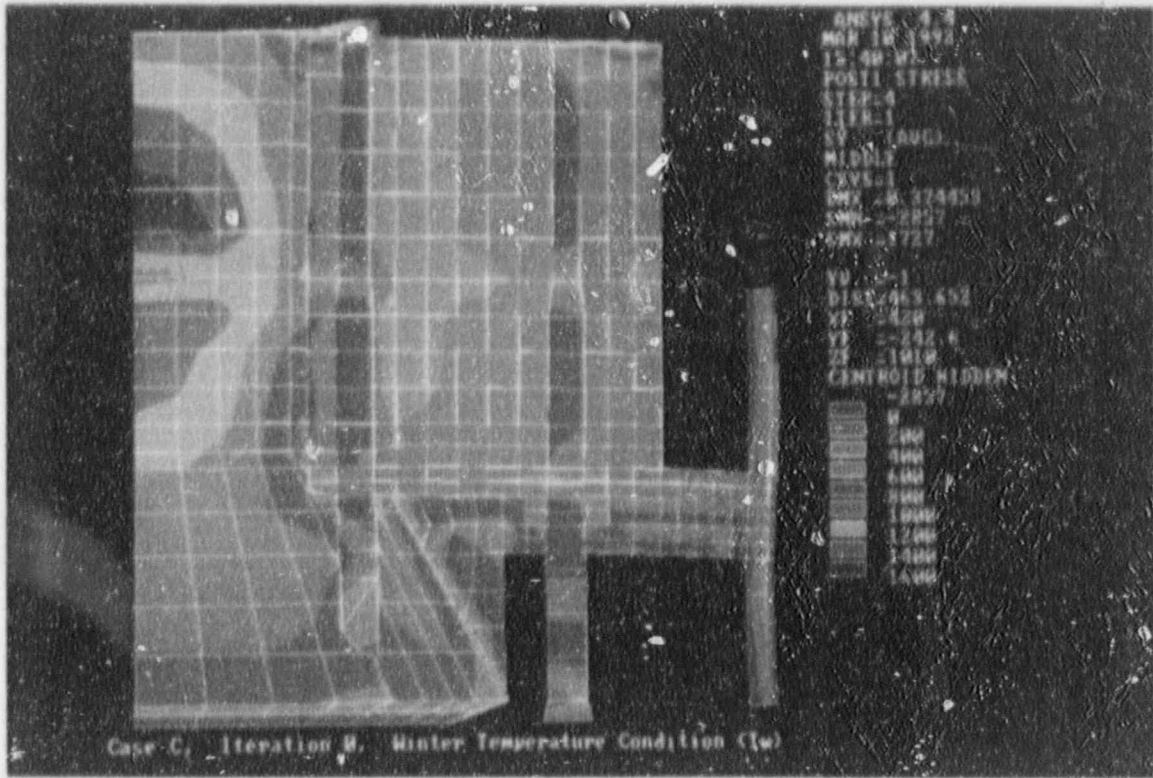


Figure 5.60

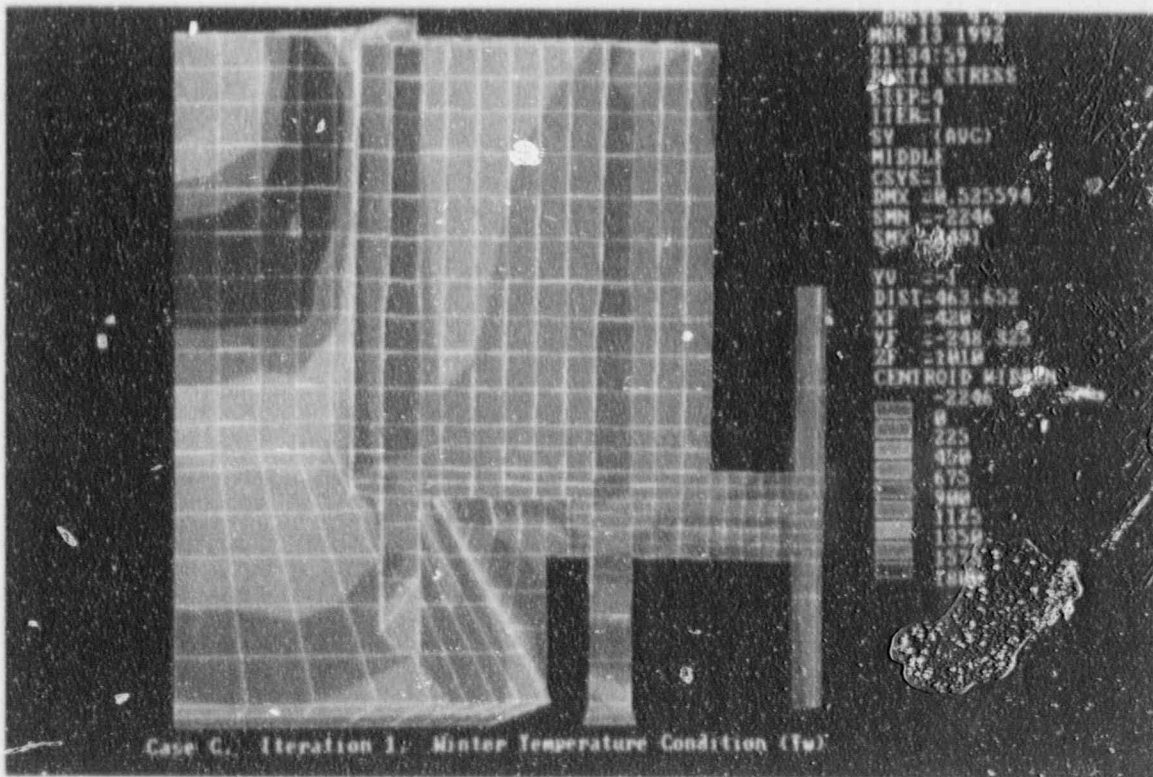


Figure 5.61

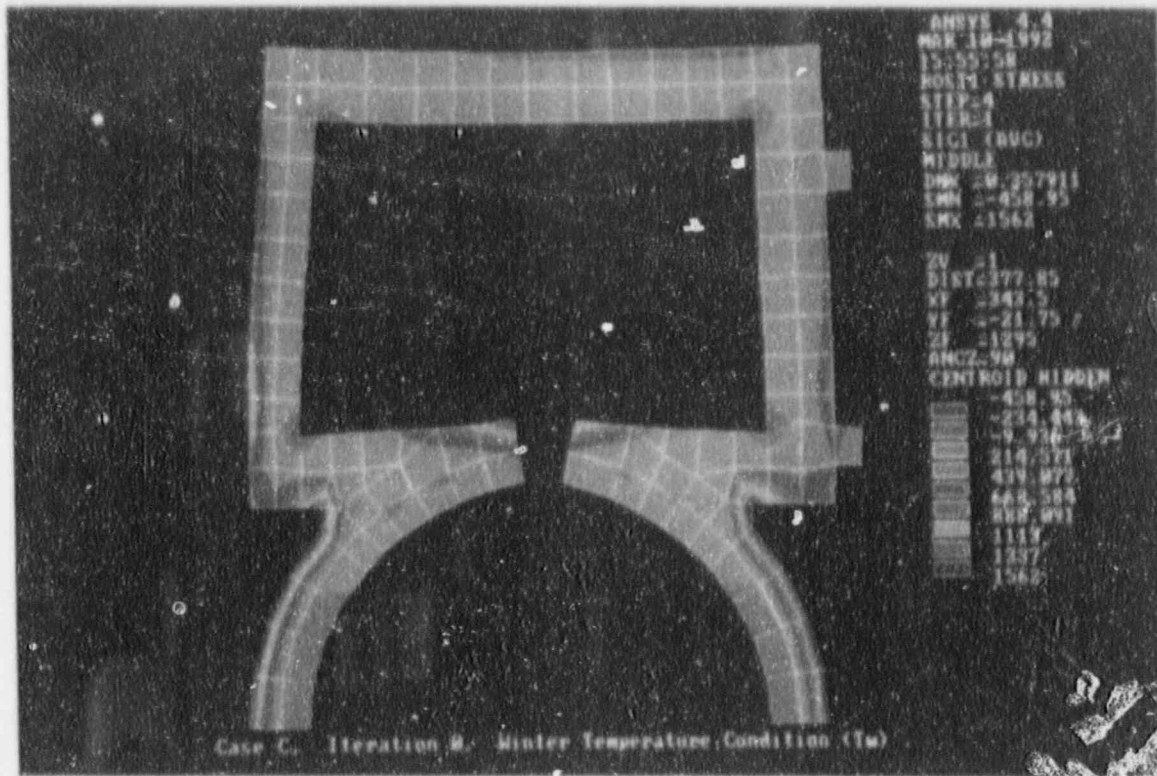


Figure 5.62

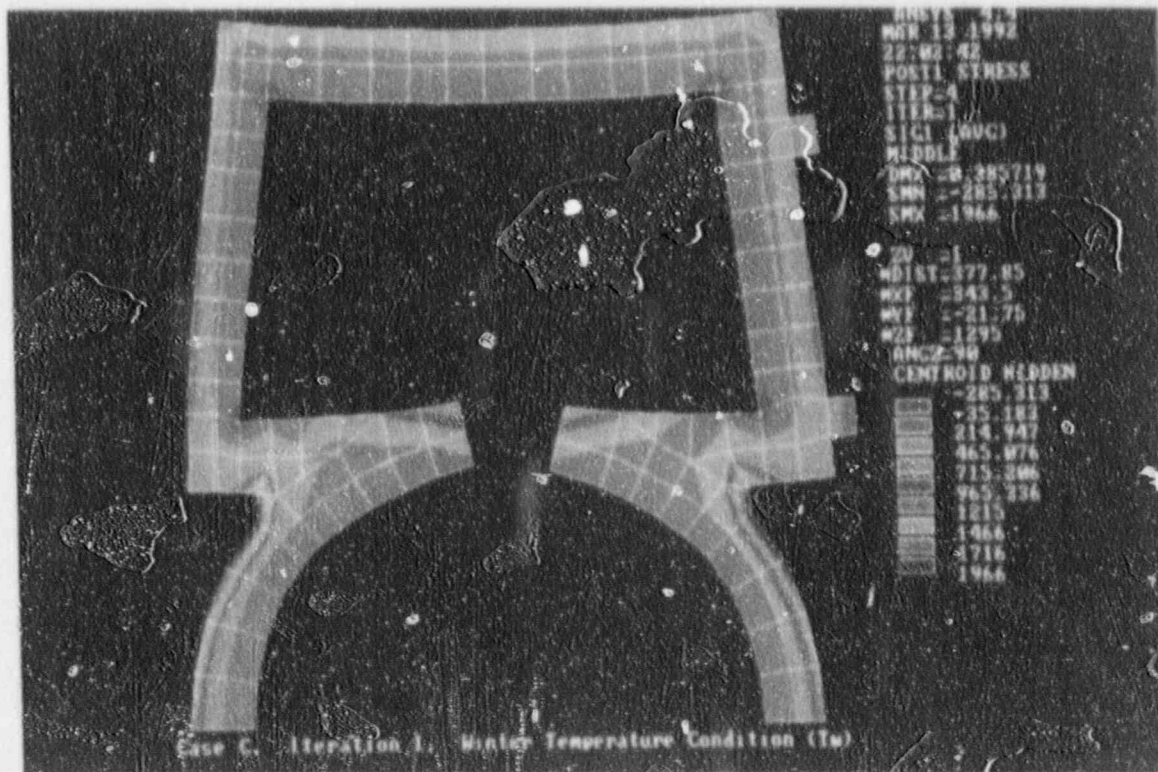


Figure 5.63

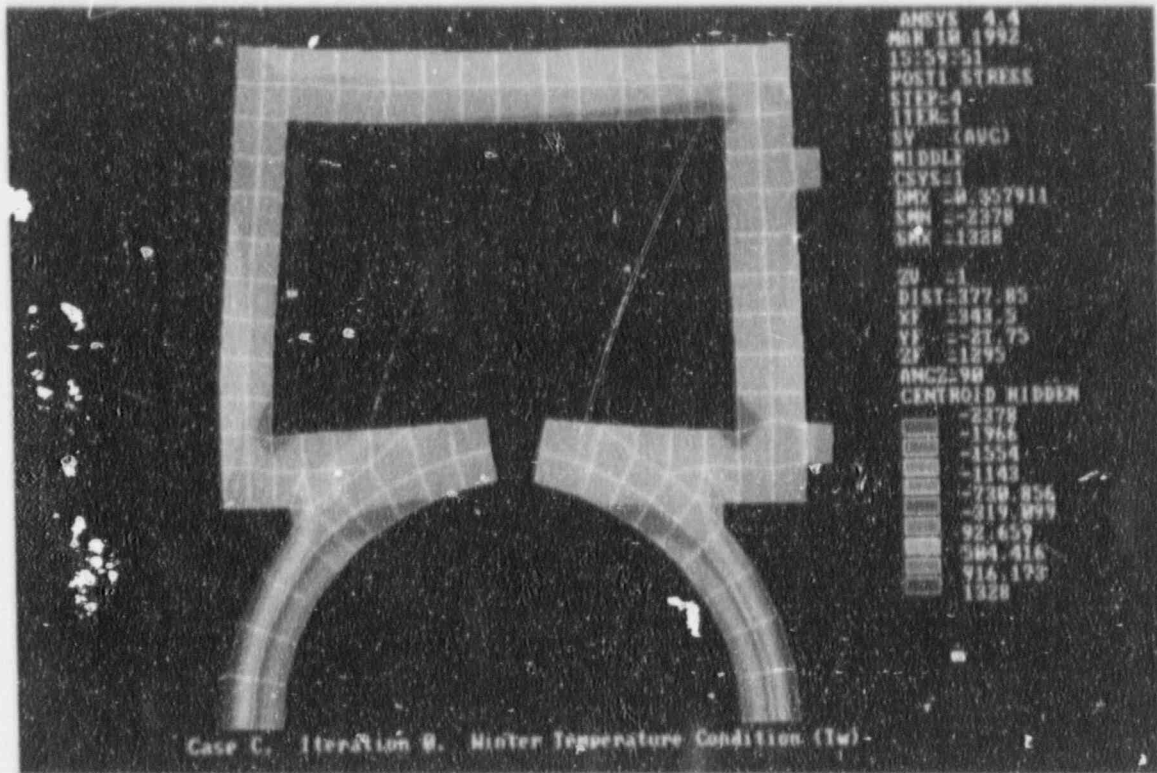


Figure 5.64

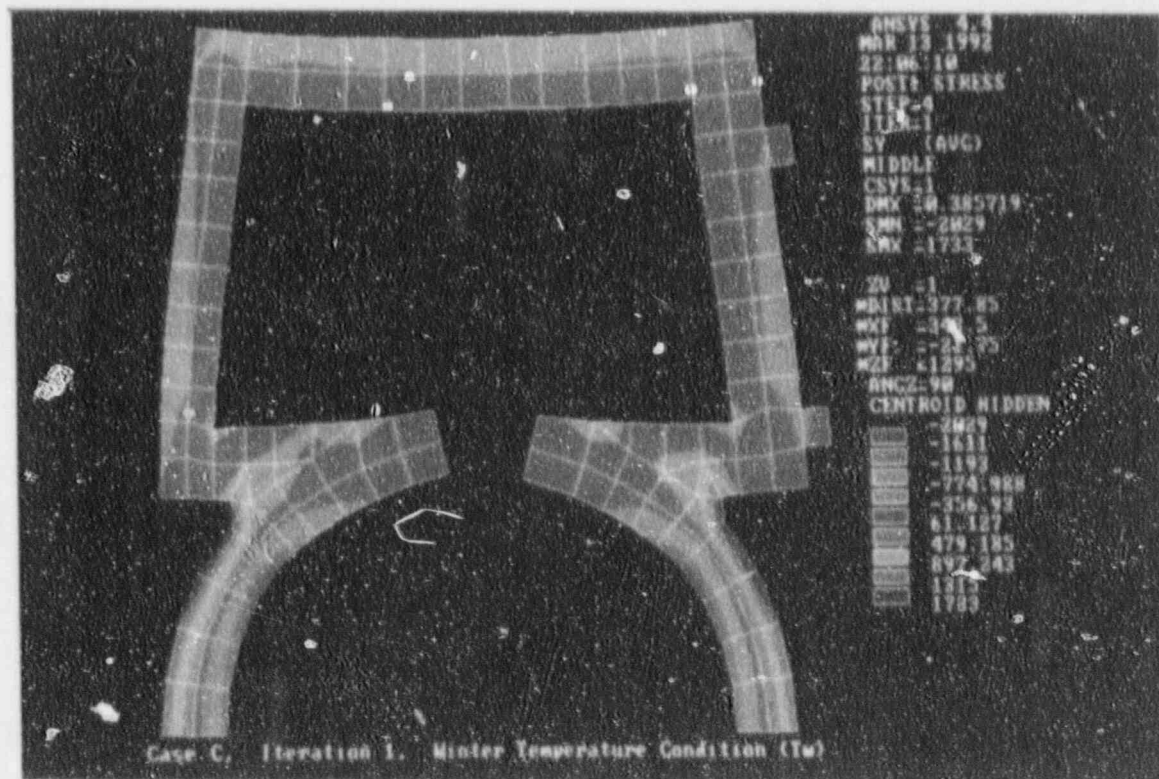


Figure 5.65

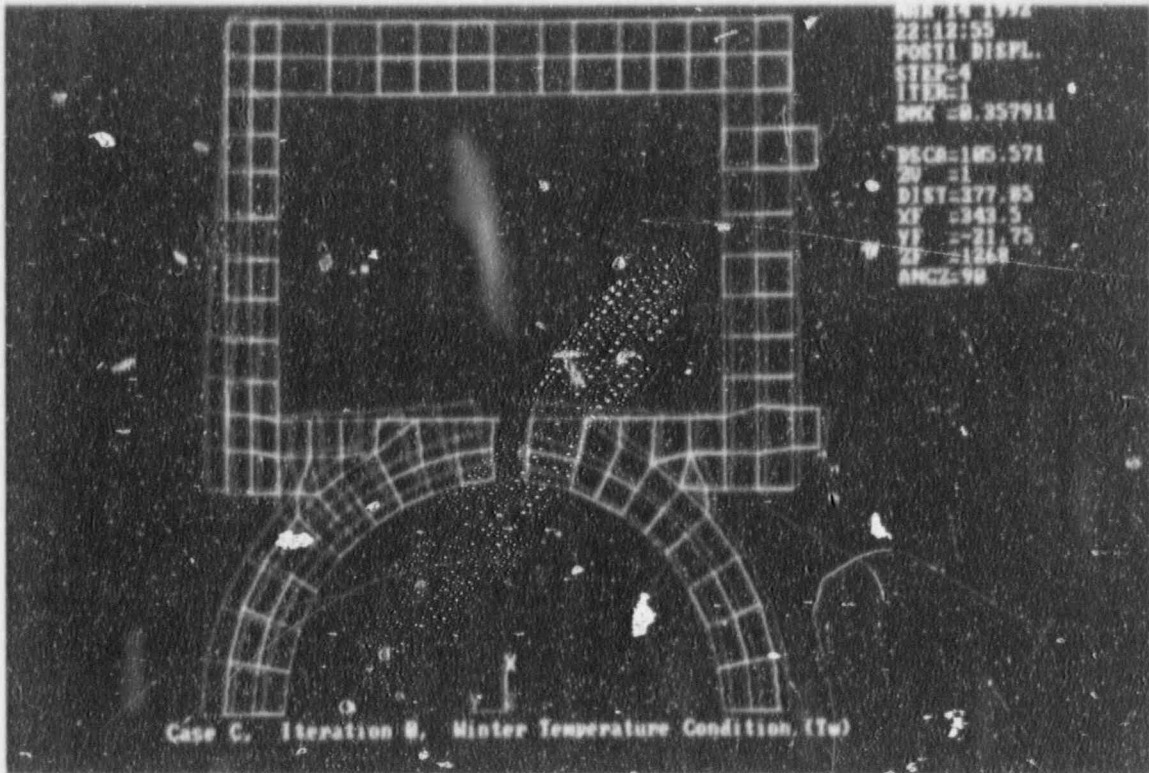


Figure 5.66

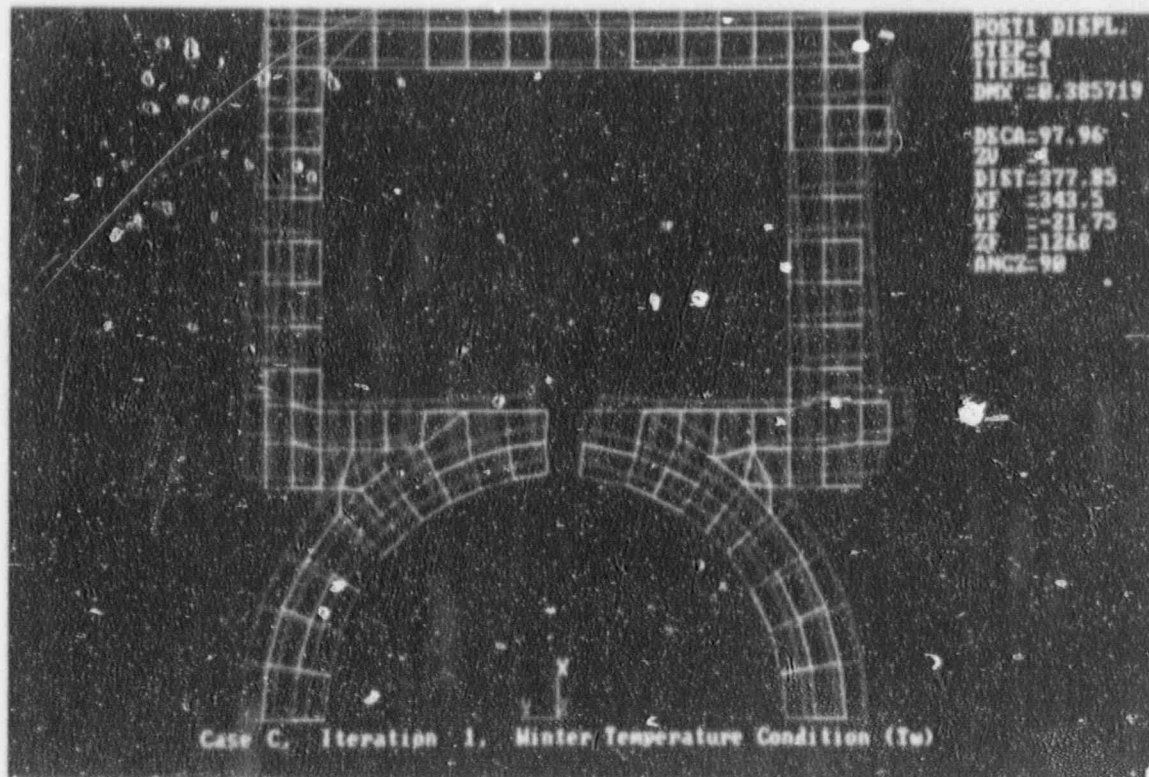


Figure 5.67

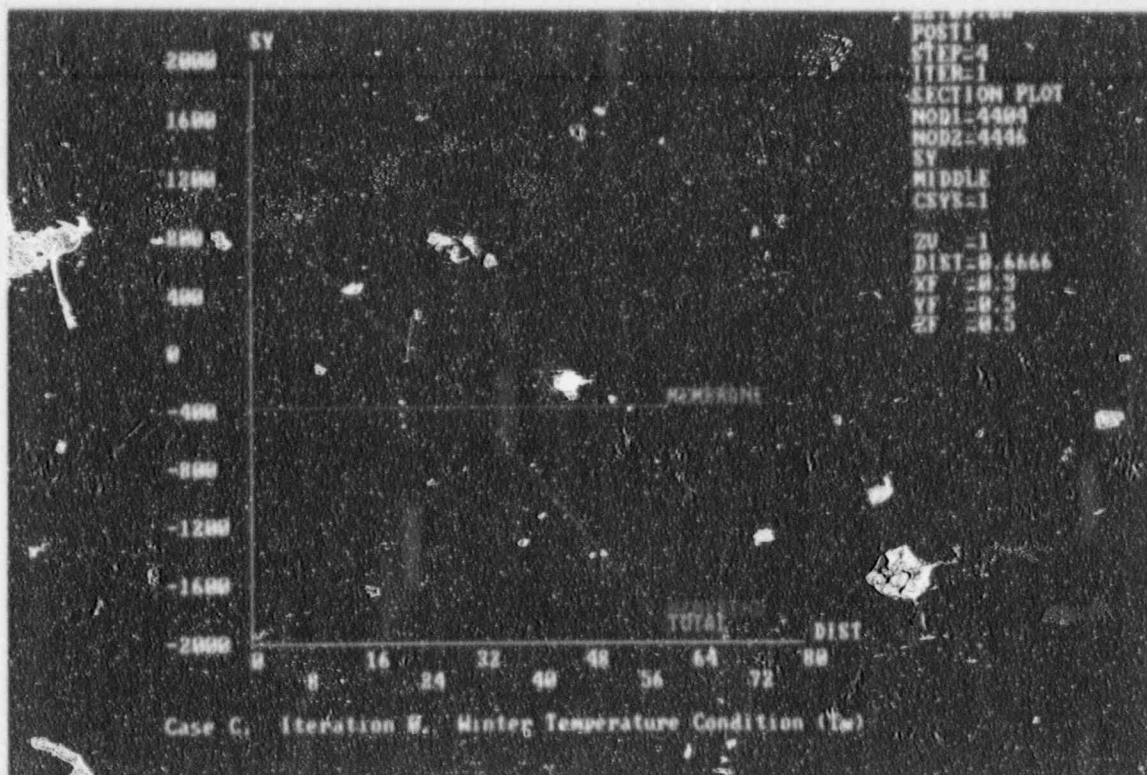


Figure 5.68

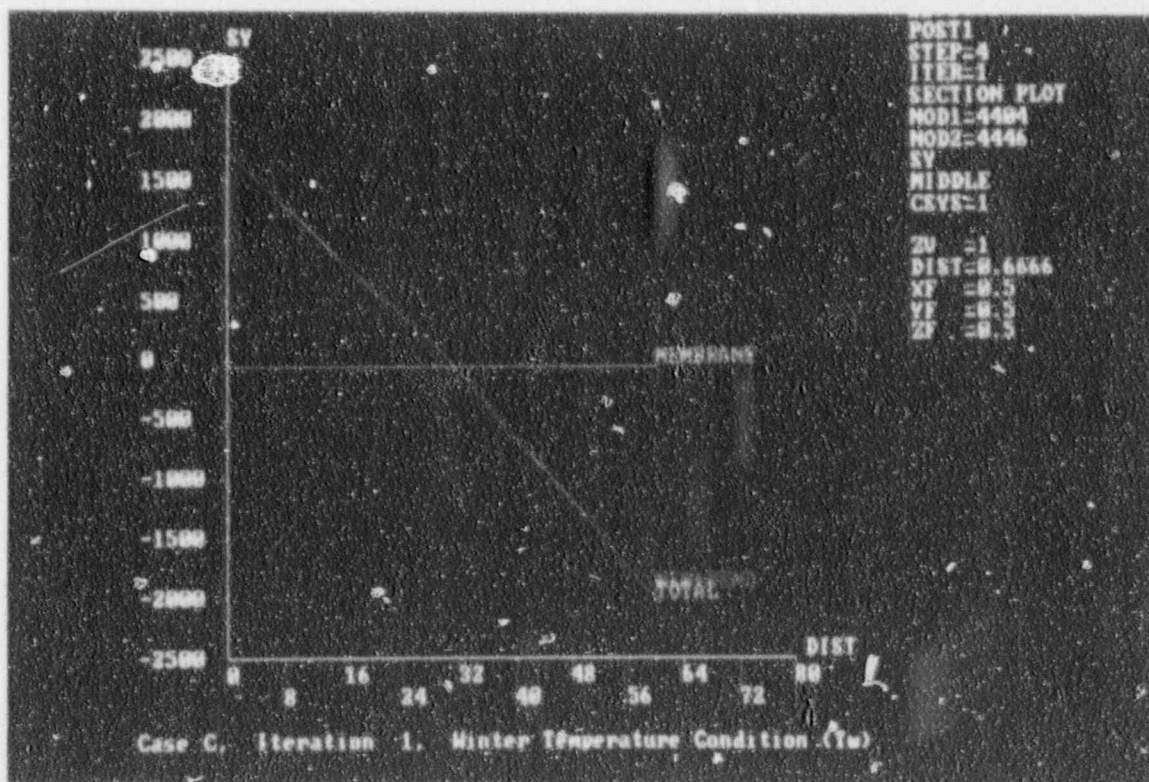


Figure 5.69

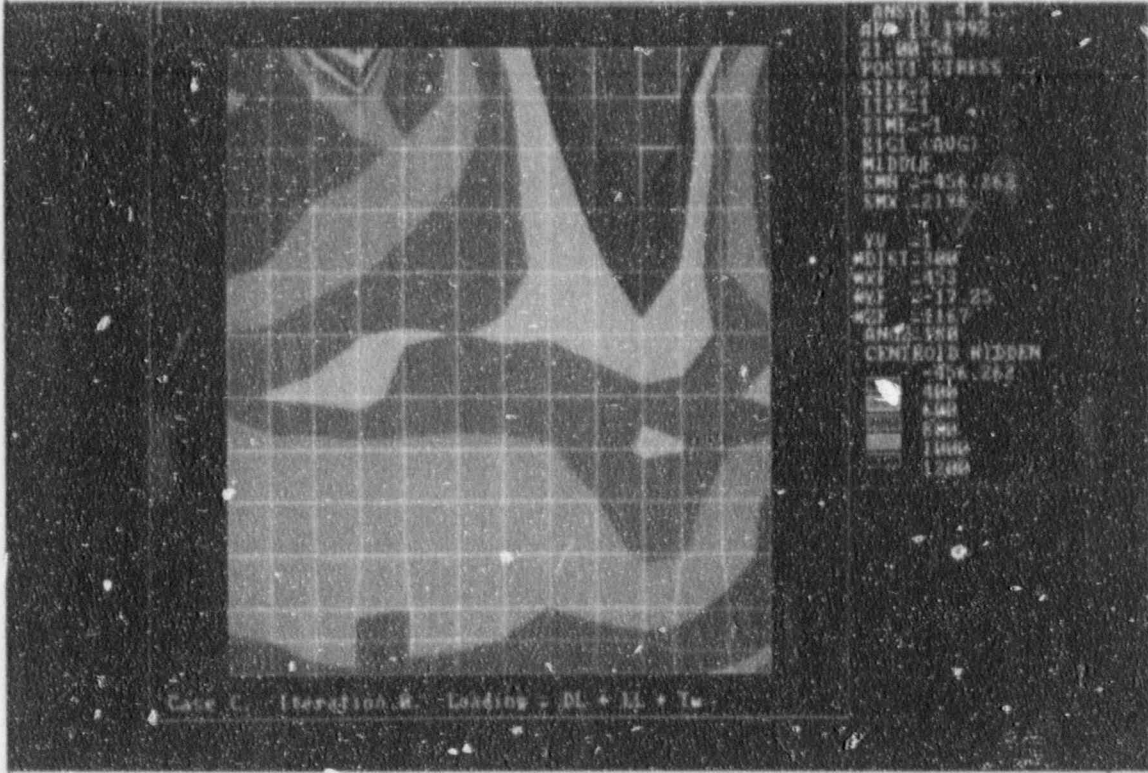


Figure 5.70

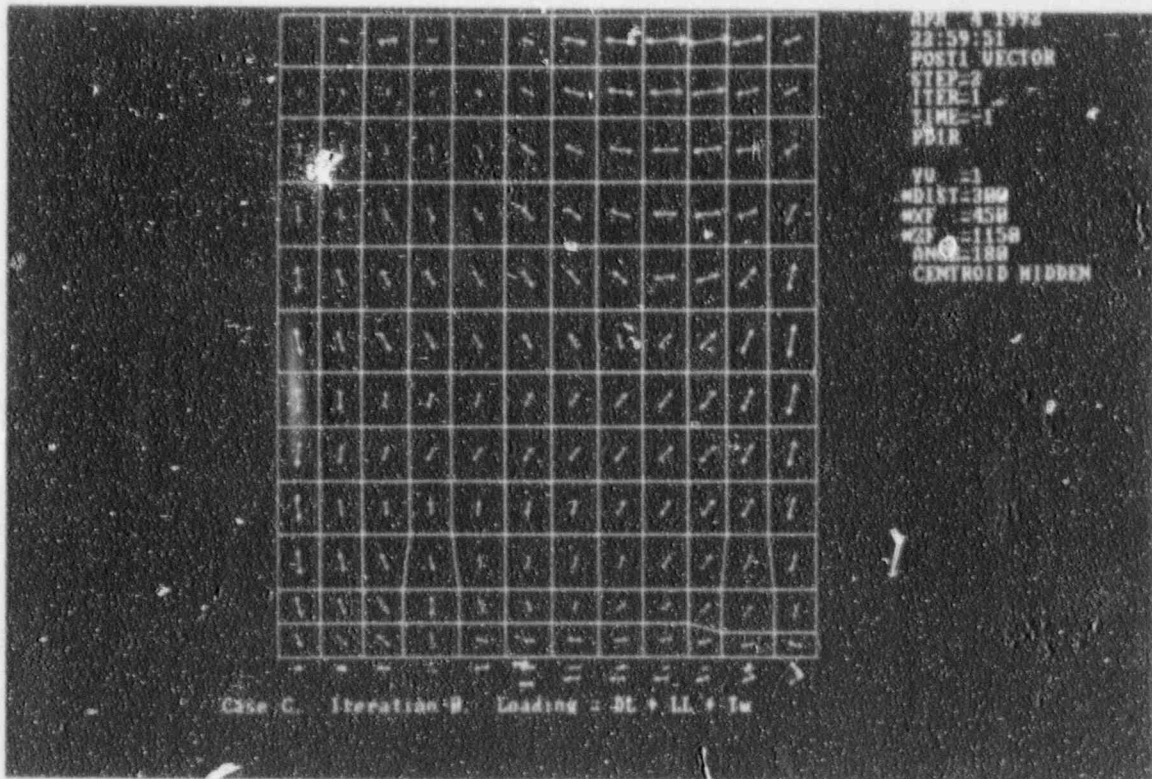


Figure 5.71

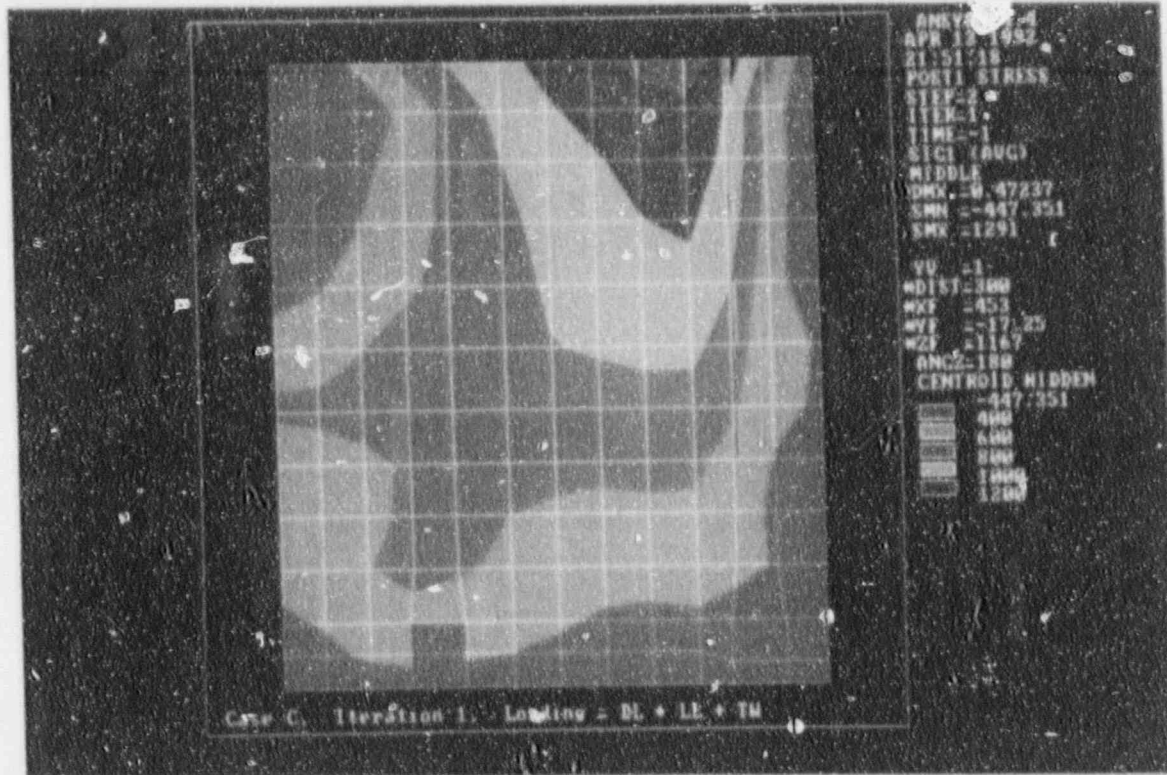


Figure 5.72

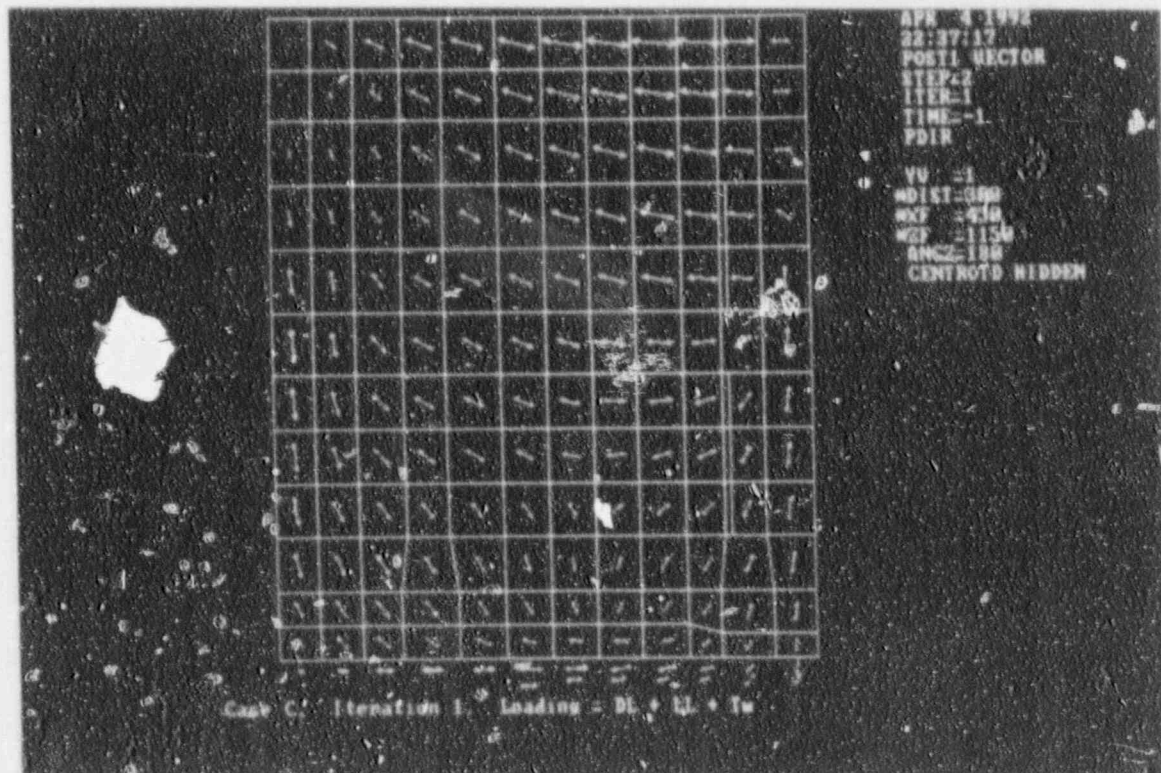


Figure 5.73

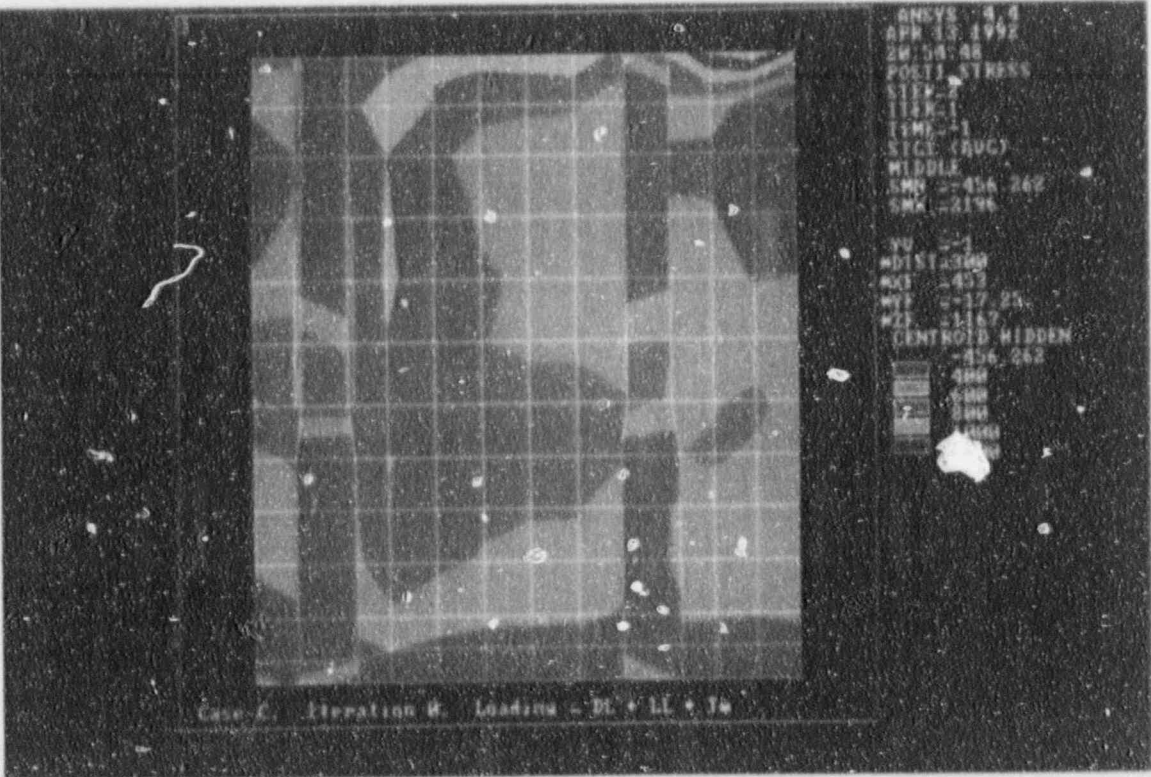


Figure 5.74

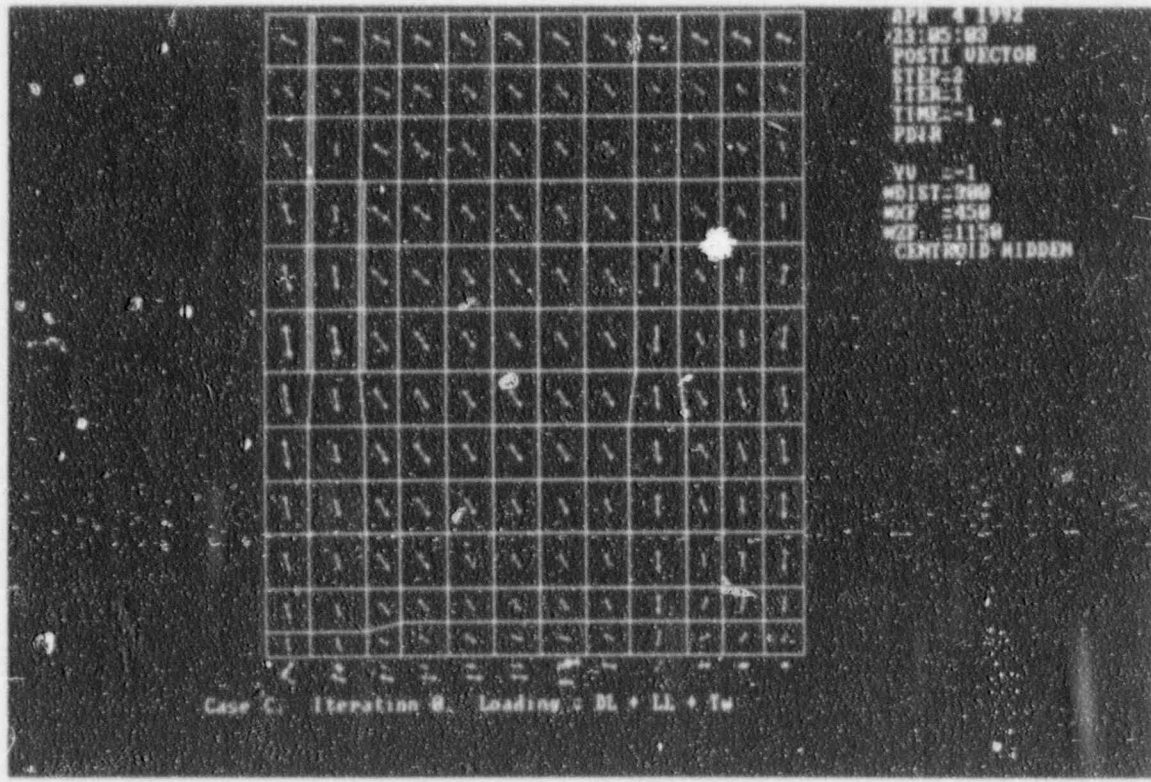


Figure 5.75

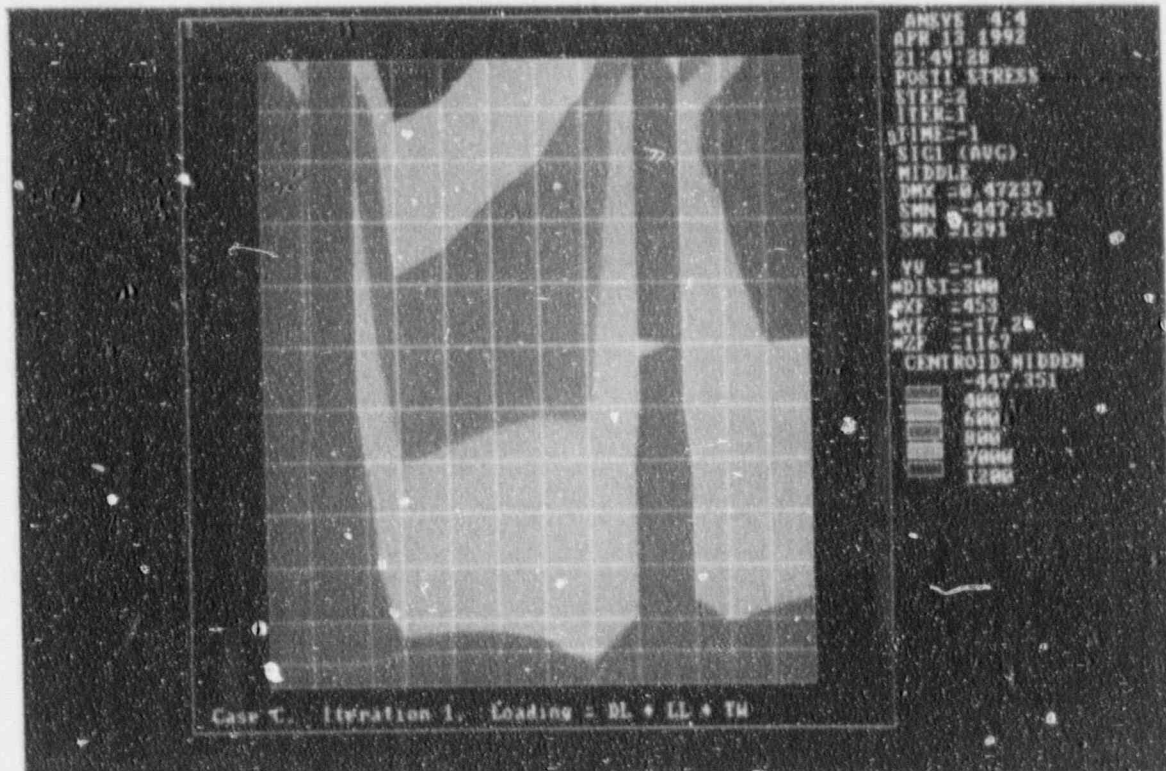


Figure 5.76

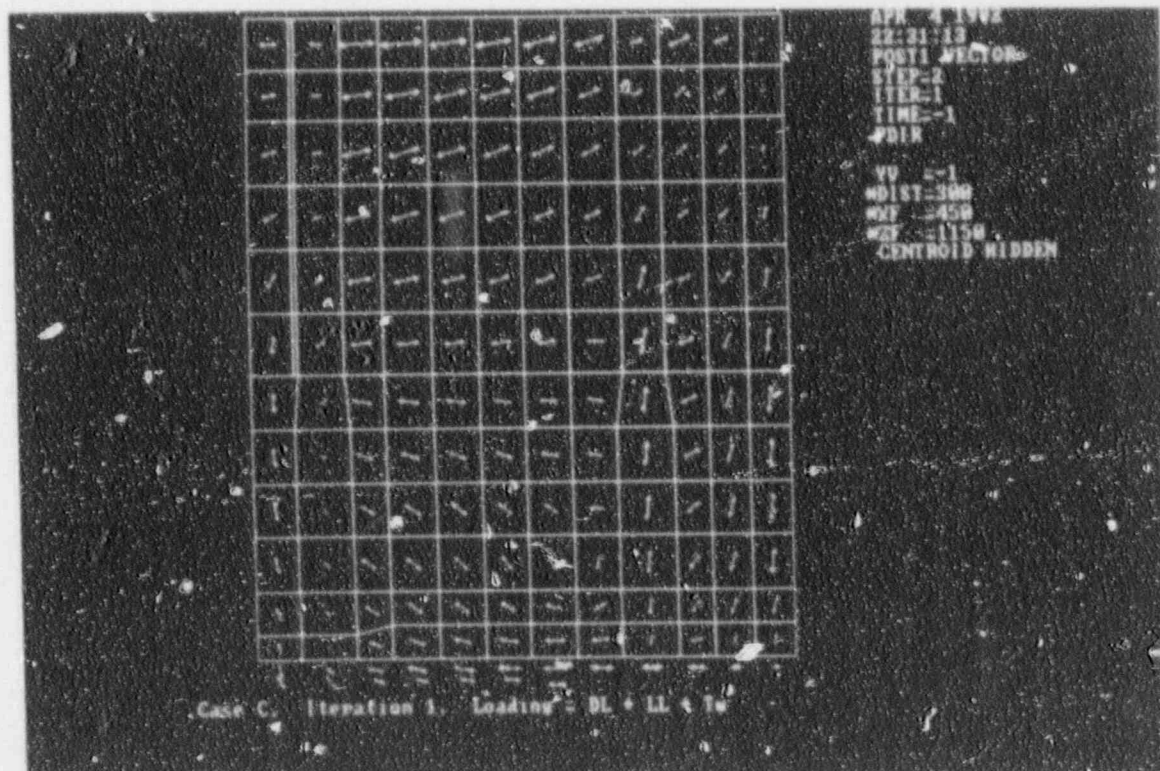


Figure 5.77

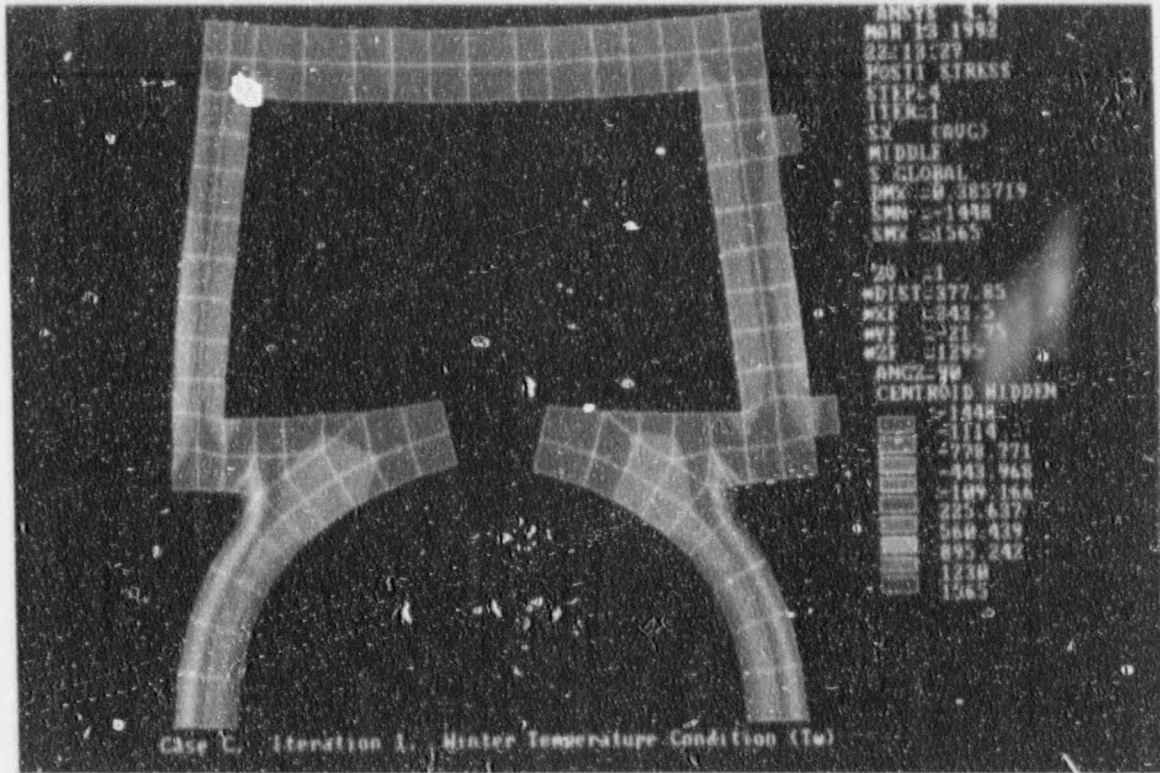


Figure 5.77A

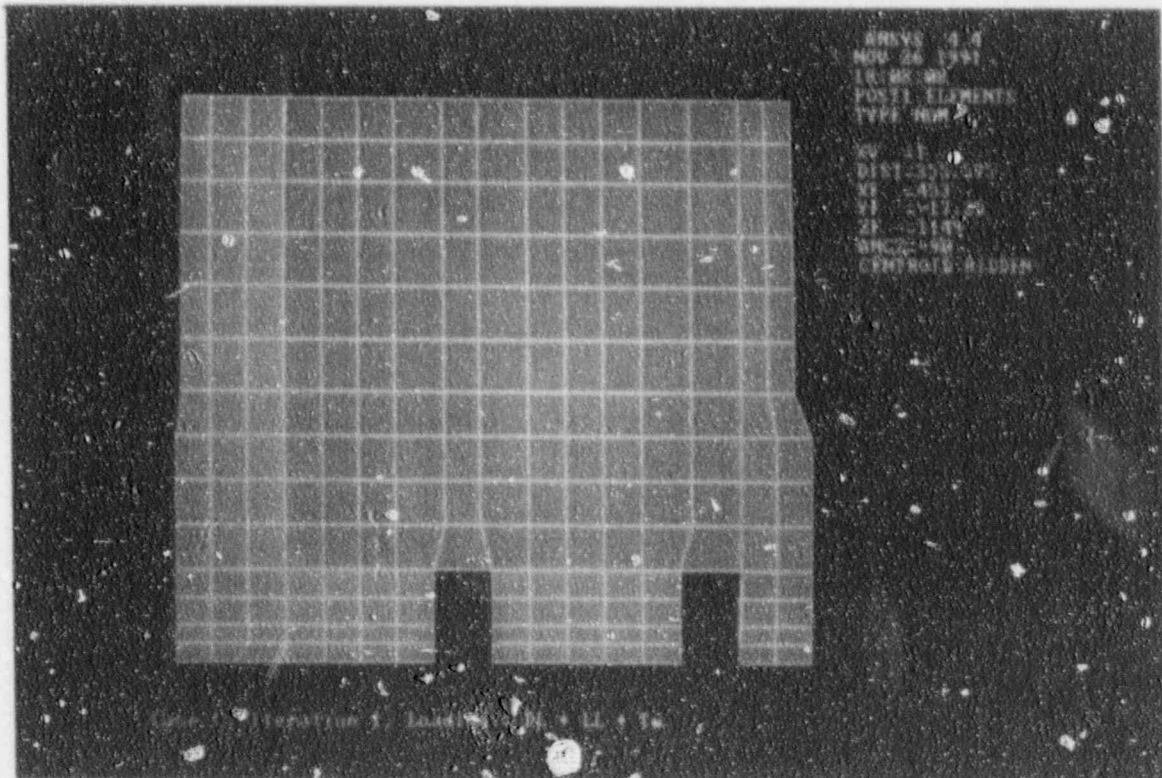


Figure 5.78

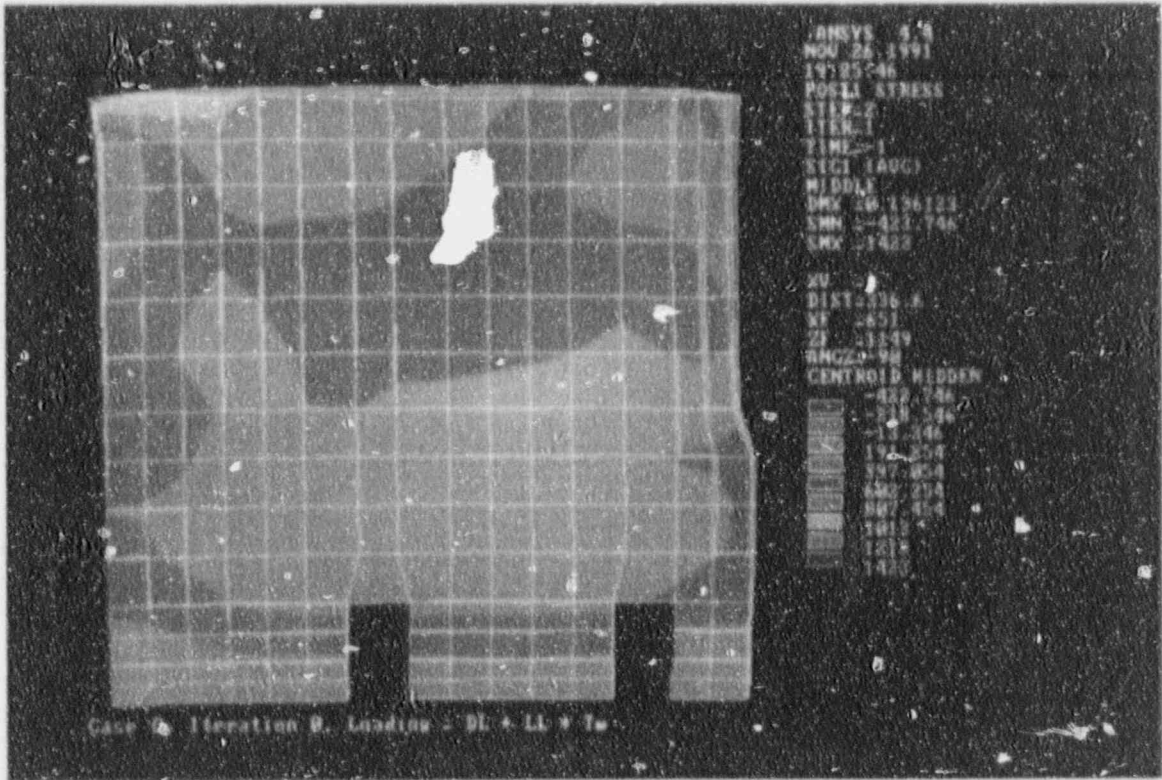


Figure 5.79

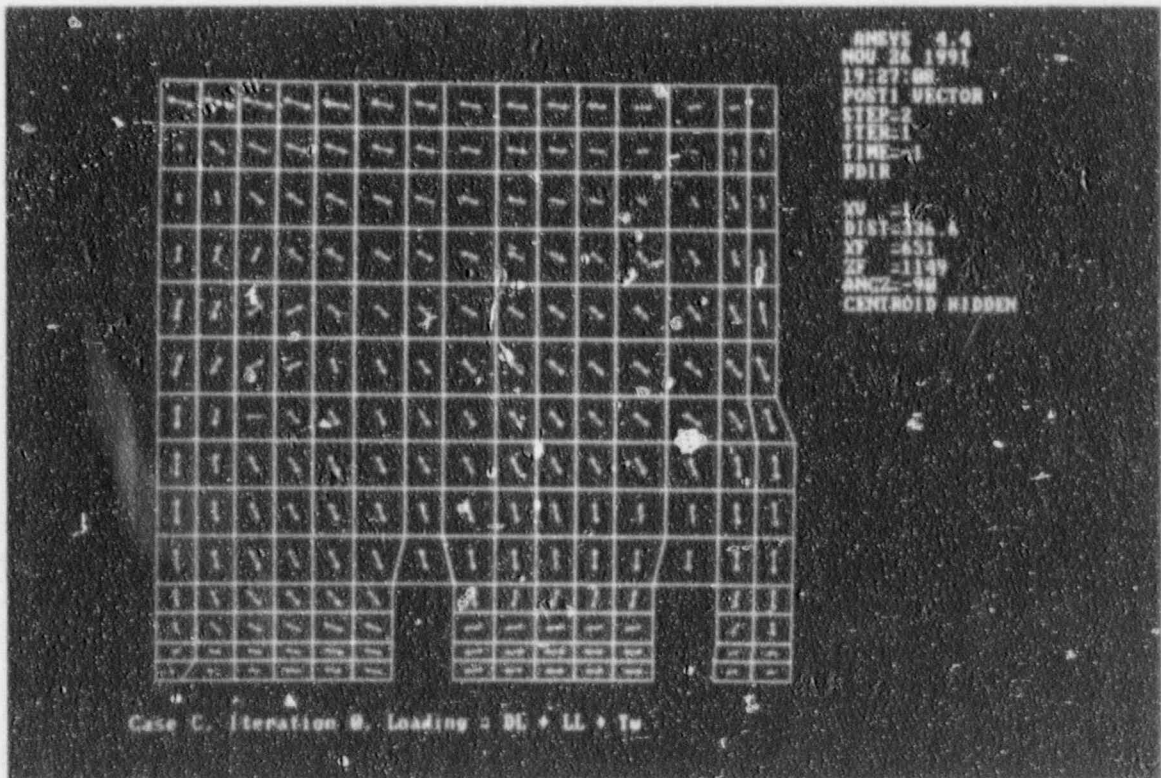


Figure 5.80

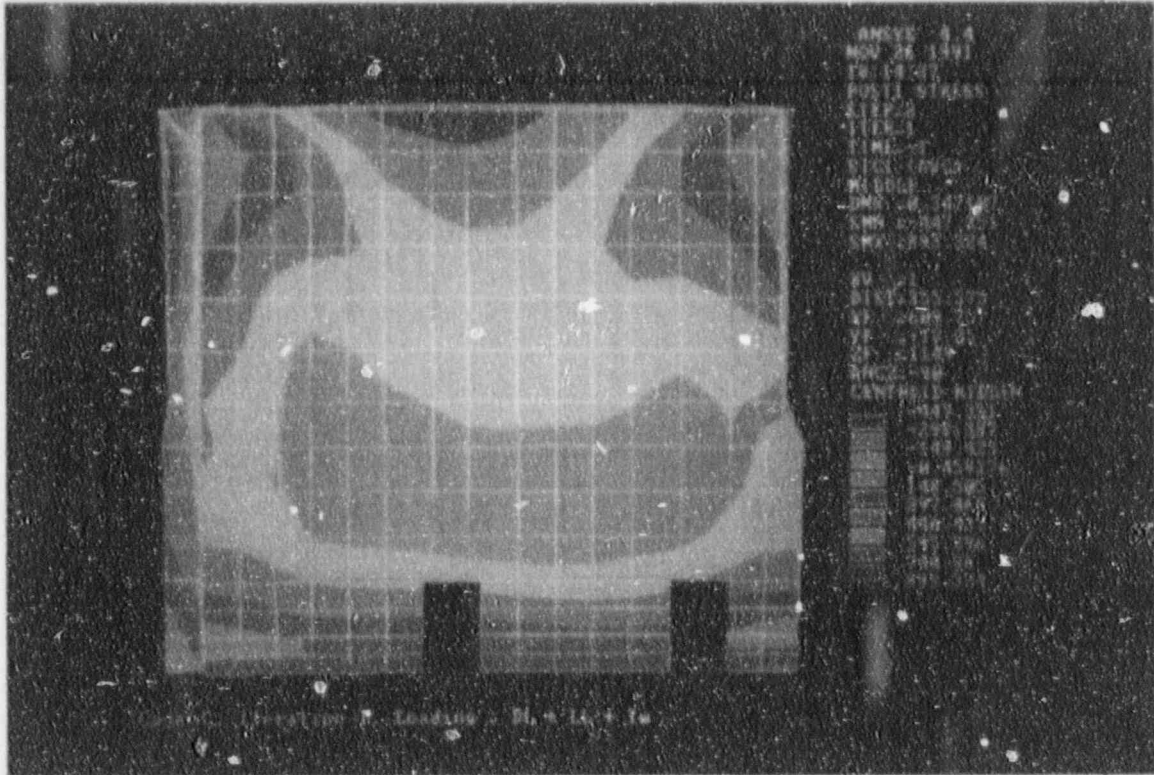


Figure 5.81

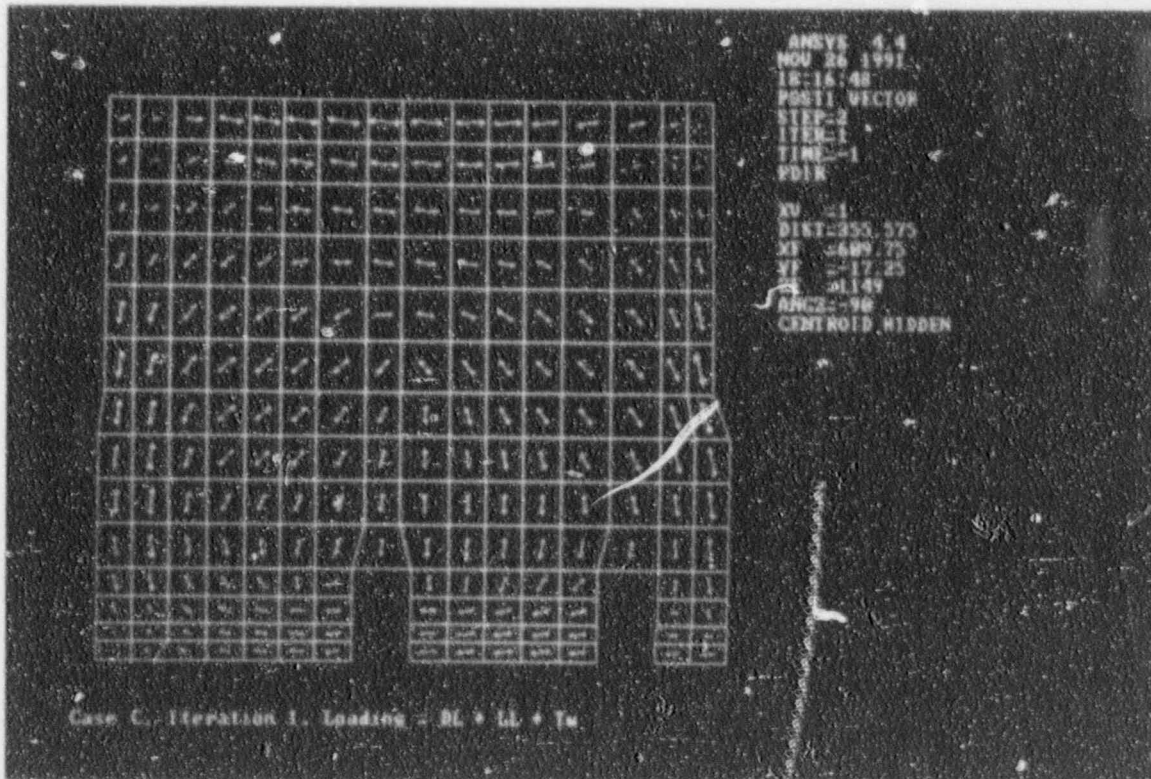
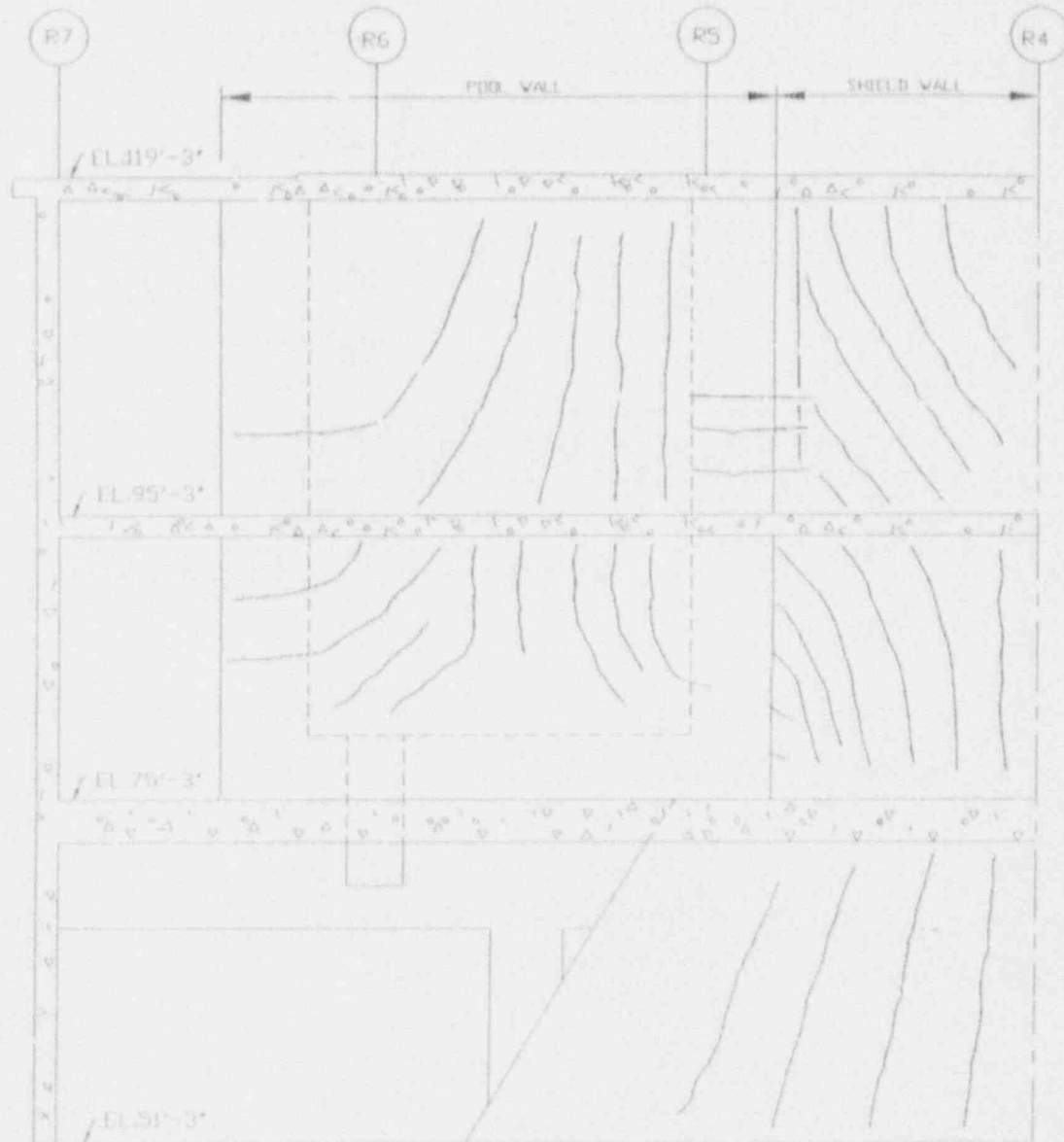


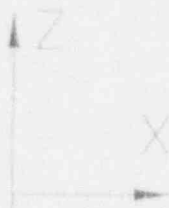
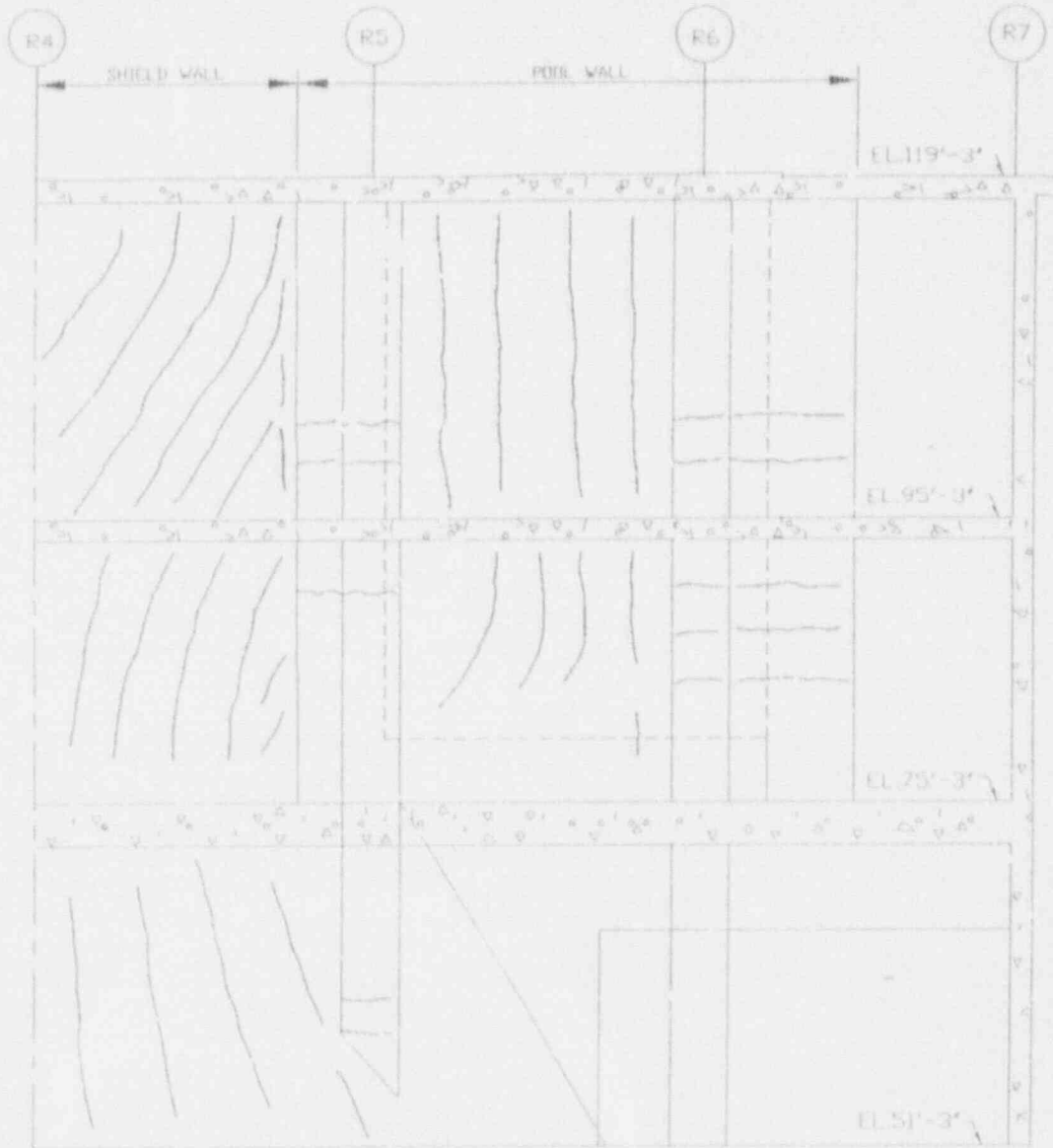
Figure 5.82



PREDICTED CRACK PATTERN ON THE WEST FACE
 OF THE SPENT FUEL POOL AND SHIELD WALL



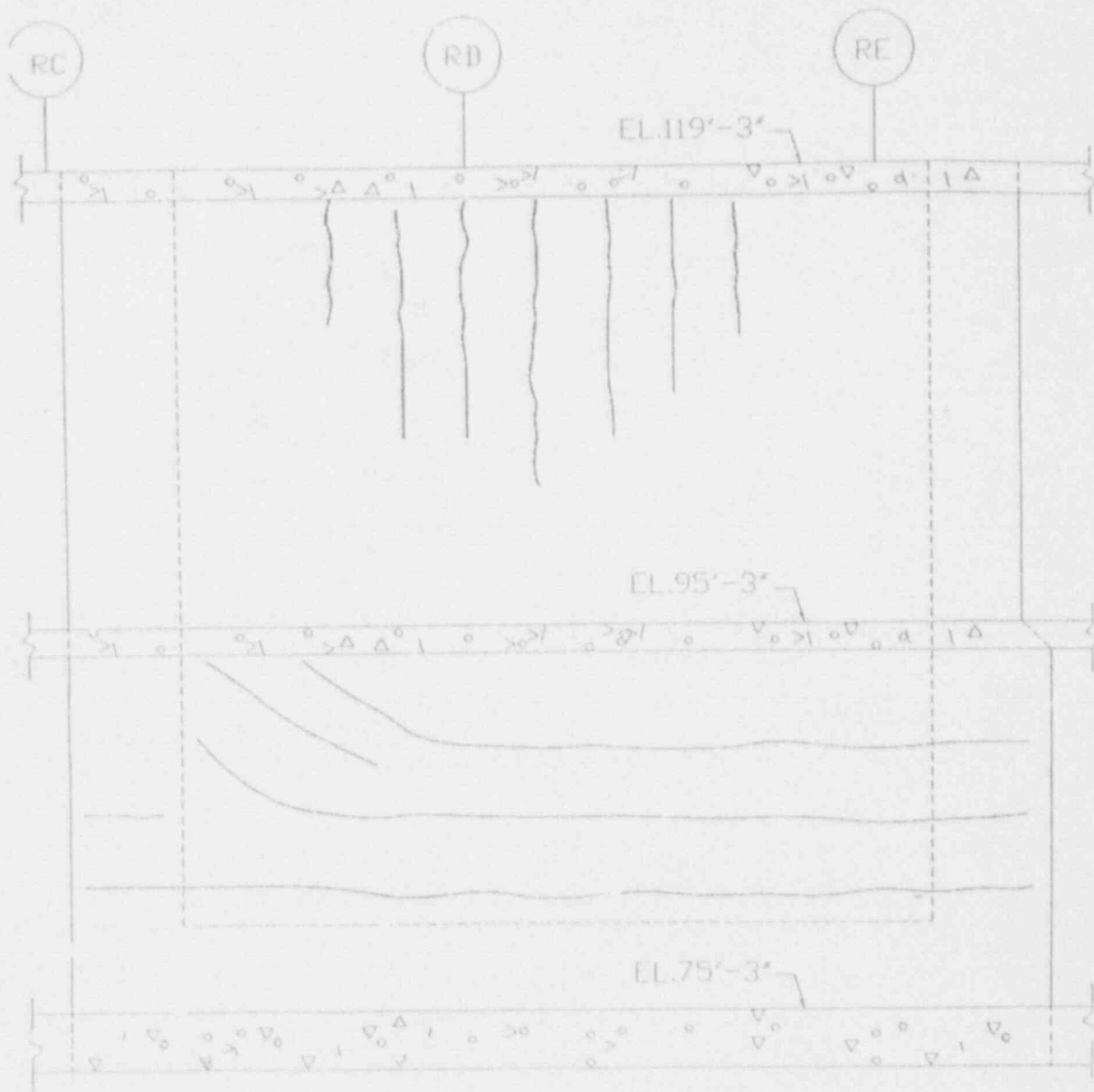
Figure 5.83



PREDICTED CRACK PATTERN FOR THE EAST FACE
OF THE SPENT FUEL POOL AND SHIELD WALL

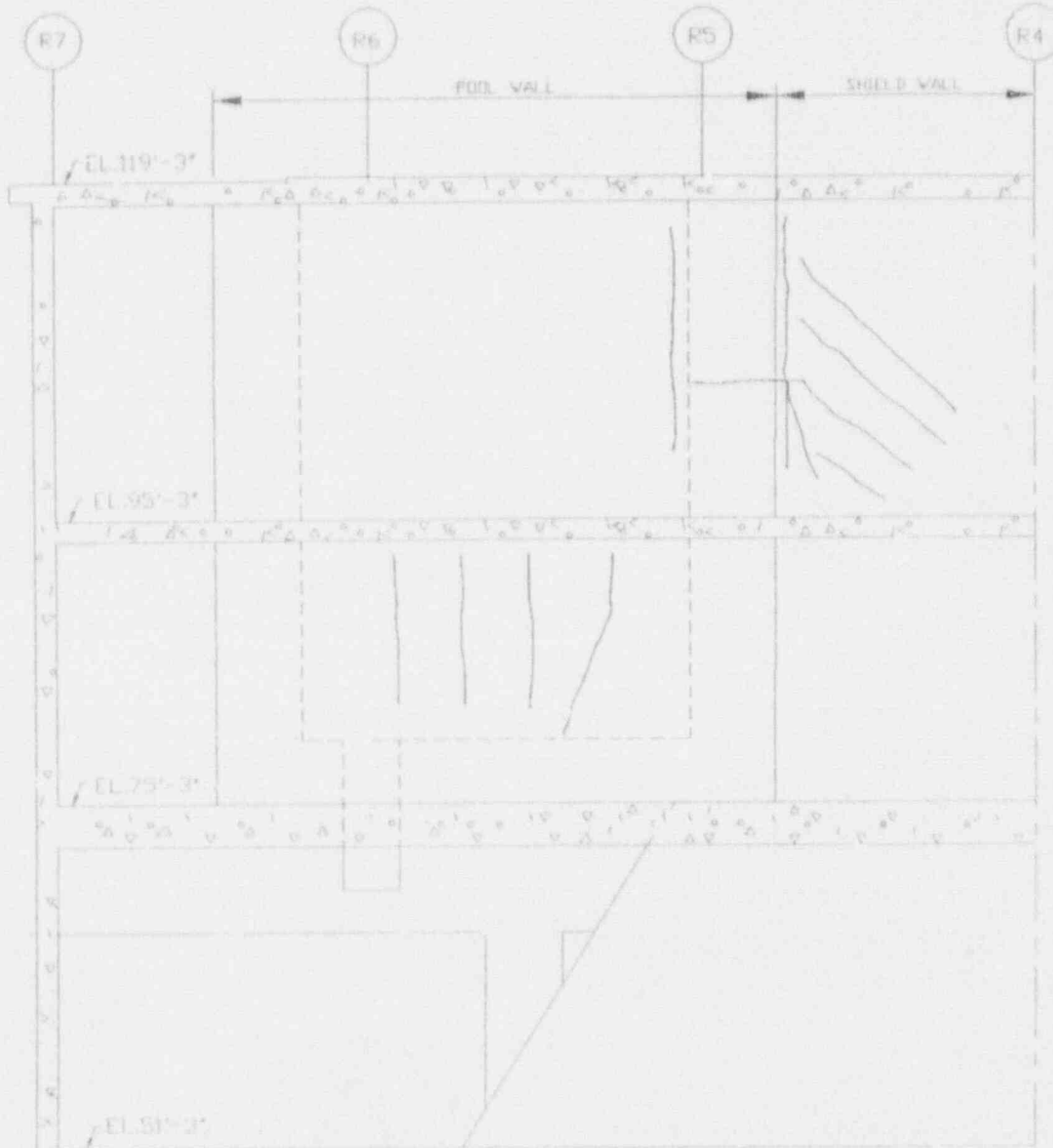
Figure 5.84

ABB Impell Corporation



PREDICTED CRACK PATTERN FOR THE NORTH FACE OF THE SPENT FUEL POOL

Figure 5.85



OBSERVED CRACKS IN THE WEST FACE OF
SPENT FUEL POOL AND SHIELD WALL

Figure 5.86

ABB Impell Corporation

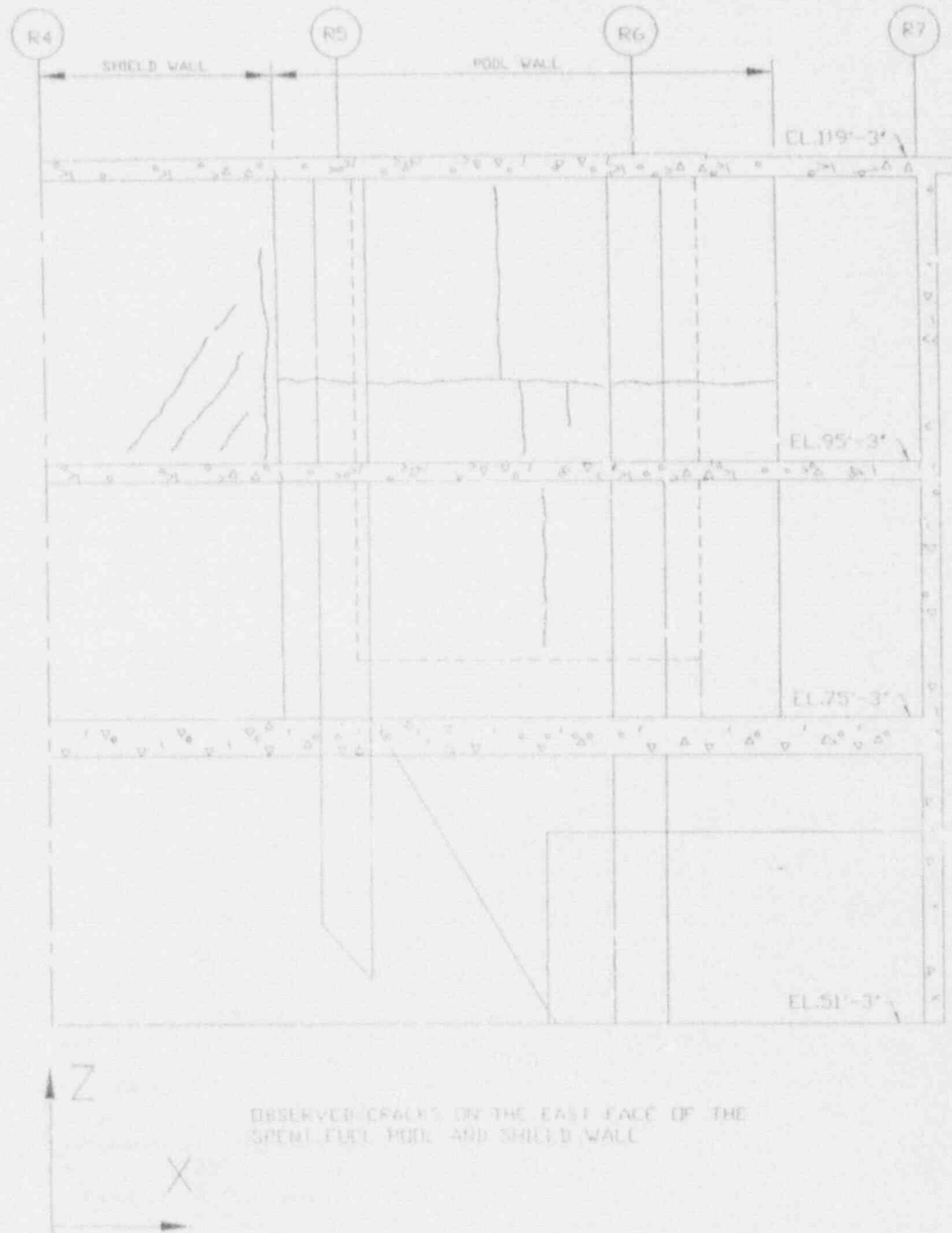
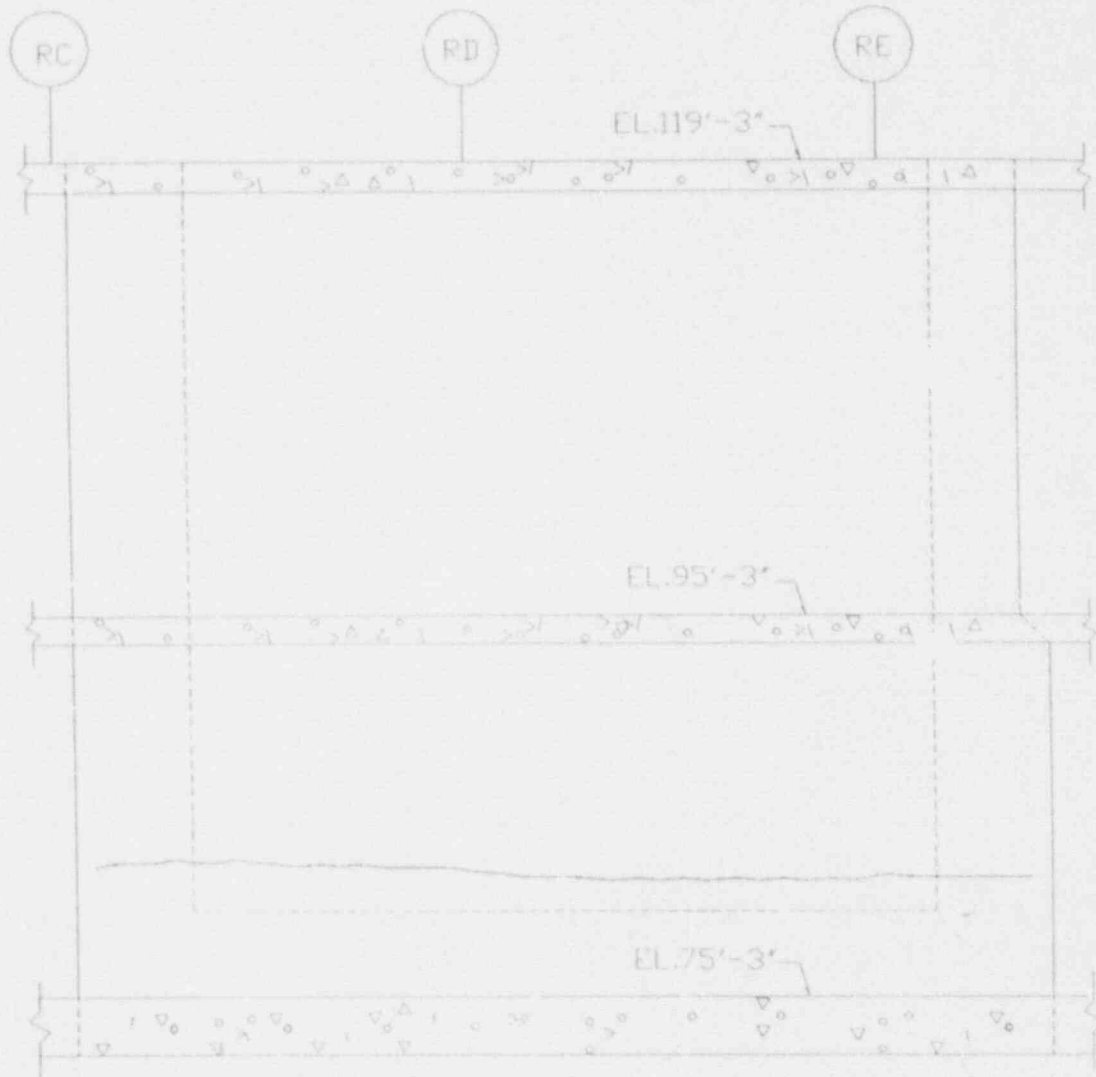


Figure 5.87

ABB Impell Corporation



OBSERVED CRACK ON THE NORTH WALL OF THE SPENT FUEL POOL

Figure 5.88

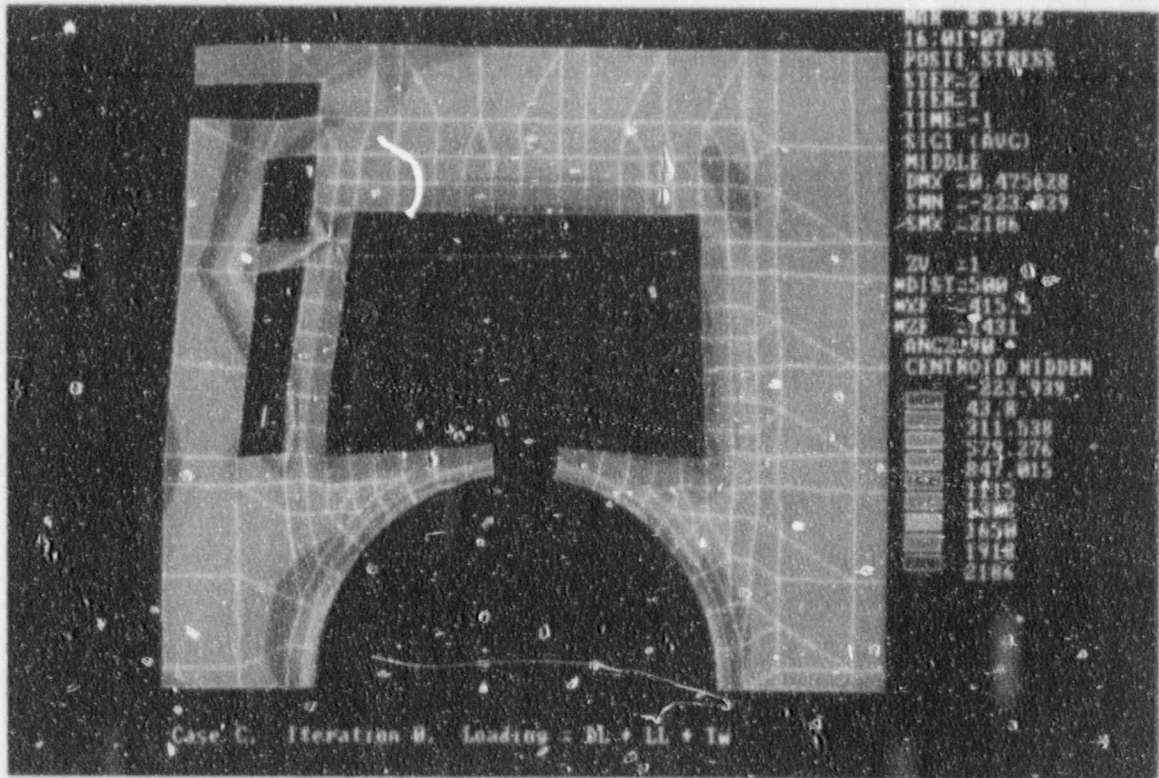


Figure 5.89

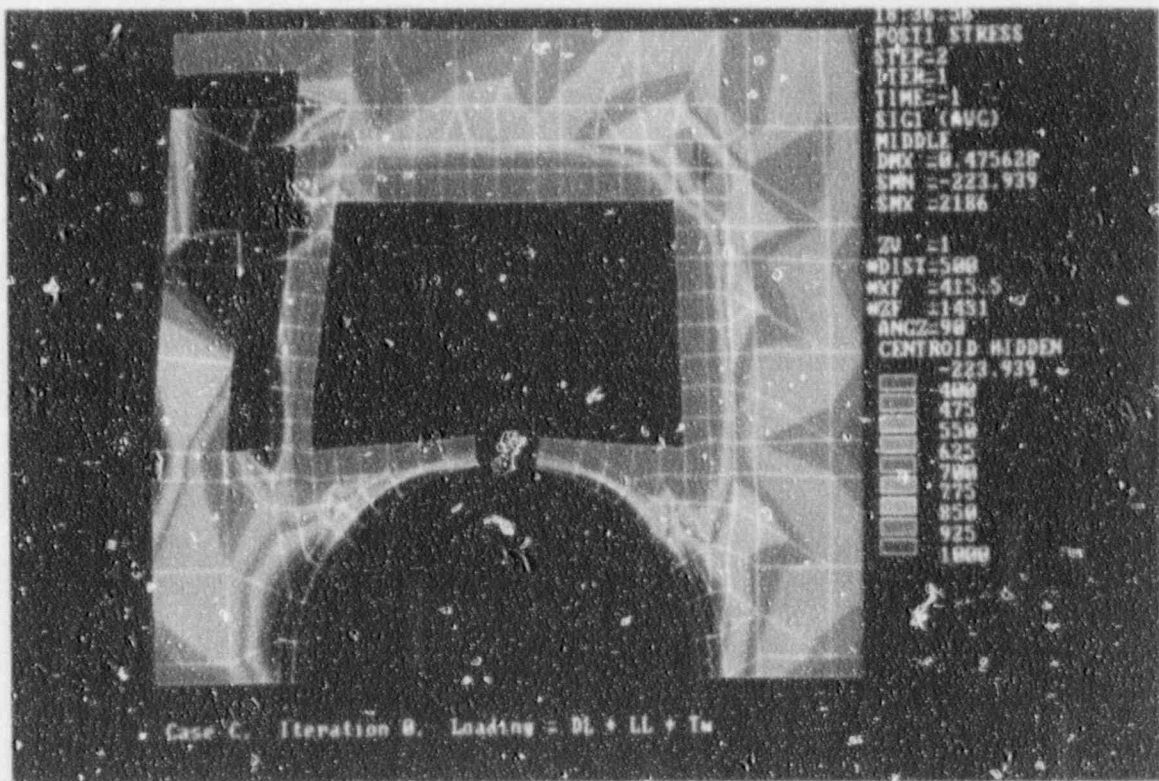


Figure 5.90

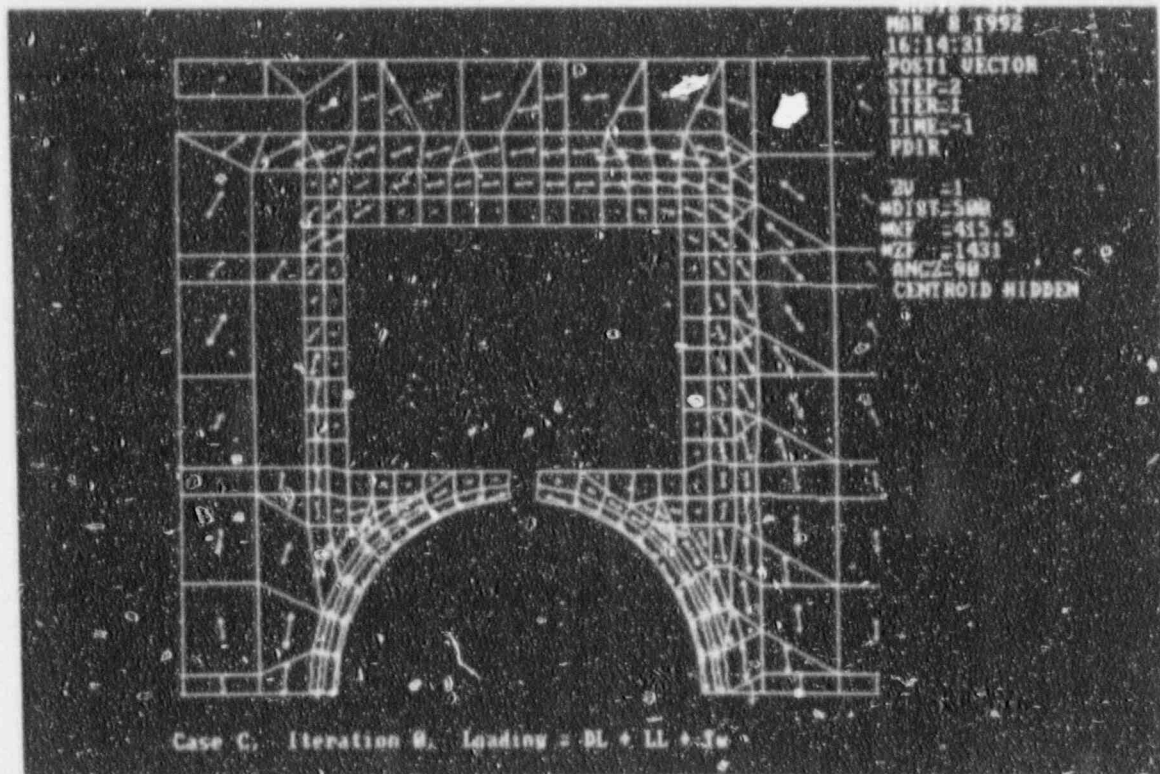


Figure 5.91

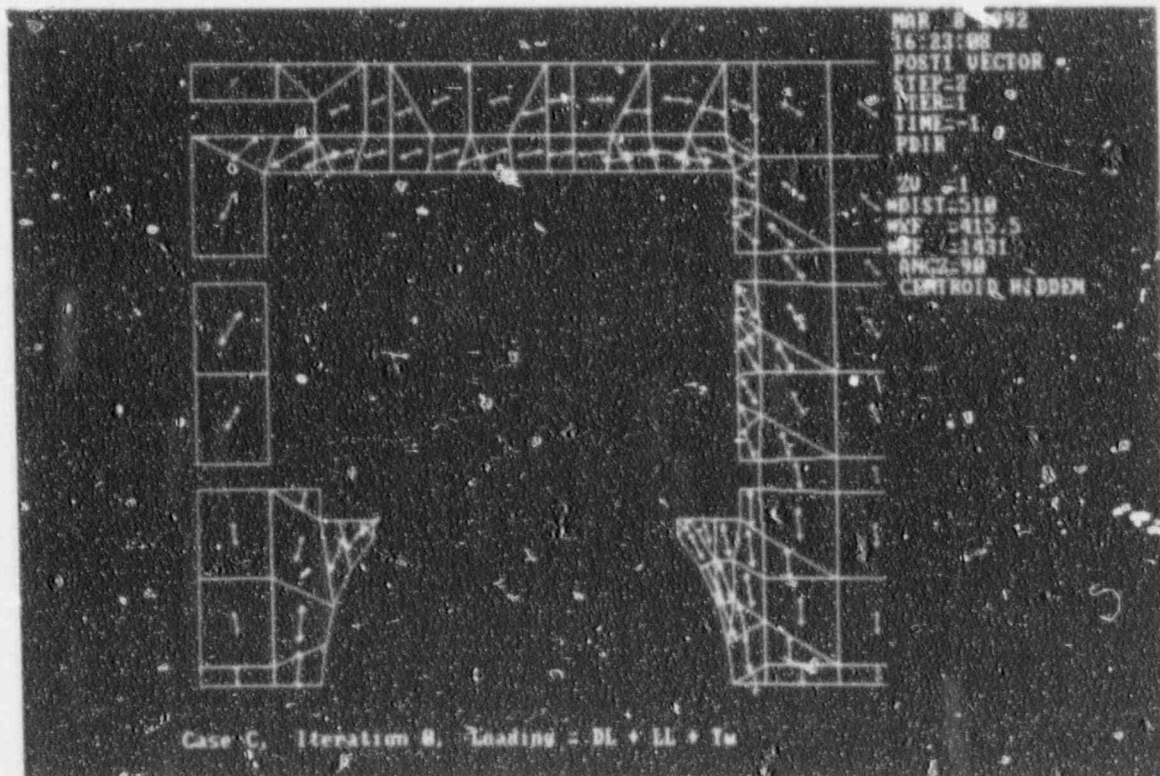


Figure 5.92

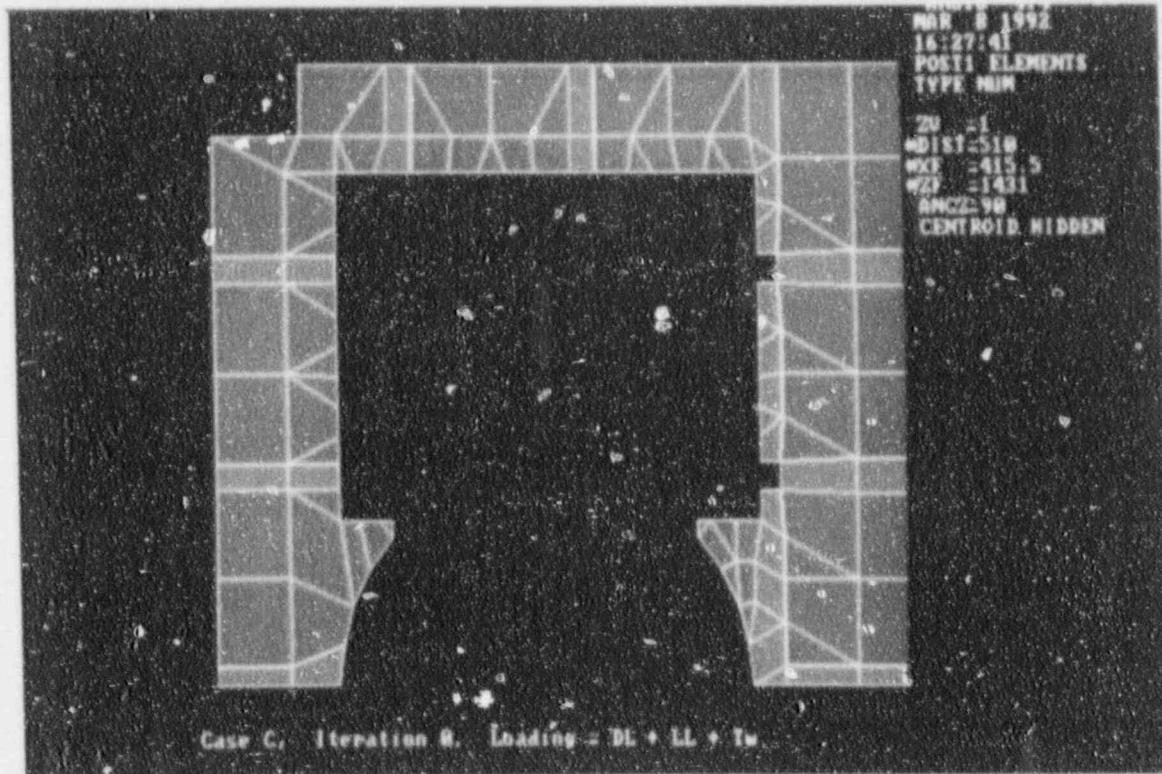


Figure 5.93

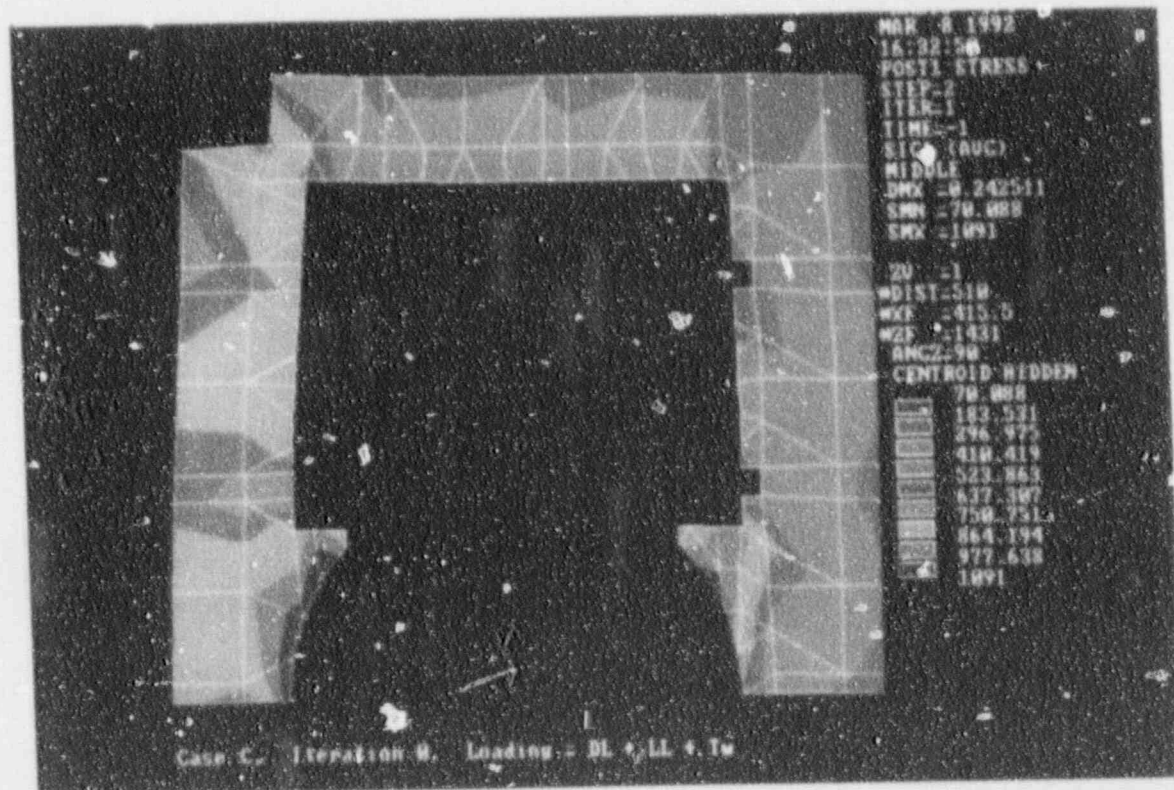


Figure 5.94

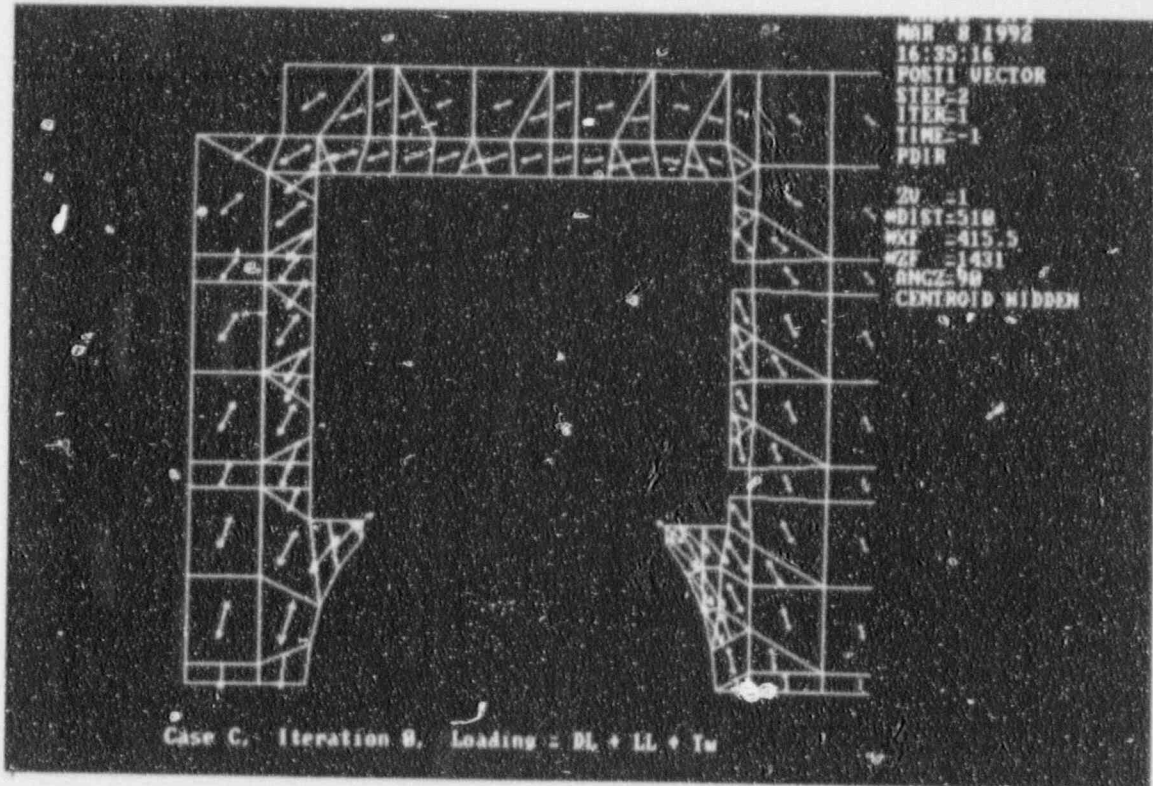


Figure 5.95

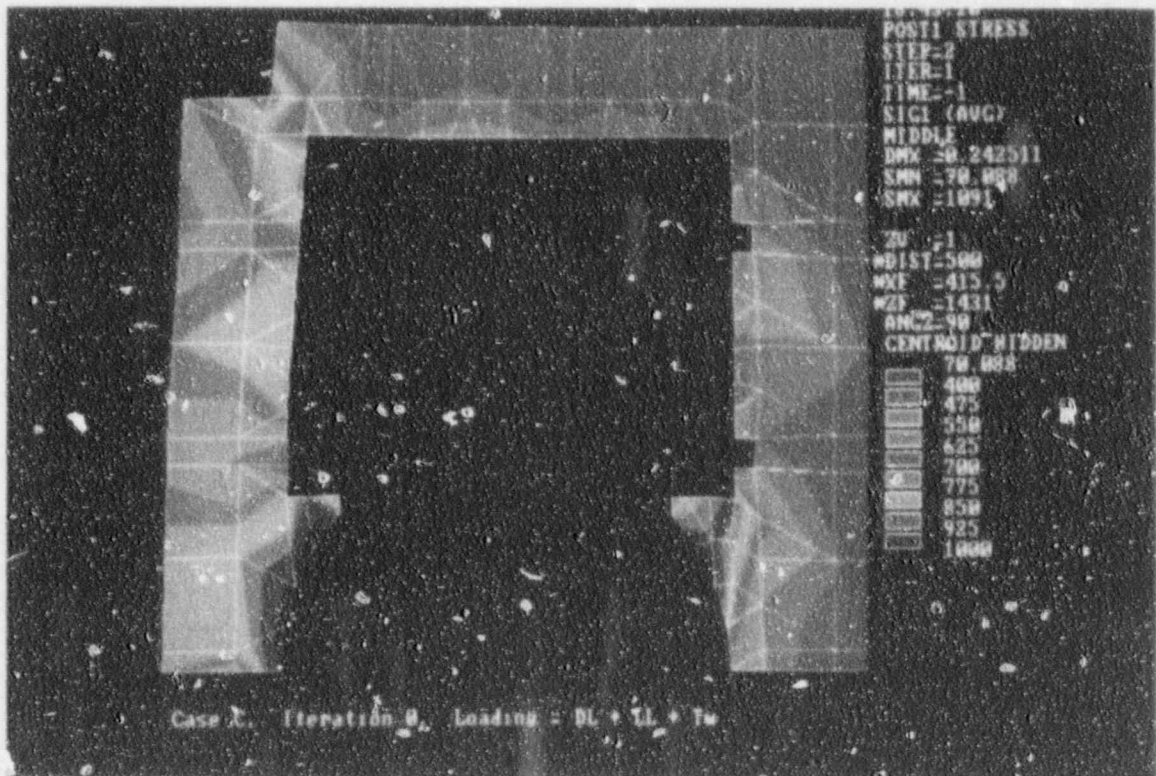


Figure 5.96

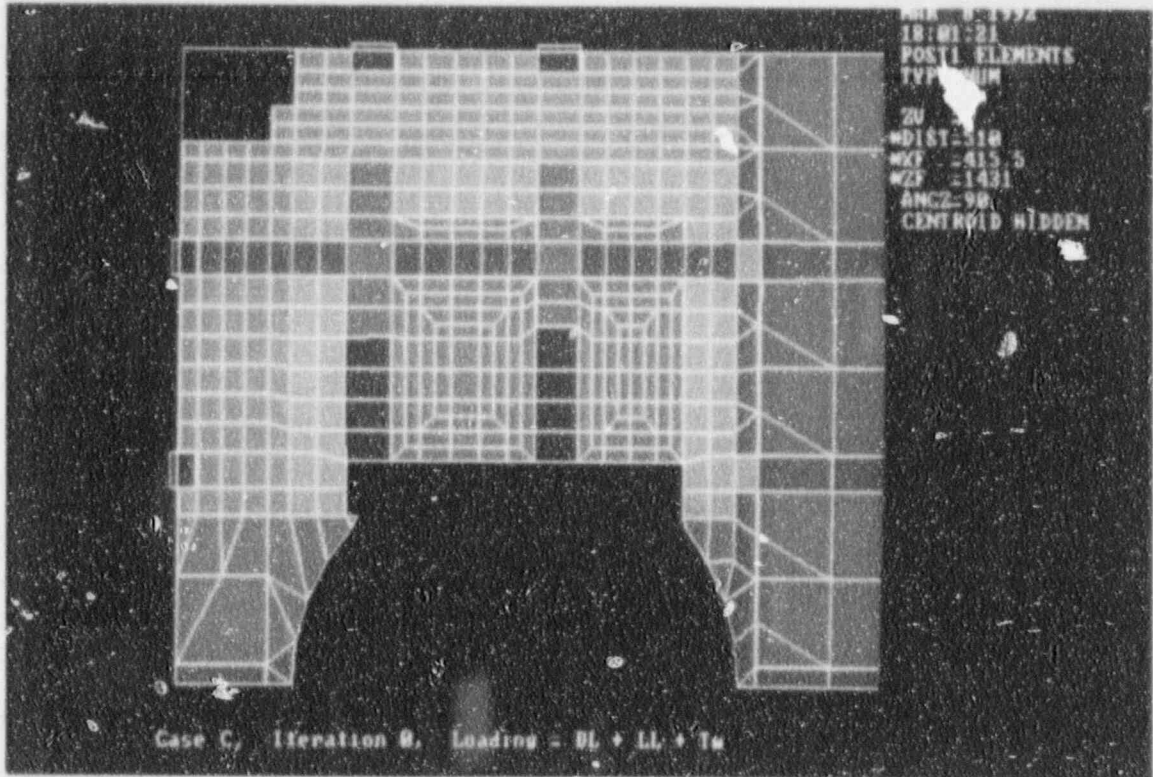


Figure 5.97

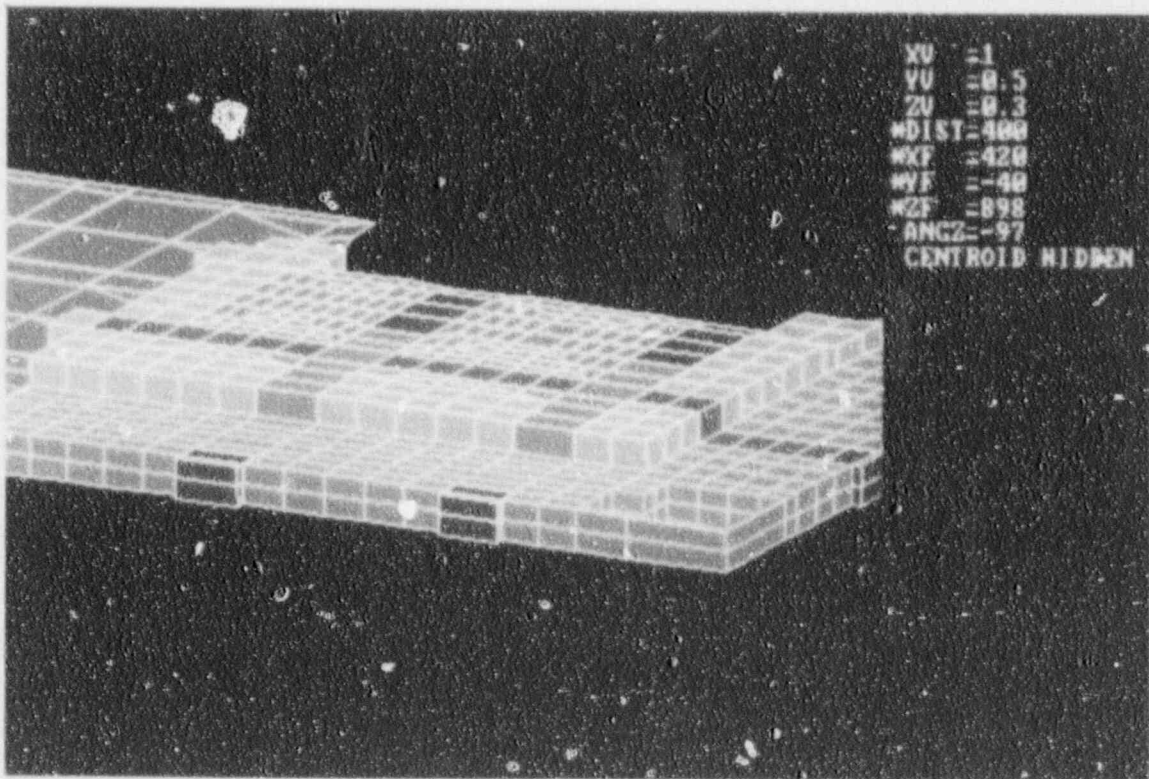


Figure 5.98

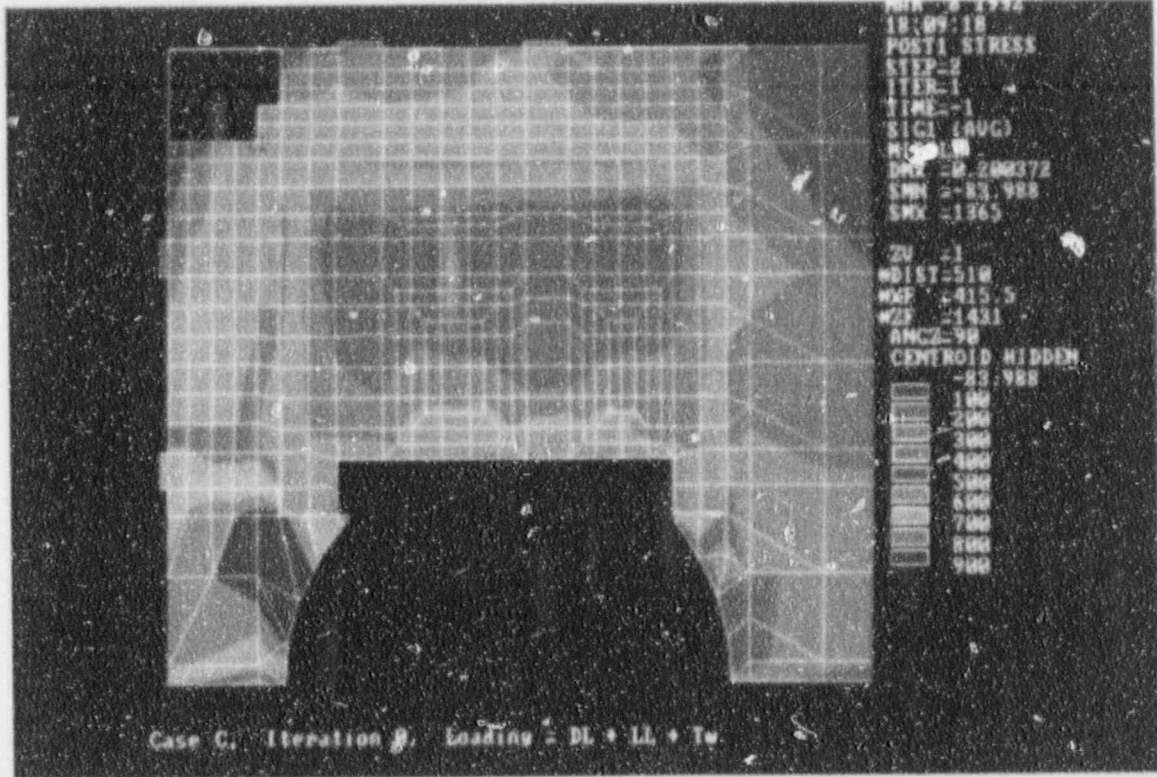


Figure 5.99

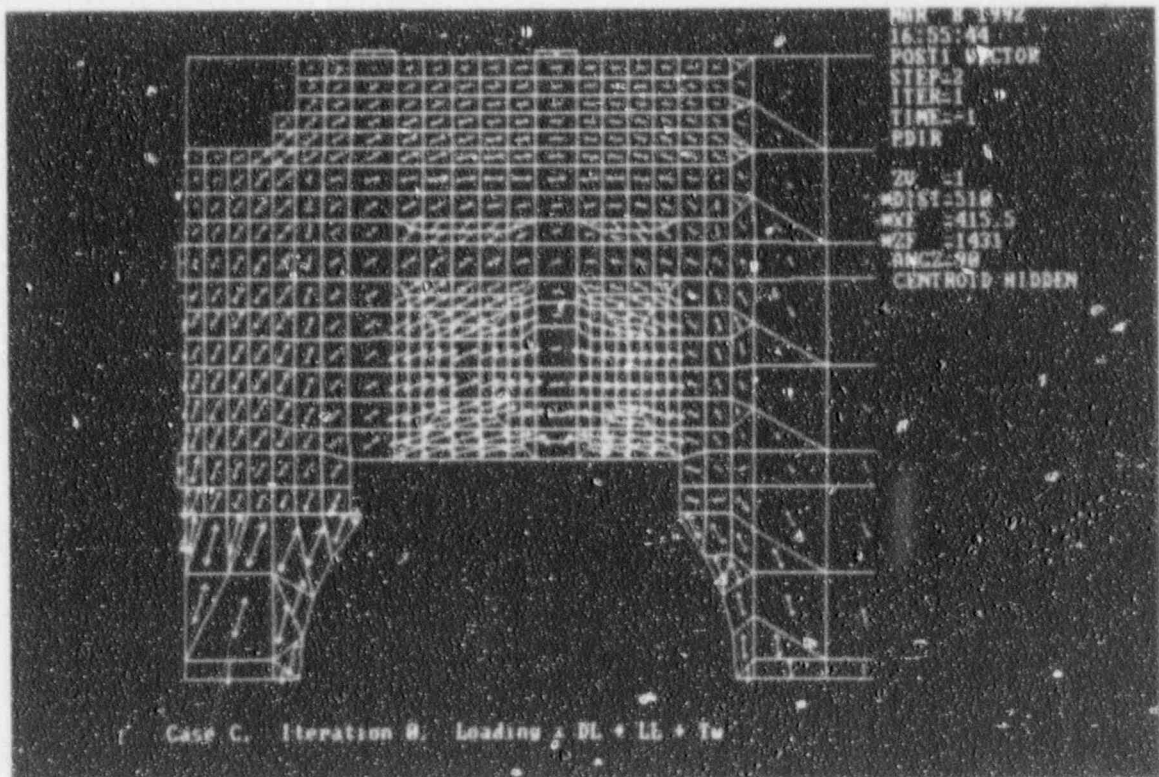
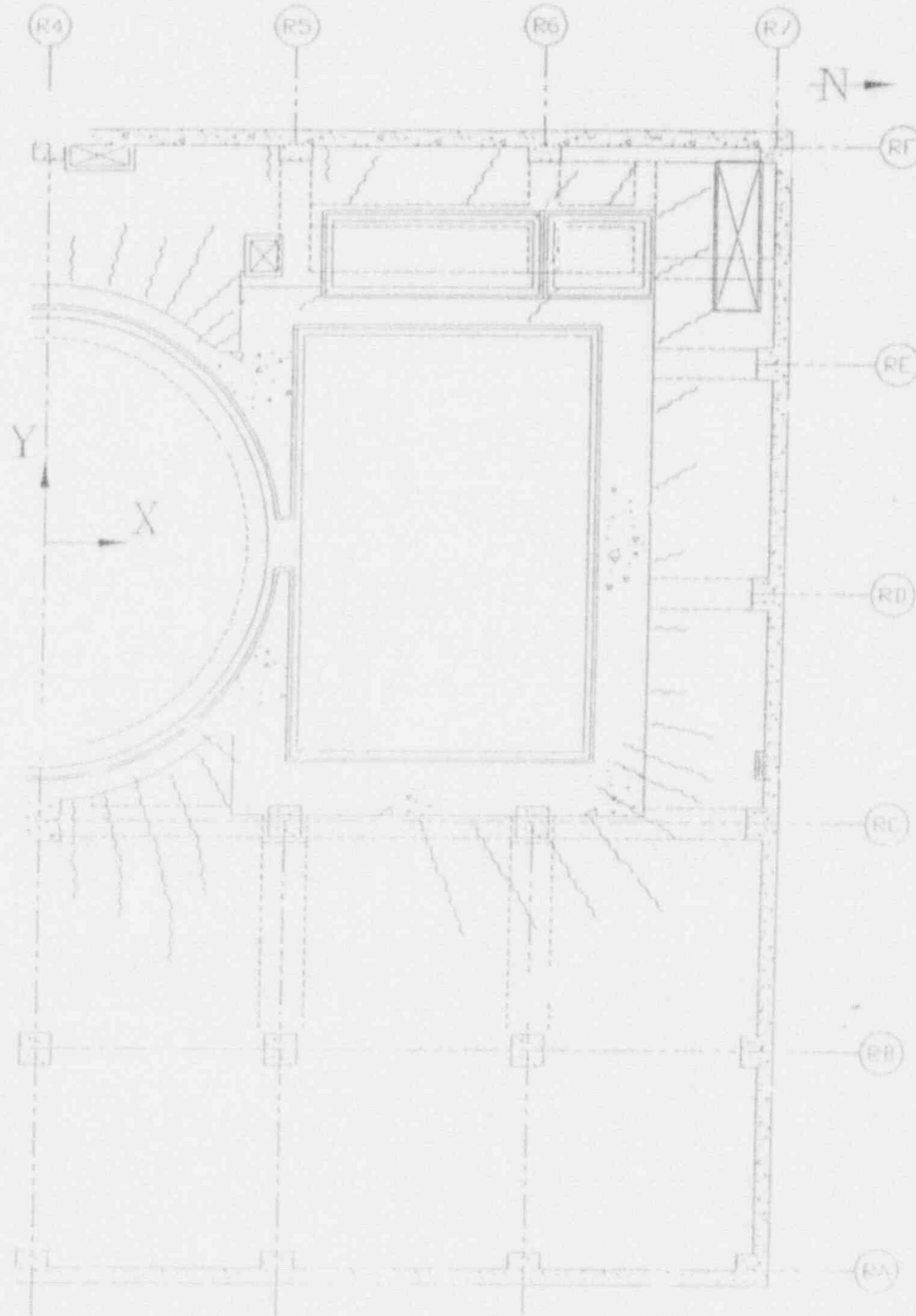


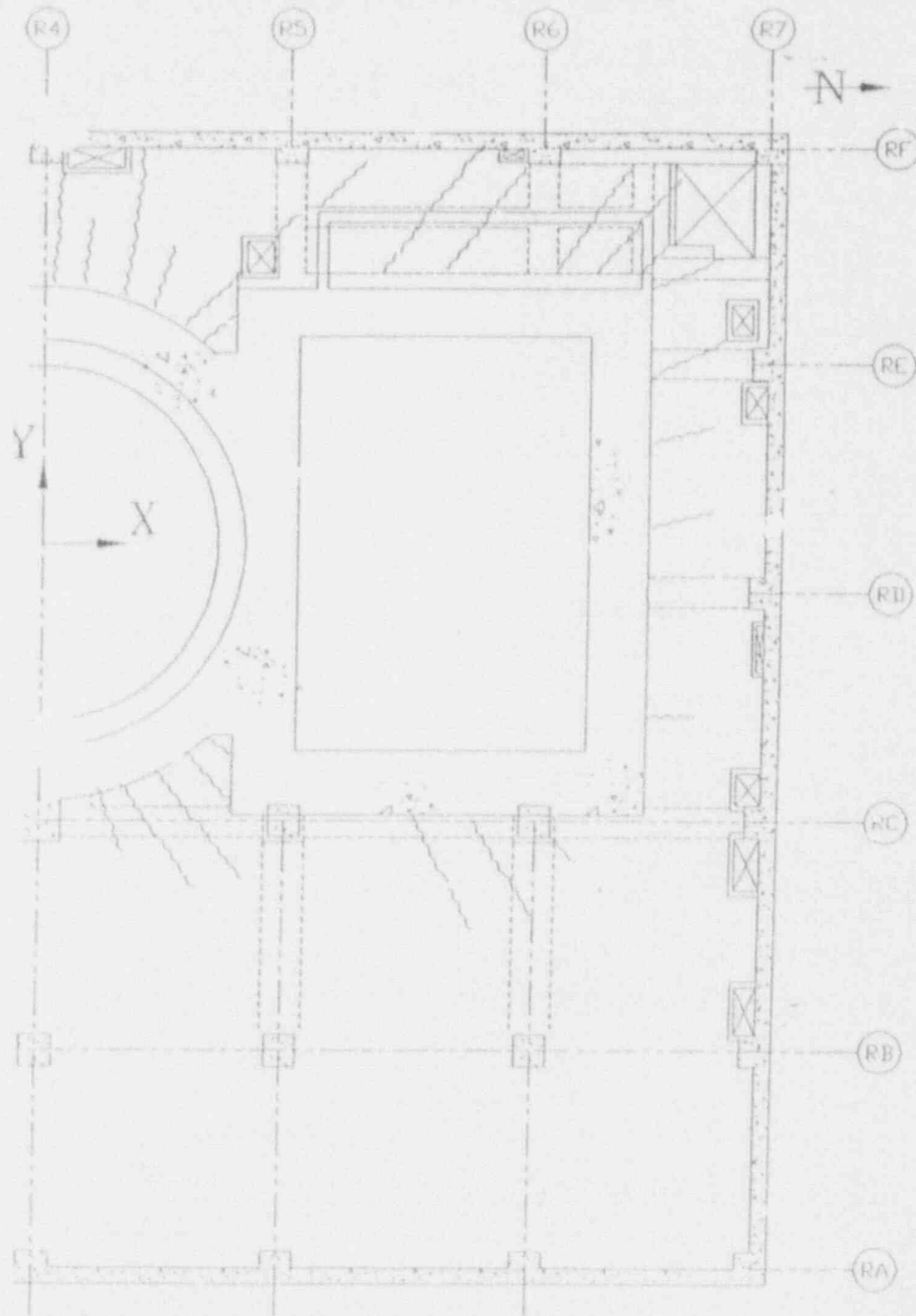
Figure 5.100

ABB Impell Corporation



PREDICTED CRACK PATTERN FOR FLOOR SLAB AT EL. 119'-3"

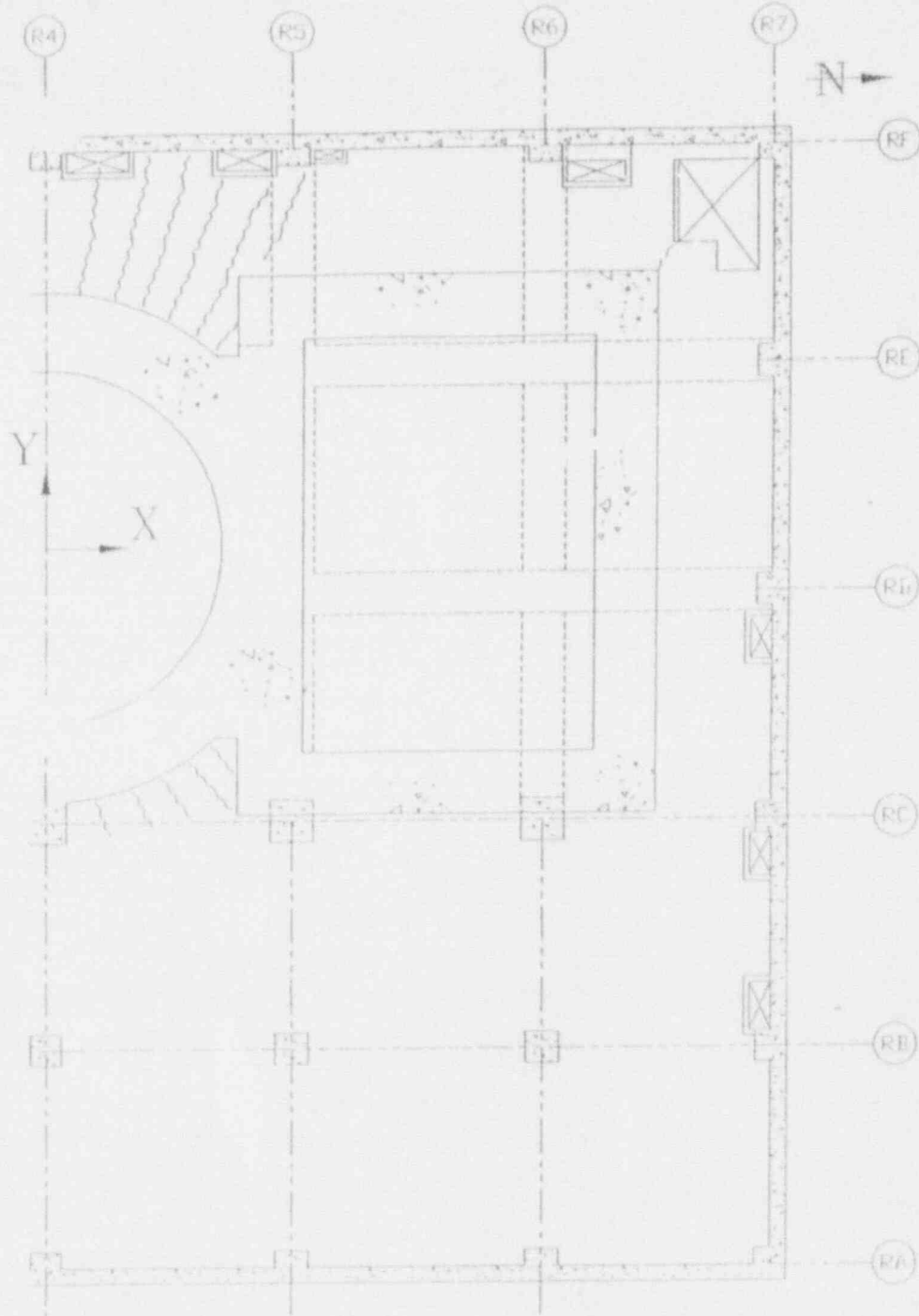
Figure 5.101



PREDICTED CRACK PATTERN FOR FLOOR SLAB AT EL. 95'-3"

Figure 5.102

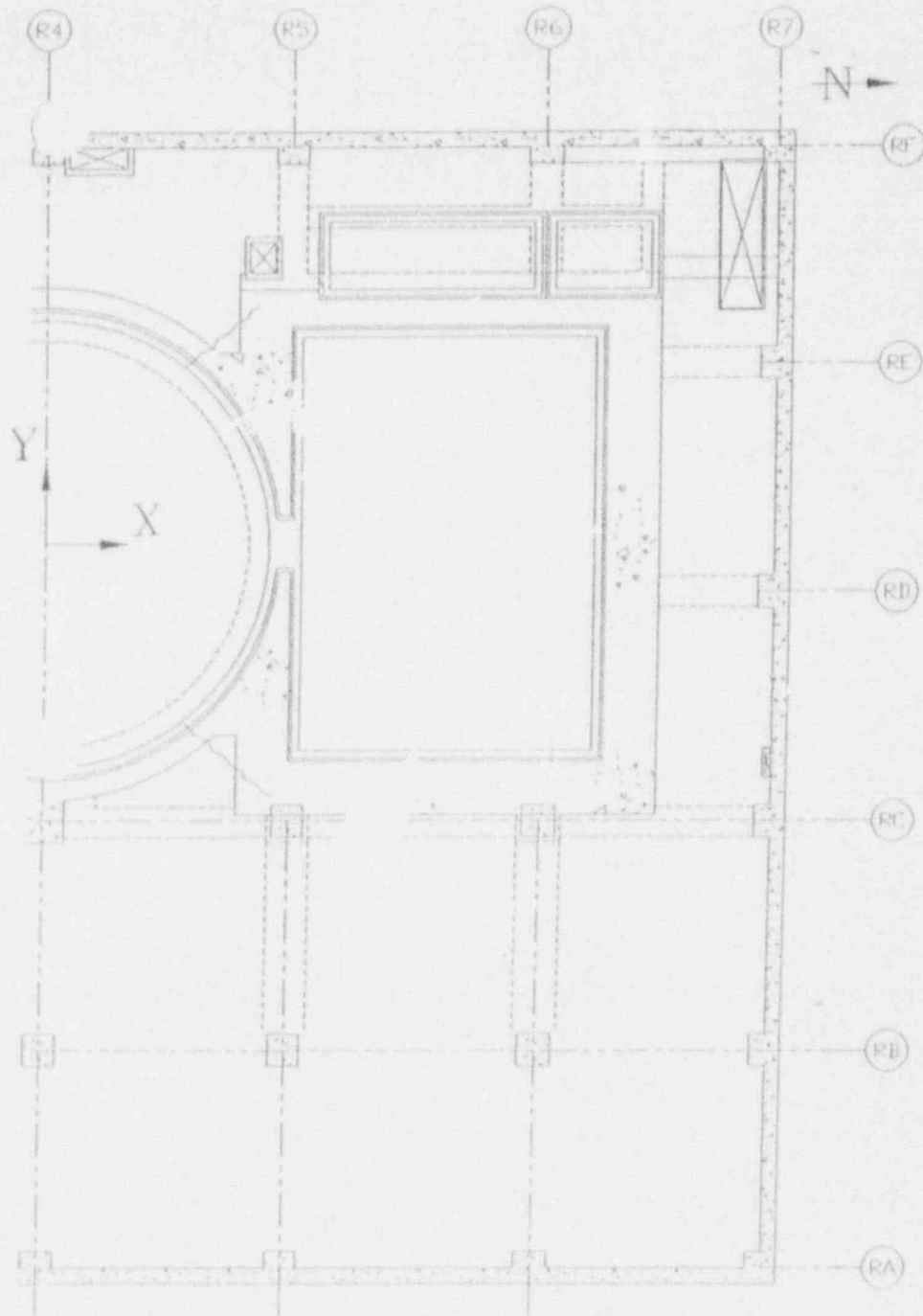
ABB Impell Corporation



PREDICTED CRACK PATTERN FOR FLOOR SLAB AT EL. 75'-3"

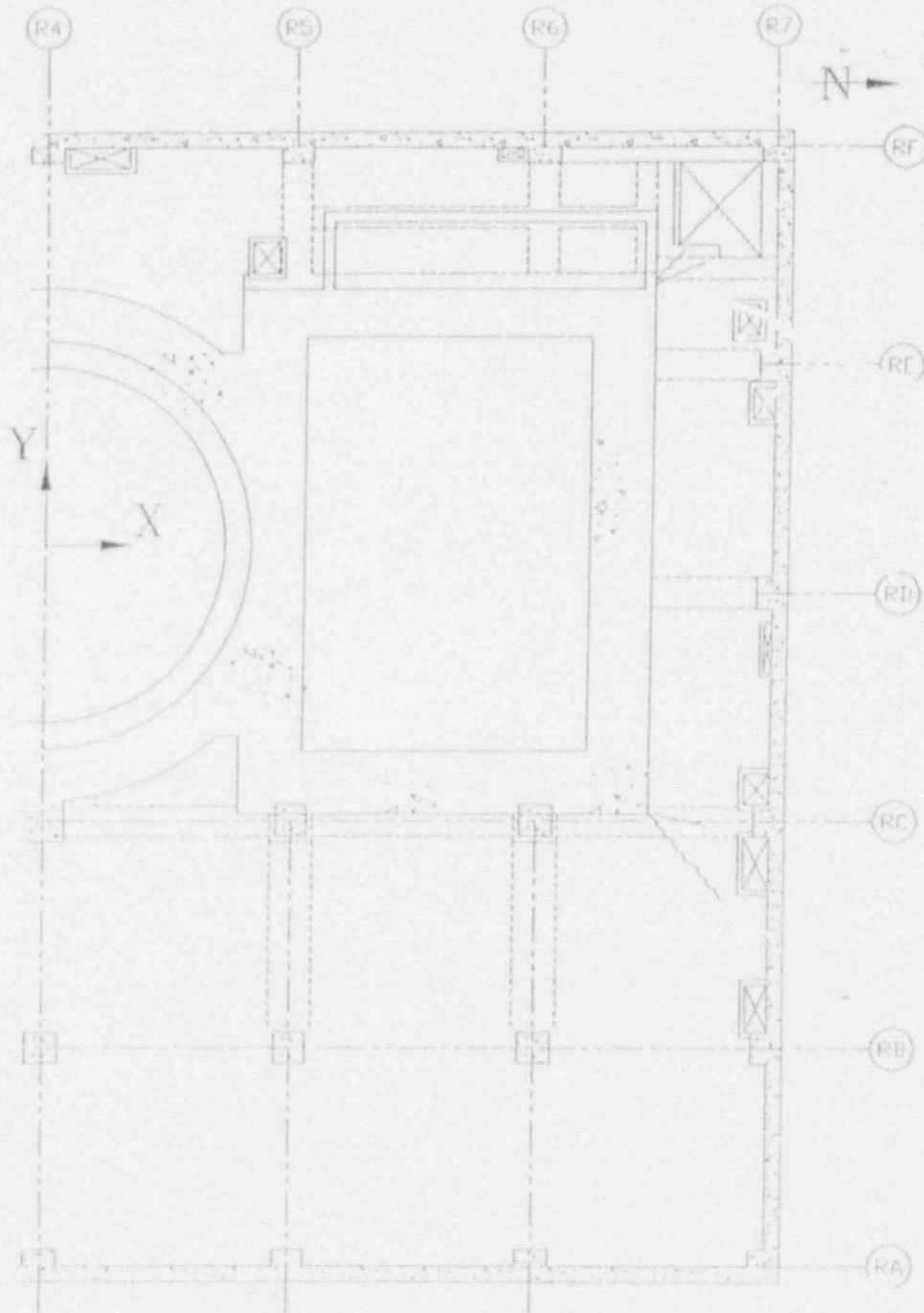
Figure 5.103

ABB Impell Corporation



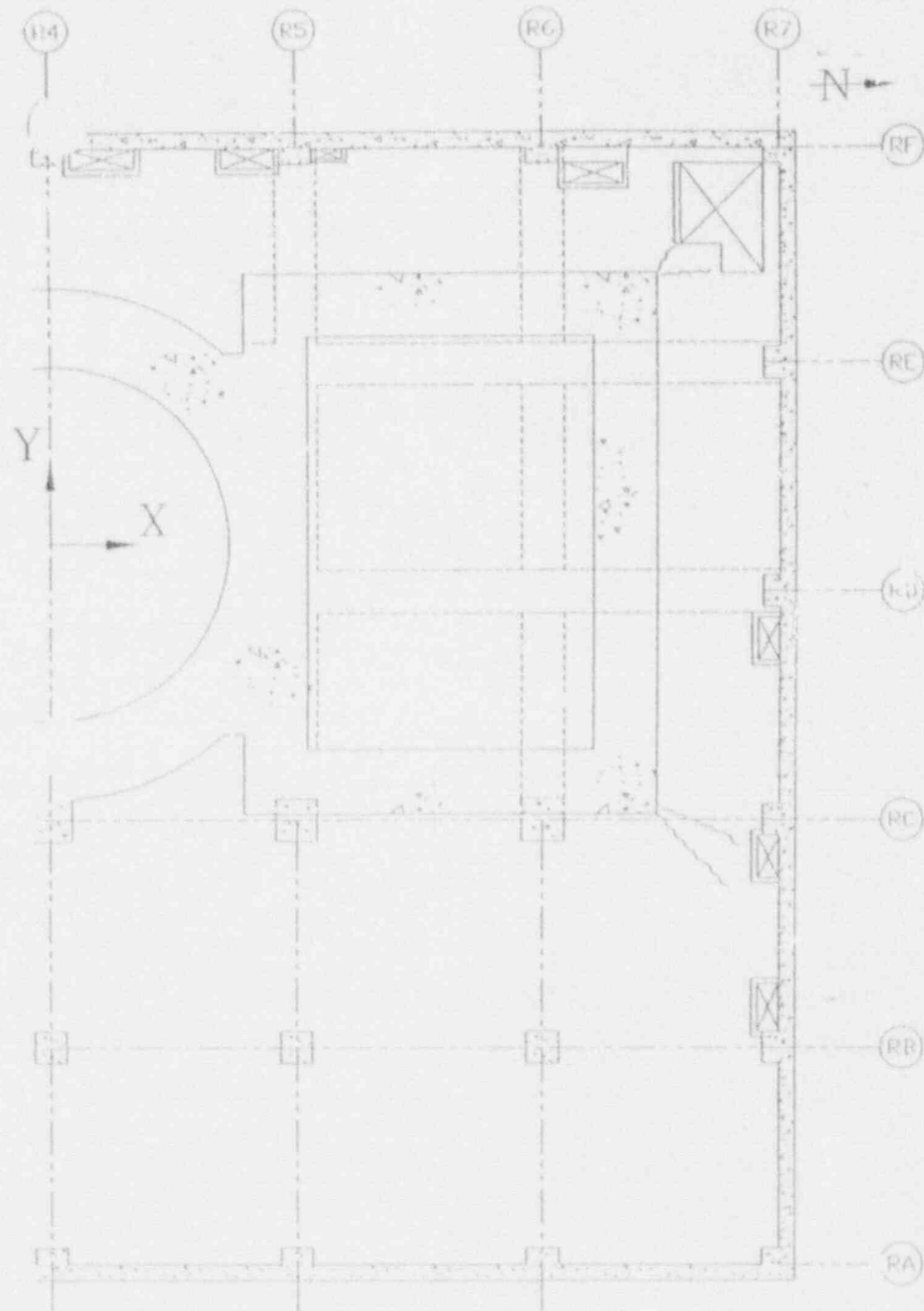
OBSERVED CRACKS IN FLOOR SLAB AT EL. 119'-3"

Figure 5.104



OBSERVED CRACK PATTERN FOR FLOOR SLAB AT EL. 95'-3"

Figure 5.105



OBSERVED CRACKS IN FLOOR SLAB AT EL. 75'-3"

Figure 5.106

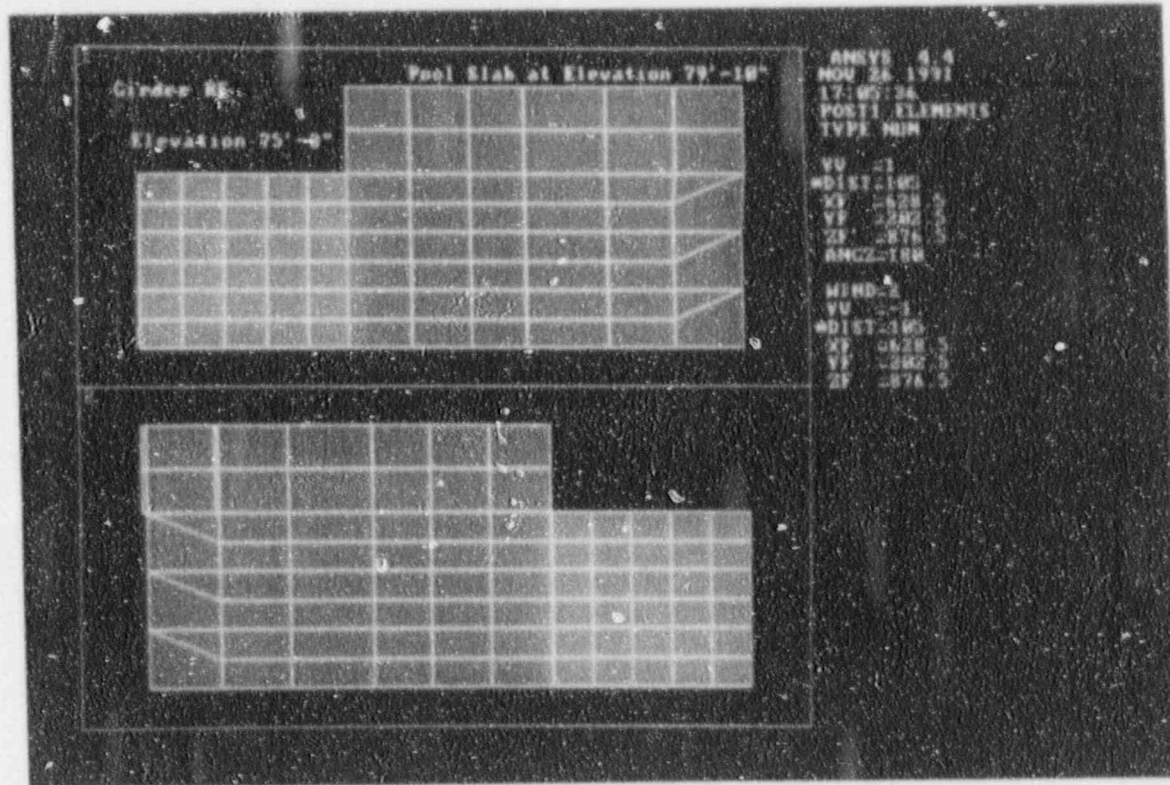


Figure 5.107

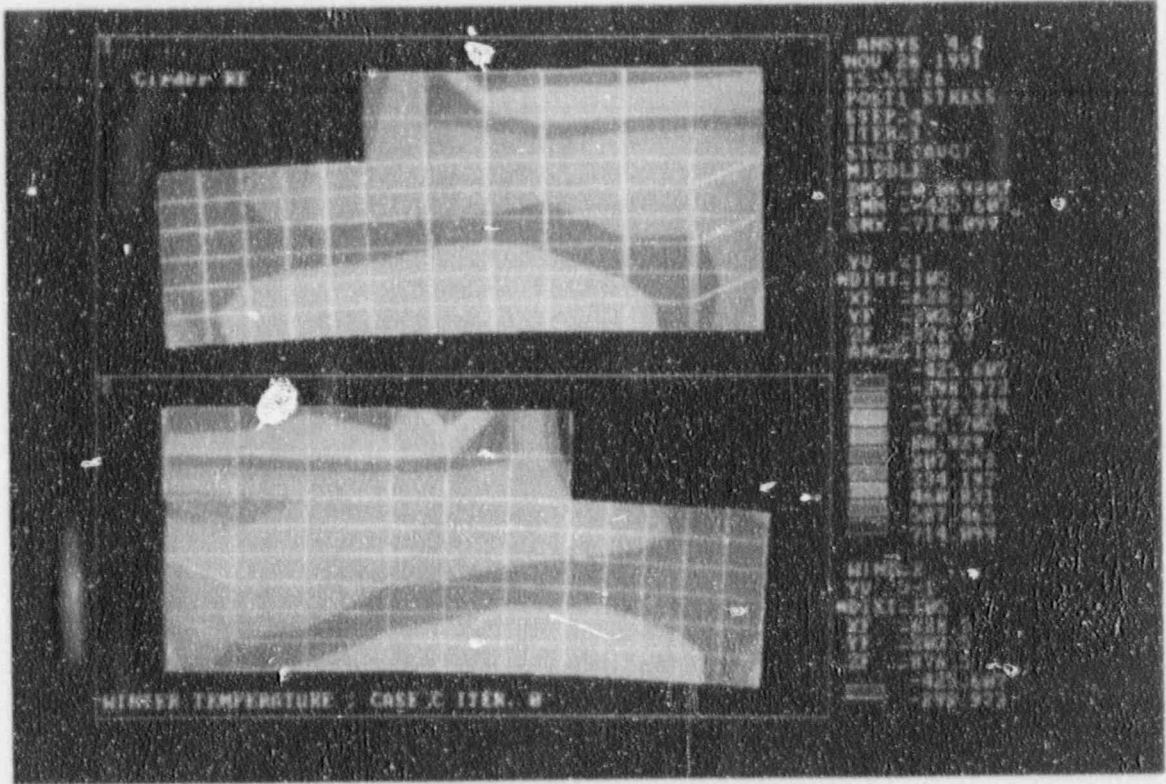


Figure 5.108

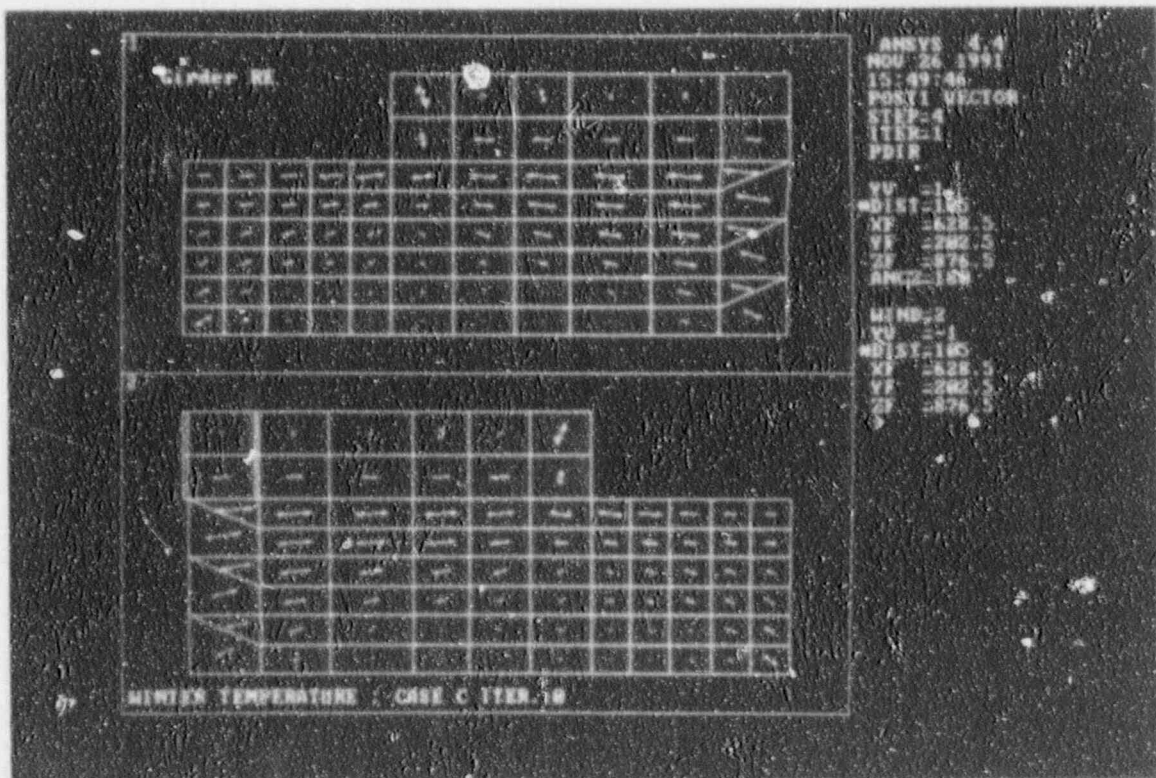


Figure 5.109

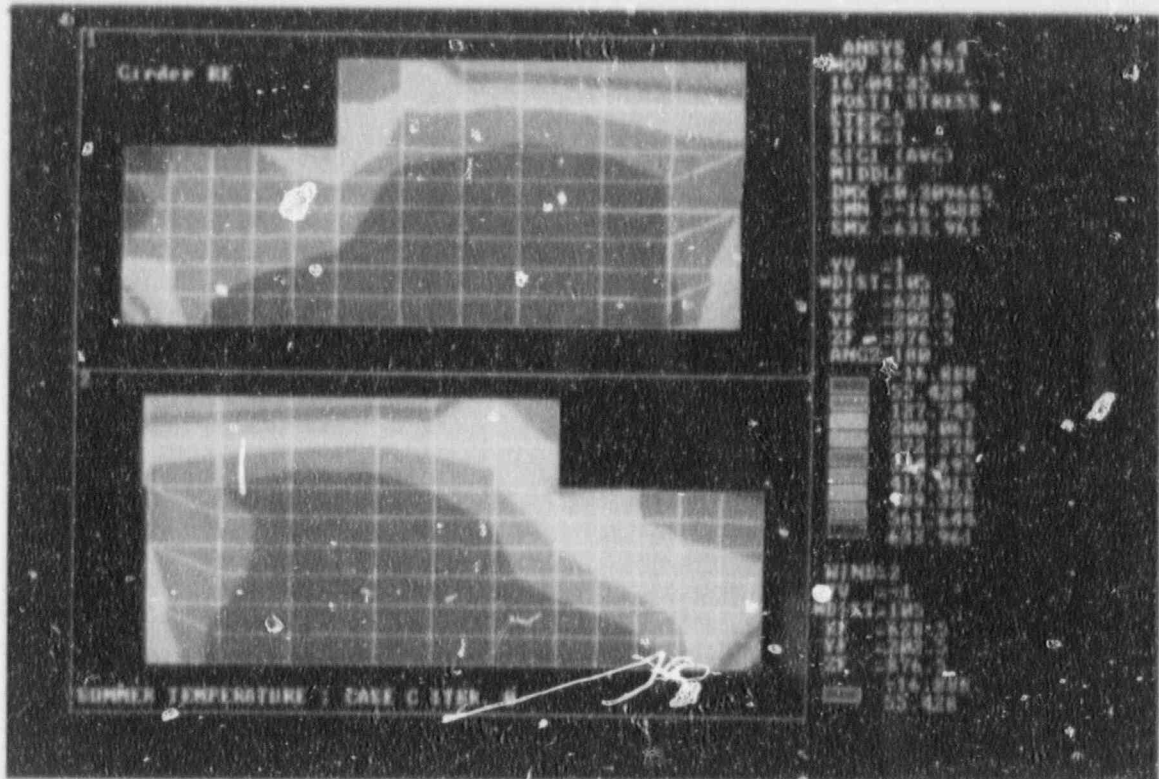


Figure 5.110

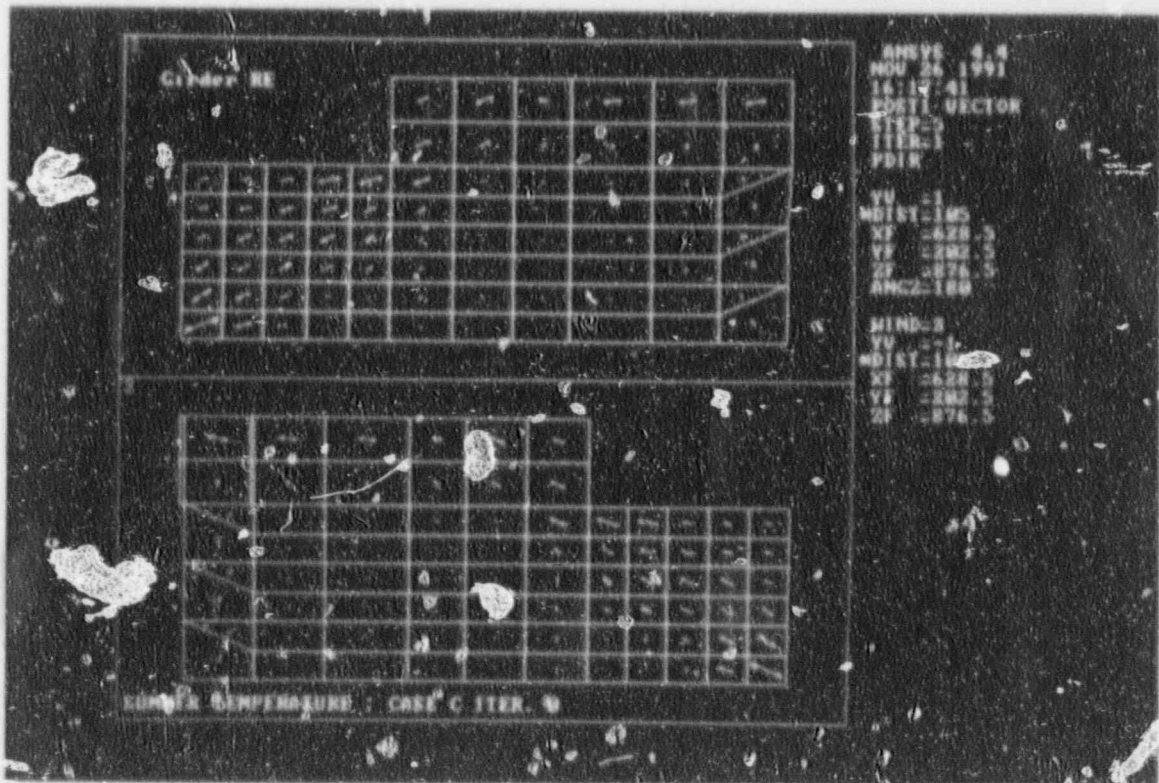


Figure 5.111

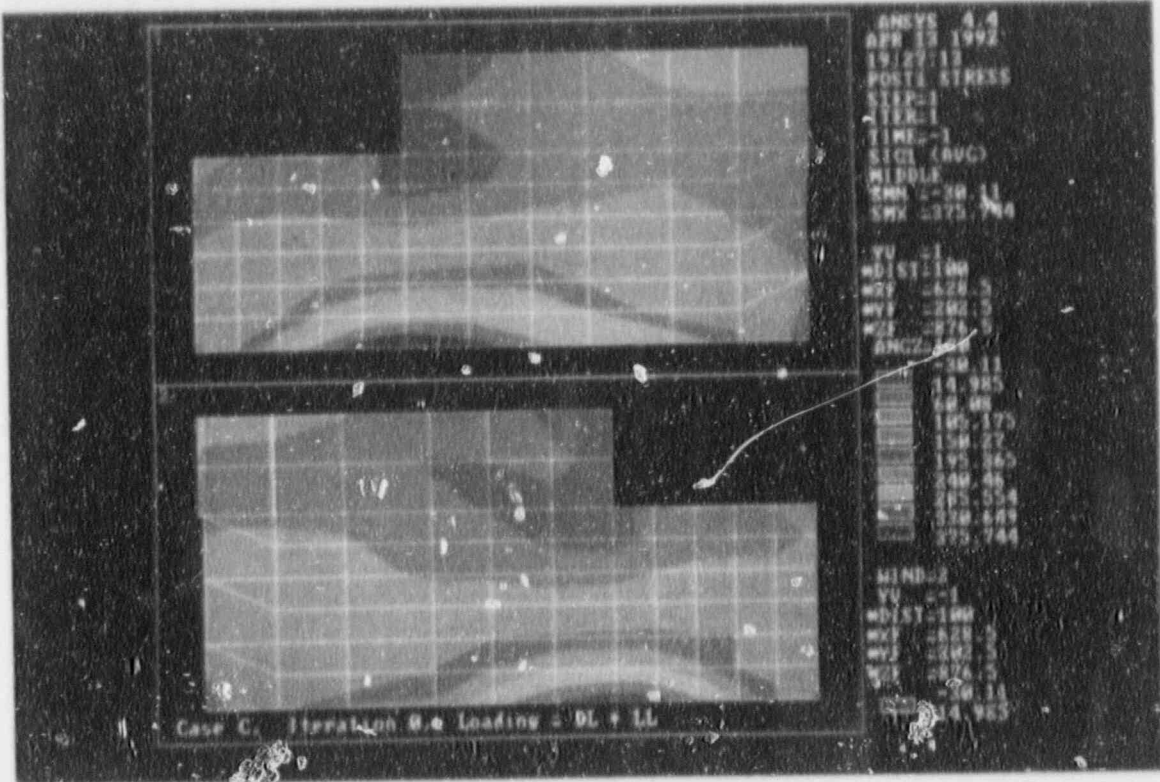


Figure 5.112

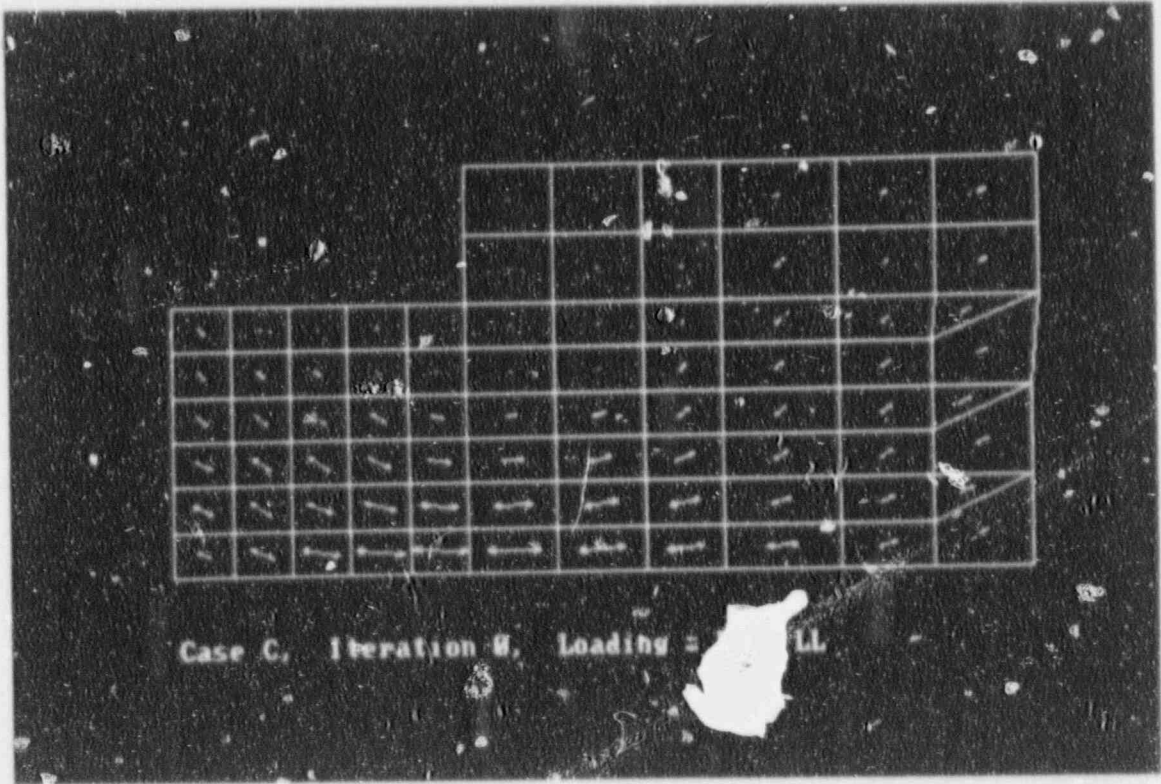


Figure 5.113

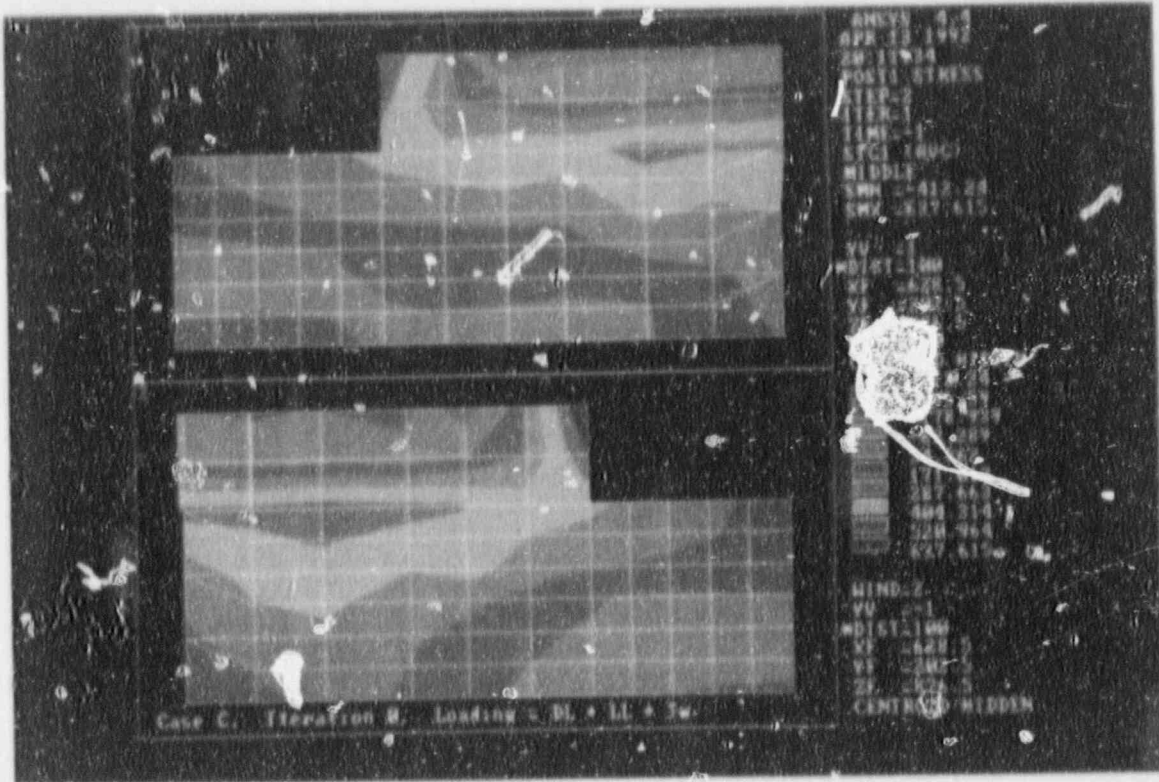


Figure 5.114

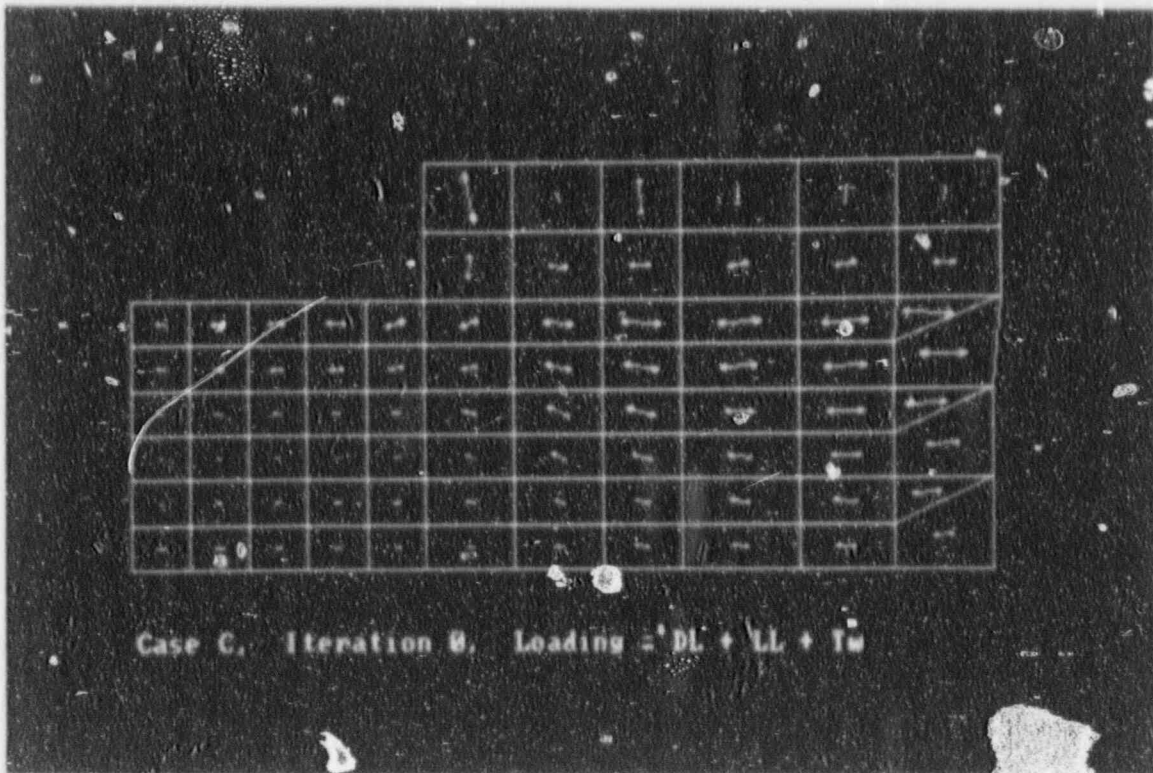


Figure 5.115

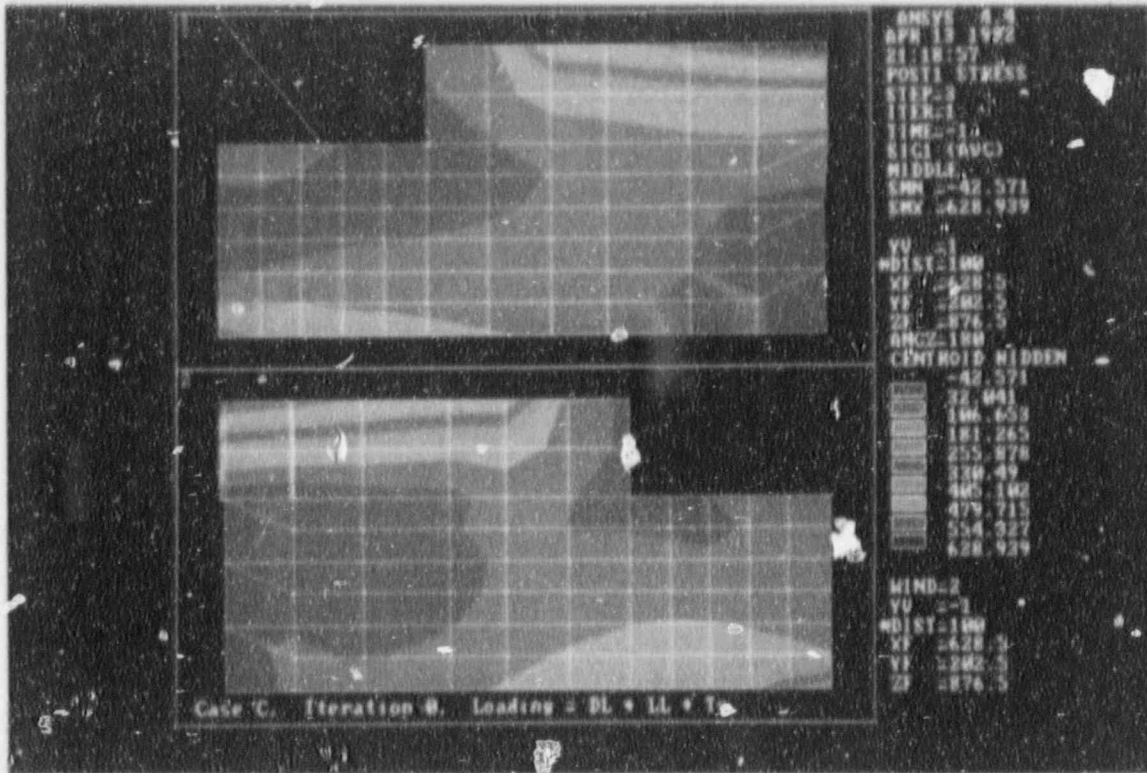


Figure 5.116

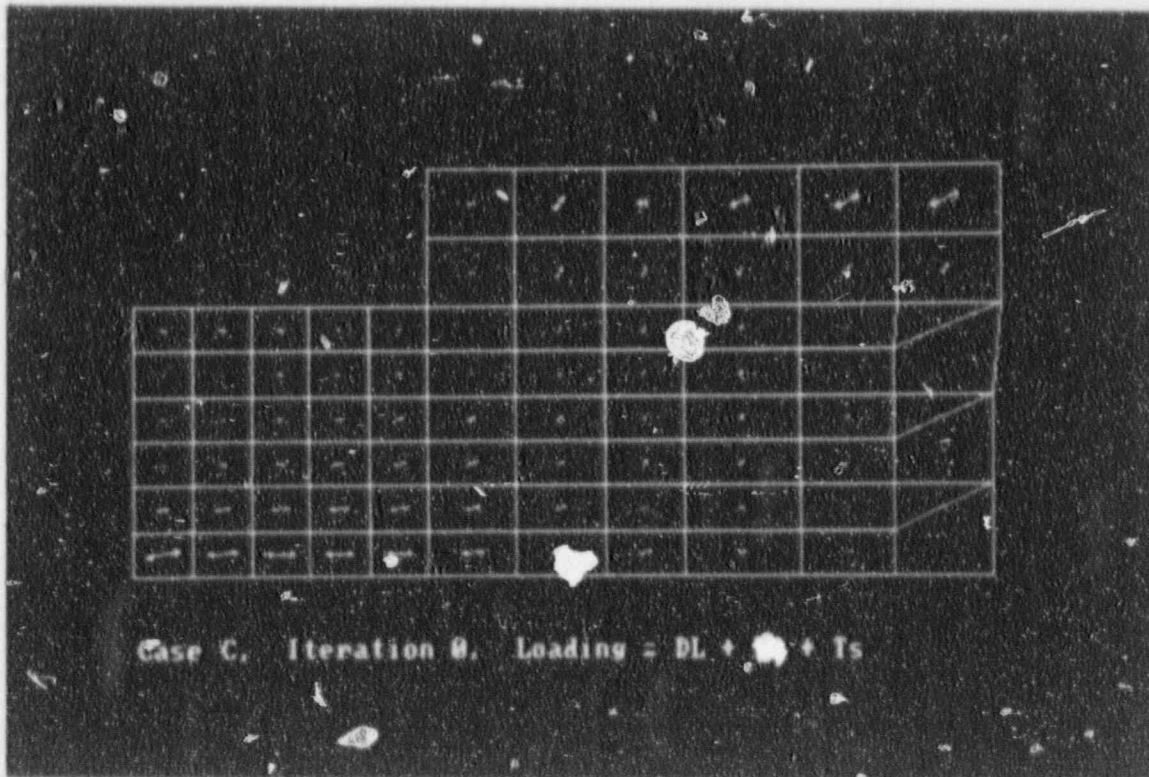


Figure 5.117

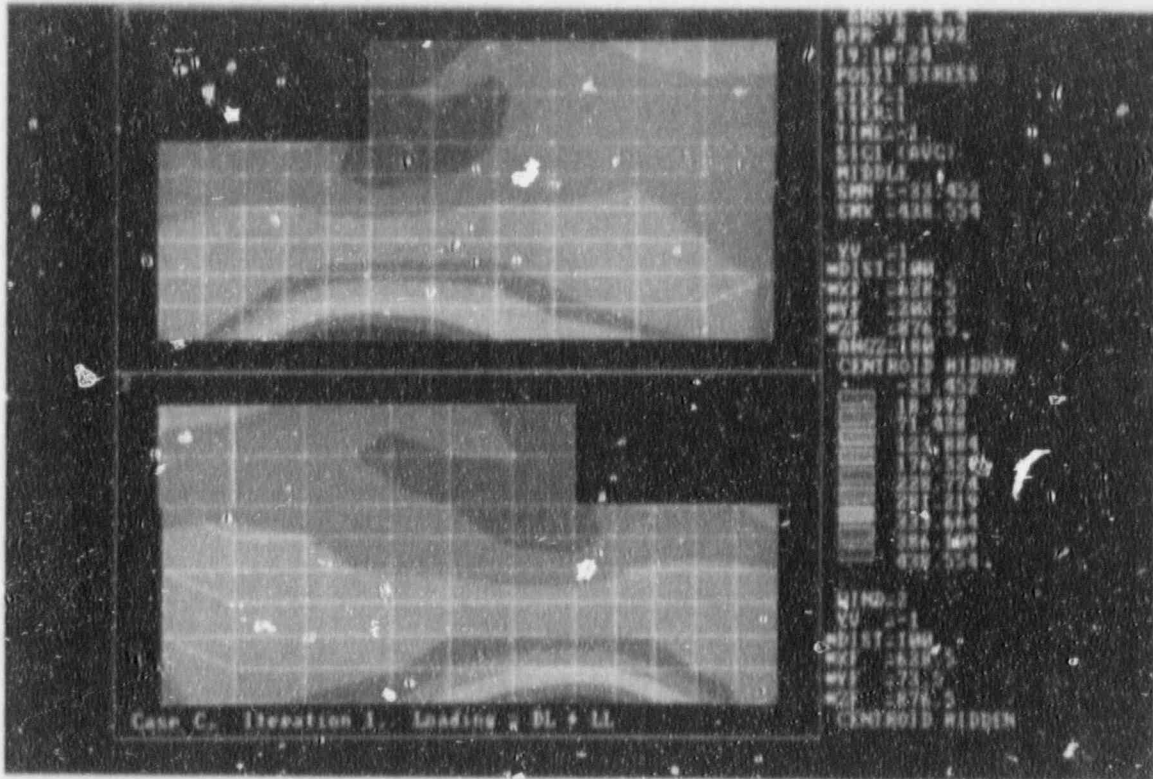


Figure 5.118

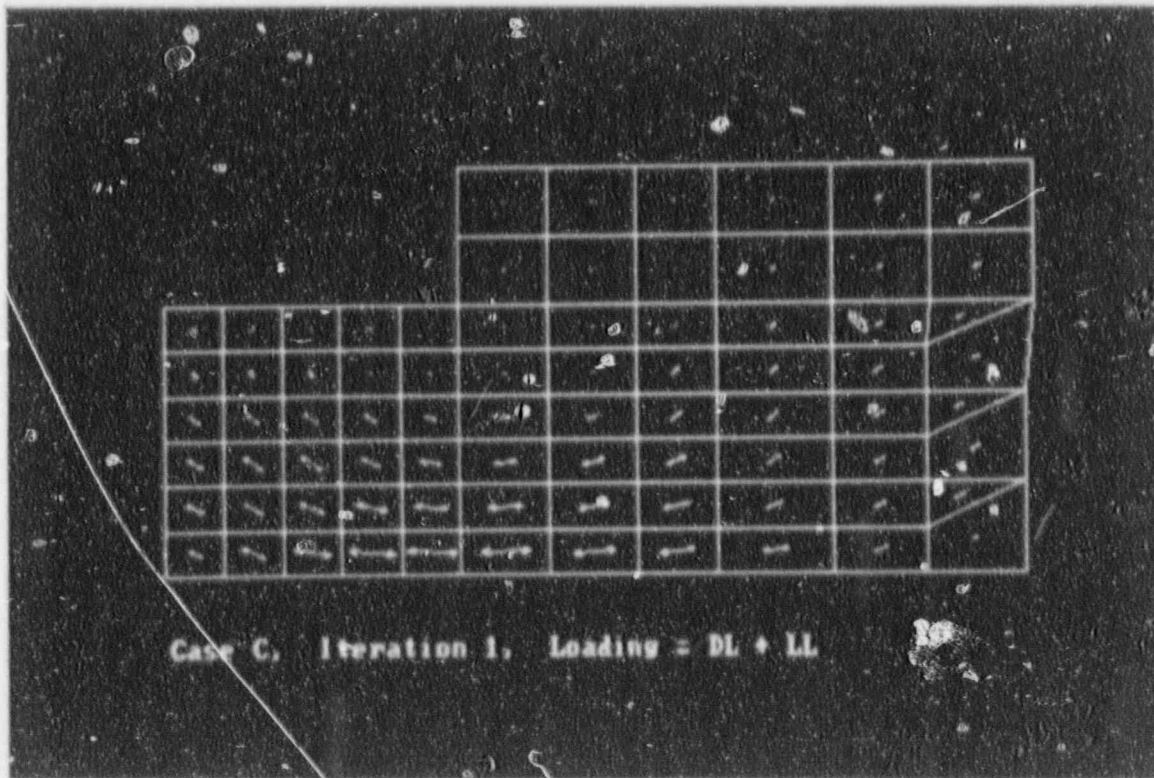


Figure 5.119

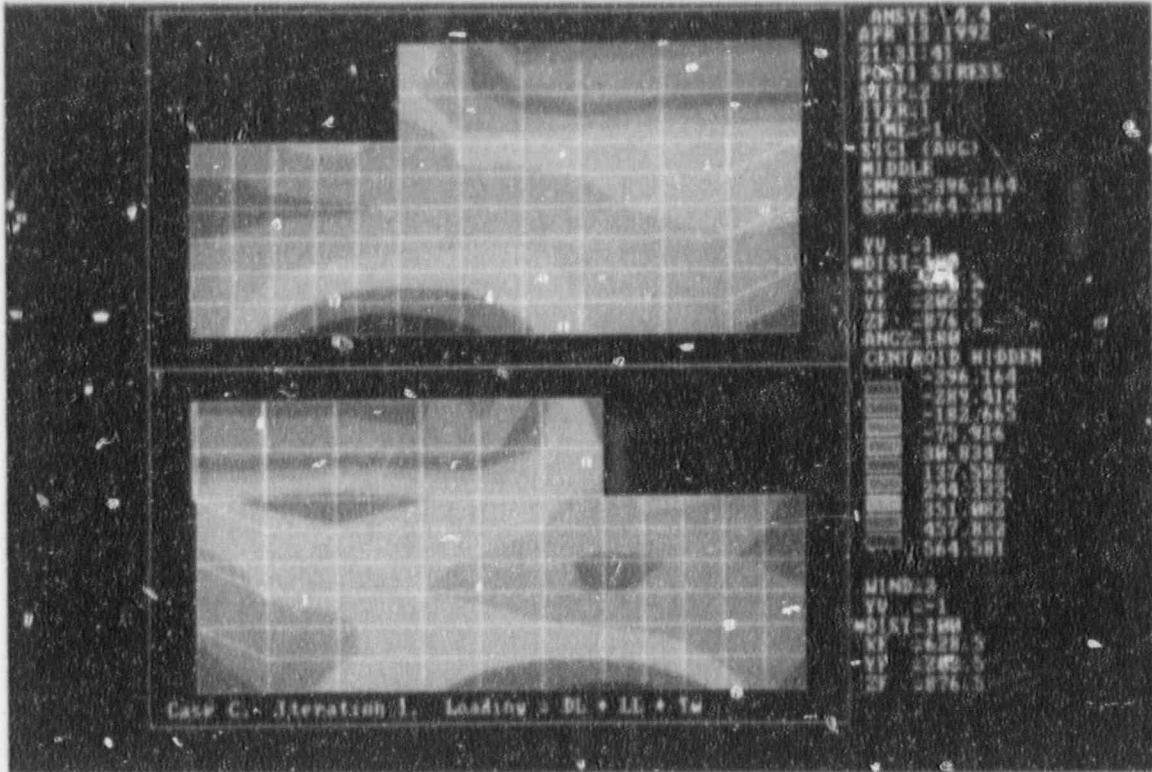


Figure 5.120

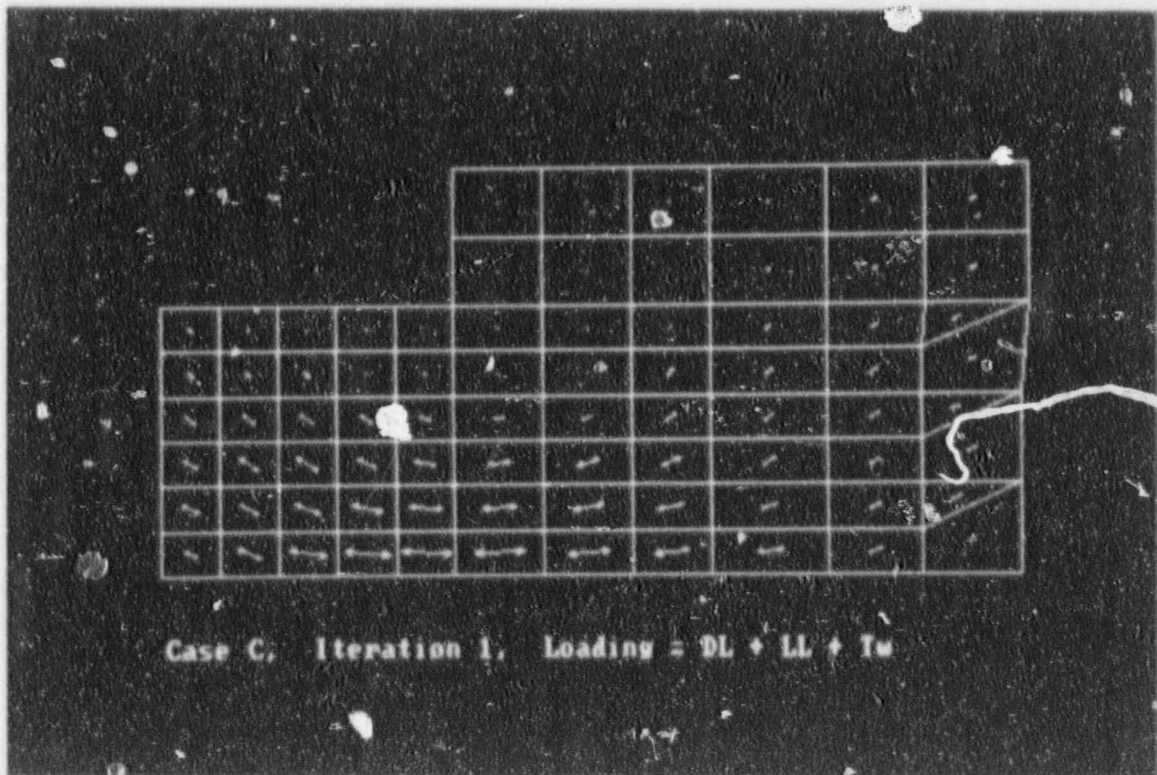


Figure 5.121

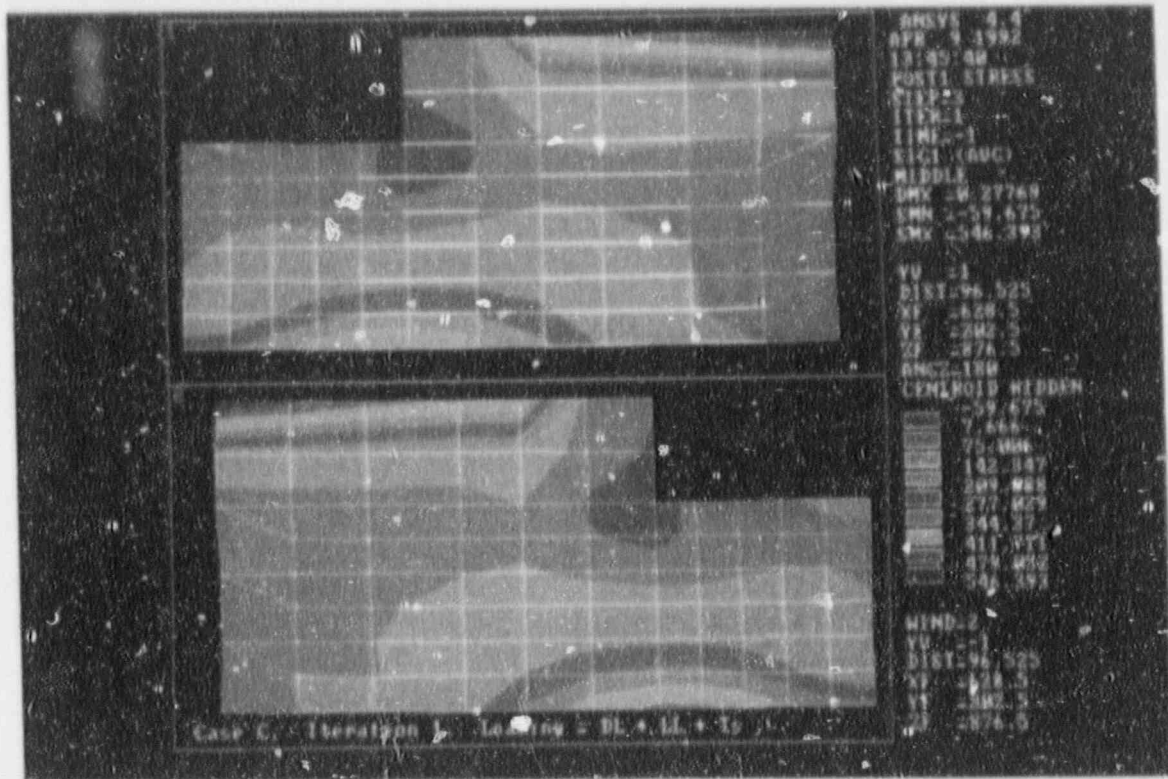


Figure 5.122

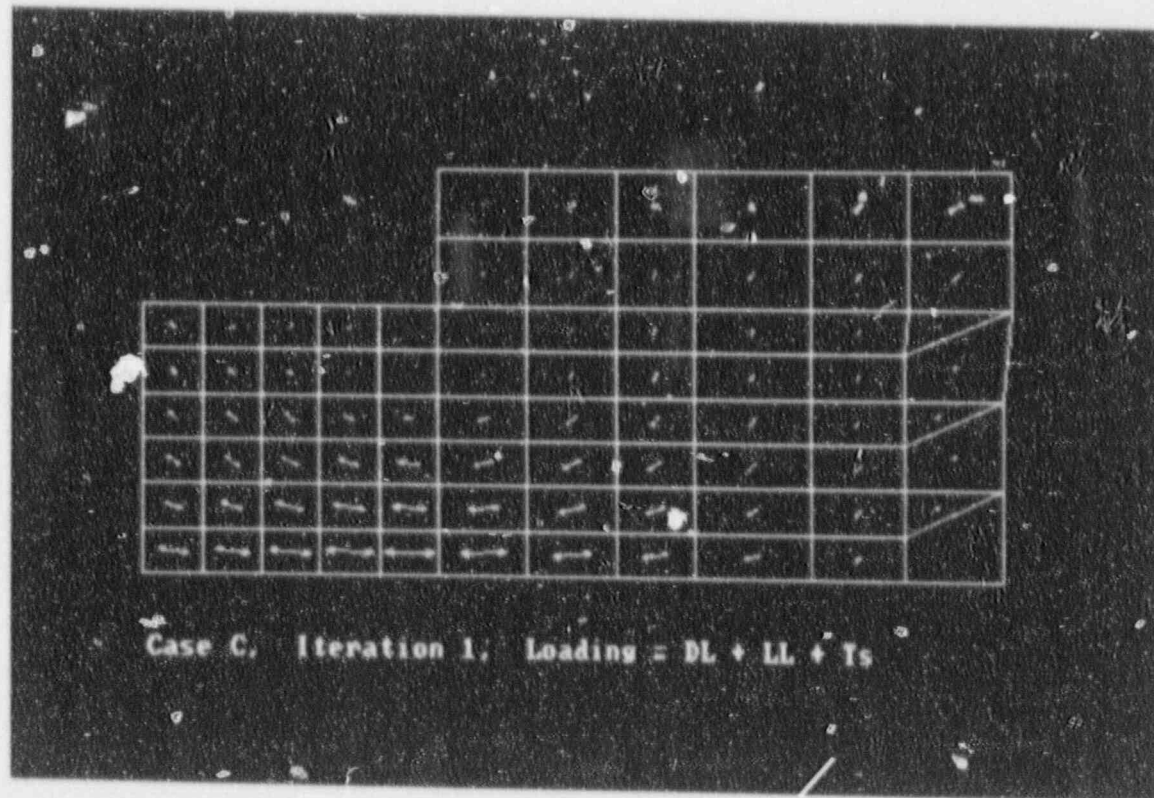


Figure 5.123

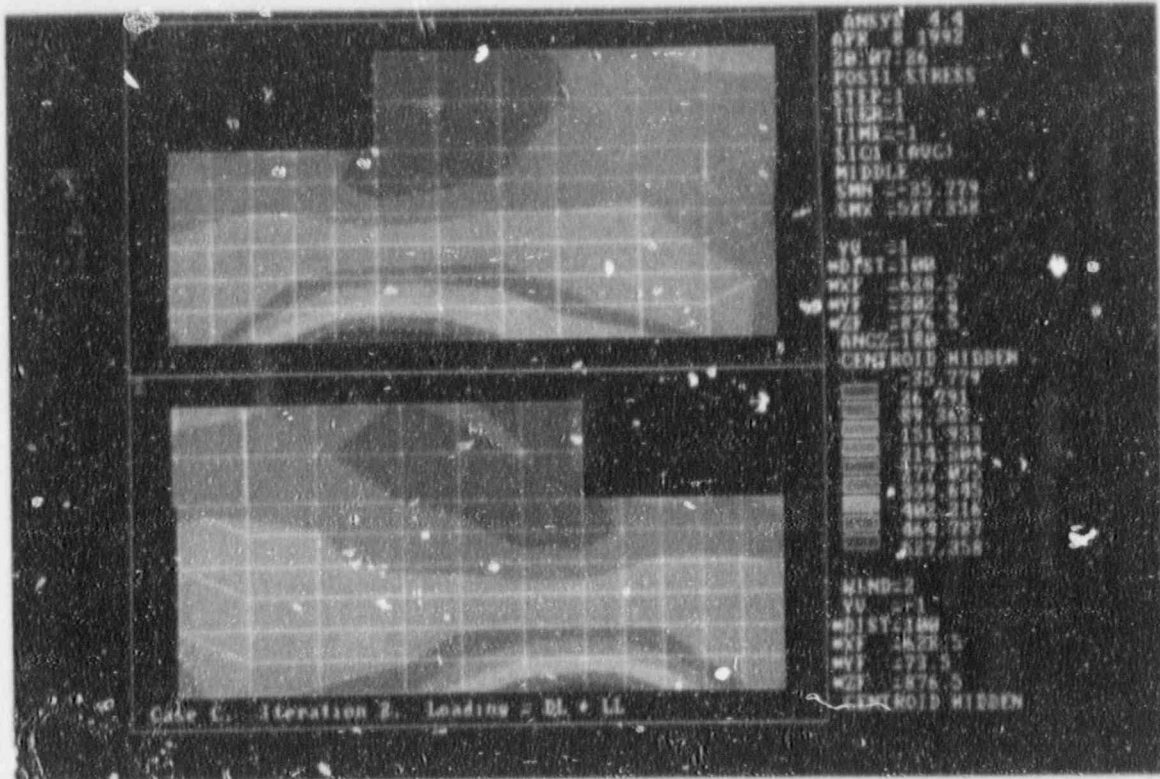


Figure 5.124

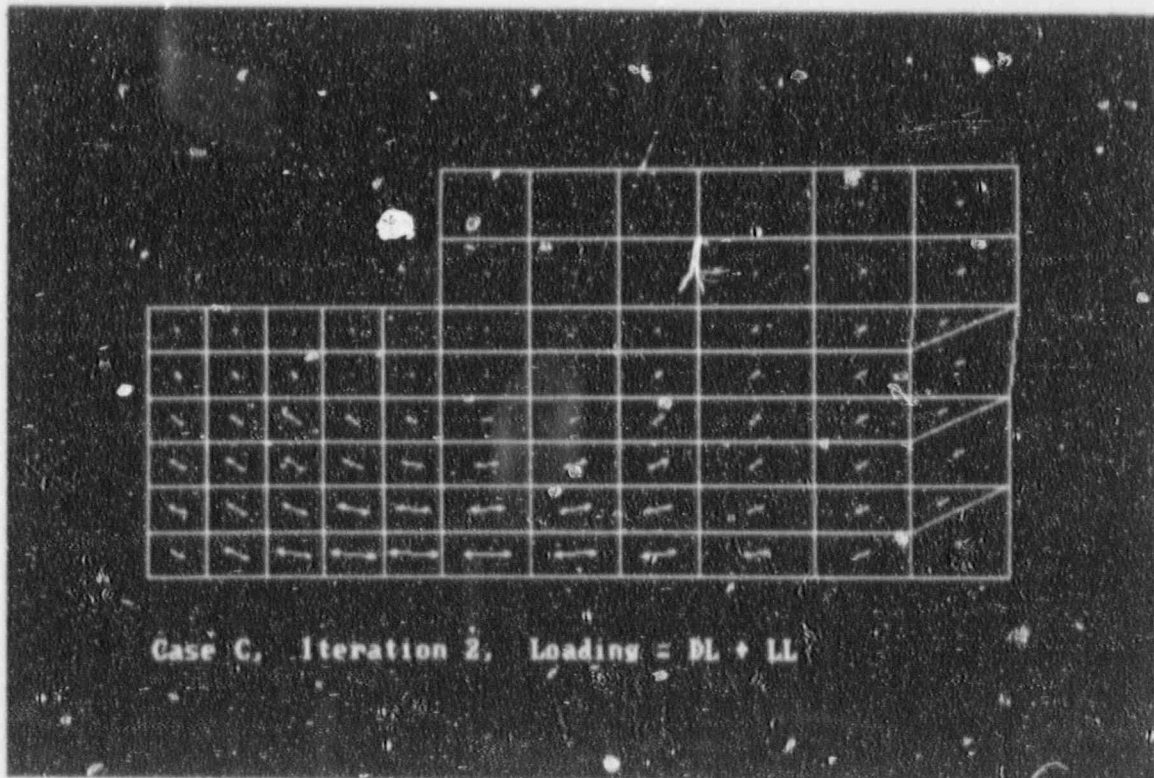


Figure 5.125

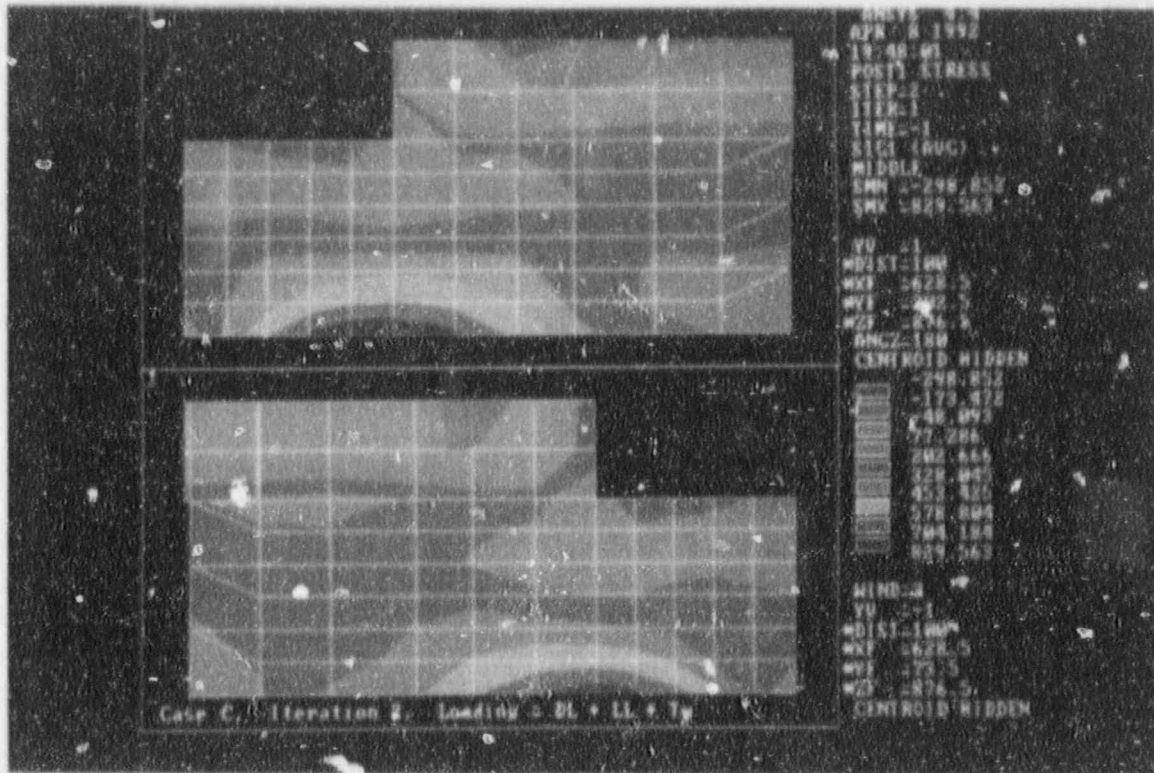


Figure 5.126

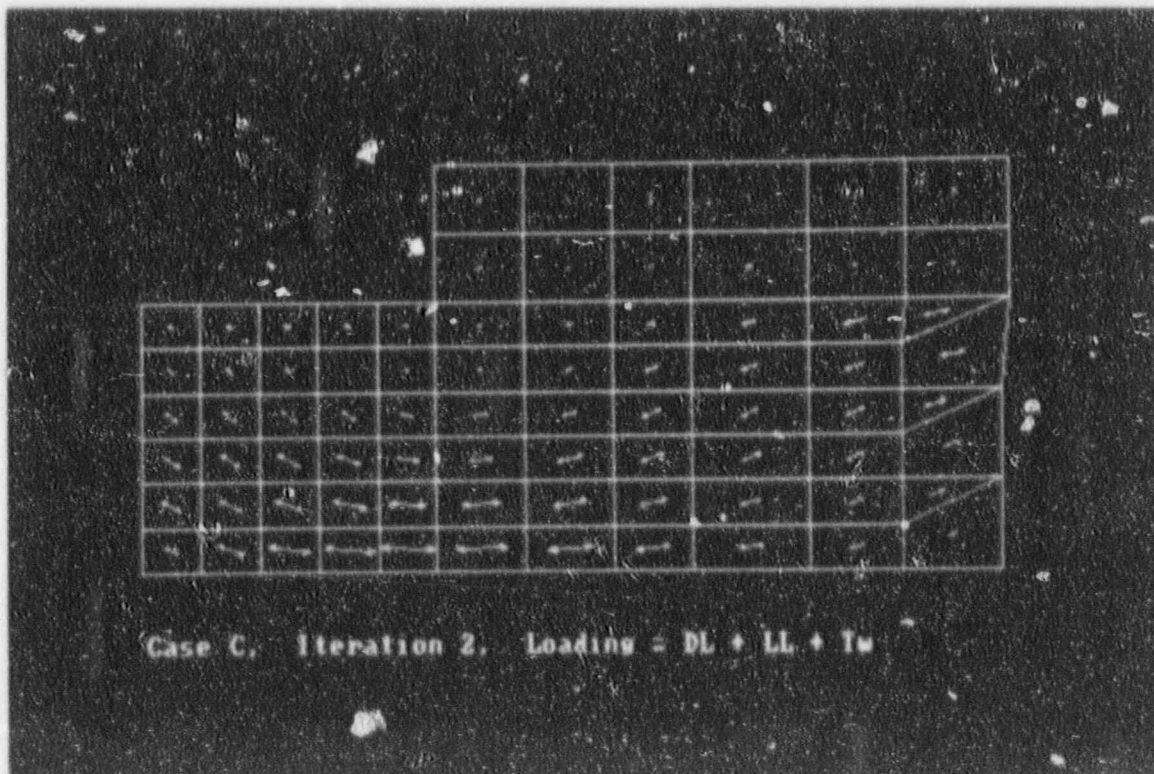


Figure 5.127

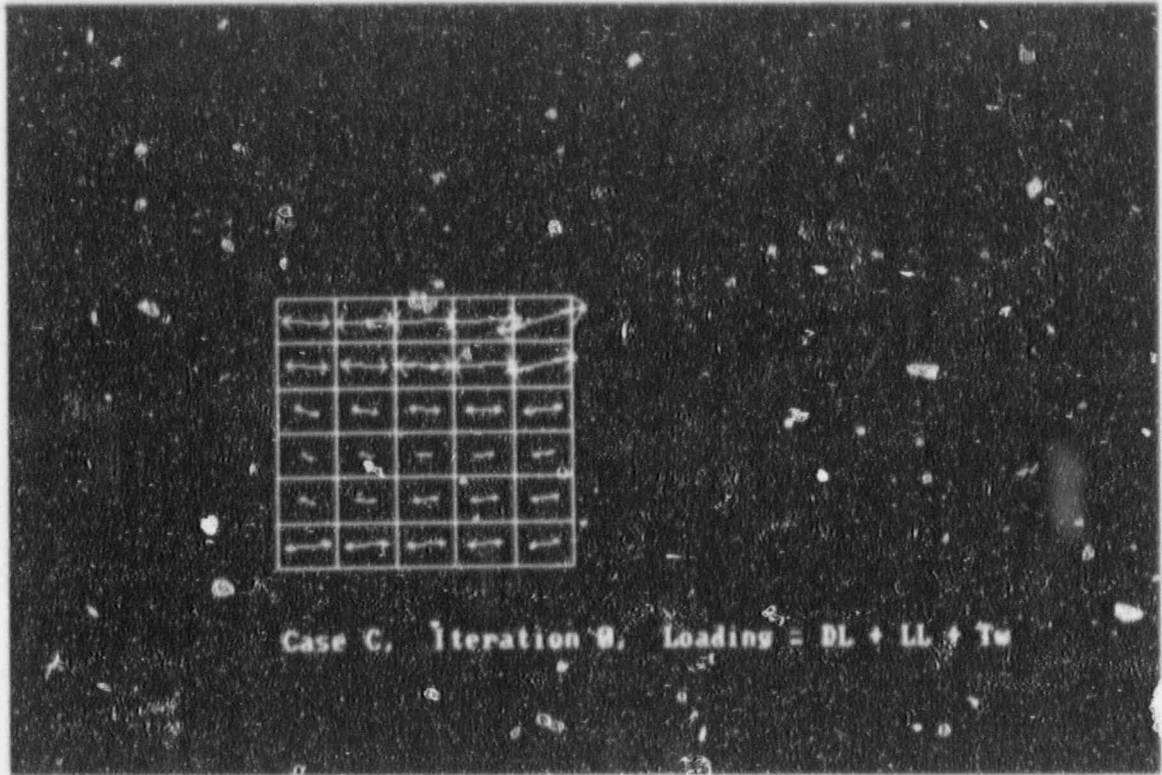


Figure 5.128

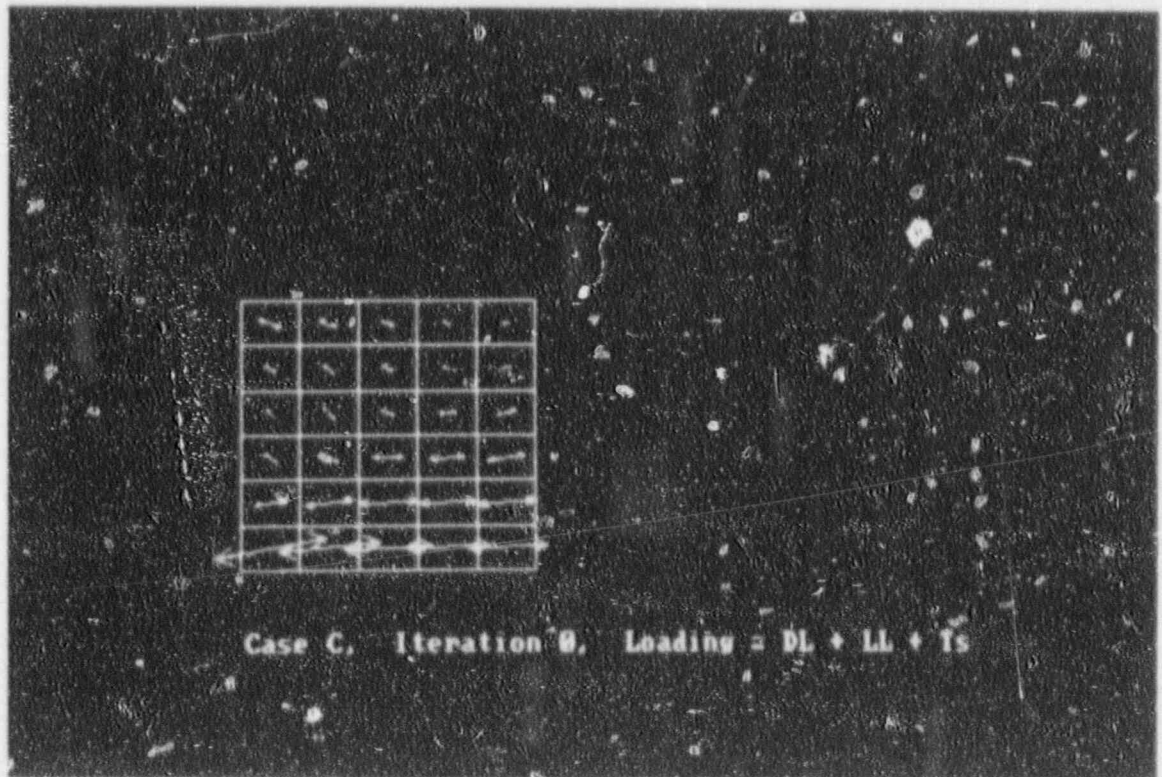
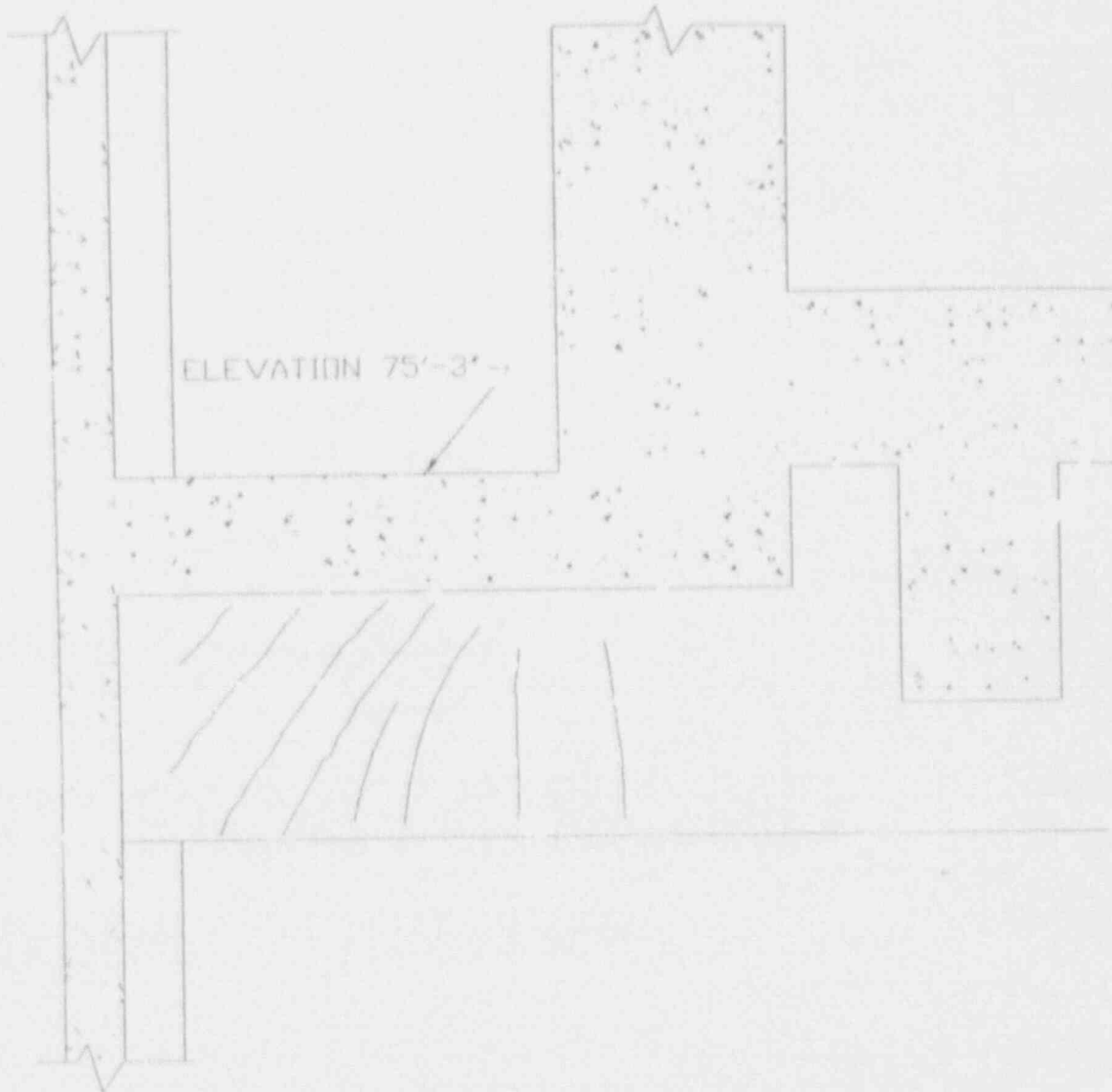


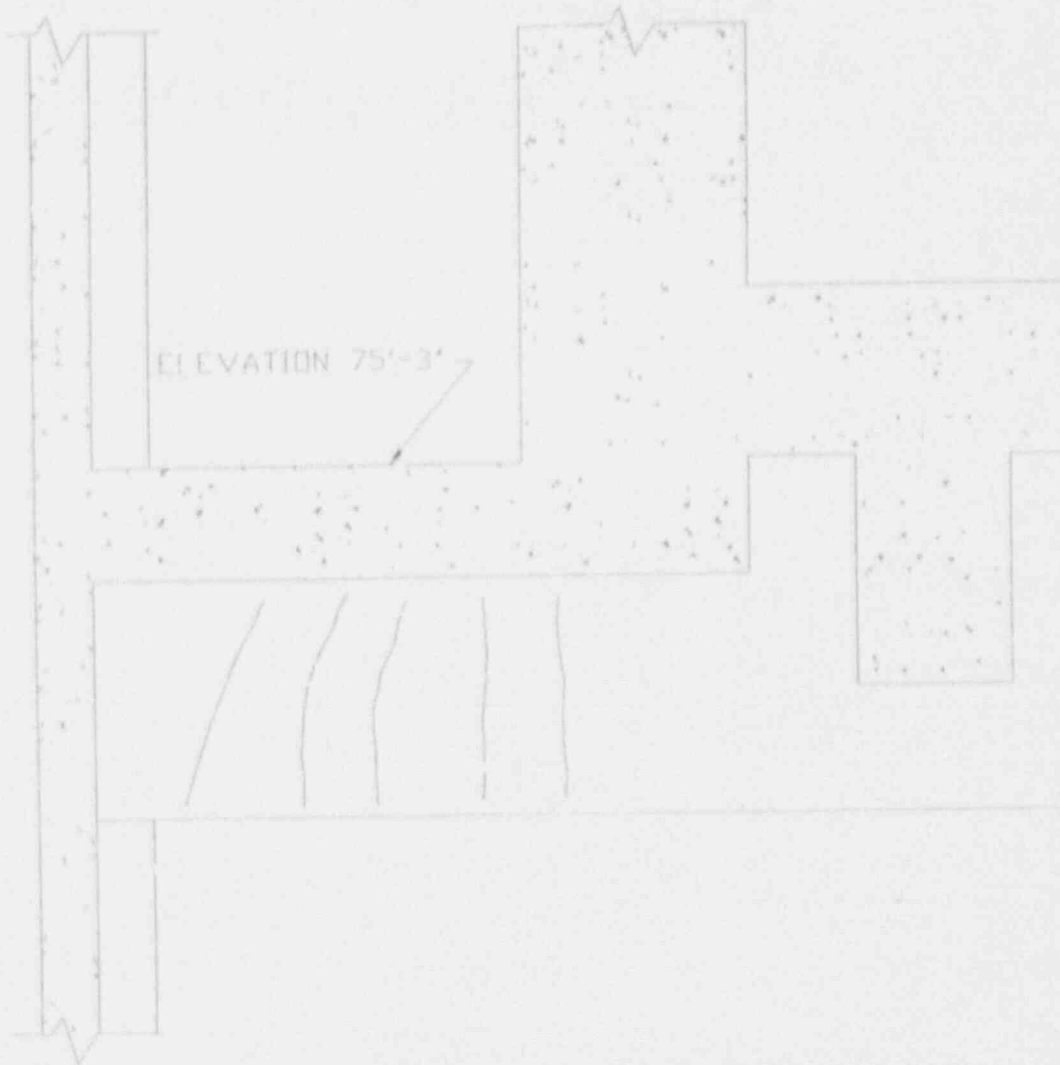
Figure 129



PREDICTED CRACK PATTERN ON THE WEST FACE
OF GIRDER RC FOR CASE C, ITERATION 2, DL+LL+Tw

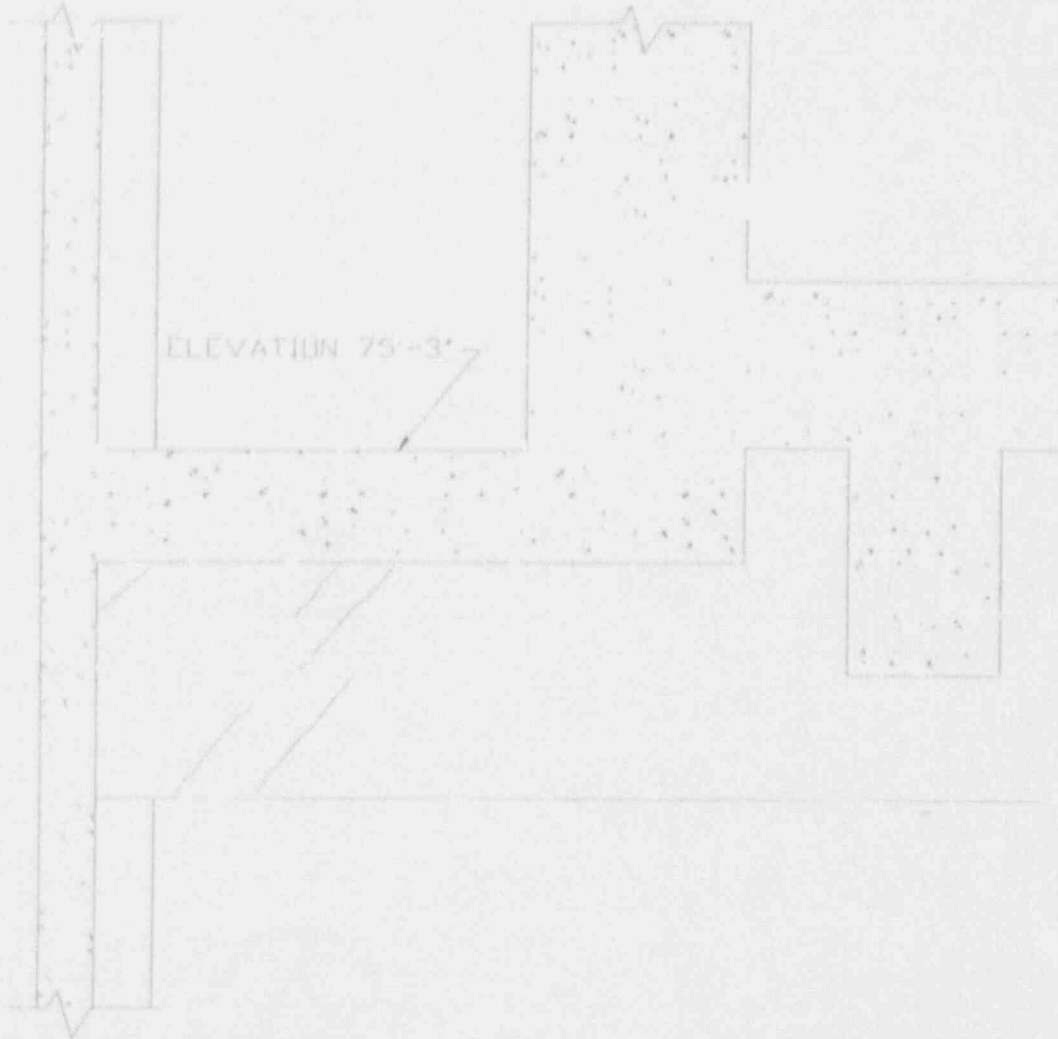
Figure 5.130

ABB Impell Corporation



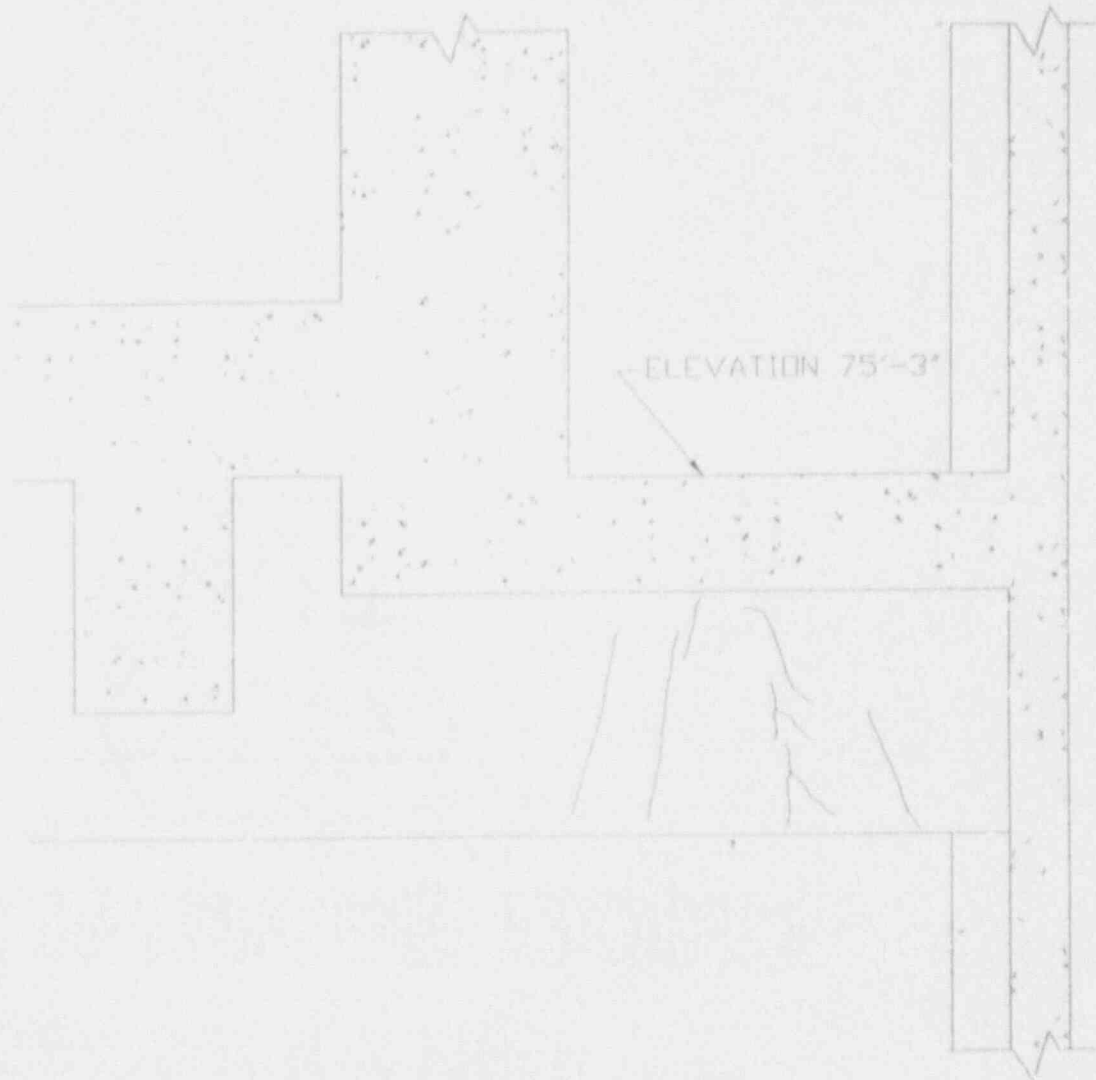
PREDICTED CRACK PATTERN ON THE WEST FACE
3" GIRDER RE FOR CASE C, DL+LL+Tw,
BASED ON AVERAGE CRACK ORIENTATION
BETWEEN ITERATION 0 AND 7.

Figure 5.131



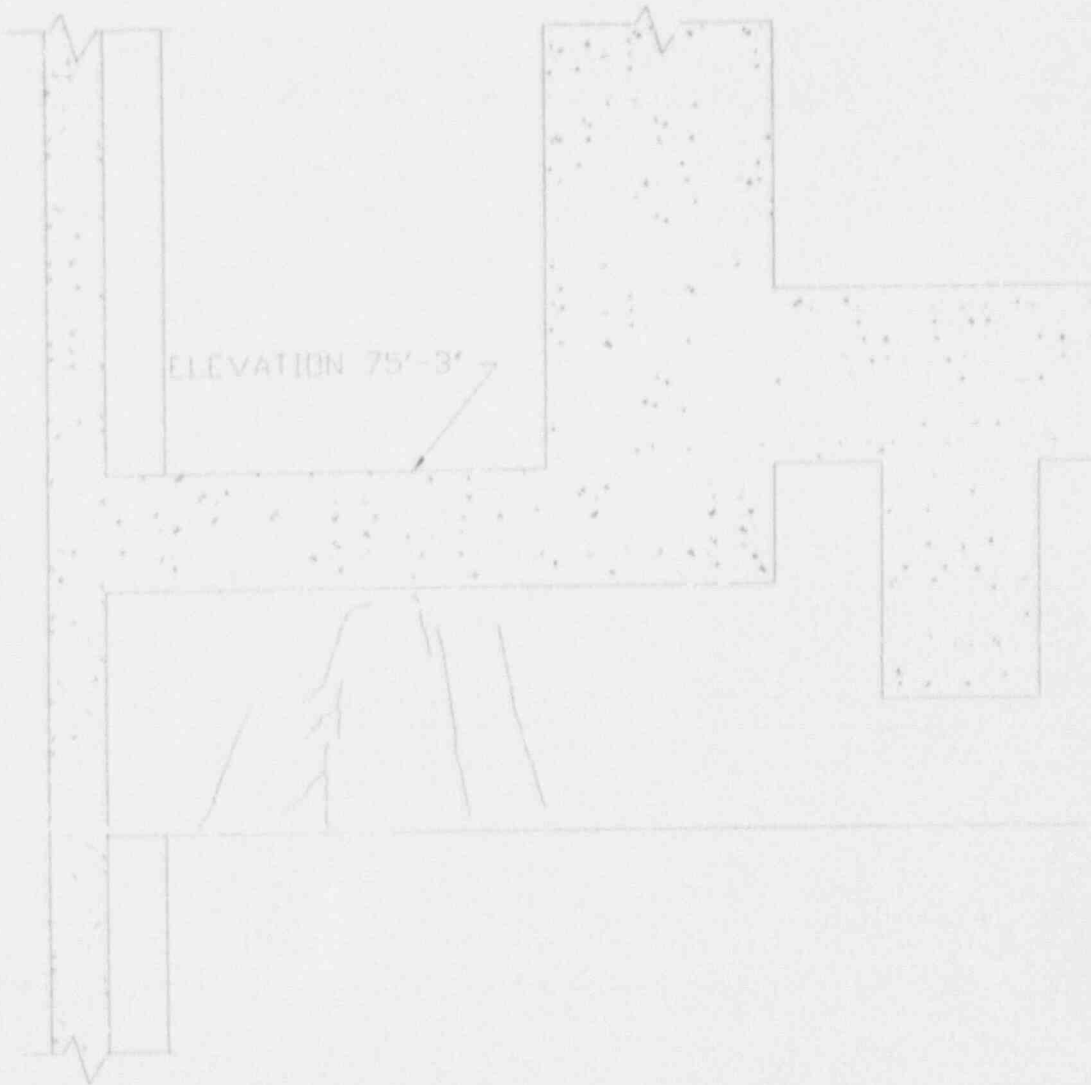
OBSERVED CRACK PATTERN IN THE WEST FACE OF GIRDER RC

ABB Impelli Corporation



OBSERVED CRACK PATTERN ON THE EAST FACE OF GIRDER RE

Figure 5.133



OBSERVED CRACK PATTERN ON THE EAST FACE OF GIRDER #E

Figure 5.134

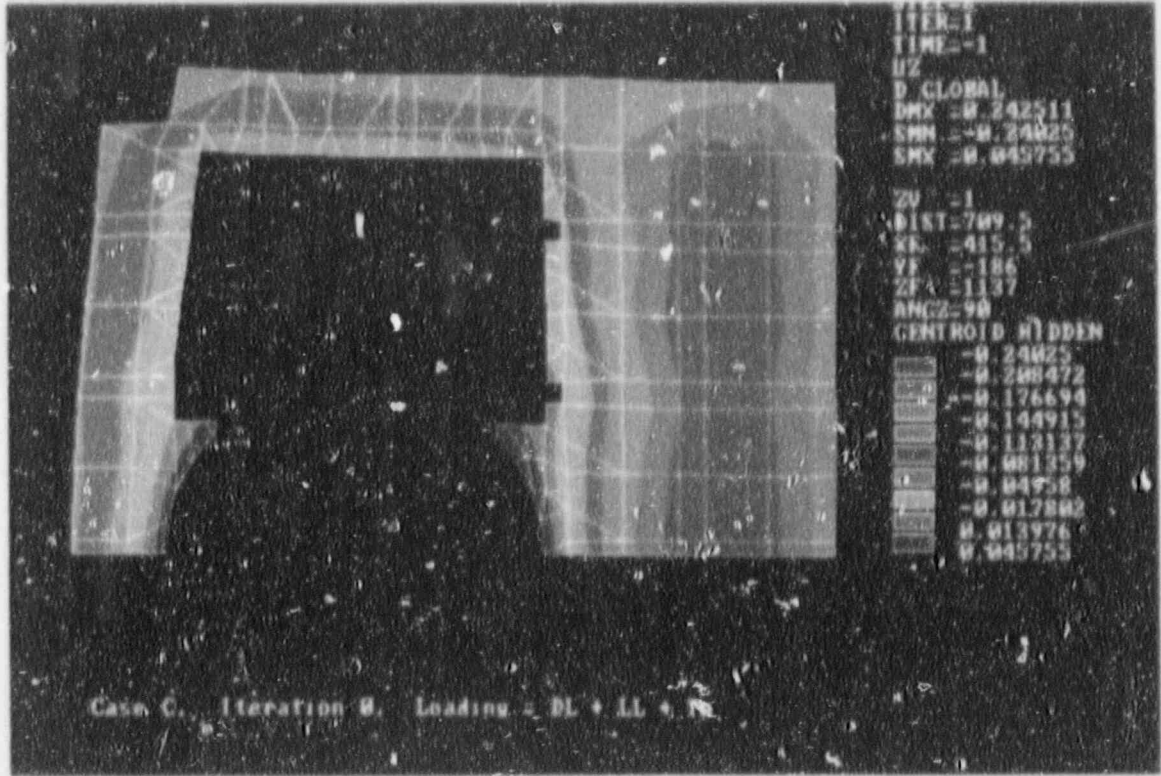


Figure 5.135

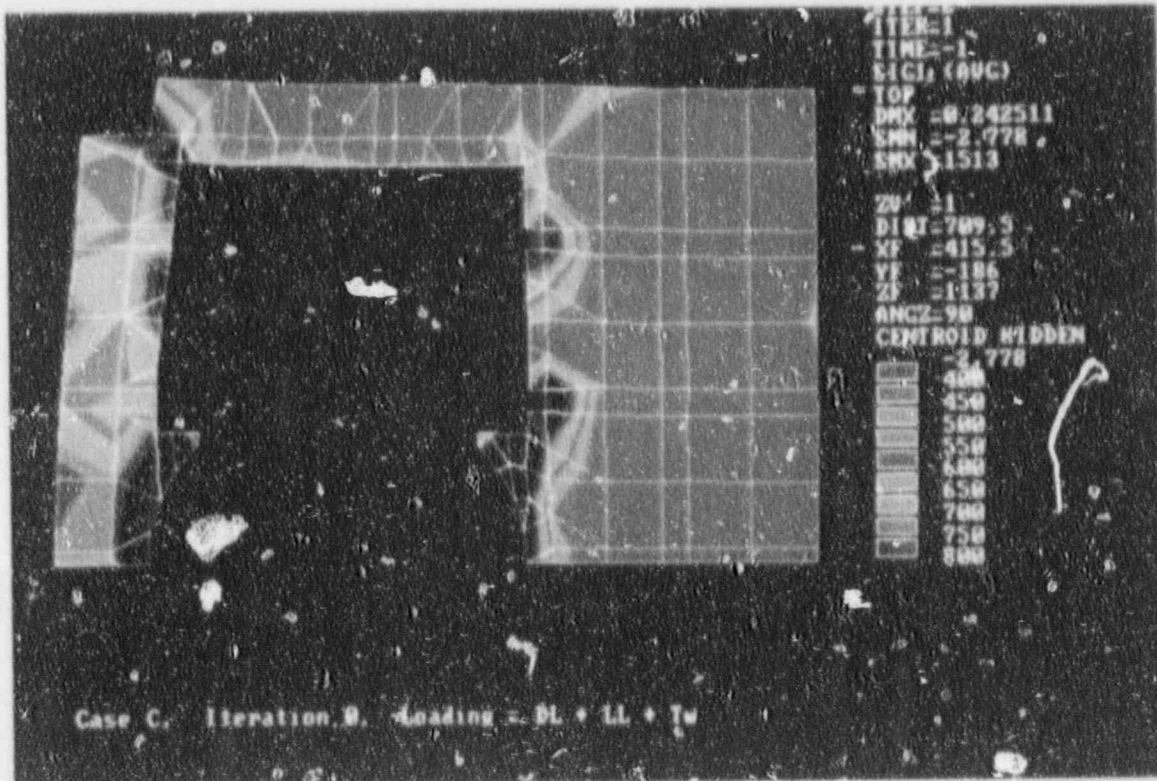


Figure 5.136

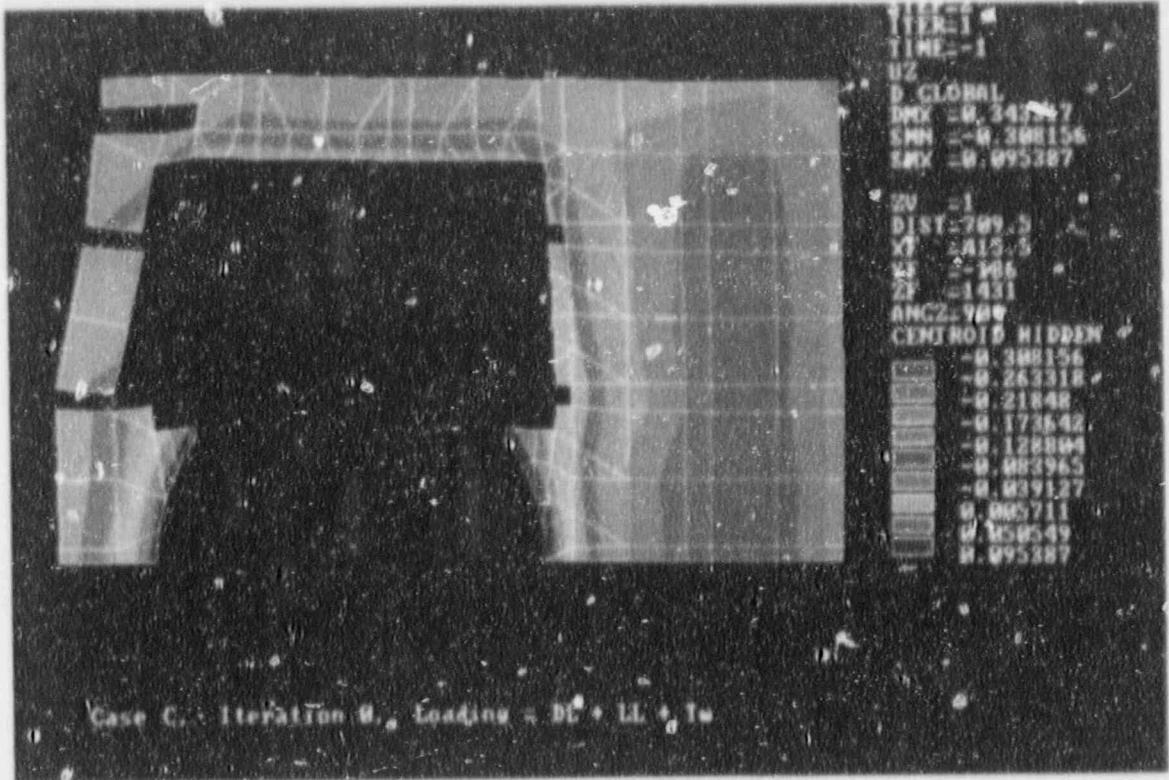


Figure 5.137

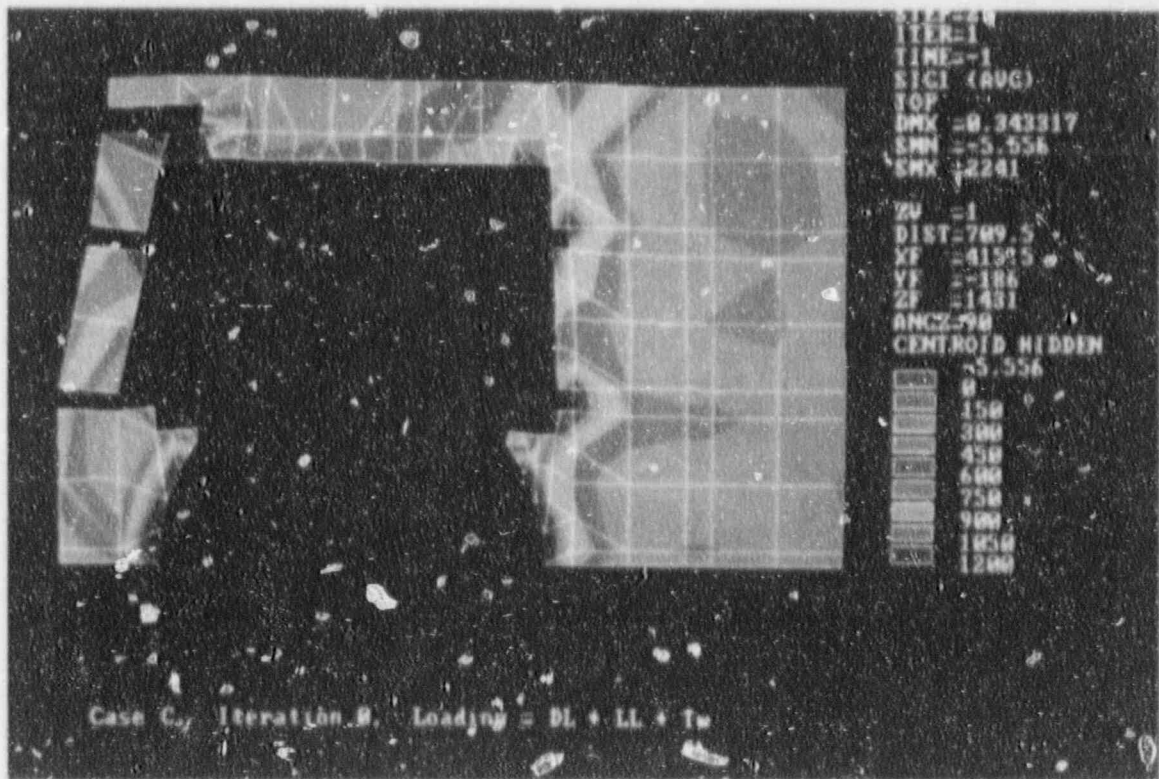


Figure 5.138



ABB Impell Corporation

LOAD COMBINATIONS

<u>EQUATION</u>	<u>LOAD COMBINATION</u>
a	$1.4D + 1.7L + 1.9E(-X-Y+Z)$
b	$0.75(1.4D + 1.7L + 1.4T_w)$
c	$0.75(1.4D + 1.7L + 1.4T_s + 1.9E(-X-Y+Z))$
d	$D + L + T_w + E'(-X-Y+Z)$
e	$D + L + T_w + C$
a'	$1.4D + 1.7L + 1.9E(-X+Y+Z)$
c'	$0.75(1.4D + 1.7L + 1.4T_w + 1.9E(-X+Y+Z))$
d'	$D + L + T_w + E'(-X+Y+Z)$
c _s	$0.75(1.4D + 1.7L + 1.4T_s + 1.9E(-X-Y+Z))$
d _s	$D + L + T_s + E'(-X-Y+Z)$
c' _s	$0.75(1.4D + 1.7L + 1.4T_s + 1.9E(-X+Y+Z))$
d' _s	$D + L + T_s + E'(-X+Y+Z)$

- D = Dead Load
 - Concrete Dead Load
 - Pool Water
 - High Density Racks and Fuel (Analysis Case C)
 - Consolidated Racks and Fuel (Analysis Case D)
 - Stored Cask
- L = Floor Design Live Loads
- T_w = Thermal Load Winter Condition
- T_s = Thermal Load Summer Condition
- E = OBE Seismic Load
- E' = SSE Seismic Load
- C = Cask Drop Accident

Table 5.1a

LOAD COMBINATIONS SPECIFICALLY DEVELOPED TO
 SHOW COMPLIANCE WITH ACI 349-80 SECTION 9.2.3

<u>EQUATION</u>	<u>LOAD COMBINATION</u>
c^*	$0.9D + 1.28L + 1.05T_w + 1.43E(-X-Y+Z)$
c'^*	$0.9D + 1.28L + 1.05T_w + 1.43E(-X+Y+Z)$
c''_1	$0.9D + 1.28L + 1.05T_x + 1.43E(-X-Y+Z)$
c''_2	$0.9D + 1.28L + 1.05T_x + 1.43E(-X+Y+Z)$
c'''	$0.9D + 1.28L + 1.05T_w + 1.43E(-X-Y-Z)$
c''''	$0.9D + 1.28L + 1.05T_w + 1.43E(-X+Y-Z)$
c'''_1	$0.9D + 1.28L + 1.05T_x + 1.43E(-X-Y-Z)$
c'''_2	$0.9D + 1.28L + 1.05T_x + 1.43E(-X+Y-Z)$

Table 5.1b



ACB Impell Corporation

SHEAR CAPACITY MARGIN IN GIRDERS RD, RE, AND R6 ANALYSIS CASE C

ITER.	EQ.	GIRDER	AXIAL FORCE* (kips)	SHEAR FORCE V_u (kips)	SHEAR CAPACITY ϕV_n (kips)	MARGIN %
3R	d'	RD	126	1,963	2,031	3
3R	d	RE	81	1,769	2,031	13
4	a	R6	45	518	982	47
4S	a	R6	45	553	1,029	46
5	a	R6	54	570	1,017	44

* A negative axial force produces a tensile axial stress on the girder cross section.

Table 5.2a

ABB Impell Corporation

SHEAR CAPACITY MARGIN (%) 1 THE GIRDERS FOR LOAD COMBINATIONS IN TABLE 5.1b
 ANALYSIS CASE C, ITERATION 48

LOCATION	LOAD COMBINATIONS (See Table 5.1b)											
	1.0SD and Seismic Upward ⁽¹⁾			0.9D and Seismic Upward			0.9D and Seismic Downward			0.9D and Seismic Downward		
	C	C'	C _s	C _s	C'	C	C _s	C _s	C'	C	C _s	C _s
Middle of the Span	24		26		30		33		40		43	
Middle of the Span	52		56		56		61		53		68	

(1) Seismic Upward means that the appropriate seismic acceleration has been applied in the upward (+Z) direction.
 (2) This table was specifically developed to demonstrate compliance with ACI 349-87 Section 9.2.3.
 (3) See Section SD of Figure 5.1.
 (4) See Section S6 of Figure 5.1.
 (5) Use data from Reference 24 for comparison.

Table 5.2b



ABB Impell Corporation

MOMENT CAPACITY MARGIN IN GIRDERS RD, RE AND R6 ANALYSIS CASE C

ITER.	EQ.	GIRDER	AXIAL FORCE* (kips)	MOMENT M_u (ft-kips)	MOMENT CAPACITY M_n (ft-kips)	MARGIN %
3R	d'	RD	126	15,897	18,982	16
3R	J	RE	78	14,065	18,931	26
4	a	R6	36	3,534	5,525	36
4S	a	R6	40	3,586	5,529	35
5	a	R6	40	3,738	5,529	32

* A negative axial force produces a tensile axial stress on the girder cross section.

Table 5.3a

ABB Impell Corporation

MOMENT CAPACITY MARGIN (%) IN THE GIRDERS FOR LOAD COMBINATIONS IN TABLE 5.1b
 ANALYSIS CASE C, ITERATION 45

LOCATION	LOAD COMBINATIONS (See Table 5.1b)												
	1.05D and Seismic Downward			0.7D and Seismic Upward			0.9D and Seismic Upward			0.9D and Seismic Downward			
	C	C'	C _s	C _s	C _s	C _s	C _s	C _s	C _s	C _s	C _s	C _s	C _s
Girder RD													
Face of the North SFP Wall		38			49			43			50		61
Girder R6													
Face of the West SFP Wall	46			59			51			64		71	

(1) Seismic Upward means that the appropriate seismic acceleration has been applied in the upward (+Z) direction.
 (2) This table was specifically developed to demonstrate compliance with ACI 349-80 Section 9.2.3.

Table 5.3b

Biaxial Moment Capacity Margin in Column C6

Iter.	Eq.	Column C6 Bending About	Axial Force* (kips)	Moment M_y (ft-kips)	Moment Capacity M_n (ft-kips)	Margin %**
3U	d	Y-axis	818	475	3,985	77
		X-axis		664		
3R	c	Y-axis	1,178	623	4,445	77
		X-axis		640		
4	d	Y-axis	1,094	606	4,341	77
		X-axis		663		
4	a'	Y-axis	2,693	664	5,268	80
		X-axis		593		
4S	c	Y-axis	1610	787	4,881	77
		X-Axis		632		
5	d	Y-axis	1,502	664	4,787	79
		X-axis		593		
5	e	Y-axis	1968	763	5,122	84
		X-axis		186		

* A negative axial force produces a tensile axial stress on the girder cross section.

** The margin was based on biaxial bending capacity.

Table 5.4

Table 5.5

MOMENT CAPACITY MARGIN IN GIRDERS RD, RE AND R6 ANALYSIS CASE D

ITER.	EQ.	GIRDER	AXIAL FORCE* (kips)	MOMENT M_u (ft-kips)	MOMENT CAPACITY M_n (ft-kips)	MARGIN %
3R	d'	RD	139	16,461	18,995	13
3R	d	RE	97	14,862	18,951	22
4	a	R6	36	3,871	5,542	30
5	a	R6	38	4,095	5,527	26

SHEAR CAPACITY MARGIN IN GIRDERS RD, RE, AND R6 ANALYSIS CASE D

ITER.	EQ.	GIRDER	AXIAL FORCE* (kips)	SHEAR FORCE V_u (kips)	SHEAR CAPACITY ϕV_n (kips)	MARGIN %
3R	d'	RD	143	2,035	2,031	0
3R	d	RE	181	1,879	2,031	7
4	a	R6	59	588	1,011	42
5	a	R6	69	646	1,029	37

* A negative axial force produces a tensile axial stress on the girder cross section.

Table 5.6

SHEAR CAPACITY MARGIN IN THE SFP SLAB FOR ANALYSIS CASE C

ITER.	EQ.	SECTION OF SLAB	AXIAL FORCE* (kips)	SHEAR FORCE V_u (kips)	SHEAR CAPACITY** ϕV_n (kips)	MARGIN %
3U	a	West of SE	-4	582	1,149	49
3U	a	South of SE	-821	338	536	37
3U	a'	East of SW	-217	646	1,111	42
3U	a	South of SW	-950	512	749	32
3R	a	West of SE	291	782	1,162	33
3R	a'	South of SE	-435	364	602	40
3R	a'	East of SW	80	771	1,153	33
3R	a	South of SW	-925	445	753	41
4	a	West of SE	304	812	1,163	30
4	a'	South of SE	-470	360	596	40
4	a'	East of SW	81	783	1,153	32
4	a	South of SW	-1,044	427	733	42
4S	a'	East of SW	177	783	1,157	32
4S	c _s	East of SW	-1,207	415	938	56
4S	d _s	East of SW	-910	641	990	35
4S	a	South of SE	-575	281	578	51
4S	d _s	South of SE	-783	195	543	64
4S	a	South of SW	-559	339	815	58
4S	d _s	South of SW	-712	257	789	67

* A negative axial force produces a tensile axial stress on the

Table 5.7a

ABB Impell Corporation

SHEAR CAPACITY MARGIN (N) IN THE SFP SLAB FOR LOAD COMBINATIONS IN TABLE 5.1b
 ANALYSIS CASE C, ITERATION 48

LOCATION ⁽²⁾	LOAD COMBINATIONS (See Tables 5.1a and 5.1b)															
	1.0SD and Seismic Upward ⁽¹⁾				0.9D and Seismic Upward				0.9D and Seismic Downward							
	C	C'	C _s	C _s '	C*	C' _s	C _s '	C _s '	C**	C' _s **	C _s **	C _s '**	C***	C' _s ***	C _s ***	C _s '***
East of SE Slab	80	64	65	67	84	68	69	72	91	76	76	78	97	80	80	80
West of SE Slab	59	75	43	58	64	79	48	64	72	89	64	64	58	74	74	74
North of SE Slab	99	97	96	99	98	97	96	99	98	98	98	98	95	100	100	100
South of SE Slab	69	66	63	59	73	70	69	67	83	78	78	78	78	76	76	76
East of SW Slab	67	51	56	38	73	56	62	44	84	67	67	67	74	55	55	55
West of SW Slab	63	79	53	71	68	84	58	77	77	93	77	77	69	87	87	87
North of SW Slab	83	83	88	83	84	84	90	90	87	97	87	87	94	94	94	94
South of SW Slab	67	65	66	67	71	72	71	72	77	79	77	77	79	80	80	80

(1) Seismic: 'ward means that the appropriate seismic acceleration has been applied in the upward (+Z) direction.
 (2) Location terminology: for example, 'East of SE Slab' means the East side critical section of the South East SFP Slab.
 (3) This table was specifically developed to demonstrate compliance with ACI 349-80 Section 9.2.3.

Table 5.7b⁽³⁾

MOMENT CAPACITY MARGIN IN THE SFP SLAB FOR ANALYSIS CASE C

ITER.	EQ.	SECTION OF SLAB	AXIAL FORCE* (kips)	MOMENT M_u *** (ft-kips)	MOMENT CAPACITY** M_c (ft-kips)	MARGIN %
3U	c	Central SE	1	164 (X)	228	28
3U	c	Central SW	43	202 (Y)	200	31
3R	c	Central SE	-13	174 (Y)	201	13
3R	a	South of SE	-51	99 (Y)	129	23
3R	c'	Central SW	17	229 (Y)	250	8
3R	a	South of SW	-40	98 (Y)	150	35
4	c	Central SE	-20	170 (Y)	187	9
4	a	South of SE	-53	102 (Y)	125	18
4	d'	Central SW	17	227 (Y)	251	10
4	a	South of SW	-44	98 (Y)	142	31
4S	c	Central SE	11	67 (X)	243	72
4S	c'	West of SE	-74	48 (X)	82	41
4S	d'	West of SE	-77	40 (X)	77	48
4S	a	South of SE	-49	53 (Y)	133	60
4S	d ₁	South of SE	-62	54 (Y)	107	50
4S	c	Central SW	-20	82 (X)	189	57
4S	c'	East of SW	-66	67 (X)	99	32
4S	d'	East of SW	-61	72 (X)	110	35
4S	a'	South of SW	-36	44 (Y)	157	72
4S	c'	South of SW	-32	52 (Y)	105	68

- * A negative axial force produces a tensile axial stress on the slab cross section. The moment capacity is based on the same axial force.
- ** Axial Force, Moment, and Moment Capacity are for a 9" wide section of slab.
- *** The letter in parenthesis is the global axis about which the moment is taken (see Figure 2.1 or 5.1).

Table 5.8a

MOMENT CAPACITY MARGIN (%) IN THE SFP SLAB FOR LOAD COMBINATIONS IN TABLE 5.1b
ANALYSIS CASE C, ITERATION 48

LOCATION ⁽²⁾	LOAD COMBINATIONS (See Table 5.1b)											
	1.0CI and Seismic Upward ⁽¹⁾				0.9D and Seismic Upward				0.9D and Seismic Downward			
	c	c'	c _s	c _i	c*	c**	c _s *	c _i *	c**	c***	c _s **	c _i **
Middle of SE Slab (SX)	79	79	91	98	79	79	91	94	81	80	91	92
Middle of SE Slab (SY)	72	69	98	95	74	70	97	95	76	72	94	92
Middle of SW Slab (SX)	75	74	97	98	76	75	97	97	77	77	95	96
Middle of SW Slab (SY)	58	59	93	91		62	55	93	65	65	99	99
East of SE Slab (SY)	63	69	95	83	1	89	95	83	82	89	95	84
West of SE Slab (SY)	91	97	40	42	94	93	44	47	100	75	51	57
North of SE Slab (SX)	82	83	90	89	82	84	91	91	82	83	91	89
East of SW Slab (SY)	94	92	46	34	90	96	51	38	81	97	61	47
West of SW Slab (SY)	100	89	48	67	97	86	53	71	71	80	60	78
North of SW Slab (SY)	89	89	83	85	89	87	84	86	88	86	86	87
South of SE Slab (SY)	100	97	51	56	98	100	57	61	94	98	67	69
South of SW Slab (SX)	97	99	67	69	99	99	71	72	98	96	77	78

- (1) Seismic Upward means that the appropriate seismic acceleration has been applied in the upward (+Z) direction
(2) Location terminology; for example, "East of SE Slab (SY)" means the East edge of the South East SFP Slab for moments which produce stress in the Y direction.
(3) This table was specifically developed to demonstrate compliance with ACI 349-83 Section 9.2.3.



ABB Impell Corporation

SHEAR IN SOUTHEAST SLAB (Kips) FOR ANALYSIS CASE C

SECTION	ITERATION 4		ITERATION 4S	
	EQUATION A SHEAR AXIAL	EQUATION A' SHEAR AXIAL	EQUATION A SHEAR AXIAL	EQUATION A' SHEAR AXIAL
East	48 364	251 -282	265 343	486 -378
West	812 303	595 -258	729 386	471 -317
North	-108 -465	-42 -362	-8 -283	35 -234
South	317 -840	360 -470	281 -575	306 -338

Table 5.9



ABB Impell Corporation

GAPS AT THE UNCOUPLED NODES IN THE SFP SLAB
CASE C ITERATION 3U LOAD COMBINATION EQUATION *B*

EAST SECTION OF SE SLAB			WEST SECTION OF SE SLAB		
Node In Slab	Adjacent Node	Gap (IN)	Node In Slab	Adjacent Node	Gap (IN)
6111	621	0.0154	6122	661	0.0187
6112	622	0.0174	6123	662	0.0092
6113	623	0.0169	6124	663	0.0048
6114	624	0.0144	6125	664	0.0014
6115	625	0.0150	6126	665	0.0032
NORTH SECTION OF NE SLAB			SOUTH SECTION OF SE SLAB		
6117	638	0.0056	6116	3569	0.0010
6119	648	0.0065	6118	3570	0.0002
6121	658	0.0055	6120	3571	0.0022
EAST SECTION OF SW SLAB			WEST SECTION OF SW SLAB		
6127	671	0.0200	6140	921	0.0150
6128	672	0.0126	6141	922	0.0138
6129	673	0.0074	6142	923	0.0117
6130	674	0.0027	6143	924	0.0271
6131	675	0.0039	6144	925	0.0086
NORTH SECTION OF NW SLAB			SOUTH SECTION OF SW SLAB		
6133	688	0.0058	6132	3511	0.0047
6135	698	0.0066	6134	3512	0.0039
6137	908	0.0061	6136	3513	0.0020
6139	918	0.0045	6138	3577	0.0020

Table 5.10



ABB Impell Corporation

SHEAR CAPACITY MARGIN IN THE SFP SLAB FOR ANALYSIS CASE D

ITER.	EQ.	SECTION OF SLAB	AXIAL FORCE* (kips)	SHEAR FORCE V_u (kips)	SHEAR CAPACITY** ϕV_u (kips)	MARGIN %
3U	a'	East of SE	500	680	1,062	36
3U	a	South of SE	-850	436	521	18
3U	a'	East of SW	-224	838	1,110	25
3U	a	South of SW	-999	698	741	5.8
3R	a	West of SE	257	884	1,161	24
3R	a	South of SE	-816	422	537	21
3R	a'	East of SW	128	972	1,155	16
3R	a	South of SW	-939	633	751	16
4	a	West of SE	255	913	1,161	20
4	a	South of SE	-862	418	529	21
4	a'	East of SW	121	990	1,155	14
4	a	South of SW	-1,064	615	729	16
4S	a'	East of SW	275	1,000	1,161	14
4S	c _s	East of SW	-941	767	985	22
4S	d _s	East of SW	-836	805	1,003	20
4S	a	South of SE	-566	377	580	35
4S	d _s	South of SE	-776	267	544	51
4S	a	South of SW	-558	484	816	41
4S	d _s	South of SW	-710	366	790	54

* A negative axial force produces a tensile axial stress on the slab cross section.

** Axial Force, Shear Force, and Shear Capacity are along the entire cross section of the slab as shown in Figure 5.1.

Table 5.11

ABB Impall Corporation

MOMENT CAPACITY MARGIN IN THE SFP SLAB FOR ANALYSIS CASE D.

ITER.	EQ.	SECTION OF SLAB	AXIAL FORCE* (kips)	MOMENT M_u (ft-kips)	MOMENT CAPACITY** M_c (ft-kips)	MARGIN %
3U	d	Central of SE X-Dir.	-6	167	219	24
3U	c'	Central of SW X-Dir.	35	222	283	22
3R	d	Central of SE X-Dir.	-21	170	170	11
3R	a	South of SE	-53	113	126	10
3R	c'	Central of SW X-Dir.	21	240	263	9
3R	a	South of SW	-41	127	149	15
4	d	Central of SE X-Dir.	-27	165	176	6
4	a	South of SE	-55	116	121	4
4	d'	Central of SW X-Dir.	11	228	248	8
4	a	South of SW	-46	128	138	7
4S	c'	West of SE	-73	54	85	36
4S	a	South of SE	-49	65	134	51
4S	d	South of SE	-65	60	101	41
4S	c'	East of SW	-63	75	104	28
4S	a'	South of SW	-36	62	158	61
4S	c'	South of SW	-32	66	167	60

* A negative axial force produces a tensile axial stress on the slab cross section. The moment capacity is based on the same axial force.
** Axial Force, Moment, and Moment Capacity are for a 9' wide section of slab.

Table 5.12

SHEAR CAPACITY MARGIN IN THE SFP WALLS ANALYSIS CASE C

ITER.	EQ.	SECTION OF WALL	AXIAL FORCE* (kips)	SHEAR FORCE V_u (kips)	SHEAR CAPACITY** ϕV_n (kips)	MARGIN %
		East-Wall				
4S	a'	North Sect.	-34	27	69	61
4S	c'	North Sect.	-27	31	71	56
		West-Wall				
4S	a	North Sect.	-43	30	48	37
4S	d _c	North Sect.	7	29	49	41
		North-Wall				
4S	d'	East Sect.	-28	26	71	63
4S	a	West Sect.	-29	31	70	56

* A negative axial force produces a tensile axial stress on the slab cross section.

** Axial Force, Shear Force, and Shear Capacity are for a 12" wide section of wall.

MOMENT CAPACITY MARGIN IN THE SFP WALLS ANALYSIS CASE C

ITER.	EQ.	SECTION OF WALL	AXIAL FORCE* (kips)	MOMENT M_u (ft-kips)	MOMENT CAPACITY** M_n (ft-kips)	MARGIN %
		East-Wall				
4S	a'	North Sect.	-34	103	166	38
4S	c'	North Sect.	-27	48	187	74
		West-Wall				
4S	a	North Sect.	-43	98	105	7
4S	d _s	North Sect.	-37	103	118	13
		North-Wall				
4S	d' _s	East Sect.	-28	122	185	34
4S	a	West Sect.	-29	107	180	40
		South-Wall @ Middle				
4S	c' _s	Y-Dir.	-39	173	192	10
4S	d	Z-Dir.	-54	44	91	51

- * A negative axial force produces a tensile axial stress on the slab cross section. The moment capacity is based on the same axial force.
- ** Axial Force, Moment, and Moment Capacity are for a 12" wide section of wall.



ABB Impell Corporation

C:\SEP\POVEL\ECTRICE.1Y6
Monday, February 25, 1991 09:26:56 am

Page: 776

ANSYS - ENGINEERING ANALYSIS SYSTEM REVISION 4.4 IMPPELL CORP. MAY 1, 1989
ANSYS(R) - COPYRIGHT(C) 1971, 1978, 1982, 1983, 1985, 1987, 1989 SWANSON ANALYSIS SYSTEMS, INC. AS UNPUBLISHED WORK.
PROPRIETARY DATA - UNAUTHORIZED USE, DISTRIBUTION OR DUPLICATION IS PROHIBITED. ALL RIGHTS RESERVED.
FOR SUPPORT CALL GORDON BUCHMAN PHONE (617) 893-2226 1M

CASE C: (ITER. 38; EQUATION C: 0.75C1.4D + 1.7L + 1.41W + 1.9E)

16.6583 FEB 20, 1991 CP= 1215.130

***** POST1 LINEARIZED STRESS LISTING *****
INSIDE NODE = 930 OUTSIDE NODE = 210

LOAD STEP = 1 (ITERATION= 1 SECTION= 1)
TIME = -1.0000 LOAD CASE = 1

THE FOLLOWING X, Y, Z STRESSES ARE IN GLOBAL COORDINATES.

** FIBERK **						
	SX	SY	SZ	SX1	SY1	SZ1
	307.9	-178.0	-419.2	-19.61	42.22	260.1
	5161	5162	5163	51	5165	
	-91.82	-119.8	-653.5	543.6	528.2	
** BENDING ** I=INSIDE C=CENTER O=OUTSIDE						
	SX	SY	SZ	SX1	SY1	SZ1
I	-1466	199.5	-520.2	-46.06	34.93	320.9
C	0.0000E+00	0.0000E+00	0.0000E+00	0.0000E+00	0.0000E+00	0.0000E+00
O	1466	199.5	-520.2	-46.06	34.93	320.9
	5161	5162	5163	51	5165	
I	195.6	-423.3	-1566.	1371.	1272.	
C	0.0000E+00	0.0000E+00	0.0000E+00	0.0000E+00	0.0000E+00	
O	195.6	-423.3	-1566.	1371.	1272.	
** MEMBRANE PLUS BENDING ** I=INSIDE C=CENTER O=OUTSIDE						
	SX	SY	SZ	SX1	SY1	SZ1
I	1775	-317.5	939.4	-60.67	77.16	581.0
C	307.9	-178.0	-419.2	-19.61	42.22	260.1
O	1158	81.53	101.0	28.44	7.296	-60.76
	5161	5162	5163	51	5165	
I	-108.0	-643.8	2077.	1765.	1626.	
O	91.82	-119.8	-653.5	543.6	528.2	
	1162	101.3	77.10	1080.	1073.	
** PEAK ** I=INSIDE C=CENTER O=OUTSIDE						
	SX	SY	SZ	SX1	SY1	SZ1
I	1027.	-110.8	-34.32	-20.01	-15.35	28.29
C	215.9	129.5	34.72	45.10	34.34	43.62
O	210.0	-85.99	-127.0	16.34	-4.368	85.02
	5161	5162	5163	51	5165	
I	30.03	113.6	-1025.	995.3	954.2	
C	238.5	129.8	7.811	250.7	199.9	
O	66.11	-93.09	-263.8	197.7	185.7	
** TOTAL ** I=INSIDE C=CENTER O=OUTSIDE						
	SX	SY	SZ	SX1	SY1	SZ1
I	2796	-428.3	-973.7	-85.67	61.81	609.8
C	91.95	7.526	-384.4	25.7	76.56	216.1
O	947.9	4.482	-25.93	10.61	2.821	24.70
	5161	5162	5163	51	5165	TEMP
I	423.2	291.6	-2985.	2584.	2400.	60.00
C	81.24	63.6.	506.4	567.7	539.7	
O	948.6	-4.229	-28.86	975.3	964.4	60.00

PRINT LINEARIZED STRESS THROUGH A SECTION
INSIDE NODE = 940 OUTSIDE NODE = 310

Table 5.15



ABB Impell Corporation

C:\APP\GRU\CC\VE\3015...
Monday, February 25, 1991 09:26:58 am

Page: 778

ANSYS - ENGINEERING ANALYSIS SYSTEM REVISION 4.4
ANSYS(R) COPY 1(C) 1971, 1978, 1982, 1983, 1985, 1987, 1989
PROPRIETARY DATA - UNAUTHORIZED USE, DISTRIBUTION OR DUPLICATION IS PROHIBITED. ALL RIGHTS RESERVED.
FOR SUPPORT CALL GORDON B. CHAMER PHONE (617) 893-2224 FAX

IMPELL CORP. MAY 1, 1989

SUBSONIC ANALYSIS SYSTEMS, INC. AN UNPUBLISHED WORK

15.0586 FEB 20, 1991 CP: 1714.280

CASE C: ITER. 58; EQUATION = 0.75(1.4D + 1.7L + 1.41W + 1.9E)

***** POST1 LINEARIZED STRESS LISTING *****
INSIDE NODE = 940 OUTSIDE NODE = 310

LOAD STEP = 1 ITERATION = 1 SECTION = 1
TIME = -1.0000 LOAD CASE = 1

THE FOLLOWING X,Y,Z STRESSES ARE IN GLOBAL COORDINATES.

** MEMBRANE **						
	SX	SY	SZ	SXY	SYZ	SXZ
I	283.0	-110.5	314.7	25.28	16.42	190.7
C	510.1	510.1	510.1	0	510.1	0
O	339.5	109.4	-372.3	711.8	623.4	0
** BENDING ** I=INSIDE C=CENTER O=OUTSIDE						
	SX	SY	SZ	SXY	SYZ	SXZ
I	114.7	-104.4	399.7	48.82	26.32	191.5
C	0.0000E+00	0.0000E+00	0.0000E+00	0.0000E+00	0.0000E+00	0.0000E+00
O	114.7	104.4	399.7	48.82	26.32	-191.5
I	510.1	510.1	510.1	0	510.1	0
C	0.0000E+00	0.0000E+00	0.0000E+00	0.0000E+00	0.0000E+00	0.0000E+00
O	114.7	104.4	399.7	48.82	26.32	191.5
** MEMBRANE PLUS BENDING ** I=INSIDE C=CENTER O=OUTSIDE						
	SX	SY	SZ	SXY	SYZ	SXZ
I	623.8	-294.9	714.3	74.10	42.74	382.2
C	283.0	-110.5	314.7	25.28	16.42	190.7
O	1430.0	71.85	84.99	21.54	9.900	-0.8073
I	510.1	510.1	510.1	0	510.1	0
C	283.0	-110.5	314.7	25.28	16.42	190.7
O	1430.0	71.85	84.99	21.54	9.900	-0.8073
** PEAK ** I=INSIDE C=CENTER O=OUTSIDE						
	SX	SY	SZ	SXY	SYZ	SXZ
I	-822.9	81.90	-52.91	22.82	9.613	10.82
C	112.4	118.7	48.98	14.89	-29.59	-22.46
O	29.97	-78.20	-105.6	11.51	12.98	35.99
I	510.1	510.1	510.1	0	510.1	0
C	69.99	84.00	-873.7	823.7	807.2	0
O	132.4	-118.8	29.79	102.6	96.16	0
O	53.93	75.81	-136.5	87.61	74.82	0
** TOTAL ** I=INSIDE C=CENTER O=OUTSIDE						
	SX	SY	SZ	SXY	SYZ	SXZ
I	1737.0	-376.8	-667.7	96.31	52.36	393.0
C	395.3	8.134	-25.7	39.91	-11.17	-160.2
O	1350.0	-4.350	-70.81	16.23	2.680	35.10
I	510.1	510.1	510.1	0	510.1	TEMP
I	368.0	-629.3	388.4	15.75	140.4	60.00
C	440.1	4.545	306.8	26.04	648.7	0
O	1351.0	-4.100	-21.85	137.5	1304.0	60.00

PRINT LINEARIZED STRESS THROUGH A SECTION
INSIDE NODE = 201 OUTSIDE NODE = 211

Table 5.16



ABB Impell Corporation

```

*****
*
* PROGRAM : RCBEAM, REV.0          CALC. NO.: _____ REV. : _____ *
* CLIENT  : GPUN                  PREP. BY : _____ DATE : _____ *
* PROJECT : SPENT FUEL POOL       CHKD. BY : _____ DATE : _____ *
* JOB NO. : 0370-187-1683        PAGE NO.: _____ OF _____ *
*
*****

```

(RUN ID: 4614.33, PAGE 1 OF 5)

ABB Impell Corporation
Engineering Division

Program: RCBEAM, Revision 0 Date: August 1990

RCBEAM is an ABB Impell project specific program for the evaluation of a reinforced concrete member of rectangular cross section. The section may be subject to axial force (compression or tension), bending moment and shear force, or alternatively, the user may input linearized normal stresses at the top and bottom edges and the average shear stress acting on the section. The evaluation is based on the Strength Method of ACI 349-80.

Reference Information:

Building Description :
Area Investigated : GIRDER PE ANALYSIS CASE C; ITER. 3R;
ANSYS Output Filename: RC13RLCS1F6 ; LOAD COMBINATION EQUATION "c"

Material Properties :

Concrete Compressive Strength	(psi)	f'c = 3000
Concrete Elastic Modulus	(psi)	Ec = 3.122E+006
Steel Yield strength	(psi)	Fy = 4.000E+004
Steel Elastic Modulus	(psi)	Es = 2.900E+007

Section Properties :

Rectangular Section

Width	(in)	b = 60.000
Total Depth	(in)	h = 108.000

Reinforcing Steel Geometry :

Rebar Area (in**2)	Distance from Top Edge (in)
As[1] = 28.090	d[1] = 104.500
As[2] = 28.080	d[2] = 101.700

Table 5.17



ABB In-pell Corporation

```

*****
*
* PROGRAM : RCBEAM, REV.0          CALC. NO.: _____ REV. : _____
* CLIENT  : GPUN                  PREP. BY : _____ DATE : _____
* PROJECT : SPENT FUEL POOL       CH'D. BY : _____ DATE : _____
* JOB NO. : 0370-187-1683        PAGE NO.: _____ OF _____
*
*****

```

(RUN ID: 4614.33, PAGE 3 OF 5)

Nominal Strength :

Point i	Load (kips)	Moment (ft-kips)	Point i	Load (kips)	Moment (ft-kips)
1	19971	0	26	7500	35138
2	19500	1727	27	7000	35206
3	19000	3561	28	6500	35072
4	18500	5396	29	6000	34803
5	18000	7230	30	5500	34397
6	17500	9064	31	5000	33855
7	17000	10898	32	4500	33177
8	16500	12732	33	4000	32363
9	16000	14566	34	3500	31412
10	15500	16400	35	3000	30326
11	15000	18235	36	2500	29103
12	14500	19950	37	2000	27744
13	14000	20920	38	1500	26249
14	13500	22785	39	1000	24617
15	13000	23595	40	500	22850
16	12500	24855	41	0	20946
17	12000	267	42	-500	18274
18	11500	27236	43	-1000	15456
19	11000	28365	44	-1500	12595
20	10500	29457	45	-2000	9727
21	10000	30517	46	-2500	6851
22	9500	31548	47	-3000	3980
23	9000	32554	48	-3500	1086
24	8500	33538	49	-3682	0
25	8000	34504			

Design Strength :

Strength reduction factors : $\Phi=0.70$ for compression and 0.90 for tension and bending, a linear transition from the value for columns to the value for beams is specified from $\rho=0.10(f'c)(A_g)$ to $\rho=0$

Point i	Load (kips)	Moment (ft-kips)	Point i	Load (kips)	Moment (ft-kips)
1	13980	0	21	4000	24211
2	13500	1759	22	3500	23699
3	13000	3591	23	3000	22991

Table 5.17 (Continued)



ABB Impell Corporation

```

*****
*
* PROGRAM : RCBEAM, REV.0          CALC. NO.: _____ REV. : _____
* CLIENT  : GPUN                  PREP. BY : _____ DATE : _____
* PROJEC  : PENT FUEL POOL        CHKD. BY : _____ DATE : _____
* JOB N.   : 79-187-1683          PAGE NO.: _____ OF _____
*
*****

```

(RUN ID: 4614.33, PAGE 4 OF 5)

4	12500	5428	24	2500	22089
5	12000	7262	25	2000	20993
6	11500	9096	26	1944	20858
7	11000	10930	27	1500	20400
8	10500	12624	28	1000	19884
9	10000	14362	29	500	19368
10	9500	15465	30	0	18852
11	9000	16772	31	-500	16172
12	8500	18008	32	-1000	13340
13	8000	19180	33	-1500	10477
14	7500	20295	34	-2000	7603
15	7000	21362	35	-2500	4731
16	6500	22388	36	-3000	1857
17	6000	23379	37	-3313	0
18	5500	24305			
19	5000	24653			
20	4500	24510			

Location No. 1 (Node Numbers: Top = 930, Bottom = 233):

Factored stresses and loads:

Normal Stress at Top Edge	(psi)	St =	-1319.0
Normal Stress at Bottom Edge	(psi)	Sb =	1294.0
Average Shear Stress	(psi)	Sv =	226.0
Factored Moment	(ft-kips)	Mu =	12699.2
Factored Axial Load	(kips)	Nu =	-81.0
Factored Shear Load	(kips)	Vu =	1464.5

Evaluation for flexure and axial loads:

Factored load Nu = 81 kips (compression)
Factored moment Mu = 12699 ft-kips

From the interaction curve, the design moment capacity is

$$M = 18938 \text{ ft-kips, at } P = 81 \text{ kips}$$

Therefore, the factored moment and axial load are O.K.

Evaluation for shear load: N/A



ABB Impell Corporation

EAST AND WEST FACE BENDING STRESSES* IN GIRDER RE

Iteration 3R				
Load Case	East Face		West Face	
	Top	Pottom	Top	Bottom
Concrete Dead Load	-231	309	-215	338
Winter Temperature	-276	196	-93	364

Iteration 2				
Load Case	East Face		West Face	
	Top	Bottom	Top	Bottom
Concrete Dead Load	-151	269	-146	291
Winter Temperature	-136	266	-121	305

* Normal stresses in X-direction, units = psi.

Table 5.18



ABB Impell Corporation

C:\V\GPM\CCV\C13PLCS.TP6
Monday, February 25, 1991 09:26:58 am

Page: 781

ANYS - ENGINEERING ANALYSIS SYSTEM REVISION 4.4
ANYS(®) COPYRIGHT(C) 1971, 1978, 1982, 1983, 1985, 1987, 1989
PROPRIETARY DATA - UNAUTHORIZED USE, DISTRIBUTION OR DUPLICATION IS PROHIBITED. ALL RIGHTS RESERVED.
FOR SUPPORT CALL GORDON BJOREM PHONE (617) 893-2224 FAX

IMPELL CORP. MAY 1, 1989

SWANSON ANALYSIS SYSTEMS, INC. AS UNPUBLISHED WORK

CASE C: ITER. 30; EQUATION C: 0.75(1.40 + 1.7L + 1.4Tw + 1.9L)

18.8593 FEB 20, 1991 CP= 1716.970

***** POST-LINEARIZED STRESS LISTING *****
INSIDE NODE = 282 OUTSIDE NODE = 212

LOAD STEP = 3 ITERATION = 1 SECTION = 1
TIME = -1.0000 LOAD CASE = 1

THE FOLLOWING X, Y, Z STRESSES ARE IN GLOBAL COORDINATES.

** MEMBRANE **						
	SX	SY	SZ	SXY	SYZ	SXZ
	218.2	-8.324	-51.40	-23.56	8.730	212.9
** BENDING **						
	SX	SY	SZ	SXY	SYZ	SXZ
1	-892.5	-10.00	-14.45	-23.02	5.123	40.52
2	892.5	10.00	14.45	23.02	-5.123	-40.52
** MEMBRANE PLUS BENDING **						
	SX	SY	SZ	SXY	SYZ	SXZ
1	-1110.7	-18.33	-65.85	-46.58	11.85	154.5
2	218.2	-8.324	-51.40	-23.56	8.730	212.9
3	674.3	-1.680	-56.95	-7.5476	3.602	123.4
** PEAK **						
	SX	SY	SZ	SXY	SYZ	SXZ
1	99.60	-23.02	23.32	0.4666	-2.054	75.9
2	20.49	12.31	-41.43	3.382	1.672	94.50
3	32.62	-4.535	31.70	-1.295	-1.635	-99.23
** TOTAL **						
	SX	SY	SZ	SXY	SYZ	SXZ
1	10.00	4.691	-42.53	-46.31	11.80	100.8
2	192.7	3.985	-92.86	-19.98	10.49	308.4
3	706.9	2.655	-5.251	-1.862	1.922	75.18

PRINT LINEARIZED STRESS THROUGH A SECTION
INSIDE NODE = 382 OUTSIDE NODE = 512

Table 5.19



ABB Impell Corporation

C:\XEN\GPA\CC\VECI3R\CS-116
Workday February 25, 1991 09:26:58 am

Page: 782

KNSTY - ENGINEERING ANALYSIS SYSTEM REVISION 4.4
ARSTY(R) COPYRIGHT(C) 1971, 1978, 1982, 1983, 1985, 1987, 1989
IMPELL CORP. MAY 1, 1989
SWANSON ANALYSIS SYSTEMS, INC. AS UNPUBLISHED WORK
PROPRIETARY DATA - UNAUTHORIZED USE, DISTRIBUTION OR DUPLICATION IS PROHIBITED. ALL RIGHTS RESERVED.
FOR SUPPORT CALL GORDON BJORKMAN PHONE (617) 893-2224 FAX

CASE C; ITER: 3R; EQUATION = 0.75(1.4D + 1.7L + 1.47W + 1.2C)

18.8596 FEB 20, 1991 CP= 1737.814

**** POST1 LINEARIZED STRESS LISTING ****
INSIDE NODE = 362 OUTSIDE NODE = 312

LOAD STEP = 3 ITERATION= 1 SECTION= 1
TIME = 1.0000 LOAD CASE= 1

THE FOLLOWING X,Y,Z STRESSES ARE IN GLOBAL COORDINATES.

** MEMBRANE **

SK	SY	SZ	SXY	SYZ	SXZ
170.8	-8.794	-41.30	23.56	-2.434	255.6
S161	S162	S163	S1	S161	
362.7	-9.440	-212.5	555.3	456.6	

** BENDING ** 1-INSIDE C-CENTER 0-OUTSIDE

SK	SY	SZ	SXY	SYZ	SXZ
C 855.5	-8.727	-10.76	-29.51	-9.518	50.13
C 0.0000E+00	0.0000E+00	0.0000E+00	0.0000E+00	0.0000E+00	0.0000E+00
O 855.5	8.727	10.76	29.51	9.518	50.13
S161	S162	S163	S1	S161	
C 0.0000E+00	0.0000E+00	0.0000E+00	0.0000E+00	0.0000E+00	0.0000E+00
O 859.5	19.01	-3.464	862.9	851.9	

** MEMBRANE PLUS BENDING ** 1-INSIDE C-CENTER 0-OUTSIDE

SK	SY	SZ	SXY	SYZ	SXZ
C 694.7	-17.52	-52.07	55.07	-11.05	305.7
C 170.8	-8.794	-41.30	23.56	-2.434	255.6
O 1026	0.6728E+01	30.57	5.3465	7.084	205.4
S161	S162	S163	S1	S161	
C 81.43	-26.91	-810.8	792.2	864.1	
C 362.7	-9.440	-212.5	555.3	456.6	
O 1065	0.3883	69.56	1435	1301	

** PEAK ** 1-INSIDE C-CENTER 0-OUTSIDE

SK	SY	SZ	SXY	SYZ	SXZ
C 37.81	18.25	12.54	-11.41	-0.5196	-167.4
C 21.32	10.96	34.22	0.1364	4.570	104.4
O 38.08	-2.885	26.46	1.280	-5.726	-114.0
S161	S162	S163	S1	S161	
C 193.2	18.77	143.7	336.9	293.8	
C 301.7	10.96	-114.6	216.3	188.1	
O 46.8	2.552	81.93	125.7	201.1	

** TOTAL ** 1-INSIDE C-CENTER 0-OUTSIDE

SK	SY	SZ	SXY	SYZ	SXZ
C 647.7	1.09	-39.52	66.48	12.47	138.1
C 197.2	2.144	-75.52	21.43	2.137	360.8
O 1065	2.971	-4.875	4.867	1.258	91.49
S161	S162	S163	S1	S161	TEMP
C 26.08	-78.64	-683.2	708.2	665.5	60.00
C 474.5	2.018	-327.7	772.2	671.8	
O 1073	1.323	83.92	1087	1081	60.00

PRINT LINEARIZED STRESS THROUGH A SECTION
INSIDE NODE = 362 OUTSIDE NODE = 312



ABB Impell Corporation

C:\SEK\GPA\CC\GCI\34\CS.176
Monday, February 25, 1991 09:26:58 am

Page: 76

ANSYS ENGINEERING ANALYSIS SYSTEM REVISION 4.4
ANSYS(R) COPYRIGHT(C) 1971, 1979, 1982, 1983, 1985, 1987, 1989
PROPRIETARY DATA - UNAUTHORIZED USE, DISTRIBUTION OR DUPLICATION IS PROHIBITED. ALL RIGHTS RESERVED.
FOR SUPPORT CALL GORDON BJORKHAR PHONE (317) 895-2224 TWX
IMPELL CORP. MAY 1, 1989
SWANSON ANALYSIS SYSTEMS, INC. AS UNPUBLISHED WORK.

CASE C, ITER. 30; EQUATION $\epsilon = 0.75(1.40 + 1.7L + 1.41W + 1.9L)$

16.8596 FEB 20, 1991 CP0 1718.670

***** POSTI LINEARIZED STRESS LISTING *****
INSIDE NODE = 285 OX/SIDE NODE = 213

LOAD STEP = 3 ITERATION = 1 SECTION = 1
TIME = 0.0000 LOAD CASE = 1

THE FOLLOWING X,Y,Z STRESSES ARE IN GLOBAL COORDINATES.

** MEMBRANE **						
S1	S7	S2	SXY	S12	S17	S27
163.6	1.655	-27.87	-24.23	2.688	274.2	
S101	S102	S103	S1	S102		
131.1	0.5439	-321.4	452.5	403.4		
** BENDING ** I=INSIDE C=CENTER O=OUTSIDE						
SX	SY	SZ	SXY	S12	S17	S27
I	-555.4	7.968	-1.342	-21.06	0.8162	-11.65
C	0.0000E+00	0.0000E+00	0.0000E+00	0.0000E+00	0.0000E+00	0.0000E+00
O	555.4	-7.968	1.348	21.06	0.8167	11.65
S101	S102	S103	S1	S102		
I	8.765	4.132	-556.4	565.2	565.9	
C	0.0000E+00	0.0000E+00	0.0000E+00	0.0000E+00	0.0000E+00	
O	-8.765	-4.132	556.4	-565.2	-565.9	
** MEMBRAN PLUS BENDING ** I=INS DE C=CENTE O=OUTSIDE						
SX	SY	SZ	SXY	S12	S17	S27
I	779.0	9.622	-32.22	45.29	-1.504	202.5
C	163.6	1.655	-27.87	-24.23	2.688	274.2
O	591.8	-6.333	23.92	-1.175	1.872	225.0
S101	S102	S103	S1	S102		
I	33.27	1.264	770.6	810.4	764.4	
C	163.6	0.5439	-321.4	452.5	403.4	
O	451.0	-6.339	122.7	613.6	564.5	
** PEAK ** I=INSIDE C=CENTER O=OUTSIDE						
SX	SY	SZ	SXY	S12	S17	S27
I	56.90	29.48	29.10	11.98	-3.654	375.2
C	10.43	7.820	20.91	4.043	2.965	103.0
O	109.5	1.307	1.436	7.883	5.412	140.3
S101	S102	S103	S1	S102		
I	189.3	30.79	61.98	253.2	219.7	
C	87.27	7.534	118.8	206.4	190.4	
O	204.9	2.051	-97.59	302.5	267.0	
** TOTAL ** I=INSIDE C=CENTER O=OUTSIDE						
SX	SY	SZ	SXY	S12	S17	S27
I	662.1	39.10	-3.116	-57.27	7.198	77.10
C	174.1	9.495	-28.82	-20.19	0.2721	317.2
O	591.5	5.006	28.96	17.06	7.294	85.60
S101	S102	S103	S1	S102	MEM	
I	48.89	0.6442	675.7	724.6	701.4	60.00
C	212.2	7.128	435.5	648.5	574	
O	515.4	2.538	-41.74	557.3	538.9	50.00

PRINT LINEARIZED STRESS THROUGH A SECTION
INSIDE NODE = 393 OX/SIDE NODE = 313

Table 5.19 (Continued)



ABB Impell Corporation

C:\ENGR\PROJECTS\BOLC-4.r6
Monday, February 25, 1991 09:26:58 am

Page: 284

ANYSYS - ENGINEERING ANALYSIS SYSTEM REVISION 4.4
ANYSYS(C) COPYRIGHT(C) 1971, 1978, 1982, 1985, 1985, 1987, 1989
IMPELL CORP. MAY 1, 1989
DUNSON ANALYSIS SYSTEMS, INC. AS UNPUBLISHED WORK.
FOR SUPPORT CALL GORDON BJORKMAR PHONE (617) 893-2224 FAX

CASE C) ITER. 3R; EQUATION = 0.75(1.40 + 1.7L + 1.41W + 1.9C)

18.3600 FLA 20.1991 CP= 1719.550

***** POST1 LINEARIZED STRESS LISTING *****
INSIDE NODE = 585 OUTSIDE NODE = 513

LOAD STEP = 3 ITERATION = 1 SECTION = 1
TIME = 1.0000 LOAD CASE = 1

THE FOLLOWING X,Y,Z STRESSES ARE IN GLOBAL COORDINATES.

** MEMBRANE **						
	SX	SY	SZ	SXY	SYZ	SXZ
I	114.7	1.577	-18.72	-24.23	2.889	266.6
C	5161	5162	5163	S1	5164	
O	323.7	1.735	-228.1	551.8	480.1	
** BENDING ** I=INSIDE C=CENTER O=OUTSIDE						
	SX	SY	SZ	SXY	SYZ	SXZ
I	-574.5	7.670	-2.807	25.35	-2.970	5.151
C	0.0000E+00	0.0000E+00	0.0000E+00	0.0000E+00	0.0000E+00	0.0000E+00
O	574.5	7.670	-2.807	25.35	-2.970	-5.151
I	5161	5162	5163	S1	5164	
C	9.596	-3.587	-575.6	585.2	578.7	
O	0.0000E+00	0.0000E+00	0.0000E+00	0.0000E+00	0.0000E+00	
D	575.6	3.587	-9.596	585.2	578.7	
** MEMBRANE PLUS BENDING ** I=INSIDE C=CENTER O=OUTSIDE						
	SX	SY	SZ	SXY	SYZ	SXZ
I	-459.8	9.048	21.54	-69.58	-0.808E-01	271.7
C	114.7	1.577	-18.72	-24.23	2.889	266.6
O	689.2	-6.293	-35.92	4.119	5.058	261.4
I	5161	5162	5163	S1	5164	
C	115.0	7.811	593.1	706.0	659.8	
O	323.7	1.735	-228.1	551.8	480.1	
D	775.5	1.617	-102.6	-678.1	834.0	
** PEAK ** I=INSIDE C=CENTER O=OUTSIDE						
	SX	SY	SZ	SXY	SYZ	SXZ
I	62.49	27.44	18.83	-15.93	4.817	-150.8
C	6.195	7.636	-14.73	2.649	-1.105	117.4
O	110.0	2.139	-6.749	5.662	-2.981	-157.6
I	5161	5162	5163	S1	5164	
C	182.2	26.57	322.0	304.7	263.5	
O	187.1	2.624	-328.0	275.1	204.4	
D	219.7	2.379	-316.7	336.4	295.2	
** TOTAL ** I=INSIDE C=CENTER O=OUTSIDE						
	SX	SY	SZ	SXY	SYZ	SXZ
I	419.3	36.49	-2.700	65.51	3.947	120.9
C	105.5	9.014	73.45	-21.58	3.783	380.0
O	895.1	-4.335	-27.67	6.283	-6.839	10.0
I	5161	5162	5163	S1	5164	TEMP
C	56.75	22.02	-447.3	515.1	500.0	60.00
O	428.9	9.879	-353.9	780.8	678.8	
D	811.4	0.2297	-39.88	852.3	831.4	60.00

LINEARIZED STRESS THROUGH A SECTION
INSIDE NODE = 294 OUTSIDE NODE = 214

Table 5.19 (Continued)



ABB Impell Corporation

Linearized stresses for Girder RE*

Nodes	Section				Average
	East Face		West Face		
	(282,212)	(283,213)	(382,312)	(383,313)	
Top (psi)	-1,111	-719	-685	-460	-744
Bottom (psi)	674	392	1026	689	696
Shear (psi)	214	214	256	267	238

* From Table 5.19

Table 5.20



ABB Impell Corporation

Report No. 03-0370-1341
Revision 0

Bendi. Evaluation in The SFP Slab (4 of 6)																	
Case C iter. 3A ANSYS filename: EC13R1CS.IF6																	
Portion: SW SLAB Print Linearized Stresses																	
Sect. / ion Surface Modes	Eq. a		Eq. b		Eq. c		Eq. d		Eq. e		Eq. a'		Eq. c'		Eq. d'		Chk Eq.
	X-DIR.	Y-DIR.	X-DIR.	Y-DIR.	X-DIR.	Y-DIR.	X-DIR.	Y-DIR.	X-DIR.	Y-DIR.	X-DIR.	Y-DIR.	X-DIR.	Y-DIR.	X-DIR.	Y-DIR.	
5985, 6085	-14, 131	617, 513	-623, 529	-599, 507	-581, 497	-12, 166	-623, 555	-599, 544	-119, 117	-315, 354	-313, 344						
6386, 6036	40, 163	645, 510	-624, 520	-601, 501	-583, 485	-32, 168	-611, 539	-599, 527	-134, 128	-321, 358	-385, 346						
6406, 6106	116, 28	-696, 554	-645, 536	-595, 504	-650, 517	160, 53	-709, 597	-685, 589	10, -41	-277, 332	-281, 329						b, c, d'
6398, 6098	167, 19	-653, 552	-622, 540	-582, 510	-616, 525	119, 91	-663, 594	-639, 586	261, 22	-264, 318	-267, 311						c'

Note: The linearized stresses shown above have units of psi. The stresses separated by a comma represent the top and bottom stresses respectively.

GAIN SFI ANALYSIS CASE C

ABB ASEA BROWN BOVERI	JOB NO: 0370-187-1683	PAGE
Impell Corporation	CALC NO: 0370-187-005	OF

Table 5.21



ABB Impell Corporation

```

*****
*
* PROGRAM : RCBEAM, REV.0          CALC. NO.: _____ REV. : _____ *
* CLIENT  : GPUN                  PREP. BY : _____ DATE : _____ *
* PROJECT : SPENT FUEL POOL       CHKD. BY : _____ DATE : _____ *
* JOB NO. : 0370-1E7-1683        PAGE NO.: _____ OF _____ *
*
*****

```

(RUN ID: 258.41, PAGE 1 OF 4)

ABB Impell Corporation
Engineering Division

Program: RCBEAM, Revision 0 Date: August 1990

RCBEAM is an ABB Impell project specific program for the evaluation of a reinforced concrete member of rectangular cross section. The section may be subject to axial force (compression or tension), bending moment and shear force, or alternatively, the user may input linearized normal stresses at the top and bottom edges and the average shear stress acting on the section. The evaluation is based on the Strength Method of ACI 349-80.

Reference Information:

Building Description :
Area Investigated : South-west SFP Slab (central location)
ANSYS Output Filename: ECL3RCLS.7F6; Load Combination Equation "c1"

Material Properties :

Concrete Compressive Strength	(psi)	f'c = 3000
Concrete Elastic Modulus	(psi)	Ec = 3.122E+06
Steel Yield strength	(psi)	fy = 4.000E+04
Steel Elastic Modulus	(psi)	Es = 2.900E+07

Section Properties :

Rectangular Section

Width	(in)	b = 9.000
Total Depth	(in)	h = 54.000

Reinforcing Steel Geometry :

Rebar Area (in**2)	Distance from Top Edge (in)
As[1] = 1.560	d[1] = 49.400
As[2] = 1.560	d[2] = 4.600

Table 5.22



ABB Impell Corporation

```

*****
*
* PROGRAM : RCBEAM, REV.0          CALC. NO.: _____ REV. : _____
* CLIENT  : GPUN                  PREP. BY : _____ DATE : _____
* PROJECT : SPENT FUEL POOL       CHKD. BY : _____ DATE : _____
* JOB NO. : 0370-187-1683        PAGE NO.: _____ OF _____
*
*****
  
```

(RUN ID: 258.41, PAGE 2 OF 4)

Load-Moment Interaction :

Plastic Centroid of the Section
(measured from the top edge of
the section)

For compressive load (inches) xc = 27.000
For tensile load (inches) xt = 27.000

Maximum Compression Capacity (kips) Pc = 1356
Maximum Tension Capacity (kips) Pt = 125

Pure Bending Moment Capacity (ft-kips) Mo = 252

At Balanced Strain Condition :

Axisl Compression (kips) Pb = 656
Bending Moment (ft-kips) Mb = 920
Load Eccentricity (inches) eb = 16.819

(measured from xc toward the
top edge of the section)
Neutral Axis (inches) xb = 33.841
(measured from the compression
edge of the section)

Point on the Interaction Curve above
which both the concrete and steel
are in compression only :

(kips) P = 1121
(ft-kip²) M = 447

Nominal Strength:

Point i	Load (kips)	Moment (ft-kips)	Point i	Load (kips)	Moment (ft-kips)
1	1356	0	21	400	838
2	1350	12	22	350	794
3	1300	107	23	300	742
4	1250	202	24	250	680

Table 5.22 (Continued)



ABB Impell Corporation

```
*****
*
* PROGRAM : RCBEAM, REV.0          CALC. NO.: _____ REV. : _____
* CLIENT  : GPUN                  PREP. BY : _____ DATE : _____
* PROJECT : SPENT FUEL POOL       CHKD. BY : _____ DATE : _____
* JOB NO. : 0370-187-1683        PAGE NO.: _____ OF _____
*
*****
```

(RUN ID: 258.41, PAGE 3 OF 4)

5	1200	297	25	200	609
6	1150	392	26	150	528
7	1100	480	27	100	439
8	1050	554	28	50	346
9	1000	620	29	0	252
10	950	680	30	-50	157
11	900	734	31	-100	55
12	850	782	32	-125	0
13	800	824			
14	750	862			
15	700	894			
16	650	921			
17	600	922			
18	550	915			
19	500	898			
20	450	873			

Design Strength :

Strength reduction factors : $\Phi=0.70$ for compression and 0.90 for tension and bending, a linear transition from the value for columns to the value for beams is specified from $P=0.10(f'c)(Ag)$ to $P=0$.

Point	Load (kips)	Moment (ft-kips)	Point	Load (kips)	Moment (ft-kips)
1			1		
1	949	0	16	300	507
2	900	94	17	150	441
3	850	189	18	146	435
4	800	284	19	100	370
5	750	366	20	50	298
6	700	434	21	0	227
7	650	493	22	-50	132
8	600	543	23	-100	27
9	550	585	24	-112	0
10	500	620			
11	450	645			
12	400	643			
13	350	629			
14	300	601			
15	250	561			

Table 5.22 (Continued)



ABB Impell Corporation

```

*****
*
* PROGRAM : RCBEAM, REV.0          CALC. NO.: _____ REV. : _____
* CLIENT   : GPUN                 PREP. BY : _____ DATE : _____
* PROJECT  : SPENT FUEL POOL      CHKD. BY : _____ DATE : _____
* JOB NO.  : 0370-187-1683       PAGE NO.: _____ OF _____
*
*****

```

(RUN ID: 258.41, PAGE 4 OF 4)

Location No. 1 (Node Numbers: Top = 6098, Bottom = 6098):

Factored stresses and loads :

Normal Stress at Top Edge	(psi)	St =	-663.0
Normal Stress at Bottom Edge	(psi)	Sb =	594.0
Average Shear Stress	(psi)	Sc =	0.0
Factored Moment	(ft-kips)	Mu =	229.1
Factored Axial Load	(kips)	Nu =	16.8
Factored Shear Load	(kips)	Vu =	0.0

Evaluation for flexure and axial loads :

Factored load Nu = 17 kips (compression)
Factored moment Mu = 229 ft-kips

From the interaction curve, the design moment capacity is

M = 250 ft-kips, at P = 16 kips

Therefore, the factored moment and axial load are O.K.

- End -



ABB Impell Corporation

C:\KUNGM\DEVEL\3R\CS_1\F6
Monday, February 25, 1991 09:26:58 am

Page: 448

***S - ENGINEERING ANALYSIS SYSTEM REVISION 4.4
ANALYSIS COPYRIGHT(C) 1971, 1978, 1982, 1983, 1985, 1987, 1989
PROPERTY DATA - UNAUTHORIZED USE, DISTRIBUTION OR DUPLICATION
FOR SUPPORT CALL GORDON BJORKMAN PHONE (617) 895-2224 FAX
IMPELL CORP. MAY 1, 1989
SWANSON ANALYSIS SYSTEMS, INC. AS UNPUBLISHED WORK,
IS PROHIBITED. ALL RIGHTS RESERVED.

CASE C: ITER. 3R; ITERATION n= 1.4D * 1.7L * 1.9E (E=X*Y*Z)

18.0759 FEB 20, 1991 CP= 1049.630

**** POSTI NODAL FORCE SUMMATION ****

LOAD STEP= 6 ITERATION= 1

THE FOLLOWING X,Y,Z FORCES ARE IN GLOBAL COORDINATES

NODE	Fx	Fy	Fz	Mx	My	Mz
886	-17595.954	-29757.648	-4436.2987	0.0000000E+00	0.0000000E+00	0.0000000E+00
726	-29645.033	30373.840	-24028.311	0.0000000E+00	0.0000000E+00	0.0000000E+00
885	-20012.936	37064.587	-11768.282	0.0000000E+00	0.0000000E+00	0.0000000E+00
3611	57284.968	-13528.083	-17158.427	0.0000000E+00	0.0000000E+00	0.0000000E+00
5711	80153.307	14561.779	-20562.921	0.0000000E+00	0.0000000E+00	0.0000000E+00
6054	-19561.190	1801.3775	-9164.3767	0.0000000E+00	0.0000000E+00	0.0000000E+00
6059	-29654.536	6259.7575	-13156.554	0.0000000E+00	0.0000000E+00	0.0000000E+00
6060	36059.501	-15353.571	-24832.408	0.0000000E+00	0.0000000E+00	0.0000000E+00
6061	-29656.383	-22748.104	-33069.604	0.0000000E+00	0.0000000E+00	0.0000000E+00
6062	-17791.462	19556.715	-35400.161	0.0000000E+00	0.0000000E+00	0.0000000E+00
6063	-5552.5869	-16723.551	-26697.430	0.0000000E+00	0.0000000E+00	0.0000000E+00
6064	4516.0689	4569.8258	-15634.77	0.0000000E+00	0.0000000E+00	0.0000000E+00
6132	1985.7666	41119.990	44421.596	0.0000000E+00	0.0000000E+00	0.0000000E+00
6205	14736.866	406.34814	-17101.856	0.0000000E+00	0.0000000E+00	0.0000000E+00
6207	28151.452	1141.6651	25581.318	0.0000000E+00	0.0000000E+00	0.0000000E+00
6216	-46095.186	9439.8985	49263.145	0.0000000E+00	0.0000000E+00	0.0000000E+00
6211	57826.468	18305.380	64904.632	0.0000000E+00	0.0000000E+00	0.0000000E+00
6212	6454.328	-10509.629	-70632.667	0.0000000E+00	0.0000000E+00	0.0000000E+00
6213	-56640.893	8263.0766	57295.985	0.0000000E+00	0.0000000E+00	0.0000000E+00
6214	54036.065	-3551.8343	-33264.254	0.0000000E+00	0.0000000E+00	0.0000000E+00
6258	4458.1676	4983.8911	-7229.3351	0.0000000E+00	0.0000000E+00	0.0000000E+00
6334	562.43301	7825.6980	-13010.654	0.0000000E+00	0.0000000E+00	0.0000000E+00
6369	9569.0605	5653.6931	-26971.458	0.0000000E+00	0.0000000E+00	0.0000000E+00
6261	28546.614	4753.1624	-36760.626	0.0000000E+00	0.0000000E+00	0.0000000E+00
6367	47136.041	10916.357	39628.541	0.0000000E+00	0.0000000E+00	0.0000000E+00
6365	-44826.490	19429.868	-31279.792	0.0000000E+00	0.0000000E+00	0.0000000E+00
6364	33801.595	5152.6782	-18039.584	0.0000000E+00	0.0000000E+00	0.0000000E+00

**** SUMMATION OF FORCES AND MOMENTS IN GLOBAL COORDINATES ****

Fx = 540768.2
Fy = 29785.63
Fz = 378661.5
Mx = 0.5268679E+00
My = 0.1783020E+09
Mz = 0.3805200E+06
F1 (R) = 0.0000000E+00
M1 (R) = 0.0000000E+00
M2 (R) = 0.0000000E+00
F3 (R) = 0.0000000E+00

SUMMATION POINT= 0.00000E+00 0.00000E+00 0.00000E+00

CASE FOR LABEL: TYPE FROM 7 10 7 81 1

Table 5.23

TENSILE STRESS (psi) AT THE MAXIMUM MOMENT SECTION OF GIRDER RE

LOAD	ANALYSIS CASE C ITERATION		
	0	1	2
DL	335	390	465
DL + T _w	50	510	765

DL = Concrete Dead Load + Hydrostatic Pressure + High Density Racks
 + Stored Cask

T_w = Winter Temperature Condition

6.0 REFERENCES

1. GPUN Contract No PC-082008, "Engineering Services for the Oyster Creek Fuel Pool Structural Analysis," October 20, 1989.
2. GPUN, "Specification for Oyster Creek Nuclear Generating Station Spent Fuel Pool Structure Qualification for Consolidated Spent Fuel Storage," SP-1302-53-047, Revision 1.
3. ABB Impell, "Analysis Criteria Document for the Structural Evaluation of the Spent Fuel Pool at Oyster Creek Nuclear Generating Station," Revision 0, dated November 16, 1990.
4. ACI 349 - "Code Requirements for Nuclear Safety Related Concrete Structures," 1980.
5. ANSYS, Version 4.4, Swanson Analysis Systems, Inc.
6. Branson, "Deformation of Concrete Structures," McGraw Hill.
7. Branson and Trost, "Unified Procedures for Predicting the Deflection and Centroidal Axis Location of Partially Cracked Nonprestressed and Prestressed Concrete Members," ACI Journal, 1982.
8. Muenow and Associates, "Nondestructive Evaluation of Two Concrete Segments Beneath Fuel Storage Pool of OCNGS," November, 1989.
9. Wang and Salmon, "Reinforced Concrete Design," Harper and Row.
10. Park and Paulay, "Reinforced Concrete Structures," Wiley-Interscience.
11. "Fluid/Structure Interaction During Seismic Excitation," Report by the ASCE Committee on Seismic Analysis of the Committee on Nuclear Structures and Materials, 1984.
12. GPUN, "Spent Fuel Pool Wall Natural Frequency," Calc. No. C-1302-161-5320-010.
13. Application for a Full Term License - Supplement No. 1 to Amendment 68-Cask Drop Protection System for OCNGS, September, 1972.
14. GPUN, DRF No. 082385, dated March 16, 1990.

ABB Impell Corporation

15. GPUN, Letter No. 5511-90-031, dated March 19, 1990.
16. GPUN, Letter No. 5511-090-046, dated April 12, 1990.
17. GPUN - OCNCS FSAR Update, Chapter 3 - "Design of Structures, Components Equipment and Systems."
18. Gilbert Associates Drawing Nos. 3E-153-02-004, Revision 3 and 3E-153-02-005. Revision 3.
19. ABB Impell Calculation No. 0370-187-002, "Development and Verification of BRANSON Program."
20. Winter and Nilson, "Design of Concrete Structures," McGraw Hill.
21. GPUN, Letter No. 5511-090-097, dated July 10, 1990.
22. GPUN, Letter No. 5511-91-014, dated January 24, 1991.
23. GPUN, Letter No. 5511-90-105, dated August 10, 1990.
24. ABB Impell Calculation No. 0370-187-005, "GPUN SFP Analysis Case C."
25. ABB Impell Calculation No. 0370-187-003, "GPUN SFP Geometry."
26. ABB Impell Calculation No. 0370-187-004, "GPUN SFP Loads."
27. ABB Impell Calculation No. 0370-187-007, "GPUN SFP Analysis Case C Using Cracked Transformed Properties."
28. ABB Impell Calculation No. 0370-187-006, "GPUN SFP Analysis Case D."
29. Burns and Roe Drawing Nos. 4055 Revision 5, and 4073 Revision 2.
30. ABB Impell ROC No. 0370-187-R07, dated October 4, 1990.
31. ABB Impell Calculation No. 0370-187-001, "Development and Verification of RCBEAM Program."
32. ABB Impell Calculation No. 0370-187-008, "GPUN SFP Analysis Case D Applying Supplemental Cracking Criteria (Fully Transformed)."
33. ABB Impell Calculation No. 0370-187-009, "GPUN SFP Analysis Case C Iteration 4S with 0.9 Dead Load."



ABB Impell Corporation

34. ABB Impell Calculation No. 0370-187-010, "GPUN SFP Analysis Case C with Antisymmetry Boundary Condition for Seismic Load in North-South Direction."



ABB Impell Corporation

Appendix A

Input Files for the Spent Fuel Pool Evaluation

Files A.1 to A.14 on Floppy No. 1
Files A.15 to A.37 on Floppy No. 2
Files A.38 to A.55 on Floppy No. 3
Files A.56 to A.65 on Floppy No. 2
Files A.66 to A.76 on Floppy No. 4



ABB Impell Corporation

Input Files for Analysis Case C (Reference 24)

The file extensions are explained as follow:

7F5: Input file for Prep7
2F5: Input file for Post27
1F5: Input file for Post1

	<u>Filename</u>	<u>Description</u>	<u>No. of Pages</u>
A.1	TEMP.7F5	Fuel Pool Heat Transfer Analysis for winter and summer conditions.	51
A.2	CCI0.7F5	Structural Analysis - Cracking Iter. 0 Prior to cracking stage.	51
A.3	CCI1.7F5	Structural Analysis - Cracking Iter. 1 Floors at elev. 75', 95' and 119' except the solid elements at elev. 75' had a reduced stiffness by one thousand.	51
A.4	CCI1LC.2F5	Load combination for equations b and e based on Iteration 1.	1
A.5	CCI1SCT.1F5	Linearized stresses for various sections in the Shield-Wall, SFP Slab and Walls based on equation e of Iteration 1.	4
A.6	CCI2.7F5	Structural Analysis - Cracking Iter. 2 Shield-Wall, SFP Slab and Walls cracked.	65
A.7	CCI2LC.2F5	Load combination for equations b and e based on Iteration 2.	1
A.8	CCI2SCT.1F5	Linearized stresses for various sections in the slab at 75' based on equation e of Iteration 2.	1
A.9	CCI3SU.7F5	Structural Analysis - Cracking Iter. 3SU SFP Slab is uncoupled. Slab at 75', solid elements, is active. "SU denotes the SFP Slab is uncoupled".	66
A.10	CCI3SULC.2F5	Load combination for equations b and e based on Iteration 3SU.	1



ABB Impell Corporation

A.11 CCI3US.7F5	Structural Analysis - Cracking Iter. 3US SFP Slab is uncoupled for seismic. All floors including the solid elements at 75' were active. *US denotes SFP slab uncoupled for seismic".	65
A.12 CCI3USLC.2F5	Load combination for different seismic directions based on iteration 3US.	1
A.13 ECI3ULC.2F5	Load combination for all equations of Case C based on Iterations 3SU and 3US.	2
A.14 ECI3ULCS.1F5	Printed results at all critical sections for evaluation based on ECI3ULC.2F5.	32
A.15 CCI3RB.7F5	Structural Analysis - Cracking Iter. 3RB Slab at 75', solid elements, is fully cracked beside all other floors. *RB denotes rectangular beam behavior".	66
A.16 CCI3RBLC.2F5	Load combination for equations b and e based on Iteration 3RB.	1
A.17 CCI3RBST.1F5	Linearized stresses for various sections in girders RD, RE and R6 based on equation e of Iteration 3RB.	2
A.18 CCI3SS.7F5	Structural Analysis - Cracking Iter. 3SS All floors are active except the solid elements at elev. 75' had negligible mass and stiffness. *SS denotes seismic with floors stiffness included".	64
A.19 CCI3SSLC.2F5	Load combination for different seismic directions based on Iteration 3SS.	1
A.20 ECI3RLC.2F5	Load combination for all equations of Case C based on Iterations 3RB and 3SS.	2
A.21 ECI3RLCS.1F5	Printed results at all critical sections for evaluation based on ECI3RLC.2F5.	34
A.22 CCI4.7F5	Structural Analysis - Cracking Iter. 4 Girders RD, RE and R6 cracked based on iteration 3RB.	67
A.23 CCI4LC.2F5	Load combination for all equations of Case C based on Iterations 4.	1



ABB Impell Corporation

A.24	CCI4SS.7F5	Structural Analysis - Cracking Iter. 4SS All floors are active except the solid elements at elev. 75' had negligible mass and stiffness. *SS denotes seismic with floors stiffness included*.	66
A.25	CCI4SSLC.2F5	Load combination for different seismic directions based on Iteration 4SS.	1
A.26	ECI4LC.2F5	Load combination for all equations of Case C based on iterations 4 and 4SS.	2
A.27	ECI4LCS.1F5	Printed results at all critical sections for evaluation based on ECI4LC.2F5.	34
A.28	CCI5.7F5	Structural Analysis - Cracking Iter. 5 Shield-Wall stiffness and mass were negligible.	65
A.29	CCI5S.7F5	Structural Analysis - Cracking Iter. 5S All floors are active except the solid elements at elev. 75' had negligible mass and stiffness. *S denotes seismic with floors stiffness included*.	64
A.30	ECI5LC.2F5	Load combination for all equations of Case C based on Iterations 5 and 5S.	2
A.31	ECI5LCS.1F5	Printed results at all critical sections for evaluation based on ECI5LC.2F5.	34
A.32	LOADDCC.1F5	Load distribution among primary members of the SFP structure for each Iteration and each load acting alone.	15
A.33	DISPCC.1F5	Displacements at critical locations in the SFP structure for each Iteration and each load acting alone.	14
A.34	SLBDISP.1F5	Displacements at the uncoupled degrees freedom in the SFP Slab for Iteration 3U for load combination equation "b".	1
A.35	ECCSLB.1F5	Shear forces and linearized stresses in the SFP Slab at an alternative south section for all eight load combination equations for Iterations 3U, 3R and 4.	5
A.36	ECCGBWX.1F5	Linearized stresses in girders for bending about weak axis, Iterations 3R, 4 & 5.	3



ABB Impell Corporation

A.37 EC15LCNM.1F5 Linearized stresses in girders RD and RE 4
for negative moment region, Iteration 5.

Input Files for Analysis Case D (Reference 28)

<u>Filename</u>	<u>Description</u>	<u>No. of Pages</u>
A.38 TEMPCD.7F5	Fuel Pool Heat Transfer Analysis for winter and summer conditions.	51
A.39 CD12.7F5	Structural Analysis - Cracking Iter. 2 Shield-Wall, SFP Slab and Walls cracked.	63
A.40 CD13SU.7F5	Structural Analysis - Cracking Iter. 3SU SFP Slab is uncoupled. Slab at 75', solid elements, is active. "SU denotes the SFP Slab is uncoupled".	64
A.41 CD13US.7F5	Structural Analysis - Cracking Iter. 3US SFP Slab is uncoupled for seismic. All floors including the solid elements at 75' were active. "US denotes SFP Slab uncoupled for seismic".	63
A.42 ED13ULC.2F5	Load combination for all equations of Case C based on iterations 3SU and 3US.	2
A.43 ED13ULCS.1F5	Printed results at all critical sections for evaluation based on EC13ULC.2F5.	32
A.44 CD13RB.7F5	Structural Analysis - Cracking Iter. 3RB Slab at 75', solid elements, is fully cracked beside all other floors. "RB denotes rectangular beam behavior".	64
A.45 CD13SS.7F5	Structural Analysis - Cracking Iter. 3SS All floors are active except the solid elements at elev. 75' had negligible mass and stiffness. "SS denotes seismic with floors stiffness included".	63
A.46 ED13RLC.2F5	Load combination for all equations of Case C based on iterations 3RB and 3SS.	2



ABB Impell Corporation

A.47	CDI3RBST.1F5	Linearized stresses for various sections in girders RD, RE and R6 based on equation e of iteration 3RB.	2
A.48	EDI3RLCS.1F5	Printed results at all critical sections for evaluation based on EDI3RLC.2F5.	35
A.49	CDI4.7F5	Structural Analysis - Cracking Iter. 4 Girders RD, RE and R6 cracked based on iteration 3RB.	65
A.50	CDI4SS.7F	Structural Analysis - Cracking Iter. 4SS All floors are active except the solid elements at elev. 75' had negligible mass and stiffness. *SS denotes seismic with floors stiffness included*.	64
A.51	EDI4LC.2F5	Load combination for all equations of Case C based on iterations 4 and 4SS.	2
A.52	EDI4LCS.1F5	Printed results at all critical sections for evaluation based on EDI4LC.2F5.	35
A.53	LOADDCD.1F5	Load distribution among primary members of the SFP structure for each iteration and each load acting alone.	7
A.54	ECDSLBS.1F5	Shear forces and linearized stresses in the SFP Slab at an alternative south section for all eight load combination equations for iterations 3U, 3R and 4.	5
A.55	ECDSLBS.1F5	Shear forces in the SFP Slab at the punching shear section for all eight load combination equations for iterations 3U, 3R and 4.	12



ABB Impeil Corporation

Input Files for Analysis Case C (Reference 27)
Applying Supplemental Cracking Criteria (Fully Transformed)

<u>Filename</u>	<u>Description</u>	<u>No. of Pages</u>
A.56 CCI4W.7F5	Structural Analysis - Cracking Iter. 4W Cracked Transformed Properties for SFP Walls and Poisson Ratio of 0.01.	61
A.57 CCI4WSS.7F5	Structural Analysis - Cracking Iter. 4WSS Seismic run for Cracking Iter. 4W In addition to changes made in iteration 4W, all floors are active except the solid elements at elev. 5' had negligible mass and stiffness. "SS denotes seismic with floors stiffness included".	60
A.58 ECI4WLC.2F5	Load combination equations (10 Eqs.) Based on iterations 4W and 4WSS.	3
A.59 CCI4S.7F5	Structural Analysis - Cracking Iter. 4S Cracked Transformed Properties for SFP Walls and Slab and Poisson Ratio of 0.01.	58
A.60 CCI4SSS.7F5	Structural Analysis - Cracking Iter. 4SSS Seismic run for Cracking Iter. 4S In addition to changes made in iteration 4S, all floors are active except the solid elements at elev. 75' had negligible mass and stiffness. "SS denotes seismic with floors stiffness included".	57
A.61 ECI4SLC.2F5	Load combination equations (10 Eqs.) Based on iterations 4S and 4SSS.	3
A.62 ECI4SLCS.1F5	Printed results at all critical sections in the SFP Slab, girders and column C-6 for evaluation based on file ECI4SLC.F10.	34



ABB Impell Corporation

A.63 ECI4SLCW.1F5	Printed results at all critical sections in the SFP Walls based on file ECI4SLC.F10.	11
A.64 LOADCI4S.1F5	Load distribution among primary members of the SFP structure for iteration 4S for each load step.	4
A.65 ECI4SLNM.1F5	Linearized stresses in girders RD and RE for negative moment region, Iteration 4S.	5

Input Files for Analysis Case D (Reference 32)
Applying Supplemental Cracking Criteria (Fully Transformed)

<u>Filename</u>	<u>Description</u>	<u>No. of Pages</u>
A.66 CDI4S.7F5	Structural Analysis Cracking Iter. 4S Cracked Transformed Properties for SFP Walls and slab and Poisson Ratio of 0.01.	58
A.67 CDI4SSS.7F5	Structural Analysis - Cracking Iter. 4SSS Seismic run for Cracking Iter. 4S. In addition to changes made in iteration 43, all floors are active except the solid elements at Elev. 75' had negligible mass and stiffness. "SS denotes seismic with floors stiffness included".	57
A.68 EDI4SLC.2F5	Load combination equations (10 Eqs.) Based on iterations 4S and 4SSS.	3
A.69 EDI4SLCS.1F5	Printed results at all critical sections in the SFP Slab, girders and Column C-6 for evaluation based on file EDI4SLC.F10.	34
A.70 LOADDI4S.1F5	Load distribution among primary members of the SFP structure for iteration 4S for each load step.	4



ABB Impell Corporation

Input Files for Analysis Case C (Reference 33)
Iteration 4S with 0.9 Dead Load

<u>Filename</u>	<u>Description</u>	<u>No. of Pages</u>
A.71 CI4SL9U.2F5	Post27 input file for all ten (10) Load combination similar to ECI4SLC.2F5 of reference 9.	3
A.72 CI4SL9US.1F5	Post1 input file to print linearized stresses and forces at the critical sections similar to ECI4SLCS.1F5 of reference 9.	34
A.73 CI4SL9D.2F5	Post27 input file for all ten (10) Load combination similar to CI4SL9D.2F59.	3
A.74 CI4SL9DS.1F5	Post1 input file to print linearized stresses and forces at the critical sections similar to CI4SL9US.1F5.	34

Input Files for Analysis Case C (Reference 34)
with Anti-Symmetry Boundary Condition
for Seismic Load in North-South Direction

<u>Filename</u>	<u>Description</u>	<u>No. of Pages</u>
A.75 CCI3SSAX.7F5	Prep7 input file. In addition to file CCI3SS.7F5 the antisymmetry boundary conditions were applied along column line R4 for seismic inertia in the north-south direction.	61
A.76 ECI3SSA.1F5	Post1 input file to print linearized stresses in girders RD, RE and R6 and column C6.	4



ABB Impell Corporation

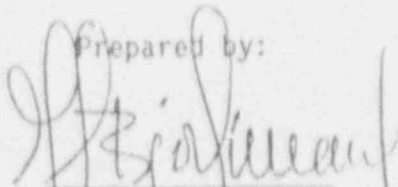
ANALYSIS CRITERIA DOCUMENT
FOR
THE STRUCTURAL EVALUATION OF THE SPENT FUEL POOL
AT
OYSTER CREEK NUCLEAR GENERATING STATION

Prepared for:

GPU Nuclear Corporation
One Upper Pond Road
Parsippany, New Jersey 07054

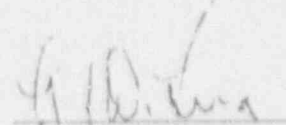
Revision 1
June 13, 1991

Prepared by:



Gordon S. Bjorkman
Technical Manager

Approved by:



L. J. DiLuna
Technical Manager

ABB Impell Corporation
800 South Street
Waltham, MA 02154



ABB Impell Corporation

Analysis Criteria Document
Revision 1
Job No. 0370-187-1683
Page 1 of 21

1.0 PURPOSE

The purpose of this document is to establish the criteria that will govern the analysis of the Spent Fuel Pool (SFP). This includes the definition of loads, load combinations, material properties, and the evaluation of section capacity. It also includes the methodology by which relative stiffness is established, the criteria that governs changes in relative stiffness due to concrete cracking, how stiffness changes are implemented, and the relationship between relative stiffness and the loading sequence. More generally the document discusses the extent of the finite element model, the boundary conditions employed, and the types of elements used.

2.0 DEFINITION OF LOADS

2.1 Dead Load

Dead load shall consist of the weight of reinforced concrete at a density of 150 lb/ft³, a 38'-9" column of water at a density of 62.4 pounds per cubic foot within the SFP, the submerged weight of fully loaded racks, and a localized load in the northeast corner of the pool to simulate a 100 ton cask temporarily stored within the Cask Drop Protection System.

The 100 ton cask dead load shall be applied as a uniform pressure to the elements within the ten (10) foot diameter circle centered as shown in Figure IV-8 of Reference 5.

Three fully loaded fuel rack cases shall be considered:

Case 1. Rack and fuel loads in place in 1983 shall be used. The rack loads shall be determined from the Wachter rack drawings listed in Reference 19. The Wachter racks are as located on Sketch No. 1 of Reference 20, except that row 6 was never installed. Approximately 980 fuel assemblies were in the pool in 1983 located in rows 1, 2 and 3 (Sketch No. 1). The weight of one fuel assembly is 680 pounds and its net volume is 2326 cubic inches including the channel.



ABB Impell Corporation

Analysis Criteria Document
Revision 1
Job No. 0370-187-1683
Page 2 of 21

- Case 2. The weights of the fully loaded high density racks presently in the pool are provided on Joseph Oat Drawing D-7475, Revision 4 (Reference 19) and their location within the pool is shown on Joseph Oat Drawing D-7472, Revision 2. The volume of the racks can be calculated from the Joseph Oat Drawings. The weight and volume of one fuel assembly are as specified for Case 1 above.
- Case 3. The weight, volume, and layout of the racks shall be the same as in Case 2 above. The net volume of a consolidated fuel assembly (i.e. fuel rods), including the canister, is 4158 cubic inches. The weight of one fuel canister fully loaded shall be 1350 lbs. (Reference 21).

Fuel and rack loads may be applied as an equivalent uniform pressure to the pool slab elements which are directly beneath the racks.

2.2 Live Load

2.2.1 Design Live Load

Design Live Load shall be as specified below:
(See Table 3.8.6 of Reference 7)

TABLE 2.2.1 - DESIGN LINE LOADING

<u>Elevation</u>	<u>Area of Loading</u>	<u>Live Load (psf)</u>
119'-3"	Columns A-C, 4-7	1000
119'-3"	Remainder	800
95'-3"	New Fuel Storage	800
95'-3"	Remainder	400 + 20 kips
75'-3"	All Floors	400

2.2.2 Equipment Live Load

Equipment Live Load shall be as specified below (Reference 21 and 23):



ABB Impoli Corporation

Analysis Criteria Document
Revision 1
Job No. 0370-187-1683
Page 3 of 21

Elevation 75'-3":

1. Two (2) Fuel Pool Heat Exchangers weighing 3200 lbs. each located near the junction of column lines R5 and RE-RF.
2. Two (2) Spent Fuel Pool Pumps weighing 5000 lbs. each located near the junction of column lines R5-R6 and RE-RF.
3. One (1) Augmented Spent Fuel Pool Heat Exchangers weighing 31,700 lbs. each located near the junction of column lines R7 and RD.
4. Two (2) Augmented Spent Fuel Pool Pumps weighing 5000 lbs. each located near the junction of column lines R7 and RE.

Elevation 95'-3":

1. Two (2) Emergency Condensers weighing 380,000 each located in the region of column lines R3-R5 and RA-RC.

2.3 Seismic Load

The Operating Basis Earthquake (OBE) horizontal acceleration in both the north-south and east-west directions shall be 0.24g. The OBE vertical acceleration shall be 0.10g (Reference 6).

The Safe Shutdown Earthquake (SSE) horizontal acceleration in both the north-south and east-west directions shall be 0.48g. The SSE vertical acceleration shall be 0.20g (Reference 6).

For the reinforced concrete of the SFP, the equivalent static seismic load shall equal the weight of the SFP walls, slab, and supporting girders multiplied by the appropriate vertical and horizontal absolute acceleration.

Except as specifically noted, all references to horizontal and vertical accelerations shall pertain to the values given above.



ABB Imnell Corporation

Analysis Criteria Document
Revision 1
Job No. 0370-187-1683
Page 4 of 21

For the pool water, the vertical inertial load on the SFP slab shall equal the weight of the 38'-9" column of water multiplied by the vertical acceleration of the SFP slab. Statically equivalent hydrodynamic loads shall be applied to the SFP walls using the methodology of Reference 10 and employing the horizontal acceleration values given above. The seismic acceleration to be used for the calculation of sloshing loads will be provided by GPUN based on the frequency of the sloshing water as provided by Impell.

To account for fuel rack impact loads during a seismic event with the pool full of racks, the buoyant weight of fully loaded racks shall be multiplied by the vertical acceleration. No horizontal inertia loading shall be applied (Reference 20).

The directions of seismic loading shall be applied independently and the results combined by SRSS.

2.4 Thermal Gradients

The stress free condition shall be 60°F for all analysis cases. The thermal gradients for Analysis Cases A, B, C and D are based on the Reactor Building air temperature varying from 40°F to 110°F, the pool water temperature varying from 85°F to 100°F, and the temperature of the interior surface of the drywell concrete varying with elevation. These variations result in two critical thermal conditions as shown in Table 2.4 (Reference 26).

Thermal Cases 1 and 2 are intended to maximize stresses in the SFP walls and slab. The maximum stresses in the concrete shield wall will result when the temperature in the drywell is a maximum and the water temperature in the pool is a minimum. Maximum stresses in the pool slab will result when the water temperature is maximum and the ambient air temperature in the reactor building is minimum, but, per Tech. Spec., this gradient may not exceed 60°F. (With the water temperature at the Tech. Spec. maximum of 125°F and the ambient temperature in the reactor building at 65°F, the same 60°F gradient will occur across the slab, but the gradient across the shield wall will be minimized and, as such, this combination does not control.)

All thermal gradients shall be considered to be steady state conditions and linearly distributed through the concrete thickness.



ABB Impell Corporation

Analysis Criteria Document
Revision 1
Job No. 0370-187-1683
Page 5 of 21

TABLE 2.4

SPENT FUEL POOL ANALYSIS TEMPERATURES (°F)

<u>ELEVATION (ft.)</u>	<u>INTERIOR SURFACE CONCRETE SHIELD WALL</u>	<u>FUEL POOL WATER</u>	<u>REACTOR BUILDING AMBIENT AIR</u>
<u>Case 1</u>			
50	105*	N/A	40
80	176*	100	40
92	200*	100	40
95	200**	100	40
110	200**	100	40
<u>Case 2</u>			
50	126*	N/A	110
80	176*	85	110
92	200*	85	110
95	200**	85	110
110	200**	85	110

* Calculated

** Measured

2.5 Cask Drop Accident

The effect of a cask drop accident shall be considered in the analysis using an equivalent static load of 1560 kips applied to the SFP slab (Reference 21). This load shall be uniformly distributed over the slab elements within a 10' diameter circle centered as shown in Figure I/-8 of Reference 5.



ABB Impell Corporation

Analysis Criteria Document

Revision 1

Job No. 0370-187-1683

Page 6 of 21

3.0 ANALYSIS CASES

3.1 Case A, Baseline Analysis

The baseline analysis assumes normal plant operation loads, the rack and fuel loads in place in 1983 as given in Section 2.1, Case 1, and two thermal gradient cases as delineated in Section 2.4. No seismic or cask drop loads shall be considered and only equipment live load shall be included for this case. Adequate embedment length of the rebar shall be assumed and pre-existing cracks shall not be included.

3.2 Case B Analysis

This analysis will use the same assumptions as in Case A, except that a reduced embedment of the bottom slab rebar into the supporting beams and walls shall be assumed.

3.3 Case C Analysis

This analysis shall assume normal plant operating loads and the high density rack and fuel loads as given in Section 2.1, Case 2. Reduced rebar embedment and the existing crack as described in Reference 6 shall be included. The thermal gradients shall be as delineated in Section 2.4. Seismic, cask drop, and design live load shall be considered.

3.4 Case D Analysis

This analysis shall assume normal plant operating loads and the maximum rack and consolidated fuel loads as given in Section 2.1, Case 3. Reduced rebar embedment and the existing crack as described in Reference 6 shall be included. The thermal gradients shall be as delineated in Section 2.4. Seismic, cask drop, and design live load shall be considered.

4.0 LOAD COMBINATIONS

4.1 Analysis Cases A and B

The following load combinations shall be considered for Analysis Cases A and B (References 6 and 21).

- a. $1.4D + 1.7L$
- b. $0.75 (1.4D + 1.7L + 1.4T_0)$



ABB Impell Corporation

Analysis Criteria Document
Revision 1
Job No. 0370-187-1683
Page 7 of 21

Where: D = dead load as specified in Section 2.1, Case 1
 L = live load as specified in Section 2.2.2
 T_0 = thermal loading due to temperature differential across the slab or wall as specified in Table 2.4

4.2 Analysis Cases C and D

The following load combinations shall be considered for Analysis Cases C and D (Reference 6 and 21).

- a. $1.4D + 1.7L \pm 1.9E$
- b. $0.75 (1.4D + 1.7L + 1.4T_0)$
- c. $0.75 (1.4D + 1.7L + 1.4T_0 \pm 1.9E)$
- d. $D + L + T_0 \pm E'$
- e. $D + L + T_0 + C$

Where: D = dead load as specified in Section 2.1, Cases 2 and 3
 L = live load as specified in Section 2.2.1
 T_0 = thermal loading due to temperature differential across the slab or wall. Two critical cases shall be considered as specified in Table 2.4.1
 E = OBE seismic load as specified in Section 2.3
 E' = SSE seismic load as specified in Section 2.3
 C = Cask drop load as specified in Section 2.5

Due to the introduction of live load in each of these equations, the load combination equations cannot be conservatively simplified to take advantage of the fact that $E' = 2E$.

4.3 Additional Considerations

In the load combination equations in Sections 4.1 and 4.2 slab live load shall be neglected if the presence of slab live load reduces the stresses due to other loads.

When live load and seismic load are specified in the same load combination, the full live load shall be considered to act with the seismic inertia load. No portion of the full live load shall be seismically amplified or be considered part of the seismic inertia load.



ABB Impell Corporation

Analysis Criteria Document
Revision .
Job No. 070-187-1683
Page 8 of 21

5.0 MATERIAL PROPERTIES AND SECTION CAPACITY

A yield strength of 40,000 psi shall be used for the reinforcing steel.

The compressive strength of the concrete shall be 3000 p.s.i. An increase in strength may be allowed for dynamic loading of the cask drop accident in accordance with Appendix C of Reference 1.

Section capacities, stresses and properties shall be determined in accordance with ACI-349 (Reference 1) and standard engineering texts on reinforced concrete analysis and design (References 12, 13, 14, and 15). Ultimate moment capacity shall be based on the fundamental assumptions of ACI-349 Section 10.2 and shall use the Whitney Stress Block for concrete as described in ACI-349 Section 10.2.7.

The surrounding structural floor slabs at Elevations 75', 95', and 119' in the SFP finite element model are expected to generate axial loads in the SFP walls and slab due to the restraint of axial thermal growth. Since compressive axial forces can have a significant effect on increasing the moment capacity of a section, the calculation of the moment capacity of a member at critical sections will account for the effects of axial load. The calculation of section capacity accounting for axial loads shall comply with ACI-349 Section 10.3.1. However, when the presence of axial force increases moment capacity the axial force shall be reduced to 90% of its value when calculating usable moment capacity.

The calculation of concrete and steel stresses at moments which are less than ultimate shall be based on the application of first principles (i.e., cross section equilibrium, linear strain distribution, strain compatibility, and the stress-strain curves for concrete and steel).

The influence of axial forces on shear capacity shall also be considered and shall comply with ACI-349 Section 11.3.1.2 and 11.3.2.3. However, when the presence of axial force increases shear capacity the axial force shall be reduced to 90% of its value when calculating usable shear capacity.



ABB Impoll Corporation

Analysis Criteria Document
Revision 1
Job No. 0370-187-1683
Page 9 of 21

6.0 THE FINITE ELEMENT ANALYSIS

6.1 The Spent Fuel Pool Model

Extent of the Model

GPUN has identified flexure and flexure-shear cracks in girder RE (Reference 16) which supports the northwest corner of the spent fuel pool slab. This cracking may be load induced, in which case a potentially significant redistribution of internal forces may have already taken place, not just locally, but on a more global scale. It is, therefore, essential to the resolution of the issues surrounding the cracking of girder RE, that the finite element model be of sufficient size and detail to properly predict where the internally redistributed forces have gone within the Reactor Building in order to achieve overall equilibrium. Thus, the finite element model shall have the capability of predicting the cracking of the concrete and the consequent redistribution of internal forces and stresses as a result of these cracks. This requires that non-linear loading increments be incorporated into the loading process to achieve a final cracked state within the structure. The SFP finite element model will be developed and analyzed using the ANSYS Computer Code Revision 4.4.

While the SFP walls and floor slab occupy a relatively small region of the Reactor Building, they are an integral part of the much larger Reactor Building structure. The south wall and south side of the SFP floor slab are integrally cast with and supported by the Reactor Shield Wall. The east, north, and west walls are supported beneath the slab by integral columns and deep girders which themselves are supported by walls along Column Lines RF and R7. In addition, the spent fuel pool walls are restrained by integral slabs at Elevations 95' and 119', and the SFP floor slab is restrained on three sides by the eccentric slab at Elevation 75'. The reactor shield wall and supporting girders provide significant bending and axial restraint to the SFP, and the slabs at Elevations 75', 95' and 119', while not providing significant bending restraint, could provide significant membrane restraint. The stiffening effects of these integral structural elements on the behavior of the SFP cannot be neglected. It is, therefore, desirable to extend the model to include adjacent portions of the reactor building structure.



ABB Impell Corporation

Analysis Criteria Document
Revision 1
Job No. 0370-187-1683
Page 10 of 21

The finite element model will provide boundary conditions for the SFP which will ensure the accurate prediction of its non-linear behavior (cracking) and subsequent internal force redistribution for a complex set of loading conditions. To accomplish this, the model will include the drywell shield wall and all columns, slabs, walls, and girders between Column Lines R4 and R7 in the north-south direction and between Column Lines RA and RF in the east-west direction. Vertically the model will extend from Elevation 51' to Elevation 119'. Extending the SFP model in all directions to incorporate all structural members integrally attached to the SFP ensures that the boundary conditions for the SFP are accurate. By including this extended region, the SFP finite element model naturally subdivides into two distinct parts; the Main SFP Model and the Extended Region Superelement.

Finite Element Types

The SFP floor slab and walls have relatively high depth to span ratios. At large depth to span ratios shear deformations become significant. In addition there exists the possibility that cracking could occur in one direction of a wall or slab but not in the other. Both of these effects can be incorporated in the model by the use of finite elements which account for shear deformation and orthotropic material behavior in their formulations. To incorporate these effects, the finite element model of the SFP slabs and walls shall be constructed of orthotropic solid elements.

Girders supporting the SFP along Column Lines RE, RD, and R6 will be modeled with a minimum of four solid elements from the top of the pool slab through the depth of the girder web. This will be done in lieu of locally thickening the slab element or using beam elements, since these techniques cannot properly account for local "tee-beam" behavior. Providing solid elements through the entire depth of the girder incorporates this behavior. This type of model can accurately incorporate the effects of cracking through the girder web by transformation of the directional elastic moduli of each element through the depth.

The south wall of the spent fuel pool is monolithically cast with the drywell shield wall and contains the thickest concrete regions of the SFP. This region of the SFP and the extended drywell shield wall shall be modeled using orthotropic solid elements.



ABB Impell Corporation

Analysis Criteria Document
Revision 1
Job No. 0370-187-1683
Page 11 of 21

The most difficult region of the SFP finite element model to construct with solid elements is the geometrically complex intersection region of the SFP slab and drywell shield wall upper cone. This area will be carefully modeled with eight node solids and tetrahedrons to ensure that the warping of element faces is avoided.

The slab at elevation 75'-3" between column lines RE and RD contains a through thickness crack at the intersection with the SFP wall/slab. This slab also forms the top flange of cracked girder RE. Based on these considerations the slabs at Elevation 75'-3" which attach to girders RE, RD, and R6 shall be modeled using solid elements to ensure that potentially complex load redistribution patterns can occur.

All of the regions discussed above, i.e., the SFP wall and slab, drywell shield wall, girders RD, RE and R6, and the selected slabs at Elevation 75'-3" constitute the Main SFP Model. The Main SFP Model shall be modeled using orthotropic solid elements with two or more elements through the member thickness. All of the elements comprising the slabs at Elevation 75', 95' and 119', and the walls of column lines RA, RF, and R7 which connect the Main SFP Model with the terminal boundaries constitute the Extended Region Superelement and shall largely be composed of plate (shell type) elements with some solid elements in sensitive transition regions.

Terminal Boundary Conditions

Due to the encompassing size of the SFP finite element model, boundary conditions need only be applied within the plane of Column Line R4 and the plane of Elevation 23'. To these planes the following terminal boundary conditions shall be applied: (To describe the boundary conditions let the positive global X axis point in the direction of north and the positive global Z axis be vertically up.)

a. Column Line R4

Symmetric boundary conditions shall be applied to all nodes along Column Line R4 from Column Line RA to Column Line RF and between Elevation 23' and Elevation 119' (i.e., translation in X and rotation about Y and Z equal zero with all other degrees of freedom unrestrained).



ABB Impell Corporation

Analysis Criteria Document
Revision 1
Job No. 0370-187-1683
Page 12 of 21

b. Elevation 23'

At Elevation 23' the nodes of the drywell shield wall and all other walls and columns shall be restrained horizontally, vertically and rotationally. The vertical (Z) degrees of freedom of column C-6 shall be either fully restrained or elastically restrained depending on the results of relative stiffness calculations for the lower elevations.

c. Remaining Degrees of Freedom

Except as specifically noted, all other degrees of freedom shall be unrestrained.

6.2 Criteria for Cracked Stiffness Properties

Application of the Branson Equation

Following the initial cracking of a slab or wall element, an effective element stiffness (elastic modulus) will be calculated based onto the use of a fourth order Branson Equation (Reference 1 and 14). The Branson Equation is the only expression explicitly recognized by ACI 349-80 for the computation of the flexural rigidity of reinforced concrete members to account for the effects of cracking.

For determining the flexural rigidity of partially cracked concrete sections the Branson Method provides a transition value between well-defined limits in the uncracked and fully cracked states. The Branson Method is based on proportioning between these limits where the proportioning factor is a function of the ratio of actual moment to cracking moment.

Since thermal loads may introduce significant compressive axial forces in the walls and slab of the SFP, the Branson Method must be adapted to account for the influence of axial load on changing flexural rigidity. This will be done by defining the cracking moment to be the actual moment on the cross section which in combination with axial load produces an extreme fiber tensile stress equal to the modulus of rupture (Reference 24).

Since the main SFP model is composed entirely of solid elements, the moments and axial forces acting on the cross section of slab or beam members cannot be obtained directly from the ANSYS output. Therefore, the moment and axial forces acting on any cross section



ABB Impell Corporation

Analysis Criteria Document
Revision 1
Job No. 0370-187-1683
Page 13 of 21

will be obtained by integrating the nodal stresses through the depth of the section. The resulting moment and axial force will be used in the Branson Equation to determine the section effective flexural stiffness.

All solid elements in the main SFP model will incorporate cracking affects by changes to the elastic modulus in the direction of cracking. The new value of elastic modulus in the cracked direction will be correlated to the relative stiffness changes predicted by the Branson equation. The influence of tension stiffening due to the uncracked concrete still bonded to the steel adjacent to the crack is implicitly incorporated in the empirical formulation of the Branson equation.

The pre-existing flexural cracks in girder RE and the slab at Elevation 75'-3" shall be modeled by modifying the elastic modulus of the elements through which the cracks pass. The effective modulus of the element in the direction perpendicular to the crack may be derived from the crack sizes given in Reference 25. To establish an effective modulus based on crack size, an approximate rebar stress at the crack will be determined from the Gergely-Lutz Equation (Reference 12). The ACI Code provisions (ACI-349 Section 10.6.4) are based on the Gergely-Lutz expression for crack width. Extensive laboratory experiments have verified that crack width is proportional to steel stress. With an approximate rebar stress based on crack width and assuming fully cracked properties at the crack plane, an estimate of the moment acting on the section can be made. This moment becomes the actual moment in the Branson Equation from which an effective modulus can be calculated.

The effective shear stiffness of the web of a member containing diagonal tension (shear) cracks shall be based on the shear reinforcement in the member and the methodology given in Reference 15. The intent of the present analysis scope is to only include pre-existing flexural cracks in the SFP model for Analysis Cases C and D. Pre-existing diagonal shear cracks shall not be included.

Insufficient or reduced rebar embedment has the effect of lowering the moment capacity of a section by not allowing the yield stress of the reinforcement to be reached prior to bar pullout. At sections of the SFP slab where moment capacity could be effected by reduced embedment, the allowable moment capacity shall be reduced in proportion to the lack of required embedment beyond the effective section depth. If the reduced moment capacity is exceeded, the effective elastic modulus of the element in the direction of the rebar shall be reduced to zero.



ABB Impell Corporation

Analysis Criteria Document
Revision 1
Job No. 0370-187-1683
Page 14 of 21

Supplemental Cracking Criteria

Sections 9.5.2 and 9.5.3 of the ACI Code (Reference 1) refer to the use of the Branson Equation to predict member stiffness changes due to cracking for both one-way construction (beams) and two-way construction (slabs and walls). Based on the Branson Equation formulation, the use of this equation to compute cracked cross-section stiffness properties implies that the section under consideration has additional moment capacity beyond the cracking moment. This may not be the case for all structural components of the spent fuel pool.

Typically, one-way construction is more heavily reinforced than two-way construction and specific provisions of the ACI Code (Reference 1 Section 10.5.1) recognize the desirability for the moment capacity to be greater than the cracking moment. For slabs and walls the minimum reinforcement requirements specified by the Code may provide less reinforcement than necessary to ensure a moment capacity greater than the cracking moment. For slabs and walls so constructed, the Branson Equation will over-predict the resulting member stiffness as cracking takes place. This is particularly significant for thermal gradients, where the over-prediction of stiffness results in higher thermal moments.

Therefore, for slabs and walls where the cracking moment exceeds the moment capacity, a revised cracking criteria may be used. In this revised criteria the stress at which cracking occurs shall equal the value of stress computed elastically with the moment capacity applied to the uncracked section. Use of this criteria is intended to avoid the situation where the factored moment from a load combination exceeds the moment capacity for a section which may not have cracked or for which cracking has been under-estimated. Should such situations occur, the analyst shall use cracked transformed properties for the section.

6.3 Load Application

Concrete dead load will be applied as a lig vertical loading on all structural elements. Hydrostatic and hydrodynamic pool loads will be applied statically as element pressures to the floor and walls of the SFP. Hydrodynamic pool loads will be calculated using the methodology given in Reference 10 and will be based on the assumption that the SFP is essentially rigid, as demonstrated by calculations performed by GPUN (Reference 18). Static and dynamic fuel rack loads corresponding to the three levels of consolidation



ABB Impell Corporation

Analysis Criteria Document
Revision 1
Job No. 0370-187-1683
Page 15 of 21

and the cask drop load will be applied statically as element pressures within the region of loading. Thermal gradients will be applied as a linear distribution of surface and mid-surface temperatures through the thickness of the elements composing the floor and walls of the SFP and the drywell shield wall. Seismic inertia loads will be applied statically to all structural elements of the SFP as the appropriate percent of gravity based on floor response spectra ZPA values.

The purpose of the proposed investigations is to focus on the cracking and capacity of the SFP and its supporting structural members. It is not the intent of this investigation to chase the normal cracking which may occur in the slabs at Elevations 75', 91' and 119' due to the application of live load, except in the case of the slab adjacent to Girder RE at Elevation 75', which is cracked.

To avoid unnecessary cracking iterations for live load, which may or may not be active, statically equivalent tributary live loads may be applied at the slab boundaries. This will avoid having to consider the normal local flexural cracking of "secondary type" members (i.e., members incorporated in the model to achieve the proper boundary conditions) which will have little or no influence on the major redistribution of internal forces and will slow convergence during each non-linear cracking iteration in the analysis.

Prior to the formalized analysis, all loading cases will be applied separately to the entire model, assuming linear elastic behavior, to determine the general effects of the loading, its relative severity with respect to other loads, and its participation in the load combination equations.

The cracking of reinforced concrete members and the resulting non-linear behavior is a nonconservative process and requires that the actual load history be reasonably well followed, since final results are load path-dependent. However, the loading sequence which has occurred over the life of the Oystec Creek SFP structure is not exactly known and thus only a reasonable approximation to the true loading sequence can be made. Therefore, in lieu of any preferred loading sequence, the general loading sequence will follow the order shown below, which is believed to closely resemble the sequence in which the loads were actually applied to the SFP.



ABB Impell Corporation

Analysis Criteria Document
Revision 1
Job No. 0370-187-1683
Page 16 of 21

1. Concrete Dead Weight
2. Hydrostatic Loading
3. Fuel Rack Loading
4. Live Load
5. Thermal Loading
6. Seismic Inertia and Hydrodynamic or Cask Drop

6.4 Analysis Strategy

As the loads are applied to the SFP structure, the distribution of internal forces which resist these loads will be dependent on the relative stiffness of the various structural elements which comprise the SFP structure. When the load level reaches a certain value, cracking begins and load is transferred from the cracked tensile concrete to the adjacent tension steel reinforcement. This results in an instantaneous change in curvature, at constant moment (i.e., a reduction in rotational stiffness). As cracking continues, the relative stiffness of the structural elements begins to change and the internal forces begin to redistribute themselves within the SFP structure. This internal redistribution of forces is a non-linear process since the stiffness is changing with increasing load.

The question arises as to how this non-linear process can best be accounted for in the analysis of the SFP structure. An analysis strategy to account for this non-linear process must incorporate the following considerations:

- (1) Since the problem is non-linear, the final result will be dependent on the sequence in which the loads were applied. However, the loading sequence which has occurred over the life of the Oyster Creek SFP structure is not exactly known and therefore only a reasonable approximation to the loading sequence can be made. Strict adherence to loading sequence is typically not concern for nuclear power plant structures (Reference 1 and 26).
- (2) Since the dead load portion of the loading sequence (i.e., concrete deadweight, pool hydrostatic and rack loads) is expected to produce monotonically increasing levels of internal forces at the most critical regions of the structure, possible minor variations in the assumed loading sequence from the true loading sequence are not expected to significantly change the final results in these critical regions.



ABB Impell Corporation

Analysis Criteria Document
Revision 1
Job No. 0370-187-1683
Page 17 of 21

- (3) Thermal gradient is the most highly non-linear portion of the loading sequence and may cause moment reversal.
- (4) Thermal loads, in contrast to mechanical loads, are reduced as the flexural rigidity of the reinforced concrete members increase due to concrete cracking. Thus, thermal loads are an actively changing loading condition.
- (5) The Branson Equations are not intended to be applied in an incremental loading manner. The calculation of the effective moment of inertia for the computation of deflections at any load level must be based on the total load, and the resulting internal forces should be computed from a linear elastic analysis using initial (uncracked) stiffnesses. This is consistent with the derivation of the Branson Equation.
- (6) The Branson Equation is intended to predict deflections (flexural rigidity) at service load levels, not at factored load levels. In theory, the factored loads most nearly correspond to the structure's lower bound limit load. At or near the limit load, deflections within the actual structure may become highly non-linear and may tend to become unbounded. (This may not be exactly true for the SFP structure for which the factored loads may be well below the lower bound limit load.) However, factored loads can be used to form the basis for the flexural rigidity of the cracked structure in structural evaluations (Reference 26). The intent in using the Branson Equation for the SFP analysis is to have a reasonable methodology to account for the changes in stiffness which occur due to cracking and the resulting redistribution of internal forces.
- (7) The nonhomogeneous nature of reinforced concrete, together with its non-linear behavior, makes it difficult to accurately predict deflections (flexural rigidity) even for the simplest cases under controlled conditions. In fact, using the most accurate expression available (the Branson Equation) to compute deflections for simply supported beams under controlled laboratory conditions, there is approximately a 90% chance that the actual deflections of a particular beam will be within $\pm 25\%$ of the calculated value (Reference 17).



33 Impell Co. ration

Analysis Criteria Document
Revision 1
Job No. 0370-187-1693
Page 18 of 21

In view of these considerations, the most appropriate analysis strategy is one which provides a balanced approach to determining the redistribution of internal forces which occurs within the SFP structure due to concrete cracking. This balanced approach is one which weighs the cost of precise incremental iterative non-linear analysis against the large uncertainties which exist in our ability to precisely quantify the fundamental behavior of a complex reinforced concrete structure.

In a balanced approach, the analysis strategy should account for the differences in the three distinct types of loading to be applied, that is, include sustained load, thermal gradient, and dynamic.

Sustained Load

The effective moment of inertia of all solid elements shall be computed from the Branson Equation and the internal forces resulting from an analysis using either service or factored loads and uncracked stiffness properties. Cracking iterations will be applied at this load level until a stable crack equilibrium condition is reached. The final stiffnesses resulting from the cracking iterations will be used as the initial stiffness for the thermal load case.

Thermal Gradient Loads

Based upon a reasonable loading sequence, thermal gradient loads are assumed to be active after all sustained loads have been applied. This loading case is the most difficult to deal with in the analysis because of its tendency to reverse the curvature established during sustained load application and the interdependency of the magnitude of the internal forces on the stiffness assumptions.

The stiffness of the SFP structure at the initial application of the thermal gradient will be the final stiffness which exists after all sustained loads have been applied. The thermal gradient will be applied in steps with cracking iterations applied at each constant load step. (Alternatively the thermal gradient may be applied in a single load step with cracking iterations applied at constant load.) During each load step, those sections (elements) of the structure which continue to deform will have their stiffness reduced in accordance with the Branson Equation, while those sections which unload will be presumed to unload along their secant



ABB Impell Corporation

Analysis Criteria Document
Revision 1
Job No. 0370-187-1683
Page 19 of 21

stiffness. When crack closure occurs (i.e., zero tensile stress is reached), the element stiffness will be increased to the gross concrete value until such time as there is further evidence of cracking or crack opening. For those sections which continue to increase their curvature after cracking, the effective stiffness will be recalculated from the Larson Equation. This iterative process will continue until a stable crack configuration has been established at the full thermal gradient.

Seismic and Cask Drop Cases

Although seismic inertia, hydrodynamic, and cask drop loads will be applied statically, they are still dynamic loads which produce oscillations about an equilibrium stiffness position. As the structure moves in one direction away from the equilibrium position, its stiffness changes as crack opening and closing occurs. When the structure moves in the other direction away from the equilibrium position, cracks which opened on the previous half cycle are now closing and vice versa. In the absence of large moment reversals, the average structural stiffness accompanying this process can be assumed to be that which exists at the static equilibrium position. Therefore, the converged structural stiffness which exists at the end of the application of all actual static loads, including thermal gradient, will be the stiffness used for the statically applied dynamic loads.

7.0 REFERENCES

1. ACI 349 - Code Requirements for Nuclear Safety Related Concrete Structures, 1980.
2. Standard Review Plan. Section 3.8.4, Other Category I Structures, 1981.
3. Standard Review Plan, Section 9.1.2, Spent Fuel Storage, 1981.
4. Licensing Report on High Density Spent Fuel Racks for OCNGS, NRC Docket No. 50-219, August 22, 1983.
5. Application for a Full Term License - Supplement No. 1 to Amendment 68 - Cask Drop Protection System for OCNGS, September 1972.
6. GPU Nuclear - Specification for OCNGS Spent Fuel Pool Structure Qualification for Consolidated Spent Fuel Storage, SP-1302-53-047, Revision 1, July 1989.



ABB Impell Corporation

Analysis Criteria Document
Revision 1
Job No. 0370-187-1683
Page 20 of 21

7. GPU Nuclear - OCNGS FSAR Update, Chapter 3 - "Design of Structures, Components, Equipment and Systems".
8. GPU Nuclear - OCNGS Upper Drywell Shield Wall Thermal Analysis, Technical Data Report No. 713, September 16, 1985.
9. GPU Nuclear - OCNGS FSAR Update Section 9.1.2.3, Revision 1, February 1986.
10. "Fluid/Structure Interaction During Seismic Excitation," Report by the ASCE Committee on Seismic Analysis of the Committee on Nuclear Structures and Materials, 1984.
11. GPU Nuclear - OCNGS Upper Drywell Shield Wall Thermal Analysis, Technical Data Report No. 713, September 16, 1985.
12. Wang and Salmon, "Reinforced Concrete Design," Harper and Row.
13. Winter and Nilson, "Design of Concrete Structures," McGraw-Hill.
14. Branson, "Deformation of Concrete Structures," McGraw-Hill.
15. Park and Paulay, "Reinforced Concrete Structures," Wiley-Interscience.
16. GPU Nuclear - Investigation of Cracks in the Concrete Slabs and Girder above the Core Spray Pumps at Elevation 51'-3" of the Reactor Building, TDR No. 809, Revision 0.
17. ACI Committee 435, "Variability of Deflections of Simply Supported Reinforced Concrete Beams," ACI Journal, Proceedings, 69, January 1972, 29-35.
18. GPU Nuclear "Spent Fuel Pool Wall Natural Frequency" Calc. No. C-1302-161-5320-010.
19. GPU Nuclear, DRF No. 082385, dated March 16, 1990.
20. GPU Nuclear, Letter No. 5511-90-031, dated March 19, 1990.
21. GPU Nuclear, Letter No. 5511-90-046, dated April 12, 1990.
22. GPU Nuclear, Letter No. 5511-90-052, dated April 19, 1990.
23. Gilbert Associates Drawing No. 3E-153-02-004, Revision 3 and 3E-153-02-005, Revision 3.



ABB Impell Corporation

Analysis Criteria Document
Revision 1
Job No. 0370-127-1683
Page 21 of 21

24. Branson and Trost, "Unified Procedures for Predicting the Deflection and Centroidal Axis Location of Partially Cracked Nonprestressed and Prestressed Concrete Members," ACI Journal, 1982.
25. Muenow and Associates, "Nondestructive Evaluation of Two Concrete Segments Beneath Fuel Storage Pool of OCNGS," November 1989.
26. ACI 349.1R-80, Reinforced Concrete Design for Thermal Effects on Nuclear Power Plant Structures, 1981.
27. GPU Nuclear, Letter No. 5511-90-097, dated July 10, 1990.